2013

Permanent deformation and resilient modulus of unbound granular materials

Jia Li
Iowa State University

Permanent deformation and resilient modulus of unbound granular materials

by

Jia Li

A thesis submitted to the graduate faculty

In partial fulfillment of the requirements for the degree of

MASTER OF SCIENCE

Major: Civil Engineering (Geotechnical Engineering)

Program of Study Committee:
David J. White, Major Professor
Pavana Vennapusa
Robert W. Stephenson

Iowa State University

Ames, Iowa

2013

TABLE OF CONTENTS

LIST OF TABLES

LIST OF FIGURES

LIST OF SYMBOLS

Symbol	Description	Unit
a, b	Regression coefficients	—
A	Original area	mm^2
A_c	Corrected area	mm^2
BI	Breakage index	—
C_c	Coefficient of curvature	—
C_u	Coefficient of uniformity	—
c_u	Undrained shear strength	
D	Sample diameter	mm
D_{10}	Diameter corresponding to 10% finer	mm
D_{30}	Diameter corresponding to 30% finer	mm
D_{60}	Diameter corresponding to 60% finer	mm
E_m	Young's modulus of membrane	kN/m^2
E_p	Permanent deformation	—
F_{200}	Fines content (materials pass No.200 sieve)	%
G_s	Specific gravity	—
H_0	Original sample height	m
ΔH	Change in sample height	m
k_1, k_2, k_3	Regression coefficients	—
k_4, k_5, k_6	Regression coefficients	—
M_r	Resilient modulus	MPa
N	Number of load cycles	—
P	Applied load at surface	N
Pa	Atmospheric pressure	MPa
RD	Relative density	%
t_m	Membrane thickness	mm
w	Moisture content	%
τ_{oct}	Octahedral shear stress	MPa
ε_1	Axial strain	%

Symbol	Description	Unit
ε_p	Permanent strain	%
ε_f	Strain at failure	%
γ_d	Dry unit weight	kN/m^3
$\sigma_1, \sigma_2, \sigma_3,$	Principal stresses	kPa
σ_B	Bulk stress	MPa
σ_c	Confining pressure	kPa
$\sigma_{contact}$	Contact stress	kPa
σ_{cyclic}	Cyclic stress	kPa
σ_d	Deviator stress	kPa
$\sigma_{d\ max}$	Maximum deviator stress	kPa

UNIT CONVERSIONS

Measurement	From Metric Units	Conversion Factor	To English Units
Length	millimeter (mm)	0.03937	inches (in.)
Length	millimeter (mm)	0.00328	feet (ft)
Length	centimeter (cm)	0.39370	inches (in.)
Length	centimeter (cm)	0.03281	feet (ft)
Length	meter (m)	39.37	inches (in.)
Length	meter (m)	3.281	feet (ft)
Weight	gram (g)	0.0022	pound (lb)
Weight	kilogram (kg)	2.205	pound (lb)
Force	Newton (N)	0.2248	pound-force (lbf)
Force	kilo Newton (kN)	224.81	pound-force (lbf)
Density	kilo gram per cubic meter (kg/m^3)	0.0624	pound per cubic feet (pcf)
Unit Weight	kilo Newton per cubic meter (kN/m^3)	6.3659	pound per cubic feet (pcf)
Pressure	kilo Pascal (kPa)	0.145	pound per square inch (psi)
Pressure	kilo Pascal (kPa)	20.89	pound per square feet (psf)
Pressure	mega Pascal (MPa)	145.04	pound per square inch (psi)
Pressure	mega Pascal (MPa)	20885.4	pound per square feet (psf)

ABSTRACT

Permanent strain and resilient modulus provide direct, quantifiable values that describe two types of deformation (irrecoverable and recoverable) of pavement foundation materials under repeated transient traffic loads. Although the permanent deformation is not directly used in pavement design calculation, it affects the long-term performances of pavement foundations. The resilient moduli are used in AASHTO 1993 pavement design and the current Mechanistic-Empirical Pavement Design Guide.

This study investigated permanent deformation and resilient modulus characteristics of unbound granular materials in relation with relative densities, fines contents, material types, stress levels, and number of load applications. Materials tested in this study included crushed limestone and recycled aggregate materials (recycled asphalt pavement and recycled portland cement concrete).

Laboratory prepared samples were tested to assess the influence of different conditions varied in situ (e.g., relative density and fines content). Varied stress levels and number of load cycles were applied to samples to assess their influence on different material types.

Results from this investigation demonstrated that 1) accumulation of permanent deformations increased with deviator stress; 2) higher fines contents (12.4%-12.6%) result in lower permanent deformations than lower fines contents (0.8%-2.2%) for the materials with laboratory reconstituted fines contents; 3) relative densities in the range of 85% to 95% does not significantly affect the permanent deformation behavior for the materials tested in this study at low deviator stress (e.g., 68.9 kPa); 4) the crushed limestone material that was tested in this study has higher resistance to permanent deformation and higher resilient moduli compared to the recycled materials that were tested in this study; 5) two recycled materials generally have the similar resilient modulus values; 6) stress levels (i.e., confining pressure and deviator stress) significantly affect the resilient modulus values; and 7) relative densities and fines contents affect the resilient moduli but they are not clearly related to the resilient modulus values of the materials tested in this study.

Due to the complexity of the test method used in this study, measurements errors related to data sampling, tests apparatus setup, and the analysis methods were studied. The analyses demonstrated that 200 readings which is the minimum value specified in AASHTO T307-99

are not sufficient in tracking the loading history and the selection of data points affects the calculated resilient modulus value at each load sequence in the resilient modulus tests.

CHAPTER 1. INTRODUCTION

This chapter presents the industry and technical problems that are addressed in this study, states the research goals and objectives, and discusses the significance of this research. The final section in this chapter describes the organization of this thesis.

Industry Problem

Recycled materials are being increasingly used in base/subbase layers under pavements to reduce costs and environmental impacts of pavement construction. However, variations in original mixtures and service history of these recycled materials lead to uncertainties in their performance as pavement foundation layers so the performance of recycled materials must be studied and compared to the conventional unbound granular materials (UGMs).

The deteriorating U.S. pavement infrastructure, increasing traffic loads, and increasing use of recycled materials are problems that require more research and improved design and pavement foundation construction. *Failure to act: The economic impact of current investment trends in surface transportation infrastructure* (ASCE 2011) reported that deficiencies in America's surface transportation systems were estimated to cost households and businesses nearly $130 billion in 2010. Many of the roads in present service were built decades ago. Repair or complete rebuild are necessary and expensive for these roads. So researchers need to understand the factors that affect the deterioration in pavement systems to improve pavements' long-term performance.

Traffic loads typically increase, and the actual growth rate might be higher than the estimated value in the original pavement design. For example, the Central Texas Regional Mobility Authority (2011) reported that from 2010 to 2011 traffic counts increased 22.6% along US 183 north of the Avery Ranch Boulevard exit. Increased traffic loads require pavement foundations to support larger loads that degrade long-term pavement performances.

A pavement structure is typically composed of three layers: the wearing surface, the base/subbase and the subgrade. The base/subbase layers are constructed with UGMs to provide high permeability, high elastic stiffness, and low variability. However, the construction process can cause degradation of UGMs and variation in densities of base/subbase layers.

Technical Problem

Deteriorating pavement infrastructure calls for advanced pavement technologies and investments to improve these technologies. One of these investments is to study the factors that affect deterioration of the pavement foundation.

Increasing traffic load will accelerate deterioration in pavement structures, so the resistance of pavement structures to large loads must be studied. Large-scale tests with actual pavement structures and real wheel loading machines are expensive and time-consuming so the use of small-scale laboratory tests that simulate the moving wheel loads on pavement foundation materials.

The repeated load triaxial (RLT) test measures permanent strain and resilient moduli of pavement foundation materials. Permanent strain provides a measure of deformation values and resilient moduli provide a measure of stiffness to help quantify long-term pavement foundation support conditions. Barksdale (1972) reported a linear relationship between accumulated permanent strain and number of load applications, and proposed a numerical model for predicting permanent strain. Other researchers (Sweere 1990, Paute et al. 1996, Lekarp and Dawson 1998, etc.) proposed different numerical models but there is no universal model for predicting permanent strain for different materials and variations in factors that affect the ability of pavement foundation materials to resist deterioration.

Recycled materials are being used more frequently in base/subbase layers during last two decades, but their performance under repeated traffic loading has not yet been fully understood. This study aims to investigate and compare permanent deformation and resilient response of these different UGMs typically used in the pavement foundation layers.

Research Goals

The goals of this study are to evaluate models for predicting permanent deformation from laboratory tests results using statistical analysis method and to better understand the permanent and resilient behavior of recycled and conventional materials under repeated traffic loading.

Research Objectives

This study has six main objectives.

- Determine permanent deformation of unbound granular materials as a function of
  - the number of load cycles;
  - stress level (deviator stress and confining pressure);
  - relative density;
  - fines content; and
  - materials type.
- Determine resilient modulus of unbound granular materials as a function of
  - relative density;
  - stress level;
  - fines content; and
  - materials type.
- Develop permanent deformation prediction equation for multi stress levels tests as the tests loading sequences specified in NCHRP 598 tests.
- Determine the significance of regression parameters of the numerical models in predicting resilient modulus.
- Discuss the possible errors in the repeated load triaxial tests to determine permanent deformation and resilient moduli.

Significance of the Research

Pavement design considers natural subgrade properties and determines the most economical subbase layer thicknesses and material types for the pavement system. Estimated traffic loads and environmental conditions are important factors. Uniform support and good, drainability are important functions of the subbase layers.

Advanced understanding of permanent deformation and resilient response aims to evaluate the functionability of base/subbase layers, slow down aging of the pavement infrastructures and improve long-term pavement performance. Resilient modulus (M_r) used to quantify resilient response is a direct input in pavement foundation design, but the resilient modulus alone does not characterize the base/subbase layers' functionability. Permanent deformation of granular base/subbase layers is one of the most important performance

measures because it can cause significant stress concentrations in the pavement layers, which in the long-term is linked to cracking. The permanent deformation behavior must be studied with the resilient modulus to fully evaluate the engineering behavior of UGMs.

FHWA recognizes that increasing use of recycled materials is necessary in U.S. highway industry because of potential cost savings, engineering performance, landfill reduction, and environment stewardship (Wright 2002). However, physical, chemical, and mechanical properties of the recycled materials need to be studied to ensure proper selection and placement of these materials.

Laboratory M_r and permanent deformation tests simulate actual roadway conditions by subjecting vibratory compacted samples to transient repeated loads and controlled stresses. This study will evaluate permanent deformation and resilient response of five pavement foundation materials and related factors (i.e., relative densities, fines contents, stress levels, etc.).

Overall, this research aims to better understand the permanent and resilient behavior of UGMs including recycled materials. The outcomes help to design economical and long lasting pavement systems.

Organization of the Document

Following this introduction chapter, this thesis is organized into five additional chapters. Chapter 2 reviews previous literature and provides background information for this study. Chapter 3 describes the laboratory test methods, and chapter 4 summarizes the tested materials' properties that characterized in laboratory tests. Chapter 5 presents the tests results and analyses and discusses findings from the analyses. Chapter 6 summarizes the conclusions and outcomes derived from this research. Moreover, chapter 6 discusses how these conclusions can be applied in construction practice and provides suggestions for future research. Supporting materials are provided as appendices that follow the list of works cited.

CHAPTER 2. BACKGROUND AND LITERATURE REVIEW

This chapter summarizes selected literature that discusses deformation behavior of unbound granular materials (UGMs) in base/subbase layers under repeated traffic loading. This literature review consists of three main sections: stresses and deformation response in base/subbase layers, permanent deformation of UGMs, and resilient response of UGMs.

Stresses and Deformation Response in Base/Subbase Layers

This section describes the stresses in base/subbase layers and discusses deformation responses of UGMs under repeated traffic load.

Stresses in base/subbase layers

Base/subbase layers are constructed to provide a working platform for upper pavement layers, to improve drainage under pavement surface, and to minimize the effects of frost heave (Saeed 2008a). UGMs are usually used in construction of base/subbase layers, because of their stiffness and permeability.

Crushed gravels and crushed limestone are two types of commonly used UGMs. However, over the last two decades, recycled materials are being increasingly used in base/subbase layers (Wright 2002). Recycled asphalt pavement (RAP) and recycled concrete pavement (RPCC) are the two primary types of recycled materials used in base/subbase construction. Performance of the recycled materials is not fully understood given the wide variation in the materials. Sivakumar et al. (2004) suggested the suitability of recycled materials in civil engineering applications must be carefully considered due the intense and cyclic nature of loading on pavements.

It is well known that the behaviors of UGMs depend on the stress state and the stress history that they experience. In pavement structures, stresses induced by moving wheel loads are complex, and they are important to the engineering behavior of the base/subbase layers.

An element in a pavement structure is subjected to stress pulses which consist of varying magnitudes of vertical, horizontal, and shear stresses. These stress pulses are transient due to the moving wheel loading. The principal stress axes rotate due to the rolling motion of the wheel loading, because the shear stresses are reversed as the load passes. In addition, the

principal stresses act on an element only in vertical and horizontal directions when the shear stresses are zero as shown in Figure 1.

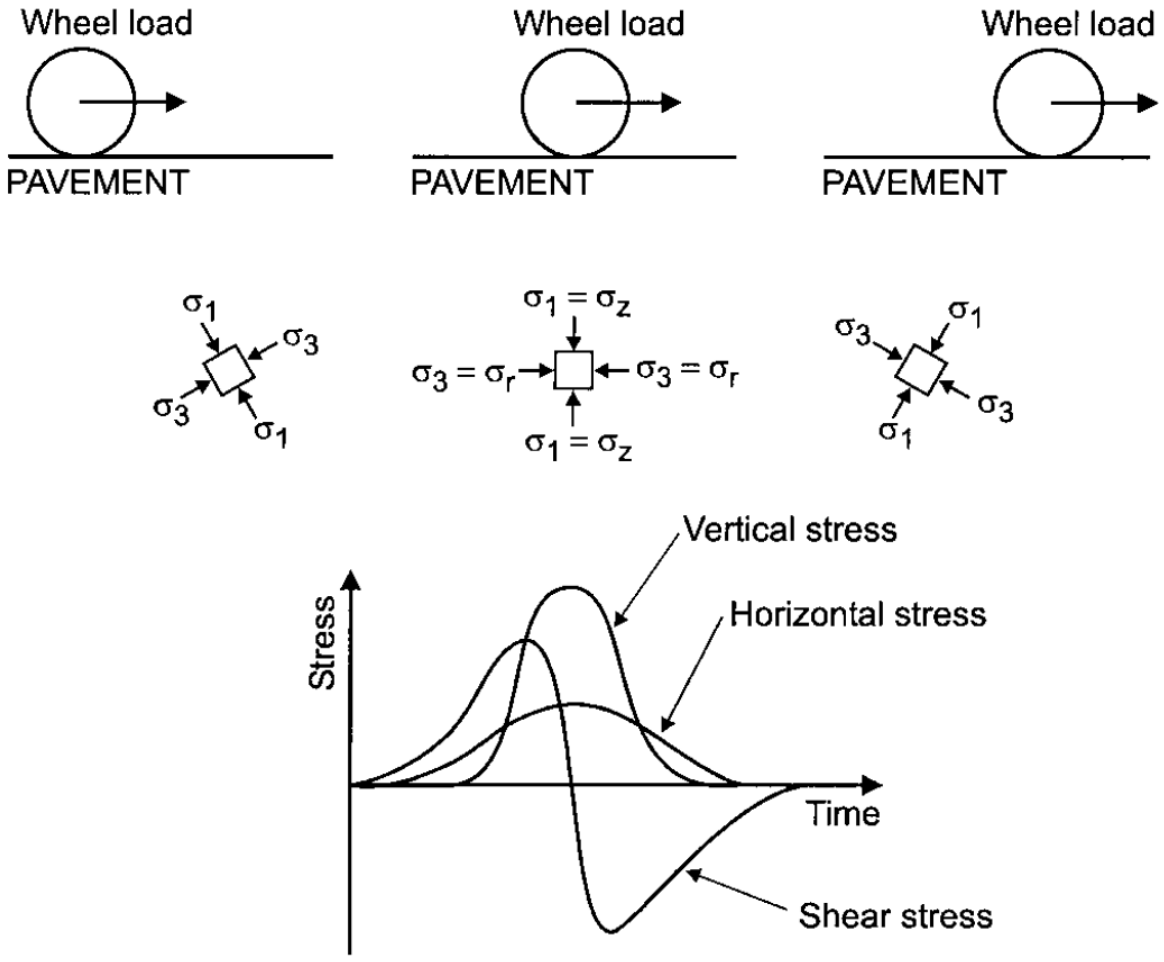

Figure 1. Stresses beneath rolling wheel load (Lakarp et al. 1997)

Saeed (2008) said the magnitude of stress, number of stress repetitions, and rates of loading are three main aspects of applied stress on foundation layers. Moving wheel load is an impulse type repeated loading.

The repeated load triaxial (RLT) testing is commonly used to simulate the transient stress pulses in laboratory to study the engineering behavior of UGMs. Various RLT test devices have been used by researchers to simulate various combinations of vertical and longitudinal stress experienced in situ in base/subbase layers. However, most RLT apparatus cannot simulate the rotation of the principal axes. So, the stresses applied in the RLT tests only simulate the stresses on an element when the wheel load is centered above the element. This

means the shear stresses in RLT tests are zero and $\sigma_1 = \sigma_z$ =vertical stress= applied cyclic stress, $\sigma_2 = \sigma_3 = \sigma_z$ = horizontal stress= confining stress. In Figure 1, σ_1 and σ_3 are shown in vertical and horizontal direction on a UGM element. σ_2 (not shown in the figure) is perpendicular to σ_1 and σ_3 planes, and is assumed to be equal to σ_3.

Deformation response mechanisms in base/subbase layers

Proper understanding of the behavior of construction materials in base/subbase layers is key for the success of mechanistic pavement design (Lekarp et al. 2000a). Werkmeister (2003) reported that the deformation resistance of UGMs is a function of the applied stress. Strain hardening and strain softening are two major behaviors of UGMs under loading (Figure 2). Strain hardening occurs at low stress levels where the stiffness of UGMs increases with increasing stress. This happens because granular particles are compacted into new interlocked positions such that particles are packed into a dense state. Some strain softening occurs at high stress levels as the volumetric strains continue to increase.

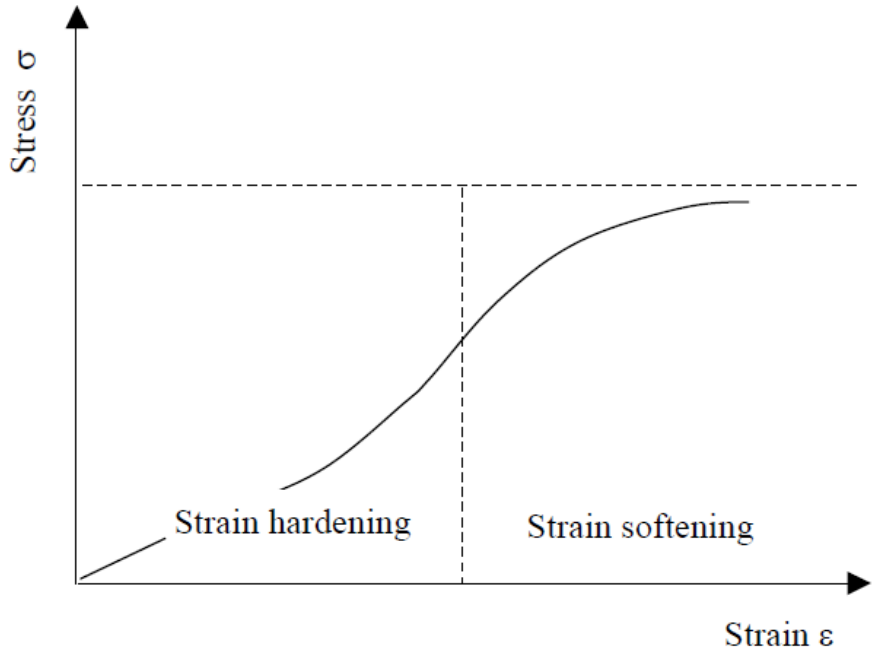

Figure 2. Stress-strain behavior of UGMs (Werkmeister 2003)

Many researchers have studied the complex deformation responses of UGMs subjected to repeated traffic loading (Thom and Brown 1989; Lekarp 1996; Werkmeister 2003; Arnold 2004). The deformation responses are typically characterized into two types: resilient

deformation and permanent deformation. UGMs exhibit both resilient strain and permanent strain under each load cycle (Figure 3). Resilient strains are the strains that are recovered after each load application and permanent strains are irrecoverable and accumulate with increasing load applications. The stress–strain relationship for UGMs can be plotted as a non-linear curve for each load cycle and forms a hysteresis loop. This indicates that less permanent deformation per load cycles occurs when more load cycles are applied compared to the first several load cycles. Werkmeister (2003) and Arnold (2004) found that permanent deformations per cycle diminished with load applications compared to the permanent deformation per cycles at first several load cycles.

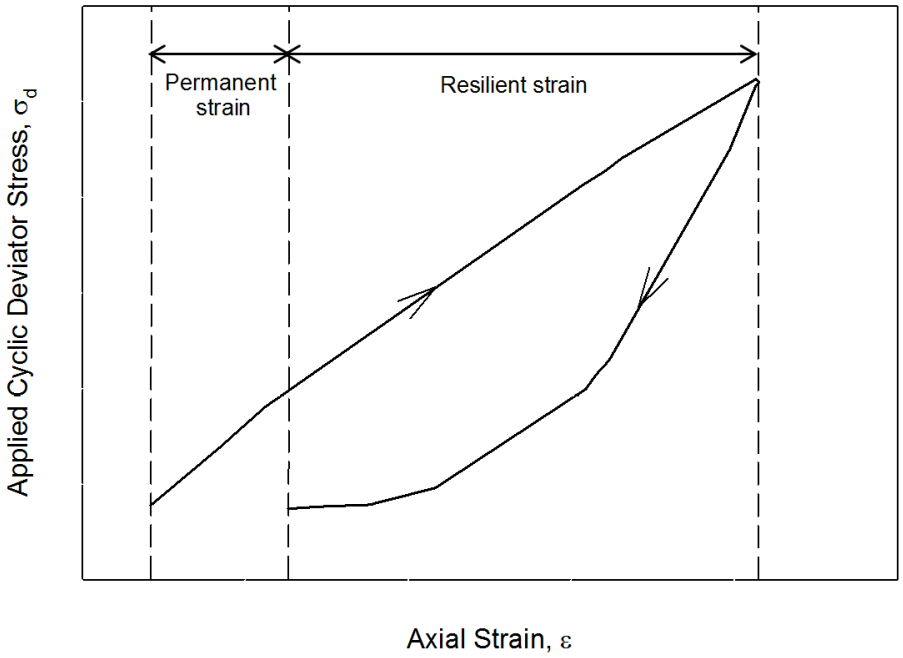

Figure 3. Stress–strain hysteresis loop in UGMs during one cyclic load application

Lekarp et al. (2000a) cited Luong (1982) who reported that permanent deformation under cyclic loading is mainly caused by three mechanisms: consolidation, distortion, and attrition. Consolidation changes the particle structure and results in volume reductions by rearranging and reorienting particles, but the inherent structures of UGMs are not modified. Distortion is characterized by three motions of individual particles: bending, sliding, and rolling and is mainly governed by the microscopic interlocking of particles and the resistance to sliding and rolling is dependent on the interparticle friction. Attrition changes the UMG's fabric and

packing, and results in crushing and breaking of the particles when the applied loads exceed the strength of the material.

Deformation of individual particles (i.e., breaking and crushing particles) is often referred to as degradation. When the contact force that transmitted by the inter-particle contacts increases, the resilient deformation of the particles decreases. Van Niekerk (2002) indicated that additional effects probably affect the non-linear resilient deformation at high stress levels. Hoff et al. (1999) and Van Niekerk (2002) found that the volume change of densely compacted granular materials increases with increasing shear strain. This is because the shear forces squeeze and push the granular particles to climb onto the other particles, because the voids between particles are relatively small in densely compacted granular materials.

Permanent Deformation of Unbound Granular Materials

This section presents the definition of permanent deformation, reviews the literature about factors that affect permanent deformation, describes shakedown theory, and discusses statistical models reported in literature for permanent deformation prediction. Additionally, the degradation of UGMs is also reviewed for quantifying particle breakage during permanent deformation accumulation under cyclic loading.

Definition of permanent deformation

Permanent deformation is quantified as the accumulated irrecoverable (permanent) strain (Figure 3) through the pavement service life. At a given number of load applications under a given stress level, the permanent strain for a laboratory test specimen is calculated using Equation 1:

$$\varepsilon_p = \frac{\Delta H}{H_o} \times 100\% \quad (1)$$

where: ε_p is the permanent deformation in percent;

ΔH is the change in specimen height after a certain number of load applications; and

H_o is the original specimen height.

Permanent deformation is one of the most important types of distresses on flexible pavements, but is also important on rigid pavements, especially in cases with non-uniform deformations. Limiting rut development or permanent deformation is one of the main

objectives in the design of flexible pavements. Permanent deformations occurred in base/subbase layers lead to low serviceability in rigid pavements.

Although permanent deformation is relatively simple to measure, the prediction of permanent deformation is comparatively complex. Lekarp et al. (2000b) proposed that the prediction of permanent deformation is not only related to the materials' characteristics but also the environmental conditions and stress distribution over the pavement service life.

Factors that affect permanent deformation

Several factors affecting permanent deformation UGMs include: applied stress, number of load cycles, moisture content, density, fines content, and material type.

Applied stress

The applied stress levels is one of the most important factors affecting UGMs ability to resist permanent deformation. Morgan (1966) reported that accumulated axial permanent strain is directly related to deviator stress and inversely related to confining pressure according to repeated load triaxial tests.

Following Morgan's research, many researchers (Lashine et al. 1971; Barksdale 1972; Boyce 1975; Brown and Hyde 1975; Werkmeister et al. 2001) have documented the influence of stress ratio (deviator stresses divided by confining pressure) on permanent deformation of granular materials.

Based on tests on crushed limestone material, Lashine et al. (1971) reported that permanent axial strain increased and finally reached a constant value at different stress ratios. These tests were performed on partially saturated samples in drained conditions to allow pore water pressures to dissipate. Barksdale (1972) confirmed Lashine et al. (1971) results showing that permanent axial strain increases as confining pressure decreases and deviator stress increases. Brown and Hyde (1975) further confirmed this conclusion by studying the response of crushed limestone material subjected to both constant and variable confining pressures during testing.

Boyce (1975) reported that the permanent strain reached a constant value before or when a low deviator to normal stress ratio was applied. When a high stress ratio (e.g. $(q/p)_{max}$ = 2.25) was applied, a larger permanent strain developed and continued to increase. Pappin

(1979) confirmed these findings and suggested that permanent axial strain is a function of the stress ratio.

Based on testing on sandy gravel material, Werkmeister et al. (2001) found that permanent strain reaches an equilibrium state at low vertical to radial stress ratio. Further, permanent deformation increased rapidly and reached to failure at high vertical to radial stress ratio.

Some researchers studied ultimate shear strength of the materials to explain the permanent deformation behavior of UGMs under repeated loading. Lekarp and Dawson (1998) stated that static failure tests induced sudden failure in granular materials, which is not in gradual process that is the case under repeated loading.

Number of load applications

Several researchers (Morgan 1966; Barksdale 1972; Kolisoja 1998; Kumar et al. 2006)) reported that permanent strain in UGMs continuously increases under repeated loading. For example, Morgan (1966) reported that permanent strain continues increasing at the end of the tests after 2,000,000 load cycles applied. Barksdale (1972) found a logarithmic relationship between the accumulated permanent strain and the number of load applications, based on testing some sand stone and crushed biotite granite gneiss materials up to 100,000 loading cycles. Barksdale (1972) indicated a sudden increase in the rate of accumulated permanent strain after up to 100,000 load applications. Kolisoja (1998) observed a progressive increase in permanent strain with number of load applications when more than 80,000 load cycles were applied, but the increasing accumulated permanent strain tends to reach an equilibrium state at 80,000 load cycles. Based on tests on crushed granite, Brown and Hyde (1975) reported that permanent strain reaches an equilibrium state after 1,000 load applications. Werkmeister et al. (2001) conducted tests on granidiorite material, which confirmed the findings reported by Brown and Hyde (1975). Werkmeister et al. (2001) also indicated that the accumulated permanent strain was clearly a function of the stress ratio (at 100,000 cycles: $\varepsilon_p = 0.05\%$ when stress ratio = 0.5, and $\varepsilon_p = 1\%$ when stress ratio = 11).

Lekarp and Dawson (1998) also reported conclusions similar to Werkmeister et al. (2001) and indicated that the accumulated permanent strain reaches a constant value when low

stresses are applied and continuous increase when high stresses are applied at a large number of load cycles.

Moisture content

High moisture content and low permeability in UGMs can lead to increasing pore water pressures (PWP) and thus resulting in low effective stress (Lekarp et al. 2000b, Werkmeister). Consequently, the UGM stiffness is reduced and deformations are increased.

Holubec (1969) reported that increasing water content contributed to higher permanent deformations based on laboratory RLT tests (with drainage channels open during testing) . The accumulated permanent strain at 1,000 load applications increased by about 300% in a waterbound macadam pavement when the water content increased from 3.1% to 5.7% and increased about 200% in a sandy gravel material when water content increased from 3% to 6.6%. Barksdale (1972) studied permanent deformation in soaked and partially saturated samples and reported a 68% increase in permanent strain from partially saturated to soaked samples. Thom and Brown (1987) agreed that permanent strain rate increase largely even with a small increase in water content. Laboratory test results reported recently by serveral researchers also agree with these findings (Kancheral 2004, Uthus et al. 2006).

Rodgers et al. (2008) reported that more rutting occurred in sandstone aggregates when a 10 mm rainfall was simulated compared to the dry state. Moreover, Ishikawa et al. (2008) studied the influence of water content on mechanical behavior of gravel by performing fixed-place loading and moving wheel loadings tests. The accumulated residual strain (permanent strain) increased due to saturation in both loading tests. They concluded that water content significantly affects mechanical behavior of gravel.

Density

The resistance of UGMs to permanent deformation under repeated wheel loading is generally improved with increasing density (Lekarp et al. 2000b). Barksdale (1972) reported an average of 185% reduction in permanent axial strain induced in samples compacted to 100% maximum density compared to samples compacted to 95% maximum density. Allen (1973) studied permanent deformation in crushed limestone and gravel under standard Proctor and modified Proctor compaction. He reported that permanent deformation reduced 80% in crushed limestone samples and reduces 22% in the gravel samples when the samples

are compacted to the maximum densities determined in the modified Proctor tests compared to the standard Proctor tests. Van Niekerk (2002) reported that higher axial stresses are required to produce the same amount of permanent axial strain in samples with 103% degree of compaction versus 97%.

Fines content and type

Fines content (passing No. 200 sieve) is typically limited to meet gradation requirements for Department of Transportation (DOT) specifications. However, fines content can vary during the pavement service life. Fines content can increase as a result of particle crushing and segregation during construction (White et al. 2004) and under traffic loading. White et al. (2004) reported that the amount of fines content affect the CBR values and hydraulic conductivities of RPCC and crushed limestone materials.

Ferguson (1972) conducted RLT tests monitoring permanent strain on crushed lime stone materials at varying fines content. His results indicated that the influence of fines content on the rate of axial strain under cyclic loading is significant above a critical fines content. Barksdale (1972), Thom and Brown (1988), Kancherla (2004), and Hussain et al. (2010) also reported that increasing fines content lead to higher permanent deformations in UGMs. Mishra et al. (2010) concluded that the uncrushed gravel has less resistance to negative effects of increasing fines content, because the voids were filled quickly in this material with low fines content. Therefore, fines content directly related to amount of permanent deformation produced in granular materials.

Mishra et al. (2009) indicated that plasticity of fines is one of the most important parameters affecting deformation behavior of UGMs at low fines content. Because plastic fines with moisture will reduce strength and lower the resistance of UGMs to permanent deformation. Excess fines content are usually produced by particles crushing under loading or compacting, so these fine materials are usually non-plastic or have low plasticity as the same as the original UGMs. However, the tests results from Belt et al. (1997) shows a increase in permanent strain of a crushed rock material as the fines content increase from about 2% to 10% and maximum grain size increase.

Material type

Allen (1973) concluded that materials with angular particles (e.g. crushed stone) have higher resistance to permanent deformation than material with rounded particles. River gravel materials which contain rounded particles are more than two times susceptible to permanent deformation than angular crushed granular materials (Barksdale and Itani 1989). Moreover, the crushed granular materials (aggregates) with blade-shaped particles have lower resistance to permanent deformation or rutting than other crushed materials (Barksdale and Itani 1989).

The researchers generally studied several different materials when they studied the permanent deformation and resilient modulus of UGMs, because there are many materials can be used as UGMs. Lekarp et al. (1996) studied permanent deformation behaviors of five different UGMs. In these five materials, granidiorite and dolomitic magnesium limestone have the highest resistance, followed by Leighton buzzard sand, and slate waste and sand with gravel. Werkmeister (2003) reported that sandy gravel (with smooth surfaces) is least resistant to permanent deformation, followed by granidiorite material (rough surface) and diabase material (rough surface). Rodgers et al. (2008) reported that sandstone had better resistance to deformation than limestone shale and sandstone was able to withstand up to 1000 kPa (145 psi) applied pressures without excessive rutting.

Werkmeister (2003) indicated that natural and crushed granular materials with similar gradation characteristics exhibit different permanent deformation behaviors b. Granular materials' angularity changes as a result of crushing. Mishra et al. (2009) agreed that aggregate type or angularity have significant effect on the permanent deformation behavior. Moreover, they indicated that the aggregate type alone does not govern aggregate behavior. Material type which governs angularity is the most important parameter at low fines content (Mishra et al. 2010). Crushed particles have higher resistance to permanent deformation than uncrushed gravels in unbound granular layers.

Bennert et al. (2000) conducted cyclic triaxial tests with a confining stress of 103 kPa (15 psi) and deviator stress of 310 kPa (45 psi) on RPCC, RAP, and dense-graded aggregate base coarse (DGABC) blended materials with different percentages. They reported that at 100,000 load applications, the amount of permanent strain is lower in 100% RPCC materials

and is higher in 100% RAP materials. Bennert et al. (2000) indicated that the amount of permanent strain at 100,000 load applications decreased with increasing percentage of RPCC and increased with increasing RAP. Kim et al. (2009) agreed that permanent deformation increased with increasing percentage of RAP in RAP and virgin aggregate blended materials. They also reported that more than four times greater permanent deformation was developed in the 100% RAP specimens than the 100% aggregate specimens.

Shakedown theory

The shakedown theory was studied in the literature to help the researchers understand the permanent deformation behaviors of UGMs under different stress levels and number of load applications.

The shakedown concept was originally introduced to analyze behavior of pressure vessels under cyclic thermal loading and behavior of metal surfaces under repeated rolling or sliding loads (Johnson 1986). Sharp and Booker (1984) developed procedures to analyze pavement shakedown under repeated cyclic loading. They suggested that pavement shakedown could be observed and satisfactorily predicted and the long term performance of weaker pavements could be conveniently estimated. The materials is said to do shakedown by an adaptation process when the accumulated permanent strain stopped increasing and the material then elastically responds to a load after a certain number of load applications (Sharp and Booker 1984).

Shakedown theory is being used widely to characterize behavior of UGMs under repeated traffic loading (Austin 2009; Tao et al. 2010; Nazzal et al. 2011; Cerni et al. 2012; Tao et al. 2010). Werkmeister (2003) indicated that shakedown analysis on a pavement layer is to determine the critical shakedown load for given material types, layer thicknesses, and environmental conditions. In addition, he suggested that adoption of the shakedown concept in modeling the permanent deformation behavior of UGMs in a pavement structure could greatly improve the accuracy and reliability. Werkmeister (2003) and Arnold (2004) categorized the behaviors of UGMs into three ranges 1, 2, and 3 as illustrated in Figure 4:

- Range 1: plastic shakedown range: at low stress level, the materials response is plastic for a finite number of load applications and the response is purely resilient after compaction is completed.

- Range 2: plastic creep shakedown range: the materials response is initially similar to Range 1 for a finite number of load application and collapse when the number of load application exceeds about 2 million. In this range, the material response is not purely resilient.
- Range 3: incremental collapse shakedown range: Increasing permanent strain with load applications.

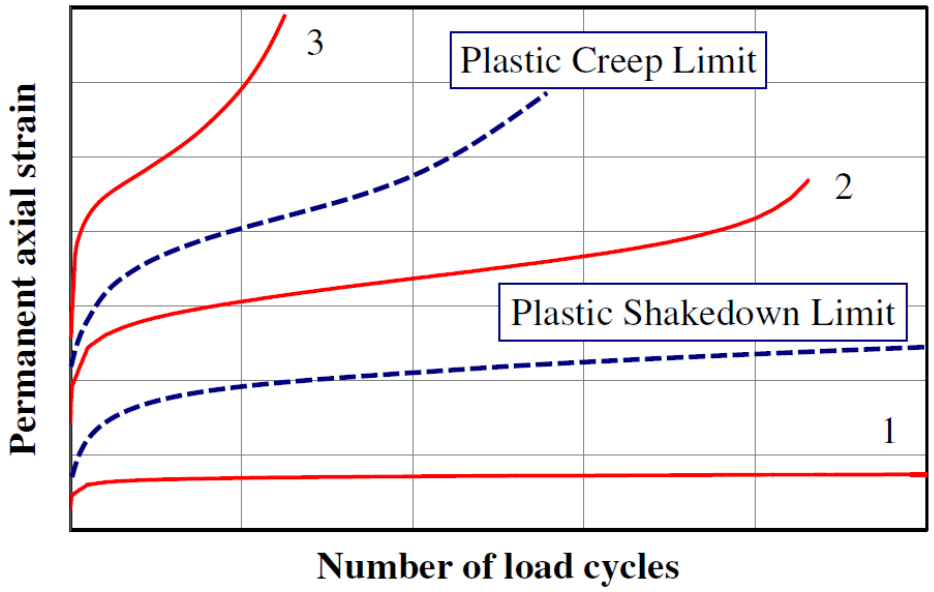

Figure 4. Shakedown ranges of typical permanent deformation behavior (Cerni et al. 2012)

For a pavement to perform well, Range 1 materials are preferred and Range 3 materials must be avoided, while Range 2 materials might be acceptable if permanent deformation is estimated with reasonable accuracy (Werkmeister 2003).

Werkmeister (2003) reported that the RLT test results could be categorized into Ranges 1, 2, and 3 by visually inspecting the shapes/slopes of vertical permanent strain rate versus vertical permanent strain curves. He also proposed that the limit criteria for Ranges 1-2 boundary is 4.5×10^{-5} mm/mm vertical permanent strains (no unit) accumulated from 3,000 to 5,000 load applications and the limit criteria for Ranges 2-3 boundary is 4.0×10^{-4} mm/mm vertical permanent strains accumulated from 3,000 to 5,000 load applications.

Numerical models for predicting permanent deformation

Many researchers have developed constitutive relationships for predicting permanent deformation of UGMs in base/subbase layers. A few selected models that are widely used are discussed in this section. Verka (1979) proposed a correlation between permanent and resilient strains of granular materials (Equation 2):

$$\varepsilon_{1,p} = \alpha \varepsilon_r N^b \quad (2)$$

where $\varepsilon_{1,p}$ = permanent strain;

ε_r = resilient strain;

a and b = regression parameters; and

N = number of load repetitions.

Sweere (1990) studied the behavior of unbound base materials and sands but could not verify Verka's correlation.

Barksdale (1972) performed RLT tests up to 10,000 load application to study the behavior of granular materials (i.e., crushed granite gneiss) that usually are used in base layer construction. He observed a logarithmic relationship between the accumulated permanent axial strain and the number of load applications as shown in Equation 3. This relationship shows that the accumulation rate of permanent axial strain decreases with increasing number of load cycles.

$$\varepsilon_{1,p} = a + b \cdot log(N) \quad (3)$$

where: $\varepsilon_{1,p}$ = accumulated permanent axial strain;

N= number of load repetitions; and

a, b = regression parameters.

Bennert et al. (2000) reported that using Equation 3, an average difference of 5.83% between the predicted and tested values was observed for RPCC, RAP, and DGABC blended materials. Sweere (1990) conducted RLT tests with 1,000,000 load applications and modified Equation 3 to a log-log model as shown in Equation 4:

$$\log(\varepsilon_{1,p}) = a + b \cdot log(N) \quad (4)$$

Paute et al. (1996) proposed Equation 5 as a function of the number of loading cycles:

$$\varepsilon_{1,p}(N) = \varepsilon_{1,p}(100) + \varepsilon^*_{1,p}(N) \quad (5)$$

where: where: $\varepsilon_{1,p}$ (N) = total accumulated permanent axial strain after the certain number of load applications;

$\varepsilon_{1,p}$ (100) = the accumulated permanent axial strain with initial 100 load applications; and

$\varepsilon^{*}_{1,p}$ (N) = the accumulated permanent axial strain after initial 100 load applications.

The accumulated permanent axial strain after the initial 100 cycles is calculated with the number of load applications (Equation 6):

$$\varepsilon^{*}_{1,p} = A\left(1 - \left(\frac{N}{100}\right)\right)^{-B} \tag{6}$$

where: N = the number of load applications; and

A, B = regression parameters (always positive).

Paute et al. (1996) state that parameter A is considered as a limit value in permanent strain accumulation as the number of load applications continues to incrase. The limit value that varies with the maximum shear stress ratio is determined with the static failure line as shown in Equation 7:

$$A = \frac{\frac{q}{(p+p^{*})}}{b\left(m - \frac{q}{(p+p^{*})}\right)} \tag{7}$$

where: q = deviator stress;

p = mean normal stress;

p* = stress parameter defined by intersection of the static failure line;

m = slope of the static failure line; and

b = regression parameter.

Lekarp and Dawson (1998) concluded from their test results that Equation 6 is only valid when low stress levels are applied and they questioned parameter A (Equation 7). Lekarp and Dawson (1998) argued that failure in granular materials occur gradually under repeated traffic loads but are not suddenly collapsed as occurs in static tests. Therefore, Parte et al. (1996) model is invalid in including effect of stress level in accumulation of permanent deformation.

Lekarp and Dawson (1998) suggested a new method that employed the shakedown approach to explain the permanent deformation behavior of granular materials. According to RLT tests on different UGMs, they determined a relationship (Equation 8) between the

accumulated permanent strain after a certain number of load applications and the stress path length (L) and the maximum deviator to normal stress ratio (q/p).

$$\frac{\varepsilon_{1,p}(N_{ref})}{(\frac{L}{p_0})} = a \cdot \left(\frac{q}{p}\right)^{b}_{max} \quad (8)$$

where: $\varepsilon_{1,p}$ (N_{ref}) = the accumulated permanent axial strain after a given number of load applications (N_{ref} >100);

L = stress path length = $\sqrt{p^2 \quad q^2}$;

p_0 = reference stress;

p = mean normal stress;

q = deviator stress;

$(q/p)_{max}$ = maximum stress ratio; and

a, b = regression parameters.

Lekarp and Dawson (1998) reported a correlation between the measured and model-predicted values. The permanent strain is accumulated at low stress ratio (q/p) to a final equilibrium state, while the permanent strain is accumulated rapidly at high stress ratio and the materials are gradually deteriorated. They suggested more research focus on determining the shakedown limit of UGMs where the gradual collapse starts occurring. If the shakedown limit method is suitable, the pavement designers are able to determine a limit to prevent excessive permanent deformation produced by controlling the induced traffic loading below the limit.

Although no standard test method was developed to determine the permanent deformation in UGMs, researchers determined several models to determine the relationship between the permanent strain and the number of load applications and the stress levels. In addition to the equations that were widely examined by other researchers as we discussed above, more equations are listed in Table 1 which summarized other models discussed by Lekarp et al. (2000b) and developed by other researchers.

Table 1. Summary of numerical prediction models for permanent response (Lekarp et al. 2000b and others)

Models	References	Parameters
Based on the number of load applications		$\varepsilon_{1,p}$ = accumulated permanent axial strain after N load cycles $\varepsilon^*_{1,p}$ = additional permanent axial strain after the first 100 load cycles $\varepsilon_{1,p}(100)$ = accumulated permanent axial strain at 100 load cycles a, b, d, $\varepsilon^0_{1,p}$, m, n, s, B = parameters m = slope of the static failure line c = apparent cohesion φ = angle of internal friction A_4, D_4 = parameters that are functions of stress ratio q/p L = length of stress path $L_{max} = \sqrt{p_{max}^2 + q_{max}^2}$ N = number of load repetitions N_{ref} = reference number of load repetitions > 100 R_f = ratio of measured strength to ultimate hyperbolic strength ratio fnN = shape factor σ_3 = confining pressure p_0=reference stress p_a = 100 kPa q = deviator stress p = mean normal stress q^0 = modified deviator stress = $\sqrt{2/3}q$ p^0 = modified mean normal stress =$\sqrt{3}p$ p^* = stress parameter defined by intersection of the static failure line
$\frac{\varepsilon_{1,p}}{N} = a \cdot N^{-b}$	Khedr (1985)	
$\varepsilon^*_{1,p} = \frac{A_4 \cdot \sqrt{N}}{\sqrt{N} + D_4}$	Paute et al. (1988)	
$\varepsilon_{1,p} = a \cdot N^b$ or $\log\left(\varepsilon_{1,p}(N)\right) = a + b \cdot \log(N)$	Sweere (1990)	
$\varepsilon_{1,p}(N) = a[1 + (N/100)^{-b}] + \varepsilon_{1,p}(100)$	Hornych (1993)	
$\varepsilon_{1,p} = (d \cdot N + a) \cdot (1 - e^{-bN})$	Wolf and Visser (1994)	
Based on stress		
$\varepsilon_{1,p} = 0.9 \cdot \frac{q}{\sigma_3}$	Lashine et al. (1971)	
$\varepsilon_{1,p} = \frac{q/a\sigma_3^b}{1 - \left[\frac{(R_f \cdot q)/2(c \cdot cos\varphi + \sigma_3 \cdot sin\varphi)}{(1 - sin\varphi)}\right]}$	Barksdale (1972)	
$\varepsilon_{1,p} = (fnN)L\left(\frac{q^0}{p^0}\right)^{2.8}_{max}$	Pappin (1979)	
$\varepsilon^*_{1,p} = a \cdot (1 - \left(\frac{N}{100}\right)^{-b})$ and $A = \frac{\frac{q}{(p+p^*)}}{a - m \cdot \frac{q}{(p+p^*)}}$	Paute et al. (1994)	
$\varepsilon_{1,p} = \varepsilon^0_{1,p} \cdot \left[1 - (\frac{N}{100})^{-B}\right]\left(\frac{L_{max}}{P_a}\right)^n \cdot \frac{1}{\left(m + \frac{s}{p_{max}} - \frac{q_{max}}{p_{max}}\right)}$	Gidel et al. (2001)	

Summary of permanent deformation research

Table 2. Summary of some previous researches on permanent deformation

Authors	Material	No. of Load Cycles	Deviator stress (kPa)	Confining Pressure (kPa)	Key Findings
Ferguson (1972)	Garner crushed stone	>10,000	384.0-930.8	68.9	Effects of fines contents below the maximum desired values on permanent deformation is small, otherwise the effects are large. The maximum desirable fines content is nearly independent of the number of load cycles.
Lekarp and Dawson (1998)	Crushed limestone, crushed dolomitic limestone, crushed slate waste, sand and gravel.	40,000 or 80,000	20.0-285.0	300.0-700.0	A new model was developed to describe the relationship between accumulated permanent axial strain and stresses at any given number of cycles (>100).
Werkmeister (2003)	Granodiorite, sandy gravel, diabase.	< 2,000,000	70.0-840.0	140.0	Three ranges were specified for the permanent deformation behavior: plastic shakedown; plastic creep; incremental collapse.
Kancherla (2004)	Crushed granite	10,000	213.7	103.5	The permanent deformation and the resilient modulus values of granular material increased. The specimen height does not influence the test results.
Kumar et al. (2006)	Coarse, stone dust, fly ash, and riverbed materials	10,000	125.0, 95.0, and 65.0	40.0, 70.0, and 100.0	The permanent strain increases with increasing number of load cycles and the deviator stress. Stone dust has least resistance to rutting compared to other three materials.
Mishra et al. (2009)	Limestone and dolomite.	1,000	103.4	103.4	The most important property at low fines contents is the aggregate type. When the fines content is low (<8%), fines do not significantly affect aggregate deformation behavior except plastic fines and high moisture content are used.

Degradation of UGMs

The integrity of the constituting particles of UGMs determines their engineering behavior in pavement foundations (Lade et al. 1996). With the accumulation of permanent deformation owing to the repeated traffic load, the particle size distribution of aggregates can be changed. The existing voids in the constructed pavement foundations could be filled with the smaller particles that are broke from large particles by repeated traffic loading. So contacts between particles were increased and the contact stresses caused particles to break into smaller sizes. Therefore, degradation of particles occurs as the permanent deformation accumulated. Nevertheless, the degradation of particles affects the strength and deformation behavior of coarse granular base/subbase (Marsal 1967).

Integrity of the constituting particles is well recognized as the important factor in determining the engineering behavior of granular coarse aggregates (Lade et al. 1996). Lade (1996) reported that if the granular aggregates subjected to a stress level above the normal geotechnical range, considerable particle breakage will exhibit in those granular aggregates.

In showing degradation of aggregate materials in numeric format, breakage index is calculated for each test. All breakage indices are calculated from the changes of overall grain-size distribution of aggregates between the unloaded materials and materials after cyclic load test (Indraratna et al. 2004). Indraratna and Salim (2002) concluded from their experimental results that the breakage of particles increased at a decreasing rate to a constant rate as the axial strain increased.

Saeed (2008) reported that RAP and RPCC degradation do not occur during constructions by comparing RAP and RPCC to the virgin aggregate materials (e.g. crushed limestone). The reason could be the asphalt coating absorbs some stresses act on the RAP particles and the hardened cement paste provides RPCC particles additional resistance to degradation. Increase in fines content in one of the indication of degradation, so Saeed (2008) reported more increase in fines content of virgin aggregate (3.6 %) than RAP (0.6 %) and RPCC (1.6 %). Housain et al. (2007) reported that particles breakage significantly affects the settlement and volumetric strains and that breakage is a function of confining pressure. Breakage occurs under dilating conditions at low confining pressure and occurs under contracting condition at higher confining pressure.

Determining degradation for UGMs

Marsal (1967) is one of the first researcher who quantified particle breakage with an independent technique and index. His particle breakage index (B_g) is the sum of the positive changes in percent of particles retained on each sieve size before and after the triaxial test. However, this B_g index is not able to quantify the breakage of smaller particles which passes the smallest sieve size. Indraratna et al. (2005) introduced the ballast breakage index (BBI) to quantify the magnitude of degradation of ballast granular materials. This method of breakage quantification was agreed by Housain et al. (2007), and they noted the particle size distribution curve move to the left with the increase in breakage. Indraratna et al. (2005) plotted the particle size distribution curves with x-axis (sieve size) started at 0 mm from left to right ended at 63 mm. The BBI was calculated as the ratio of change in passing fraction through a range of sieve size due to load applications to the difference between the original particle size distribution and the determined arbitrary boundary of maximum breakage (Figure 5).

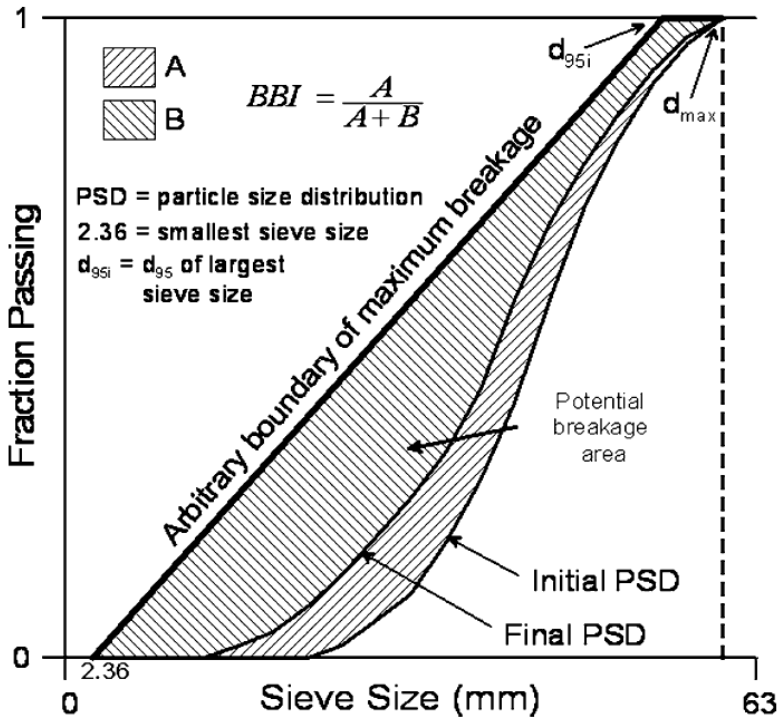

Figure 5. Definition of ballast breakage index (BBI) (Indraratna et al. 2005)

Although this BBI is developed for ballast degradation under cyclic triaxial loading, the same concept could be employed on UGMs. Because both of ballast materials and UGMs are granular materials with large particles and they experience same type of loading (transient and repeated). Consequently, breakage model (Equation 9) introduced model is able to be used to quantify degradation occurred in UGMs under repeated traffic loads.

$$BBI = \frac{A}{A+B} \tag{9}$$

where: BBI = ballast breakage index;

A = area between initial particle size distribution and final particle size distribution curves; and

B = area between initial particle size distribution curve and the arbitrary boundary of maximum breakage.

Resilient Modulus of Unbound Granular Materials

This section defines resilient modulus, discusses the factors that affect the resilient response of UGMs and numerical models for predicting resilient modulus, and listed typical resilient modulus design values.

Definition of resilient modulus

Resilient modulus (M_r) is a basic property of UGMs in characterizing stiffness of UGMs and resilient deformation in base/subbase layers. In mechanistic-empirical pavement design method, M_r is a key parameter to determine the thickness of each layer. M_r is defined as the ratio of the cyclic deviator stress to the resilient strain in each load cycle. As the AASHTO T307 suggested, resilient modulus is calculated according to Equation 10

$$M_r = \frac{\sigma_d}{\varepsilon_r} \tag{10}$$

where: M_r = resilient modulus,

σ_d = cyclic deviator stress (the difference between applied deviator stress and the contact stress), and

ε_r = resilient strain.

When certain deviator stresses were applied, the variation in M_r decreases between load cycles. Therefore, in the AASHTO T307 standard, the mean value of M_r in 96–100 cycles is

determined to represent the M_r of the materials under certain applied stress. Figure 3 shows the axial strain recovered when the applied load released which is defined as resilient response of the materials.

Hveem (1955) is the first person who attempts to observe the resilient properties of UGMs. However, Seed et al. (1962) first introduced the actual concept of M_r. AASHTO T307 "Standard method of test for determining the resilient modulus of soils and aggregate materials" is most used in determination of M_r for materials used in subgrade and base/subbase layers. Groeger et al. (2003) introduced the history of current AASHTO T307 developed. The current AASHTO T307 standard is developed based on the Long Term Pavement Performance (LTPP) Protocol P46. This LTPP Protocol P46 is the revised procedure based on AASHTO T274 in 1982 which is the first standard to determine M_r. AASHTO T274 is developed according to studies on vehicle speed, deflections, and effect of depth on vertical stress pulses. In 1999, LTPP Protocol P46 was modified to AASHTO T307 to include the allowed type of loading system, cycle durations, number of readings per cycle, and allowed sample compaction methods. As Groeger et al. (2003) indicated, these modifications allow the AASHTO standard to be used by more testing agencies.

Factors that affect resilient modulus

Lekarp et al. (2000b) mentioned the importance of learning variation in resilient modulus of pavement foundation materials with change in different factors. Resilient moduli of granular materials have been shown to be dependent on several factors such as stress, density, physical properties, fines content, and material type.

Stress

Kolisoja (1997) concluded that stress level is a factor that significantly affects the resilient response of granular materials. Many researchers (Morgan 1966; Hicks and Monismith 1971; Brown and Hyde 1975; Sweere 1990; Kolisoja 1997) have found that resilient response which is quantifies by M_r of UGMs is highly dependent on sum of principal stresses and confining stress. M_r increases rapidly with increasing sum of principal stresses and confining stress.

Morgan (1966) reported that the M_r slightly decreases with increasing deviator stress and constant confining stress. However, Hicks (1970) and Stolle et al. (2009) suggested that the

magnitude of applied deviator stresses practically did not affect the M_r or could be neglected. On the other hand, Hicks and Monismith (1971) reported that the materials exhibit a slight softening when low deviator stress was applied and a slight stiffening when higher deviator stress was applied. They also reported that the M_r increased as the confining stress increased. Brown and Hyde (1975) agreed with this conclusion. Moreover, they found that the deviator stress and the permanent strain after 10,000 load cycles are in proportion when constant confining stress was applied.

Both of constant confining pressure (CCP) and variable confining pressure (VCP) are used in laboratory resilient modulus tests. Allen and Thompson (1974) reported that higher M_r is calculated with CCP test data compared to VCP test (Figure 6). Brown and Hyde (1975) suggested that the same M_r values were obtained from CCP and VCP tests when the constant confining pressure in the CCP tests is equal to the average value of variable confining pressures in the VCP tests.

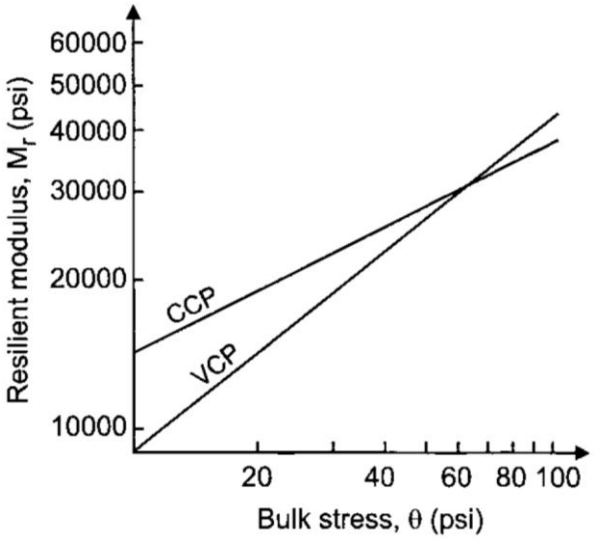

Figure 6. Triaxial test results example with CCP and VCP (Allen and Thompson 1974)

Density

Generally, the density increases in granular materials would cause the base/subbase layer to be stiffer and resilient and permanent deformation subjected to repeated load to be reduced. Many researchers (e.g., Seed et al. 1962; Trollope et al. 1962; Hicks and Monismith 1971; Thom and Brown 1989; Barksdale and Itani 1989; Kolisoja 1997; Andrei 2009) contributed to study the effects of density on resilient responses and this topic has not been

fully understood. Some researchers suggested that increasing densities generally cause increases in the M_r values. Trollope et al. (1962) concluded that the M_r increased up to 50% from loose to dense samples according to the slow repeated load tests on a uniform sand. Kolisoja (1997) also observed that the M_r increases with increased density. The reason is that the number of particle contacts increases when additional compaction is applied to reach the higher target density. More particle contacts reduce the contact stress per particle contact and then reduce the deformation in particle contacts.

Nevertheless, Thom and Brown (1989) stated the effect of density is relatively insignificant. Some factors such as material types, stress levels have impacts on significance of density's impacts on M_r. Hicks and Monismith (1971) reported that the M_r increases with increasing relative density according to tests on the partially crushed aggregates and they observed almost same M_r values for the fully crushed aggregates with increasing relative density. They further found the effect of density is less significant when granular materials (aggregates) contain more fines content. The M_r increased rapidly with increasing density at low stress levels, whereas at higher stress levels, effect of density is relatively insignificant (Barksdale and Itani 1989). The M_r is not very sensitive to density when density is higher than the optimum value. Seed et al. (1962) reported that M_r is lower in less densified samples with low moisture contents. However, M_r is higher in more densified samples with high moisture contents. Their observations are shown in Figure 7.

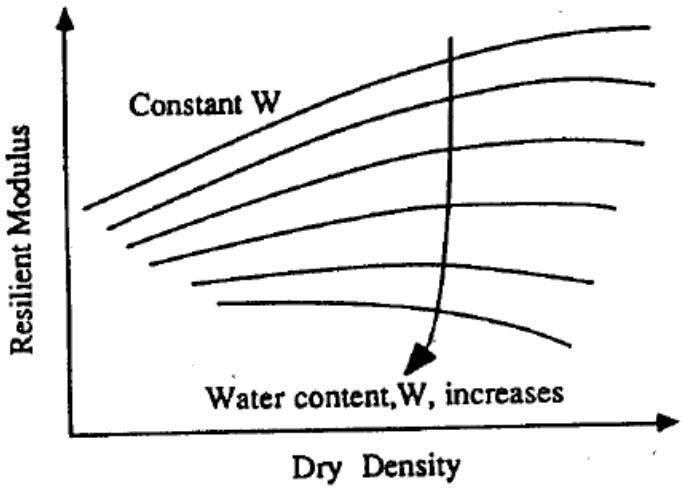

Figure 7. Influence of dry density on resilient modulus at difference moisture content levels (Seed et al. 1962)

According to 96 tests performed on Arizona DOT materials with NCHRP 1-28A test protocol, Andrei (2009) agreed that density strongly affects the relationship between M_r and moisture content and suggested adding density as a predictor to the M_r model which developed based on moisture contents. Alam et al. (2010) studied RAP and virgin granular materials mixture. They reported that dry density has a positive and moisture content has a negative influence on M_r.

Fines content

The impact of fines content on materials stiffness has not been fully understood, but some researchers (Hicks and Monismith 1971; Thom and Brown 1987; Barksdale and Itani 1989; Kamal et al. 1993) studied this topic.

Hicks and Monismith (1971) studied the impact of fine content on two types of crushed aggregates which are partially and fully crushed aggregates. They had different observations in these two granular materials. M_r of the partially crushed aggregates reduced with increasing fines content, whereas opposite effect was reported for fully crushed aggregates. Moreover, Hicks and Monismith (1971) suggested that fines content had a minor impact on M_r when it was in the range of 2-10%.

However, Barksdale and Itani (1989) reported that M_r reduced 60% when fines content increased from 0% to 10%. Thom and Brown (1987), Kamal et al. (1993), Kancherla (2004) agreed that M_r generally decreases in samples contains more fines. Stolle et al. (2009) reported that fines nature importantly affects the moisture sensitivity of aggregates M_r values even at low percentage.

Material type

Variation in material types called several researchers (Hicks 1970; Hicks and Monismith 1971; Barksdale and Itani 1989; Thom and Brown 1989; Heydinger et al. 1996) to study the impact of material type on resilient response. Heydinger et al. (1996) performed M_r tests on limestone, gravel, and slag. They reported that gravel has the highest M_r and then limestone while slag has the lowest M_r.

However, many other researchers (Hicks 1970; Hicks and Monismith 1971; Barksdale and Itani 1989; Thom and Brown 1989) reported that crushed aggregates which contain particles in angular to subangular shape spread load better and have higher M_r values than

uncrushed gravels which contain particles in round or sub-round shapes. Particle shape is one of the main characteristics used to describe different material types. Brown and Itani (1989) reported that the rough and angular crushed materials had about 50% more M_r than the rounded uncrushed gravels at low mean normal stress and about 25% more at high mean normal stress.

Recycled materials are more used as pavement foundation materials since last two decades, and researchers expand their study on effect of material types on M_r to include the most used recycles materials. RPCC and RAP are two most used materials in base/subbase constructions. The hydration of residual concrete might affect RPCC samples (Nataatmadja and Tan 2001; Mayrberger and Hodek 2007).

Granular materials typically showed a decrease in M_r values with increased moisture content, whereas, RPCC specimens had increased M_r with increased moisture content and longer mellowing time. The asphalt coating on particles might affect properties of RAP materials. Bennert et al. (2000) conducted cyclic triaxial tests on the RPCC, RAP, and dense-graded aggregate base coarse (DGABC) blended materials with different percentages. They concluded that the 100% RPCC and 100% RAP materials had higher M_r values than the 100% DGABC materials. Moreover, they reported from the tests results that the M_r values increased with increasing percentage of RPCC and RAP at bulk stresses of 144.7 kPa (21 psi) and 344.7 kPa (50 psi).

Alam et al. (2010) agreed that the M_r values increased with increased RAP content in RAP and virgin granular materials mixture. They also reported that M_r is increasing at both high and low bulk stress levels. They concluded that increasing RAP content decreases pavement surface distresses according to the in situ tests. Kang et al. (2011) concluded that M_r generally increased when RPCC or RAP was added into virgin granular materials and suggested that RAP and RPCC would be good substitutes for virgin materials used in base/subbase construction. However, Leite et al. (2011) suggested that recycled construction and demolition waste materials and a standard well-graded crushed stone had similar M_r values determined in laboratory tests.

Numerical models for predicting resilient modulus

During last six decades, researchers made many efforts to investigate the resilient moduli of the granular materials and proposed several models to predict M_r in different materials and conditions. The proposed models are developed according to the test data by using different test methods and pavement materials. Different test methods and pavement types determine the certain M_r values in designing specific layers. These resilient moduli models are used to predict the nonlinear behavior of a soil layer and this help on developing more rational pavement design procedures.

Some models were widely used to predict resilient modulus and examined in many research works. Seed et al. (1962) proposed the bulk stress model to indicate the simple hyperbolic relationship between resilient modulus and bulk stress. As the result of the simplicity, the bulk stress model was widely used to characterize materials stiffness related to stress conditions. This model is shown as Equation 11:

$$M_r = k_1 \sigma_B^{k_2} \tag{11}$$

where: σ_B = bulk stress (MPa) = $\sigma_1 + \sigma_2 + \sigma_3$; and

k_1, k_2 = regression coefficients.

However, several drawbacks were found by other researchers. A constant Poisson's ratio was assumed in calculating radial strain. Hicks and Monishmith (1971) and Sweere (1990) proposed that applied stresses caused variation in Poisson's ratio so Poisson's ratio is not a constant. Sweere (1990) reported good prediction of axial strain by using the bulk stress model, but radial and volumetric strains were rather poorly predicted by assuming the constant Poisson's ratio. Another drawback is that the bulk stress model only uses the sum of the principal stresses to account for effect of stress on M_r. However, May and Witczak (1981) reported that shear strain induced mainly by shear or deviator stress is a plausible factor related to the M_r of granular materials.

MEPDG (NCHRP 2004) recommends the universal constitutive model developed by Witczak and Uzan (1988) to account for effects of bulk stress and shear stress on M_r (Equation 12):

$$M_r = k_1 P_a \left(\frac{\sigma_B}{P_a}\right)^{k_2} \left(1 + \frac{\tau_{oct}}{P_a}\right)^{k_3} \tag{12}$$

where: P_a = atmospheric pressure (MPa);

τ_{oct} = octahedral shear stress (MPa) $=\frac{\sqrt{(\sigma_1-\sigma_2)^2+(\sigma_2-\sigma_3)^2+(\sigma_3-\sigma_1)^2}}{3}$

σ_B= bulk stress (MPa) = $\sigma_1+ \sigma_2+ \sigma_3$;

k_1, k_2, k_3 = regression coefficients; and

σ_1, σ_2, σ_3 = principal stresses (MPa).

NCHRP (2004) gave a general idea about the values of regression coefficient and this idea helps researchers to understand the application of this model in different materials and conditions. k_1 is a regression coefficient proportional to Young's modulus. The value of k_1 is positive according to positive M_r in real application. k_2 is also a positive regression coefficient because stiffening response caused by increasing bulk stress will result in larger M_r values. However, k_3 should be a negative regression coefficient to account the softening response. Because increasing shear stress results in softening response and lower M_r values (NCHRP 2004).

However, Stolle et al. (2009) reported shortcomings in application of the universal model and demonstrated relatively linear relationship between bulk stresses and M_r for the granular base/subbase materials. They suggested a simplified linear M_r–σ_B model (Equation 13) developed by Stolle et al. (2006) is better in predicting the test data.

$$M_r = m\left(\frac{\sigma_B}{p_a}\right) + b \tag{13}$$

where: P_a = atmospheric pressure (MPa);

σ_B= bulk stress (MPa) = $\sigma_1+ \sigma_2+ \sigma_3$; and

m, b = regression coefficients.

The efficiency of the developed M_r models in predicting resilient moduli are based on the studied materials and accurate measurements of parameters employed in the models. Puppala (2008) listed some resilient moduli equations that developed by other researchers for cohesive and/or granular materials. Some resilient modulus models used for granular soils are summarized in Table 3 on next page.

Table 3. Summary of resilient modulus models (Puppala 2008 and additional models)

Models	Original References	Parameters
$M_r = k_1 P_a \left(\frac{\sigma_3}{P_a}\right)^{k_2}$	Dunlap (1963)	k_1, k_2, k_3, k_4, k_6, k_7 = regression coefficients P_a = atmospheric pressure σ_1, σ_2, σ_3 = principal stresses σ_B= bulk stress = σ_1+ σ_2+ σ_3 $\sigma_d = \sigma_1 - \sigma_3$ = deviator stress τ_{oct} = octahedral shear stress $=\frac{\sqrt{(\sigma_1-\sigma_2)^2+(\sigma_2-\sigma_3)^2+(\sigma_3-\sigma_1)^2}}{3}$ $(\mu_a - \mu_w)$ = matric suction; and α_1, β_1 = regression constants n, n_{max} = porosity of the aggregate
$M_r = k_1 P_a \left(\frac{\sigma_B}{P_a}\right)^{k_2}$	Seed et al. (1967)	
$M_r = k_1 P_a \left(\frac{\sigma_B}{P_a}\right)^{k_2} \left(\frac{\sigma_d}{P_a}\right)^{k_3}$	Uzan (1985)	
$M_r = k_1 P_a \left(\frac{\sigma_B}{P_a}\right)^{k_2} \left(\frac{\tau_{oct}}{P_a}\right)^{k_3}$	Witczak and Uzan (1988)	
$M_r = k_1 P_a \left(\frac{\sigma_3}{P_a}\right)^{k_2} \left(\frac{\sigma_d}{P_a}\right)^{k_3}$	Pezo (1993)	
$M_r = k_1 (n_{max} - n) P_a \left(\frac{\sigma_B}{P_a}\right)^{0.5}$ and $M_r = k_2 (n_{max} - n) P_a \left(\frac{\sigma_B}{P_a}\right)^{0.7} \left(\frac{\sigma_d}{P_a}\right)^{-0.02}$	Kolisoja (1998)	
$M_r = k_1 P_a \left(1 + \frac{\sigma_3}{P_a}\right)^{k_2} \left(1 + \frac{\sigma_d}{P_a}\right)^{k_3}$	Ni et al. (2002)	
$M_r = k_1 P_a \left(1 + \frac{\sigma_B}{P_a}\right)^{k_2} \left(1 + \frac{\sigma_d}{P_a}\right)^{k_3}$ $M_r = k_1 P_a \left(1 + \frac{\sigma_B}{P_a}\right)^{k_2} \left(1 + \frac{\tau_{oct}}{P_a}\right)^{k_3}$	Ooi et al. (2004)	
$M_r = k_1 P_a \left(\frac{\sigma_B}{P_a}\right)^{k_2} \left(1 + \frac{\tau_{oct}}{P_a}\right)^{k_3}$	NCHRP project 1-28 and MEPDG recommended	
$M_r = k_1 P_a \left(\frac{\sigma_B - 3k_6}{P_a}\right)^{k_2} \times \left(k_7 + \frac{\tau_{oct}}{P_a}\right)^{k_3} + \alpha_1 (\mu_\alpha - \mu_w)^{\beta_1}$	Gupta et al. (2007)	

Typical resilient modulus design values

The typical M_r values for unbound granular and subgrade materials at optimum moisture content without modification for climate are recommended in NCHRP 1-37A (2004). These values help researchers compare the M_r values of tested materials and required design input

values. Table 4 shows the ranges and typical M_r values of soils according to both AASHTO and USCS classification systems.

Table 4. Typical M_r values for pavement foundation layers at optimum moisture content (NCHRP 1-37A)

Material Classification	M_r Range				Typical M_r	
	Low		High		psi	MPa
	psi	MPa	psi	MPa		
A-1-a	38,500	265.4	42,000	289.6	40,000	275.8
A-1-b	35,500	244.8	40,000	275.8	38,000	262.0
A-2-4	28,000	193.1	37,500	258.6	32,000	220.6
A-2-5	24,000	165.5	33,000	227.5	28,000	193.1
A-2-6	21,500	148.2	31,000	213.7	26,000	179.3
A-2-7	21,500	148.2	28,000	193.1	24,000	165.5
A-3	24,500	168.9	35,500	244.8	29,000	199.9
A-4	21,500	148.2	29,000	199.9	24,000	165.5
A-5	17,000	117.2	25,500	175.8	20,000	137.9
A-6	13,500	93.1	24,000	165.5	17,000	117.2
A-7-5	8,000	55.2	17,500	120.7	12,000	82.7
A-7-6	5,000	34.5	13,500	93.1	8,000	55.2
CH	5,000	34.5	13,500	93.1	8,000	55.2
MH	8,000	55.2	17,500	120.7	11,500	79.3
CL	13,500	93.1	24,000	165.5	17,000	117.2
ML	17,000	117.2	25,500	175.8	20,000	137.9
SW	28,000	193.1	37,500	258.6	32,000	220.6
SP	24,000	165.5	33,000	227.5	28,000	193.1
SW-SC	21,500	148.2	31,000	148.2	25,500	175.8
SW-SM	24,000	165.5	33,000	227.5	28,000	193.1
SP-SC	21,500	148.2	31,000	148.2	25,500	175.8
SP-SM	24,000	165.5	33,000	227.5	28,000	193.1
SC	21,500	148.2	28,000	193.1	24,000	165.5
SM	28,000	193.1	37,500	258.6	32,000	220.6
GW	39,500	272.3	42,000	289.6	41,000	282.7
GP	35,500	244.8	40,000	275.8	38,000	262.0
GW-GC	28,000	193.1	40,000	275.8	34,500	237.9
GW-GM	35,500	244.8	40,500	279.2	38,500	265.4
GP-GC	28,000	193.1	39,000	268.9	34,000	234.4
GP-GM	31,000	148.2	40,000	275.8	36,000	248.2
GC	24,000	165.5	37,500	258.6	31,000	148.2
GM	33,000	227.5	42,000	289.6	38,500	265.4

CHAPTER 3. METHODS

This chapter describes the laboratory test methods and standards employed to address the goals and objectives of the research design.

Research Design

The goals of this study are to better understand the permanent and resilient deformation behavior of recycled and conventional unbound granular materials (UGMs) under repeated traffic loading and to evaluate numerical models for predicting permanent deformation from laboratory tests results. The six objectives of the study are as follows:

- Determine permanent deformation of UGMs as functions of the number of load applications; relative density; confining pressure and deviator stress; and fines content.
- Determine breakage index of UGMs after permanent deformation tests.
- Determine resilient moduli of UGMs as functions of relative density; confining pressure and deviator stress; and fines content.
- Determine unconsolidated undrained strength of UGMs after resilient modulus tests.
- Compare permanent deformation and resilient moduli of different unbound granular materials.
- Evaluate numerical models that were developed and widely used in other research works for predicting permanent strain.
- Determine the significance of regression parameters in the universal model for predicting resilient moduli.

To characterize the engineering properties of the unbound granular materials used in this study, basic soil index properties and relative density tests were conducted. Special sample preparation techniques were used and are discussed. Permanent deformation, degradation, resilient modulus (M_r), and undrained shear strength tests were performed. Test standards have not been published for determining permanent strain and breakage index values of pavement foundation materials, so the specific procedures will be described in the permanent deformation and degradation tests sections. Table 5 summarizes the laboratory tests and standards used in this study, and any differences from the test standards are described.

Table 5. Standards used for laboratory soil tests

Laboratory test	Test method
Standard Test Method for Particle-Size Analysis of Soils	ASTM D422-63
Standard Test Methods for Laboratory Determination of Water (moisture) Content of Soil and Rock by Mass	ASTM D2216-10
Standard Test Method for Density, Relative Density (Specific Gravity), and Absorption of Coarse Aggregate	ASTM C127-07
Standard Test Methods for Specific Gravity of Soil Solids by Water Pycnometer	ASTM D854-10
Standard Test Methods for Laboratory Compaction Characteristics of Soil Using Standard Effort (12,400 ft-lbf/ft^3 (600 kN-m/m^3))	ASTM D698-07
Standard Test Methods for Maximum Index Density and Unit Weight of Soils Using a Vibratory Table	ASTM D4253-00
Standard Test Methods for Minimum Index Density and Unit Weight of Soils and Calculation of Relative Density	ASTM D4254-00
Iowa Modified Relative Density Test for Determination of Bulking Moisture Contents of Cohesionless Soils	White el al. 2002
Standard Method of Test for Determining the Resilient Modulus of Soils and Aggregate Materials	AASHTO T307-99
Quick Shear Test	AASHTO T307-99
Standard Test method for Unconsolidated-Undrained Compression Test on Cohesive Soils	ASTM D2850-03a

Soil Index Property Tests

Soil index properties were determined through particle size distribution analysis, soil classification, and specific gravity tests.

Particle size distribution

Mechanical sieve analysis and hydrometer analysis tests to determine particle size distributions of the UGMs were conducted according to ASTM D422-63. Samples of UGMs were first divided into two portions by sieving the material through a No. 10 sieve. Mechanical sieve analyses were conducted on washed and dried materials retained on No. 10 sieve. Usually, a set of 1.5 in., 1 in., 3/4 in., 3/8 in., No. 4, and No. 10 sieves was used in mechanical sieve analysis, but in some cases other sieves were used for capture more detailed particle size information. Hydrometer test on material passing the No. 10 sieve was used to determine particles sizes on materials smaller than the No. 200 sieve. A calibrated 152H

hydrometer was used. Timers were used to record hydrometer readings at 2 min, 5 min, 15 min, 30 min, 60 min, 250 min, and 1440 min from the hydrometer test jars were sit stably (Figure 8). After the hydrometer tests, the material was washed though No. 200 sieve and material retained on No. 200 sieve was saved and oven dried for analysis with a set of No. 20, No. 40, No. 60, No. 100, and No. 200 sieves.

Figure 8. A hydrometer test in process

Soil classification

AASHTO and Unified Soil Classification System (USCS) soil classifications were followed to classify the UGMs. These two systems use Atterberg limits and particle size to classify materials. However, the UGMs in this study were non-plastic, so they were classified solely based on their particle size distributions.

Specific gravity

Two test methods were used to determine the sample average specific gravity (ASTM D854-10 and ASTM C127-07). Method B in ASTM D854-10 was followed for oven-dried materials passing the No. 4 sieve, and ASTM C127-07 was followed for materials retained on the No. 4 sieve. Materials passing the No. 4 sieve were weighed in the pycnometer (Figure 9a), and coarse granular materials retained on the No. 4 sieve were weighed in a basket submerged in water (Figure 9b). In addition, temperatures of materials were recorded during the tests and temperature corrections were made in the specific gravity calculations.

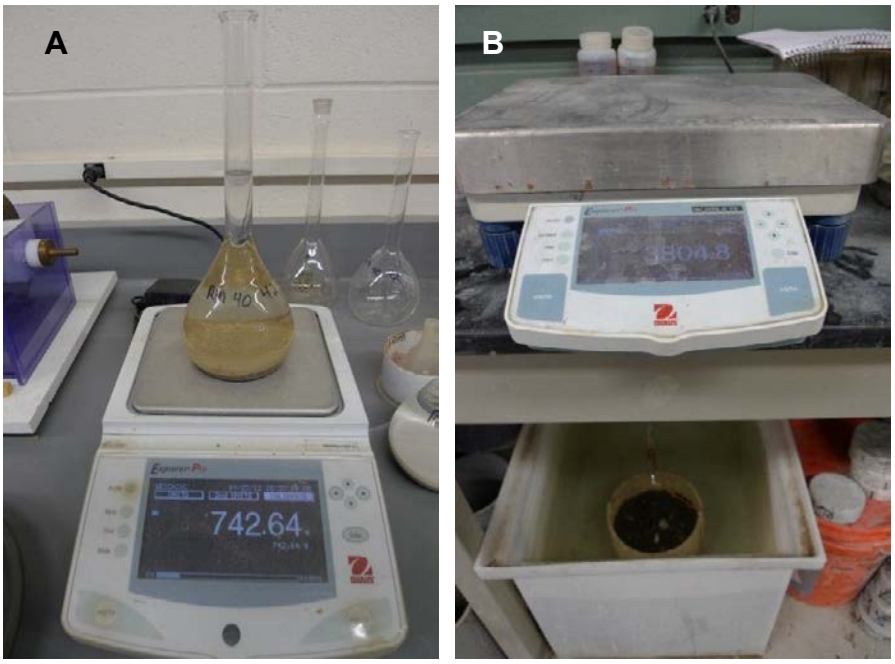

Figure 9. Specific gravity: pycnometer test (A); coarse aggregate test (B)

Materials in this study all contained particles both retained on and passed No. 4 sieve, so Equation 14 (ASTM D854-10) was used to calculate the average specific gravity.

$$G_{ave@20°C} = \frac{1}{\frac{R}{100 \cdot G_{1@20°C}} + \frac{P}{100 \cdot G_{2@20°C}}} \quad (14)$$

where: R = percent of soil retained on No. 4 sieve;

P = percent of soil passing the No. 4 sieve;

$G_{1@20°C}$ = apparent specific gravity of soils retained on the No. 4 sieve as determined by ASTM C127-07, corrected to 20°C; and

$G_{2@20°C}$ = apparent specific gravity of soils passing the No. 4 sieve as determined by ASTM D854-10, corrected to 20°C.

Moisture content

Moisture contents were determined according to ASTM D2216-10 by oven drying samples at 110 ± 5°C (230 ± 9°F) to a constant mass, except for recycled asphalt pavement (RAP) and recycled portland cement concrete samples with less than about 10% RAP (RPCC/RAP). Asphalt binder on the particles melts at 110°C (230°F), and this liquid asphalt binds aggregate particles when it cools to room temperature and changes particle size distribution of original materials. Consequently, the oven temperature for RAP samples was

controlled at 38°C (100°F) and at 60°C (140°F) for RPCC with RAP. These drying temperatures allowed more representative particle size distributions so the same RAP and RPCC/RAP samples could be used for mechanical sieve analysis.

Relative Density Tests

Relative density tests were conducted to determine the relationships between dry unit weights and moisture contents. Material gradation requirements determine which compaction method should be used.

Maximum and minimum relative densities of cohesionless free-draining soils were calculated by performing relative density tests with a vibrating table according to ASTM D4253-00 and ASTM D4254-00 respectively. This test method is applicable for materials which particles passing the 3 in. sieve and not more than 15 percent pass No. 200 sieve by mass. In addition, moisture contents of the material were varied according to methods introduced by White et al. (2002) to determine moisture–dry unit weight relationships. Moreover, the bulking moisture content can be determined from the moisture-dry unit weight relationships.

Sample preparation

Samples for permanent deformation and M_r tests were prepared according to AASHTO T307-99. The untreated materials were classified as Type I or II. Type I materials are untreated base, subbase, and subgrade that have less than 70 percent particles smaller than 2.00 mm and less than 20 percent particles smaller than 75 μm, and plasticity index equal to or less than 10. Type II materials include all untreated pavement foundation materials that do not satisfy requirements for Type I materials. All UGMs in this study are classified as Type I materials, so sample preparation procedures for Type I materials were followed for this study.

Due to particle size requirements in AASHTO T307-99, special methods were applied to materials preparation. For non-cohesive Type I materials, vibratory compaction was used to reconstitute the materials. The following sections described detailed procedures for materials preparation and sample compaction.

Material preparation

Due to sample size limitations, oversized particles where either scalped and replaced (method SR), or scalped only (method S). Method SR was used for studying permanent deformation response of test specimens that made of untrimmed slag and RPCC materials. Method S was used for studying permanent deformation and resilient modulus behaviors under various conditions (i.e., relative densities and fines contents) of tests samples that made of crushed limestone, RAP, and RPCC/RAP materials.

The fines contents were varied for each material that was prepared with scalp only method to study effects of fines contents on permanent deformation and resilient modulus of UGMs. Four fines contents of each UGM were studied and included natural fines content which is the original fines content as the materials were produced and three reconstituted fines contents. To reconstitute fines contents, the materials were first oven dried and then sieved through No. 200 sieve. For the 0% target fines content materials, no more fines was added and for 6% or 12% target fines contents, more fines that were produced by crushing larger particles from the same material type.

Both the method SR and S were used to prepare samples that satisfied the requirements in AASHTO T307-99. First requirement is that the minimum diameter of the mold used to fabricate samples should be equal to five times the maximum particle size of the materials. Second requirement is that particles should be scalped if their size exceeds 25 percent of the mold diameter. Equipment used for M_r and permanent deformation tests in this research is not capable to fit 152.4 mm (6 in.) diameter samples, so the maximum diameter of mold used is 101.6 mm (4 in.). Samples were compacted in 101.6 mm (4 in.) diameter molds so the maximum particle size of the test materials should be less than 20.3 mm (0.8 in.).

Scalp and replace method

Method SR is to remove particles retained on 19.1 mm (3/4 in.) sieve and replace them with same percentage by weight of the same material that retained on the No. 4 sieve and passed 19.1 mm (3/4 in.) sieve. This method was used for two materials that were collected from I-94, Michigan and US-30, Iowa to modify their particle size distribution to meet requirement in AASHTO T307-99.

Scalp only method

Method S is to remove particles that are retained on the 19.1 mm (3/4 in.) sieve without replacement. This method was used for three materials that were collected from Martin Marietta Materials, Inc. and Manatt's, Inc. quarries.

Sample compaction

Before vibratory compaction, prepared materials were in moisture conditions and mellowed in sealed bags for at least three to six hours to allow particles to absorb water. Equipment for preparing vibratory compacted samples includes the base of the triaxial chamber, 101.6 mm (4 in.) diameter split mold (Figure 10), porous stones, filter paper, rubber O-rings, rubber membranes, a steel compaction plate with rod, and an electric rotary hammer drill (Figure 11).

Figure 10. Split mold sit on pressure chamber base

Figure 11. Compaction plate with rod and electric rotary hammer drill

When the diameter of the hole in the flat compaction plate was bigger than the diameter of the steel rod, the compaction rod slid during compaction which caused the plate to tilt and create an uneven top surface for the samples. A tapered compaction plate was made to prevent the compaction rod from sliding. The tapered plate had a tapered hole at the center of the plate to tightly fit the modified compaction rod which had a tapered head (Figure 12).

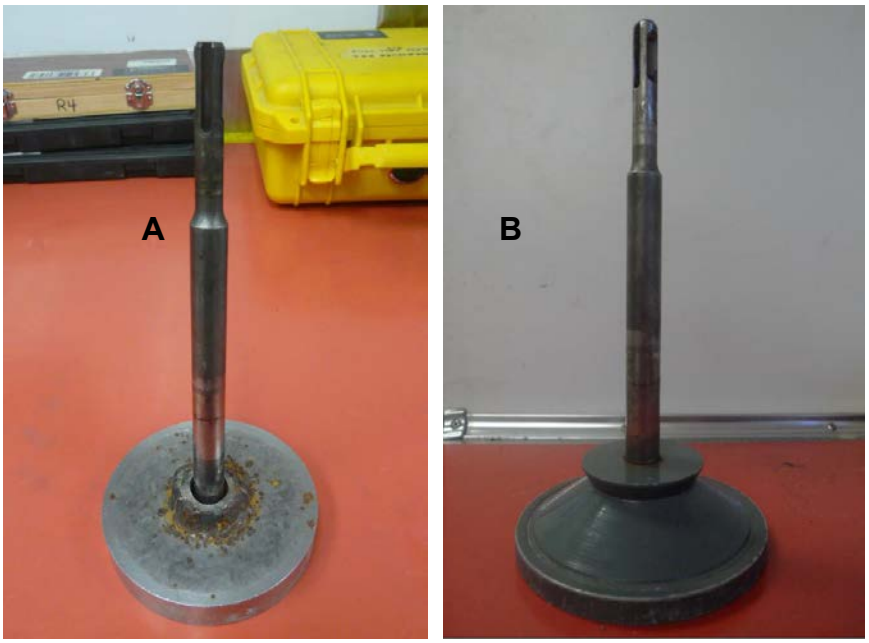

Figure 12. Compaction plate and rod: flat (A) and tapered (B)

The split mold was designed for compacting 8 in. high by 4 in. diameter samples, and the height to diameter ratio is 2 as required in AASHTO T307-99 to sufficiently eliminate the end effects on measuring strength as suggested by Lekarp et al. (1996). They also proposed that membranes might slightly reduce deformation of samples as result of restraining effect of the membranes. However, the reduction is very small compared to the total amount of permanent deformation of UGM samples, so the reduction of deformation caused by membranes can be ignored and accounted by membrane correction in calculating the applied deviator stresses.

During vibratory compaction, materials were restrained by the 4 in. inner diameter split mold and compacted in five lifts of equal mass and thickness by using an electric rotary hammer drill (Figure 13 A). The uniform thickness of each lift was controlled with caliper measurements (Figure 13 B). Density gradient verification tests were conducted to see if the densities of compacted sample match requirements of AASHTO T307-99.

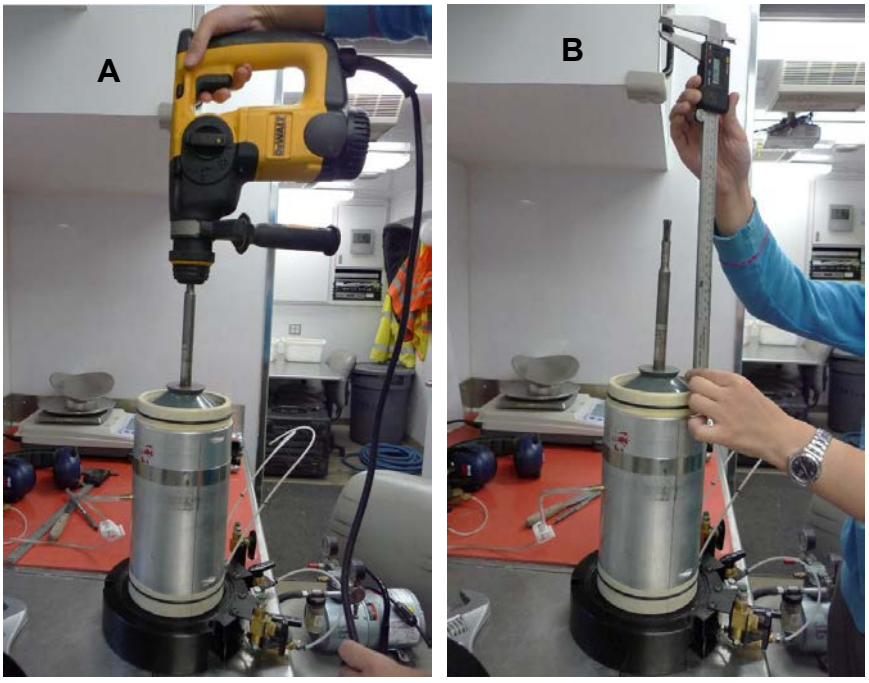

Figure 13. Compaction of UGMs in split mold (A) and thickness verification (B)

Thickness of each lift was verified by caliper measurement and constant mass of each lift was controlled, so reduction in time cost might indicates density gradient for whole sample. RPCC and RAP subbase materials were tested to verify achievement of uniform density of

the whole compacted samples. Three methods were used to determine the densities and the compaction time for each lift. All of the tools used in these tests except the rubber membranes and O-rings are shown in Figure 14.

Figure 14. Density gradient verification test tools

Method 1 is using filter paper to separate two adjacent compacted layers and measure the height after each layer was compacted. In addition, when all layers were compacted, the post-compaction height of each layer was measured by taking out one compacted layer at each time. Method 2 is compacting sample in general procedures that are same for all M_r and permanent deformation tests samples. In method 2, 1 in. materials from the top of each compacted layer were scarified to loosen the compacted materials to produce better conjunction between two layers. Method 3 is to use polypropylene (PP) strapping band between two layers and measured the layer thickness when each of following layers was compacted. The PP strapping bands were bending to form a right angle and looks like a "L" as the red strapping bands shown in Figure 14. A PP strapping band was put inside the split mold that short side was parallel to and long side was perpendicular to the mold base before each layer was compacted (Figure 15(3)). When the subsequent layers were compacted, the

former layers were also compacted and the new thicknesses were measured to compare with the original layer thickness. The detailed procedures are shown in Figure 15.

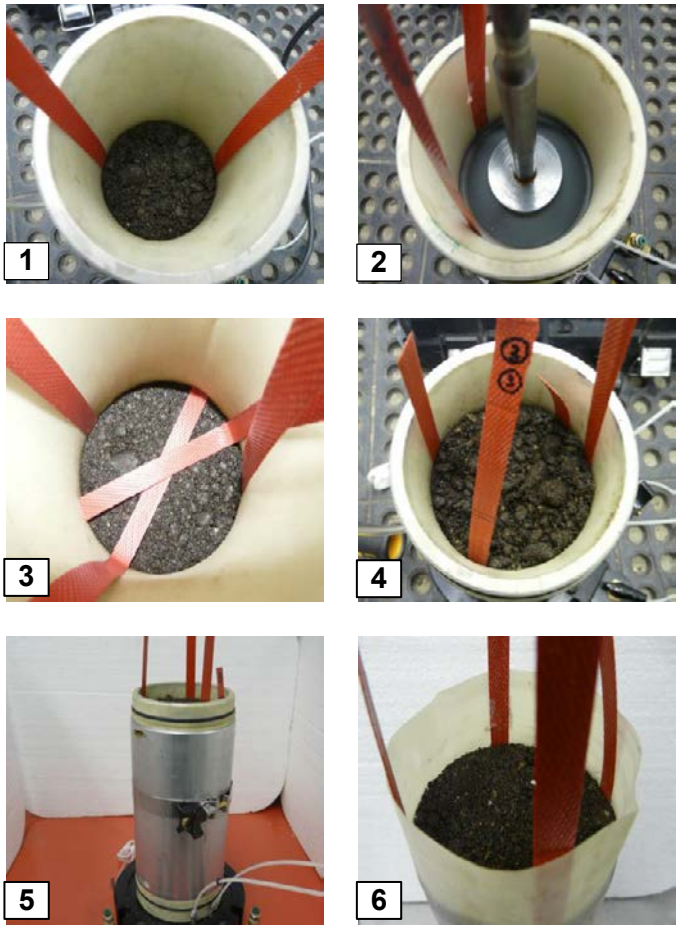

Figure 15. Basic steps for compacting samples with Method 3 (PP strapping band)

The compacted wet density should not vary more than ±3% of target wet density (AASHTO T307-99). Six samples were compacted for checking the sample density gradient with the three methods that were described above. The compacted wet density of each was calculated for the compacted samples and the percentages of differences between the measured and target wet densities were also calculated. Moreover, the compaction time for each layer was recorded.

Method 1 was used on three samples that two were made of RPCC and one was made of RAP materials. The average compacted wet density of five layers for all three samples is less than -1% from the target wet density. However, the first layer which is the bottom layer of each sample generally show the largest difference between the measured and the target wet

density while the last layer which is the top layer of each sample generally show the least difference. Although the compaction time that was consumed in compacting each layer was varied, the last layer generally need the least compaction time.

Method 2 was used on one sample that was made of RAP materials. The average compacted wet density of five layers is about -0.1% from the target wet density and the last layer consumed the least compaction time. However, this method only calculated the wet density of each layer before subsequent layers were compacted and compaction of the subsequent layers could result in higher wet density for the first four layers.

Method 3 was used on two samples that were made of RAP materials. The average compacted wet density of five layers for all two samples is less than 0.7% from the target wet density. The compaction time that was consumed in compacting the last layer is shortest compared to other four layers for both samples, but the decrease in compaction time was small.

These six samples all shows differences between the measured layer wet densities and the target sample density, but the differences are within the ±3% limit from target value as AASHTO T307-99 specified. Therefore, the differences are acceptable as the standard does not specify the requirement for each compacted layer. The results for all six samples are summarized in Table 6.

Table 6. Density gradient tests

Method	Material	Target wet density (kN/m^3)	Layer	Actual wet density (kN/m^3)	Actual wet density off target value (%)	Compaction time (s)
1 Filter paper	IA Hyw-30 Clean RPCC subbase	18.37	1	17.97	-2.2%	19
			2	18.79	2.3%	16
			3	18.04	-1.8%	14
			4	18.36	-0.1%	17
			5	18.38	0.1%	17
			Avg	18.31	-0.3%	—
1 Filter paper	IA Hyw-30 Clean RPCC subbase	18.94	1	18.35	-3.1%	23
			2	18.85	-0.5%	20
			3	19.07	0.7%	20
			4	18.81	-0.7%	20
			5	18.90	-0.2%	17
			Avg	18.94	-0.8%	—
1 Filter paper	Manatt's Inc. RAP	18.57	1	19.79	6.6%	44
			2	18.94	2.0%	63
			3	17.92	-3.5%	50
			4	18.29	-1.5%	51
			5	17.91	-3.6%	32
			Avg	18.57	0.0%	—
2 No separation	Manatt's Inc. RAP	18.57	1	18.43	-0.8%	60
			2	18.63	0.3%	42
			3	18.52	-0.3%	51
			4	18.69	0.6%	44
			5	18.53	-0.2%	31
			Avg	18.57	-0.1%	—
3 PP strapping band	Manatt's Inc. RAP	17.59	1	18.73	6.5%	7
			2	17.23	-2.0%	7
			3	17.51	-0.5%	6
			4	17.99	2.3%	4
			5	17.07	-3.0%	4
			Avg	17.59	0.7%	—
3 PP strapping band	Manatt's Inc. RAP	18.57	1	19.79	6.6%	26
			2	18.94	2.0%	26
			3	17.92	-3.5%	28
			4	18.29	-1.5%	25
			5	17.91	-4.0%	24
			Avg	18.57	0.0%	—

Notes: —means no value; the layer was numbered from the bottom to the top of each sample

Permanent Deformation Tests

This section discusses testing procedures and data analyses to determine the permanent deformation of samples.

Permanent deformation tests to determine permanent deformation of the UGMs were conducted according to three methods which include ISU 100k, ISU 1k, and NCHRP 598 (Saeed 2008a) methods. The sample compactions were the same by following the requirements in AASHTO T307-99. However, the loading sequences are designed with different number of load applications, confining pressures, and deviator stresses. In ISU 100k tests, the loading sequences were modified to produce large permanent deformation because high stresses and large number of load applications could produce large deformation that might occur in pavement service life.

The automated M_r test system that meets the AASHTO T307-99 requirements was used to determine the permanent deformation of samples. This system consisted of fully automated unit and a computer for data acquisition. The automated unit consists of a load frame, a cyclic-RM unit, a load cell, and electro-pneumatic air pressure regulator, a triaxial pressure chamber with two spring-loaded linear variable differential transducers (LVDT). The cyclic-RM unit was used to apply cyclic load with haversine pulse for 0.1 s and rest for 0.9 s in each loading cycle. A 11.1 kN (2500 lbf) load cell was used in this tests to apply up to 198.9 psi stress on cylindrical samples with diameter of101.6 mm (4 in.) by height of 203.2 mm (8 in.). The electro-pneumatic air pressure regulator automatically maintained and increased air pressure in triaxial chamber.

Two LVDTs were installed at opposite side and equal distance from the piston rod to measure the axial deformation of samples externally. Average values of the measurements of two LVDTs were used for calculating axial strains. RM5 software was installed in the computer for system parameters input and data acquisition and the version is 1.0.9.289. This system uses a proportional-integral-derivative (PID) controller to adjust the system control parameters in real-time as the stiffness of the sample changes during each test, so the applied loads were corrected to meet the target values. Figure 16 shows triaxial pressure chamber, load frame, and the computer used for permanent deformation and M_r tests.

Figure 16. Triaxial pressure chamber, load unit, and computer used for permanent deformation and M_r tests.

ISU 100 k, ISU 1k, and NCHRP 598 tests are three permanent deformation tests that were conducted in this study. They were performed on different materials and using the same test machine as shown in Figure 16. In addition, drainage valves of triaxial pressure chamber remained open during the permanent deformation tests.

The loading sequences and the number of readings per cycle were different in the permanent deformation tests from the M_r tests. The ISU 100k test consists of 4 loading sequences with 25,000 load cycles in each under constant confining stress and axial stress, because the capacity of each sequence was limited to about 33,000 cycles in the program used in this study. 20 instead of 200 readings per cycle which is the minimum requirement in AASHTO T307-99 were collected in each load cycle of the permanent deformation tests, because the permanent strain is calculated by using the first and last readings of each load cycle. Samples were considered as failed for both ISU 100k and ISU 1k tests when an axial strain of 5% obtained as AASHTO T307-99 specified.

ISU 100k tests were performed on the samples that were made of untrimmed slag subbase materials from I-94, MI and RPCC subbase materials from US-30, IA. ISU 1k tests were performed on the samples that were made of RPCC subbase materials from US-30, IA.

Dry unit weights, moisture contents, fines contents, confining pressures, and maximum axial stresses were varied for different tests to determine effects of these factors on resistance of materials to permanent deformation. An example of ISU 100k test setup is shown in Table 7 and an example of ISU 1k test setup is shown in Table 8.

Table 7. Repeated load triaxial test sequences and stress values (ISU 100 k test)

Sequence No.	Confining Pressure		Maximum Axial Stress		No. of Cycles
	(kPa)	(psi)	(kPa)	(psi)	
1	103.4	15.0	68.9	10.0	100,000

Table 8. Repeated load triaxial test sequences and stress values (ISU 1 k test)

Sequence No.	Confining Pressure		Maximum Axial Stress		No. of Cycles
	(kPa)	(psi)	(kPa)	(psi)	
1	103.4	15.0	68.9	10.0	1,000

NCHRP 598 test used in this study was introduced by National Cooperative Highway Research Program (NCHRP) report 598, and it consists of 1 preconditioning (PC) sequence and 10 loading sequences with same confining pressure and various cyclic stresses for each loading sequence as shown in Table 9. The PC with 50 load cycles was first performed on the sample to minimize the effects of unflatten top surfaces of the test samples which lead to imperfect contacts between the test samples and the sample cap which sit on the top surface of the samples. After PC sequence, 10 loading sequences with 1,000 cycles for each were applied on the sample with constant confining pressure of 103.4 kPa (15 psi) and increasing cyclic stress from 68.9 kPa (10 psi) to 1241.1 kPa (180 psi) with increment of 137.9 kPa (20 psi).

Table 9. Repeated load triaxial test sequences and stress values (NCHRP report 598)

Sequence No.	Confining Pressure		Maximum Axial Stress		No. of Cycles
	(kPa)	(psi)	(kPa)	(psi)	
PC	103.4	15.0	68.9	10.0	50
1	103.4	15.0	68.9	10.0	1000
2	103.4	15.0	137.9	20.0	1000
3	103.4	15.0	275.8	40.0	1000
4	103.4	15.0	413.7	60.0	1000
5	103.4	15.0	551.6	80.0	1000
6	103.4	15.0	689.5	100.0	1000
7	103.4	15.0	827.4	120.0	1000
8	103.4	15.0	965.3	140.0	1000
9	103.4	15.0	1103.2	160.0	1000
10	103.4	15.0	1241.1	180.0	1000

Saeed (2008) suggested that the NCHRP 598 tests loading sequences are applicable for M_r and permanent deformation tests and 200 readings per load application were recorded for calculating M_r and permanent strain. However, this NCHRP 598 test method was only applied for permanent deformation tests in this study, so 20 readings per load application was suggested for calculating permanent strain of the tested samples. The NCHRP 598 tests were completed when either all loading cycles applied or 10% permanent strain of the test samples reached. The NCHRP 598 tests were performed on RPCC/RAP and RAP subbase materials from Manatt's, In., IA and crushed limestone subbase materials from Martin Marietta Materials, Inc., IA. Dry unit weights and fines contents were varied to find their effects on resistance of the tested materials to permanent deformation.

Data analysis of permanent deformation tests

Data analysis for ISU 100k, ISU 1k and NCHRP 598 tests were basically the same. Permanent defamation in this study was quantified as accumulated permanent axial strain which is the ratio of the amount of unrecoverable change in sample height to the original sample height. The original heights of samples were measured when the samples were compacted and vacuumed with a vacuum pump before the permanent deformation tests. In addition, the accumulated permanent strain was calculated at every load cycle for all three permanent deformation test methods.

The displacements measured by two LVDTs were first averaged and then the average value at the end of each load cycle was divided by the original sample height to calculate the accumulated permanent strain at that load cycle. After the permanent strains of all load applications were calculated, the permanent strains were plotted with number of load cycles to observe the change in the accumulated permanent strains with increasing loading cycles. The accumulated permanent strain versus number of load cycles for ISU 100k and ISU 1k tests is a single parabola curve with increasing number of loading cycles, because constant confining pressure and cyclic stress were applied in each test. The accumulated permanent strains obtained in NCHRP 598 tests were plotted with increasing number of load cycles in stair-step parabola curve, because increasing deviator stress and constant confining pressure were applied in these tests.

According to literature studies, one widely used equation for permanent deformation prediction was selected for data analysis in this research. This equation was proposed by Barksdale (1972) and indicated a linear relationship between the accumulated permanent strain and logarithm number of load applications (Equation 15).

$$\varepsilon_{1,p} = a + b \cdot log(N) \tag{15}$$

where: $\varepsilon_{1,p}$ = accumulated permanent axial strain;

N= number of load repetitions; and

a, b = regression parameters.

This equation was also modified to predict the permanent strain obtained in the NCHRP 598 tests according to the applied deviator stresses (Equation 16):

$$\varepsilon_{1,p} = k_1 + k_2 \cdot \sigma_d + k_3 \cdot \sigma_d^2 + \left[k_4 + \frac{k_5 \cdot (e^{k_6 \cdot \sigma_d} - 1)}{k_6}\right] \cdot \log_{10}[N - 1000 \cdot (S - 1)] \tag{16}$$

where: $\varepsilon_{1,p}$ = accumulated permanent axial strain;

N = number of load cycles;

S = number of load sequences;

k_1, k_2, k_3, k_4, k_5, and k_6 = regression parameters; and

σ_d = deviator stress (kPa).

Degradation Tests

Mechanical sieve analyses were conducted according to ASTM D422-63 to determine degradations of UGMs caused by permanent deformation tests. Breakage index (BI) was defined as the change in particle size distributions of the tested materials due to test loadings, and BI was developed based on the ballast breakage index (BBI) that is used for quantifying ballasts degradations due to cyclic loading and developed by Indraratna et al. (2005).

If the original particle size distribution curve below the particle size distribution curve after permanent deformations, the difference between two curves indicates that particles broke down to smaller particles under the test loading. The loads can cause particles breakages are from two sources: permanent deformation test loading and sample compactions. Certain forces are applied in compacting materials to reach target densities. However, breakage caused by sample compaction is hard to be differentiated from samples variations. Consequently, total breakages caused by the applied forces from sample compaction and permanent deformation test were determined. The base line at 0% passing was determined as the reference line for calculating degradation in whole sample (Figure 17).

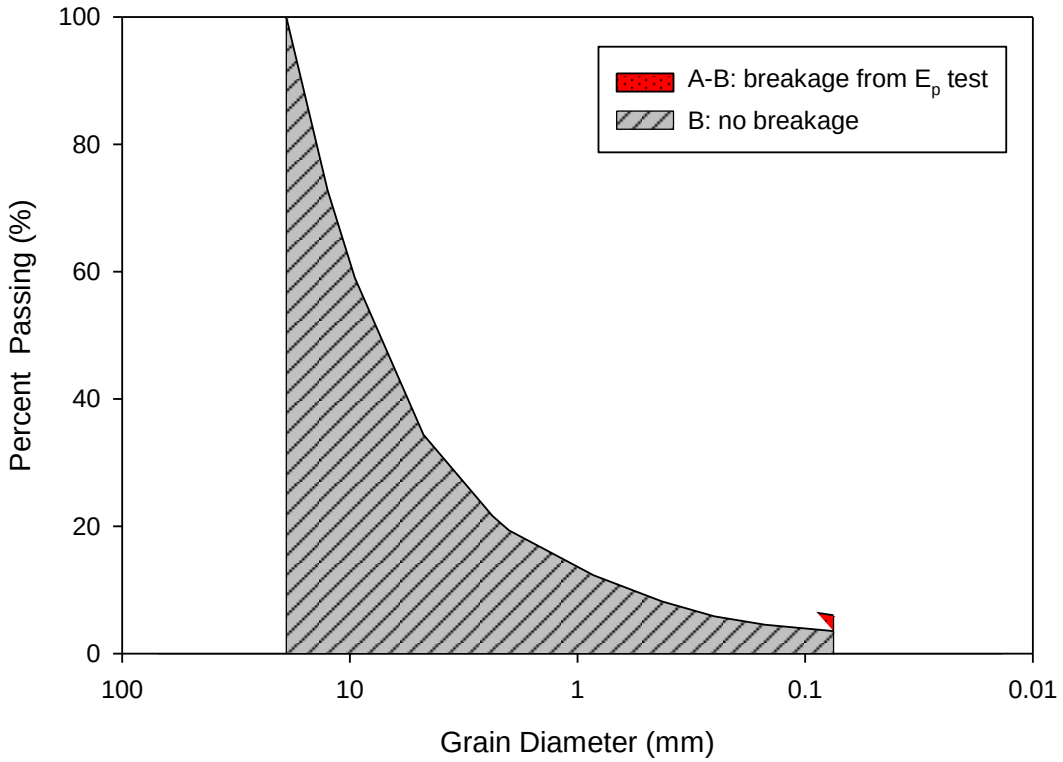

Figure 17. Example for calculating BI

Data analysis of degradation tests

Each degradation test includes two mechanical sieve analyses that one is for the materials before permanent deformation test and another one is for the materials after the test. Therefore, two particle size distribution curves that were plotted on the same figure (Figure 17) to calculate breakage index. Equation 17 was modified based on the BBI method that was developed by Indraratna et al. (2005), and each parameter was described.

$$BI=\frac{A-B}{B} \quad (17)$$

where: BI= breakage index;

A=area between the particle size distribution curve of the original materials and after the permanent deformation test; and

B= area between the particle size distribution curve of the original materials and the 0% passing base line.

Resilient Modulus Tests

This section discusses the testing and data analysis procedures for determining resilient modulus (M_r). Same sample preparation procedures, test equipment, and data acquisition system that were used in permanent deformation tests (Figure 16) were used in M_r tests. M_r tests were conducted according to AASHTO T307-99 with an automated M_r test system (Figure 16).

In this study, M_r tests were conducted on the cylindrical samples with diameter of 101.6 mm (4 in.) by height of 203.2 mm (8 in.), because the triaxial chamber used in this study could not fit larger samples (e.g., 6 in. diameter sample). Drainage valves of the triaxial pressure chamber were kept open to provide drained condition during M_r tests. The samples were air vacuuming before the M_r tests starts to maintain the samples shape. A computer software was also used for data acquisition during M_r tests, and the PID controller was used to adjust the system control parameters in real-time to correct the applied loads to reach the target values.

Although Saeed (2008) reported that the data from the cyclic triaxial tests with loading sequences (Table 9) was analyzed to determine not only the permanent deformations of the samples but also the M_r, AASHTO T307-99 is more widely used and followed in this study to determine resilient modulus values under different stress conditions.

In AASHTO T307-99, two different loading sequences were specified to simulate the stress conditions under traffic loading at different locations in a pavement foundation structure. One series of loading sequences is designed for subgrade materials with low confining and axial stresses and the other series of loading sequences is designed for base and subbase materials has higher stresses. In both series, the first loading sequence is a preconditioning sequence that is used to minimize the effect of imperfect contact between the sample surface and load cap. The PC sequence has 500 to 1000 cycles, and 500 cycles was used in this study. When the PC sequence completed, 15 loading sequences were continuously applied with 100 load cycles in each to determine the M_r at specified stress conditions. In this study, the granular materials that used for subbase layers were tested, so only the loading sequences specified for base and subbase materials are used (Table 10).

Table 10. Resilient modulus test sequences and stress values for base and subbase materials (AASHTO T307-99)

Sequence No.	Confining Pressure		Max. Axial Stress		No. of Cycles
	(kPa)	(psi)	(kPa)	(psi)	
PC	103.4	15	103.4	15	500-1000
1	20.7	3	20.7	3	100
2	20.7	3	41.4	6	100
3	20.7	3	62.1	9	100
4	34.5	5	34.5	5	100
5	34.5	5	68.9	10	100
6	34.5	5	103.4	15	100
7	68.9	10	68.9	10	100
8	68.9	10	137.9	20	100
9	68.9	10	206.8	30	100
10	103.4	15	68.9	10	100
11	103.4	15	103.4	15	100
12	103.4	15	206.8	30	100
13	137.9	20	103.4	15	100
14	137.9	20	137.9	20	100
15	137.9	20	275.8	40	100

The M_r tests were completed when either all test sequences completed or 5% permanent strain of the samples reached. When the M_r tests were finished, quick shear tests were conducted on the same samples that were used for M_r tests to determine the stress–strain

relationships of the samples if less than 5% accumulated permanent axial strain was obtained when the M_r tests completed. M_r tests were performed on RPCC/RAP and RAP subbase materials from Manatt's, In., IA and crushed limestone subbase materials from Martin Marietta Materials, Inc., IA. Dry unit weights and fines contents were varied to study their effects on resilient moduli of UGMs.

Data analysis of resilient modulus tests

Test readings of every load cycles in each sequence were calculated according to AASHTO T307-99 to determine the resilient moduli under various combinations of confining pressure and deviator stress. In the table summary report that was automatically generated in the computer program when M_r test was completed, M_r was calculated by averaging M_r values of the last five load cycles for each loading sequence. Manual calculations were performed according to AASHTO T307-99 to check the results from system summary report.

The raw data which consists of displacement 1 and 2, confining pressure, and load were recorded for each of 200 readings in one load cycle during M_r tests. Two displacement readings were averaged to calculate accumulated axial strain of each reading by dividing the average displacement by original heights of test samples. The difference between the maximum axial strain and the last axial strain in the 200 axial strains of each load cycle is the resilient strain of this load cycle. Axial stresses of each reading were calculated by dividing the load by the area of test samples. Cyclic stress is the difference between the maximum axial stress and the minimum axial stress in 200 readings for each load application. M_r of each load cycle was calculated through dividing the cyclic stress by the resilient strain. The manually calculated resilient moduli of last five cycles in each load sequence were summarized to compare to the values from system output.

The calculated M_r values for each sample were analyzed by fitting the M_r prediction model by Witczak and Uzan (1988). This prediction model was recommended by MEPDG (NCHRP 2004) and also called Universal model (Equation 18):

$$M_r = k_1 P_a \left(\frac{\sigma_B}{P_a}\right)^{k_2} \left(1 + \frac{\tau_{oct}}{P_a}\right)^{k_3} \quad (18)$$

where: P_a = atmospheric pressure (MPa);

τ_{oct} = octahedral shear stress (MPa) = $\frac{\sqrt{(\sigma_1-\sigma_2)^2+(\sigma_2-\sigma_3)^2+(\sigma_3-\sigma_1)^2}}{3}$

σ_B= bulk stress (MPa) = $\sigma_1+ \sigma_2+ \sigma_3$;

k_1, k_2, k_3 = regression coefficients; and

σ_1, σ_2, σ_3 = principal stresses (MPa).

Unconsolidated Undrained Tests

Unconsolidated undrained tests (quick shear test in AASHTO T307-99) were conducted to determine the undrained shear strengths of the UGMs according to AASHTO T307-99. The quick shear test was conducted only when a sample experienced less than 5% permanent strain during a M_r test and was conducted as soon as possible after the M_r test.

In this study, only UGMs used for subbase construction were studied, so 34.5 kPa (5 psi) confining stress was controlled for all quick shear tests. During the quick shear tests, the confining stresses were controlled by the M_r test computer program while data was acquired by another computer program which is for quick shear tests. This quick shear tests program also controlled the strain rate that compresses samples at 1% axial strain per minute according to AASHTO T307-99. In addition, the valves of the triaxial pressure chamber were turned off during quick shear tests to maintain undrained conditions. Undrained shear strength were determined as half of the peak values before the load values decrease with increasing strain. The quick shear tests completed when either undrained shear strengths were determined, 5% permanent strain reached, or load capacity of load cell reached.

Data analysis of shear strength tests

Stress–strain relationships were presented by plotting accumulated axial strains with deviator stresses. Deviator stresses were calculated according to ASTM D2850-03a using raw data from quick shear tests, and axial strains were corrected by counting the permanent strains from the M_r tests on the sample. Strains were calculated by dividing the displacements by the sample height that was calculated after M_r test. Then, the cross area of test sample was corrected by accounting strain effects on sample. Membrane corrections for stress difference were calculated to subtract the effects of membranes used in each test (Equation 19) as introduced in ASTM D2850-03a.

$$\Delta(\sigma_1 - \sigma_3) = \frac{4E_m t_m \varepsilon_1}{D} \quad (19)$$

where: $\Delta (\sigma_1 - \sigma_3)$ = correction to be subtracted from the measured principal stress difference;

D= $\sqrt{4A/}$ = diameter of sample;

E_m = Young's modulus for the membrane material;

t_m = thickness of the membrane; and

ε_1 = axial strain.

Typical value of E_m for latex membrane is 1400 kN/m^2 (ASTM D2850-03a) and this value was used for membrane correction in this study. Membrane thickness was doubled to account the effect of two membranes that used on each sample. The actual deviator stresses were calculated by dividing the axial loads with the corrected areas and subtracting the membrane corrections. Changes in original sample height due to load applications in M_r tests were accounted for correcting axial strain in the quick shear test. Finally, the stress-strain relationship and the undrained shear strength of each sample were determined.

CHAPTER 4. MATERIALS

This chapter summarizes the index properties of granular materials used in this study (Table 11). Materials from project sites were collected from pavement foundation layers of newly constructed or reconstructed pavements. Materials from Iowa quarries were produced to meet requirements of Iowa Department of Transportation (Iowa DOT) for pavement foundation materials. All materials were non-plastic with low fines content (percentage of materials passing No. 200 sieve). In addition to mechanical sieve analysis, hydrometer tests were conducted on samples of recycled portland cement concrete pavement (RPCC), RPCC with recycled asphalt pavement mixture (RPCC/RAP), recycled asphalt pavement (RAP), and crushed limestone materials.

Table 11. Site locations and subbase materials

State	Site Location	Subbase Material
Michigan	I-94, St. Clair and Macomb Counties	Untrimmed slag
Iowa	US-30, Story County	RPCC
	Manatt's, Inc., Ames	RPCC/RAP
		RAP
	Martin Marietta Materials, Inc., Ames	Crushed limestone

These unbound granular materials (UGMs) were investigated in two stages that required different preparation methods and involved different test matrices. In stage one, the main objectives were to determine permanent deformations of two UGMs (untrimmed slag subbase and RPCC) and to observe the factors that affect permanent deformation response, so the test materials were prepared using the scalp and replace method to reduce the maximum particle size per test standards. In stage two, a new test matrix was created to study permanent deformation response of the remaining three materials (RPCC/RAP, RAP, and crushed limestone) and to perform other laboratory tests to observe relationships between permanent deformation and other properties (e.g., M_r, permeability). The test materials tested in stage two were prepared by scalping off large particles (retained on 3/4in. sieve) only to maintain nearly the same particle size distribution for materials used in different tests.

Both the scalp and replace and scalp only samples were prepared to meet the requirements in AASHTO T307-99. The requirement of the M_r test is that the minimum diameter of the mold used to fabricate samples should be equal to five times the maximum

particle size of the materials. Samples that were subjected for M_r and permanent deformation tests were compacted in 101.6 mm (4 in.) diameter molds so the maximum particle size of the test materials should be less than 20.3 mm (0.8 in.). For each material in the study, soil index properties were determined by conducting mechanical sieve analysis, hydrometer tests, relative density tests, and specific gravity tests.

Untrimmed Slag Subbase

The untrimmed slag subbase material from Michigan I-94 was sampled from St. Clair and Macomb Counties in Michigan (Figure 18). Table 12 shows the soil index properties of the original untrimmed slag subbase and same material after the scalp and replace process.

Figure 18. Untrimmed slag subbase in situ

Table 12. Untrimmed slag subbase soil index properties

Soil Index Property	Original	Scalp and Replaced
USCS classification	GP	GP
AASHTO classification	A–1–a	A–1–a
Coefficient of uniformity (C_u)	2.00	13.14
Coefficient of curvature (C_c)	1.10	3.71
Specific gravity (G_s)	—	—
Min dry unit weight (kN/m^3) relative density at 0% moisture content	14.05	—
Max dry unit weight (kN/m^3) relative density at 0% moisture content	16.24	—
D_{10} (mm)	13.44	0.59
D_{30} (mm)	19.57	4.09
D_{60} (mm)	26.18	7.71
F_{200} (%)	2.2	0.8

Note: — indicates tests not performed

Both the original untrimmed slag subbase material and the material after the scalped and replace process were classified as GP in accordance with USCS and A–1–a in accordance with AASHTO classification systems. The particle size distribution curve of the scalp and replace material moved to the right side of the original material as expected, because more particles passed ¾ in. (19 mm) sieve and no materials were retained on 1 in. (25 mm) sieve. These particle size distribution curves are shown in Figure 19.

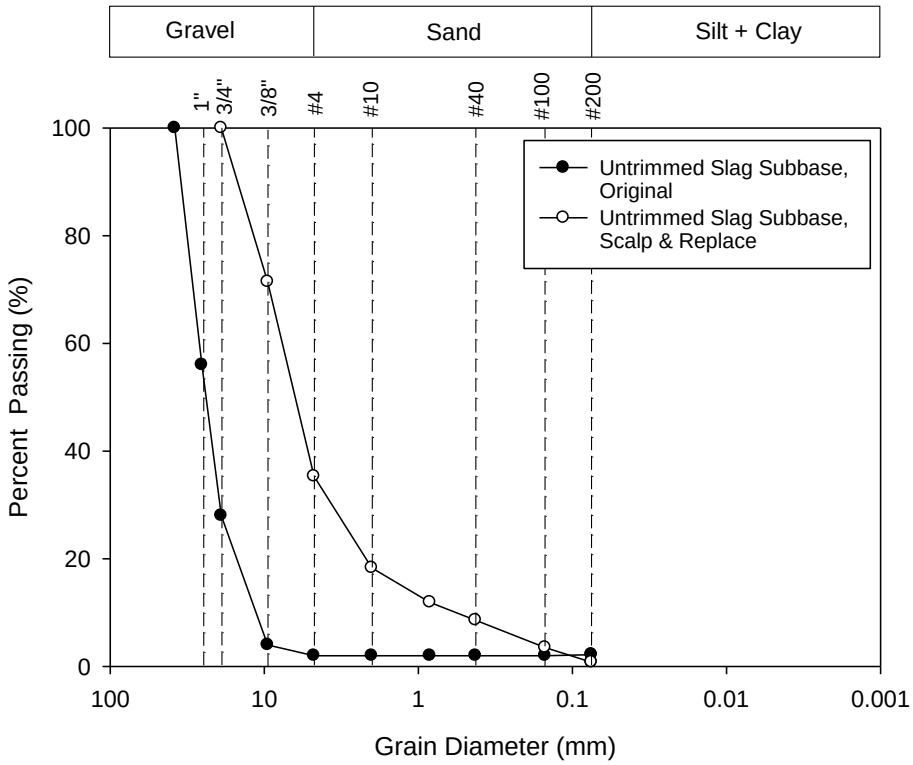

Figure 19. Untrimmed slag subbase particle size distribution

Laboratory relative density tests were conducted to determine the maximum and minimum dry unit weights. The actual moisture content and dry unit weight for each resilient modulus tests was determined to cover the range of maximum and minimum dry unit weights. The moisture contents and dry unit weights were similar for all permanent deformation test samples because the main variable in this test set was fines content. Figure 20 shows the maximum and minimum dry unit weights that were determined in the relative density test at 0% moisture content and the actual moisture contents and dry unit weights of samples that were prepared for permanent deformation and resilient modulus tests.

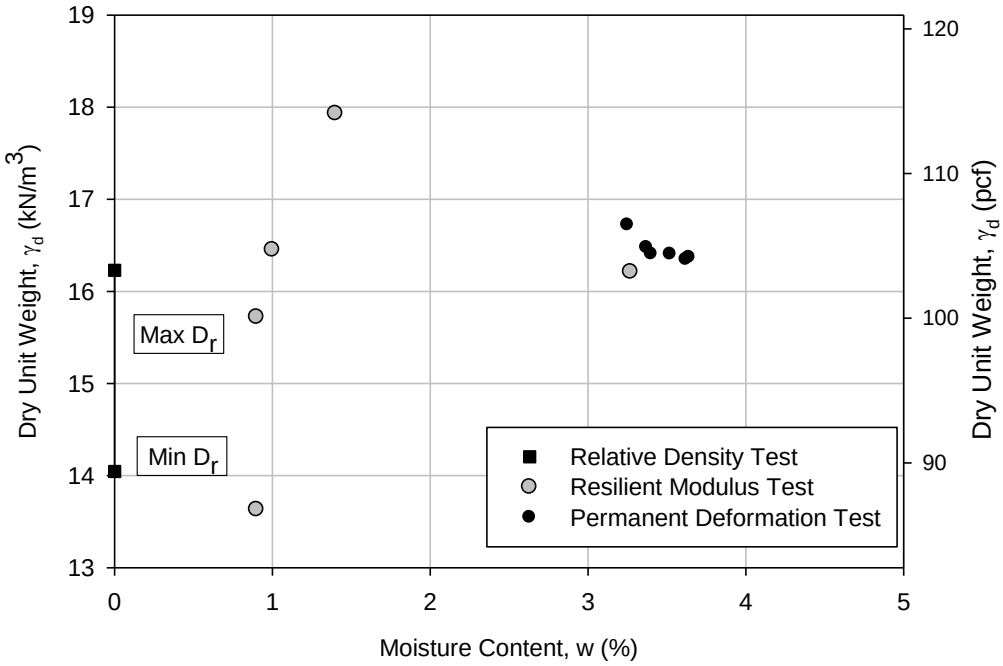

Figure 20. Untrimmed slag subbase moisture–dry unit weight relationships

RPCC

The RPCC subbase material was sampled from a stockpile at a project site on US 30 in Story County, Iowa (Figure 21). Table 13 shows the soil index properties of the original RPCC and the same material after the scalp and replace process.

Figure 21. RPCC (US–30) air dried

Table 13. RPCC (US 30) soil index properties

Soil Index Property	Original	Scalp and Replaced
USCS classification	GP–GM	GP–GM
AASHTO classification	A–1–a	A–1–a
Coefficient of uniformity (C_u)	44.34	36.17
Coefficient of curvature (C_c)	4.48	5.39
Specific gravity (G_s)	2.57	—
Min dry unit weight (kN/m^3) relative density at 0% moisture content	13.49	—
Max dry unit weight (kN/m^3) relative density at 0% moisture content	17.40	—
D_{10} (mm)	0.27	0.28
D_{30} (mm)	3.85	3.84
D_{60} (mm)	12.12	9.95
F_{200} (%)	5.2	5.6

Note: — indicates tests not performed

The original RPCC material and the RPCC material after the scalp and replace process were classified as GP–GM in accordance with USCS and A–1–a in accordance with AASHTO classification systems. As a result of the scalp and replace process, the RPCC coefficient of uniformity decreased about 20% and the coefficient of curvature increased about 20%. D_{60} decreased about 18% compared to the original material, but values of D_{10}, D_{30}, and F_{200} changed within 8%. The larger change in D_{60} is because the scalp and replace process that add more materials without particles retained on ¾" (19 mm) and passed No. 4 (4.75 mm) sieve.

To further characterize the gradation of the material, a mechanical sieve analysis was conducted on a sample compacted in preparation for permanent deformation testing. This sieve analysis indicates the breakage of particles due to sample compaction. Sample compaction broke particles, so higher percent of materials passing each sieve. All of these three particle distribution curves are plotted in Figure 22.

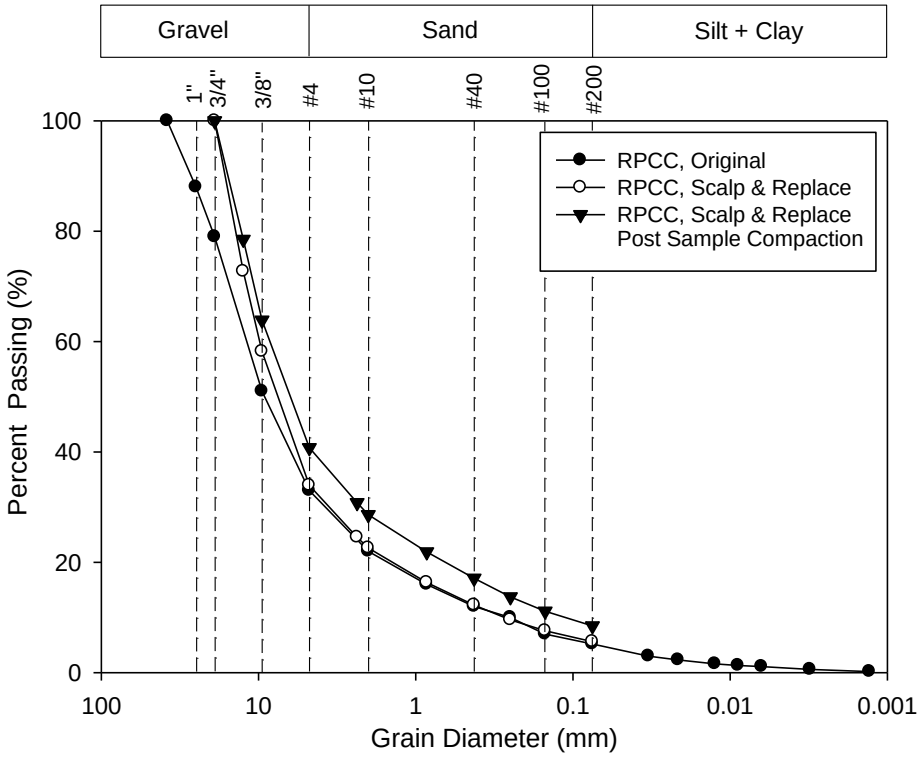

Figure 22. RPCC (US–30) subbase particle size distribution

A relative density test was conducted to determine the maximum and minimum dry unit weights for the material with 0% moisture content. In addition, the specific gravity test was conducted to determine specific gravity for this RPCC material as 2.57. Then, the zero air voids (ZAV) curve was plotted based on the calculation with the determined specific gravity. The actual moisture content and dry unit weight values were calculated for each permanent deformation test sample. The moisture contents for all ISU 100k and ISU 1k permanent deformation tests were around 10% except one ISU100k test specimen at about 8%. Dry unit weights of all permanent deformation tests were about1% to 6% higher than the maximum dry unit weight which was determined in the relative density test.

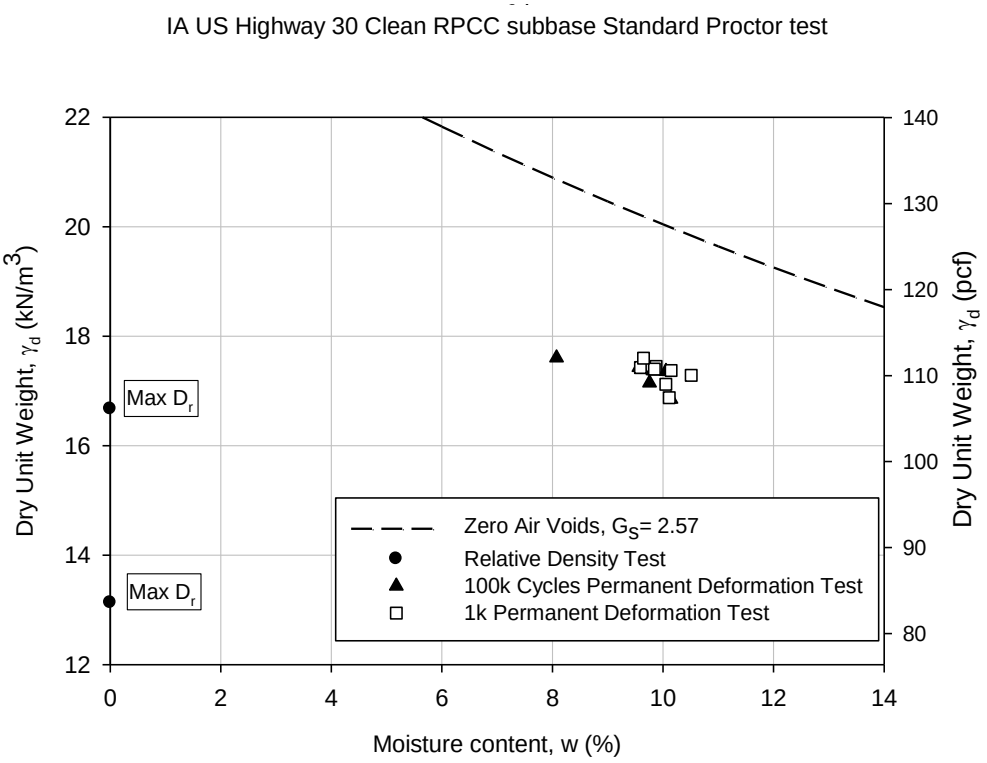

Figure 23. RPCC (US–30) subbase moisture–dry unit weight relationships

RPCC/RAP

The RPCC/RAP material was produced by Manatt's, Inc. (Figure 24). Although RAP particles were observed, the percent of RAP in this mixed material was not reported. Particle size distribution of this material was produced to meet the requirements of the Iowa DOT on subbase aggregate materials with gradation No. 12a (Iowa DOT 2008). In addition, this material had moisture content of 5.98% as tested in Laboratory when the researchers transport it from quarry to laboratory in sealed buckets. Table 14 shows the soil index properties of the original RPCC/RAP and the same material after the scalp only process and contains four different fines content.

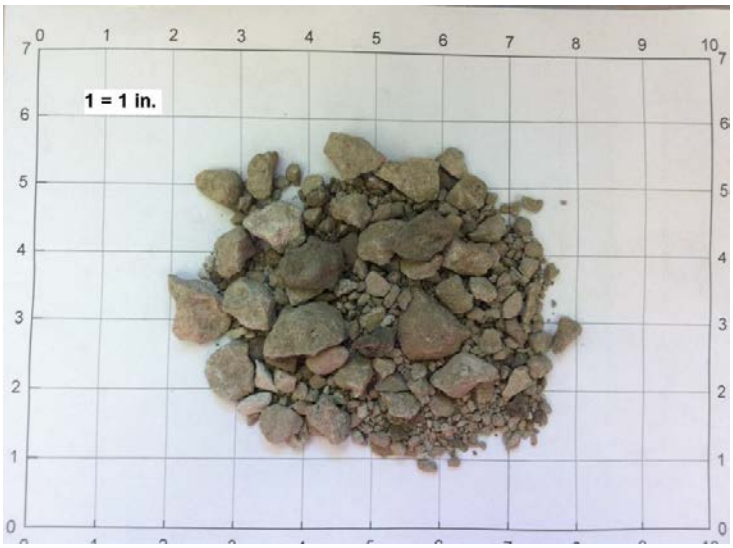

Figure 24. RPCC/RAP (Iowa Manatt's) oven-dried

Table 14. RPCC/RAP (Iowa Manatt's) soil index properties

Soil Index Property	Natural % Fines		0% Fines	6% Fines	12% Fines
	Original	Scalped only			
USCS classification	GW	GW	GW	GW–GM	GM
AASHTO classification	A–1–a	A–1–a	A–1–a	A–1–a	A–1–a
Coefficient of uniformity (C_u)	10.7	15.73	11.03	29.89	*
Coefficient of curvature (C_c)	2.63	2.61	1.86	1.89	*
Specific gravity (G_s)	2.62	—	—	—	—
Min dry unit weight (kN/m^3) relative density at 0% moisture content	14.65	12.88	12.93	13.96	14.69
Max dry unit weight (kN/m^3) relative density at 0% moisture content	16.42	14.97	15.57	17.38	18.17
D_{10} (mm)	1.39	0.62	0.82	0.26	*
D_{30} (mm)	7.36	3.99	3.71	1.99	1.87
D_{60} (mm)	14.84	9.78	9.02	7.92	7.51
F_{200} (%)	2.2	3.1	0.8	5.8	12.4

Note: — indicates tests not performed
* indicates cannot be calculated

The original, scalp only, 0% fines content RPCC/RAP materials were classified as GW in accordance with USCS. The 6% and 12% fines content materials were classified as GW–GM and GM separately in accordance with USCS. However, all of these five materials were classified as A–1–a in accordance with AASHTO. The target fines contents were determined as the 0%, 100%, and 200% of the maximum fines content that is specified by Iowa DOT (2008) on granular subbase materials (gradation No. 12a). Therefore, fines content was made to reach the target values of 0%, 6%, and 12%, but actual fines contents were measured and not exactly as the target values. Coefficient of uniformity, coefficient of curvature, and D_{10} values could not be calculated for materials with >10% target fines content. All the particle size distribution curves were plotted in Figure 25.

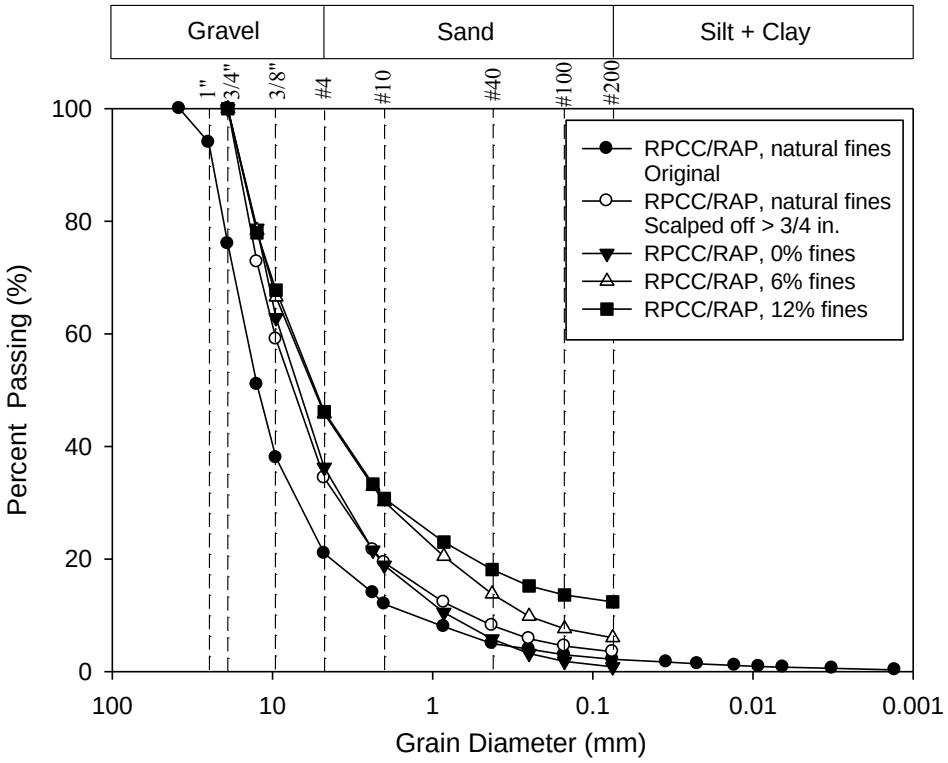

Figure 25. RPCC/RAP (Iowa Manatt's) particle size distribution

Relative density tests were conducted on the original RPCC/RAP material to determine the maximum and minimum dry unit weights at 0% moisture content and a moisture-dry unit weight relationship. The bulking moisture content effect was identified by varying the moisture content of samples in small increment. The actual moisture content and dry unit

weight for each sample after permanent deformation testing or resilient modulus testing was determ

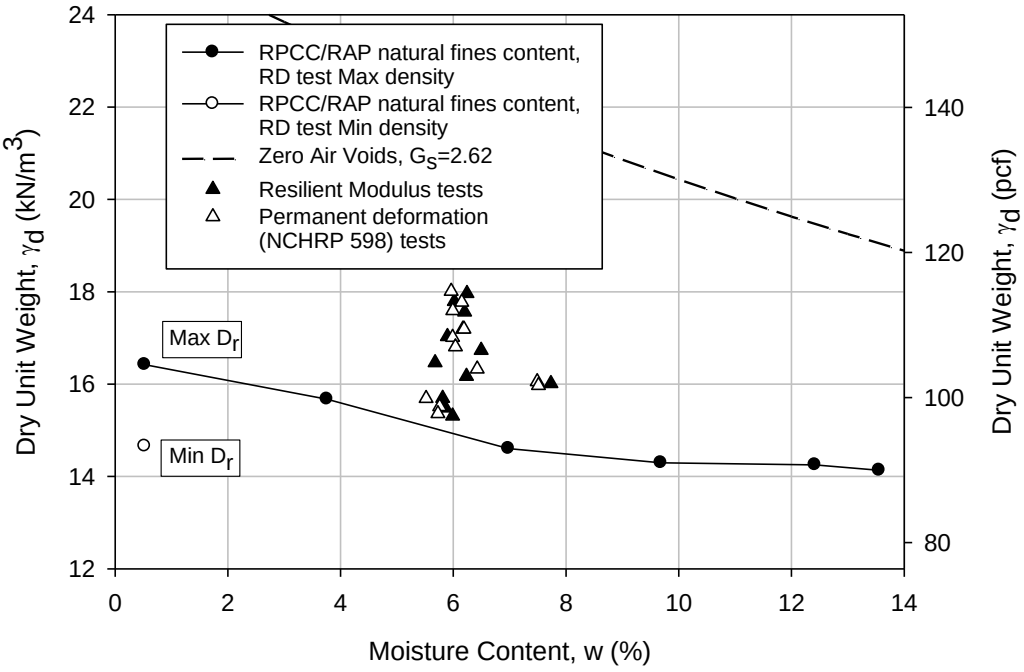

Figure 26. RPCC/RAP (Iowa Manatt's) moisture–dry unit weight relationships

Moreover, relative density tests were conducted on the materials with different target fines contents. The maximum and minimum dry unit weights of materials increased with increasing fines content for 0% to 12%. Fine materials increased in percentage of the total materials from 0% to 12%, so more voids between particles were filled with fine materials and dry unit weight increased. The maximum and minimum dry unit weights of all relative density tests were reported in Figure 27.

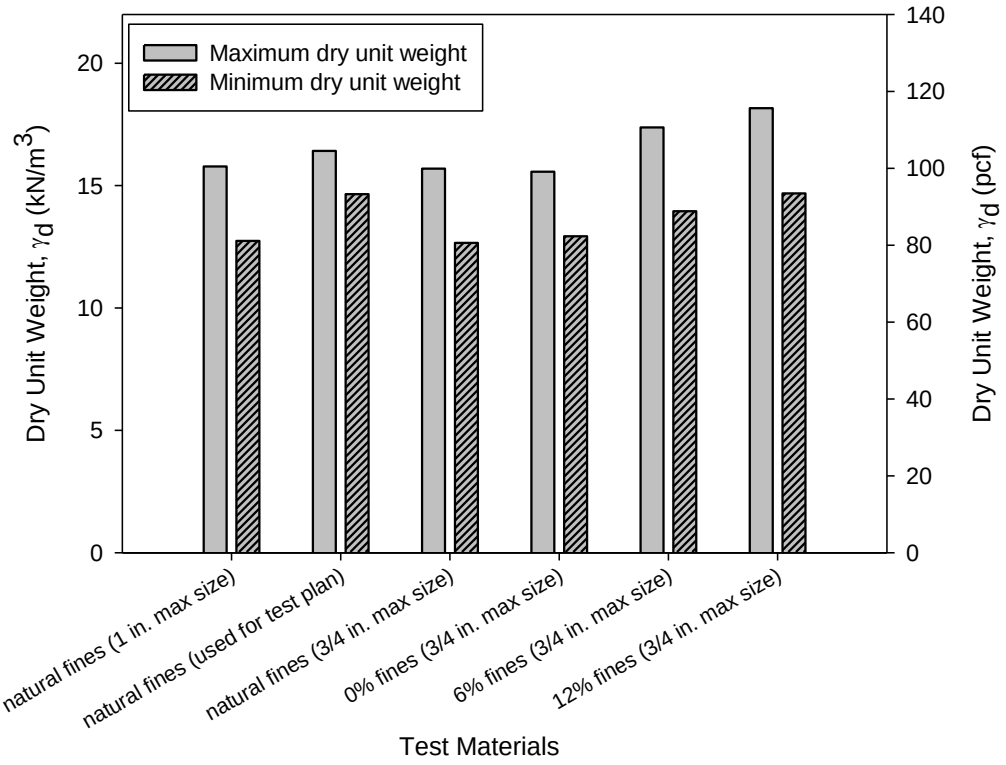

Figure 27. RPCC/RAP (Iowa Manatt's) with varied fines content dry unit weight

RAP

The RAP material was produced by Manatt's, Inc. (Figure 28). Particle size distribution of this material was produced to meet the requirement of Iowa DOT on subbase aggregate materials with gradation No. 12a (Iowa DOT 2008). In addition, this material had moisture content of 2.86% as tested in Laboratory when the researchers transport it from quarry to laboratory in sealed buckets. Table 15 shows the soil index properties of the original RAP material and the materials after the scalp only process and contained four different fines content.

Figure 28. RAP with 4.8% moisture content

Table 15. RAP soil index properties

Laboratory Property	Natural % Fines		0% Fines	6% Fines	12% Fines
	Original	Scalped only			
USCS classification	GW	GW	SW	SW–SM	SM
AASHTO classification	A–1–a	A–1–a	A–1–a	A–1–a	A–1–a
Coefficient of uniformity (C_u)	13.28	10.89	11.78	15.74	*
Coefficient of curvature (C_c)	1.38	1.38	1.11	1.29	*
Specific gravity (G_s)	2.47	—	—	—	—
Min dry unit weight (kN/m^3) relative density at 0% moisture content	13.67	12.88	13.70	14.51	14.97
Max dry unit weight (kN/m^3) relative density at 0% moisture content	14.35	14.97	16.15	17.50	18.20
D_{10} (mm)	0.51	0.57	0.50	0.37	*
D_{30} (mm)	2.17	2.21	1.81	1.66	1.01
D_{60} (mm)	6.73	6.22	5.90	5.80	4.12
F_{200} (%)	2.9	2.0	1.6	5.6	12.5

Note: — indicates tests not performed
* indicates cannot be calculated

Average specific gravity of this RAP material is 2.47 from calculation of coarse aggregate specific gravity and water pycnometer tests. The actual fines content of materials with 0% target fines content was 1.6%, because the dry sieve process that to separate fines

cannot clearly separate the fine materials from asphalt binder coated large particles. When 6% or 12% target fines content were desired, additional fines that were produced by crushing or washing and drying RAP materials were added to the materials after the scalp only process.

Both of the original RAP material and the RAP material after scalped off the materials retained on 3/4 in. sieve were classified as GW in accordance with USCS. However, materials with target fines content of 0%, 6%, and 12% were classified as SW, SW–SM, and SM separately. Moreover, all materials were classified as A–1–a in accordance with AASHTO classification system. Coefficient of curvature and uniformity and D_{10} values were not reported for materials with >10% target fines content. All particle size distribution curves were plotted in Figure 29. The particle size distribution curve moved to the right as target fines increased.

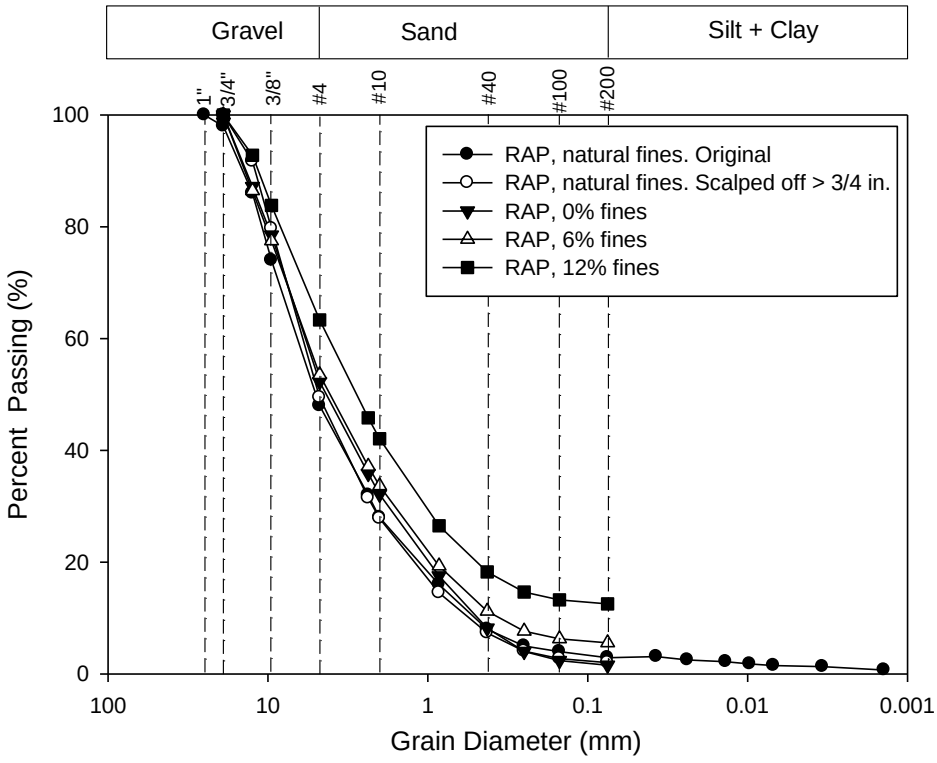

Figure 29. RAP particle size distribution

Relative density tests were conducted on the original RAP material to determine the maximum and minimum dry unit weights and a moisture-dry unit weight relationship. The

bulking moisture content effect was identified by varying the moisture content in small increments and up to about 13%. In addition, the actual moisture contents and dry unit weights of all samples for permanent deformation and resilient modulus tests were reported.

Dry unit weight of all permanent deformation and resilient modulus tests were higher than the maximum dry unit weight of the original RAP materials (Figure 30) because the target dry unit weight for each sample was determined based on the maximum and minimum dry unit weights on the materials in the same conditions (e.g., same fines content and after scalp only process). The moisture–dry unit weight relationship of the original RAP materials, and dry unit weights and moisture contents for all permanent deformation and resilient modul

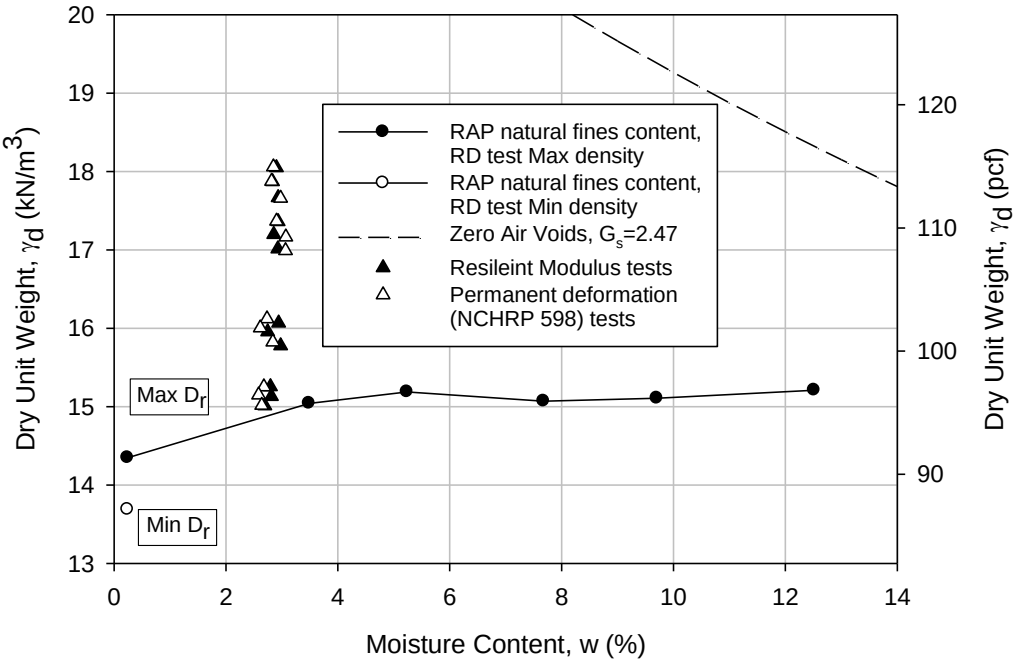

Figure 30. RAP moisture–dry unit weight relationships

In addition, the maximum and minimum dry unit weights for RAP with different fines content after scalped off oversize particles and the original RAP were determined by conducting relative density tests. The maximum and minimum dry unit weight increased with increasing fines content for 0% to 12%. Although fines content of materials after scalped off with natural fines content is about 30% higher than the materials with 0% target fines

content, the maximum and minimum dry unit weights of materials with 0% target fines content

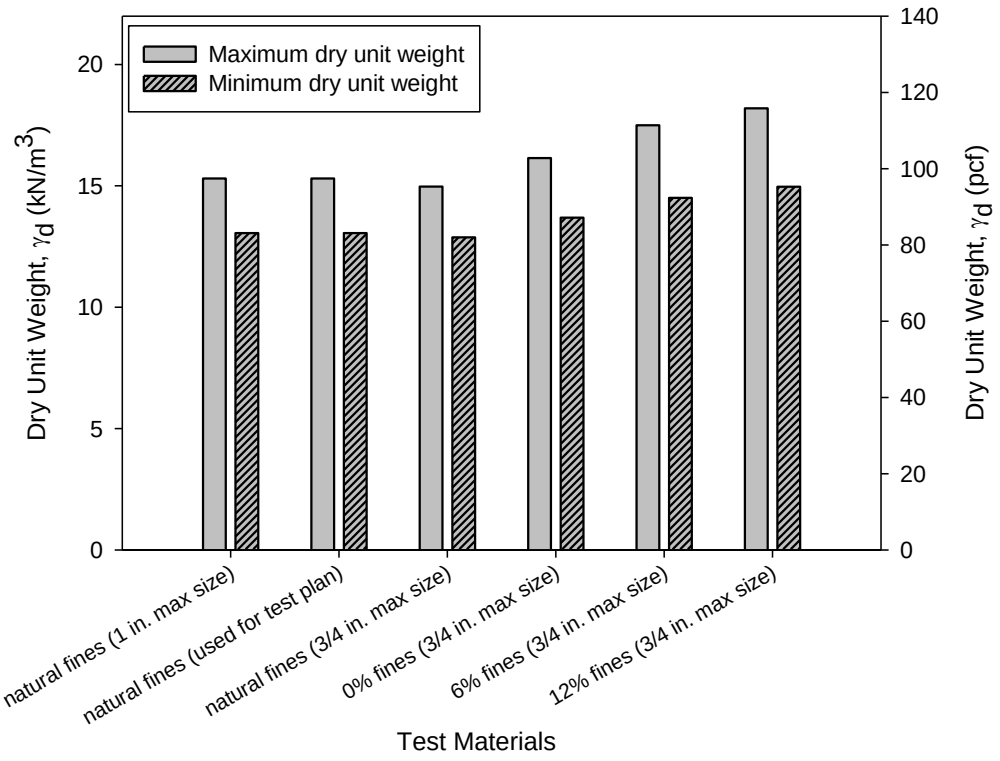

Figure 31. RAP with varied fines content dry unit weight

Crushed Limestone

This crushed limestone was produced by Martin Marietta Materials, Inc.. Particle size distribution of this material should meet the requirement of Iowa DOT on subbase aggregate materials with gradation No. 12a (Iowa DOT 2008). In addition, this material had moisture content of 2.32% as tested in Laboratory when the researchers transport it from quarry to laboratory in sealed buckets. Fine grains around the large crushed limestone particles make it in grey color as Figure 32 shows. Table 16 shows the soil index properties of the original crushed limestone material and the same material after the scalp only process and contains different fines contents.

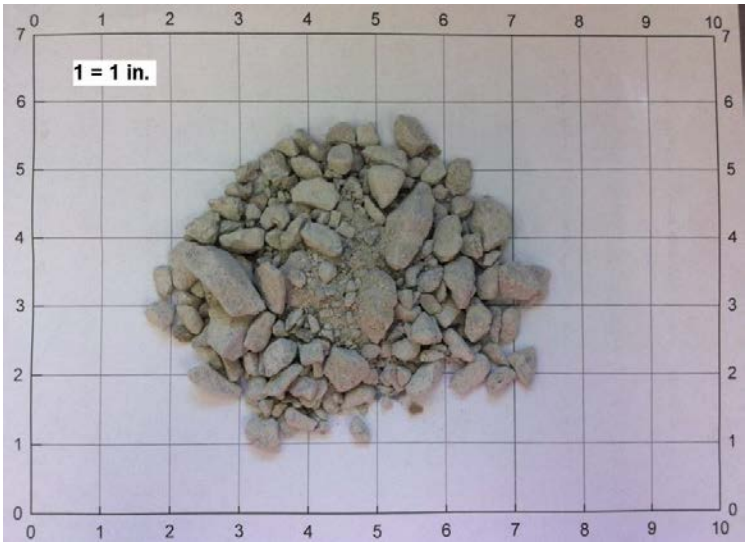

Figure 32. Crushed limestone oven-dried

Table 16. Crushed limestone soil index properties

Soil Index Property	Natural % Fines		0% Fines	6% Fines	12% Fines
	Original	Scalped only			
USCS classification	GP–GM	GP–GM	GP	GP–GM	GM
AASHTO classification	A–1–a	A–1–a	A–1–a	A–1–a	A–1–a
Coefficient of uniformity (C_u)	61.88	*	22.33	35.78	*
Coefficient of curvature (C_c)	11.41	*	4.36	5.69	*
Specific gravity (G_s)	2.71	—	—	—	—
Min dry unit weight (kN/m^3) relative density at 0% moisture content	16.76	16.94	16.15	16.15	16.64
Max dry unit weight (kN/m^3) relative density at 0% moisture content	17.83	21.06	19.60	20.20	20.60
D_{10} (mm)	0.17	*	0.45	0.28	*
D_{30} (mm)	4.54	1.84	4.40	3.98	3.34
D_{60} (mm)	10.56	8.91	9.96	9.98	10.42
F_{200} (%)	7.8	10.1	2.2	5.8	12.6

Note: — indicates tests not performed
* indicates cannot be calculated

Average specific gravity of the crushed limestone material is 2.71 from calculation of coarse aggregate specific gravity and water pycnometer tests. Although 0% fines content was desired, the actual fines content of materials with 0% target fines content was 2.2%. When

6% or 12% target fines content were desired, additional fines that were produced by crushing oven-dried crushed limestone materials were added to the materials after the scalp only process.

The original crushed limestone materials and the scalped only materials with natural and 6% target fines content were classified as GP–GM in accordance with USCS. Moreover, the scalped only materials with 0% and 12% target fines content were classified as GP and GM separately in accordance with USCS. However, all materials were classified as A–1–a in accordance with AASHTO classification system. Coefficient of curvature and uniformity and D_{10} were not reported for materials with 12% target and natural fines content after scalped off oversize particles, because the percentage of fines in these materials were over 10%. The particle size distribution curve moved to the right as target fines increased. All particle size distribution curves were plotted in Figure 33.

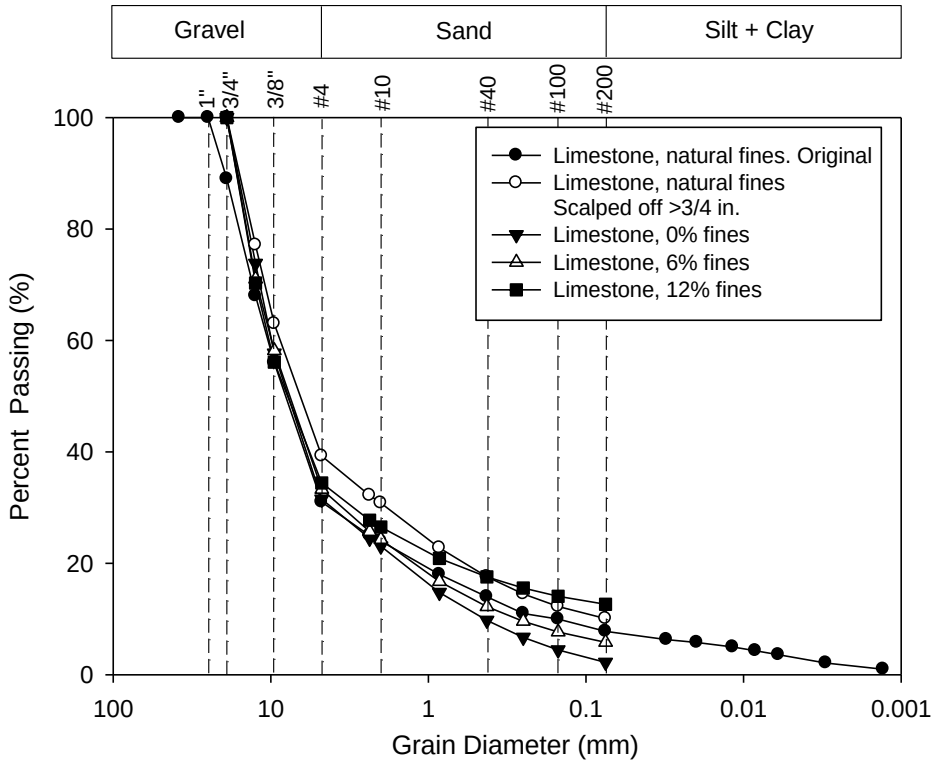

Figure 33. Crushed limestone particle size distribution

Relative density tests were conducted on the original materials to determine the maximum and minimum dry unit weights and a moisture-dry unit weight relationship. The

bulking moisture content effect was identified by varying moisture content of samples in small increments and up to 9%. The lowest dry unit weight of the original materials reached when moisture content was about 2.9%. This bulking moisture content is close to 2.32% which is the target moisture content for all permanent deformation and resilient modulus tests samples. Dry unit weight of all permanent deformation and resilient modulus testing samples were higher than the maximum dry unit weight of the original materials (Figure 34), because the target dry unit weight for each sample was determined based on relative density tests of the materials in the same conditions (fines content, scalped off or not). Actual dry unit weights and moisture contents for all permanent deformation and resilient modulus testing were s

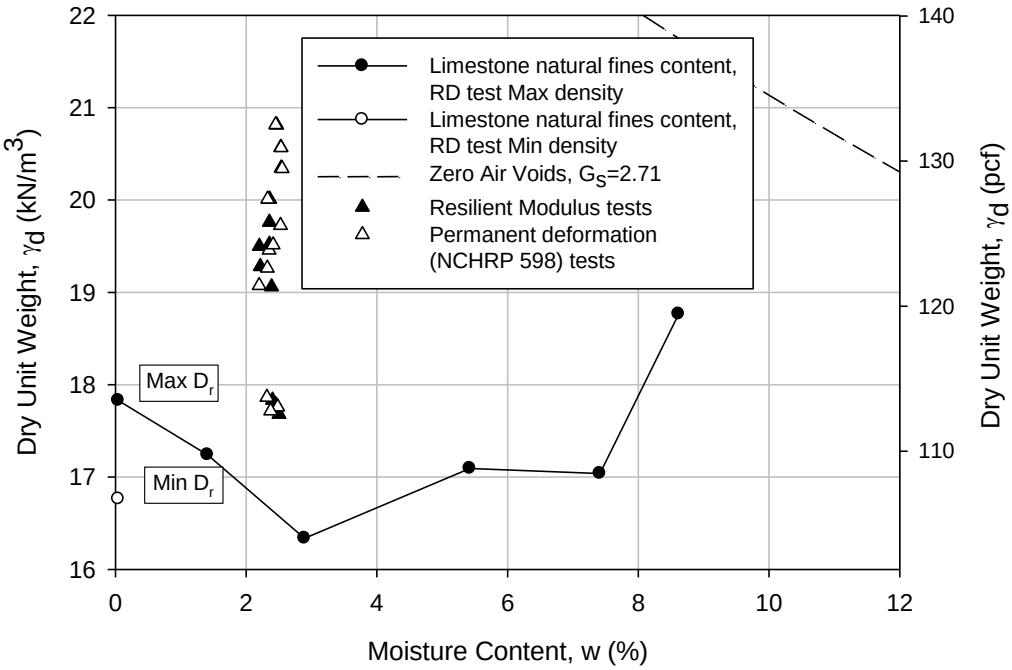

Figure 34. Crushed limestone moisture–dry unit weight relationships

The maximum and minimum dry unit weight increased about 3% and 5% separately as target fines content of the scalped only crushed limestone materials increased from 0% to 12%. However, the maximum and minimum dry unit weight of scalped off crushed limestone materials with natural fines content were about 3% higher than the values of materials with 12% target fines content. The second relative density test determined the maximum and minimum dry unit weight that used for determining the target dry unit weight for samples

made with natural scalped off materials in the test plan. However, another relative density test was conducted on scalped only materials with natural fines content. The maximum dry unit weights of these two relative density tests showed about 15% in difference, because two tests were conducted on materials sampled from different soil buckets and fines content of materials were varied among soil buckets. The minimum dry unit weights that determined in all relative density testes were within about 14% in difference. However, the difference between the highest and the lowest maximum dry unit weighs was about 20%. All dry unit weight

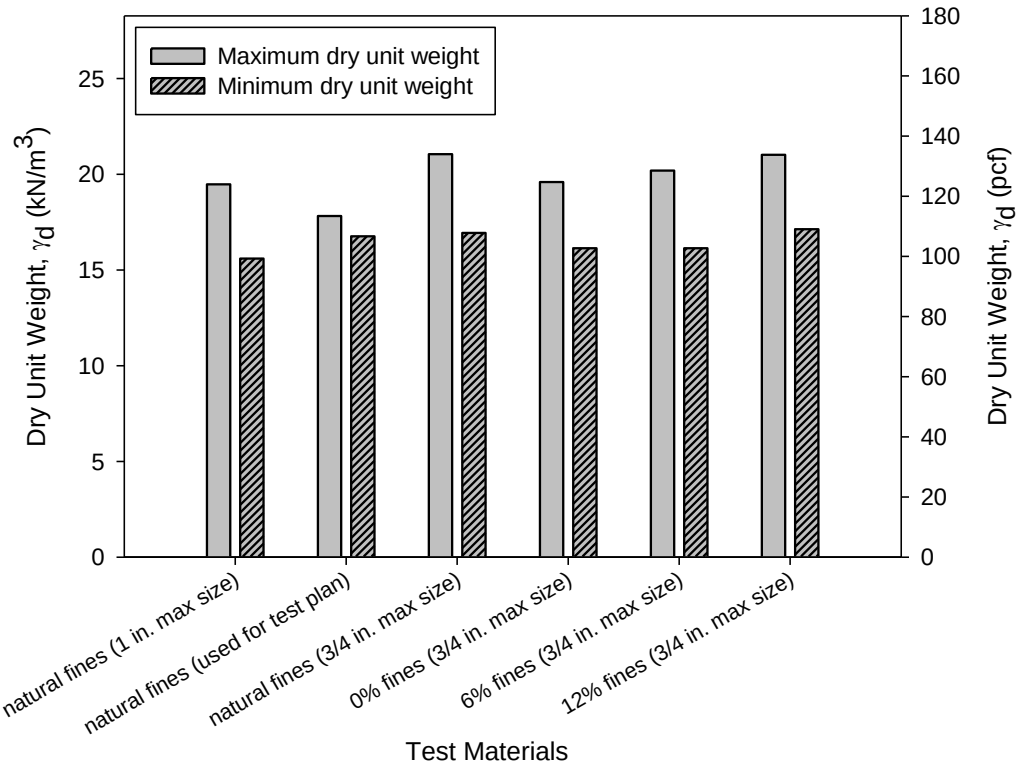

Figure 35. Crushed limestone with varied fines content dry unit weight

CHAPTER 5. RESULTS AND DISCUSSION

This chapter presents and discusses the test results from accumulated permanent strain (ε_p) and resilient modulus (M_r) studies. The ε_p was studied by performing permanent deformation tests on five materials to determine the significance of factors affecting ε_p, to generate a model for predicting accumulated permanent axial strain (ε_p), and to quantify particles breakage of unbound granular materials (UGMs) due to sample compaction and cyclic loading. The M_r study was performed on three materials to observe measurement errors in the M_r tests, to find significance of factors affecting M_r, to predict M_r using the universal model, and to determine the unconsolidated undrained (UU) strength. The number and types of tests that were performed on each material are summarized in Table 17 and detailed information about the variables for each tests are summarized in related tests sections.

Table 17. Summary of tests performed

No. of Tests Performed / Materials	Permanent Deformation Tests			Resilient modulus tests
	ISU 100k	ISU 100k	NCHRP 598	
Untrimmed slag	6	0	0	0
Recycled portland cement concrete	8	8	0	0
Crushed Limestone	0	0	12	12
Recycled portland cement concrete with recycled asphalt pavements	0	0	12	12
Recycled asphalt pavements	0	0	12	12

Permanent Deformation

Results related to E_p tests are presented in four sections, significance of samples characteristics, permanent deformation prediction model, and breakage index. Three test methods, ISU 100k, ISU 1k, and NCHRP 598 tests, were used to study E_p behavior of UGMs. The ISU 100k tests were conducted by loading the samples up to 100,000 cycles to observe the effect of cycle numbers on accumulated ε_p. Moreover, the effects of relative densities (RD), deviator stress (σ_d), and fines content (F_{200}) were studied by conducting the ISU 100k tests on the untrimmed slag material.

The ISU 1k tests were conducted by loading the samples up to 1,000 cycles to observe the difference from the ISU 100k tests. In addition, the effects of relative densities (RD) and deviator stress (σ_d) were studied by conducting the ISU 100k and ISU 1k tests on the recycled portland cement concrete (RPCC) materials that were collected from US-30, IA. The NCHRP 598 tests were conducted by loading samples with incrementally increasing σ_d up to 180 psi to measure the effect of σ_d. The results of the NCHRP 598 tests were analyzed by assuming that stress history did not have significant effects on measuring permanent strain of one sample that were subjected to different stress levels. Moreover, the effects of RD, fines content (F_{200}), and materials type were studied by conducting NCHRP 598 tests on crushed limestone, recycled asphalt pavement (RAP), and recycled portland cement concrete with recycled asphalt pavement (RPCC/RAP) that were collected from two quarries in Iowa.

Each test was conducted on a unique sample that was prepared to meet the target values of designed sample characteristics and the actual values of the samples characteristics were determined. Moreover, the test number was assigned for each test to avoid repeated descriptions of samples characteristics.

The ISU 100k tests that were conducted on untrimmed slag samples were numbered from D-A1 to D-A6 and the target and the actual values of samples characteristics were summarized (Table 18). Actual F_{200} are about 1.0% higher than the target values. Actual moisture contents (w) are about 0.1% to 0.3% higher than the target w. The actual relative densities are about 15% higher than the target values.

Table 18. The target and actual characteristics of ISU 100k tests untrimmed slag samples

Test no.	F_{200} (%)		w (%)		RD (%)		γ_d (kN/m^3)	
	Target	Actual	Target	Actual	Target	Actual	Target	Actual
D-A1	2.0	3.3	3.3	3.6	90.0	104.3	15.99	16.35
D-A2		3.3		3.3	100.0	118.8	16.24	16.73
D-A3	4.0	4.5		3.6	90.0	105.1	15.99	16.37
D-A4		4.5		3.5		106.3		16.40
D-A5	6.0	7.0		3.4		109.3		16.48
D-A6	8.0	9.0		3.4		106.3		16.40

The ISU 100k tests were also conducted on RPCC materials. The actual moisture contents generally are less than 0.4% different from the target w, except the sample D-A8,

which has moisture content about 1.9% less than the target value. The actual relative densities are about 15% higher than the target values. The ISU 100k tests that were conducted on RPCC samples were numbered from D-A8 to D-A15 and the target and the actual values of samples characteristics were summarized (Table 19).

Table 19. The target and actual characteristics of ISU 100k tests RPCC samples

Test no.	F_{200} (%)		w (%)		RD (%)		γ_d (kN/m^3)	
	Target	Actual	Target	Actual	Target	Actual	Target	Actual
D-A8	natural	6.2	10.0	8.1	95.0	104.1	17.14	17.61
D-A9				9.6	90.0	100.4	16.90	17.42
D-A10				9.9		99.4		17.37
D-A11				9.8		99.4		17.37
D-A12				9.6		99.8		17.39
D-A13				10.1		99.2		17.36
D-A14				10.1	80.0	88.7	16.44	16.85
D-A15				9.8	85.0	95.0	16.67	17.15

The RPCC materials were also studied by using the ISU 1k method. The actual moisture contents are within ±4% from the target w. The actual RD are about 10% higher than the target RD. The ISU 1k tests that were conducted on RPCC samples were numbered from D-B1 to D-B8 and the target and the actual values of samples characteristics were summarized (Table 20).

Table 20. The target and actual characteristics of ISU 1k tests RPCC samples

Test no.	F_{200} (%)		w (%)		RD (%)		γ_d (kN/m^3)	
	Target	Actual	Target	Actual	Target	Actual	Target	Actual
D-B1	natural	5.6	10.0	9.65	95.0	103.7	17.14	17.59
D-B2				10.15	90.0	99.4	16.90	17.37
D-B3				9.59		100.4		17.42
D-B4				9.88		101.0		17.45
D-B5				9.84		100.0		17.40
D-B6				10.51		98.0		17.30
D-B7				10.11	80.0	89.2	16.44	16.87
D-B8				10.05	85.0	94.4	16.67	17.12

The NCHRP 598 method was used to study the ε_p behavior of crushed limestone, RAP, and RPCC/RAP materials. Each material was studied with four target fines contents and three relative densities.

The actual w of crushed limestone samples are within ±0.2, of RAP samples are within ±0.3%, and of RPCC/RAP samples are within ±0.4% from the target moisture contents values, except three RPCC/RAP samples that two have 3.5% and one has 0.8% fines contents.

The actual RD of crushed limestone samples are less than 9% RD, of RAP samples are less than 5% RD, and of RPCC/RAP samples are less than 7% RD different from the target RD values. Generally, the dry unit weights of materials with natural fines content are smaller than the materials with target fines contents. The materials with natural fines contents usually have small fine particles adhered on the large particles surfaces. The wet and dry process hardened the fine particles layer and made the particles bigger so less free fine particles in the material could fill the voids.

Actual F_{200} for three materials that contain natural fines content are varied. The natural F_{200} of crushed limestone was measured as 7.9% which is the highest compared to other two recycles materials. Natural F_{200} were determined as the original F_{200} of the materials that were transported from the quarries to the lab. The natural F_{200} might be different if the materials were collected from different locations or different productions. The 0% target F_{200} was not reached for all materials because the large particles attracted fines on the rough surfaces and particles could break down when the mechanical sieve analysis was conducted to determine the F_{200} of the material. The actual F_{200} for the materials with 6% target F_{200} are <0.4% lower than 6% and the actual F_{200} for the materials with 12% target F_{200} are <0.6% higher than 12%.

The crushed limestone samples were numbered from D-C1 to D-C12, the RAP samples were numbered from D-C13 to D-C24, the RPCC/RAP samples were numbered from D-C25 to D-C36 and the target and the actual values of all samples characteristics were also summarized (Table 21).

Table 21. The target and actual characteristics of NCHRP 598 tests samples

Test No.	F_{200} (%)		w (%)		RD (%)		γ_d (kN/m^3)	
	Target	Actual	Target	Actual	Target	Actual	Target	Actual
D-C1	0.0	2.2	2.3	2.2	85.0	87.0	18.99	19.08
D-C2	6.0	5.8		2.4		86.0	19.47	19.52
D-C3	natural	7.9		2.4		90.7	17.65	17.72
D-C4	12.0	12.6		2.6		85.3	20.33	20.34
D-C5	0.0	2.2		2.3	90.0	91.7	19.19	19.26
D-C6	6.0	5.8		2.5		90.4	19.70	19.73
D-C7	natural	7.9		2.5		94.6	17.71	17.76
D-C8	12.0	12.6		2.5		90.4	20.55	20.57
D-C9	0.0	2.2		2.4	95.0	96.4	19.40	19.46
D-C10	6.0	5.8		2.3		96.2	19.95	20.01
D-C11	natural	7.9		2.3		103.7	17.76	17.86
D-C12	12.0	12.6		2.5		95.7	20.78	20.82
D-C13	0.0	1.6	2.9	2.8	85.0	87.7	15.75	15.83
D-C14	natural	2.0		2.7		88.9	14.92	15.02
D-C15	6.0	5.6		3.1		85.6	16.97	16.99
D-C16	12.0	12.5		3.0		85.9	17.62	17.66
D-C17	0.0	1.6		2.6	90.0	94.2	15.89	16.01
D-C18	natural	2.0		2.6		94.0	15.05	15.15
D-C19	6.0	5.6		3.1		90.7	17.14	17.17
D-C20	12.0	12.5		2.8		91.7	17.81	17.87
D-C21	0.0	1.6		2.7	95.0	98.2	16.03	16.12
D-C22	natural	2.0		2.7		98.0	15.17	15.25
D-C23	6.0	5.6		2.9		96.4	17.32	17.37
D-C24	12.0	12.5		2.8		96.5	18.00	18.06
D-C25	0.0	0.8	6.0	5.7	85.0	88.5	15.26	15.36
D-C26	natural	3.5		7.5		77.0	16.12	15.97
D-C27	6.0	6.0		6.0		86.1	16.76	16.81
D-C28	12.0	12.4		6.0		86.3	17.54	17.60
D-C29	0.0	0.8		5.8	90.0	93.3	15.41	15.51
D-C30	natural	3.5		7.5		81.2	16.22	16.05
D-C31	6.0	6.0		6.0		91.3	16.96	17.01
D-C32	12.0	12.4		6.2		90.7	17.74	17.77
D-C33	0.0	0.8		5.5	95.0	99.0	15.56	15.69
D-C34	natural	3.5		6.4		95.4	16.44	16.33
D-C35	6.0	6.0		6.2		95.6	17.17	17.19
D-C36	12.0	12.4		6.0		96.4	17.95	18.01

Two deviator stresses (41.4 kPa, 62.1 kPa), four target fines contents (2.0%, 4.0%, 6.0%, 8.0%), and two target relative densities (90.0%, 100.0%) were studied for the untrimmed slag materials by performing the ISU 100k tests. The accumulated permanent strain at the test end doubled as the σ_d increased from 41.4 kPa to 62.1 kPa. In addition, the accumulated permanent strain at the test end is the highest for the sample with 7.0% F_{200} at about 0.71% and within the 0.35 ± 0.03% range for other three samples. Moreover, the accumulated ε_p at the test end doubled when the target RD decreased from 118.8% to 104.3%. The ε_p at the test end, confining pressure (σ_c), and σ_d for all ISU 100k tests that conducted on untrimmed slag materials are summarized (Table 22).

Table 22. ε_p values (%) at the end of the tests for untrimmed slag samples (ISU 100k)

Test no.	ε_p at the test end	σ_c		σ_d	
	%	kPa	psi	kPa	psi
D-A1	0.38	20.7	3.0	41.4	6.0
D-A2	0.16				
D-A3	0.32				
D-A4	0.66			62.1	9.0
D-A5	0.71			41.4	6.0
D-A6	0.34				

Five deviator stresses (20.7 kPa, 41.4 kPa, 62.1 kPa, 82.7 kPa, and 103.4 kPa), and four target relative densities (80.0%, 85.0%, 90.0%, and 95.0%) were studied for the RPCC materials by performing the ISU 100k tests and the ISU 1k tests separately. The accumulated ε_p at all ISU 100k test ends are within the range of 0.10 ± 0.04% and do not show a clear trend as the σ_d increased. The accumulated ε_p at all ISU 100k test ends are less than 0.11% and do not show a clear trend as the RD increases. The accumulated permanent strain in these ISU 100k tests were not continuously increasing as expected, but show decrease in some samples. However, the reason cause the decrease is not determined while the same machine and materials were used for IUS 1k tests and no decrease was observed. The ε_p at the test end, σ_c, and σ_d for all ISU 100k tests that conducted on RPCC materials are summarized (Table 23).

Table 23. ε_p values (%) at the end of the tests for RPCC samples (ISU 100k)

Test no.	ε_p at the test end	σ_c		σ_d	
	%	kPa	psi	kPa	psi
D-A8	0.02	103.4	15.0	20.7	3.0
D-A9	0.06			20.7	3.0
D-A10	0.07			41.4	6.0
D-A11	0.13			62.1	9.0
D-A12	0.11			82.7	12.0
D-A13	0.11			103.4	15.0
D-A14	0.003			20.7	3.0
D-A15	0.06			20.7	3.0

The accumulated ε_p at all ISU 1k test ends are within the range of 0.08 ± 0.05% and do not show a clear trend as the σ_d increased. The accumulated ε_p at all ISU 1k test ends are less than 0.10% and do not show a clear trend as the RD increased. The differences of the accumulated ε_p between the ISU 1k tests and the ISU 100k tests conducted on the samples with the same target characteristics are within ±0.07%. The small differences could be the results of small permanent deformation occurred in the RPCC materials, the low stress level, the internal error of the test machine, and the inaccuracy in the ISU 100k tests that were conducted on the RPCC materials. Moreover, this is an indicator that the number of load cycles does not have significant effects on permanent deformation at deviator stress up to 103.4 kPa, though the 1,000 times load cycles were applied. The ε_p at the test end, σ_c, and σ_d for all ISU 1k tests that conducted on RPCC materials are summarized (Table 24).

Table 24. ε_p values (%) at the end of the tests for RPCC samples (ISU 1k)

Test no.	ε_p at the test end	σ_c		σ_d	
	%	kPa	psi	kPa	psi
D-B1	0.02	103.4	15.0	20.7	3.0
D-B2	0.01			20.7	3.0
D-B3	0.03			41.4	6.0
D-B4	0.05			62.1	9.0
D-B5	0.05			82.7	12.0
D-B6	0.09			103.4	15.0
D-B7	0.03			20.7	3.0
D-B8	0.03			20.7	3.0

The accumulated ε_p at the NCHRP 598 test sequence (S) end was calculated using the change of samples height at the end of the 1000 load cycles to the 0-point height measurement (sample height was measured at the end of preconditioning (PC) sequence) to be divided by the initial sample height (sample height was measured at the end of sample compaction).

Saeed (2008 a) suggested that the NCHRP 598 test may be ceased and the samples were considered failed when 10% ε_p reached. Consequently, the tests might be terminated at any number of load cycles in any load sequence. So the ε_p at the sequence end was only calculated for the load sequences were completely finished. The accumulated ε_p at the sequence end increased as the σ_d increased from 68.9 kPa up to 1241.1 kPa for all NCHRP 598 tests that were conducted on crushed limestone (Table 25), RAP (Table 26), and RPCC/RAP (Table 27).

Table 25. ε_p values (%) at the end of all load sequences for all crushed limestone samples (NCHRP 598)

Test No.	S1	S2	S3	S4	S5	S6	S7	S8	S9	S10
D-C1	0.020	0.062	0.156	0.417	1.337	3.339	6.870	—	—	—
D-C2	0.013	0.033	0.087	0.232	0.875	2.246	5.309	—	—	—
D-C3	0.068	0.322	1.464	3.338	5.658	8.648	—	—	—	—
D-C4	0.022	0.052	0.102	0.144	0.187	0.276	0.982	2.476	4.425	7.811
D-C5	0.005	0.032	0.096	0.187	0.573	1.669	3.951	8.483	—	—
D-C6	0.008	0.035	0.089	0.151	0.295	0.980	2.455	5.138	—	—
D-C7	0.050	0.239	1.158	3.067	5.488	8.250	—	—	—	—
D-C8	0.007	0.020	0.046	0.062	0.077	0.097	0.141	0.309	1.322	4.577
D-C9	0.018	0.057	0.141	0.300	0.870	2.116	4.705	9.347	—	—
D-C10	0.010	0.032	0.074	0.113	0.209	0.750	1.947	5.054	10.380	—
D-C11	0.093	0.420	1.788	3.783	6.154	8.849	—	—	—	—
D-C12	0.004	0.019	0.041	0.060	0.078	0.093	0.115	0.153	0.419	6.304

Notes: — means the test ended at this load sequence or previous load sequence.

Table 26. ε_p values (%) at the end of all load sequences for all RAP samples (NCHRP 598)

Test No.	S1	S2	S3	S4	S5	S6	S7	S8	S9	S10
D-C13	1.533	2.752	5.286	8.083	—	—	—	—	—	—
D-C14	1.850	3.281	6.058	—	—	—	—	—	—	—
D-C15	0.491	1.048	2.491	4.585	7.118	10.000	—	—	—	—
D-C16	0.232	0.533	1.340	2.693	4.576	6.872	9.679	—	—	—
D-C17	1.268	2.383	4.741	7.381	—	—	—	—	—	—
D-C18	1.750	3.049	5.647	—	—	—	—	—	—	—
D-C19	0.346	0.780	1.934	3.699	5.996	8.704	—	—	—	—
D-C20	0.217	0.473	1.223	2.548	4.479	6.948	10.095	—	—	—
D-C21	1.014	1.919	3.930	6.373	9.078	—	—	—	—	—
D-C22	1.374	2.675	5.326	8.292	—	—	—	—	—	—
D-C23	0.255	0.595	1.514	3.062	5.242	7.936	—	—	—	—
D-C24	0.185	0.425	1.119	2.389	4.217	6.514	9.307	—	—	—

Notes: — means the test ended at this load sequence or previous load sequence.

Table 27. ε_p values (%) at the end of all load sequences for all RPCC/RAP samples (NCHRP 598)

Test No.	S1	S2	S3	S4	S5	S6	S7	S8	S9	S10
D-C25	0.076	0.362	1.352	2.694	4.624	7.440	—	—	—	—
D-C26	0.011	0.051	0.196	0.599	2.102	6.459	—	—	—	—
D-C27	0.022	0.141	0.741	1.685	2.953	4.445	7.122	—	—	—
D-C28	0.006	0.039	0.130	0.404	0.971	1.704	2.816	5.258	—	—
D-C29	0.078	0.330	1.336	2.620	4.122	6.496	—	—	—	—
D-C30	0.016	0.062	0.194	0.500	1.635	4.388	8.894	—	—	—
D-C31	0.024	0.146	0.711	1.558	2.568	3.770	5.395	7.695	—	—
D-C32	0.015	0.050	0.162	0.404	0.895	1.622	2.572	4.262	—	—
D-C33	0.066	0.279	1.073	2.208	3.789	5.756	10.176	—	—	—
D-C34	0.017	0.071	0.255	0.639	1.802	3.740	7.217	—	—	—
D-C35	0.016	0.075	0.389	1.001	1.845	2.905	4.272	6.610	—	—
D-C36	0.007	0.031	0.106	0.240	0.551	1.078	1.772	3.002	—	—

Notes: — means the test ended at this load sequence or previous load sequence.

Significance of samples characteristics

Various factors that were expected to affect the permanent deformation behavior of UGMs were identified in the literature review. The number of load cycles, deviator stresses, relative densities, fines contents, and materials types are investigated in this research.

Number of load cycles

Permanent strain in UGMs is continuously increasing under repeated loading (Morgan 1966; Barksdale 1972; Kolisoja 1998; Kumar et al. 2006) and identified as an important factor affecting permanent deformation behavior of pavement subbase layers.

The ISU 100k test was designed to determine the effect of number of load cycles by loading the samples up to 100,000 cycles. The permanent strain of untrimmed slag samples nearly continuously increased with increasing number of load cycles and reached a constant value at the end of the test. However, some samples shows about 0.025% decrease in permanent strain at a large number of load cycles while the permanent strain at the end of all untrimmed slag sample are less than1.0%. The reasons might be the small amount of permanent strain developed during the ISU 100k tests and the temperature caused shrinkage and expansion of aggregates. Moreover, the ISU 100k tests were also conducted on RPCC materials and the permanent strains at the end of test are less than 0.15%. The ε_p is not continuously increasing with the number of load cycles. The reasons might be the small amount of strain was developed in the test, hydration of the cementitious materials on the particles surfaces, expansion and shrinkage of particles under varied temperature as the ISU 100k required about 28 hours to be finished, and the workability of the test machine as it might need to be calibrated at that period.

The finding that constant values are reached for several ISU 100k tests depart from the conclusion proposed by Morgan (1966) and Kolisoja (1998) that permanent strain continues increasing at the end of the tests after large number of load cycles applied. The reason is that they only applied high stress levels to have the conclusion.

The ISU 1k tests were also conducted on the RPCC materials with the same target characteristics as the ISU 100 test RPCC samples by applying up to 1,000 cycles. The ε_p is continuously increasing with the number of load cycles to a constant value. However, the permanent strains at the end of all ISU 1k tests on the RPCC materials are also less than 0.15% that is similar to the values that were produced by the ISU 100k tests.

ISU 1k tests results shows a large increase of permanent strain at first several load cycles (Figure 36), and the increase of permanent strain with increasing number of load cycles from 50 to 1000 is relatively small (Figure 37) compared to the permanent strain that was

produced in first 50 load cycles. These large increases of permanent strain at first 50 load cycles could be the results of initial sample setting.

Therefore, as Saeed (2008a) specified in NCHRP report 598, the preconditioning sequence of 50 load cycles was applied for every NCHRP 598 tests to subtracting the effect of initial sample setting. As the results of ISU 100k tests indicate that the permanent strain will be negative if subtract the permanent strain accumulated during first 50 load cycles. The ISU 1k and NCHRP 598 tests results are analyzed with less effects of initial sample setting.

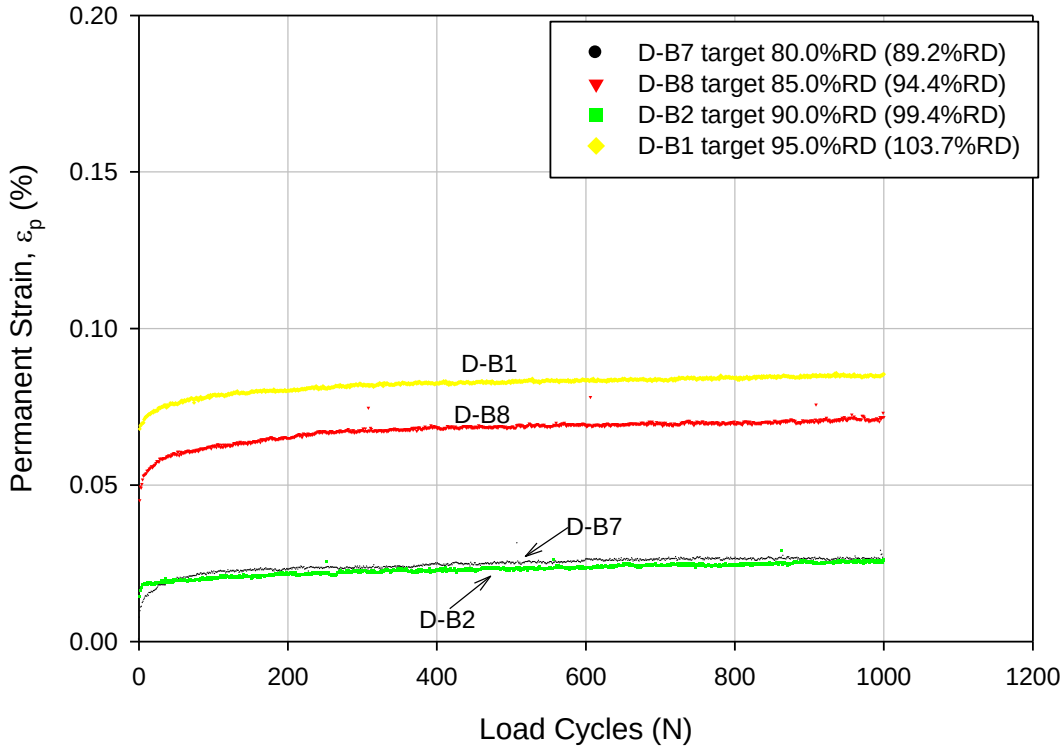

Figure 36. ISU 1k tests results without subtraction of first 50 load cycles

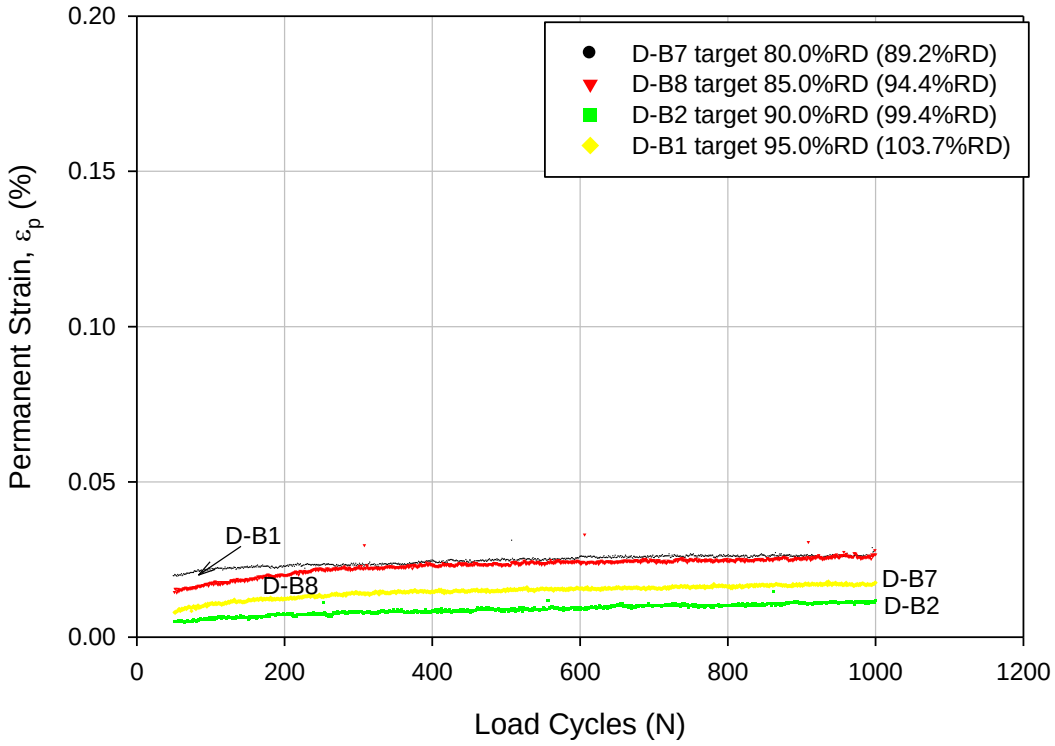

Figure 37. ISU 1k tests results with subtraction of first 50 load cycles

The NCHRP 598 tests show the ε_p of crushed limestone is continuously increasing with the applied number of load cycles in each load sequence. The ε_p reaches a constant value at the end of first several load sequences where the strain rate decreases to about 0. The strain rate is used to present the trend of ε_p developed with the number of load cycles. The strain rate might not decrease with the number of load cycles at later load sequences in the test. For example, the ε_p of the D-C12 remains below 0.5% for the first nine sequences and continuously increases with the applied number of load cycles until the test terminated at the last sequence.

The NCHRP 598 tests show the ε_p of RAP is continuously increasing with the applied number of load cycles in each load sequence with different strain rates. Because the strain rate at the end of each load sequence is lower than the value at the beginning of the test, except the last sequence before the sample failed, a constant value of ε_p could be obtained after certain number of load cycles were applied. The same observations of RAP could be concluded on the ε_p development of RPCC/RAP with the number of load cycles. Except that the RPCC/RAP materials shows instant fail and lead to tests termination.

The finding that the constant permanent strains were not obtained at the end of 1,000 load cycles depart from the conclusion reported by Brown and Hyde (1975) that the permanent strain reaches an equilibrium state after approximately 1,000 load cycles. The reason could be that the different materials were used in the research, because they studied crushed granite materials.

In conclusion, the constant ε_p could be obtained at the end of large number of load cycles (up to 100,000) when the low deviator stress is applied and the continuous increasing ε_p could be obtained at the end of small number of load cycles (1,000). Barksdale (1972) indicated a sudden increase in strain rate after a large number of load cycles was applied. In this study, the ε_p of crushed limestone shows a sudden increase in strain rate in the last several sequences in each NCHRP 598 test. However, the number of load cycles is 1,000 and is not large. This indicates that the sudden increase in strain rate could be the results of several factors.

The number of load cycles is a significant factor on ε_p based on statistical analyses. The parameters of statistical analysis are summarized for ISU 100k tests on untrimmed slag (Table 28) and RPCC materials (Table 29), ISU 1k tests on RPCC materials (Table 30), and NCHRP 598 tests (Table 31) on crushed limestone, RAP, and RPCC/RAP.

Table 28. Significance of load cycles on ε_p for ISU 100k untrimmed slag samples

Test No.	Sum of Squares	F Ratio	Probability >F	R^2	Significant?
D-A1	19.6258	196431.7	<0.0001	0.6627	Yes
D-A2	49.8620	65641.7	<0.0001	0.3963	Yes
D-A3	46.0794	267208.5	<0.0001	0.7277	Yes
D-A4	226.2940	112434.2	<0.0001	0.5293	Yes
D-A5	198.0317	224042.6	<0.0001	0.6914	Yes
D-A6	100.0025	263886.3	<0.0001	0.7252	Yes

Table 29. Significance of load cycles on ε_p for ISU 100k RPCC samples

Test No.	Sum of Squares	F Ratio	Probability >F	R^2	Significant?
D-A8	1.8542	38097.9	<0.0001	0.2759	Yes
D-A9	1.4748	28862.7	<0.0001	0.2240	Yes
D-A10	0.2983	5521.5	<0.0001	0.0524	Yes
D-A11	1.8699	14857.1	<0.0001	0.1294	Yes
D-A12	5.3579	69598.8	<0.0001	0.4104	Yes
D-A13	0.1972	10060.3	<0.0001	0.0914	Yes
D-A14	1.7034	23590.3	<0.0001	0.1909	Yes
D-A15	0.9985	41710.2	<0.0001	0.2943	Yes

Table 30. Significance of load cycles on ε_p for ISU 1k RPCC samples

Test No.	Sum of Squares	F Ratio	Probability >F	R^2	Significant?
D-B1	0.0059	2856.6	<0.0001	0.7411	Yes
D-B2	0.0033	9528.2	<0.0001	0.9052	Yes
D-B3	0.0114	2044.2	<0.0001	0.6720	Yes
D-B4	0.0203	2183.9	<0.0001	0.6864	Yes
D-B5	0.0105	798.5	<0.0001	0.4445	Yes
D-B6	0.0657	2660.6	<0.0001	0.7272	Yes
D-B7	0.0044	1823.4	<0.0001	0.6463	Yes
D-B8	0.0096	2371.0	<0.0001	0.7038	Yes

Table 31. Significance of load cycles on ε_p for NCHRP 598 test samples

Test No.	Sum of Squares	F Ratio	Probability >F	R^2	Significant?
D-C1	33976.8	17122.8	<0.0001	0.6972	Yes
D-C2	23117.1	11839.9	<0.0001	0.6120	Yes
D-C3	48552.3	64875.1	<0.0001	0.913	Yes
D-C4	26021.4	17588.9	<0.0001	0.6376	Yes
D-C5	33892.6	15028.3	<0.0001	0.6464	Yes
D-C6	22690.7	12432.6	<0.0001	0.5923	Yes
D-C7	47574.3	57847.6	<0.0001	0.9023	Yes
D-C8	3592.2	6769.2	<0.0001	0.4037	Yes
D-C9	45786.2	17788.6	<0.0001	0.6832	Yes
D-C10	37896.0	13239.8	<0.0001	0.5921	Yes
D-C11	51829.1	86324.8	<0.0001	0.9334	Yes
D-C12	2854.0	3273.6	<0.0001	0.2467	Yes
D-C13	29521.1	145400.8	<0.0001	0.9711	Yes
D-C14	20930.2	115736.7	<0.0001	0.9687	Yes
D-C15	60047.5	102735.7	<0.0001	0.9436	Yes
D-C16	61525.5	78312.2	<0.0001	0.9166	Yes
D-C17	37085.4	155972.7	<0.0001	0.9705	Yes
D-C18	22394.1	125791.9	<0.0001	0.9696	Yes
D-C19	61125.9	85350.5	<0.0001	0.9291	Yes
D-C20	61104.2	63074.6	<0.0001	0.8995	Yes
D-C21	40755.8	141659.6	<0.0001	0.9649	Yes
D-C22	30208.4	134747.7	<0.0001	0.9694	Yes
D-C23	64052.5	66703.8	<0.0001	0.9077	Yes
D-C24	59918.4	67877.3	<0.0001	0.9041	Yes
D-C25	43257.6	56185.4	<0.0001	0.8987	Yes
D-C26	19824.8	11389.4	<0.0001	0.6478	Yes
D-C27	36817.9	54469.9	<0.0001	0.8836	Yes
D-C28	16597.4	28129.9	<0.0001	0.7767	Yes
D-C29	49625.4	57763.2	<0.0001	0.8956	Yes
D-C30	33428.7	17061.0	<0.0001	0.7074	Yes
D-C31	46339.5	87472.9	<0.0001	0.9147	Yes
D-C32	13189.8	33209.6	<0.0001	0.8026	Yes
D-C33	55009.5	47813.1	<0.0001	0.9683	Yes
D-C34	30221.0	21806.1	<0.0001	0.7517	Yes
D-C35	32633.0	48058.3	<0.0001	0.8550	Yes
D-C36	7768.6	14397.0	<0.0001	0.6359	Yes

Deviator stress

Stress levels (confining pressure and deviator stress) or stress ratio was identified to have effects on the permanent deformation behavior of UGMs. In this study, the constant confining pressures were used for each test method so the increase in deviator stress indicates increase in stress ratio (deviator stress to confining pressure ratio).

Two deviator stresses of 41.4 kPa and 62.1 kPa were studied in the ISU 100k tests on untrimmed slag materials. The ε_p of the sample under 62.1 kPa is as twice as the ε_p of the sample under 41.4 kPa (Figure 38). Five deviator stresses were studied in the ISU 100k tests on RPCC materials. The ε_p of the sample under high σ_d is higher than the ε_p of the sample under low σ_d (Figure 39), but the clear trend of ε_p under increasing σ_d is not shown in this test set. Same conclusion could be drawn for RPCC materials under ISU 1k tests (Figure 40).

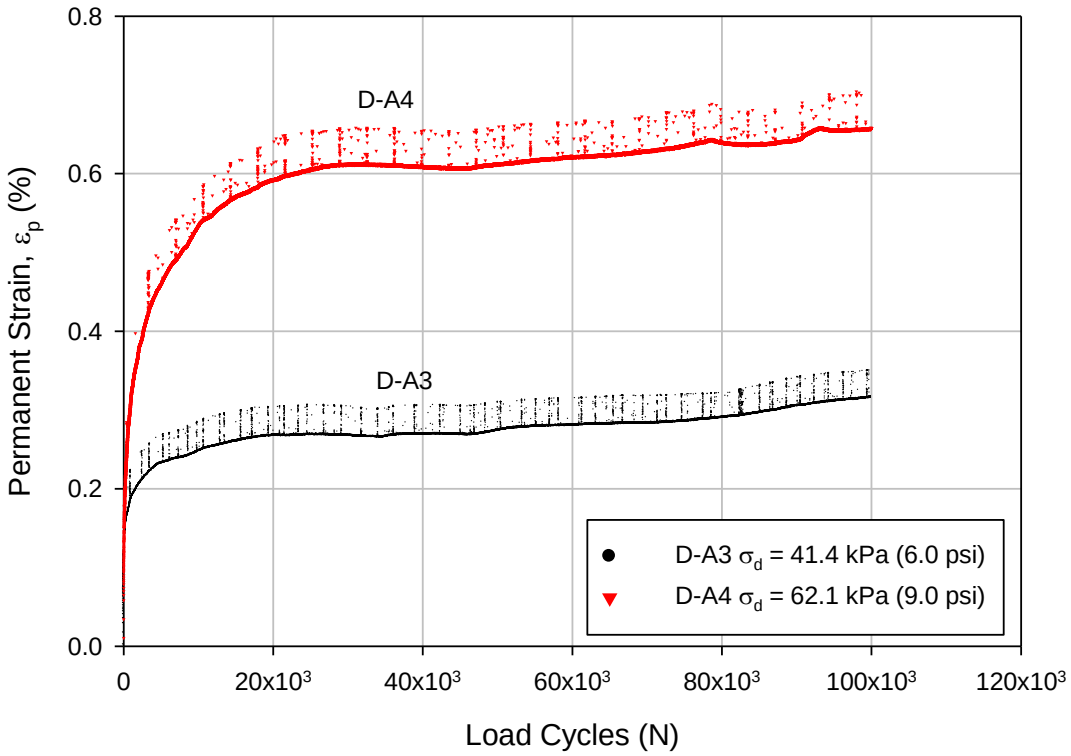

Figure 38. ε_p at 4.5% F_{200} for untrimmed slag samples (ISU 100k)

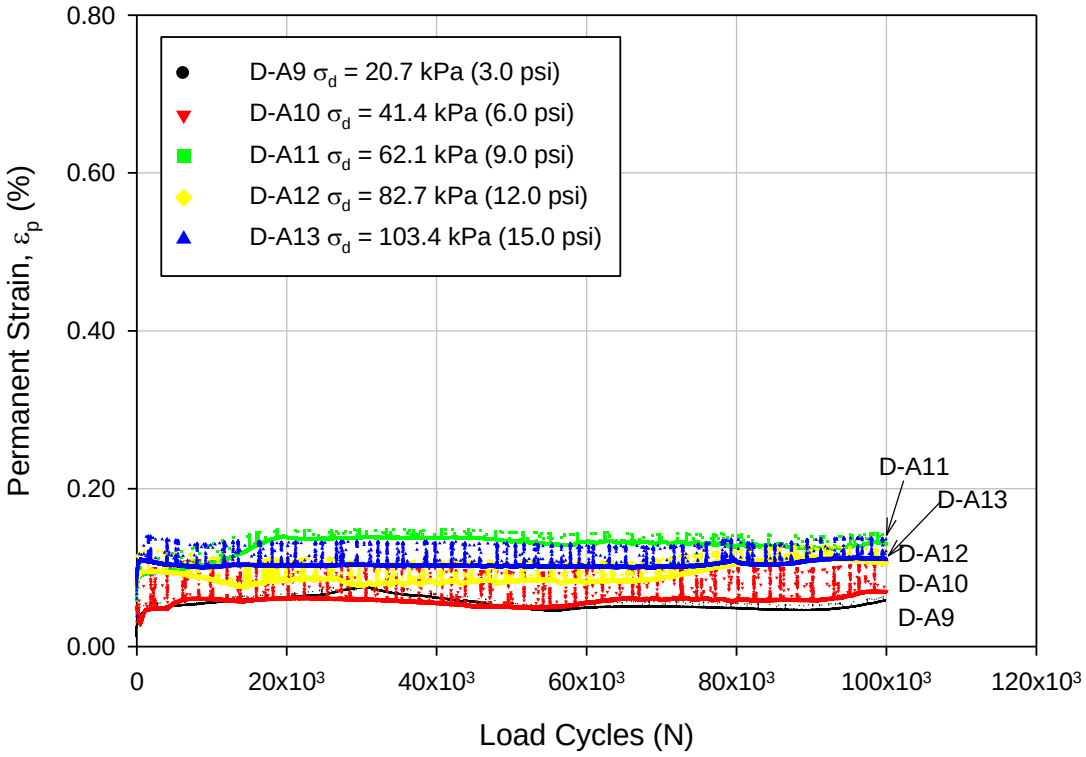

Figure 39. ε_p at 90% target RD for RPCC samples (ISU 100k)

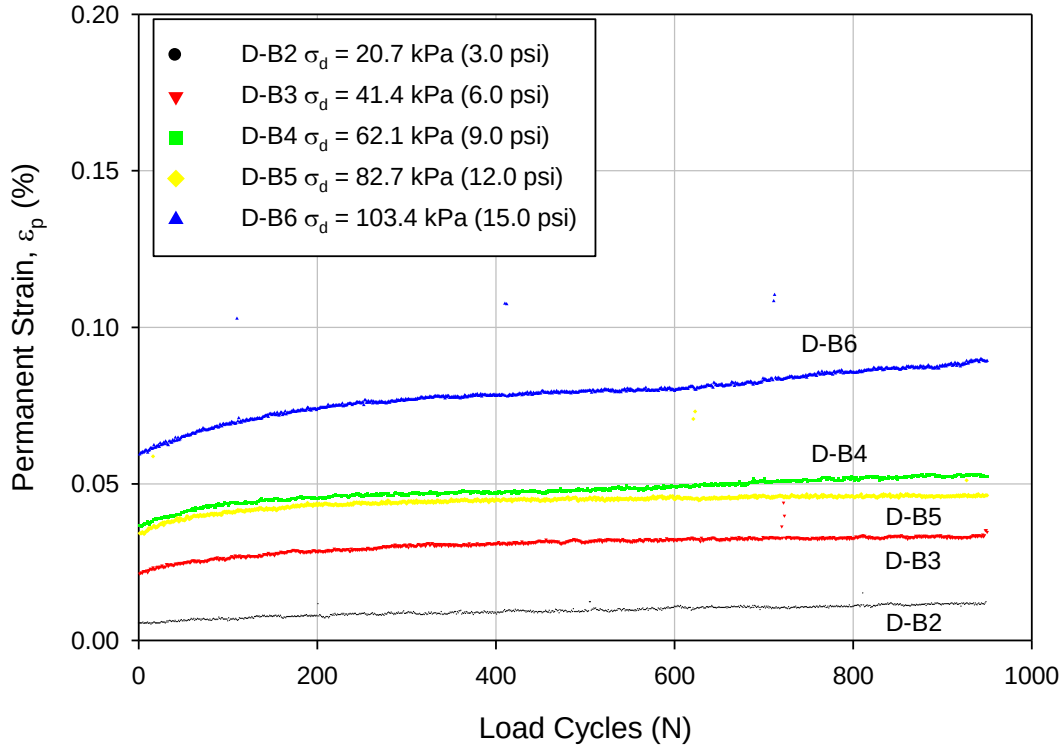

Figure 40. ε_p at 90% target RD for RPCC samples (ISU 1k)

The permanent strain at the end of each load sequence in all NCHRP 598 tests in this study increases with increasing deviator stress. The statistical analyses were conducted on first six deviator stresses for crushed limestone, first three deviator stresses for RAP, and first six deviator stresses for RPCC/RAP with the permanent strains at the end of load sequences where the selected σ_d was applied. In the statistical analyses, only the completely finished sequences in the NCHRP 598 tests for each material were studied. The deviator stress is concluded as significant factor affecting the permanent deformation behavior of the studied materials. The statistical analysis parameters are summarized (Figure 53).

Table 32. Statistical analysis summary for significance of deviator stress affecting ε_p

Materials	Degree of Freedom	Sum of Squares	F Ratio	Probability >F	R^2	Significant?
Crushed Limestone	5	85.5934	4.9923	0.0006	0.2744	Yes
RAP	2	39.5048	6.0275	0.0059	0.2676	Yes
RPCC/RAP	5	151.6650	24.1431	<0.0001	0.6465	Yes

The deviator stress is concluded to have direct effect on increasing permanent strain or stress ratio (σ_d/σ_c) as the confining pressure (σ_c) is constant. This conclusion is confirmed to Morgan (1966), Lashine et al. (1971), Barksdale and Hyde (1975), and Boyce (1975). Moreover, the permanent strain is found to reach a constant value at low deviator stresses and continue increasing with high strain rate at the end of the load sequence while high deviator stresses were applied. This finding confirmed the conclusion of Lashine et al. (1971) that permanent axial strain increases and reaches a constant value directly related to stress ratio. This also confirmed the conclusion reported by Boyce (1975) that the permanent strain reaches a constant value when a low stress level was applied and a large permanent strain develops and continues increasing at the end of the test.

Relative density

The resistance of UGMs to permanent deformation under repeated wheel loading is generally improved by increasing density (Lekarp et al. 2000b). In the field site the 95% relative density is a general target value for subbase compaction but the actual values might be varied throughout the field site. Consequently, the density which is specified as relative density in this study is important for studying the permanent deformation behavior of UGMs.

Although the target RD is varied in different levels, the target dry unit weight is varied at each RD level for different materials and same materials with different fines contents. The actual RD is also determined for each test and shown in the parenthesis in the legend of each figure which is shown in the following parts.

Two relative densities of 104.3% and 118.8% were studied by conducting the ISU 100k tests on untrimmed slag materials. The 104.3% RD sample has about one time higher ε_p at the end of the test than the 118.8% RD sample (Figure 41). Four measured relative densities of 88.7%, 95.0%, 100.4%, and 104.1% were studied by conducting the ISU 100k tests on RPCC materials. The ε_p at the end of these tests does not show a clear relationship with RD (Figure 42). The reason could be the errors in the ISU 100k tests on RPCC that indicted by the ε_p changes in a wave form with increasing number of load applications. The same findings were concluded for the ISU 1k tests on RPCC materials (Figure 43).

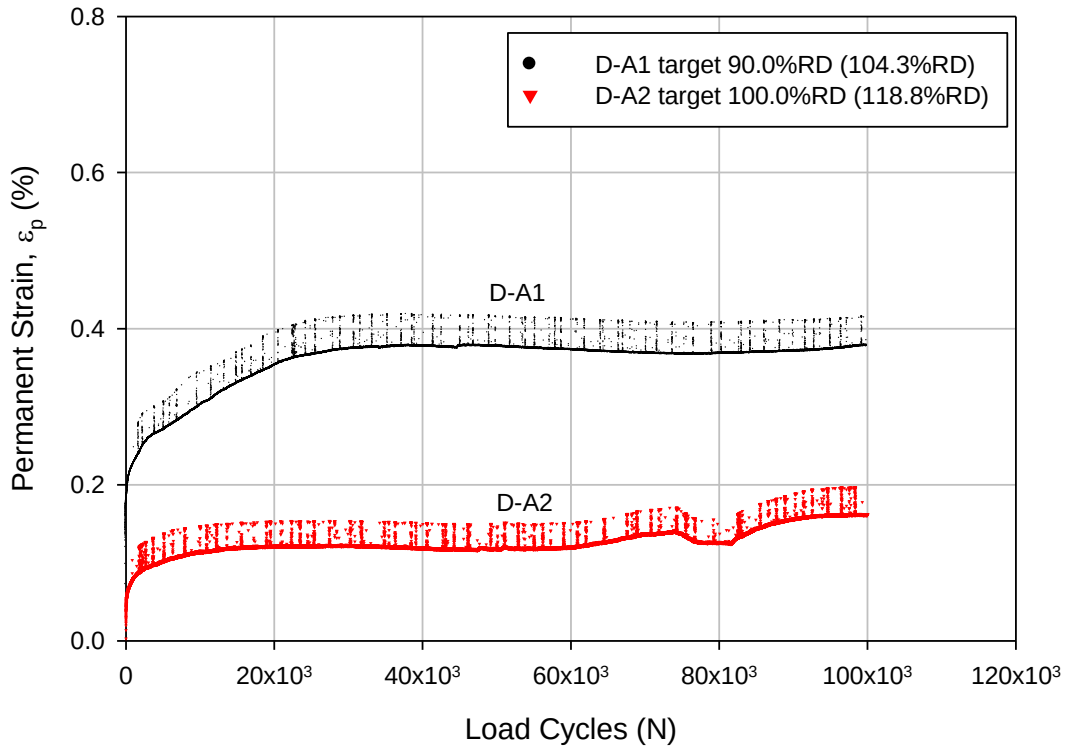

Figure 41. ε_p at 3.3% F_{200} for untrimmed slag samples (ISU 100k)

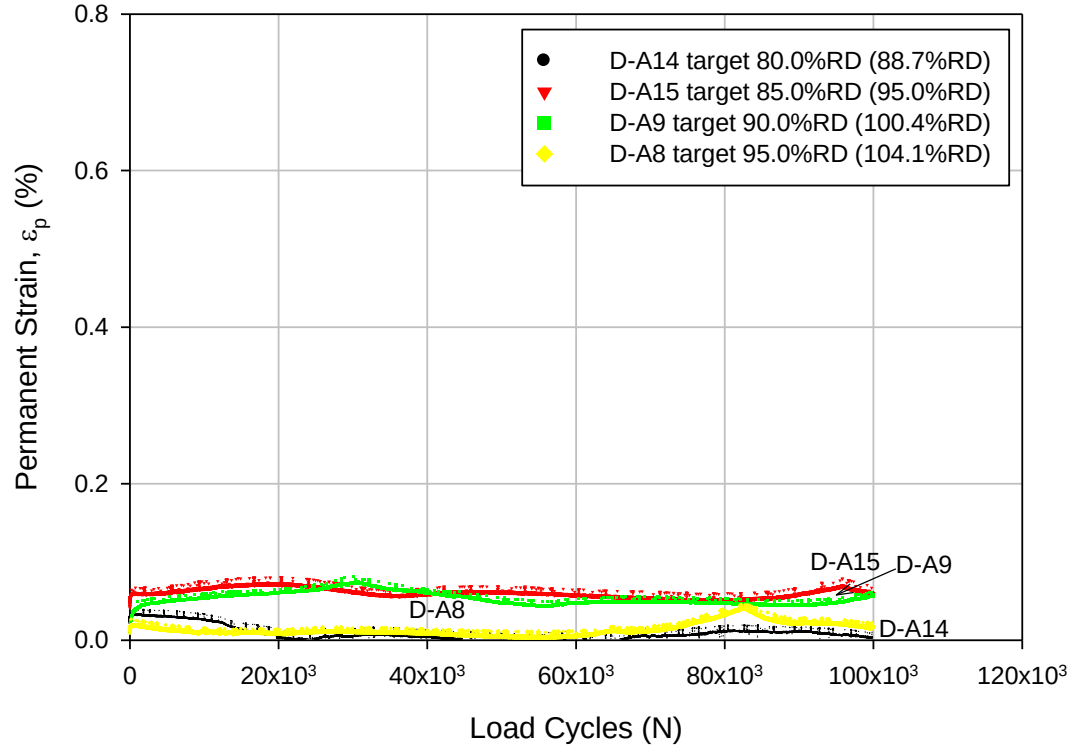

Figure 42. ε_p at 20.7 kPa (3.0 psi) σ_d for RPCC samples (ISU 100k)

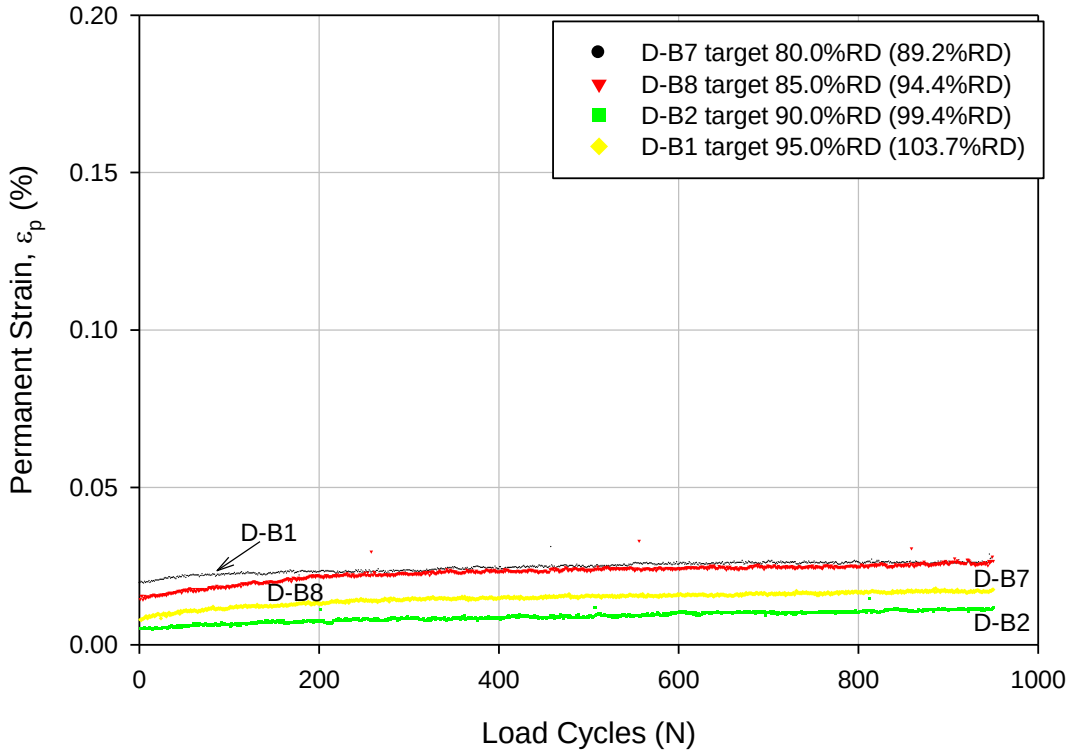

Figure 43. ε_p at 20.7 kPa (3.0 psi) σ_d for RPCC samples (ISU 1k)

Three target relative densities of 85.0%, 90.0%, and 95.0% were studied by conducting the NCHRP 598 tests. The measured relative density values are varied for each target level. When natural F_{200} of 7.9% was specified for crushed limestone samples, the 94.6% RD (target 90% RD) sample has the lowest ε_p at the end of each load sequence and the 103.7% RD (target 95% RD) sample has the highest ε_p for all load sequences (Figure 44). When 2.2% F_{200} was specified, the 91.7% RD sample has the lowest ε_p at the end of each load sequence and the 87.0% RD sample has the highest ε_p for all load sequences (Figure 45). When 5.8% F_{200} was specified, the 96.2% RD sample has the lowest ε_p at the end of each load sequence and the 86.0% RD sample has the highest ε_p for all load sequences (Figure 46). When 12.6% F_{200} was specified, the 95.7% RD sample has the lowest ε_p at the end of each load sequence except the last sequence and the 85.3% RD sample has the highest ε_p for all load sequences (Figure 47). In the last load sequence, the ε_p of the sample with 90.4% target RD increases at a higher rate than the samples with 95.7% and 85.3% target relative densities. The accumulated ε_p of the sample with 90.4% target RD exceed the accumulated ε_p of the sample with 95.7% target RD before the sequence ended (Figure 47).

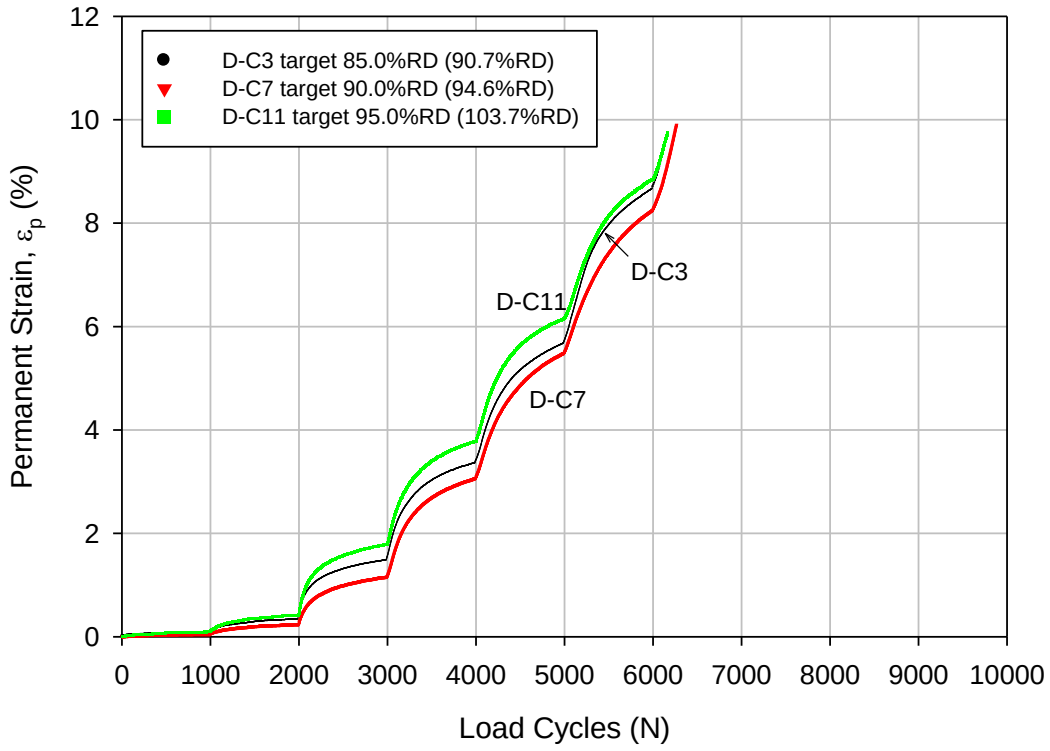

Figure 44. ε_p at natural 7.9% F_{200} for crushed limestone samples (NCHRP 598)

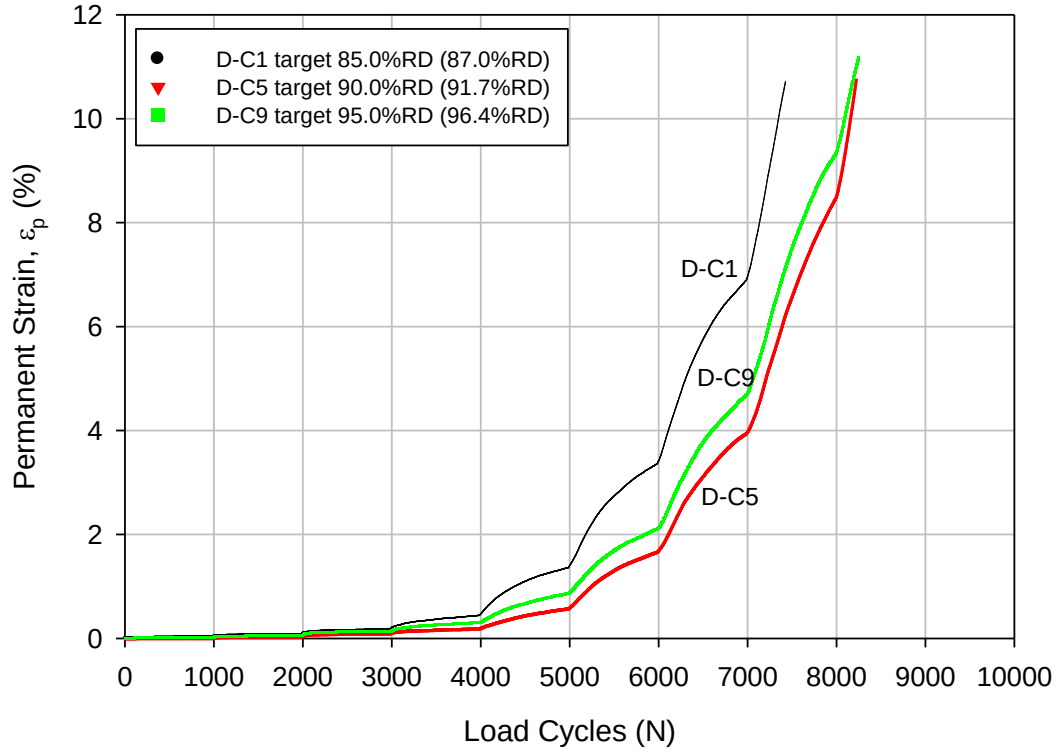

Figure 45. ε_p at reconstituted 2.2% F_{200} for crushed limestone samples (NCHRP 598)

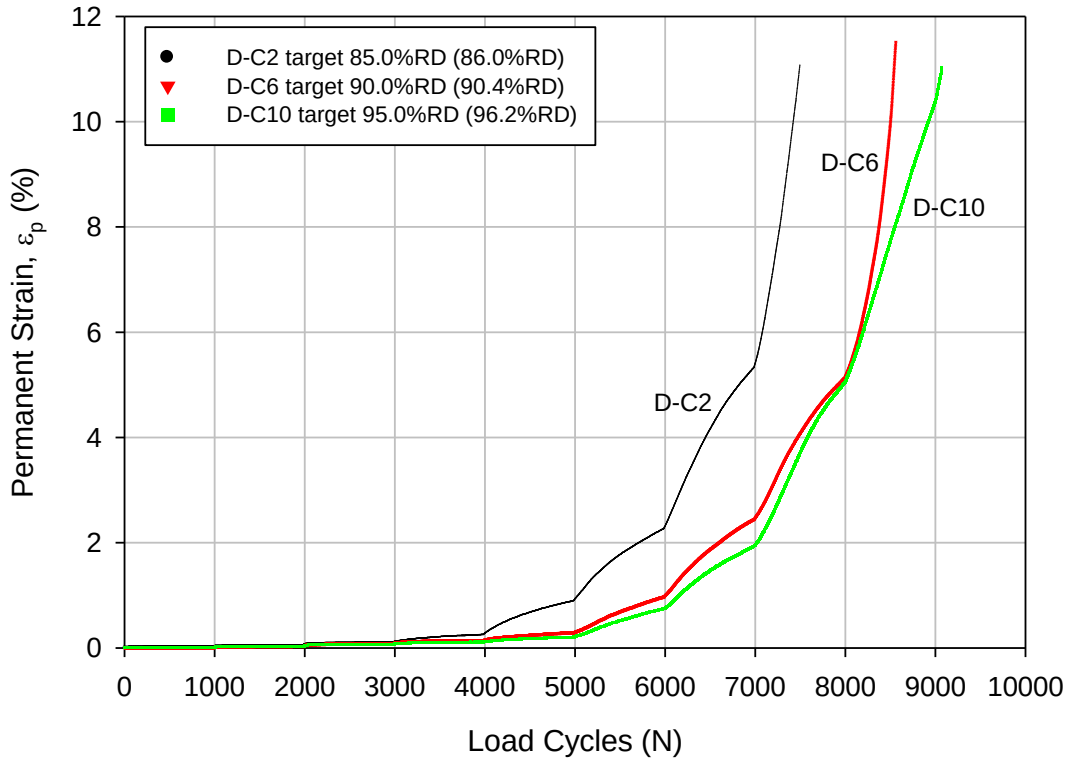

Figure 46. ε_p at reconstituted 5.8% F_{200} for crushed limestone samples (NCHRP 598)

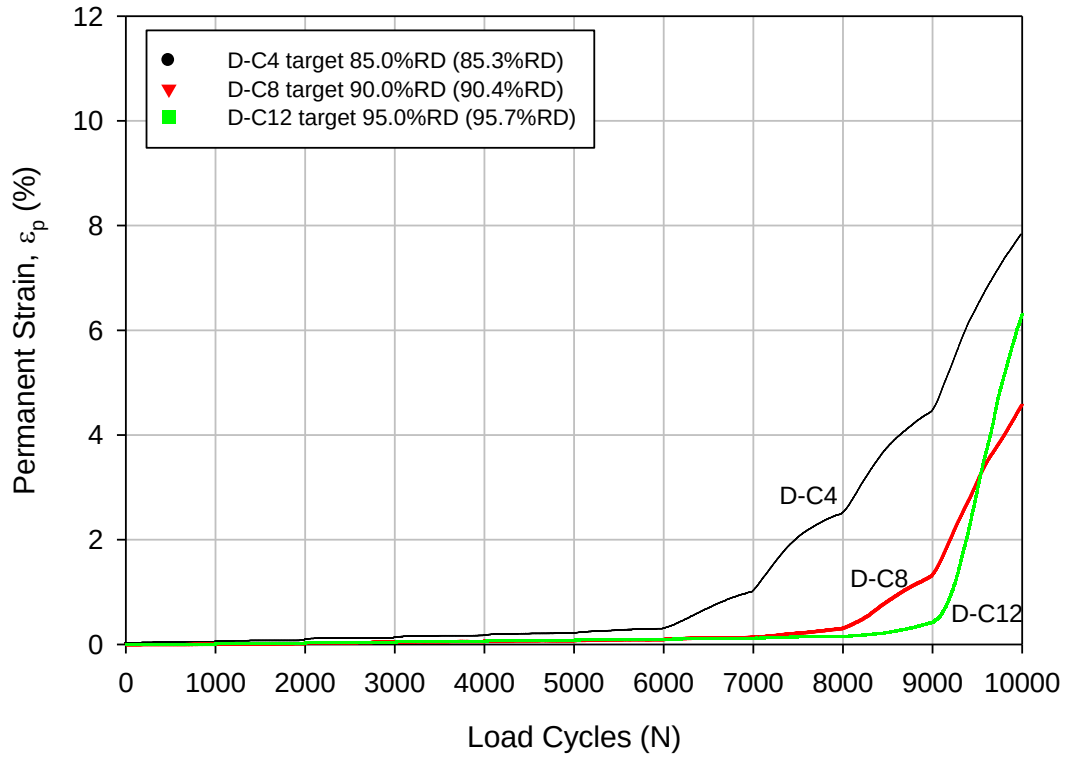

Figure 47. ε_p at reconstituted 12.6% F_{200} for crushed limestone samples (NCHRP 598)

When natural F_{200} of 2.0% was specified for RAP samples, the 98.0% RD sample has the lowest ε_p at the end of each load sequence and the 88.9% RD sample has the highest ε_p for all load sequences (Figure 48). When 1.6% F_{200} was specified, the 98.2% RD sample has the lowest ε_p at the end of each load sequence and the 87.7% RD sample has the highest ε_p for all load sequences (Figure 49). When 5.6% F_{200} was specified, the 96.4% RD sample has the lowest ε_p at the end of each load sequence and the 85.6% RD sample has the highest ε_p for all load sequences (Figure 50). When 12.5% F_{200} was specified, the 96.5% RD sample has the lowest ε_p at the end of each load sequence and the 85.6% RD sample has the highest ε_p for first five load sequences in the tests (Figure 51). The ε_p of the sample with 91.7% RD increases at a higher rate than the samples with 96.5% and 85.6% target relative densities. The accumulated ε_p of the sample with 91.7% RD exceed the accumulated ε_p of the other two samples at sequence No. 6 and the following sequences. Generally, the RAP materials indicate that increased permanent strain is a result of increasing relative densities.

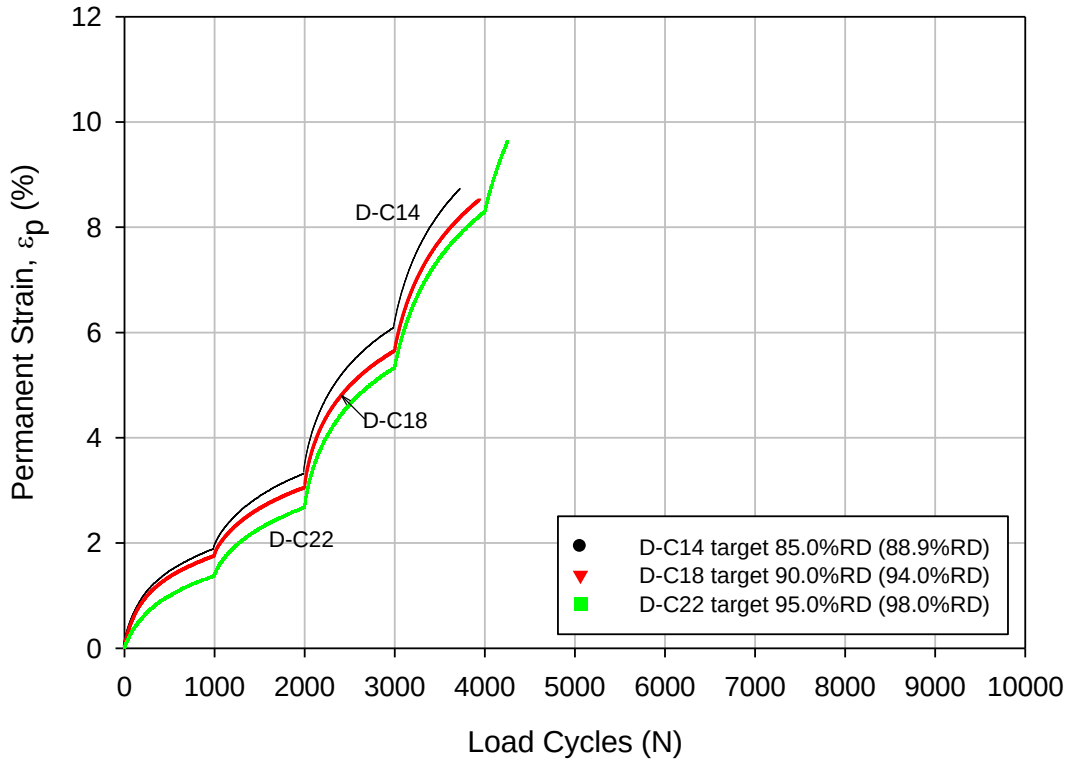

Figure 48. ε_p at natural 2.0% F_{200} for RAP samples (NCHRP 598)

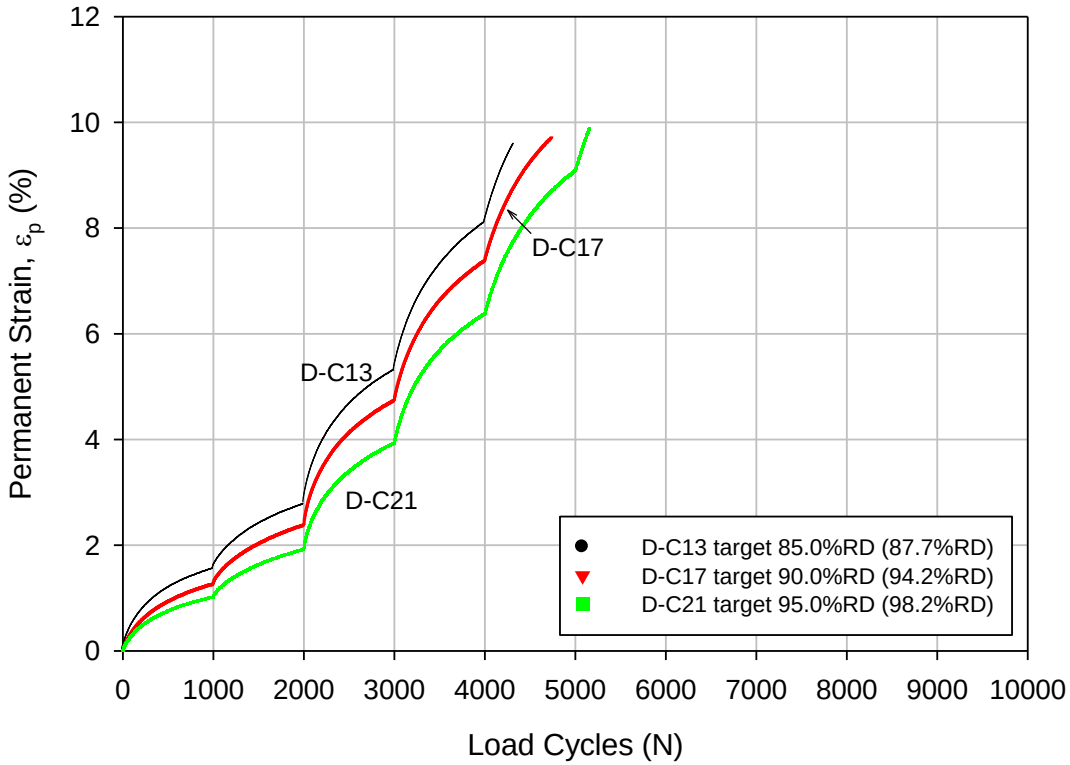

Figure 49. ε_p at reconstituted 1.6% F_{200} for RAP samples (NCHRP 598)

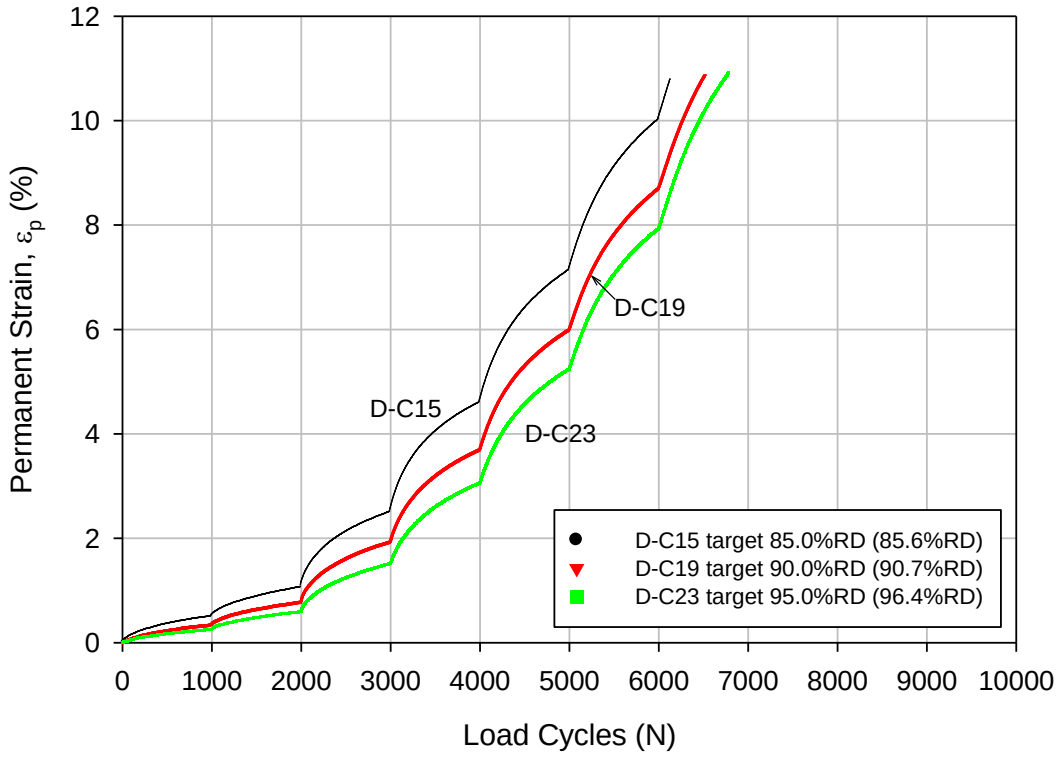

Figure 50. ε_p at reconstituted 5.6% F_{200} for RAP samples (NCHRP 598)

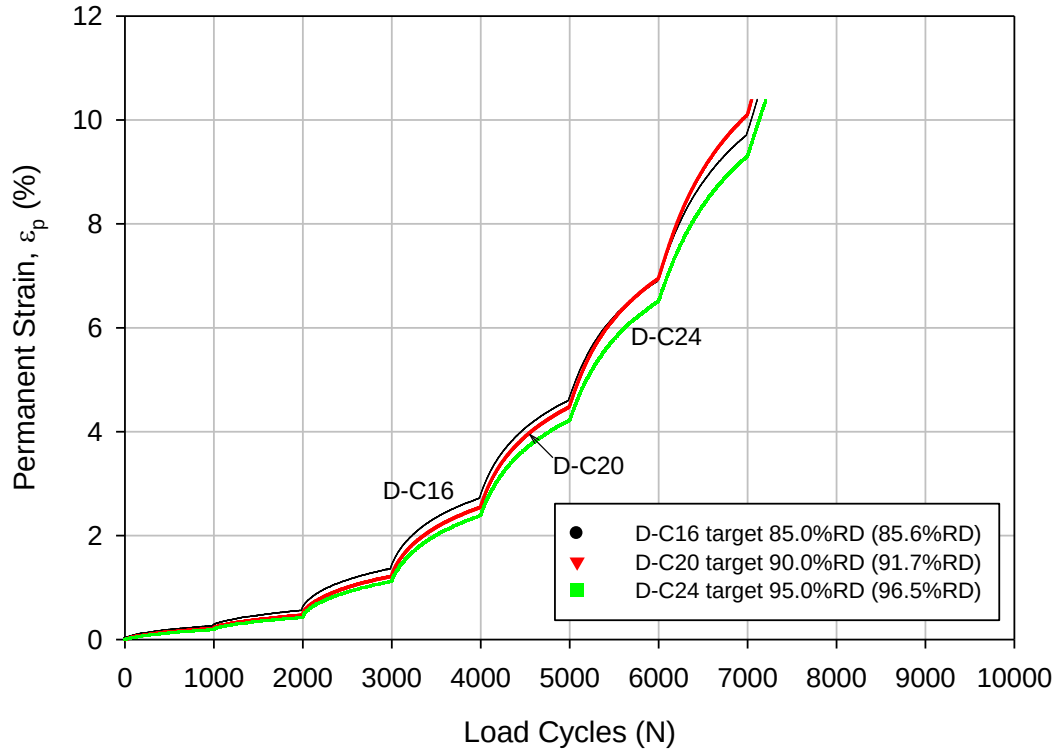

Figure 51. ε_p at reconstituted 12.5% F_{200} for RAP samples (NCHRP 598)

When natural F_{200} of 3.5% was specified for RPCC/RAP samples, the 81.2% RD sample has the lowest ε_p at the end of the first five load sequences and the 77.0% RD sample has the highest ε_p for all load sequences (Figure 52). The ε_p of the sample with 81.2% RD increases at a higher rate than the samples with 95.4% RD. The accumulated ε_p of the sample with 81.2% RD exceed the accumulated ε_p of the sample 95.4% RD at sequence No. 6 and the rest following sequences. The reason could be the large difference of approximately 9% between the target and the actual RD values. When 0.8% F_{200} was specified, the 99.0% RD sample has the lowest ε_p at the end of each load sequence and the 88.5% RD sample has the highest ε_p for all load sequences (Figure 53). When 6.0% F_{200} was specified, the 95.6% RD sample has the lowest ε_p at the end of each load sequence and the 86.3% RD sample has the highest ε_p for all load sequences (Figure 54). When 12.4% F_{200} was specified, the 95.6% RD sample has the lowest ε_p at the end of each load sequence and the 86.3% RD sample has the highest ε_p for all load sequences (Figure 55). Generally, the RPCC/RAP materials indicates that increased permanent strain with increasing relative densities

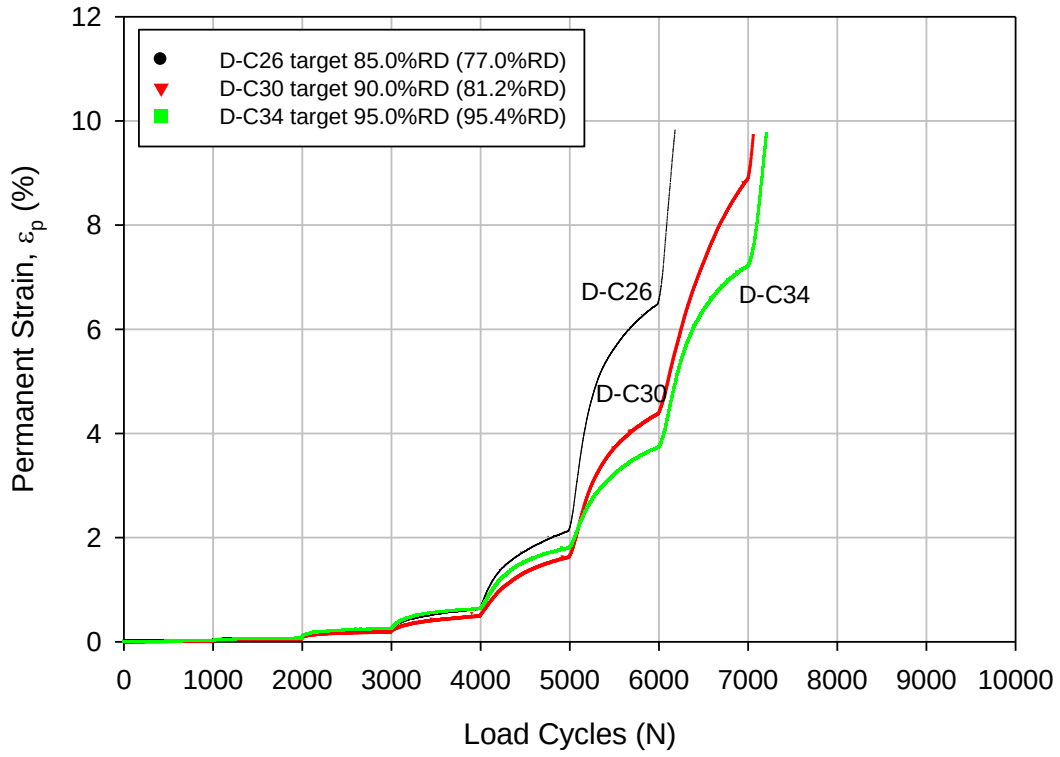

Figure 52. ε_p at natural 3.5% F_{200} for RPCC/RAP samples (NCHRP 598)

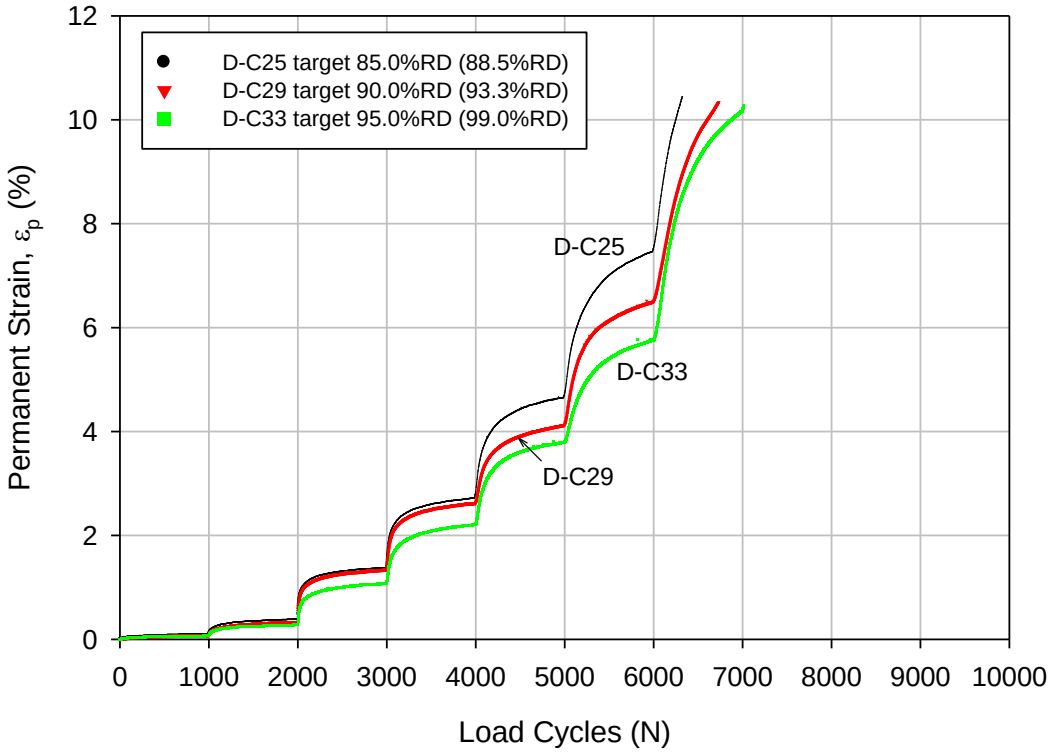

Figure 53. ε_p at reconstituted 0.8% F_{200} for RPCC/RAP samples (NCHRP 598)

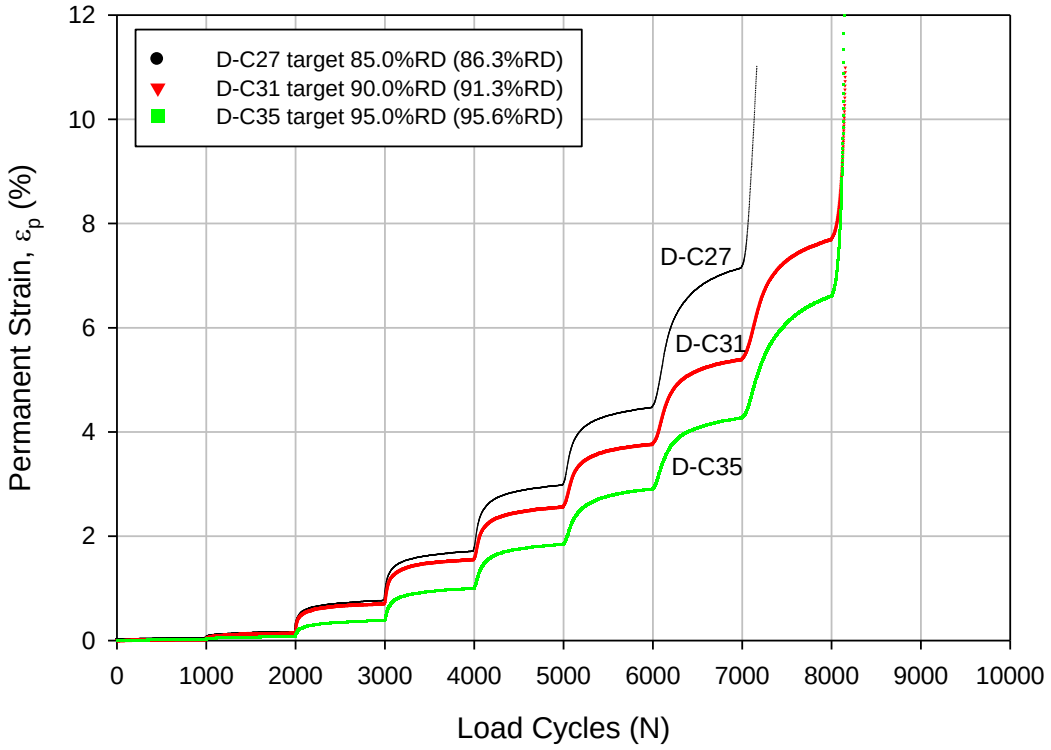

Figure 54. ε_p at reconstituted 6.0% F_{200} for RPCC/RAP samples (NCHRP 598)

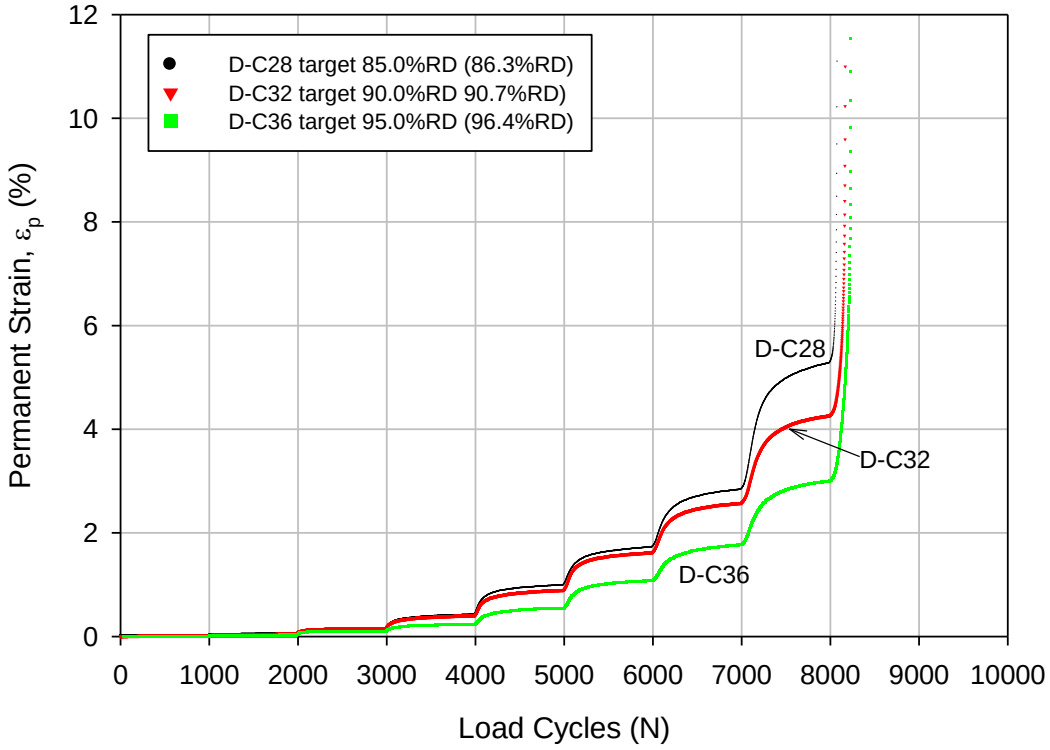

Figure 55. ε_p at reconstituted 12.4% F_{200} for RPCC/RAP samples (NCHRP 598)

The statistical analysis for RD affecting the accumulated permanent strain at the end of each load sequence, six complete sequences were selected from the NCHRP 598 tests on crushed limestone samples, four complete sequences were selected for RAP samples, and six complete sequences were selected for RPCC/RAP samples.

The statistical analyses conclude the RD is an insignificant factor for crushed limestone. The parameters of statistical analyses that were conducted for each material separately are summarized in Table 33.

Table 33. Statistical analysis for RD affecting ε_p of different materials samples

Materials	Sequence No.	Degree of Freedom	Sum of Squares	F Ratio	Probability >F	R^2	SIG ?
Crushed limestone	S1	2	0.0042	0.6811	0.5304	0.1315	No
	S2		0.0126	0.2117	0.8131	0.0450	No
	S3		0.0729	0.0697	0.9332	0.0152	No
	S4		0.1154	0.0216	0.9787	0.0048	No
	S5		0.3819	0.0265	0.9739	0.0059	No
	S6		1.7930	0.0621	0.9402	0.0136	No
RAP	S1		0.9686	0.3198	0.7342	0.0664	No
	S2		1.5207	0.2538	0.7812	0.0534	No
	S3		2.8280	0.2045	0.8187	0.0434	No
RPCC/RAP	S1		0.0005	0.0435	0.9576	0.0096	No
	S2		0.0045	0.0689	0.9339	0.0151	No
	S3		0.0622	0.0967	0.9088	0.0210	No
	S4		0.2427	0.1132	0.8942	0.0245	No
	S5		0.9246	0.2141	0.0811	0.0454	No
	S6		5.5228	0.5668	0.5863	0.1119	No

Notes: SIG is abbreviation for significant

The significance of RD affecting ε_p was also studied by conducting the statistical analysis on all sample without differentiate the load sequence number. These statistical analyses indicate that RD does not have significant factor affecting ε_p. The parameters of statistical analyses that were conducted for all materials are summarized in Table 34.

Table 34. Statistical analysis for significance of RD affecting ε_p at the sequence end

Materials	Degree of Freedom	Sum of Squares	F Ratio	Probability >F	R^2	Significant ?
Crushed Limestone	2	1.0674	0.1185	0.8885	0.0034	No
RAP		5.0584	0.5853	0.5626	0.0343	No
RPCC/RAP		2.7926	0.4156	0.6616	0.0119	No

The general finding from the NCHRP 598 tests confirmed the conclusion reported by Barksdale (1972) and Allen (1973) that the permanent strain decreases with increasing relative densities. However, for some tests, the permanent strain for samples with 90.0%

target RD could be varied. The statistical analyses results indicate possible effects of deviator stresses and material types on RD affecting permanent deformation behavior of UGMs.

Fines content

Fines content (F_{200}) is the percentage of the materials passing the No. 200 sieve and can vary for UGMs during the entire pavement service life. Migration of fine materials from subbase to pavement surface lead to loss of pavement support and finally induced pavement distresses. The fines content was specified as a factor influencing permanent deformation behavior of UGMs in the literature review. Four fines contents of 3.3%, 4.5%, 7.0%, and 9.0% were studied in the ISU 100k tests that were performed on the untrimmed slag materials. Although the sample with 7.0% F_{200} has higher ε_p at the test end than the sample with 3.3% F_{200}, the permanent strains at the test ends of samples with 4.5% and 9.0% F_{200} are lowest in the four tests. The clear relationship between F_{200} and the accumulated permanent strain is not observed in the tests (Figure 56).

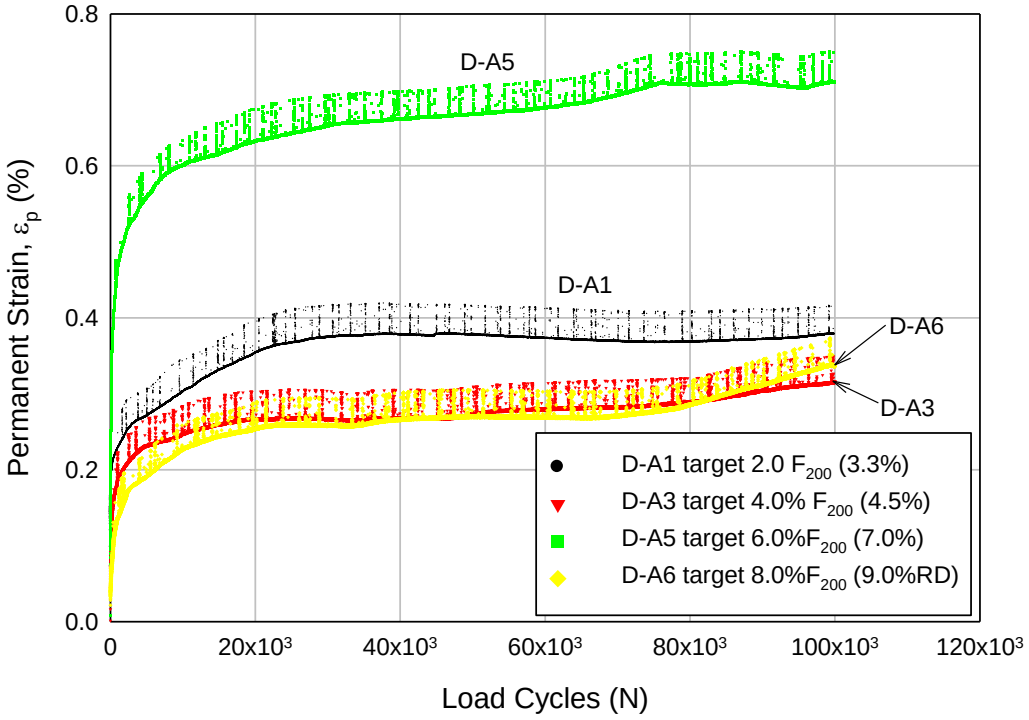

Figure 56. ε_p at 41.2 kPa σ_d for untrimmed slag samples (ISU 100k)

When 85.0% target RD was specified for the crushed limestone samples, the natural 7.9% F_{200} sample has the highest permanent strain and the other samples show that the fines

contents are inversely related to the accumulated ε_p at the end of each load sequence (Figure 57). Permanent strain of the sample with 12.6% F_{200} accumulates at very low strain rate and close to 0%/N at the first several load sequences where lower σ_d was applied and accumulates at higher strain rate when higher σ_d was applied. The same observations of fines contents affecting permanent deformation of crushed limestone materials are concluded on the samples with 90.0% target RD (Figure 58) and 95.0% target RD (Figure 59).

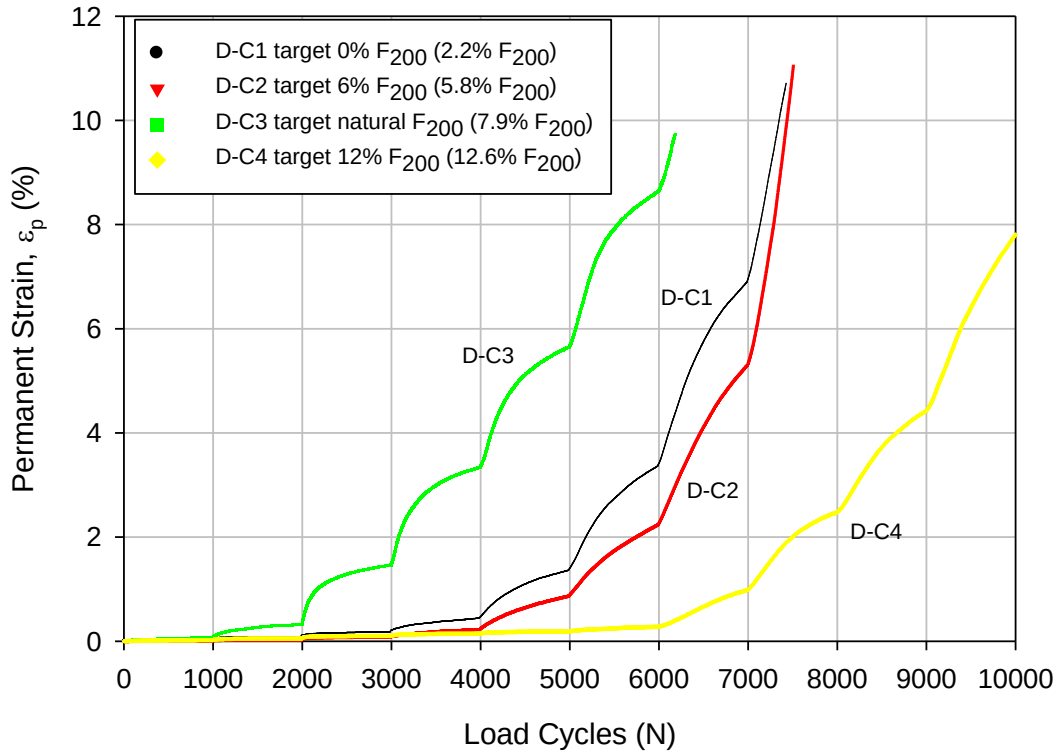

Figure 57. ε_p at 85% target RD for crushed limestone samples (NCHRP 598)

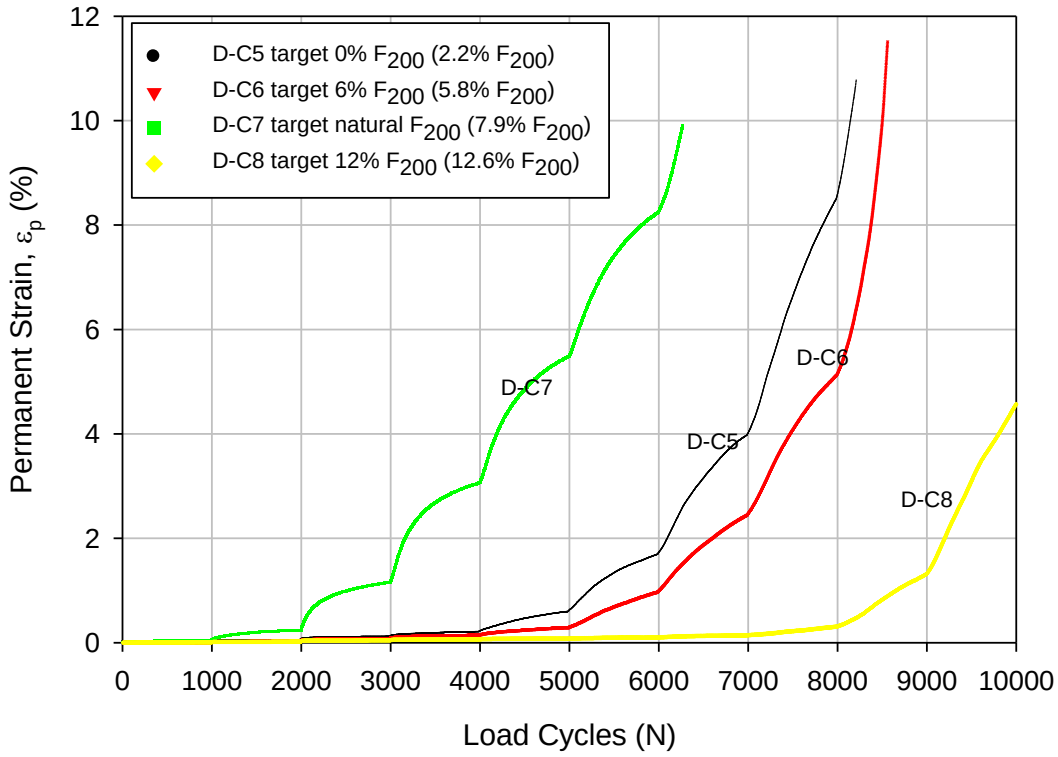

Figure 58. ε_p at 90% target RD for crushed limestone samples (NCHRP 598)

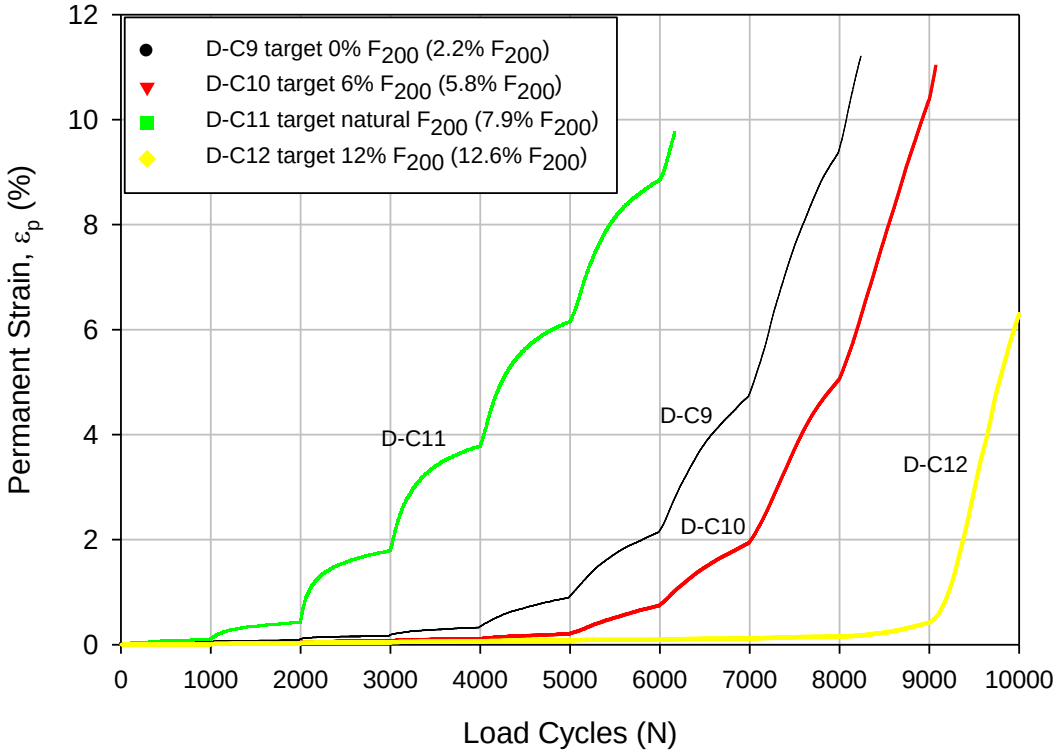

Figure 59. ε_p at 95% target RD for crushed limestone samples (NCHRP 598)

When 85.0% target RD was specified for the RAP samples, the natural 2.0% F_{200} sample has the highest permanent strain and the other samples show that the fines contents inversely relates to the accumulated ε_p at the end of each load sequence (Figure 60). The 12.5% F_{200} sample has the lowest ε_p for all load sequences compared to other three samples has the same target RD and different fines contents. The same observations of fines contents affecting permanent deformation of RAP materials are drawn on the samples with 90.0% target RD (Figure 61) and 95.0% target RD (Figure 62Figure 58).

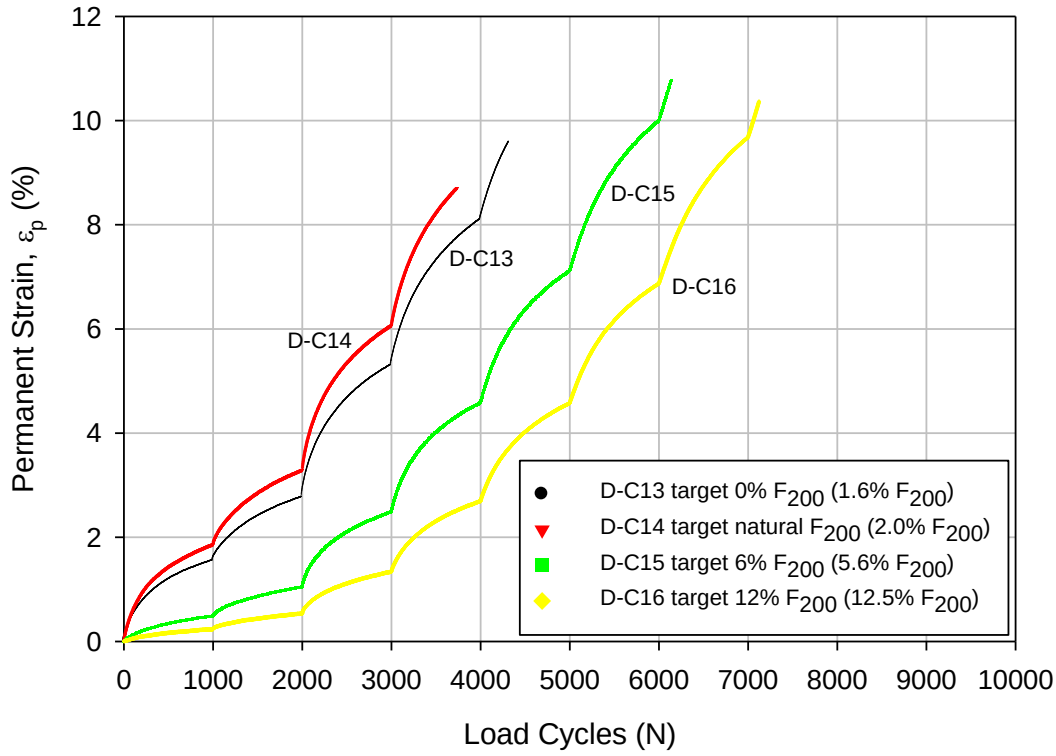

Figure 60. ε_p at 85% target RD for RAP samples (NCHRP 598)

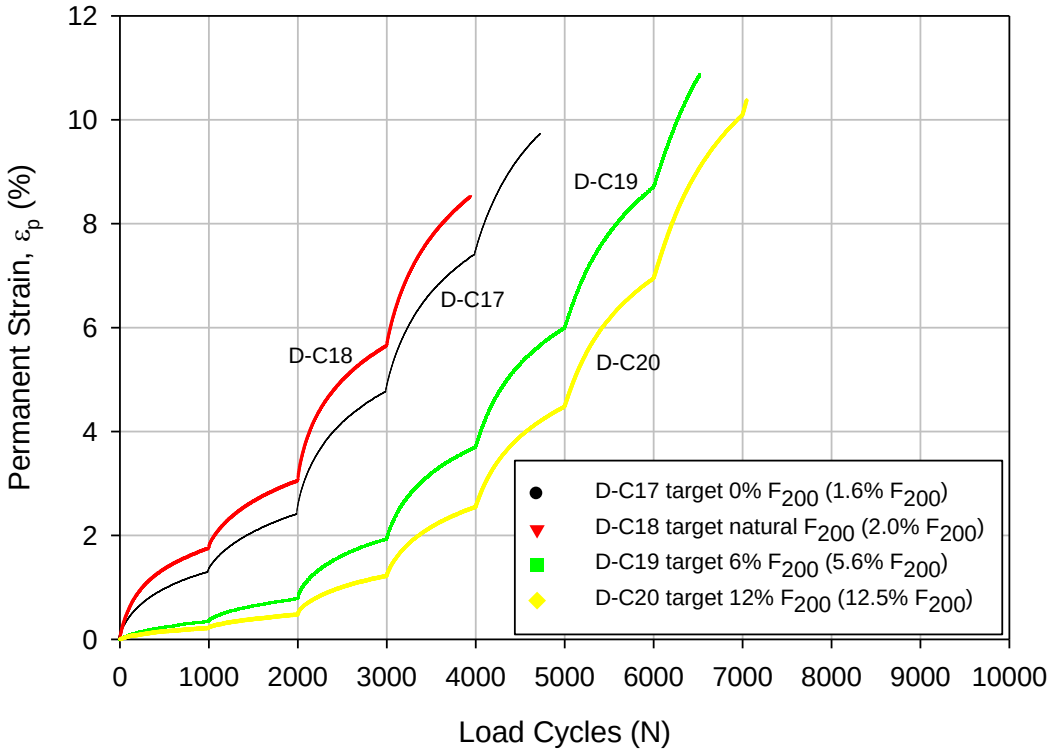

Figure 61. ε_p at 90% target RD for RAP samples (NCHRP 598)

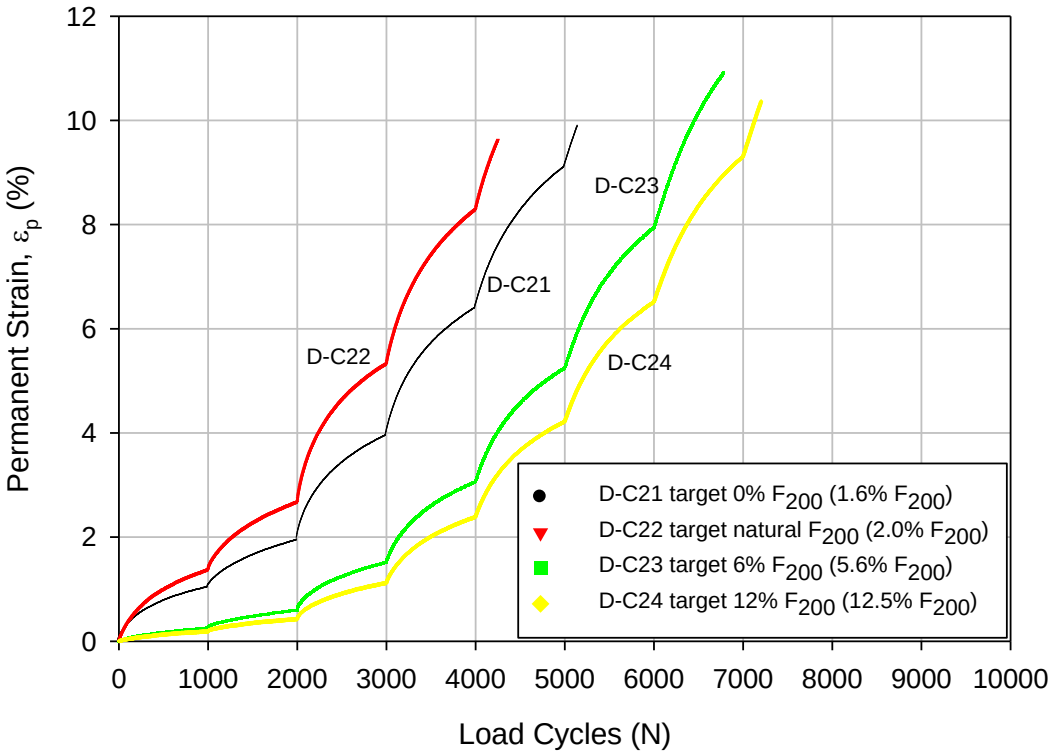

Figure 62. ε_p at 95% target RD for RAP samples (NCHRP 598)

When 85.0% target RD was specified for the RPCC/RAP samples, the samples with fines contents of 0.8%, 6.0%, and 12.4% show that the fines contents inversely relates to the accumulated ε_p at the end of each load sequence and the sample with 0.8% fines content has the highest ε_p for all load sequences (Figure 63). However, the natural F_{200} sample has higher strain rate than the other three samples. The ε_p of the natural F_{200} sample are lower than the ε_p of the 0.8% and 6.0% F_{200} samples at the first five load sequences, but the ε_p of the natural F_{200} sample increases to be higher than the ε_p of the 0.8% F_{200} sample and closer to the ε_p of the 6.0% F_{200} sample.

The same observations of fines contents affecting permanent deformation of RPCC/RAP materials are drawn on the samples with 90.0% target RD (Figure 64) and 95.0% target RD (Figure 65). The plots of ε_p accumulated with the number of load cycles for RPCC/RAP samples with different fines contents are shown in next two pages.

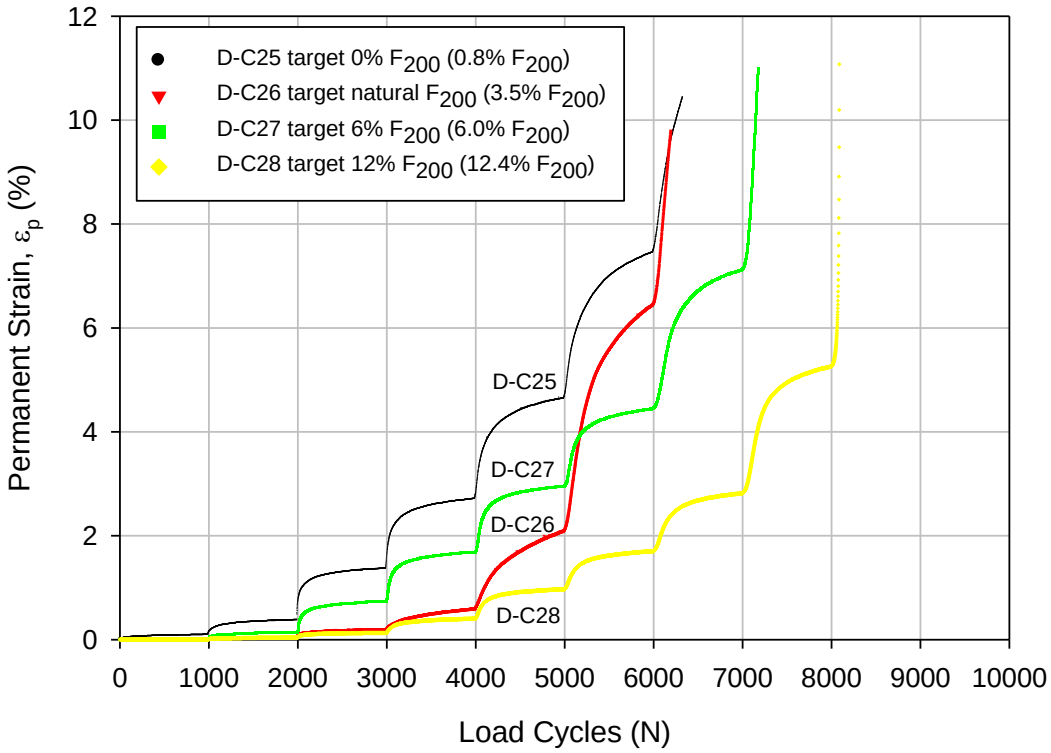

Figure 63. ε_p at 85% target RD for RPCC/RAP samples (NCHRP 598)

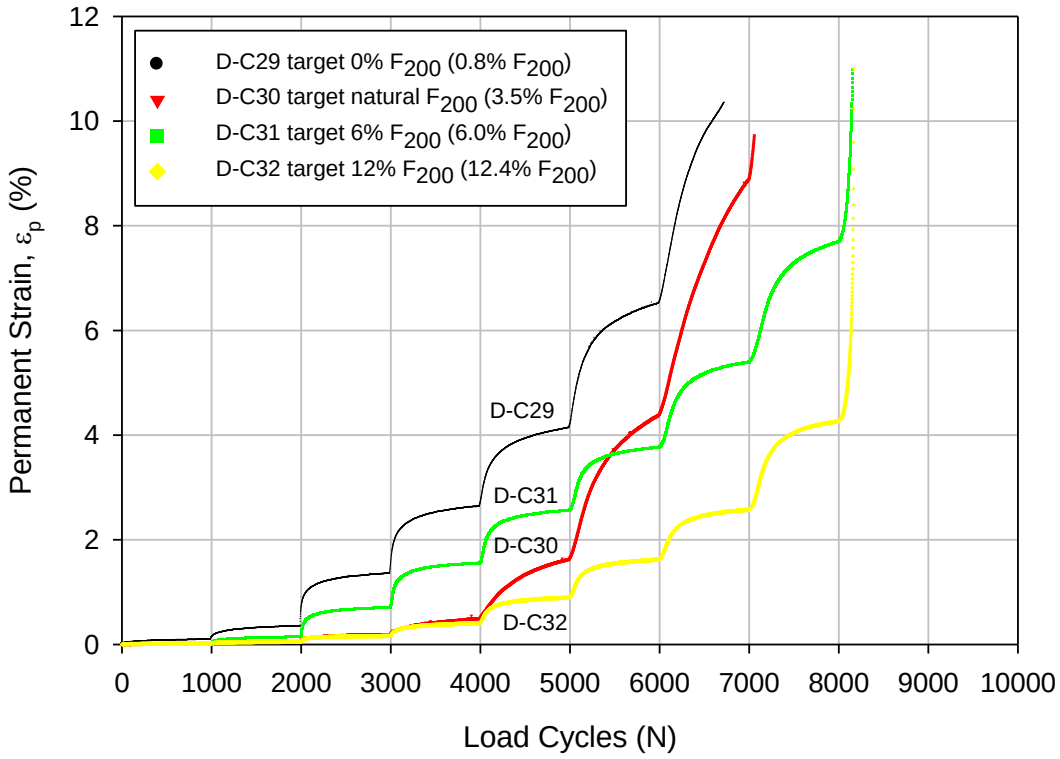

Figure 64. ε_p at 90% target RD for RPCC/RAP samples (NCHRP 598)

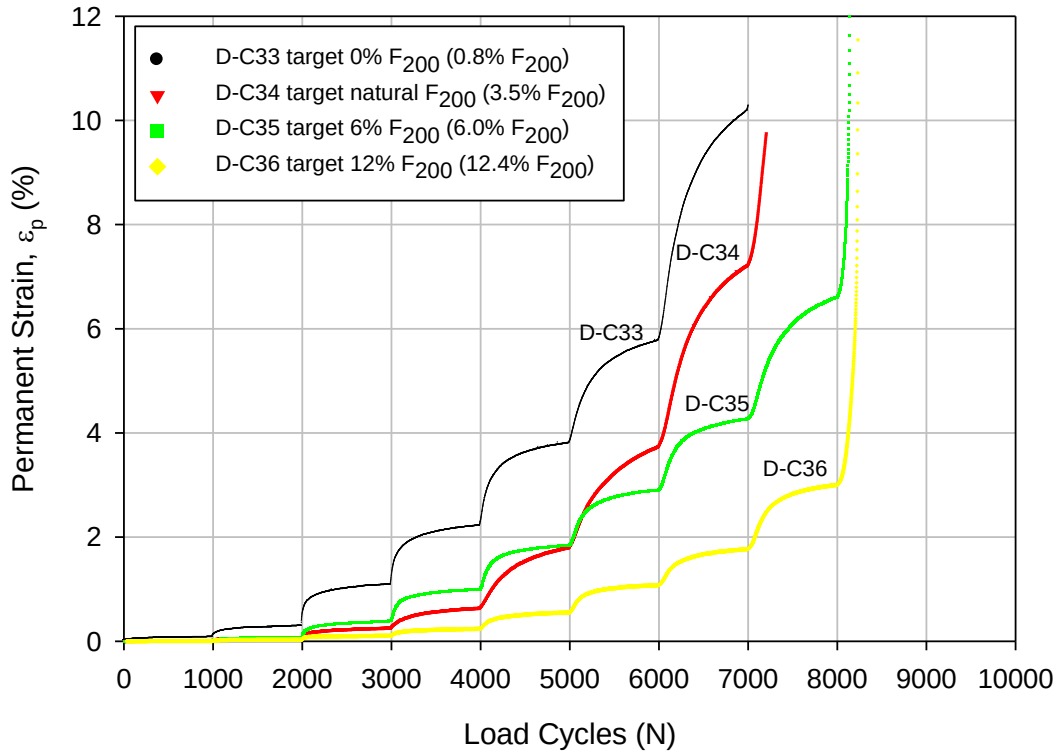

Figure 65. ε_p at 95% target RD for RPCC/RAP samples (NCHRP 598)

The samples with natural fines contents are always show much different trends that the permanent strain was accumulated with increasing number of load cycles in different strain rate. The RPCC/RAP samples with natural fines content have the permanent strains increase to be higher than the permanent strains of the 6.0% F_{200} samples at the same number of load cycles after first five load sequences. Moreover, the crushed limestone and RAP samples with natural fines contents always have higher permanent strain than the samples with 0% target F_{200}.

One reason could be the materials preparation methods. The materials were prepared by adding more fines to or removing extra fines from the dried original materials which were used to prepare natural F_{200} sample. The structures between fine particles and large particles were changed. For example, the extra fine particles were added to the original materials and the fine particles might be adhered to form larger particles while they were expected to adhere to the larger particles surface.

Low dry unit weights were determined in the relative density testes for the natural F_{200} samples could be another reason. Although the target relative densities were specified for all tests samples, the dry unit weights of all crushed limestone and RAP samples with natural F_{200} are lower than the dry unit weights of the samples with target fines contents and the dry unit weights of all RPCC samples with natural fines content are close to the dry unit weights of the samples with 0% target F_{200}. Therefore, the observations that were concluded on relations between the ε_p of the natural and the target F_{200} samples for the crushed limestone and RAP materials are different from the observation on the RPCC/RAP materials. The dry unit weights of each material were calculated based on the maximum and minimum dry unit weights that were obtained by conducting the RD tests at 0.0% moisture content. However, the original materials have more fines adhered to the larger particles surface and fewer fines fill the voids among particles. The materials with target fines contents were dried and sieved in materials preparation so these materials have less fines adhere to the larger particles surface and more fines fill the voids between particles. The difference in the proportion of fines adhered to larger particles surface might cause lower dry unit weights and higher ε_p at the same fines content.

According to the ε_p at the end of each load sequence for 0.0%, 6.0%, and 12.0% target F_{200} samples of crushed limestone, RAP, and RPCC/RAP materials, the permanent strains are inversely related to fines contents. This finding are conflict with the conclusion reported by Barksdale (1972), Thom and Brown (1988), Kancherla (2004), Mishra et al. (2009) and Hussian et al. (2010) that increasing fines content causes decrease in resistance of UGMs to permanent deformation.

The higher permanent strain at the same deviator stress and number of load cycles indicate lower resistance to permanent deformation. The possible reason caused the different conclusion might be the samples were compacted to the same level of RD not the same values of dry unit weight in this research while other researchers compacted the samples to the same dry unit weight (Hussian et al. 2010) or similar dry unit weights with less than 1 kN/m^3 difference (Mishra et al. 2009).

However, Belt et al. (1997) reported a similar results with the conclusion in this study that higher fines content results in lower fines content except the fines content is very high (>15%). Moreover, Mishra et al. (2009) also found the permanent deformation is lower in dolomite materials with 8% fines than the same materials with 4% fines, although they also found that the permanent deformation in gravel materials increased with increasing fines content from 4% to 16%. The stress level has been identified as important factor affecting permanent deformation, so another reason lead to different conclusions in study from some findings in previous studies on relationship between fines content and the accumulated permanent strain could be stress level. Crushed limestone materials do not show purely increase in ε_p with increasing fines content (Figure 66).

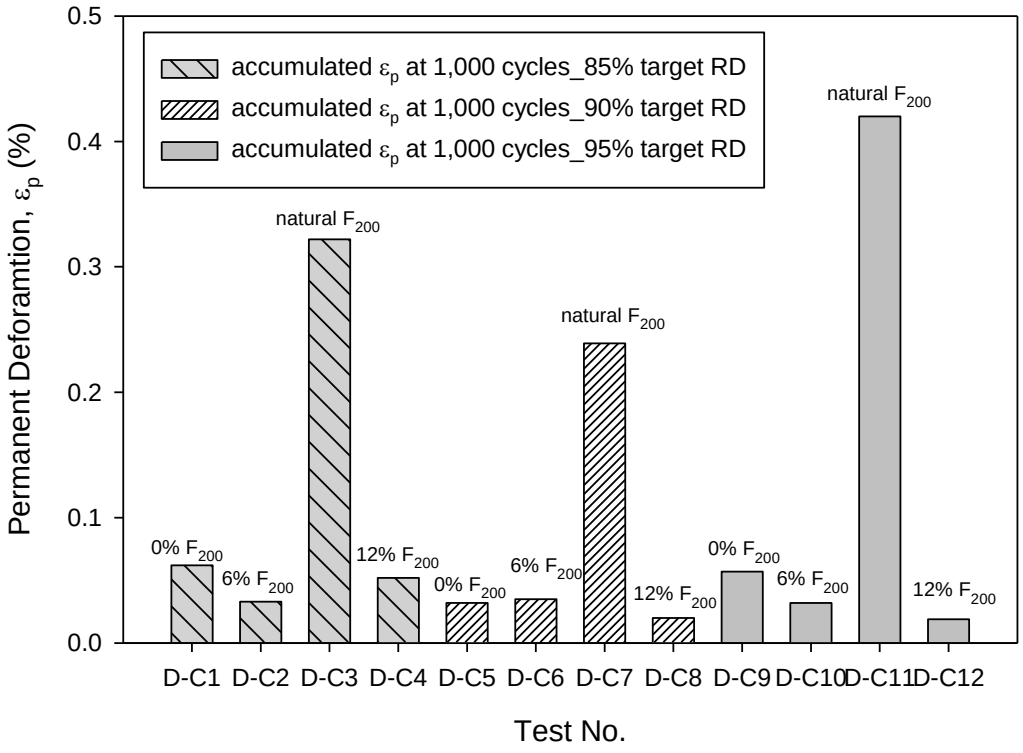

Figure 66. The accumulated ε_p at load sequence 1 end for crushed limestone samples

All four fines contents are studied to determine the significance of fines content affecting permanent deformation behavior on first six load sequences for crushed limestone samples, on first three load sequences for RAP samples, and on first size load sequences for RPCC/RAP samples. The fines content is determined to have significant effect on permanent strain for each material (Table 35).

Table 35. Statistical analysis for F_{200} affecting ε_p for all samples of each material

Materials	Sequence No.	Degree of Freedom	Sum of Squares	F Ratio	Probability >F	R^2	SIG ?
Crushed limestone	S1	3	0.0232	6.8853	0.0132	0.7208	Yes
	S2		0.2467	18.9518	0.0005	0.8766	Yes
	S3		4.5344	48.5349	<0.0001	0.9479	Yes
	S4		23.8617	181.4911	<0.0001	0.9855	Yes
	S5		64.4158	200.6485	<0.0001	0.9869	Yes
	S6		128.6572	111.5199	<0.0001	0.9766	Yes
RAP	S1		12.8867	20.0877	0.0004	0.8828	Yes
	S2		26.1983	30.5358	<0.0001	0.9197	Yes
	S3		61.4095	44.8792	<0.0001	0.9439	Yes
RPCC/RAP	S1		0.0533	45.5114	<0.0001	0.9447	Yes
	S2		0.2818	52.8763	<0.0001	0.9520	Yes
	S3		2.8128	52.0217	<0.0001	0.9512	Yes
	S4		9.4309	54.9623	<0.0001	0.9537	Yes
	S5		19.0970	40.4824	<0.0001	0.9382	Yes
	S6		42.3812	16.1748	0.0009	0.8585	Yes

Notes: SIG is abbreviation for significant

However, the fines content is determined to have insignificant effect on permanent strain when materials types were not differentiated (Table 36) and only three target fines contents were studied because the natural fines content are largely different (up to 75%) for the three tested materials.

Table 36. Statistical analysis for significance of F_{200} affecting ε_p for all samples

Materials	Degree of Freedom	Sum of Squares	F Ratio	Probability >F	R^2	Significant ?
Crushed Limestone	3	121.0120	14.3687	<0.0001	0.3880	Yes
RAP		91.1498	17.2092	<0.0001	0.6174	Yes
RPCC/RAP		40.9308	4.7908	0.0044	0.1745	Yes

Materials type

The materials type is an important factor affecting the permanent deformation behavior. The researchers (Lerkarp et al. 1996; Bernertet al. 2000; Rodgers et al. 2008; Werkmeister 2003) all reported different resistance to deformation levels for different materials. The

materials used for subbase construction are varied, and the crushed limestone, RAP, and RPCC/RAP were selected for this study to learn the difference in the resistance to permanent deformation of virgin materials and recycled materials.

The NCHRP 598 tests results for all the samples indicate that RAP usually have the lowest resistance, followed by RPCC/RAP, and the crushed limestone have the highest resistance to the permanent deformation when same target fines content, relative density, and deviator stress were specified.

The permanent strain of RAP samples continuously increased with small increase in the strain rate at different deviator stress and shows the trend to reach a constant value at the end of each load cycles. RAP has the highest permanent strain at the end of each load sequence compared to other two materials. The reasons might be the void ratio of the asphalt coating on the particles surfaces is higher than the void ratio of aggregates and the asphalt coating break down under high deviator stresses to fill the voids between particles.

The permanent strain of RPCC/RAP samples also continuously increased with small increase in the strain rate at different deviator stress and shows a sudden failure in the test. For example, the permanent strain of sample D-C36 is about 3.0% at the end of the 8th load sequence and reaches 10% at the 230 load cycles of the 9th load sequence. The sudden increase in the permanent strain for the RPCC/RAP samples is because the sample cannot support the high deviator stress (i.e. 1103.2 kPa) and cracks. The RAP particles in this RPCC/RAP material are very low in proportion and not specified in this study.

The permanent strain of crushed limestone samples continuously increased with small increase in the strain rate at the low deviator stress and with large increase in the strain rate at the high stress level. For example, the permanent strain of sample D-C8 has less than 0.2% accumulated at the end of the 8th load sequence and reaches 1.3% at the end of the 9th load sequence and 4.6% at the test end. This indicates the crushed limestone samples starts to form crack and losing interlocking between particles.

This study confirmed the finding reported by Bennert et al. (2000) that the RPCC materials have lower permanent strain than the RAP materials. Materials type is proved using statistical analysis to have significance effect on permanent strain at the end of first four load sequences. The parameters of statistical analysis are summarized (Table 37).

Table 37. Statistical analysis for significance of materials type affecting ε_p at the end of the sequence

Sequence No.	Degree of Freedom	Sum of Squares	F Ratio	Probability >F	R^2	Significant ?
S1	2	4.6196	9.7212	0.0008	0.4475	Yes
S2		11.8058	11.6294	0.0003	0.4926	Yes
S3		39.8884	14.8260	<0.0001	0.5527	Yes
S4		103.9763	21.1735	<0.0001	0.6383	Yes

Permanent deformation prediction model

The accumulated permanent strain was predicted with the applied number of load cycles (N) by using the Barksdale (1972) model (Equation 20) in this study:

$$\varepsilon_{1,p} = a + b \cdot log(N) \quad (20)$$

where: $\varepsilon_{1,p}$ = accumulated permanent axial strain;

N= number of load cycles; and

a, b = regression parameters.

Bennert et al. (2000) reported a good fit by using the Barksdale model to fit the accumulated permanent strain of RPCC, RAP, and aggregate base course materials. The Barksdale model is used as the start in studying the permanent deformation prediction.

Two samples from each of the ISU 100k tests and the ISU 1k tests were fitted by using the Barksdale model. The large differences between the predicted and the measured permanent strain are observed on the ISU 100k tests because the measured values are not constant (Figure 67). The small difference between the predicted and the measured permanent strain are observed on the ISU 1k tests (Figure 68). This model predicts the trend of the permanent strain to reach a constant value at certain number of load cycles. However, the ISU 100k and ISU 1k tests were conducted with low deviator stress less than 103.4 kPa. According to the study on important factors affecting the permanent deformation behavior of UGMs, the Barksdale model is also used to fit the measured accumulated permanent strains.

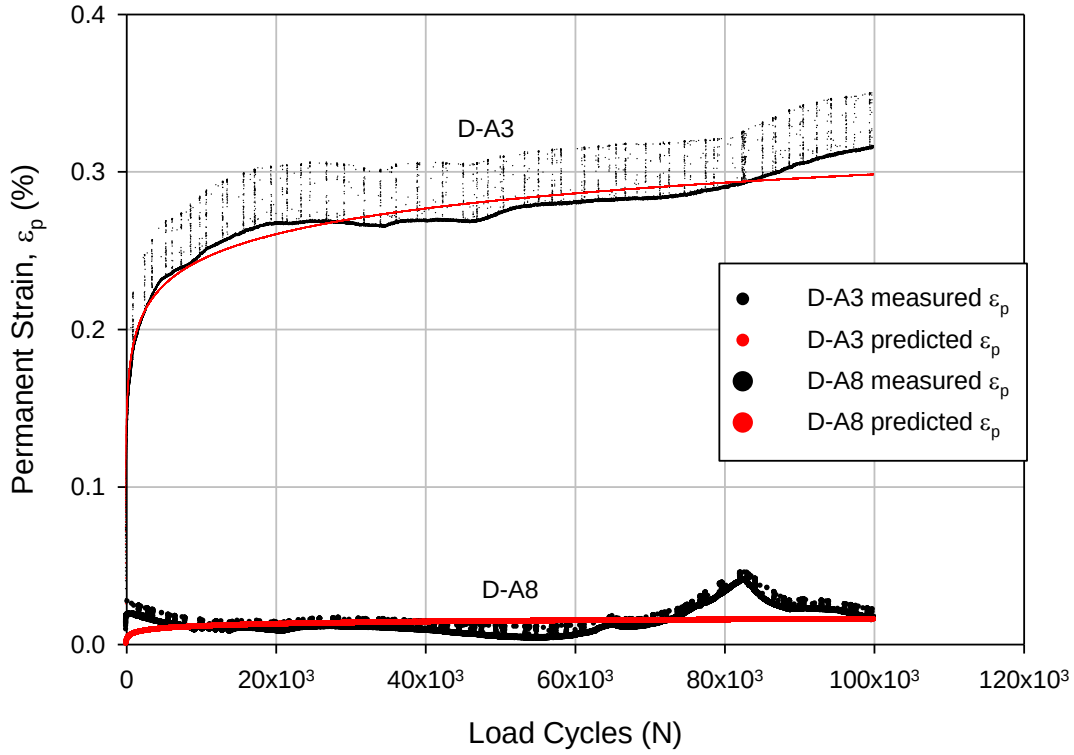

Figure 67. Predicting ε_p using Barksdale model on two ISU 100k ε_p test samples

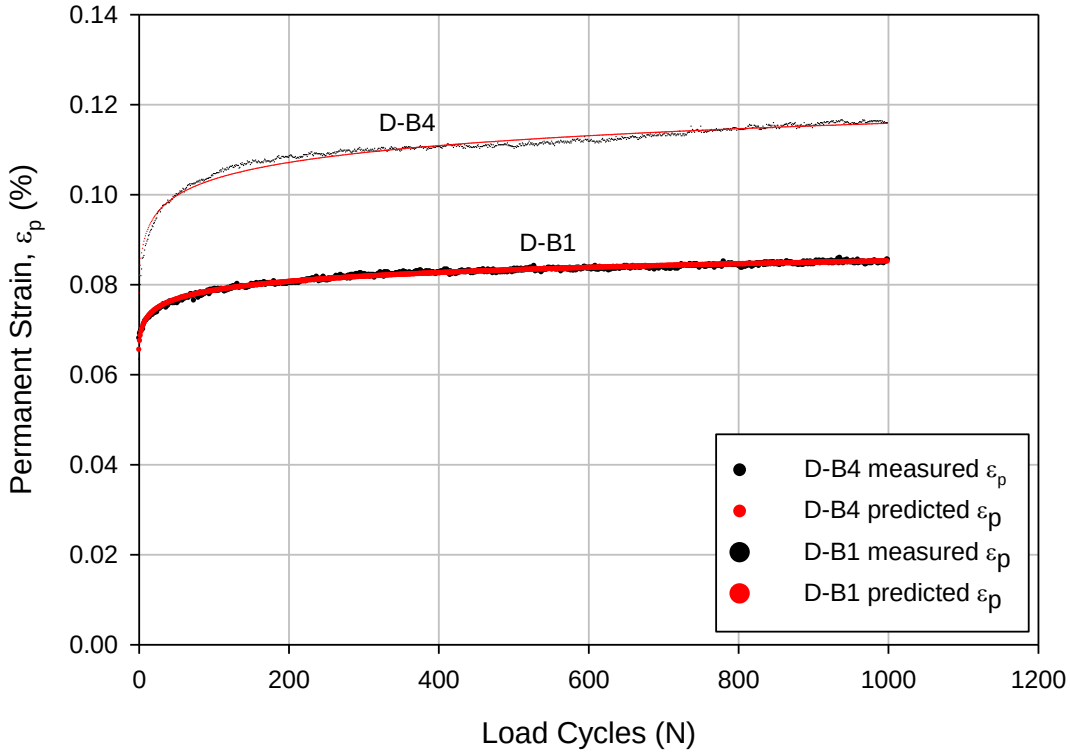

Figure 68. Predicting ε_p using Barksdale model on two ISU 1k ε_p test samples

The prediction of sample D-A8 has very low R^2 value of 0.0593 which indicates only 5.93% of the measured data points could be explained by the prediction model. The predictions of permanent strain for other three samples are better to fit the measured data points as indicated by the high R^2 values. This statistical conclusion confirmed the observations that were discussed earlier. The Barksdale's model parameters were summarized for two ISU 100k and two ISU 1k tests.

Table 38. Barksdale's model parameters for two ISU 100k and two ISU 1k samples

Test No.	a	b	R^2
D-A3	0.0250	0.0545	0.8848
D-A8	-0.0075	0.0046	0.0593
D-B4	0.0780	0.0125	0.9652
D-B1	0.0653	0.0066	0.9876

The NCHRP 598 tests were designed to include up to 10 deviator stress levels, so the Barksdale model is used to fit the measured accumulated permanent strain for each load sequence separately. The Barksdale model fitted the accumulated permanent strain of two crushed limestone samples with natural fines content and 0.0% target fines content. The number of load cycles (N) is from 51 to 1051 to void the effects of (0, 0) origin on determine the parameters a and b. At low deviator stress up to 413.7 kPa, the model shows a good fit to the measured permanent strain. At high deviator stress from 551.6 kPa to 827.4 kPa, the differences between the predicted and measured permanent strain are clearer (Figure 69). The predicted values are negative at the beginning of the load sequences where the high deviator stresses were applied. The negative value is due to the reversed S shape transition of permanent strain between two load sequences under high deviator stresses. The reversed S shape describes the accumulated permanent strain first increases with increasing strain rate then increases with decreasing stain rate. This reversed S shape might be an indicator of the effects of stress history in the tests and the question to the assumption of no effect from previous load sequences in the NCHRP 598 tests.

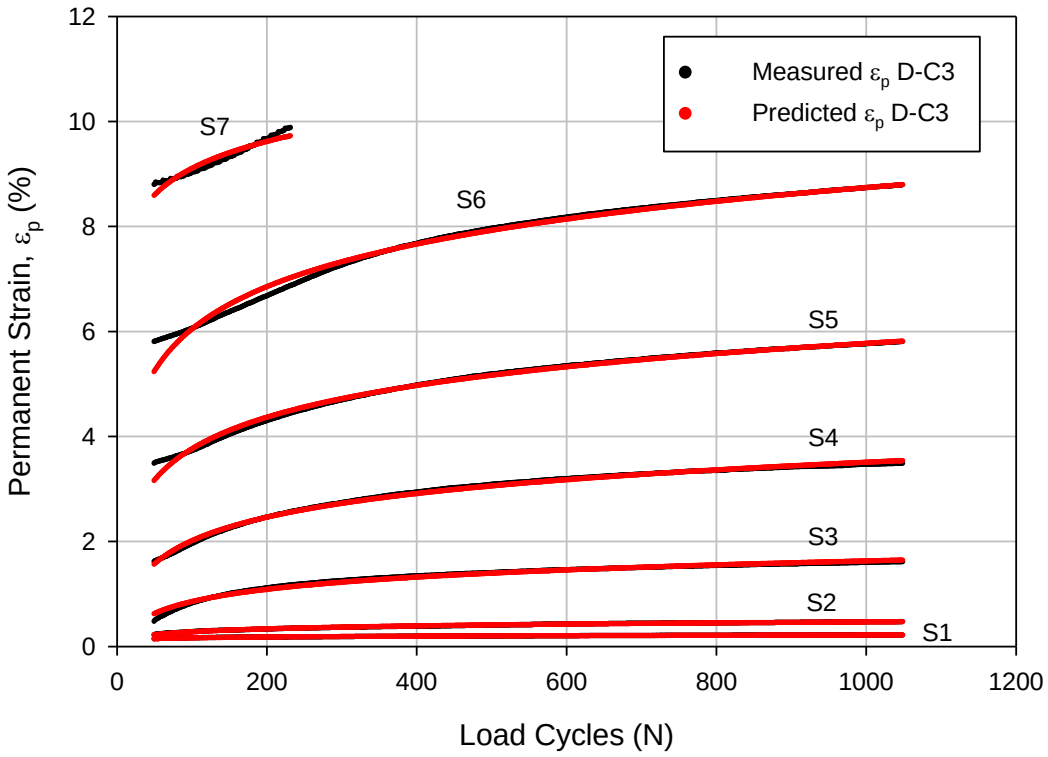

Figure 69. Measured and Barksdale's model predicted ε_p for one NCHRP 598 ε_p test sample (D-C3)

The similar observations are concluded on the crushed limestone sample with 0.0% target fines content (D-C1) as the crushed limestone sample with natural fines content (D-C3). The large difference between the predicted and the measured permanent strains in the last load cycle, because small amount of data points were collected for this load sequence as the test was terminated after 10.0% ε_p reached. The lower accumulated permanent strain at the end of load sequence No. 7 was predicted than the measured value. The reason could be the Barksdale's model always predicts a trend to reach constant permanent strain after certain number of load cycles was applied. This lead to a question of different models could be used at different deviator stresses.

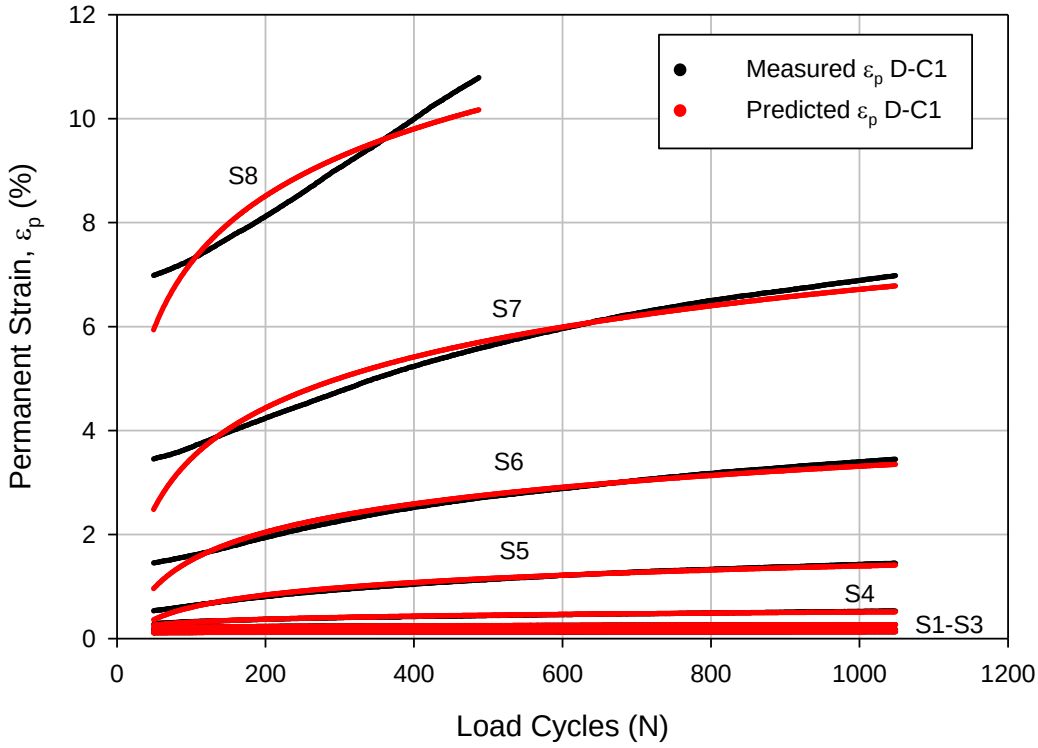

Figure 70. Measured and Barksdale's model predicted ε_p for one NCHRP 598 ε_p test sample (D-C1)

According to the statistical analyses on the prediction of accumulated strain from the applied number of load cycles, the prediction is good to fit the measured data points as R^2 is higher than 0.9 for all load sequences in two tests on the crushed limestone samples. The differences between the predicted and measured permanent strain are indicated as lower R^2 values for load sequences with high deviator stresses (Table 39).

Table 39. Barksdale's model parameters for two crushed limestone samples

Sequence No.	Sample D-C1			Sample D-C3		
	a	b	R^2	a	b	R^2
S1	0.0586	0.0147	0.9682	0.0336	0.0529	0.9936
S2	0.0881	0.0193	0.9838	-0.1262	0.1895	0.9964
S3	0.0902	0.0499	0.9905	-0.7291	0.7776	0.9877
S4	-0.1022	0.1950	0.9833	-1.0255	1.5028	0.9969
S5	-1.0311	0.8000	0.9834	-0.3145	2.0205	0.9947
S6	-2.1728	1.8194	0.9746	0.5819	2.7104	0.9883
S7	-3.1367	3.2748	0.9646	5.6270	1.7212	0.9237
S8	-1.4480	4.3106	0.9086	—	—	—

Notes: — means no value

The parameters a and b of Barksdale's model for each load sequence except the last load sequence where the tests were terminated are plotted with the deviator stresses, because the deviator stress was determined as an important factor affecting accumulated permanent strain. The parameter a for two crushed limestone samples are shown in Figure 71, and quadratic polynomial relationship (Equation 21) is specified to describe the relationship between the parameter a and the deviator stress.

$$a = k_1 + k_2 \cdot \sigma_d + k_3 \cdot \sigma_d^2 \quad (21)$$

where: a = parameter a in Barksdale's model;

k_1, k_2, and k_3 = regression parameters; and

σ_d = deviator stress (kPa).

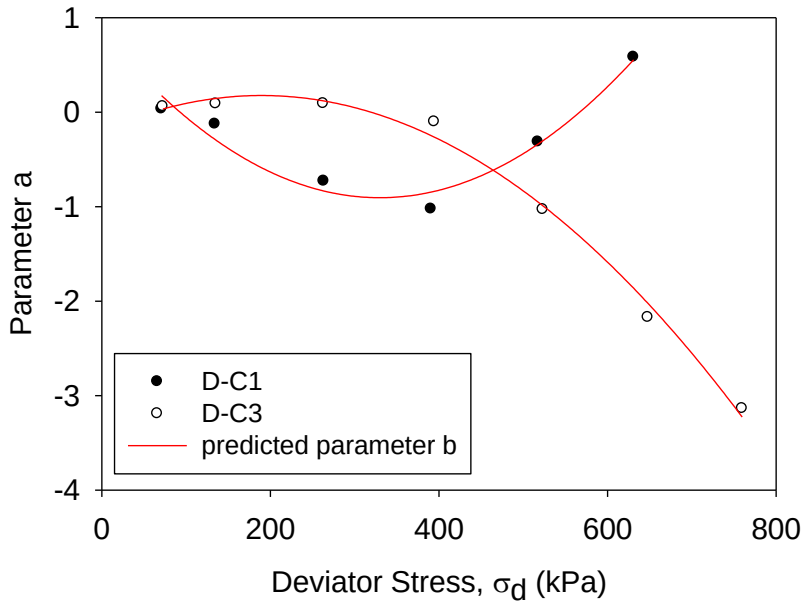

Figure 71. Parameter a of Barksdale's model at different σ_d for two samples

The parameter b for two crushed limestone samples are shown in Figure 74, and exponential growth with stirling model (Equation 22) relationship is specified to describe the relationship between the parameter b and the deviator stress.

$$b = k_4 + \frac{k_5 \cdot (e^{k_6 \cdot \sigma_d} - 1)}{k_6} \quad (22)$$

where: b = parameter a in Barksdale's model;

k_4, k_5, and k_6 = regression parameters; and

σ_d = deviator stress (kPa).

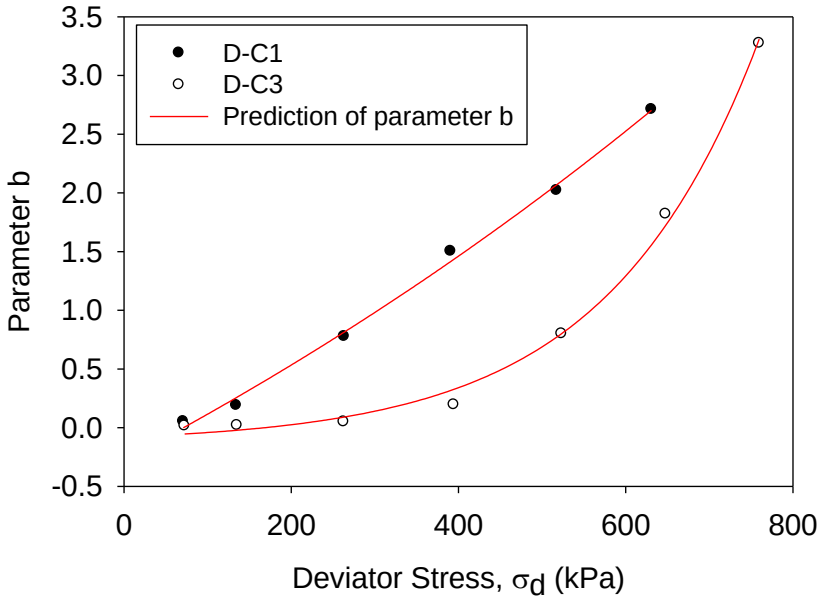

Figure 72. Parameter b of Barksdale's model at different σ_d for two samples

Based on the relationships between the parameters a and b of Barksdale's model and the deviator stresses, a modified model was proposed as (Equation 23):

$$\varepsilon_{1,p} = k_1 + k_2 \cdot \sigma_d + k_3 \cdot \sigma_d^2 + \left[k_4 + \frac{k_5 \cdot (e^{k_6 \cdot \sigma_d} - 1)}{k_6}\right] \cdot \log_{10}[N - 1000 \cdot (S - 1)] \quad (23)$$

where: $\varepsilon_{1,p}$ = accumulated permanent axial strain;

N = number of load cycles;

S = number of load sequences;

k_1, k_2, k_3, k_4, k_5, and k_6 = regression parameters; and

σ_d = deviator stress (kPa).

This modified model accounts for the effects of deviator stresses on permanent deformation. Moreover, this model is modified to fit the data points obtained in NCHRP 598 tests. This modified model is used to predict the accumulated permanent strain with increasing number of load cycles and deviator stresses on the two crushed limestone samples which were used for finding the relationship between the Barksdale's model regression parameters deviator stress (Figure 73). The good fits are shown in the figure, but the predicted permanent stains are much lower than the measured values. The reason could be the transitions of permanent strains between two load sequences are not explained by the

Barksdale's model. The parameters of modified model predicting accumulated permanent strain for two crushed limestone samples (Figure 73) are summarized in Table 40.

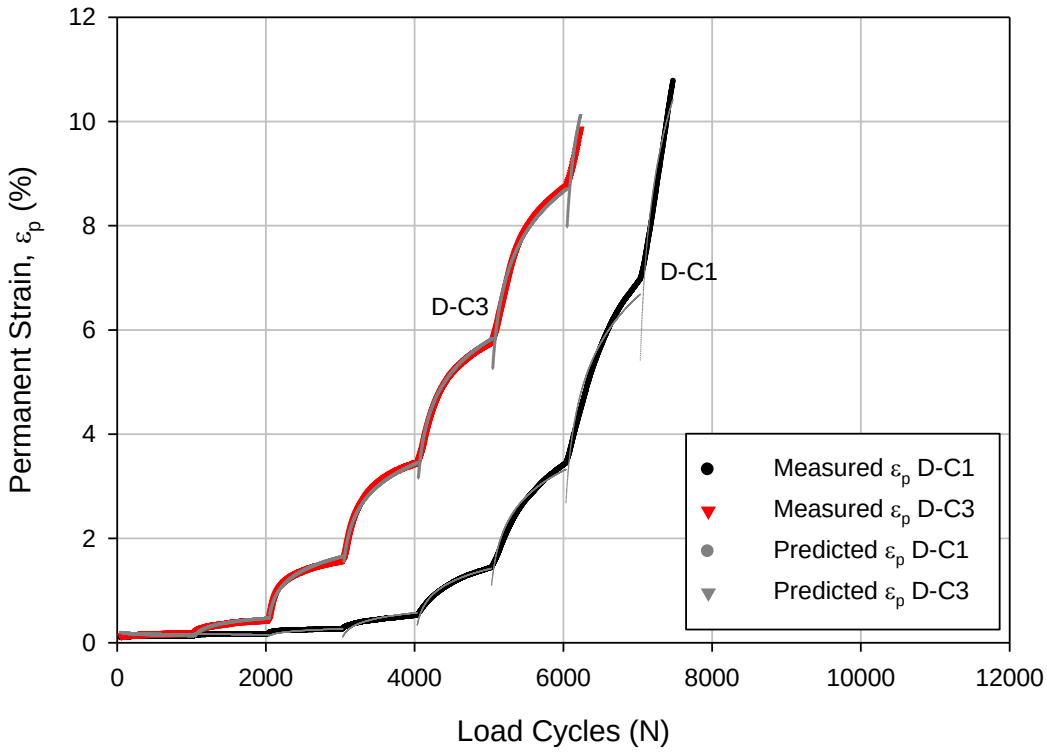

Figure 73. Predicting ε_p with increasing N using modified model on an NCHRP 598 ε_p test sample

Table 40. Modified model parameters for two crushed limestone samples

Parameters	D-C1	D-C3
k1	2.83E-01	1.15E+00
k2	-1.38E-04	-1.36E-02
k3	-4.68E-06	2.14E-05
k4	-8.08E-02	-3.71E-01
k5	3.33E-04	4.50E-03
k6	5.11E-03	2.98E-04
R2	9.97E-01	9.99E-01

The modified model is also used to predict the accumulated permanent strain for test No.D-C12, D-C24, and D-C36. However, the modified model does not provide good fit for these three tests especially for the D-C12 samples with 12.0% target F_{200} and 95.0% target RD. The large offset in the predicted values from the measure values indicates the model

regression parameters might also be affected by fines contents and relative densities. The predicted and measured permanent strains for the three samples are compared in Figure 74.

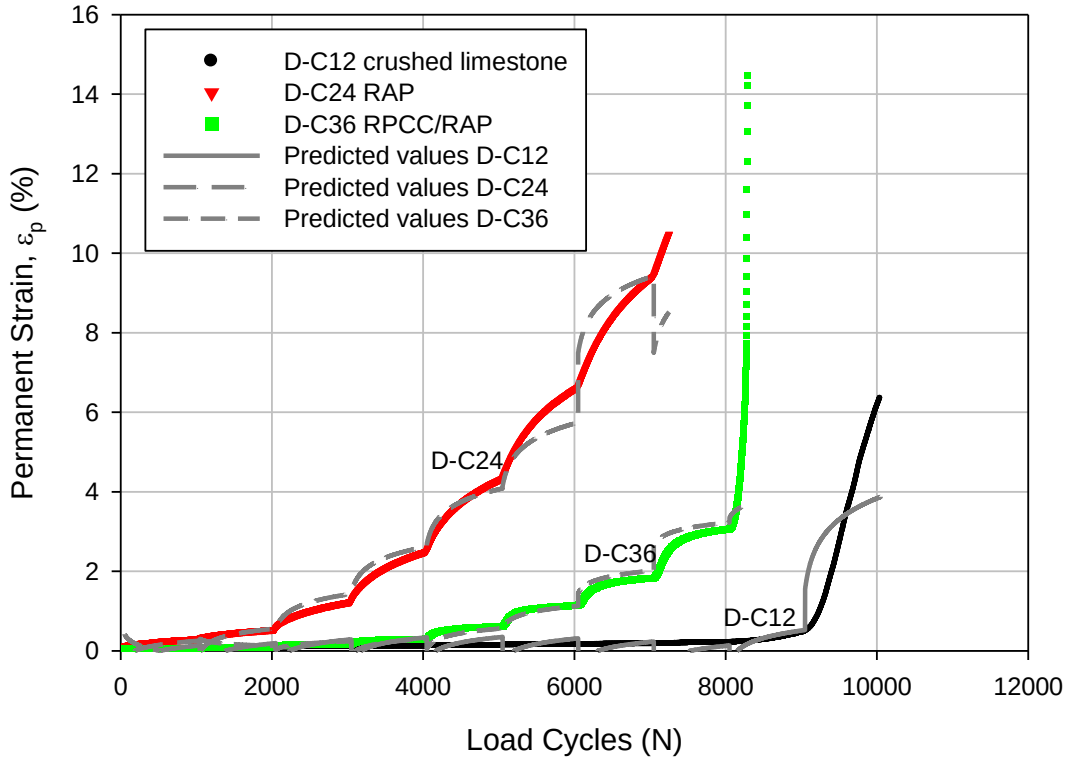

Figure 74. Predicting ε_p with increasing N using modified model on three NCHRP 598 ε_p test sample

The regression parameters of the modified model for the three samples (Figure 74) are listed in (Table 41).

Table 41. Modified model parameters for three materials samples

Parameters	D-C12	D-C24	D-C36
k1	-1.26E+00	-6.12E-01	1.92E+00
k2	1.17E-03	-2.93E-03	-1.15E-02
k3	-1.15E-06	1.13E-05	1.28E-05
k4	5.39E-15	1.96E-01	-8.76E-01
k5	2.52E-02	1.92E-03	7.59E-03
k6	4.37E-01	-5.89E-04	-5.75E-03
R2	8.03E-01	9.76E-01	8.15E-01

Breakage index

To quantify the degradation of aggregate particles due to sample compaction and ε_p test, BI was calculated for each ε_p test using Equation 24.

$$BI=\frac{A-B}{B} \quad (24)$$

where: BI= breakage index;

A=area between the particle size distribution curve of the original materials and after the permanent deformation test; and

B= area between the particle size distribution curve of the original materials and the 0% passing base line.

The breakage of particles was calculated based on the change in particle size distribution curves. In this study, the BI was calculated for each test sample to quantify the change in particle size due to both of sample compaction and ε_p test loading. The BI due to sample compaction was not calculated as result of the variance in particle size distribution among samples. The difference in the particle size distribution of the materials before and after the NCHRP 598 test on a crushed limestone sample are shown in Figure 75. The area between two particle size distribution curves of this crushed limestone sample is very small compared to the area below the particle size distribution curve to the reference line (0% passing).

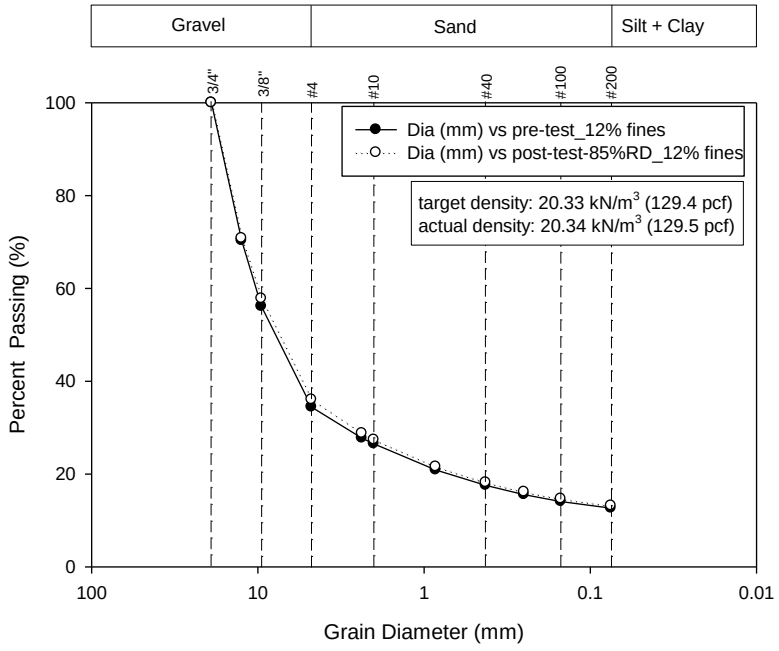

Figure 75. Gradation curves used for calculating BI for a crushed limestone sample

BI was calculated for each sample for NCHRP 598 test. Crushed limestone samples have BI less than 4.5% and most samples have positive BI values. RAP samples have BI varied in large approximate range of -7 to +2%. The large negative values of BI for RAP samples might be due to the regroup of the particles. The large applied force in the NCHRP tests pushed the asphalt coating into the voids and the asphalt coating binds the small particles to the large particles and forms larger particles. The sample materials were broken down by hand force and oven-dried for mechanical sieve analysis. When the sample cools to the room temperature, the asphalt binder hardened from the relative soft state and larger particles can resist force from mechanical sieve analysis to break down. RPCC/RAP samples have BI varied in the approximate range from -2 to +4%. The negative values might be due to regroup of the particles and variance between the materials sample. Because the material used to determine the pre-test particle size distribution is a sample from a large amount of materials and the material used to determine the post-test particle size distribution is another sample from the same materials source. However, the variance of particles in sampling is not able be fully eliminated. Variance in sampling might has larger effect on the samples with low BI. The BI for all NCHRP 598 test samples are plotted with the actual fines contents of the samples () and the detailed data are listed in Figure 76.

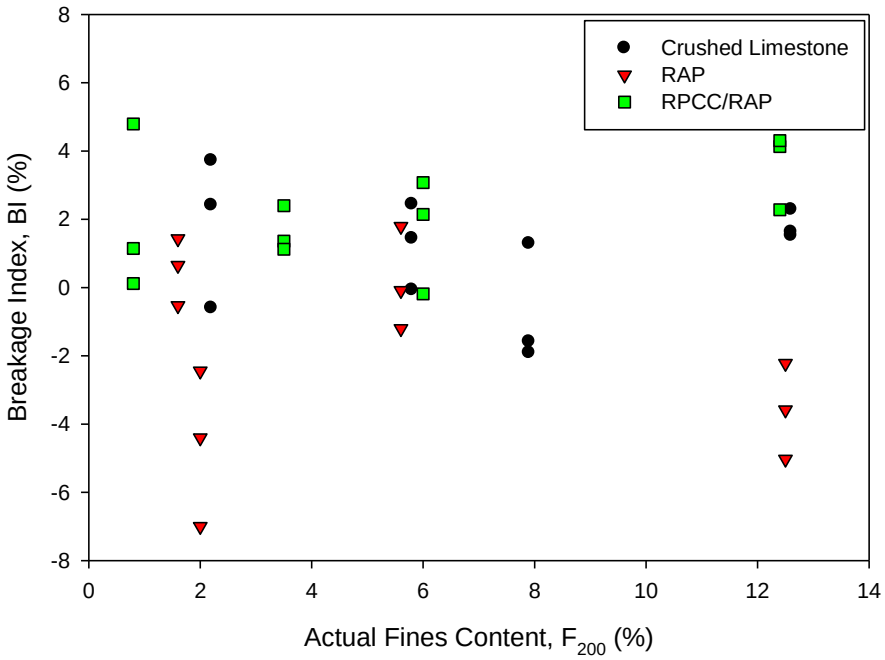

Figure 76. BI for all NCHRP 598 test samples

Table 42. BI summary for all NCHRP 598 ε_p test samples

Materials	Test No.	Fines content (%)			BI (%)
		Target	Pre-test	Post-test	
Crushed Limestone	D-C1	0.0	2.2	3.0	2.4092
	D-C2	6.0	5.8	6.6	1.4394
	D-C3	natural	7.9	9.6	-1.5901
	D-C4	12.0	12.6	13.2	1.6270
	D-C5	0.0	2.2	2.8	-0.5998
	D-C6	6.0	5.8	6.3	-0.0711
	D-C7	natural	7.9	9.8	-1.9122
	D-C8	12.0	12.6	12.9	2.2822
	D-C9	0.0	2.2	3.1	3.7179
	D-C10	6.0	5.8	6.6	2.4385
	D-C11	natural	7.9	10.3	1.2880
	D-C12	12.0	12.6	12.8	1.5195
RAP	D-C13	0.0	1.6	2.1	-0.5312
	D-C14	natural	2.0	2.2	-7.0029
	D-C15	6.0	5.6	6.4	-0.0873
	D-C16	12.0	12.5	10.1	-3.5844
	D-C17	0.0	1.6	1.6	0.6453
	D-C18	natural	2.0	2.4	-2.4497
	D-C19	6.0	5.6	5.4	-1.2036
	D-C20	12.0	12.5	10.0	-2.2259
	D-C21	0.0	1.6	2.0	1.4263
	D-C22	natural	2.0	2.5	-4.4030
	D-C23	6.0	5.6	6.1	1.7918
	D-C24	12.0	12.5	8.7	-5.0307
RPCC/RAP	D-C25	0.0	0.8	1.4	4.7950
	D-C26	natural	3.5	3.7	1.3578
	D-C27	6.0	6.0	6.3	3.0762
	D-C28	12.0	12.4	12.2	2.2793
	D-C29	0.0	0.8	1.4	1.1468
	D-C30	natural	3.5	3.5	1.1242
	D-C31	6.0	6.0	6.7	2.1408
	D-C32	12.0	12.4	13.2	4.1308
	D-C33	0.0	0.8	1.4	0.1188
	D-C34	natural	3.5	3.5	2.3974
	D-C35	6.0	6.0	6.1	-0.1834
	D-C36	12.0	12.4	13.3	4.3033

Resilient Modulus

Results related to resilient modulus (M_r) are presented in four sections, significance of samples characteristics, resilient moduli prediction, assessment of possible errors in M_r tests, and unconsolidated undrained shear strength.

Resilient modulus tests were conducted on crushed limestone, RAP, and RPCC/RAP materials for studying the resilient modulus behavior of different UGMs. Fines contents and relative densities are varied for studying the effects on the resilient modulus behavior of all the UGMs. M_r values were directly calculated by averaging the system generated data of last five cycles in each load sequence. Stress levels and number of load cycles are same as AASHTO T-307 (99) specified load sequences for base/subbase materials that were summarized in Methods chapter. Appendix B provides resilient modulus sample calculations.

The actual moisture contents (w) of all samples are within ±0.2% from the target moisture content of each material. The actual RD of crushed limestone samples are less than 7% RD, of RAP samples are less than 4% RD, and of RPCC/RAP samples are less than 11% RD different from the target RD. The crushed limestone samples were numbered from M1 to M12, the RAP samples were numbered from M13 to M24, the RPCC/RAP samples were numbered from M25 to M36 and the target and the actual values of all samples characteristics were also summarized in Table 43 for crushed limestone samples, in Table 44 for RAP samples, and in Table 45 for RPCC/RAP samples.

Table 43. The target and actual characteristics of M_r tests crushed limestone samples

Test No.	F_{200} (%)		w (%)		RD (%)		γ_d (kN/m^3)	
	Target	Actual	Target	Actual	Target	Actual	Target	Actual
M1	0.0	2.2	2.3	2.4	85.0	86.6	18.99	19.06
M2	6.0	5.8		2.4		86.2	19.47	19.52
M3	natural	7.9		2.5		87.4	17.65	17.68
M4	12.0	12.6		2.5		85.5	20.33	20.35
M5	0.0	2.2		2.2	90.0	92.1	19.19	19.28
M6	6.0	5.8		2.4		91.2	19.70	19.76
M7	natural	7.9		2.5		96.3	17.71	17.78
M8	12.0	12.6		2.5		90.4	20.55	20.57
M9	0.0	2.2		2.2	95.0	97.5	19.40	19.50
M10	6.0	5.8		2.4		96.2	19.95	20.01
M11	natural	7.9		2.4		101.0	17.76	17.83
M12	12.0	12.6		2.5		95.7	20.78	20.81

Table 44. The target and actual characteristics of M_r tests RAP samples

Test No.	F_{200} (%)		w (%)		RD (%)		γ_d (kN/m^3)	
	Target	Actual	Target	Actual	Target	Actual	Target	Actual
M13	0.0	1.6	2.9	3.0	85.0	86.0	15.75	15.78
M14	natural	2.0		2.7		88.6	14.92	15.01
M15	6.0	5.6		2.9		86.2	17.01	17.01
M16	12.0	12.5		2.9		86.1	17.62	17.67
M17	0.0	1.6		2.7	90.0	92.4	15.89	15.96
M18	natural	2.0		2.8		93.3	15.05	15.13
M19	6.0	5.6		2.9		91.6	17.14	17.20
M20	12.0	12.5		2.8		91.6	17.81	17.87
M21	0.0	1.6		2.9	95.0	96.3	16.03	16.07
M22	natural	2.0		2.8		98.1	15.17	15.25
M23	6.0	5.6		2.9		96.3	17.30	17.36
M24	12.0	12.5		2.9		96.3	18.00	18.05

Table 45. The target and actual characteristics of M_r tests RPCC/RAP samples

Test No.	F_{200} (%)		w (%)		RD (%)		γ_d (kN/m^3)	
	Target	Actual	Target	Actual	Target	Actual	Target	Actual
M25	0.0	0.8	6.0	6.0	85.0	86.8	15.26	15.31
M26	natural	3.5		6.2		87.3	16.12	16.17
M27	6.0	6.0		6.5		84.3	16.77	16.73
M28	12.0	12.4		6.2		85.5	17.54	17.56
M29	0.0	0.8		5.9	90.0	92.5	15.41	15.48
M30	natural	3.5		7.7		79.1	16.22	16.01
M31	6.0	6.0		5.9		91.7	16.96	17.03
M32	12.0	12.4		6.0		91.2	17.74	17.79
M33	0.0	0.8		5.8	95.0	99.1	15.56	15.69
M34	natural	3.5		5.7		102.5	16.32	16.47
M35	6.0	6.0		6.2		95.6	17.17	17.19
M36	12.0	12.4		6.2		95.2	17.95	17.96

The average resilient modulus value of last five cycles in each load sequence was calculated for all load sequences and plotted with load sequence number for all M_r tests conducted on each material separately. The M_r values are within the range of 50 to 1,100 MPa for crushed limestone samples (Figure 77). The M_r values are within the range of 50 MPa to 700 MPa for RAP samples (Figure 78). The M_r values are within the range of 50 MPa to 600 MPa for RPCC/RAP samples (Figure 79).

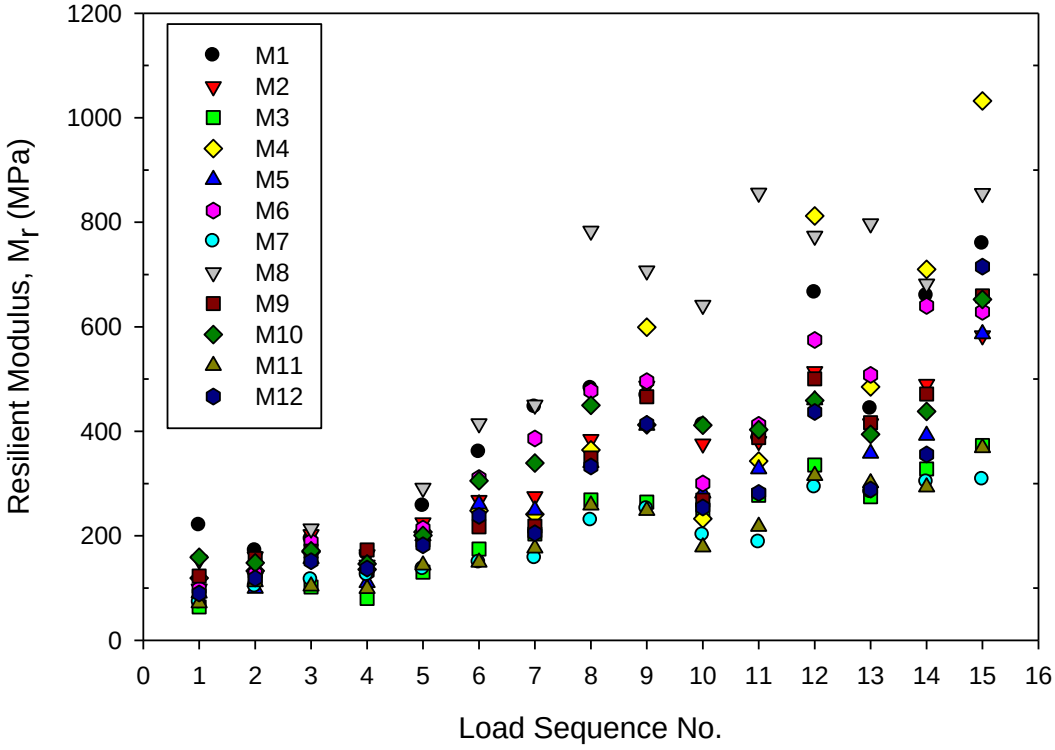

Figure 77. Resilient moduli summary for M_r tests on crushed limestone samples

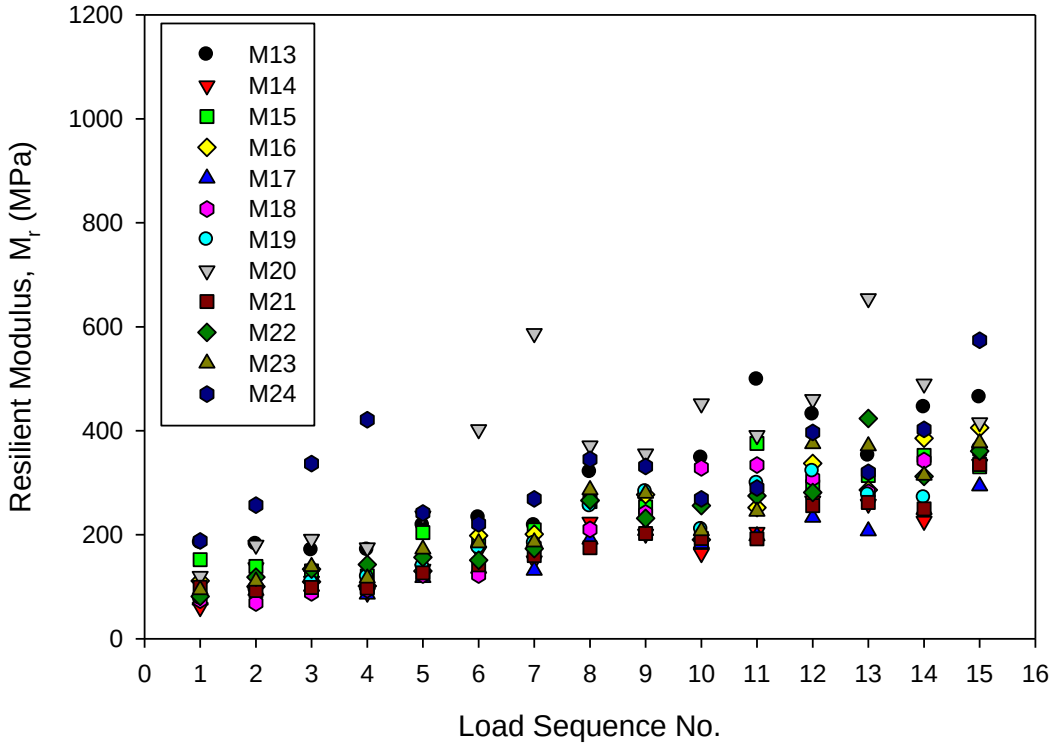

Figure 78. Resilient moduli summary for M_r tests on RAP samples

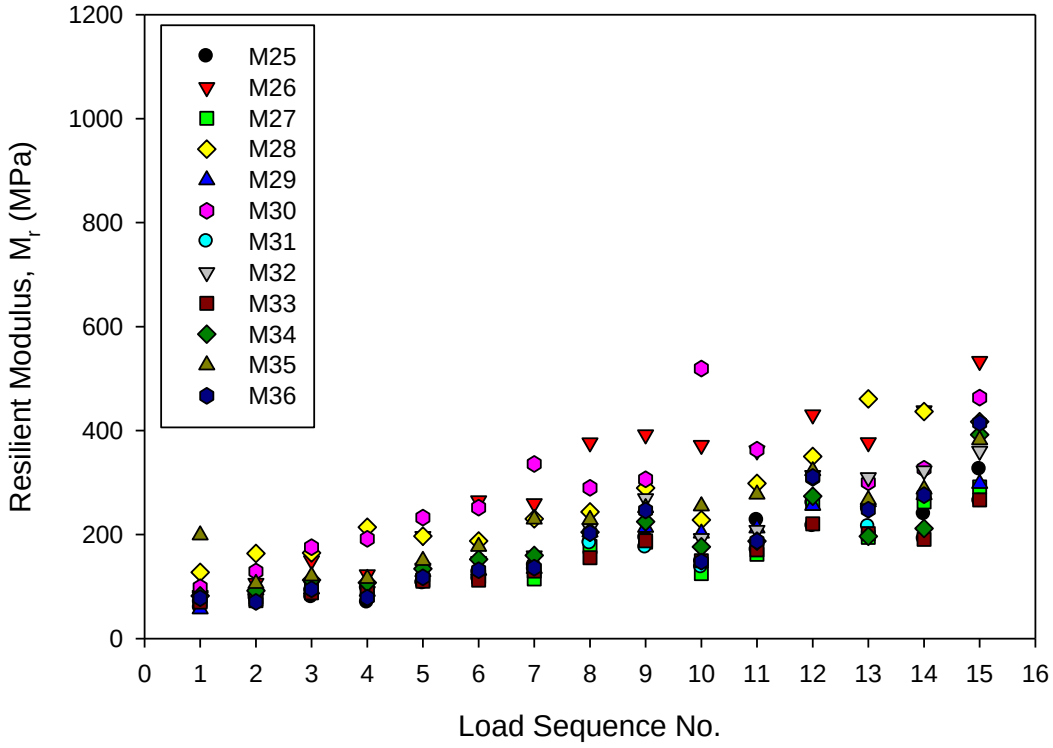

Figure 79. Resilient moduli summary for M_r tests on RPCC/RAP samples

Significance of samples characteristics

The first important factor is stress level which many researchers (Morgan 1966; Hicks and Monismith 1971; Brown and Hyde 1975; Sweere 1990; Kolisoja 1997; Wolfe 2011) concluded have significant effect on resilient modulus of UGMs. Fines contents, relative densities, and materials type are three important samples characteristics that were also identified in the literature review to have effect on resilient modulus in the literature. This section discusses the significance of stress level, relative density, fines content, and material type on affecting resilient modulus.

Stress level

Several stress levels of confining pressures (σ_d) and deviator stresses (σ_c) were designed in the AASHTO T307-99 M_r tests. These stresses were selected to represent the stress states that the UGMs likely to be experienced in the in situ pavement foundation structures.

The variance of M_r values at each load sequence is higher in the load sequences where high stress levels were applied than the load sequences where the low stress levels were applied. Two outliers are found as sample M20 and M24 that lead to increase in variance of

M_r values at low stress levels for RAP materials (Figure 78). Although the trend of increasing M_r could be obtained at higher stress levels are observed, the M_r values are not continuously increasing with increasing stress levels. This finding is not fully agreed the conclusion that reported by Sweere (1990) and Kolisoja (1997) that Mr increases rapidly with increasing sum of principal stresses and confining pressure and the conclusion that drawn by Wolfe (2011) that resilient moduli of granular materials increased with load sequences. Because M_r values are observed to decrease when increasing σ_d and constant σ_c were applied. Morgan (1996) also reported that the M_r slightly decreases with increasing σ_d and constant σ_c, but continuous decreases in M_r values are not observed in this study. M_r values are not linearly related to the sum of deviator stress and confining pressure. Stress levels have significant effects on the resilient modulus for UGMs while the statistical analysis was conducted on each material separately (Table 46).

Table 46. Statistical analysis on significance of RD affecting Mr values

Materials	Degree of Freedom	Sum of Squares	F Ratio	Probability >F	R^2	Significant ?
Crushed limestone	14	4141510.1	19.5378	<0.0001	0.6237	Yes
RAP		1281584.6	14.7797	<0.0001	0.5564	Yes
RPCC/RAP		1163992.0	19.3927	<0.0001	0.6220	Yes

Relative density

Generally, the density increases in granular materials would cause the base/subbase layer to be stiffer and resilient deformation subjected to repeated load to be reduced. This indicates that higher densities generally result in higher resilient moduli at the same stress levels. However, the literature review does not conclude a clear effect of density on resilient response.

Four randomly selected examples for the three tested material are shown in this section and the entire results could be found in Appendix B. The M_r values are different for the samples with different relative density, but no clear relationship between the M_r and RD could be drawn. Because M_r values of the samples at different relative densities reach the maximum at different load sequences.

For example (Figure 80), the 96.2% RD sample has maximum M_r value at sequence 15 ($\sigma_B \approx 0.71$), the 91.2% RD sample has maximum M_r value at sequence 7 ($\sigma_B \approx 0.3$), and the 86.2% RD sample has maximum M_r value at sequence 1 ($\sigma_B \approx 0.09$). Moreover, the 90.4% RD sample nearly has the highest M_r values for all load sequences except the last three compared to other two samples (85.5% and 95.7% RD) of this crushed limestone material with 12.6% F_{200} (Figure 81). However, the 86.0% RD sample has the highest M_r values for all load sequences compared to other two samples (92.4% and 98.1% RD) of this RAP material with 1.6% F_{200} (Figure 82). The same observation that 85.5% RD sample has the highest M_r values can be concluded for the RPCC/RAP materials with 12.4% F_{200} (Figure 83). However, the higher M_r cannot be specified between the sample with 91.2% and 95.2% RD samples.

Therefore, the same conclusion is not bale to be drawn for all samples. This confirmed the conclusion that reported by Thom and Brown (1989) and Wolfe (2011) that the effect of density is relatively insignificant and the M_r values are not clearly influenced by the density alone. The statistical analysis show that the relative density does not have significant effect on M_r values for all three samples and the statistical analysis was conducted separately for each material (Table 47).

Table 47. Statistical analysis on significance of RD affecting Mr values

Materials	Degree of Freedom	Sum of Squares	F Ratio	Probability >F	R^2	SIG?
Crushed limestone	2	123784.57	1.6812	0.1891	0.0186	No
RAP		685.49	0.0263	0.9740	0.0003	No
RPCC/RAP		41839.50	2.0239	0.1352	0.0224	No

Notes: SIG is abbreviation for significant

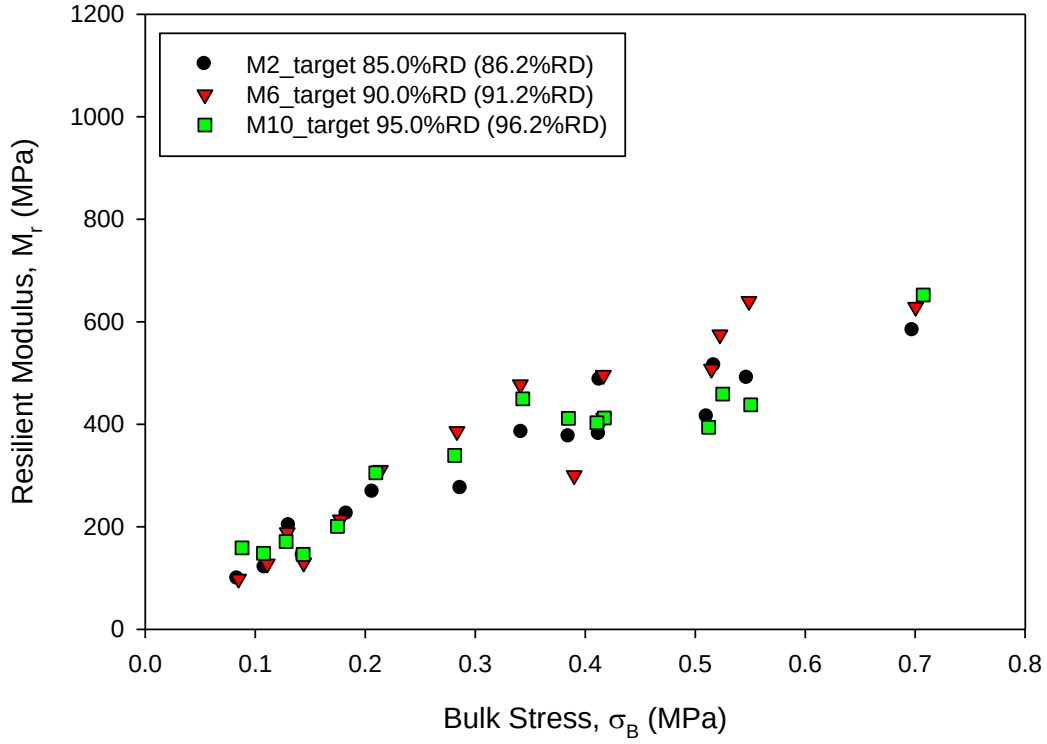

Figure 80. Comparison of M_r at reconstituted 5.8% F_{200} for crushed limestone samples

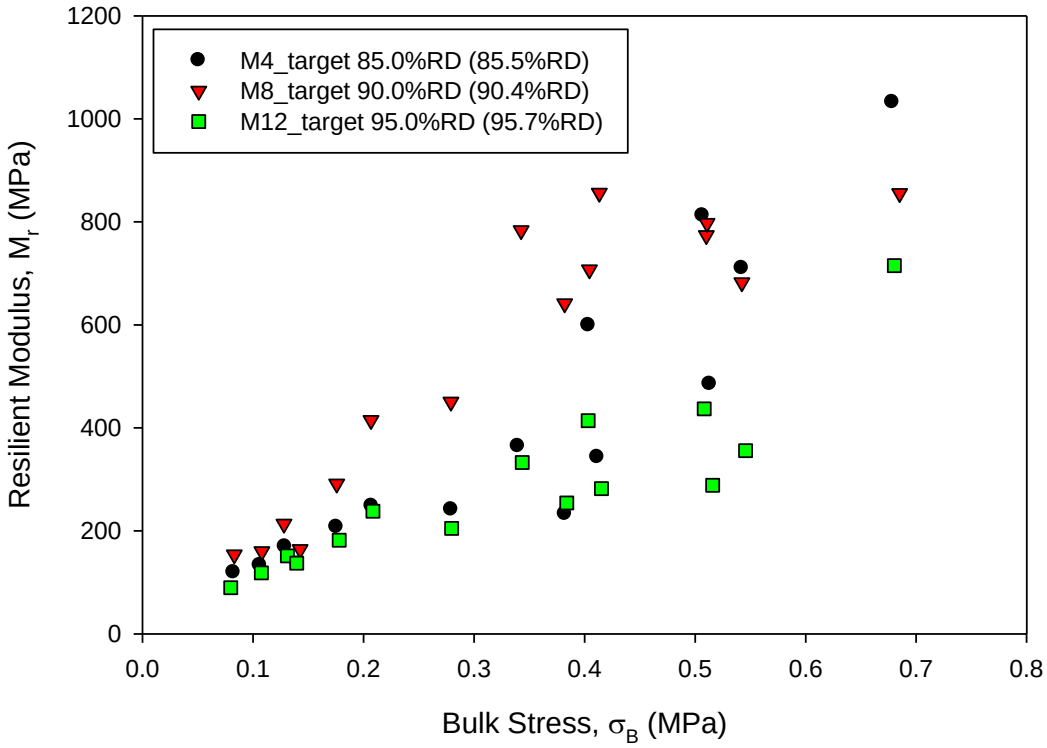

Figure 81. Comparison of M_r at reconstituted 12.6% F_{200} for crushed limestone samples

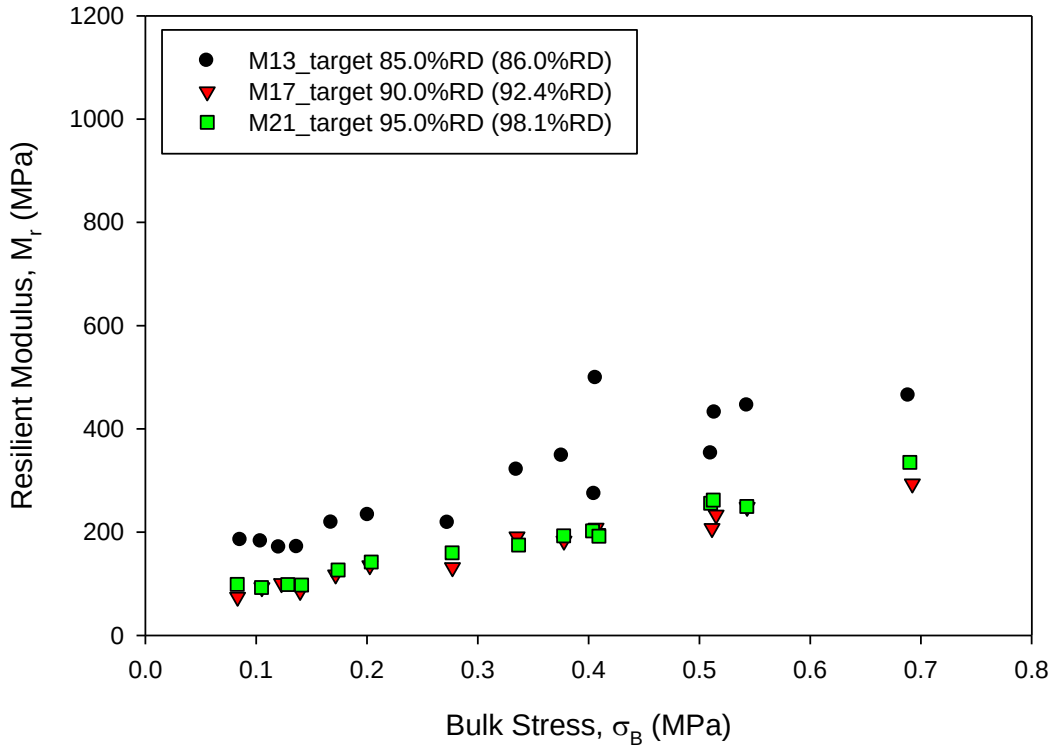

Figure 82. Comparison of M_r at reconstituted 1.6% F_{200} for RAP samples

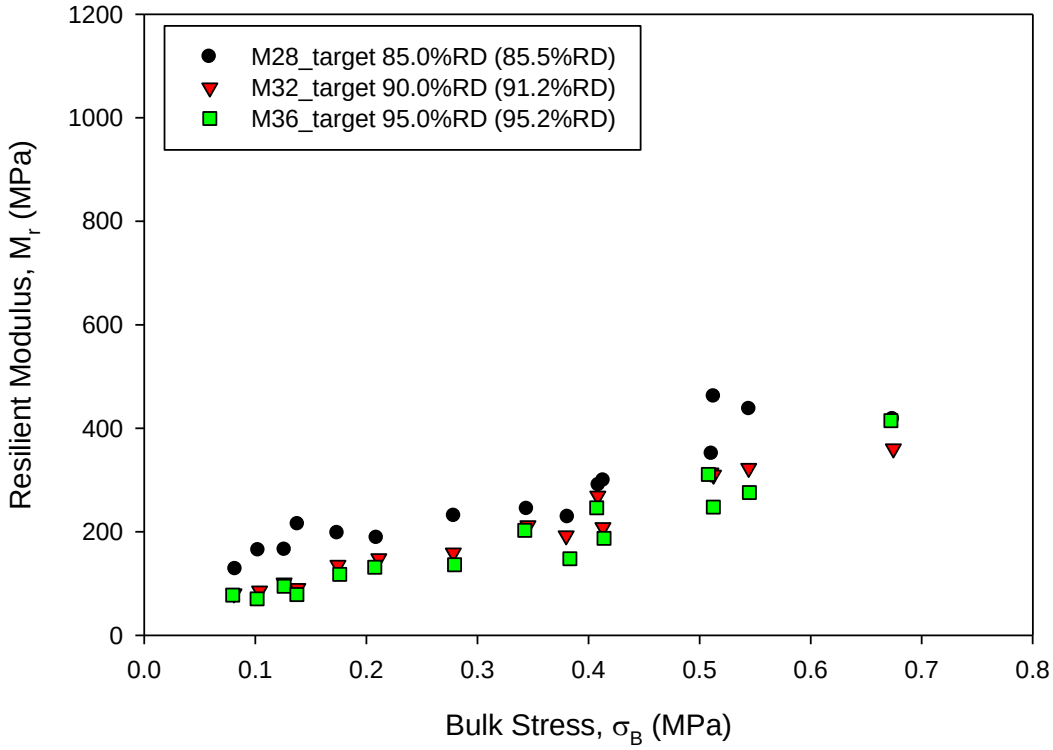

Figure 83. Comparison of M_r at reconstituted 12.4% F_{200} for RPCC/RAP samples

Fines content

Fines content is not a fully understood factor that could affect resilient modulus values in the literature review. Measured M_r values are not indicating a good relationship to the fines contents in this study. However, the M_r data points are plotted for the samples with varied fines content at the same target relative densities to learn the effect of fines content. Although no consistent conclusion could be drawn to define the linear relationship between fines content and resilient moduli, the difference in M_r values between samples with varied fines contents are clear.

The natural fines content samples always have large difference from the three target fines content samples, so the target fines content samples are compared separately from the natural fines content samples. The samples with about 12.0% fines content have the largest M_r values in some examples, like 85.0% (Figure 84) and 90.0% (Figure 85) target RD crushed limestone samples, 90.0% (Figure 88) and 95.0% (Figure 89) target RD RAP samples, and all RPCC samples. This finding is conflict with the conclusion reported by Thom and Brown (1987), Kamal et al. (1993), and Kancherla (2004) that the resilient modulus generally decreases with increasing fines content. However, Hicks and Monismith (1971) observed some increase in resilient modulus with increasing fines content for fully crushed aggregates and confirmed the findings from some samples in this study. Relationships between 6.0% target F_{200} and 0.0% target F_{200} affecting M_r values is not determined. The 0.0% target F_{200} samples could have the higher M_r values than the 6.0% target F_{200} samples for some materials, like the 85.0% target RD crushed limestone materials (Figure 84), 85.0% target RD RAP materials (Figure 84), and 85.0% target RD RPCC/RAP materials (Figure 90). The 6.0% target F_{200} samples could have the higher M_r values than the 0.0% target F_{200} samples for some materials, like the 90.0% (Figure 85) and 95.0% (Figure 86) target RD crushed limestone materials, 95.0% target RD RAP materials (Figure 89), and 90.0% (Figure 91) and 95.0% (Figure 92) target RD RPCC/RAP materials.

These findings indicate the fines content have effect on M_r values and correlated to relative densities. The resilient modulus generally increases with increasing fines content when high relative densities (95.0% RD) are reached and the lowest resilient modulus generally reached at 6.0% fines content when low relative densities (85.0%RD) are reached.

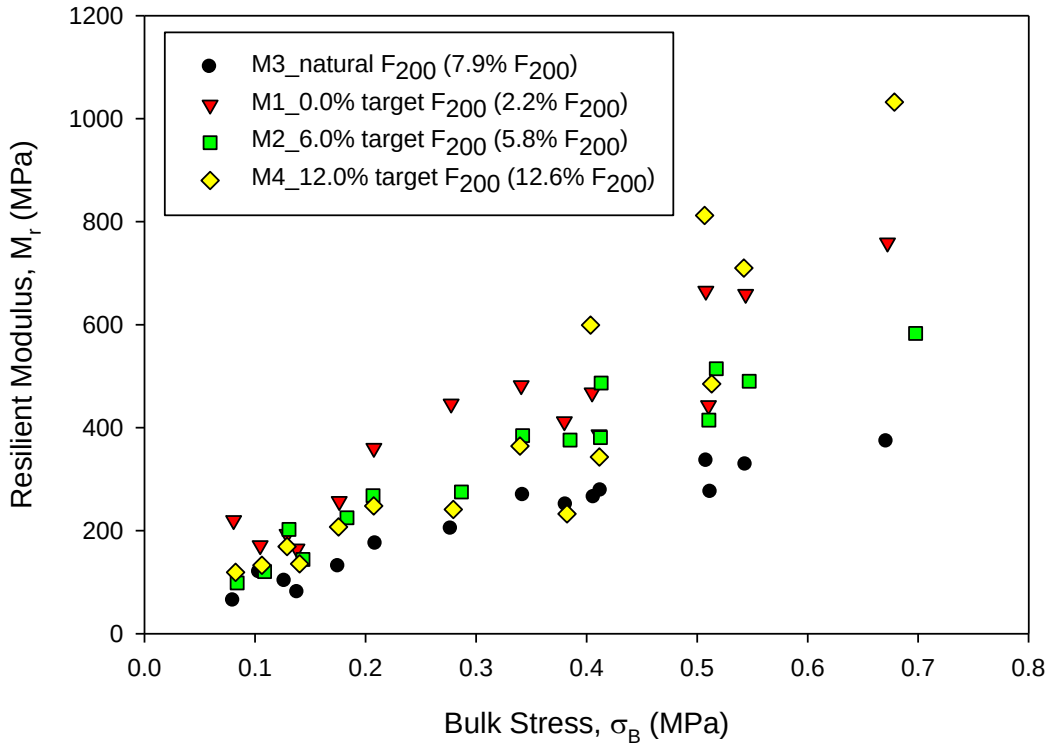

Figure 84. Comparison of M_r at 85% RD for crushed limestone samples

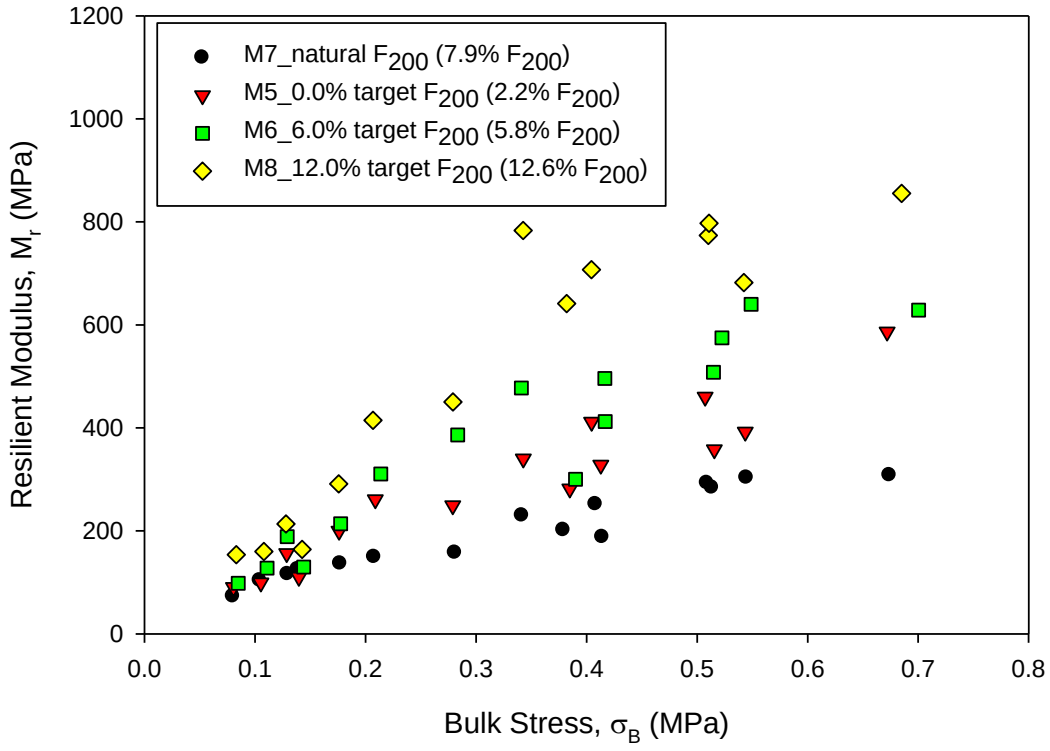

Figure 85. Comparison of M_r at 90% RD for crushed limestone samples

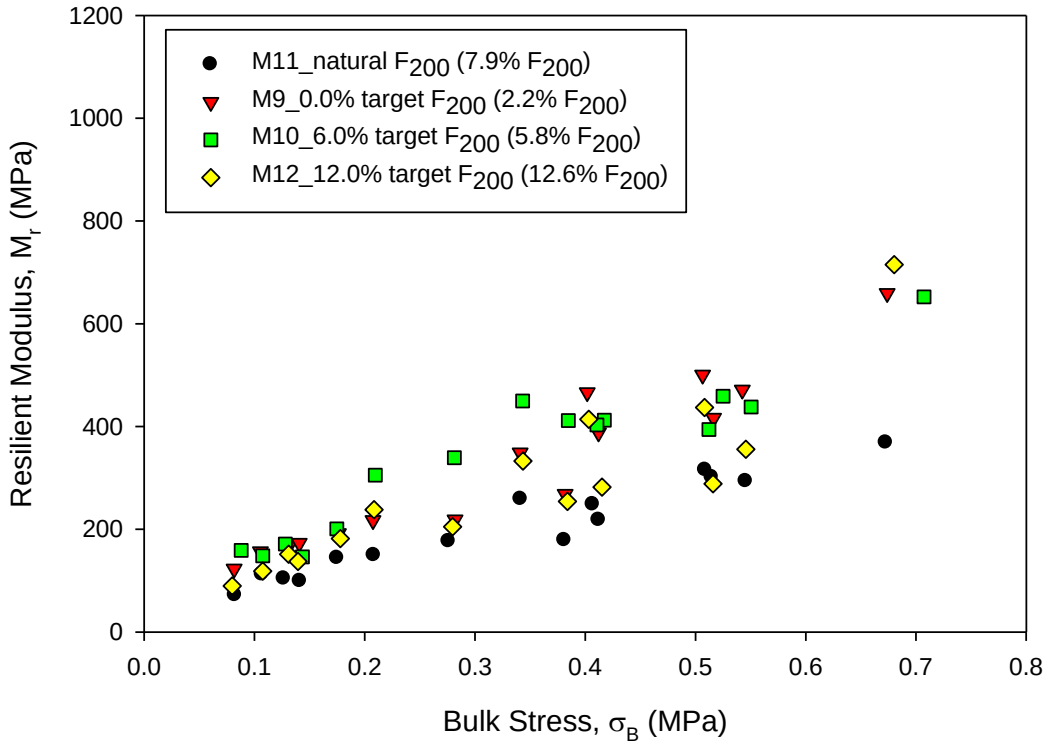

Figure 86. Comparison of M_r at 95% RD for crushed limestone samples

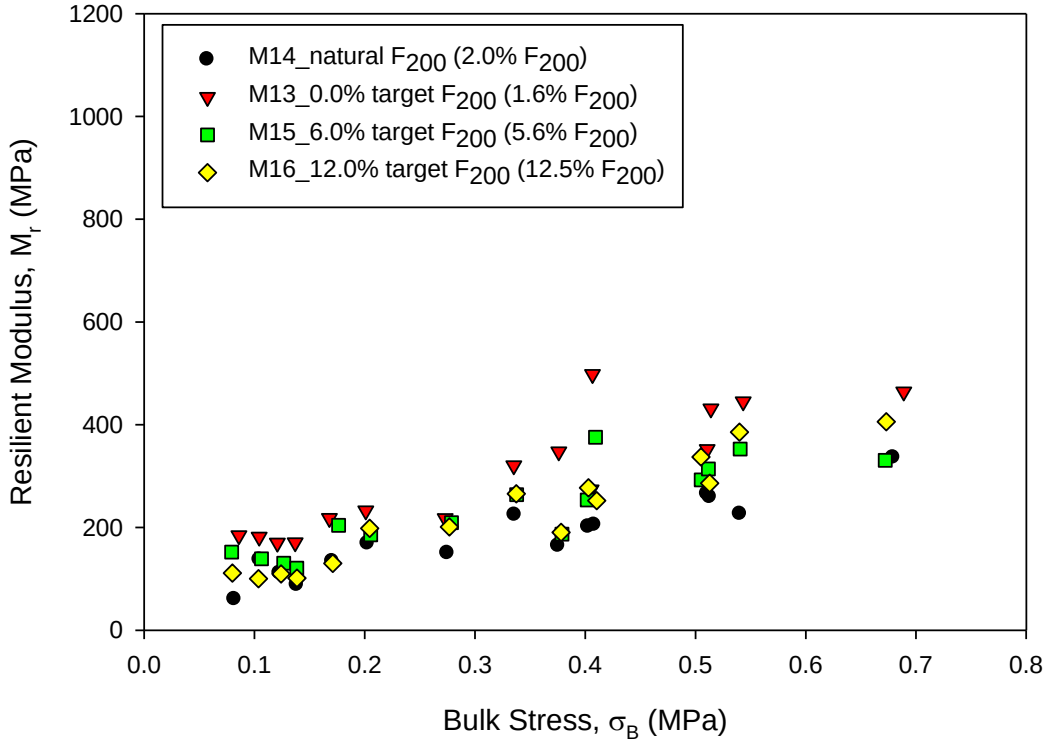

Figure 87. Comparison of M_r at 85% RD for RAP samples

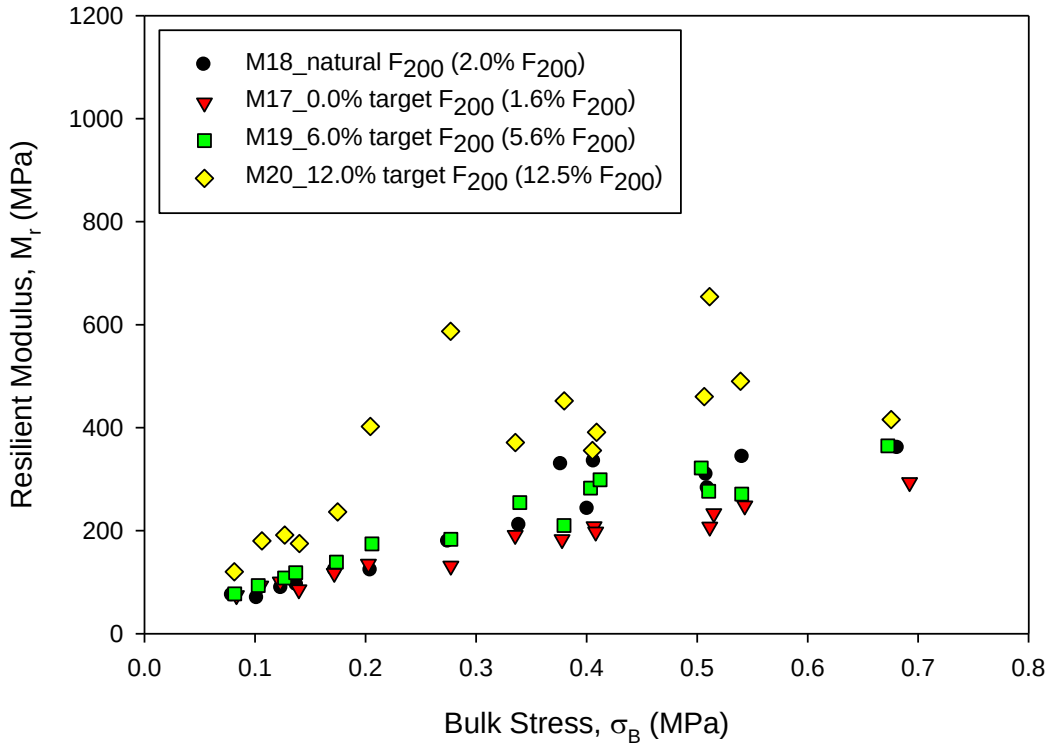

Figure 88. Comparison of M_r at 90% RD for RAP samples

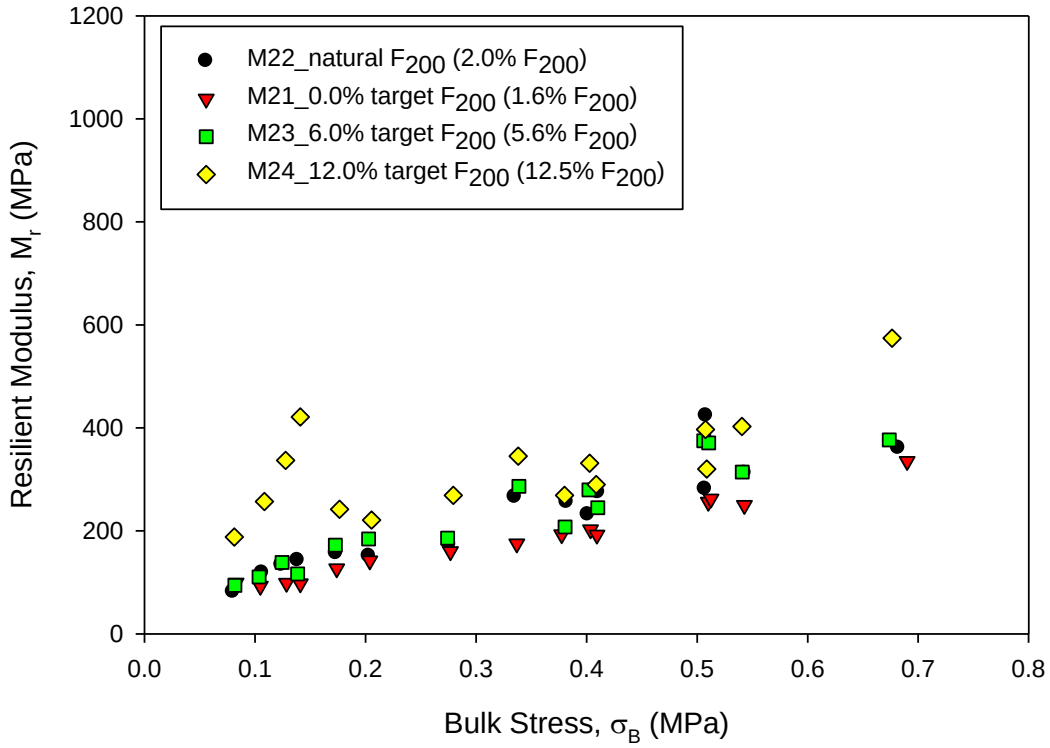

Figure 89. Comparison of M_r at 95% RD for RAP samples

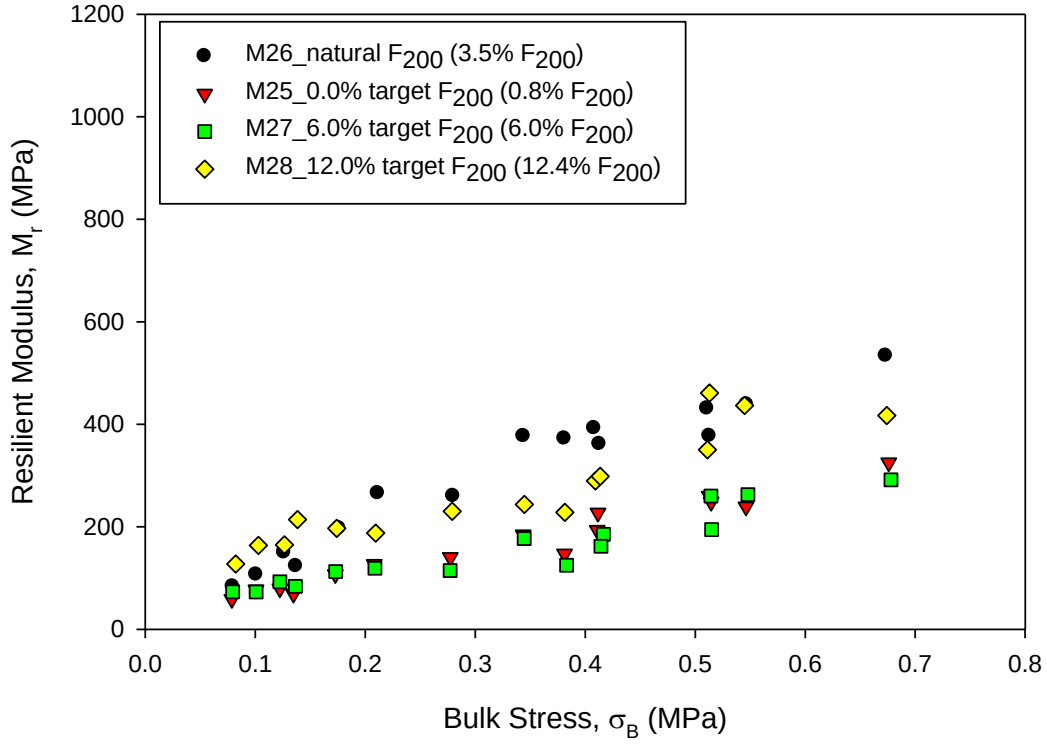

Figure 90. Comparison of M_r at 85% RD for RPCC/RAP samples

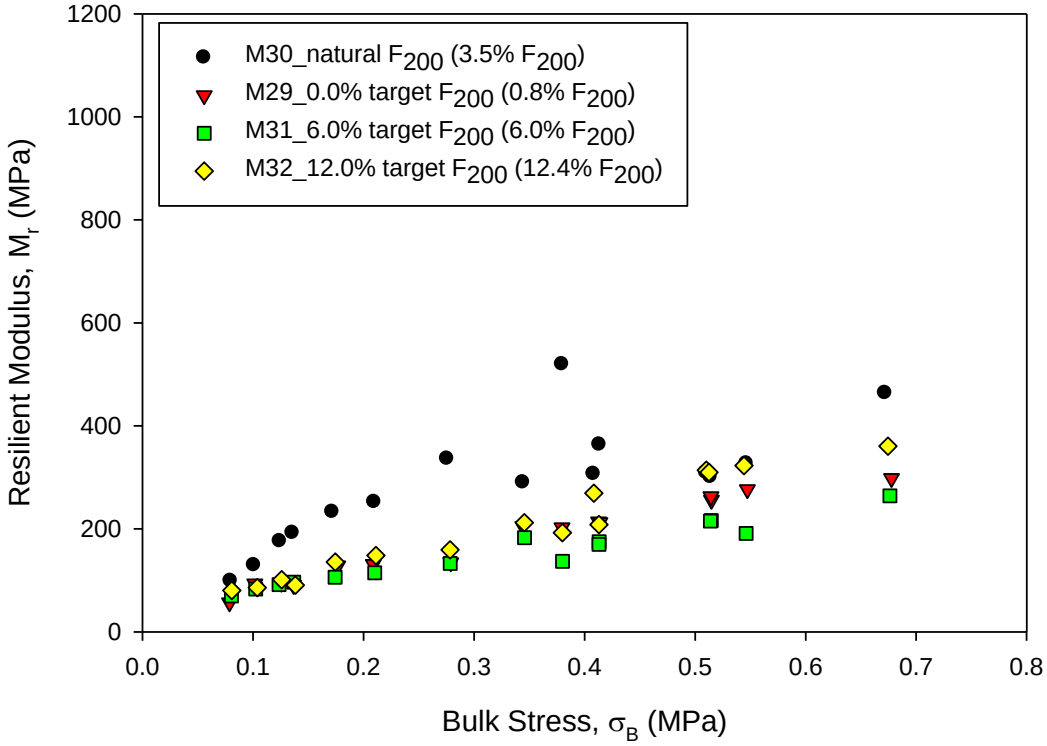

Figure 91. Comparison of M_r at 90% RD for RPCC/RAP samples

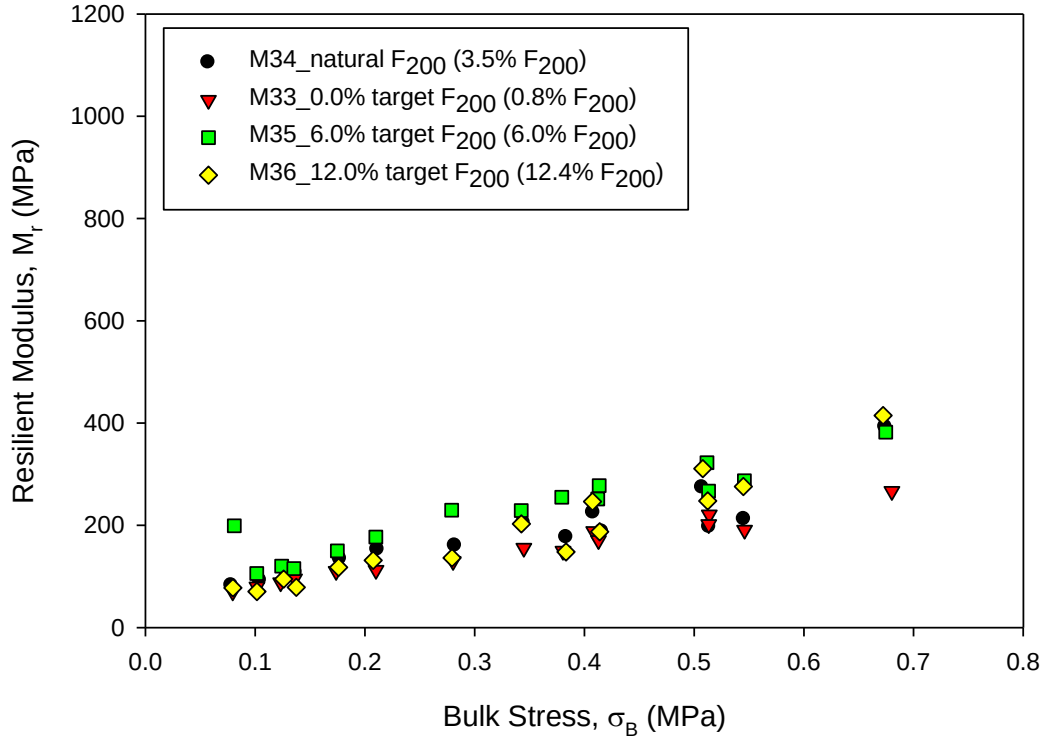

Figure 92. Comparison of M_r at 95% RD for RPCC/RAP samples

Statistical analyses were separately conducted on each material to determine the significance of fines content affecting resilient modulus values. All four different fines content were used for the statistical analyses. The statistical analysis results proved that fines content has significant effect on resilient modulus and the statistical analyses were performed separately for each material (Table 48).

Table 48. Statistical analysis for significance of F_{200} affecting M_r values

Materials	Degree of Freedom	Sum of Squares	F Ratio	Probability >F	R^2	Significant ?
Crushed limestone	3	927597.32	9.5268	<0.0001	0.1397	Yes
RAP		276369.63	7.9981	<0.0001	0.1200	Yes
RPCC/RAP		229746.04	8.2103	<0.0001	0.1228	Yes

Material type

The resilient modulus tests results shows the crushed limestone has the highest M_r values while RAP and RPCC have similar M_r values. The reason could be that crushed limestone

which contain angular to subangular shape particles spread load better than the recycled materials which always have coating materials (e.g., asphalt binder, cement hydration products) on the particles surface. Hicks (1970), Barksdale and Itani (1989) and Thom and Brown (1989) all reported that angular crushed aggregates have higher M_r values than round uncrushed gravels. Bennert et al. (2000) also studied the resilient modulus of RAP and RPCC and concluded similar values for these two materials up to 600 MPa which is close to the values obtained for the RAP and RPCC/RAP materials tested in this study.

The significance of material types, RD, and F_{200} affecting the M_r values of UGMs were concluded by using the statistical method. In order to conduct the statistical analyses, the samples with natural fines content were excluded from the analyses. The natural F_{200} of each material were varied in the range of 40% to 75% so the natural F_{200} is not a fixed factor in the analysis on all samples. The conclusion from the statistical analysis on all samples agreed with the conclusion from the statistical analysis on each material. RD is concluded as a factor insignificantly affecting M_r of UGMs while it ranges from 80% to 95%. F_{200} is concluded as a factor significantly affecting M_r of UGMs while it ranges from 0% to 12%. Moreover, material type is concluded as a factor significantly affecting M_r of UGMs when the crushed limestone, RAP, and RPCC/RAP were studied. The statistical analysis that was performed for all samples except the samples with natural F_{200} determined the significance of each factor (Table 49).

Table 49. Statistical analysis summary for significance of F_{200}, RD, and materials type affecting M_r of all samples

Factors	Degree of Freedom	Sum of Squares	F Ratio	Probability >F	R^2	SIG?
Material type	2	2126319.2	51.1181	<0.0001	0.2028	Yes

Notes: SIG is abbreviation for significant

Resilient modulus prediction model

Resilient moduli data are used to determine regression coefficients (k values) for finite element analysis or to determine a single resilient modulus value to indicate the stiffness of pavement foundation support materials in current structural pavement design. The National Highway Cooperative Research Program (NCHRP) Project 1-28A (2004a) suggested that a

representative resilient modulus value could be determined using the universal model (Equation 25) with cyclic stress of 103.4 kPa and confining pressure of 34.5 kPa for granular base/subbase materials. The cyclic stress is determined using the maximum applied stress minus the contact stress (the minimum applied stress).

$$M_r = k_1 P_a \left(\frac{\sigma_B - 3k_6}{P_a}\right)^{k_2} \left(\frac{\tau_{oct}}{P_a} + k_7\right)^{k_3} \quad (25)$$

where: P_a = atmospheric pressure (MPa);

τ_{oct} = octahedral shear stress (MPa) $= \frac{\sqrt{(\sigma_1-\sigma_2)^2+(\sigma_2-\sigma_3)^2+(\sigma_3-\sigma_1)^2}}{3}$;

σ_B= bulk stress (MPa) = $\sigma_1 + \sigma_2 + \sigma_3$;

σ_1, σ_2, σ_3 = principal stresses (MPa); and

k_1, k_2, k_3, k_6, k_7 = regression coefficients.

In the NCHRP (2004a) suggested universal model, the regression coefficients k_1 and k_2 are generally positive, k_3 and k_6 are generally positive, and k_7 is generally larger than 1. Another universal model suggested by Mechanistic-Empirical Pavement Design Guide (MEPDG) (Witczak and Uzan 1988) is nearly same as the NCHRP (2004a) suggested universal model but has less regression coefficients by using $k_6 = 0$ and $k_7 = 1$. The three parameter universal model (Equation 26) is used to predict M_r values in this study.

$$M_r = k_1 P_a \left(\frac{\sigma_B}{P_a}\right)^{k_2} \left(1 + \frac{\tau_{oct}}{P_a}\right)^{k_3} \quad (26)$$

where: P_a = atmospheric pressure (MPa);

τ_{oct} = octahedral shear stress (MPa) $= \frac{\sqrt{(\sigma_1-\sigma_2)^2+(\sigma_2-\sigma_3)^2+(\sigma_3-\sigma_1)^2}}{3}$;

σ_B= bulk stress (MPa) = $\sigma_1 + \sigma_2 + \sigma_3$;

σ_1, σ_2, σ_3 = principal stresses (MPa); and

k_1, k_2, k_3 = regression coefficients.

The "k" coefficients for the universal model were determined through regression analysis. The k_1 will be positive because it is proportional to the M_r. The k_2 will be positive because it is the exponent of the σ_B and increased σ_B results in a higher M_r. The k_3 will typically be slightly negative because it is the exponent of the τ_{oct} and increased τ_{oct} likely weaken the materials resulting lower M_r values.

However, the single resilient modulus value is not really representative for a given UGM. The resilient modulus for UGMs is highly dependent on stress state (i.e., bulk stress, octahedral shear stress) which is a function of the position in the pavement structure where the materials at and volume of traffic loading. Resilient moduli values were predicted using the universal model and compared to the measured values for all M_r test samples (Appendix B). Three samples of each crushed limestone (Figure 93), RAP (Figure 94), and RPCC/RAP (Figure 95) materials with 6% target F_{200} were shown as examples for studying the prediction equations in this section. The predicted resilient moduli are shown in line with symbol format and the measured resilient moduli are shown in symbol format in all M_r versus σ_B plots. The predicted values could present the change of M_r values due to increasing bulk stresses and good to fit M_r values at all applied stress states.

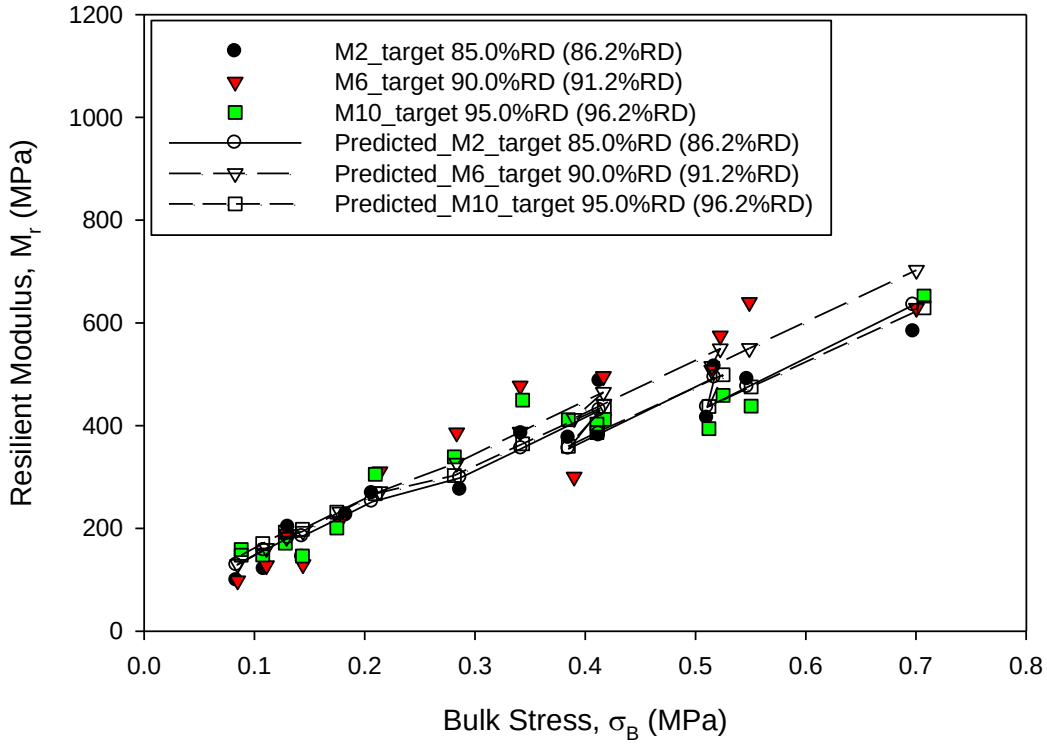

Figure 93. M_r vs. σ_B on crushed limestone samples with reconstituted 5.8% F_{200}

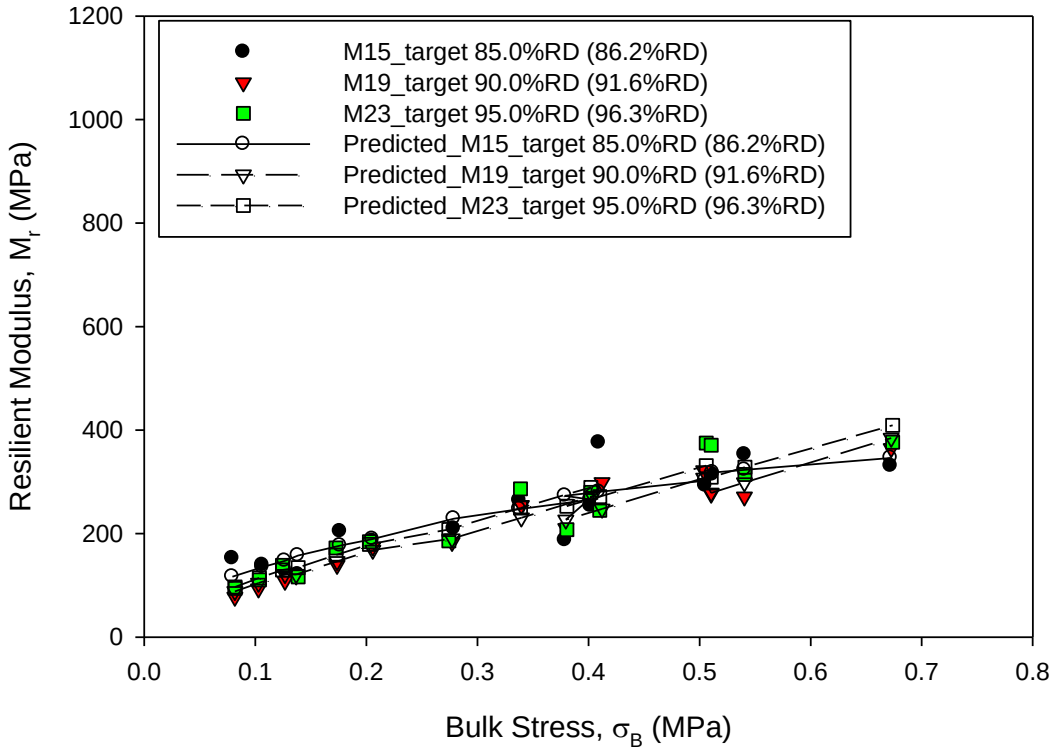

Figure 94. M_r vs. σ_B on RAP samples with reconstituted 5.6% F_{200}

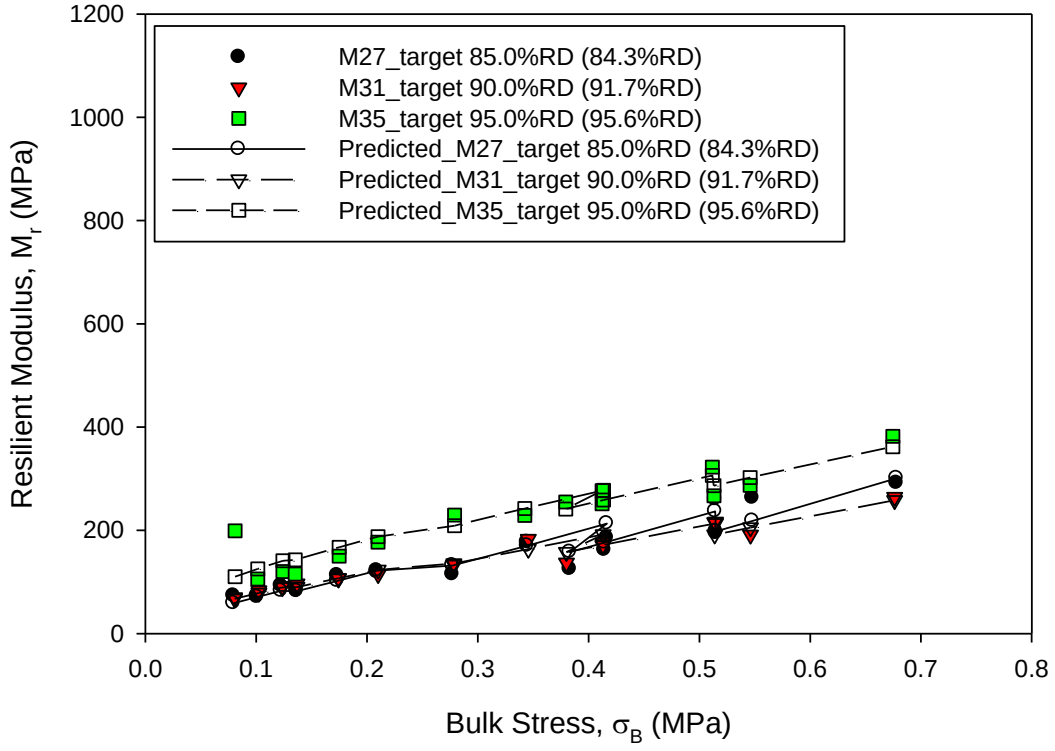

Figure 95. M_r vs. σ_B on RPCC/RAP samples with reconstituted 6.0% F_{200}

Values of regression coefficients k_1, k_2, and k_3 and P-values for every regression coefficients that were determined in statistical analyses are summarized in Table 50 for crushed limestone samples, Table 51 for RAP samples, and Table 52 for RPCC/RAP samples.

k_1 values range from 800 to 2300 for crushed limestone samples, from 800 to 2400 for RAP samples, and from 550 to 1800 for RPCC/RAP samples. Larger k_1 value generally indicates higher resilient modulus. k_1 regression coefficient is significant in the 3-parameter universal mode as the statistical analyses indicate for all samples. k_2 values range from 0.3 to 0.9 for crushed limestone samples, from 0.4 to 1.0 for RAP samples except one outlier, and from 0.3 to 0.8 for RPCC/RAP samples. One outlier is the RAP sample with 12.5% F_{200} and 96.3% RD which has a k_2 of 0.064 that is out the range from 0.4 to 1.0. The same sample has R^2 is about 0.51 which means only 51% measured M_r values can be represented by the predicted M_r values. k_2 regression coefficient is significant except the outlier. However, k_3 values range from -0.2 to 1.8 for crushed limestone samples, from -1.1 to 1.0 for RAP samples except one outlier, and from -0.3 to 1.3 for RPCC/RAP samples. The k_3 values are either negative or positive and are not always significant in the 3-parameter universal model.

Table 50. Statistical analysis for the parameters in M_r prediction of crushed limestone samples

Test No.	k_1			k_2			k_3			R^2
	Values	P-value	SIG ?	Values	P-value	SIG ?	Values	P-value	SIG ?	
M1	1685.60	<0.0001	Y	0.549	<0.0001	Y	0.594	0.0413	Y	0.8990
M2	1373.59	<0.0001	Y	0.614	<0.0001	Y	0.393	0.0234	Y	0.9592
M3	917.67	<0.0001	Y	0.687	<0.0001	Y	0.178	0.3401	N	0.9577
M4	841.53	<0.0001	Y	0.740	<0.0001	Y	1.418	<0.0001	Y	0.9494
M5	1068.93	<0.0001	Y	0.511	<0.0001	Y	0.942	<0.0001	Y	0.9835
M6	1436.54	<0.0001	Y	0.734	<0.0001	Y	0.183	0.5342	N	0.8996
M7	910.53	<0.0001	Y	0.600	<0.0001	Y	0.187	0.3607	N	0.9377
M8	2227.49	<0.0001	Y	0.829	<0.0001	Y	-0.188	1.4020	N	0.8624
M9	1121.10	<0.0001	Y	0.562	<0.0001	Y	0.898	<0.0001	Y	0.9773
M10	1512.07	<0.0001	Y	0.556	<0.0001	Y	0.384	0.0832	N	0.9229
M11	836.61	<0.0001	Y	0.608	<0.0001	Y	0.439	0.0229	Y	0.9545
M12	862.90	<0.0001	Y	0.334	<0.0001	Y	1.767	<0.0001	Y	0.9894

Note: SIG= significant; R^2 = coefficient of determination; Y = yes; and N = no.

Table 51. Statistical analysis for the parameters in M_r prediction of RAP samples

Test No.	k_1			k_2			k_3			R^2
	Values	P-value	SIG ?	Values	P-value	SIG ?	Values	P-value	SIG ?	
M13	1625.30	<0.0001	Y	0.631	0.0129	Y	-0.218	1.4978	N	0.8074
M14	867.39	<0.0001	Y	0.452	<0.0001	Y	0.565	0.0189	Y	0.9098
M15	1337.79	<0.0001	Y	0.566	<0.0001	Y	-0.168	1.3653	N	0.7783
M16	928.79	<0.0001	Y	0.615	<0.0001	Y	0.427	0.0659	N	0.9331
M17	787.44	<0.0001	Y	0.550	<0.0001	Y	0.307	0.0055	Y	0.9787
M18	856.93	<0.0001	Y	0.991	<0.0001	Y	-0.570	1.9764	N	0.9300
M19	951.70	<0.0001	Y	0.561	<0.0001	Y	0.404	0.0305	Y	0.9530
M20	2322.10	<0.0001	Y	0.821	<0.0001	Y	-1.125	1.9860	N	0.7377
M21	804.08	<0.0001	Y	0.610	<0.0001	Y	0.243	0.0772	N	0.9688
M22	1080.99	<0.0001	Y	0.854	<0.0001	Y	-0.581	1.9742	N	0.9041
M23	1057.41	<0.0001	Y	0.590	<0.0001	Y	0.279	0.2722	N	0.9103
M24	2079.20	<0.0001	Y	0.064	0.7021	N	0.902	0.0550	N	0.5149

Note: SIG= significant; R^2 = coefficient of determination; Y = yes; and N = no.

Table 52. Statistical analysis for the parameters in M_r prediction of RPCC/RAP samples

Test No.	k_1			k_2			k_3			R^2
	Values	P-value	SIG ?	Values	P-value	SIG ?	Values	P-value	SIG ?	
M25	626.21	<0.0001	Y	0.726	<0.0001	Y	0.310	0.0811	N	0.9645
M26	1247.67	<0.0001	Y	0.662	<0.0001	Y	0.271	0.1346	N	0.9611
M27	627.83	<0.0001	Y	0.541	<0.0001	Y	0.652	0.0093	Y	0.9250
M28	1360.70	<0.0001	Y	0.704	<0.0001	Y	-0.297	1.6519	N	0.8420
M29	779.56	<0.0001	Y	0.731	<0.0001	Y	-0.038	1.2378	N	0.9779
M30	1780.75	<0.0001	Y	0.632	0.0003	Y	-0.533	1.7439	N	0.6848
M31	721.84	<0.0001	Y	0.498	<0.0001	Y	0.394	0.0153	Y	0.9558
M32	766.61	<0.0001	Y	0.728	<0.0001	Y	0.265	0.1295	N	0.9642
M33	701.84	<0.0001	Y	0.486	<0.0001	Y	0.470	<0.0001	Y	0.9845
M34	728.98	<0.0001	Y	0.317	<0.0001	Y	1.247	<0.0001	Y	0.9659
M35	1184.37	<0.0001	Y	0.476	<0.0001	Y	0.251	0.3681	N	0.8557
M36	570.83	<0.0001	Y	0.603	<0.0001	Y	1.040	<0.0001	Y	0.9813

Note: SIG= significant; R^2 = coefficient of determination; Y = yes; and N = no.

Assessment of measurements errors in M_r tests

The resilient modulus tests were conducted by following the procedures in AASHTO T307-99. This section discusses five major possible sources lead to errors in measuring resilient moduli values as selection of load cycles, load cell location, linear variable differential transducers (LVDTs) location, load pulse shape, and number of points per cycle.

Load cycles selection

A general assumption in the M_r tests is that M_r increases with increasing number of load applications and reaches at a constant value when a certain number of load cycles were applied. The AASHTO T307-99 standard requires using the average value of the last five cycles at the end of each load sequence to represent the M_r value of this load sequence. However, according to the program generated M_r values with the number of load application, the constant M_r values are not generated at the sequence end. M_r values could increase, decrease, or vary as the number of load cycles applied in different loading sequences.

An example that M_r increases first and then decreases to the sequence end where it was assumed a constant value reached is shown on Figure 96. Another example that M_r increases first and then decreases in about every 9 load cycles is shown on Figure 97.

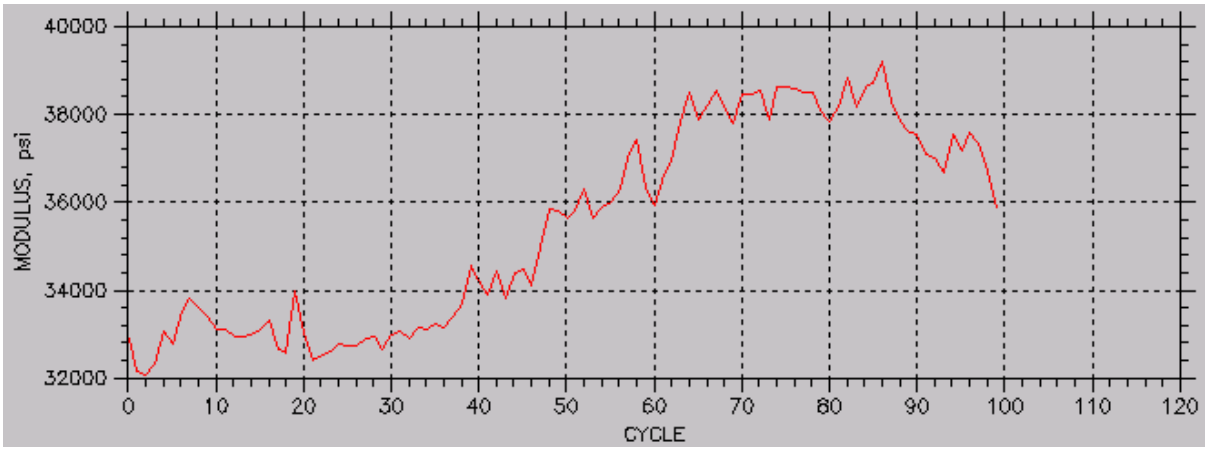

Figure 96. Example 1 of M_r vs. load cycles from program output for one load sequence

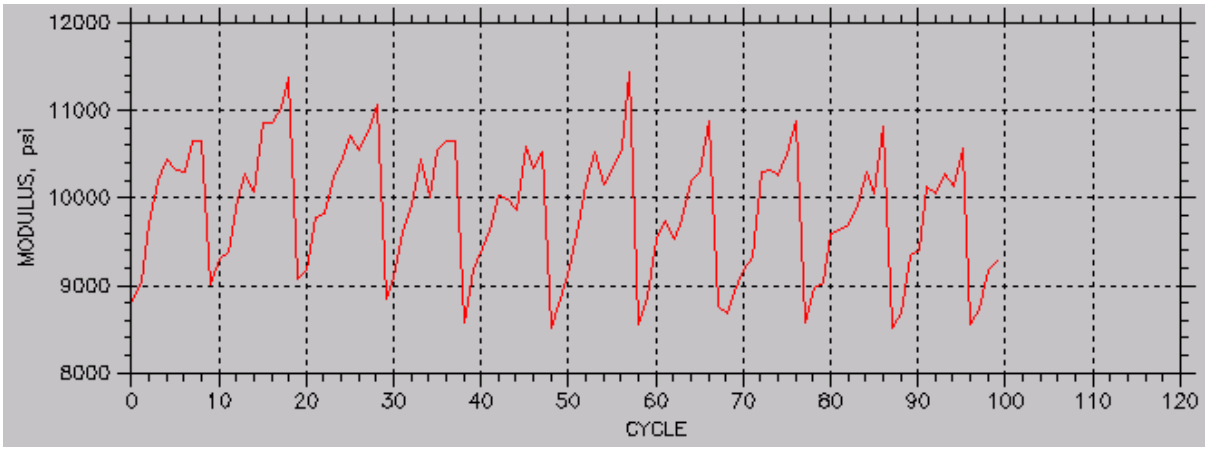

Figure 97. Example 2 of M_r vs. load cycles from program output for one load sequence

Therefore, the differences between the average M_r values of the maximum and adjacent four points, minimum and adjacent four points, and the standard last five cycles are studied in this study.

One load sequence from each M_r test was randomly selected and the maximum, minimum, and standard average M_r values were directly read from the program generated resilient modulus versus load cycles plots. The maximum average M_r value was determined as the average value of the maximum and adjacent four M_r values. The minimum average M_r value was determined as the average value of the minimum and adjacent four M_r values. The standard M_r value was determined as the average M_r values at the last five cycles. A summary of the average M_r values which were calculated using the maximum, minimum, and standard methods is shown in Figure 98 for observing difference in M_r values. Generally, the difference between the maximum and minimum average M_r values increases with increasing standard average M_r values.

Statistical analysis was conducted to find the significance of the three methods on affecting M_r values. The mean M_r values of each method are different, but the range of variation in M_r values is similar. The plot of the distributions of M_r values for the three methods were plotted in Figure 99 where the (shown as the horizontal line at the center of each diamond) indicates the mean M_r value. Although three different methods result in different M_r values, statistical analysis of variance (ANOVA) showed that the method does not have a significant effect on M_r values. The reason is that the selected data are obtained at different stress levels that have significant effects on affecting M_r values.

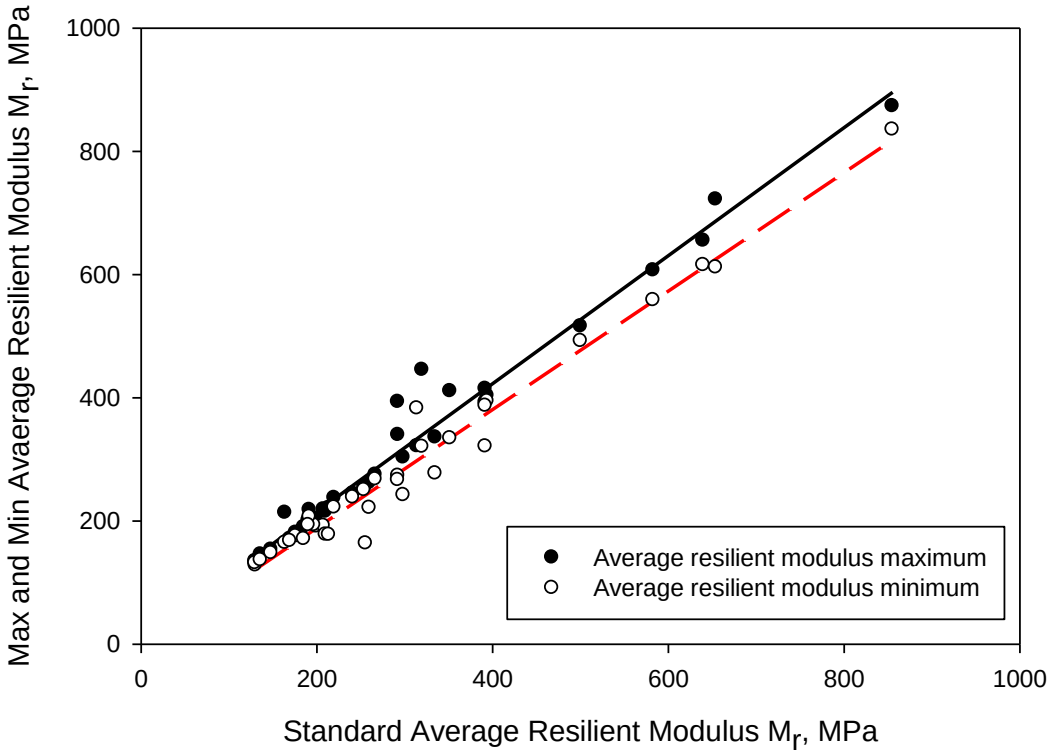

Figure 98. Average M_r determined with standard, maximum, and minimum methods

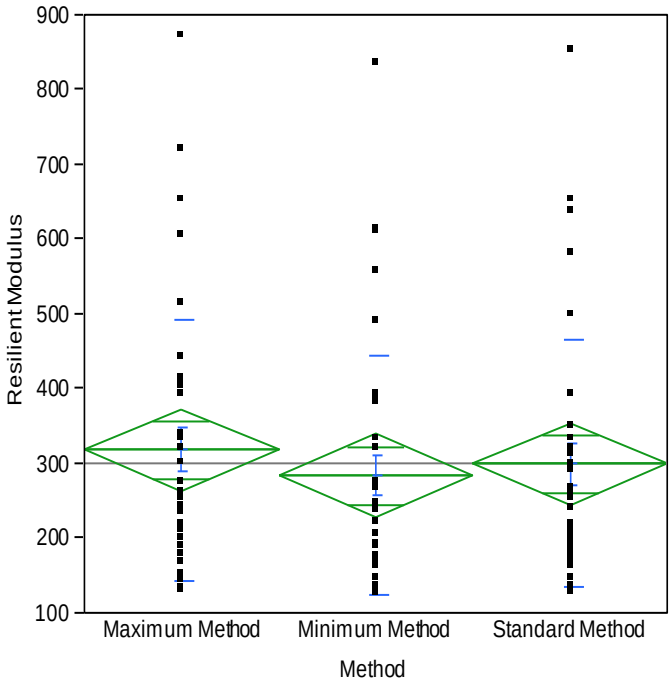

Figure 99. Statistical analysis of M_r values determined with maximum, minimum, and standard methods.

Table 53. Statistical ANOVA summary in determine the significance of load cycles selections in affecting calculated M_r values

Source	Degree of Freedom	Sum of Squares	Mean Squares	F Ratio	Probability >F
Method	2	21075.4	10537.7	0.3784	0.6859
Error	105	2923727.4	27845.0	—	—
Corrected Total	107	2944802.8	—	—	—

Notes: —means no data

Load cell location

The standard require the outside mounted load cell used outside of the triaxial chamber. The inside load cells mounted within the triaxial chamber are also suitable, and allows for more precise control and more accurate reading of the loads applied on the specimens.

LVDTs type

The AASHTO T307 requires use of outside mounted LVDTs because LVDTs mounted on the specimen may slip during testing. This action might not be observed by the operator during the tests and the results will be inaccurate (Groeger et al. 2003). However, Groeger et al. (2003) also suggest that the advantage of using the LVDTs mounted on the specimens could negate any slop in the system and alleviate concerns with stress concentration at the ends of the specimens. The internal deflection measurements were taken by using the LVDTs mounted on samples and the external deflection measurements were taken using the outside mounted LVDTs. Camargo et al. 2012 reported that higher resilient moduli values are determined on the same sample using the internal deflection measurements than the external measurements.

Load pulse shape

Load pulse shape should be a harversine waveform. The first 20 data points in one load cycle indicates duration of 0.1 s for a cycle with 200 readings were recorded. One load cycle is selected to verify the harversine shape of load pulse (Figure 100). The raw data points are nearly followed the harversine waveform fitted line but the peak value is lower the fitted peak value.

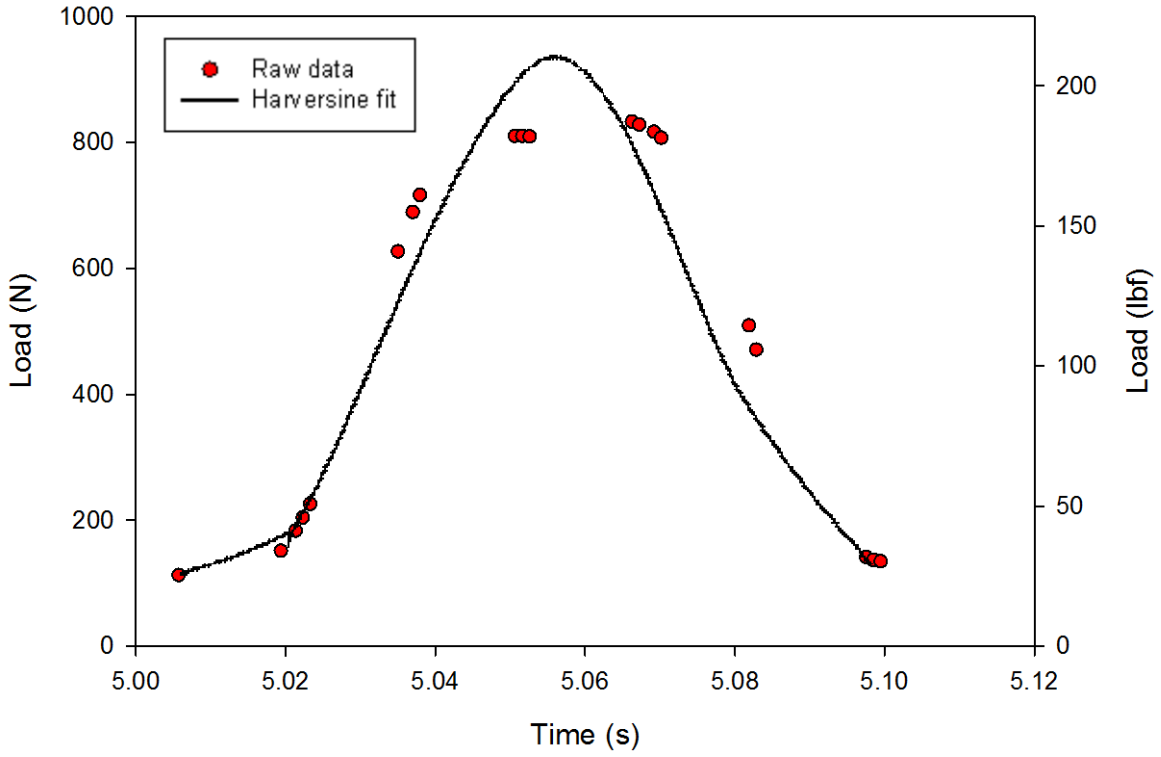

Figure 100. Compare the actual load pulse shape with the harversine waveform for the loading duration in one load cycle

Number of points per cycle

However, the raw data points shown on Figure 100 are distributed in groups of about 3 points. This indicates the 200 readings of a single load cycle are not sampling at a constant rate which is assumed in the standard method (Groeger et al. 2003). The inconstant sampling rate causes increase sampling error because the peak value might be lost. In addition, Groeger et al. (2003) suggested using 500 points instead of 200 points per second, because 200 points are not adequate to fully characterize the true shape of the curve. The NCHRP report 598 (Saeed, 2008b) also suggest to use a data acquisition rate of 500 data points per second to record values.

The system generated M_r values are different from the hand calculated M_r values with the collected raw data points. This might be the result of insufficient data acquisition and missing the true value on the curve.

Unconsolidated undrained shear strength

The unconsolidated undrained triaxial (UU) tests or quick shear tests were conducted on the same sample when 5% of the permanent axial strain is not obtained at the end of the M_r tests. All M_r test samples were used for UU tests except the RAP samples with natural fines contents that obtained5% ε_p at the M_r tests ends. In addition, the UU test data was overwrote and not reported for the RPCC/RAP sample with 12% target F_{200} and 90% target RD. Another outlier is the crushed limestone sample with natural F_{200} and 95% target RD which did not give the maximum deviator stress when the UU test was terminated. The possible reason might the strain hardening of this sample that the interlocking between the particles is stronger.

The undrained shear strength (c_u) is in the range of 80 to 400 kPa for crushed limestone samples, 60 to 110 kPa for RAP samples, and 70 to 140 kPa for RPCC/RAP samples. The average strain at failure for RAP samples is the smallest, followed by crushed limestone samples and the RPCC/RAP samples have the highest average strain at failure. All the UU test samples were used for M_r tests so the same test number is specified for the UU test samples as the M_r tests. The sample height changed for each sample due to the load applications in the M_r tests, so the appropriate calibrations of sample characteristics are done for analyzing UU tests data.

Detailed sample data analysis could be found in Appendix B. The maximum deviator stress (σ_{dmax}), strain at failure (ε_f), and c_u are summarized for all UU tests in Table 54.

Table 54. Undrained strength summary

Test No.	$\sigma_{d\ max}$ (kPa)	ε_f (%)	c_u (kPa)
M1	254	0.48	127
M2	364	0.70	182
M3	166	2.04	83
M4	364	0.29	182
M5	505	0.77	253
M6	515	0.77	257
M7	164	0.48	82
M8	326	0.47	163
M9	478	0.62	239
M10	474	0.80	237
M11	462	5.08	231
M12	797	0.58	398
M13	209	0.86	104
M15	143	0.50	72
M16	170	0.49	85
M17	135	0.66	68
M19	123	0.50	62
M20	189	0.64	95
M21	162	0.66	81
M23	155	0.48	77
M24	202	0.46	101
M25	153	1.35	76
M26	279	0.65	139
M27	146	0.83	73
M28	217	0.65	108
M29	250	3.94	125
M30	279	1.15	139
M31	170	2.56	85
M33	236	3.24	118
M34	251	3.57	126
M35	180	2.72	90
M36	237	0.46	118

The statistical least square fit analysis was conducted to find the significance of variables that include materials type, target F_{200}, and target RD on affecting c_u. In order to conduct the statistical analysis, the varied natural fines contents were excluded from the analysis. In addition, it needs to be noted that the c_u value of the RPCC/RAP with 12% target F_{200} and 90% target RD was lost in the analysis. The materials type was found as the factor that has

significant effect on c_u values while target F_{200} and RD do not have significant effects. The statistical analysis results for studying the effects of the three variables on undrained shear strength are summarized in Table 55.

Table 55. Least square fit analysis of factors significance on c_u

Factors	Degree of Freedom	Sum of Squares	F Ratio	Probability >F	Significant ?
Materials type	2	108619.48	26.0098	<0.0001	Yes
F_{200}		2923.33	0.7000	0.5089	No
RD		11258.07	2.6958	0.0932	No

CHAPTER 6. CONCLUSIONS AND RECOMMENDATIONS

This chapter presents an overview of the scientific value gained from the study, an overview of the lessons learned, and recommendations based on the lessons learned.

The conclusions are grouped into the following categories: permanent deformation, resilient modulus, materials, and prediction models. The last part of this chapter presents recommendations for immediate impact, long-term impact, and implications for the future to advance the knowledge gained from this study.

Permanent Deformation

Permanent deformation is a measure to indicate the support capacity of the unbound granular materials (UGMs) in long-term performance. This study examined the influence of the following variables on the permanent deformation behavior of UGMs: number of load cycles, deviator stress level, relative density (RD), fines content (F_{200}), and material type. The results showed that four of these variables are important factors except RD at influencing the resistance of UGMs to permanent deformation under traffic loads, but have different levels of importance. The results of statistical analyses results are summarized in Table 56.

Table 56. Importance of five factors affecting permanent deformation of UGMs

Factors	Materials	Probability >F	Significant?	R^2	Rank
Number of load cycles	All	<0.0001	Yes	0.2467-0.9711	1
Deviator Stresses	Crushed limestone	0.0006	Yes	0.2744	3
	RAP	0.0059	Yes	0.2676	
	RPCC/RAP	<0.0001	Yes	0.6465	
Relative Density	Crushed limestone	0.8885	No	0.0034	—
	RAP	0.5626	No	0.0343	
	RPCC/RAP	0.6616	No	0.0119	
Fines Contents	Crushed limestone	<0.0001	Yes	0.3880	3
	RAP	<0.0001	Yes	0.6174	
	RPCC/RAP	0.0044	Yes	0.1745	
Material Types	All	<0.0001-0.0008	Yes	0.4475-0.6383	2

Notes: the range of P-values is determined as the summary of all completed load sequences.
—means no significant effects

Number of load cycles

Results and analysis indicated that the number of load cycles is the most important factor affecting the long-term performance of the UGMs. The ISU 100k test results indicate that the untrimmed slag and the recycled portland cement concrete pavements (RPCC) have high resistance to permanent deformation at low stress levels (<103.4 kPa) with less than 1.0% permanent strains at 100,000 load cycles. The ISU 1k tests results highlighted that the initial permanent strain produced in the first several load cycles is due to sample setting.

The NCHRP 598 tests were conducted on crushed limestone, recycled asphalt pavement (RAP), and recycled portland cement concrete with recycled asphalt pavement (RPCC/RAP). The permanent deformation (ε_p) of crushed limestone materials reached a constant value (varied with other factors) at 1,000 load cycles at low deviator stresses (i.e., 137.9 kPa). However, deformation increased at 1,000 load cycles at high deviator stresses (i.e., 551.6 kPa). Permanent deformation of RAP materials tends to increase at the 1,000 load cycles for all stress levels, except on RAP materials with about 12.5% fines content which showed a relatively constant ε_p value at 1,000 cycles at 68.9 kPa and 137.9 kPa deviator stress levels. RPCC/RAP materials generally showed a constant ε_p value at the 1,000 load cycles for all stress levels except the very high stress levels (i.e., >551.6 kPa for 0.8% fines content, >689.5 kPa for 12.4% fines content) where the samples tend to fail.

Deviator stress level

Stress history and traffic loading applied at the pavement surface is important in predicting the long-term service life of the designed pavement structure. In this study, the confining pressures are kept the same for each UGM, so only deviator stresses were studied for UGMs permanent deformation. The ISU 100k tests on the untrimmed slag materials indicate that two times more permanent deformation accumulated at 100,000 load cycles when the applied deviator stress is increased from 41.4 kPa to 62.1 kPa. Tests on the RPCC materials also showed a similar finding.

The NCHRP 598 tests applied up to 10 levels of deviator stress with constant confining pressure to study the permanent deformation of the UGMs with various stress levels. Increasing stress levels are applied as increasing deviator stresses with constant confining pressure in this study by following the procedures specified in NCHRP report 598 (Saeed

2008a). The permanent deformations of the crushed limestone materials at 1,000 cycles increased up to 100% with increasing deviator stress with every 137.9 kPa deviator stress increment applied. However, the crushed limestone materials with 12.6% fines content did not show large permanent deformation increases with increasing deviator stress until >827.4 kPa was applied. Permanent deformations of both RAP and RPCC/RAP materials at the 1,000 cycles increase about 40% to 100% with every 137.9 kPa deviator stress increment applied.

Consequently, all materials have less resistance to permanent deformation as deviator stresses increases. The deviator stress level has a significant effect on permanent deformation for all materials based on the statistical analysis. The increasing rate of permanent deformation with increasing deviator stress is lower, however, for recycled materials compared to crushed limestone materials at higher deviator stresses.

Relative density

Relative densities of the compacted base/subbase materials are generally varied through the project sites. This lead to a study of the effects of the relative density on the resistance of the UGMs to the permanent deformation.

The ISU 100k tests on the untrimmed slag materials shows that permanent deformation at 100,000 cycles increased two times when the relative density decreased from 118.8% to 104.3%. The NCHRP 598 tests were conducted to compare 3 levels of relative densities (85%, 90%, and 95% target RD that are varied in actual values). The permanent deformations of the 7.9% F_{200} crushed limestone materials are highest at 103.7% RD and decreased from 90.7% to 94.6% RD. The permanent deformations of the 2.2% F_{200} crushed limestone materials are highest at 87% RD and decreased from 96.4% to 91.7% relative densities. However, the permanent deformations of the 5.8% and 12.5% target fines crushed limestone materials are highest at around 85.5% RD followed by 90.4% and around 96% RD that show similar permanent deformations values. The permanent deformation of crushed limestone materials is generally higher at around 85.5% RD than higher relative densities except the natural 7.9% F_{200} materials. However, the differences in permanent deformation between about 90.4% and 96% RD are smaller compared to the difference from 85.5%RD. The reason is that the actual RD values of the natural 7.9% F_{200} samples are about 5% higher

than the target RD values. The difference in permanent deformation between samples at high RD is smaller. The reason is that higher relative density required higher forces to compact the materials and breakage of the materials that produces more small particles while breakage indexes for crushed limestone is up to 4%.

Permanent deformations of the RAP and RPCC/RAP materials all increase with decreasing relative densities. This finding confirmed the conclusions from literature review that resistance to permanent deformation could be highly improved with increased density (Lekarp et al. 2000b). Larger permanent deformation values reflect lower resistance to permanent deformation.

Statistical analysis shows that relative density does not have a significant effect on permanent deformation of all three materials tested in this study but the differences in permanent strain between different relative densities were found in the tests results. Therefore, the significant effects of relative densities might be concluded on different materials or same materials with wider range of relative densities.

Fines content

Particle breakage of UGMs can produce more fine materials. Moreover, migration of fine materials generally leads to loss of fines content in lower pavement foundation layers and increase in fines content of upper pavement foundation layers. Studying on fines content affecting the permanent deformation of UGMs helps designer understand distress of rigid pavement (i.e., pumping, corner cracks, and joint cracks).

In this study, the NCHRP 598 tests were conducted to study four fines contents of three materials that include 7.9%, 2.2%, 5.8%, and12.6% F_{200} in crushed limestone, 2.0%, 1.6%, 5.6, and 12.5% F_{200} in RAP, 3.5%, 0.8%, 6.0%, and 12.4% F_{200} in RPCC/RAP materials to cover the range of 0% to 6% F_{200} that IOWA DOT specified for crushed subbase materials. The natural fines contents mean that the fines content is the same as the materials were produced and collected from the quarry. However, the reconstituted fines contents are produced by subtracting or adding more fines that were produced by crushing the same material type. The different materials preparation processes could be the reason that caused the natural fines contents (7.9%, 2.0%, and 3.5%) for all materials to have large different permanent deformation behavior from other three reconstituted fines contents.

Permanent deformations of all materials increase with increasing fines content from approximate 1% to 12% at same relative density level except the natural fines materials. This finding diverges from the conclusion reported by some researchers (Barksdale 1972; Thom and Brown 1988; Kancherla 2004; Mishra et al. 2009; Hussian et al. 2010) that increasing fines content causes decrease in resistance of UGMs to permanent deformation. One reason is that some previous researchers prepared limited samples to studying effects of fines contents up to 20% which is not included in this study. Another reason is that some previous researchers tested the samples with low deviator stress (i.e., <200 kPa). In this study, permanent deformation of crushed limestone at 1,000 cycles under <200 kPa deviator stresses did not show increased fines content caused decreasing permanent strain.

Statistical analysis shows that the effect of fines content on permanent deformation is significant for each material separately.

Material type

The NCHRP 598 tests results for all the samples indicate that RAP usually have the lowest resistance, followed by RPCC/RAP, and the crushed limestone have the highest resistance to the permanent deformation when the same target fines content, relative density, and deviator stress are specified. Moreover, the permanent deformation in the RAP is up to 300% higher than the permanent deformations in the crushed limestone and RPCC/RAP materials while other factors are the same. The RPCC/RAP materials also show sudden failures when the 965.3 kPa deviator stress is applied.

Statistical analysis shows that material type has significant effects on permanent deformation of all samples.

Resilient Modulus

Resilient modulus is a measure of the stiffness of the UGMs and is used as an input in pavement designs. Resilient modulus tests were conducted over a range of confining and deviator stress conditions. In this study, relative density, fines content, and material type were identified as important factors influencing the laboratory resilient modulus. The statistical analyses results were summarized in Table 57.

Table 57. Importance of four factors affecting laboratory resilient moduli of UGMs

Factors	Materials	Probability >F	Significant?	R^2	Rank
Stress levels	Crushed limestone	<0.0001	Yes	0.6237	1
	RAP	<0.0001		0.5564	
	RPCC/RAP	<0.0001		0.6220	
RD	Crushed limestone	0.1891	No	0.0186	—
	RAP	0.9740		0.0003	
	RPCC/RAP	0.1352		0.0224	
F_{200}	Crushed limestone	<0.0001	Yes	0.1397	3
	RAP	<0.0001		0.1200	
	RPCC/RAP	<0.0001		0.1228	
Material type	All	<0.0001	Yes	0.2028	2

Note: — means no significant effects

Stress level

The AASHTO T307-99 standard test covers a range of confining and deviator stress conditions. In general, resilient moduli of the tested materials are higher when higher bulk stresses (sum of deviator stress and confining pressure) are applied. However, the effects of stress levels on resilient modulus values are not linearly related to the bulk stress. Statistical analysis showed that stress levels have significant effects on laboratory resilient modulus of all samples.

Relative density

Results from testing a number of samples with relative density values from about 86% to 100% (target 85% to 95%) showed no clear relationship between resilient moduli and relative densities. However, statistical analysis showed that relative density has significant effects on laboratory resilient modulus of all samples.

Fines content

Fines content affects resilient modulus values and is correlated to relative densities. The resilient modulus generally increases with increasing fines content at relatively high relative densities (about 96.0% RD). Moreover, in this study fines content is not important for resilient modulus at low relative densities (about 85%) because the testing results did not

show a clear relationship between resilient modulus and fines content. Statistical analysis shows that fines content has a significant effect on laboratory resilient moduli of UGMs. However, a clear relationship between resilient modulus values and fines contents cannot be concluded.

Material type

The crushed limestone material has the highest resilient modulus values of up to 1,000 MPa compared to the RAP and RPCC/RAP materials that have the similar resilient modulus values of up to 600 MPa. The material type has significant effect on resilient modulus as the statistical analysis shows by comparing the crushed limestone, RAP, and RPCC/RAP materials.

Prediction Models

The models for predicting permanent deformations and resilient moduli of UGMs are discussed in this study separately.

Permanent deformation prediction

Barksdale's model is used to predict permanent deformations of UGMs under a single stress level, and a new model based on NCHRP 598 test results was developed in this study to predict permanent deformations of UGMs under multiple stress levels (i.e., varying deviator stresses and constant confining pressure).

- The new model cannot predict the transition between two stress levels if several stresses were applied on the same sample in one test (e.g., NCHRP 598 specified test sequences).
- The new model shows good fit to the natural and low fines content materials but cannot predict the permanent deformations of the high fines content materials.

Resilient moduli prediction

The three-parameter universal model was used to predict the resilient modulus of the UGMs. Moreover, statistical analyses were conducted to determine the significances of each regression parameters on predicting resilient moduli for UGMs.

- The three regression coefficients (k_1, k_2, and k_3) account for nonlinear soil and are related to the specific stress parameters.

- The k_1 values are always positive and vary from hundreds to thousands. Regression coefficient k_1 has a significant effect on predicting resilient moduli.
- The positive k_2 values indicate the dependence of resilient moduli on bulk stresses. The k_2 values are generally less than one and have a significant effect on predicting resilient moduli.
- The k_3 values could be either negative or positive and are close to zero. Moreover, the regression parameter k_3 does not always have a significant effect on predicting resilient moduli.

Conclusions from Testing

The materials with natural fines content showed large differences in permanent deformations from the materials with target fines contents.

- Relative densities of the natural fines content materials are much lower than the target fines content materials. This difference is related to the use of crushed fines in the reconstituted specimens.
- Laboratory resilient modulus values are not continuously increasing with the number of load applications. Therefore, the last five cycles of each load sequence cannot precisely represent the actual resilient moduli.
- Following AASHTO T307-99, LVDTs were installed outside and at the top of the pressure chamber in this study, so the measured values may not accurately represent resilient behavior through the whole sample height.
- Numbers of reading points are set to be 200 per load cycle which is the minimum value specified in AASHTO T307-99. However, the system did not record the data at a constant rate and 200 readings are not enough to represent the harversine shape load pulse.

Immediate Impact

This study has shown that care needs to be taken when migration of fines in pavement foundation structures are present in situ because the stiffness of subbase layers is significantly affected by fines content. Although materials with reconstituted fines contents from about 1% to 12% have decreasing permanent strain, materials with natural fines content

(>2%) may have larger permanent deformation than the materials with about 1%-2% fines contents. This indicates that reconstituted materials should be prepared with similar procedures as materials produced in quarries and attention should be paid to the preparation process.

Long-term Impact

The industry problem discussed in the introduction chapter involved the need to use more recycled materials in pavement foundation construction and to better predict the permanent and resilient deformation of UGMs.

Increasing the use of recycled materials reduces costs associated with repairing deteriorated pavements or constructing new pavement structures. Permanent deformation and resilient modulus tests show the acceptable workability of recycled materials based on their permanent deformation and resilient moduli over a range of conditions (e.g., varying stress levels, relative densities) compared to the conventional crushed limestone materials.

Accurate prediction of permanent deformation in UGMs has not been determined, but deviator stress, fines contents, and relative densities must be correlated in predicting the permanent deformation in addition to the present focus on the number of load cycles. More accurate prediction for permanent deformation would help pavement designer to design a pavement to serve longer and decrease the possible pavement deteriorations.

Recommendations for Future Research

The research presented in previous chapters is based on investigations of the permanent and resilient deformation of a limited number of variables. Additional investigations are necessary to advance pavement foundation design.

- The movement of fine particles between foundation layers had been identified as an important issue affecting permeability, uniformity, strength of pavement foundation layers. Future research should include fines from subgrade in composite samples to study the effects of subgrade fines migration. Different amounts of subgrade fines should be studied to learn the severity of fines migration.

- Deformation behavior could be affected by the support from lower layers in pavement foundation structures. Future study should include composite samples in studying the permanent deformation and resilient modulus of UGMs.
- The different deformation behaviors of recycled and conventional materials at different stress levels warrant further study of combinations of RAP, RPCC, and limestone materials in different proportion.
- The effects of freezing and thawing of UGMs reduce the serviceability of pavement structures. Future study of permanent deformation and resilient modulus could be conducted on UGM samples after freeze-thaw cycles have been applied.
- The permeability of pavement foundation layers is important, so it should be included in future studies to understand whether materials that can resist higher permanent deformation also can provide acceptable permeability.
- Actual stresses in the field are not constant, so future study should investigate the permanent deformation of UGMs under varying confining pressures.
- The discrepancies between predictions made using the new permanent deformation model and measured permanent strains should be examined to test the assumption that stress history does not affect tests results in multiple stage tests.

WORKS CITED

AASHTO T307-99. (2007). "Standard method of test for determining the resilient modulus of soils and aggregate materials." American Association of State Highway and Transportation Officials (AASHTO), Washington, D.C.

Alam, T.B., Abdelrahman, M., and Schram, S.A. (2010). "Laboratory Characterization of recycled asphalt pavement as a base layer." International Journal of Pavement Engineering, Taylor & Francis, 11(2), 123–131.

Allen, J.J. (1973). "The effect of non-constant lateral pressures of the resilient response of granular materials." Ph.D. dissertation, University of Illinois at Urbana-Champaign, Urbana, IL.

Allen, J.J., and Thompson, M.R. (1974). "Resilient response of granular materials subjected to time dependent lateral stresses." Transportation Research Record, 510, Transportation Research Board, Washington, D.C., 1–13.

American Society of Civil Engineers. (2011). *Failure to act: The economic impact of current investment trends in surface transportation infrastructure*. (Nov 19, 2012). http://www.asce.org/uploadedFiles/Infrastructure/Report_Card/ASCE-FailureToActFinal.pdf

Arnold, G.K. (2004). "Rutting of granular pavements." Ph.D. dissertation, The University of Nottingham, United Kingdom.

ASTM C127-07. Standard test method for density, relative density (specific gravity), and absorption of coarse aggregate. American Standards for Testing Methods (ASTM), West Conshohocken, PA.

ASTM D422-63. Standard test method for particle-size analysis of soils. American Standards for Testing Methods (ASTM), West Conshohocken, PA.

ASTM D698-07. Standard test method for laboratory compaction characteristics of soil using standard effort (12,400 ft-lbf/ft3 (600 kN-m/m3)). American Standards for Testing Methods, West Conshohocken, PA.

ASTM D2216-10. Standard test methods for laboratory determination of water (moisture) content of soil and rock by mass. American Standards for Testing Methods (ASTM), West Conshohocken, PA.

ASTM D2850-03a. Standard test methods for unconsolidated-undrained triaxial compression test on cohesive soils. American Standards for Testing Methods (ASTM), West Conshohocken, PA.

ASTM D4253-00. Standard test methods for maximum index density and unit weight of soils using a vibratory table. American Standards for Testing Methods (ASTM), West Conshohocken, PA.

ASTM D4254-00. Standard test methods for minimum index density and unit weight of soils and calculation of relative density. American Standards for Testing Methods (ASTM), West Conshohocken, PA.

Austin, A. (2009). "Fundamental characterization of unbound base course materials under cyclic loading." M.S. thesis, Louisiana State University, LA

Barksdale, R.D. (1972). "Laboratory evaluation of rutting in base course materials." Proceedings of the Third International Conference on Structural Design of Asphalt Pavements, London, 1972, 161–174.

Barksdale, R.D., and Itani, S.Y. (1989). "Influence of aggregate shape on base behavior." Transportation Research Record, 1227, Transportation Research Board, Washington, D.C., 173–182.

Bennert, T., Papp, W.J., Macher, A., and Gucunski, N. (2000). "Utilization of construction and demolition debris under traffic-type loading in base and subbase applications." Transportation Research Record, 1714, Transportation Research Board, Washington, D.C., 33–39.

Belt, J., Ryynänen, T., and Ehrola, E. (1997). "Mechanical properties of unbound base course." Proceedings of the 8th International Conference on Asphalt Pavements, Seattle, 1, 771-781

Boyce, J.R. (1976). "The behavior of a granular material under repeated loading." Ph.D. dissertation, The University of Nottingham, United Kingdom.

Bozyurt, O., Tinjum, J.M., Son, Y-H, Edil, T.B., and Benson, C.H. (2012). "Resilient modulus of recycled asphalt pavement and recycled concrete aggregate." *GeoCongress 2012: State of the Art and Practice in Geotechnical Engineering*, Oakland, CA. ASCE, 3901–3910.

Brown, S.F., and Hyde, A.F.L. (1975). "Significance of cyclic confining stress in repeated-load triaxial testing of granular material." Transportation Research Record, 537, Transportation Research Board, Washington, D.C., 49–58.

Camargo,F., Benson, C., and Edil, T. (2012). "An assessment of resilient modulus testing: internal and external deflection measurements." *Geotechnical Testing Journal*, 35(6), 1-8.

Central Texas Regional Mobility Authority. (2011). "2011 traffic surveys and travel time studies 183A area roadways." (Nov 19, 2012). http://www.mobilityauthority.com/183A%20Area%20Roadways%20Traffic%20Study_December_2011.pdf

Cerni, G., Cardone, F., Virgili, A., and Camilli, S. (2012). "Characterization of permanent deformation behavior of unbound granular materials under repeated triaxial loading." Construction and Building Materials, 28(1), 79–87.

Ferguson, E.G. (1972). "Repetitive triaxial compression of granular base course material with variable fines content." Ph. D. dissertation, Iowa State University, Ames, IA.

Gidel, G., Hornych, P., Chaauvin, J-J., Breysse, D., and Denis, A. (2001). "A new approach for investigating the permanent deformation behavior of unbound granular material using the repeated load triaxial apparatus." Bulletin des Laboratoires des Ponts et Chaussées. 233(4), 5–21.

Groeger, J.L., Rada, G.R., and Lopez, A. (2003). "AASHTO T307–Background and discussion." Resilient Modulus Testing for Pavement Components, *ASTM STP 1437*, Durham, G.N., Marr, W.A., and De Groff, W.L., (eds.), ASTM International, West Conshohocken, PA, 16–29.

Guimarães, A.C.R., and da Motta, L.M.G. (2008) "A study on permanent deformation of lateritic soils including the shakedown concept." Advances in Transportation Geotechnics, Ellis, E., Thom, N., Yu, H.S., Dawson, A., and McDowell, G. (eds.), 147–155.

Heydinger, A.G., Xie, Q.L., Randolph, B.W., and Gupta, J.D. (1996). "Analysis of resilient modulus of dense and open-graded aggregates." Transportation Research Record, 1547. Transportation Research Board, Washington, D.C., 1–6.

Hicks, R.G. (1970). "Factors influencing the resilient properties of granular materials." Ph.D. dissertation, University of California, Berkeley, Calif.

Hicks, R.G., and Monismith, C.L. (1971). "Factors influencing the resilient properties of granular materials." Highway Research Board Record, 345, 15–31.

Hoff, I., Nordal, S., and Nordal, R.S. (1999) "Constitutive model for unbound granular materials based on hyperelasticity." Proceedings of an International Workshop on Modelling and Advanced Testing for Unbound Granular Materials, Lisbon, Balkema 1999, 187–196.

Holubec, I. (1969). "Cyclic creep of granular materials." D.H.O. report No. RR147. Department of Highways, Ontario.

Hossain, Z., Indraratna, B., Darve, F., and Thakur, P.K. (2007). "DEM analysis of granular ballast breakage under cyclic loading." Geomechanics and Geoengineering: International Journal, 2(3), 175–182.

Hussain, J., Wilson, D.J., Henning, T.F.P., Black, P., and Alabaster, D. (2010). "Investigating the permanent deformation of unbound greywacke road base considering geology, gradation and moisture conditions." Presentation at Annual Meeting of Transportation Research Board and Publication in Transportation Research Record.

Hveem, F.N. (1955). "Pavement deflections and fatigue failures." Bulletin No.114, Highway Research Board, Washington, D.C., 43-87.

Iowa DOT (2008). "Aggregate gradation table (English)." Iowa Department of Transportation. (Jan 20, 2012). http://www.iowadot.gov/erl/archives/Apr_2008/GS/common/english_gradations.htm

Indraratna, B., and Salim, W. (2002). "Modelling of particle breakage of coarse aggregates incorporating strength and dilatancy." Proceedings of the Institution of Civil Engineers, London, 155 (4), 243–252.

Indraratna, B., and Salim, W. (2004). "A new elastoplastic constitutive model for coarse granular aggregates incorporating particle breakage." Canadian Geotechnical Journal, 41 (4), August, 657–671.

Indraratna, B., Lackenby, J., and Christie, D. (2005). "Effect of confining pressure on the degradation of ballast under cyclic loading." Géotechnique, 55 (4), 325 –328.

Ishikawa, T., Hosoda, M., Miura, S., and Sekine, E. (2008). "Influence of water content on mechanical behavior of gravel under moving wheel loads." Advances in Transportation Geotechnics, Ellis, E., Thom, N., Yu, H.S., Dawson, A., and McDowell, G. (eds.), 185–191.

Johnson, K.L. (1986). "Plastic flow, residual stresses, and shakedown in rolling contact." Proceedings of 2nd International Conference on Contact Mechanics and Wear of Rail/Wheel Systems, University of Rhode Island, Waterloo Ontario, Canada.

Kancherla, A. (2004). "Resilient modulus and permanent deformation testing of unbound granular materials." M.S. thesis, Texas A&M University, College Station, TX.

Kang, D-H., Gupta, S.C., Ranaivoson, A.Z., Siekmeier, J., and Roberson, R. (2011). "Recycled materials as substitutes for virgin aggregates in road construction: I. Hydraulic and mechanical characteristic." Soil Science Society of America Journal, 75(4), 1265–1275.

Kenis, W.J. (1978). "Predictive design procedures, VESYS users manual—an interim design method for flexible pavements using the VESYS structural subsystem." Final Report No. FHWA-RD-77-154, U.S. Dept. of Transp., Washington, D.C.

Kim, W., Lim, J., and Labuz, J.F. (2009). "Cyclic triaxial testing of recycled asphalt pavement and aggregate base." Transportation Research Board 88th Annual Meeting CD-ROM, TRB Paper 09-1604, Transportation Research Board, Washington, D.C.,

Kolisoja, P. (1998). "Large scale dynamic triaxial tests." III. Delprosjektrapport 20, Arbeidsfelleskapet KPG, Oslo, Norway.

Kumar, P., Chandra, S., and Vishal, R. (2006). "Comparative study of different subbase materials." Journal of Materials in Civil Engineering, 18 (4), 576–578.

Lade, P.V., Yamamuro, J.A., and Bopp, P.A. (1996). "Significance of particle crushing in granular materials." Journal of Geotechnical Engineering, ASCE, 122 (4), 309–316.

Lashine, A.K., Brown, S.F., and Pell, P.S. (1971). "Dynamic properties of soils." Report No.2 Submitted to Koninklijke/Shell Laboratorium. University of Nottingham, United Kingdom.

Leite, F.C., Motta, R.S., Vasconcelos, K.L., and Bernucci, L. (2011). "Laboratory evaluation of recycled construction and demolition waste for pavements." Construction and Building Materials, 25(6), 2972–2979.

Lekarp, F., Richardson, I. R., and Dawson, A. (1996). "Influences on permanent deformation behavior of unbound granular materials." Transportation Research Record, 1547. Transportation Research Board, Washington, D.C., 68–75.

Lekarp, F., and Dawson, A. (1998). "Modelling permanent deformation behaviour of unbound granular materials." Construction and Building Materials, 12 (1), 9–18.

Lekarp, F., Isacsson, U., and Dawson, A. (2000a). "State of the art. I: Resilient response of unbound aggregates." Journal of Transportation Engineering, ASCE, 126(1), 66–75.

Lekarp, F., Isacsson, U., and Dawson, A. (2000b). "State of the art. II: Permanent strain response of unbound aggregates." Journal of Transportation Engineering, ASCE, 126(1), 76–83.

Luong, M.P. (1982). "Mechanical aspects and thermal effects of cohesionless soils under cyclic and transient loading." Deformation and Failure of Granular materials. Vermeer, P.A., and Luger, H.J. (eds.), Balkema, Rotterdam, The Netherlands. 239–246.

Marsal, R.J. (1967). "Large scale testing of rockfill materials." Journal of the Soil Mechanics and Foundations Division, ASCE, 93(SM2), 27–43.

May, R.W., and Witczak, M.W. (1981). "Effective granular modulus to model pavement responses." Transportation Research Record, 810, Transportation Research Board, Washington, D.C., 1-9.

Mayrberger, T, and Hodek, R.J. (2007). "Resilient modulus at the limits of gradation and varying degrees of saturation." Final Report Research Report RC-1497. Michigan Department of Transportation, Lansing, MI.

Mishra, D., Tutumluer, E., Kern, J. and Butt, A. (2009). "Characterizing aggregate permanent deformation behavior based on types and amounts of fines." Proceedings of the 8th International Conference on the Bearing Capacity of Roads, Railways, and Airfields, Champaign, 2009, 237–246.

Mishra, D., Tutumluer, E., and Butt, A.A. (2010). "Quantifying effects of particle shape and type and amount of fines on unbound aggregate performance through controlled gradation." Transportation Research Record, 2167. Transportation Research Board, Washington, D.C. 61–71.

Morgan, J.R. (1966). "The response of granular materials to repeated loading." Proceedings of 3rd Conference, Australian Road Research Board, 1178–1192.

Nataatmadja, A., and Tan, Y.L. (2001). "Resilient response of recycled concrete road aggregates." Journal of Transportation Engineering, 127(5), 450–453.

National Cooperative Highway Research Program (NCHRP). (2004a). "Laboratory determination of resilient modulus for flexible pavement design." NCHRP resultsdigest for NCHRP 1-28A project, Washington, D.C.

National Cooperative Highway Research Program (NCHRP). (2004b). "Guide for mechanical-empirical design of new and rehabilitated pavement structures." NCHRP final report for NCHRP 1-37A project, Washington, D.C. (Oct 10, 2012). http://onlinepubs.trb.org/onlinepubs/archive/mepdg/guide.htm

Nazzal, M.D., Mohammad, L.N., and Austin, A. (2011). "Evaluation of the shakedown behavior of unbound granular base materials." Geo-Frontiers, ASCE, 4752–4761.

Paute, J.L., Hornych, P., and Benaben, J.P, (1996). "Repeated load triaxial testing of granular materials in the French network of Laboratories des Ponts et Chaussées." Flexible

Pavements, Proc., Eur. Symp. Euroflex 1993, Correia, A.G. (ed.), Balkema, Rotterdam, The Netherlands, 53–64.

Pappin, J.W. (1979). "Characteristics of granular material for pavement analysis." Ph.D. dissertation, University of Nottingham, Nottingham, United Kingdom.

Puppala, A. J. (2008). "Estimating stiffness of subgrade and unbound materials for pavement design: A synthesis of highway practice." NCHRP Synthesis 382, Transportation Research Board, Washington, D.C.

Rodgers, M., Hayes, G., and Healy, M.G. (2008). "Cyclic loading tests on sandstone and limestone shale aggregates used in unbound forest roads." Construction and Building Materials, 23 (6), June 2009, 2421–2427.

Saeed, A. (2008a). "Performance-related tests of recycled aggregates for use in unbound pavement layers." NCHRP report 598, Transportation Research Board, Washington, D.C.

Saeed, A. (2008b). Appendixes to NCHRP Report 598. National Cooperative Highway Research Program. Web-only document 119. Transportation Research Board, Washington, D.C.

Seed, H.B., Chan, C.K., Lee, C.E. (1962). "Resilience characteristics of subgrade soils and their relation to fatigue failures in asphalt pavements." Proceedings International Conference on the Structural Design of Asphalt Pavements. University of Michigan, Ann Arbor, MI, 611–636.

Seed, H.B., Mitry, F.G., Monismith, C.L., and Chan, C.K. (1967). "Prediction of flexible pavement deflections from laboratory repeated load tests." NCHRP Rep. No.35, National Cooperative Highway Research Program.

Shane, B. (2007). "Resilient modulus: what, why, and how?" Vulcan Materials Company. (Feb 20, 2013). http://www.vulcaninnovations.com/resource-center/

Sharp, R.W., and Booker, J.R. (1984). "Shakedown of pavements under moving surface loads." Journal of Transportation Engineering, ASCE, 110(1), 1–14.

Sivakumar, V., Mckinley, J.D., and Ferguson, D. (2004). "Reuse of construction waste: performance under repeated loading." Proceedings of the Institution of Civil Engineers on Geotechnical Engineering, 157(2), 91–96.

Stolle, D., Guo, P., and Liu, Y. (2006). "Resilient modulus properties of typical granular base materials of Ontario." Proceedings of 59th Canadian Geotechnical Conference, Vancouver, B.C., 1–4.

Stolle, D., Peijun, G., and Ying, L. (2009). "Resilient modulus properties of granular highway materials." Canadian Journal of Civil Engineering, 36(4), 639-654.

Sweere, G.T.H. (1990). "Unbound granular basis for roads." Ph.D. dissertation, University of Delft, Delft, The Netherlands.

Tao, M., Mohammad, L.N., Nazzal, M.D., Zhang, Z., and Wu, Z. (2010). "Application of shakedown theory in characterizing traditional and recycled pavement base materials." Journal of Transportation Engineering, 136(3), 214–222.

Thom, N.H., and Brown, S.F. (1987). "Effect of moisture on the structural performance of a crushed-limestone road base." Transportation Research Record, 1121. Transportation Research Board, Washington, D.C., 50–56.

Thom, N.H., and Brown, S.F. (1988). "The effect of grading and density on the mechanical properties of a crushed dolomitic limestone." Proceedings of 14th ARRB Conference, Part 7, 94–100.

Thom, N.H., and Brown, S.F. (1989). "The mechanical properties of unbound aggregates from various sources." Unbound Aggregates in Roads: Proceedings of the Fifth International Symposium on Unbound Aggregates in Roads, Dawson, A. (ed.), UNBAR 5, Nottingham, United Kingdom, 130–142.

Trollope, E.H., Lee, I.K., and Morris, J. (1962). "Stresses and deformation in two-layer pavement structures under slow repeated loading." Proc., ARRB, Vol. 1, Part 2, 693–718.

Tutumluer, E., Mishra, D., and Butt, A.A. (2009). "Characterization of Illinois aggregates for subgrade replacement and subbase." Research Report ICT-09-060, Illinois Center for Transportation, Urbana, IL.

Uthus, L., Hermansson, Å., Horvli, I., and Hoff, I. (2006). "A study on the influence of water and fines on the deformation properties and frost heave of unbound aggregates." Proceedings of 13th International Conference on Cold Regions Engineering, 2006, ASCE, doi: 10.1061/40836(210)65.

Van Niekerk, A.A. (2002). "Mechanical behavior and performance of granular bases and sub-bases in pavements." Ph.D. dissertation, Delft University of Technology, Delft, The Netherlands.

Veverka, V. (1979). "Raming van de spoordiepte bij wegen met een bitumineuze verharding." De Wegentechniek, 24(3), 25–45 (in Dutch).

Werkmeister, S. (2003). "Permanent deformation behaviour of unbound granular materials in pavement constructions." Ph.D. dissertation, Dresden University of Technology, Dresden, Germany.

Werkmeister, S., Dawson, A. R., and Wellner, F. (2001). "Permanent deformation behavior of granular materials and the shakedown concept." Transportation Research Record, 1757. Transportation Research Board, Washington, D.C. 75–81.

White, D.J., Bergeson, K.L. Jahren, C.T. (2002). *Embankment Quality: Phase III*, Center for Transportation Research and Education, Iowa State University, Ames, IA.

White, D.J., Vennapusa, P., and Jahren, C.J. (2004). "Determination of the optimum base characteristics for pavements." Iowa DOT project TR-482, Iowa Department of Transportation and Iowa Highway Research Board.

Witczak, M., and Uzan, J. (1988). "The universal airport design system, report I of IV: Granular material characterization." Department of Civil Engineering, University of Maryland, College Park, MD.

Wolfe, A.J. (2011). "Behavior of composite pavement foundation materials subjected to cyclic loading." M.S. thesis, Iowa State University, Ames, IA.

Wright, F.G. (2002). "FHWA recycled materials policy." United States Department of Transportation Federal Highway Administration. (Feb 19, 2012) http://www.fhwa.dot.gov/legsregs/directives/policy/recmatpolicy.htm

APPENDIX A. PERMANENT DEFORMATION TESTS ANALYSES

Permanent Deformation Calculation

Permanent deformation at each load repetition was calculated as the accumulated vertical permanent strain using Equation 27.

$$\varepsilon_p = \frac{\Delta H}{H_0} = \frac{0.004363}{7.989634} \times 100\% = 0.0546\% \quad (27)$$

Test methods

Method #1 ISU 100k tests

ISU 100k tests were conducted on the I–94 untrimmed slag subbase and US–30 RPCC materials (Table 58). The 100k load repetitions were divided into 4 load sequences because the program cannot run 100k load repetitions in a single load sequence. This method is designed to terminate the tests when the 5% permanent strain reached. The deviator stresses were varied for different tests, and the values could be 20.7 kPa (3 psi), 41.4 kPa (6 psi), 62.1 kPa (9 psi), 82.7 psi (12 psi), and 103.4 kPa (15 psi). The confining stresses were 20.7 kPa (3 psi) for the I–94 untrimmed slag subbase and were 103.4 kPa (15 psi) for US–30 RPCC materials.

Table 58. Permanent deformation test sequences and stress values for ISU 100k tests on a subbase sample

Sequence No.	Confining Stress		Deviator Stress		No. of Load Repetitions
	kPa	Psi	kPa	Psi	
1	103.4	15	41.4	6	25,000
2	103.4	15	41.4	6	25,000
3	103.4	15	41.4	6	25,000
4	103.4	15	41.4	6	25,000

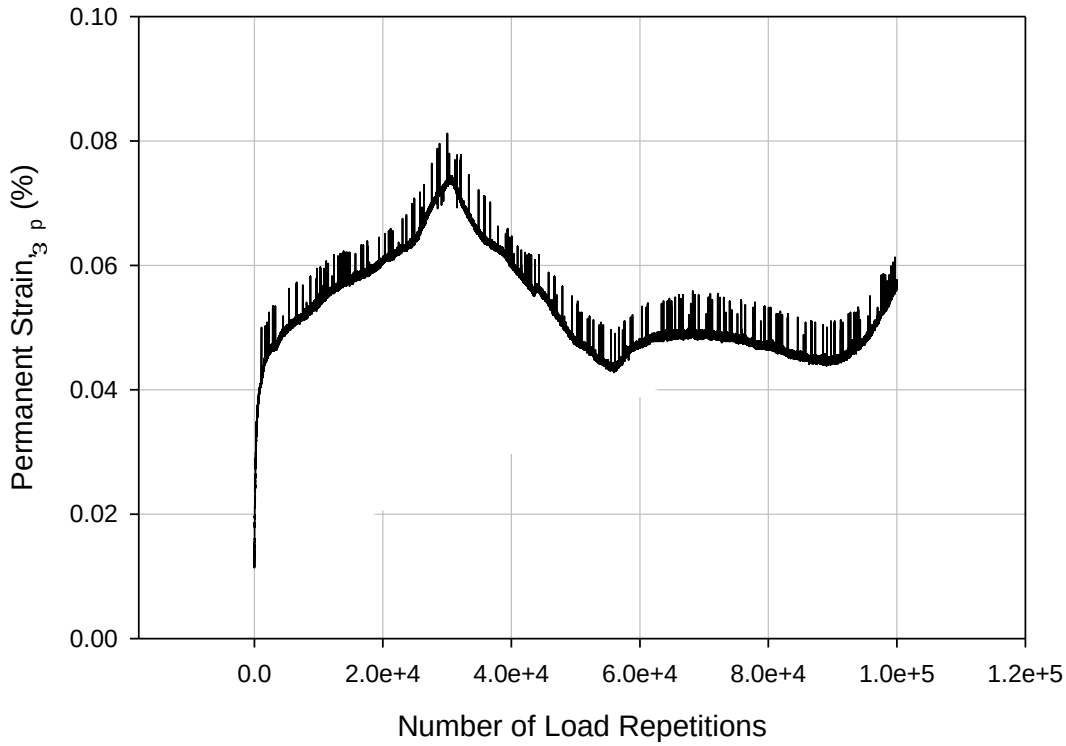

Figure 101. Permanent deformation accumulated with number of load repetitions for a subbase sample using ISU 100k method

Method #2 ISU 1k tests

ISU 1000k tests were conducted on Iowa US–30 recycled portland cement concrete materials (Table 59). This test method was designed to terminate the tests when permanent strain of 5% reached.

Table 59. Permanent deformation test sequence and stress values for ISU 1k tests

Sequence No.	Confining Stress		Deviator Stress		No. of Load Repetitions
	kPa	Psi	kPa	Psi	
1	103.4	15	20.7	3	1000

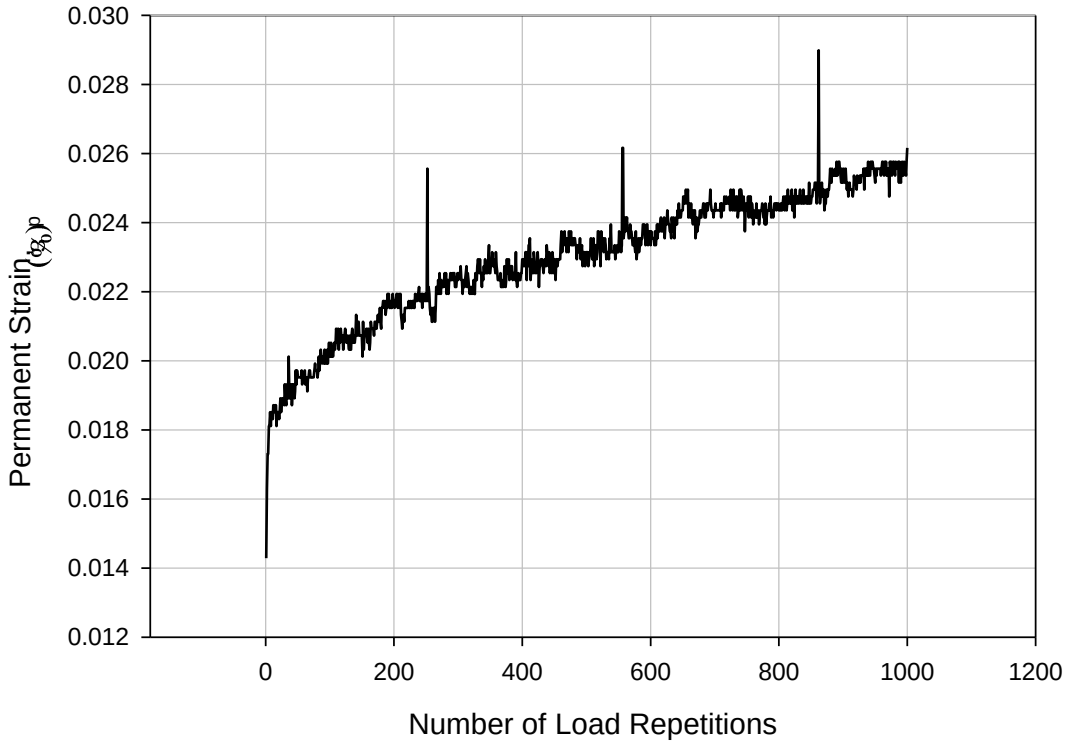

Figure 102. Permanent deformation accumulated with number of load repetitions for a subbase sample using ISU 1k method

Method #3 NCHRP 598 tests

NCHRP 598 tests were conducted on Martin Marietta crushed limestone, Manatt's RPCC/RAP, and Manatt's RAP materials (Table 60).

Table 60. Permanent deformation test sequences and stress values for NCHRP 598 tests

Sequence No.	Confining Pressure		Cyclic Stress		No. of Cycles
	(kPa)	(psi)	(kPa)	(psi)	
PC	103.4	15	68.9	10	50
1	103.4	15	68.9	10	1000
2	103.4	15	137.9	20	1000
3	103.4	15	275.8	40	1000
4	103.4	15	413.7	60	1000
5	103.4	15	551.6	80	1000
6	103.4	15	689.5	100	1000
7	103.4	15	827.4	120	1000
8	103.4	15	965.3	140	1000
9	103.4	15	1103.2	160	1000
10	103.4	15	1241.1	180	1000

Note: In system output, the sequences were numbered from 1 to 11 instead of PC to 10.

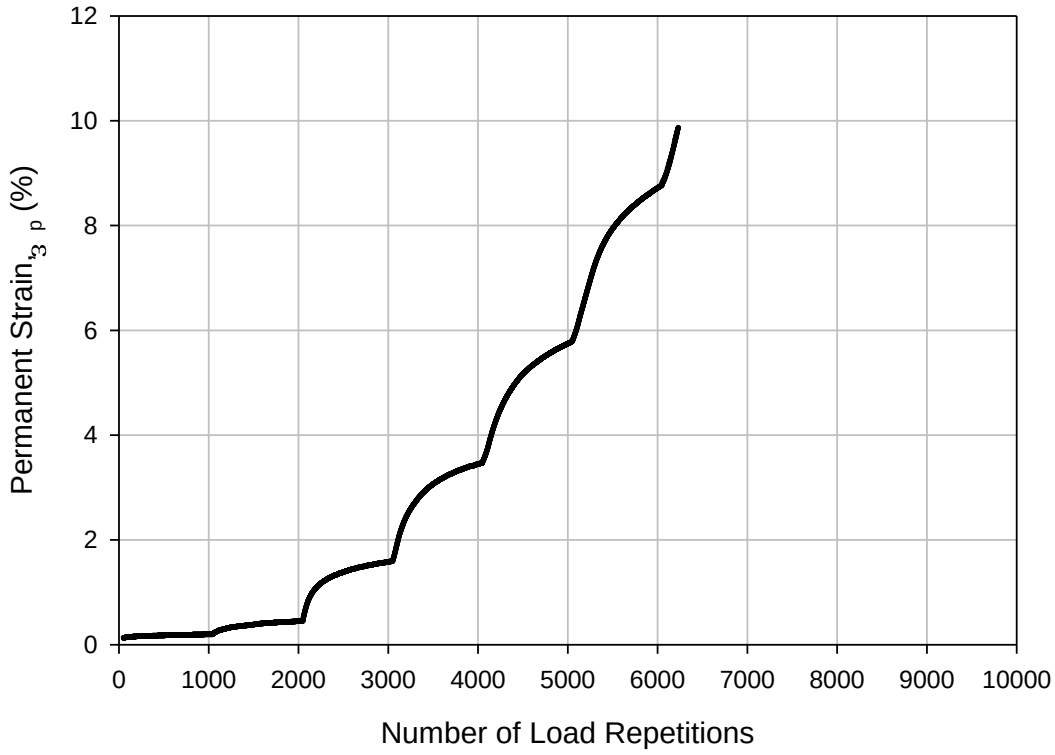

Figure 103. Permanent deformation accumulated with number of load repetitions for a subbase sample using NCHRP 598 method

Statistical analysis

Prediction model

Barksdale permanent deformation prediction model (Equation 28) was used to predict the permanent strain at given number of load repetitions.

$$\varepsilon_p = a + b \cdot \log_{10}(N) \quad (28)$$

1. Calculate and input the permanent strain with related number of load cycles into JMP.
2. Create the third column named as "% Ep Predicted" with formula

a b $\log_{10}$ (N) where a and b are assumed parameters and N is the actual number of load repetitions in first column. If the NCHRP 598 tests results are analyzed, the

a b $\log_{10}$ (N-n×1000) formula will be used and n is the load sequence number.

3. Run Analyze→ Modeling→ Nonlinear→ % Ep Predicted as Y, Response and %Ep as X, Predictor Formula. An example result for the nonlinear fit is shown in Figure 104 for ISU 100k test and is shown in Figure 105 for one load sequence in a NCHRP 598 test.

Nonlinear Fit

Prediction Model

Response: D-A3, Predictor: Column 8

Control Panel

Converged in Gradient

Warning: 3 missing Y's. 3 missing Models.

Criterion	Current	Stop Limit
Iteration	1	60
Obj Change	14971.027515	1e-15
Relative Gradient	1.472759e-10	0.000001
Gradient	1.475493e-10	0.000001

Parameter	Current Value	Lock
a	0.0249533192	
b	0.0545236158	

SSE 7.2955752819

N 99997

Edit Alpha	0.050
Convergence Criterion	0.00001
Goal SSE for CL	.

Plot

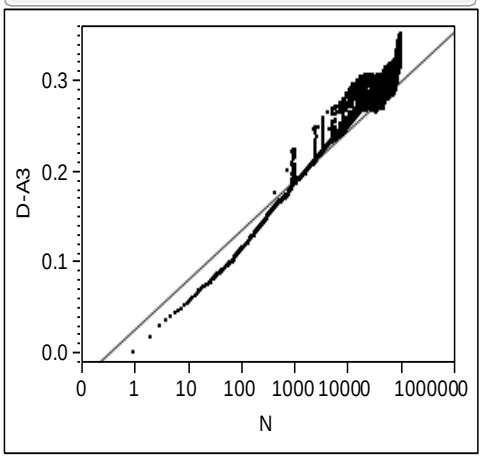

Parameter	Estimate	Low	High
a	0.0249533192	5	15
b	0.0545236158	0.0005	0.0015

Solution

SSE	DFE	MSE	RMSE
7.2955752819	99995	7.2959e-5	0.0085416

Parameter	Estimate	ApproxStdErr
a	0.0249533192	0.00028536
b	0.0545236158	0.00006222

Solved By: Analytic Gauss-Newton

Figure 104. Statistical nonlinear analysis on prediction of ε_p on a ISU 100k test sample

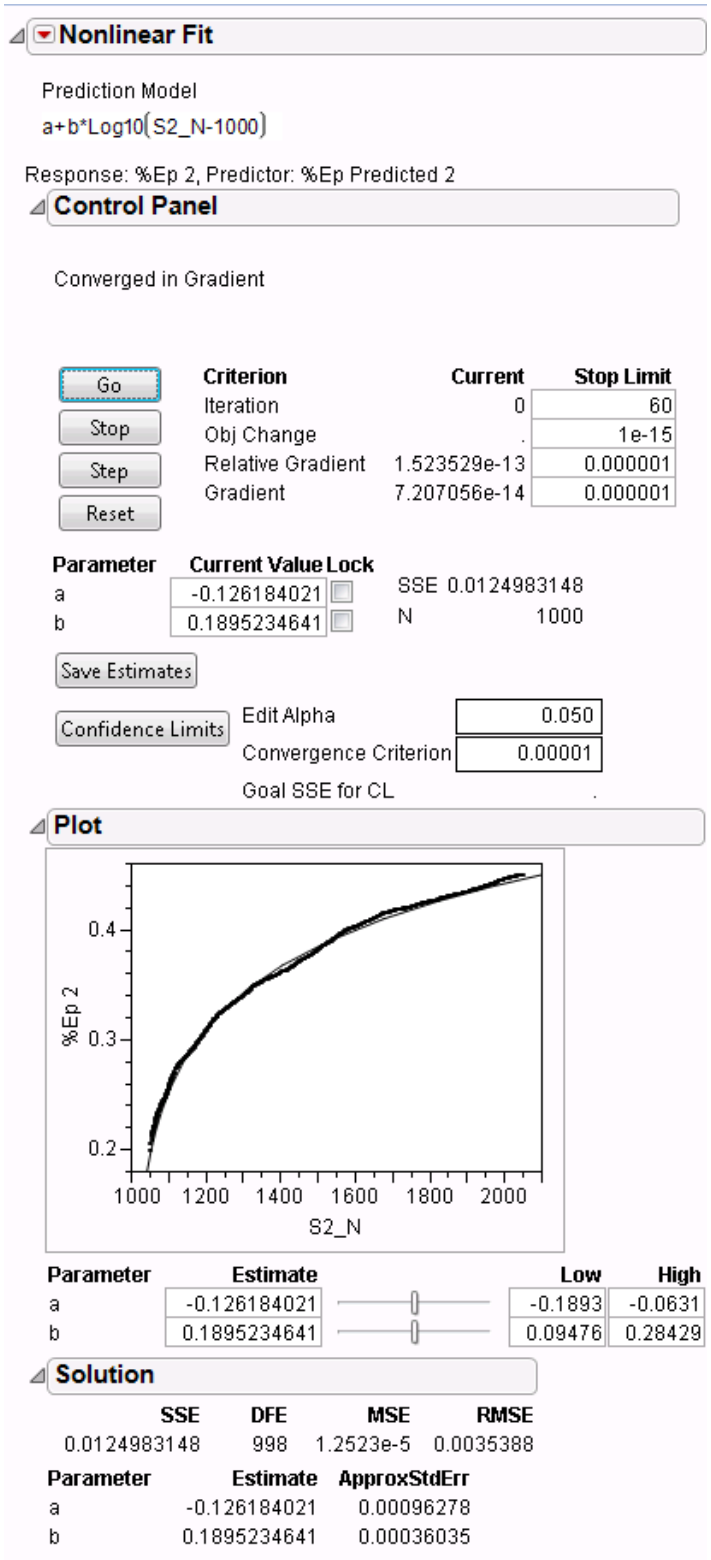

Figure 105. Statistical nonlinear analysis on prediction of ε_p on one load sequence for a NCHRP 598 test sample

The modified prediction model also fitted to the calculated permanent strains for NCHRP 598 test samples and the same statistical analysis procedures that were used for fitting Barksdale model are sued in obtain the regression coefficients in the modified model (Equation 29). The predicted permanent strains for one NCHRP 598 test sample are shown in Figure 106.

$$\varepsilon_{1,p} = k_1 + k_2 \cdot \sigma_d + k_3 \cdot \sigma_d^2 + \left[k_4 + \frac{k_5 \cdot (e^{k_6 \cdot \sigma_d} - 1)}{k_6}\right] \cdot \log_{10}[N - 1000 \cdot (S - 1)] \qquad (29)$$

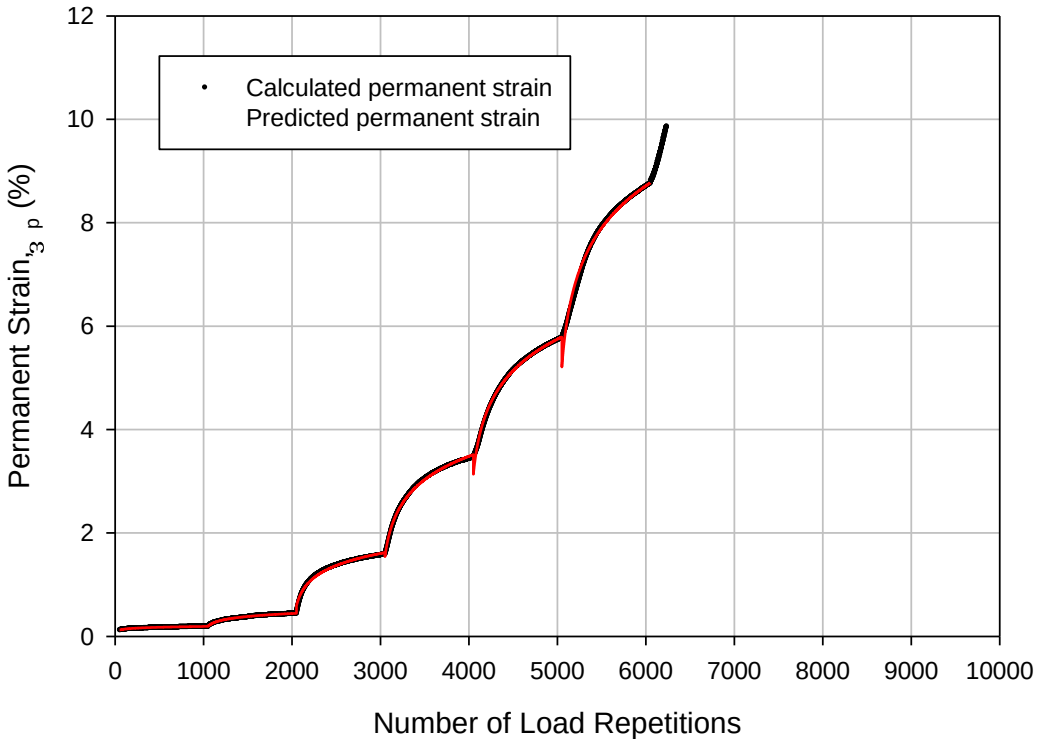

Figure 106. Modified model predicted permanent strain for a NCHRP 598 test sample

Significance of factors

The permanent strains (ε_p) at the end of each load sequence were summarized when the load sequences were completely finished. For example, if the ε_p reached 10% at 500 load repetitions in sequence 6, the permanent strains of up to sequence 5 were recorded for this test. In order to analysis the effects of materials, target fines content, and target relative density on accumulated permanent strain at the end of the load sequences, only permanent strain at the end of load sequence No. 1 (S1), sequence No. 2 (S2), sequence No. 3 (S3), sequence No. 4 (S4) were used as summarized.

Table 61. Factor analysis for permanent deformation tests

Source	Materials	Target Fines Content	Target RD	PC	ε_p at S1 (%)	ε_p at S2 (%)	ε_p at S3 (%)	ε_p at S4 (%)
Martin Marietta	Crushed Limestone	0%	85%	0.0855	0.1051	0.1478	0.2418	0.5029
		6%		0.0390	0.0524	0.0716	0.1257	0.2706
		12%		0.0657	0.0875	0.1176	0.1675	0.2100
		0%	90%	0.0570	0.0624	0.0888	0.1533	0.2435
		6%		0.0460	0.0542	0.0811	0.1350	0.1969
		12%		0.0427	0.0499	0.0627	0.0888	0.1050
		0%	95%	0.0714	0.0896	0.1283	0.2127	0.3712
		6%		0.0557	0.0654	0.0876	0.1293	0.1691
		12%		0.0388	0.0432	0.0577	0.0797	0.0985
Manatt's	RAP	0%	85%	1.0153	2.5484	3.7677	6.3011	9.0985
		6%		0.2188	0.7100	1.2667	2.7099	4.8042
		12%		0.1596	0.3920	0.6930	1.4991	2.8531
		0%	90%	0.6928	1.9612	3.0762	5.4340	8.0740
		6%		0.1404	0.4860	0.9208	2.0742	3.8392
		12%		0.1541	0.3711	0.6274	1.3767	2.7017
		0%	95%	0.5892	1.6027	2.5079	4.5193	6.9621
		6%		0.1312	0.3857	0.7263	1.6454	3.1927
		12%		0.1179	0.3030	0.5427	1.2373	2.5064
	RPCC/RAP	0%	85%	0.1853	0.2617	0.5469	1.5372	2.8798
		6%		0.0819	0.1041	0.2226	0.8231	1.7669
		12%		0.0488	0.0552	0.0879	0.1789	0.4524
		0%	90%	0.1193	0.1973	0.4496	1.4557	2.7389
		6%		0.0847	0.1084	0.2304	0.7960	1.6427
		12%		0.0509	0.0659	0.1009	0.2132	0.4553
		0%	95%	0.1306	0.1964	0.4099	1.2036	2.3384
		6%		0.0744	0.0908	0.1498	0.4638	1.0754
		12%		0.0579	0.0653	0.0894	0.1637	0.2976

JMP analysis on permanent strain at the end of first four load sequences

Whole Model

Actual by Predicted Plot

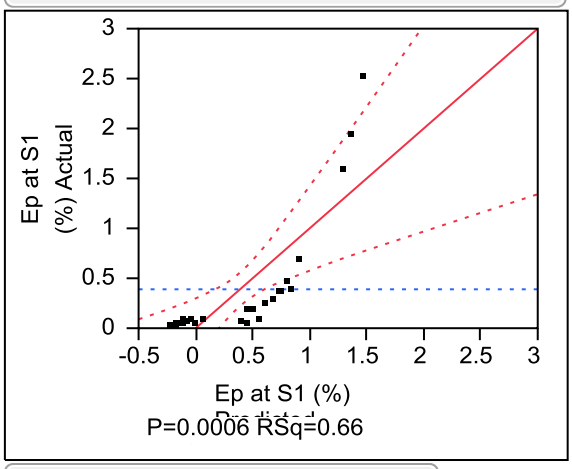

Summary of Fit

RSquare	0.66178
RSquare Adj	0.560314
Root Mean Square Error	0.417758
Mean of Response	0.389441
Observations (or Sum Wgts)	27

Analysis of Variance

Source	DF	Sum of Squares	Mean Square	F Ratio
Model	6	6.829591	1.13827	6.5222
Error	20	3.490437	0.17452	Prob > F
C. Total	26	10.320028		0.0006 *

Effect Tests

Source	Nparm	DF	Sum of Squares	F Ratio	Prob > F
Materials	2	2	4.6186629	13.2323	0.0002 *
Target Fines Content	2	2	2.0864962	5.9778	0.0092 *
Target RD (%)	2	2	0.1244320	0.3565	0.7045

Figure 107. JMP analysis on permanent strain at the end of load sequence No.1

Whole Model

Actual by Predicted Plot

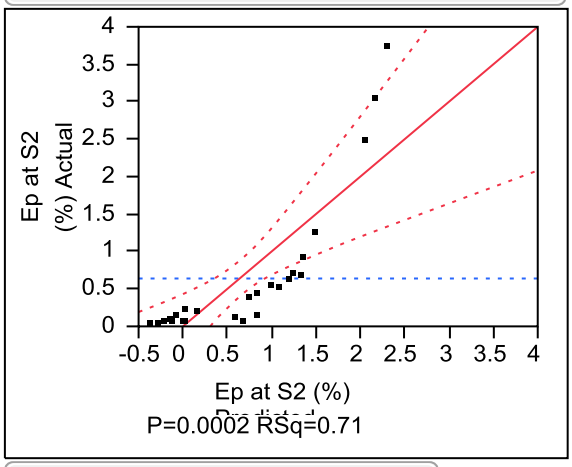

Summary of Fit

RSquare	0.709026
RSquare Adj	0.621734
Root Mean Square Error	0.590543
Mean of Response	0.639233
Observations (or Sum Wgts)	27

Analysis of Variance

Source	DF	Sum of Squares	Mean Square	F Ratio
Model	6	16.995789	2.83263	8.1224
Error	20	6.974831	0.34874	Prob > F
C. Total	26	23.970620		0.0002 *

Effect Tests

Source	Nparm	DF	Sum of Squares	F Ratio	Prob > F
Materials	2	2	11.807652	16.9289	<.0001 *
Target Fines Content	2	2	4.911582	7.0419	0.0048 *
Target RD (%)	2	2	0.276555	0.3965	0.6778

Figure 108. JMP analysis on permanent strain at the end of load sequence No.2

Whole Model

Actual by Predicted Plot

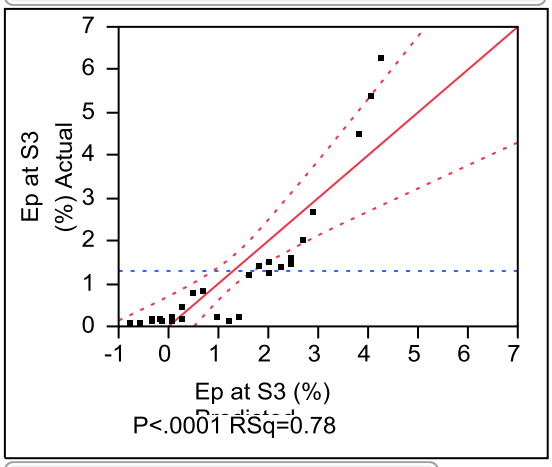

Summary of Fit

RSquare	0.780427
RSquare Adj	0.714555
Root Mean Square Error	0.890204
Mean of Response	1.295037
Observations (or Sum Wgts)	27

Analysis of Variance

Source	DF	Sum of Squares	Mean Square	F Ratio
Model	6	56.332909	9.38882	11.8476
Error	20	15.849259	0.79246	Prob > F
C. Total	26	72.182168		<.0001 *

Effect Tests

Source	Nparm	DF	Sum of Squares	F Ratio	Prob > F
Materials	2	2	39.893089	25.1703	<.0001 *
Target Fines Content	2	2	15.581134	9.8308	0.0011 *
Target RD (%)	2	2	0.858685	0.5418	0.5900

Figure 109. JMP analysis on permanent strain at the end of load sequence No.3

Whole Model

Actual by Predicted Plot

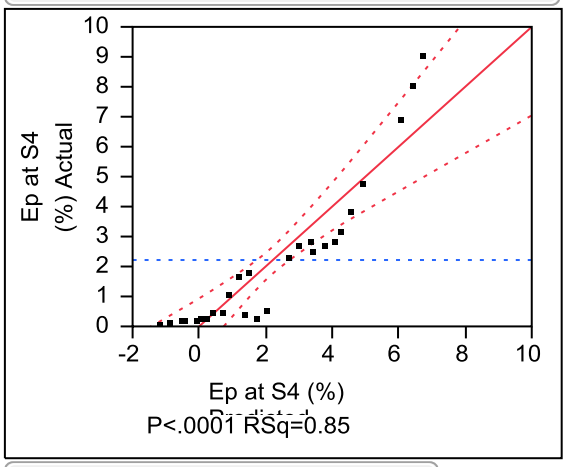

Summary of Fit

RSquare	0.847788
RSquare Adj	0.802124
Root Mean Square Error	1.113515
Mean of Response	2.216556
Observations (or Sum Wgts)	27

Analysis of Variance

Source	DF	Sum of Squares	Mean Square	F Ratio
Model	6	138.12079	23.0201	18.5659
Error	20	24.79831	1.2399	Prob > F
C. Total	26	162.91910		<.0001 *

Effect Tests

Source	Nparm	DF	Sum of Squares	F Ratio	Prob > F
Materials	2	2	103.98565	41.9326	<.0001 *
Target Fines Content	2	2	32.24842	13.0043	0.0002 *
Target RD (%)	2	2	1.88672	0.7608	0.4803

Figure 110. JMP analysis on permanent strain at the end of load sequence No.4

APPENDIX B. RESILIENT MODULUS TESTS ANALYSES

Resilient Moduli Calculation

Resilient modulus (M_r) tests were conducted on crushed limestone, recycled asphalt pavement (RAP), and recycled portland cement concrete (RPCC) materials. According to AASHTO T307-99 (2009), average resilient strain and applied maximum deviator stress were calculated separately for last five load repetitions in each load sequence (Table 62) for calculating resilient modulus. The parameters in prediction model were determined according to the average resilient moduli for all load sequences and calculated octahedral stress (T_{oct}) and bulk stress (σ_B) as example shown on Table 62.

Table 62. Last five load repetitions in load sequence 1 of resilient modulus test for a subbase sample

No. of Load Repetition	Applied Max Dev Stress, σd (kPa)	Applied Cyclic Dev Stress, σcyclic (kPa)	Applied Contact Dev Stress, σc (kPa)	Deflection LVDT (mm)	Resilient Strain, εr (%)	Resilient Modulus, Mr (MPa)
96	17.793	16.003	1.78981	0.04464	0.021981	72.8
97	17.370	15.323	2.04698	0.05276	0.025978	59.0
98	17.835	15.617	2.21804	0.05276	0.025978	60.1
99	18.303	16.422	1.88117	0.05276	0.025978	63.2
100	18.474	16.635	1.83911	0.05276	0.025978	64.0
Average	17.955	16.000	1.95501	0.05114	0.025178	63.8

Using data shown in Table 62, the resilient moduli for the last five load repetitions in Sequence No.1 were calculated using Equation 30 and the average resilient modulus was also calculated.

$$M_r = \frac{\text{Applied Cyclic Deviator Stress}}{\text{Resilient Strain}} \quad (30)$$

$$M_r(96th) = \frac{16.003}{0.021981\% \times 1000} = 72.8MPa$$

$$M_r(97th) = \frac{15.323}{0.025978\% \times 1000} = 59.0MPa$$

$$M_r(98th) = \frac{15.617}{0.025978\% \times 1000} = 60.1MPa$$

$$M_r(99th) = \frac{16.422}{0.025978\% \times 1000} = 63.2MPa$$

$$M_r(100th) = \frac{16.635}{0.025978\% \times 1000} = 64.0MPa$$

$$M_r(\text{Sequence 1}) = \frac{1}{5} \times (72.8 + 59.0 + 60.1 + 63.2 + 64.0) = 63.8MPa$$

Using the same procedures, the average M_r was calculated for each load sequence. In addition, using confining pressure and maximum deviator stress, the σ_B was calculated using Equation 31 and the T_{oct} was calculated using Equation 32 in Sequence No.1.

$$\sigma_B = 3 \times \sigma_c + \sigma_d = 3 \times 40.9 + 18.0 = 140.7\text{kPa} \quad (31)$$

$$T_{oct} = \frac{1}{3} \times \sqrt{2 \times (\sigma_d)^2} = \frac{1}{3} \times \sqrt{2 \times (18.0)^2} \times \frac{1}{1000} = 0.0085MPa \quad (32)$$

Table 63. All load sequences for a subbase sample

Sequence No.	Confining Pressure, σ_c (kPa)	Max Deviator Stress, σ_d (kPa)	Mean Bulk Stress, σ_B (MPa)	Avgerage M_r (MPa)	T_{oct} (MPa)
PC	41.4	27.6	0.0804	249.2	
1	40.9	18.0	0.1038	63.8	0.0085
2	41.1	42.0	0.1270	119.2	0.0198
3	40.9	65.4	0.1385	102.0	0.0308
4	40.9	34.6	0.1755	80.2	0.0163
5	40.7	72.0	0.2092	130.5	0.0339
6	27.1	105.3	0.2774	174.7	0.0496
7	26.9	70.6	0.3427	203.6	0.0333
8	27.2	135.7	0.4067	268.8	0.0639
9	27.0	198.6	0.3814	264.6	0.0936
10	27.1	70.5	0.4129	250.2	0.0332
11	13.4	102.8	0.5086	277.4	0.0485
12	13.2	197.7	0.5123	335.7	0.0932
13	13.4	102.1	0.5440	274.6	0.0481
14	13.4	133.6	0.6715	327.8	0.0630
15	13.5	260.3	0.0804	372.7	0.1227

Statistical Analysis

Prediction model

The calculated resilient moduli were used to fit the universal model (Equation 33) to determine the parameters k_1, k_2, and k_3 based on the calculated T_{oct} and σ_B in Table 63. In this calculation, the atmospheric pressure P_a value was assumed to be constant as 0.101325

$$M_r = k1 \times P_a \times \left(\frac{\sigma_B}{P_a}\right)^{k2} \times \left(1 + \frac{T_{oct}}{P_a}\right)^{k3} \quad (33)$$

The statistical nonlinear modeling analysis was conducted to determine the values of regression coefficients k_1, k_2, and k_3.

4. Input the bulk stress, octahedral stress, calculated M_r, and a column named "M_r Pred" with formula of Equation 33.
5. Run Analyze→ Modeling→ Nonlinear→ M_r as Y, Response and M_r Pred as X, Predictor Formula (Figure 111).

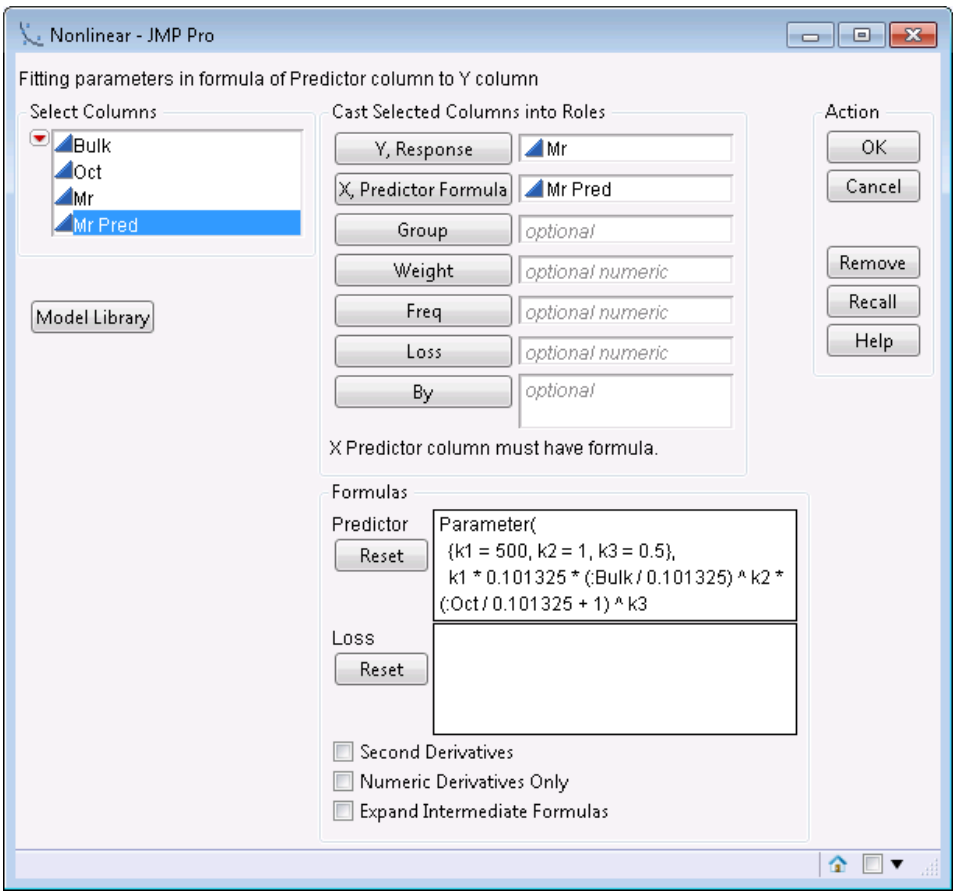

Figure 111. Nonlinear statistical analysis dialog in JMP program

6. Run analysis and determine k1, k2, and k3 values and record SSE values that are shown in the generated nonlinear analysis report. An example of the generated report is shown in Figure 112.

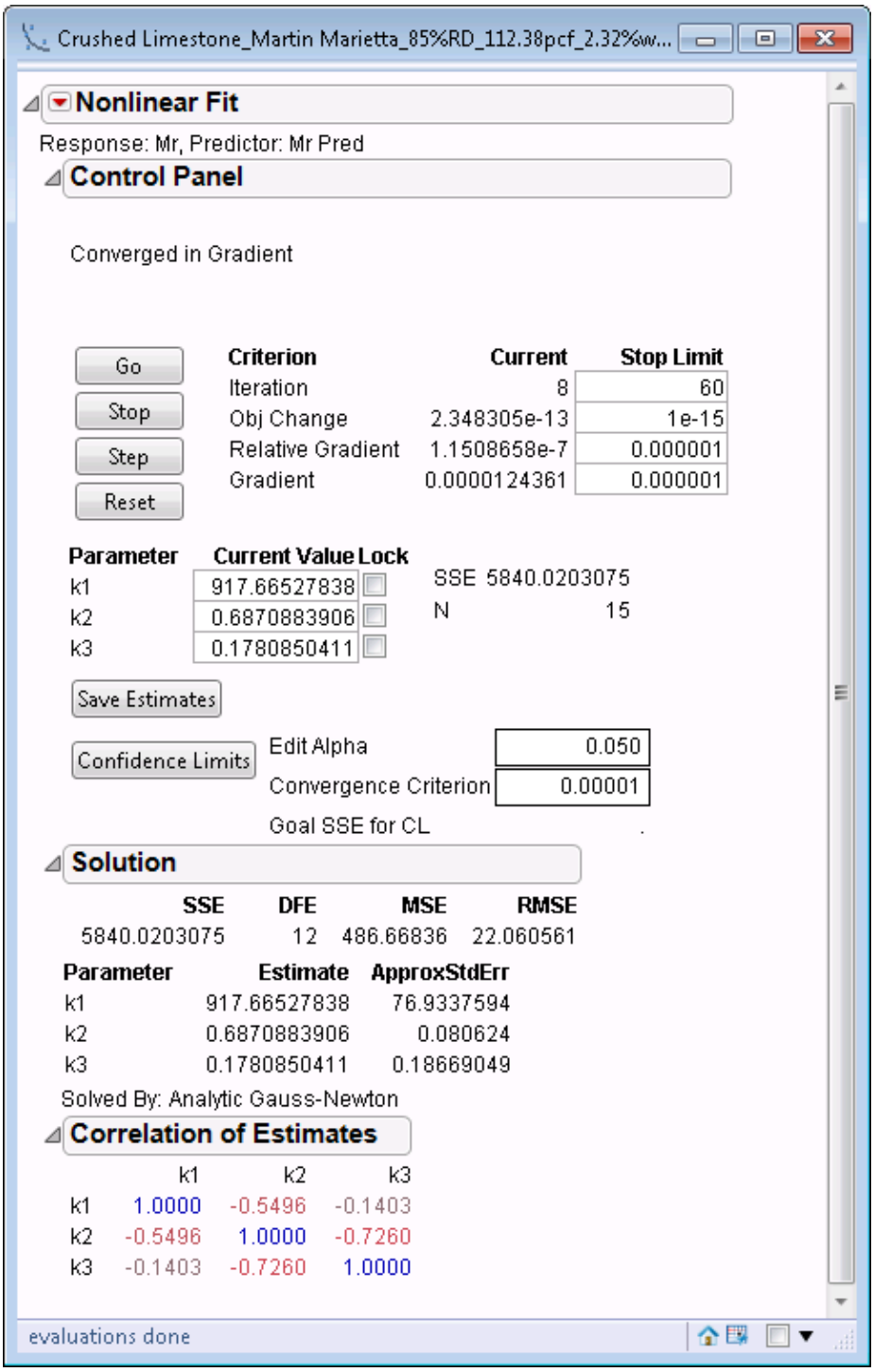

Figure 112. An example of the JMP generated nonlinear analysis report

7. Run Analyze→ Distribution→ Set M_r as Y column → Record Standard Deviation→ Determine R^2. An example of the M_r distribution is shown in Figure 113.

$$R^2 = \frac{SS_{Model}}{SS_{Total}} = 1 - \frac{SS_{Error}}{SS_{Total}}$$

$$SS_{Total} = (N-1) \times (Standard\ Deviation)^2 = (15-1) \times (99.299603)^2$$
$$= 138045.76$$

$$R^2 = 1 - \frac{SS_{Error}}{SS_{Total}} = 1 - \frac{5840.0203}{138045.76} = 0.9577$$

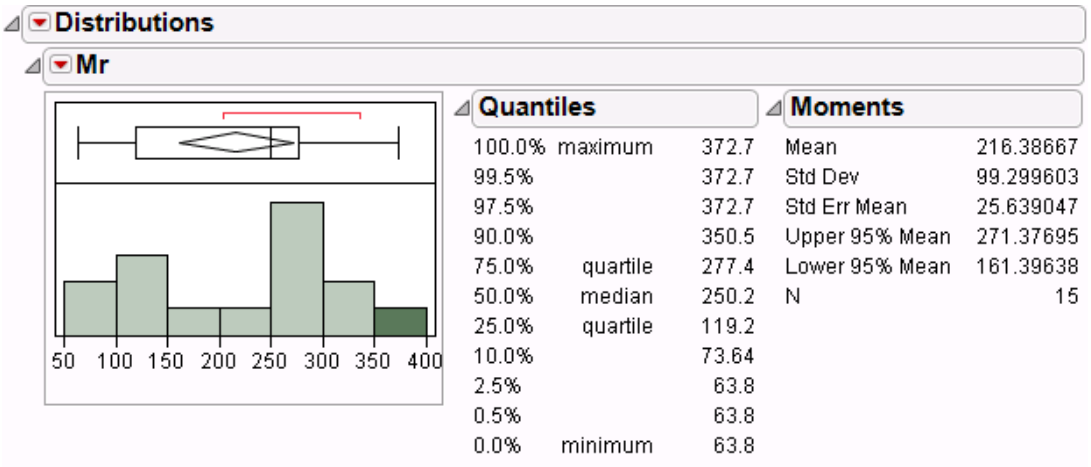

Figure 113. An example of histogram of M_r values

Significance of parameters

According to JMP nonlinear analysis on predicting resilient modulus, k1, k2, and k3 are three parameters concluded for the universal model.

8. Estimate and approximate standard error (Approx Std Err) from nonlinear modeling M_r were recorded and imputed into two new columns in JMP program
9. Create a new column named as "Z" with formula $\frac{Estimate}{ApproxStdErr}$
10. Create another new column named as "p-value" with formula$2 \times [1 - Normal\ Distribution\ (Z)]$
11. If p-value < 0.05, the parameter was concluded as significant with null hypothesis that H_o: k=0 is true.

Significance of factors

Materials type, fines content, and relative density were tested for their effects on prediction parameters k_1, k_2, and k_3. In order to run statistical analysis, the natural fines content was excluded and the target values were used to test the effects of the factors. The factors and universal prediction model's parameters were summarized in JMP worksheet (Figure 114). The sequence No. indicates the stress levels as Table 63 summarized.

Whole Model

Actual by Predicted Plot

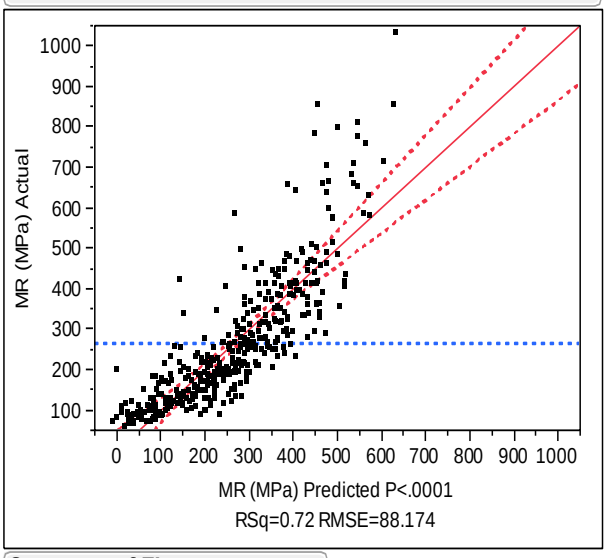

Summary of Fit

RSquare	0.715322
RSquare Adj	0.700495
Root Mean Square Error	88.1739
Mean of Response	264.9058
Observations (or Sum Wgts)	405

Analysis of Variance

Source	DF	Sum of Squares	Mean Square	F Ratio
Model	20	7501689	375084	48.2446
Error	384	2985460	7775	Prob > F
C. Total	404	10487149		<.0001*

Effect Tests

Source	Nparm	DF	Sum of Squares	F Ratio	Prob > F
Material	2	2	2126319.2	136.7472	<.0001*
RD (%)	2	2	62078.6	3.9924	0.0192*
F200 (%)	2	2	362501.3	23.3131	<.0001*
Sequence No.	14	14	4950789.8	45.4848	<.0001*

Figure 114. Statistical analysis for significance of all factors affecting M_r

Material

Leverage Plot

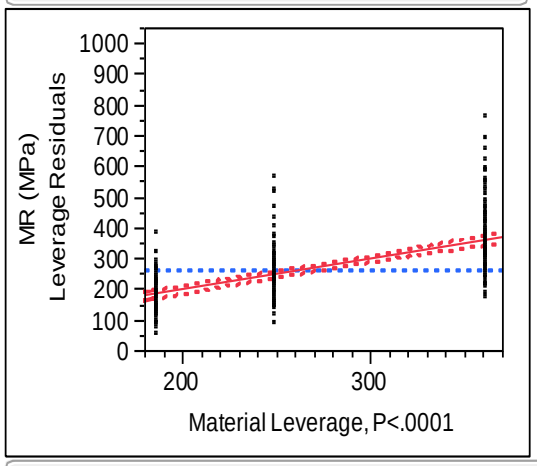

Least Squares Means Table

Level	Least Sq Mean	Std Error	Mean
Crushed Limestone	360.75347	7.5888010	360.753
RAP	248.36964	7.5888010	248.370
RPCC/RAP	185.59443	7.5888010	185.594

LSMeans Differences Student's t

a= 0.050 t= 1.96616

Level		Least Sq Mean
Crushed Limestone	A	360.75347
RAP	B	248.36964
RPCC/RAP	C	185.59443

Levels not connected by same letter are significantly different.

Figure 115. Statistical analysis for significance of material types affecting M_r

RD (%)

Leverage Plot

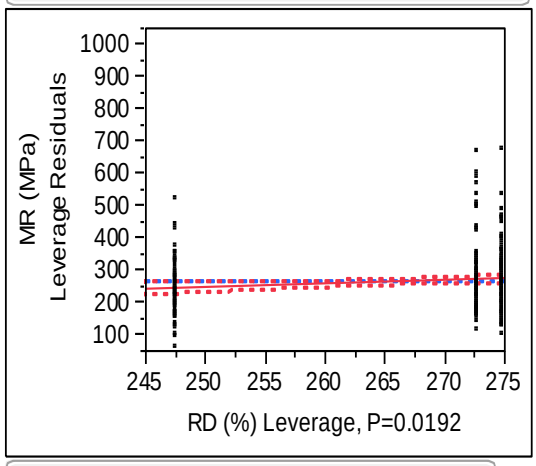

Least Squares Means Table

Level	Least Sq Mean	Std Error	Mean
85	274.62551	7.5888010	274.626
90	272.65818	7.5888010	272.658
95	247.43384	7.5888010	247.434

LSMeans Differences Student's t

a= 0.050 t= 1.96616

Level		Least Sq Mean
85	A	274.62551
90	A	272.65818
95	B	247.43384

Levels not connected by same letter are significantly different.

Figure 116. Statistical analysis for significance of RD affecting M_r

F200 (%)

Leverage Plot

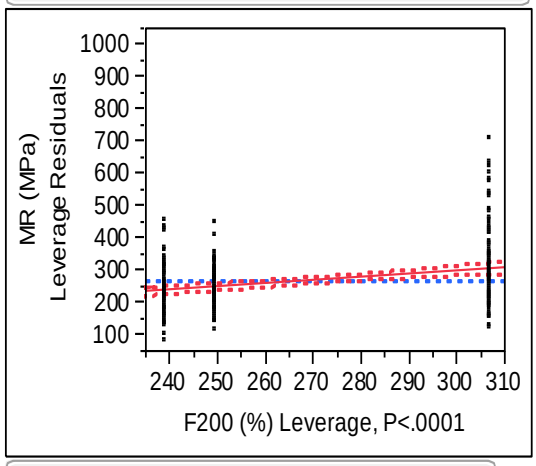

Least Squares Means Table

Level	Least Sq Mean	Std Error	Mean
0	238.79765	7.5888010	238.798
12	306.79341	7.5888010	306.793
6	249.12648	7.5888010	249.126

LSMeans Differences Student's t

a= 0.050 t= 1.96616

Level		Least Sq Mean
12	A	306.79341
6	B	249.12648
0	B	238.79765

Levels not connected by same letter are significantly different.

Figure 117. Statistical analysis for significance of F_{200} affecting M_r

Sequence No.

Leverage Plot

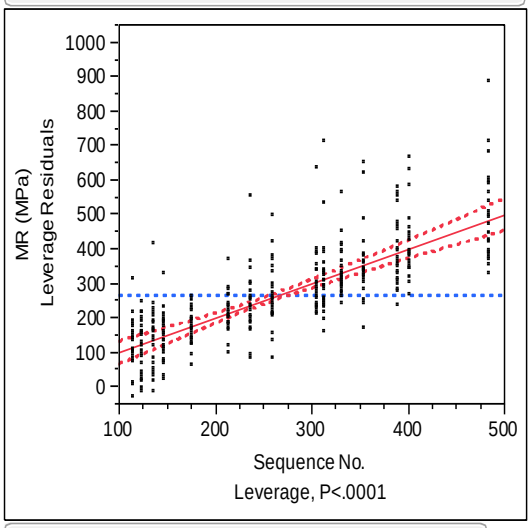

LSMeans Differences Student's t

a= 0.050 t= 1.96616

Level		Least Sq Mean
S15	A	483.41415
S12	B	400.39082
S14	B	388.16743
S13	B C	353.94288
S9	C D	330.96853
S11	C D	312.31641
S8	D E	304.76691
S10	E F	259.35166
S7	F	235.72206
S6	F G	212.87002
S5	G H	174.78566
S3	H I	145.51999
S4	H I	135.05665
S2	I	122.77061
S1	I	113.54392

Levels not connected by same letter are significantly different.

LS Means Plot

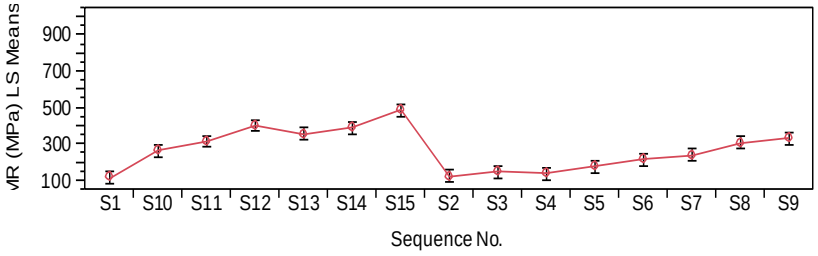

Figure 118. Statistical analysis for significance of stress levels affecting M_r

Summary of Statistical Analysis on Resilient Moduli

Test number was assigned for each M_r test and related target sample properties were summarized in Table 64.

Table 64. Test numbers and sample target properties

Crushed Limestone					RAP					RPCC/RAP				
Test No.	Fines Content (%)	w (%)	RD (%)	γ_d (pcf)	Test No.	Fines Content (%)	w (%)	RD (%)	γ_d (pcf)	Test No.	Fines Content (%)	w (%)	RD (%)	γ_d (pcf)
M1	0.0	2.3	85.0	120.9	M13	0.0	2.9	85.0	100.3	M25	0.0	6.0	85.0	97.1
M2	6.0	2.3	85.0	123.9	M14	2.0	2.9	85.0	95.0	M26	3.5	6.0	85.0	102.7
M3	7.9	2.3	85.0	112.4	M15	6.0	2.9	85.0	108.3	M27	6.0	6.0	85.0	106.8
M4	12.0	2.3	85.0	129.4	M16	12.0	2.9	85.0	112.2	M28	12.0	6.0	85.0	111.7
M5	0.0	2.3	90.0	122.2	M17	0.0	2.9	90.0	101.1	M29	0.0	6.0	90.0	98.1
M6	6.0	2.3	90.0	125.4	M18	2.0	2.9	90.0	95.8	M30	3.5	6.0	90.0	103.3
M7	7.9	2.3	90.0	112.7	M19	6.0	2.9	90.0	109.1	M31	6.0	6.0	90.0	108.0
M8	12.0	2.3	90.0	130.8	M20	12.0	2.9	90.0	113.4	M32	12.0	6.0	90.0	113.0
M9	0.0	2.3	95.0	123.5	M21	0.0	2.9	95.0	102.0	M33	0.0	6.0	95.0	99.1
M10	6.0	2.3	95.0	127.0	M22	2.0	2.9	95.0	96.6	M34	3.5	6.0	95.0	103.9
M11	7.9	2.3	95.0	113.1	M23	6.0	2.9	95.0	110.1	M35	6.0	6.0	95.0	109.3
M12	12.0	2.3	95.0	132.3	M24	12.0	2.9	95.0	114.6	M36	12.0	6.0	95.0	114.3

Note: w = moisture content; RD = relative density; γ_d = dry unit weight.

Table 65. Prediction model summary for resilient modulus tests on crushed limestone materials

Test No.	Equation parameters												
	k1			k2			k3			SSE	SD (Mr)	R^2	MSE
	Value	P-value	SIG Y/N	Value	P-value	SIG Y/N	Value	P-value	SIG Y/N				
M1	1685.60	<0.0001	Y	0.549	<0.0001	Y	0.594	0.0413	Y	49094.2	186.36	0.8990	4091.2
M2	1373.59	<0.0001	Y	0.614	<0.0001	Y	0.393	0.0234	Y	13422.0	153.37	0.9592	1118.5
M3	917.67	<0.0001	Y	0.687	<0.0001	Y	0.178	0.3401	N	5840.0	99.30	0.9577	486.7
M4	841.53	<0.0001	Y	0.740	<0.0001	Y	1.418	<0.0001	Y	55760.9	280.56	0.9494	4646.7
M5	1068.93	<0.0001	Y	0.511	<0.0001	Y	0.942	<0.0001	Y	4746.3	143.30	0.9835	395.5
M6	1436.54	<0.0001	Y	0.734	<0.0001	Y	0.183	0.5342	N	48798.0	186.29	0.8996	4066.5
M7	910.53	<0.0001	Y	0.600	<0.0001	Y	0.187	0.3607	N	5476.5	79.21	0.9377	456.4
M8	2227.49	<0.0001	Y	0.829	<0.0001	Y	-0.188	1.402	N	146230.6	275.55	0.8624	12185.9
M9	1121.10	<0.0001	Y	0.562	<0.0001	Y	0.898	<0.0001	Y	8078.1	159.43	0.9773	673.2
M10	1512.07	<0.0001	Y	0.556	<0.0001	Y	0.384	0.0832	N	23624.5	147.97	0.9229	1968.7
M11	836.61	<0.0001	Y	0.608	<0.0001	Y	0.439	0.0229	Y	5328.1	91.48	0.9545	444.0
M12	862.90	<0.0001	Y	0.334	<0.0001	Y	1.767	<0.0001	Y	3789.3	159.79	0.9894	315.8

Note: SIG = significant; Y = yes; N = no; SSE= Sum squares error; SD = standard deviation; MSE = mean squares error.

Table 66. Prediction model summary for resilient modulus tests on RAP materials

Test No.	Equation parameters											
	k1			k2			k3			SSE	SD (Mr)	R^2	MSE
	Value	P-value	SIG Y/N	Value	P-value	SIG Y/N	Value	P-value	SIG Y/N				
M13	1625.30	<0.0001	Y	0.631	0.0129	Y	-0.218	1.4978	N	36522.7	116.38	0.8074	3043.6
M14	867.39	<0.0001	Y	0.452	<0.0001	Y	0.565	0.0189	Y	6832.5	73.54	0.9098	569.4
M15	1337.79	<0.0001	Y	0.566	<0.0001	Y	-0.168	1.3653	N	22113.1	84.40	0.7783	1842.8
M16	928.79	<0.0001	Y	0.615	<0.0001	Y	0.427	0.0659	N	9932.5	102.97	0.9331	827.7
M17	787.44	<0.0001	Y	0.550	<0.0001	Y	0.307	0.0055	Y	1318.8	66.55	0.9787	109.9
M18	856.93	<0.0001	Y	0.991	<0.0001	Y	-0.570	1.9764	N	11777.5	109.65	0.9300	981.5
M19	951.70	<0.0001	Y	0.561	<0.0001	Y	0.404	0.0305	Y	5485.3	91.26	0.9530	457.1
M20	2322.10	<0.0001	Y	0.821	<0.0001	Y	-1.125	1.986	N	91014.3	157.44	0.7377	7584.5
M21	804.08	<0.0001	Y	0.610	<0.0001	Y	0.243	0.0772	N	2330.1	72.98	0.9688	194.2
M22	1080.99	<0.0001	Y	0.854	<0.0001	Y	-0.581	1.9742	N	12835.4	97.76	0.9041	1069.6
M23	1057.41	<0.0001	Y	0.590	<0.0001	Y	0.279	0.2722	N	12296.1	98.98	0.9103	1024.7
M24	2079.20	<0.0001	Y	0.064	0.7021	N	0.902	0.055	N	63918.9	97.01	0.5149	5326.6

Note: SIG = significant; Y = yes; N = no; SSE= Sum squares error; SD = standard deviation; MSE = mean squares error.

Table 67. Prediction model summary for resilient modulus tests on RPCC/RAP materials

Test No.	Equation parameters											
	k1			k2			k3			SSE	SD (M_r)	R^2	MSE
	Values	P-value	SIG Y/N	Values	P-value	SIG Y/N	Values	P-value	SIG Y/N				
M25	626.21	<0.0001	Y	0.7259	<0.0001	Y	0.3095	0.0811	N	3318.33	81.72	0.9645	276.5
M26	1247.67	<0.0001	Y	0.6622	<0.0001	Y	0.2706	0.1346	N	10548.53	139.25	0.9611	879.0
M27	627.83	<0.0001	Y	0.5410	<0.0001	Y	0.6520	0.0093	Y	5430.60	71.89	0.9250	452.5
M28	1360.70	<0.0001	Y	0.7036	<0.0001	Y	-0.2967	1.6519	N	24535.87	105.32	0.8420	2044.7
M29	779.56	<0.0001	Y	0.7313	<0.0001	Y	-0.0379	1.2378	N	1855.29	77.45	0.9779	154.6
M30	1780.75	<0.0001	Y	0.6320	0.0003	Y	-0.5330	1.7439	N	57382.74	114.03	0.6848	4781.90
M31	721.84	<0.0001	Y	0.4978	<0.0001	Y	0.3939	0.0153	Y	2044.31	57.47	0.9558	170.4
M32	766.61	<0.0001	Y	0.7278	<0.0001	Y	0.2654	0.1295	N	4596.04	95.79	0.9642	383.0
M33	701.84	<0.0001	Y	0.4864	<0.0001	Y	0.4704	<0.0001	Y	718.84	57.54	0.9845	59.9
M34	728.98	<0.0001	Y	0.3169	<0.0001	Y	1.2468	<0.0001	Y	3002.48	79.36	0.9659	250.2
M35	1184.37	<0.0001	Y	0.4760	<0.0001	Y	0.2512	0.3681	N	12988.62	80.19	0.8557	1082.4
M36	570.83	<0.0001	Y	0.6027	<0.0001	Y	1.0400	<0.0001	Y	2626.39	100.05	0.9813	218.9

Note: SIG = significant; Y = yes; N = no; SSE= Sum squares error; SD = standard deviation; MSE = mean squares error.

Resulient Modulus versus Bulk Stess

This section summarizes the relationships between the M_r values and the bulk stresses on the plots. In addition to the actual measured M_r values, the predicted M_r values are also shown in the plots. The predicted M_r values were calculated by fitting the universal model (Equation 33) to the actual values. The test numbers (e.g., M3, M7, M11) that were denoted in the results chapter and the target relative density (RD) are shown in the figure legends for reference. Moreover, the actual RD values are shown in the parentheses in the legends.

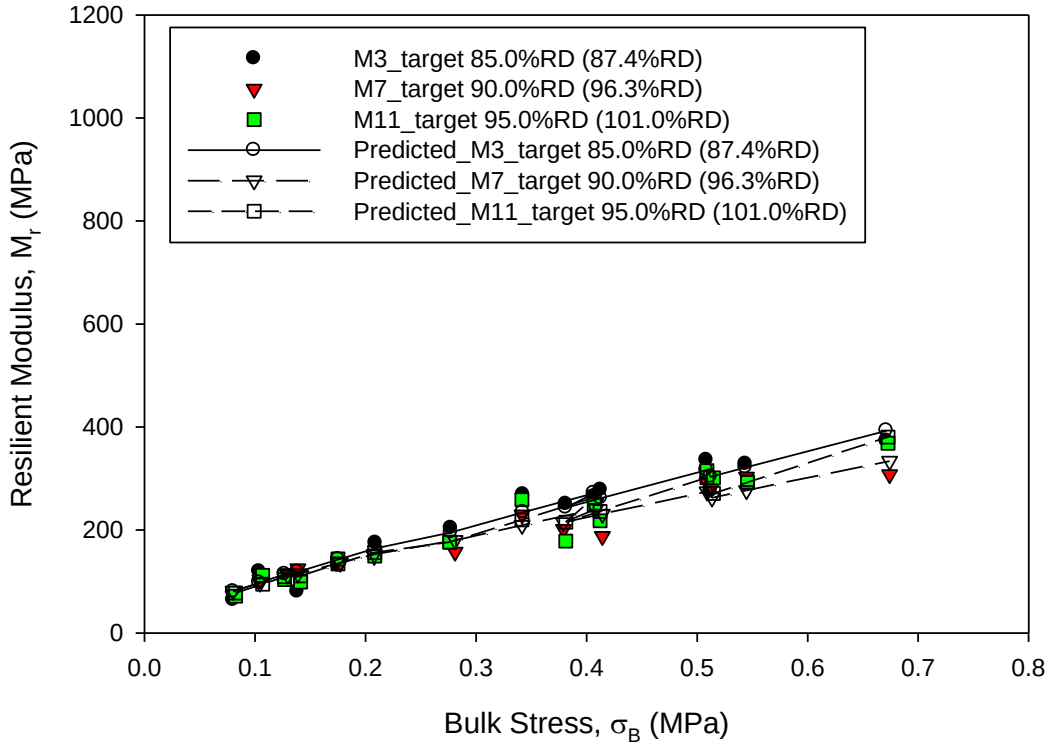

Figure 119. M_r vs. σ_B on crushed limestone sample with natural F_{200}

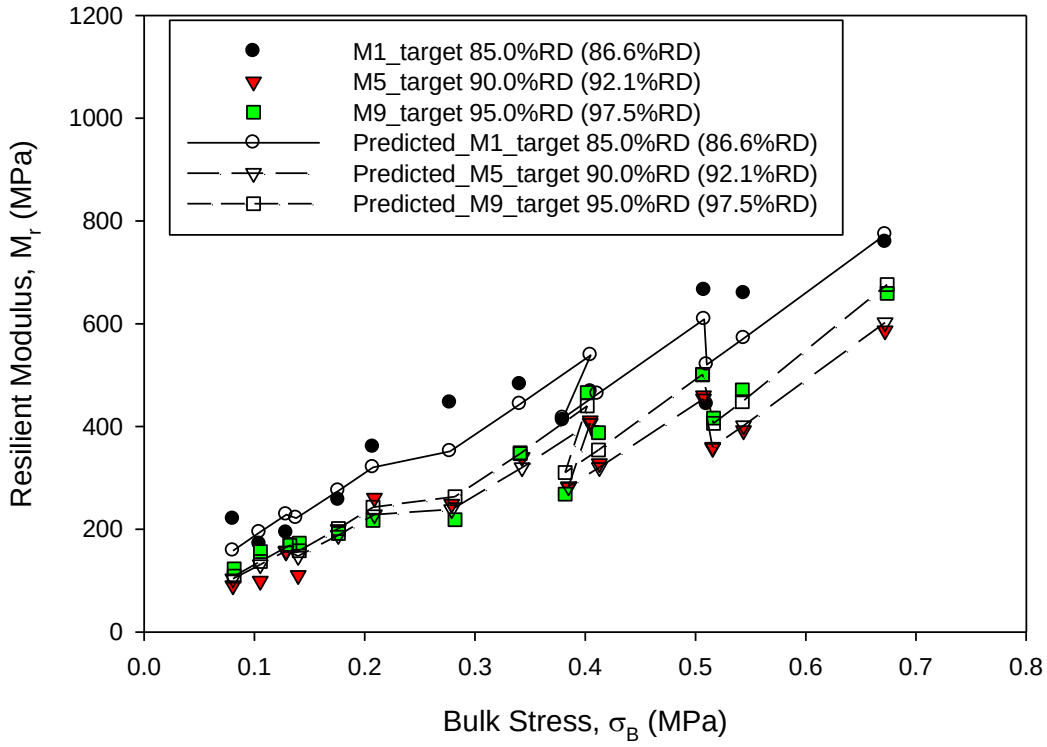

Figure 120. M_r vs. σ_B on crushed limestone sample with target 0% F_{200}

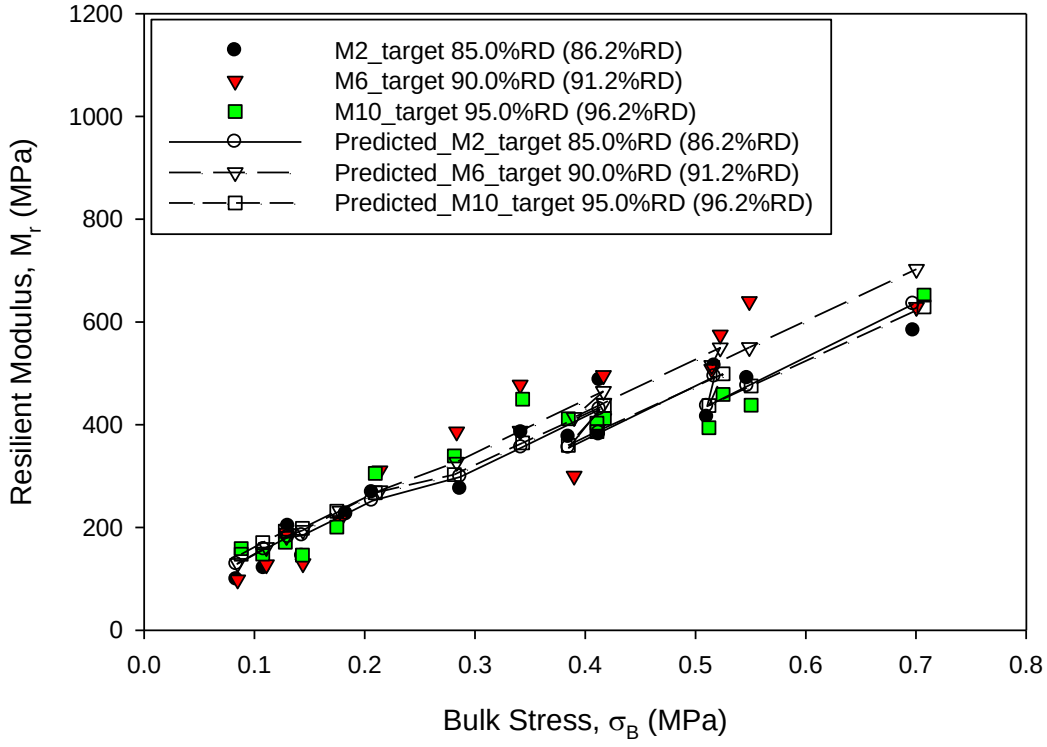

Figure 121. M_r vs. σ_B on crushed limestone sample with target 6% F_{200}

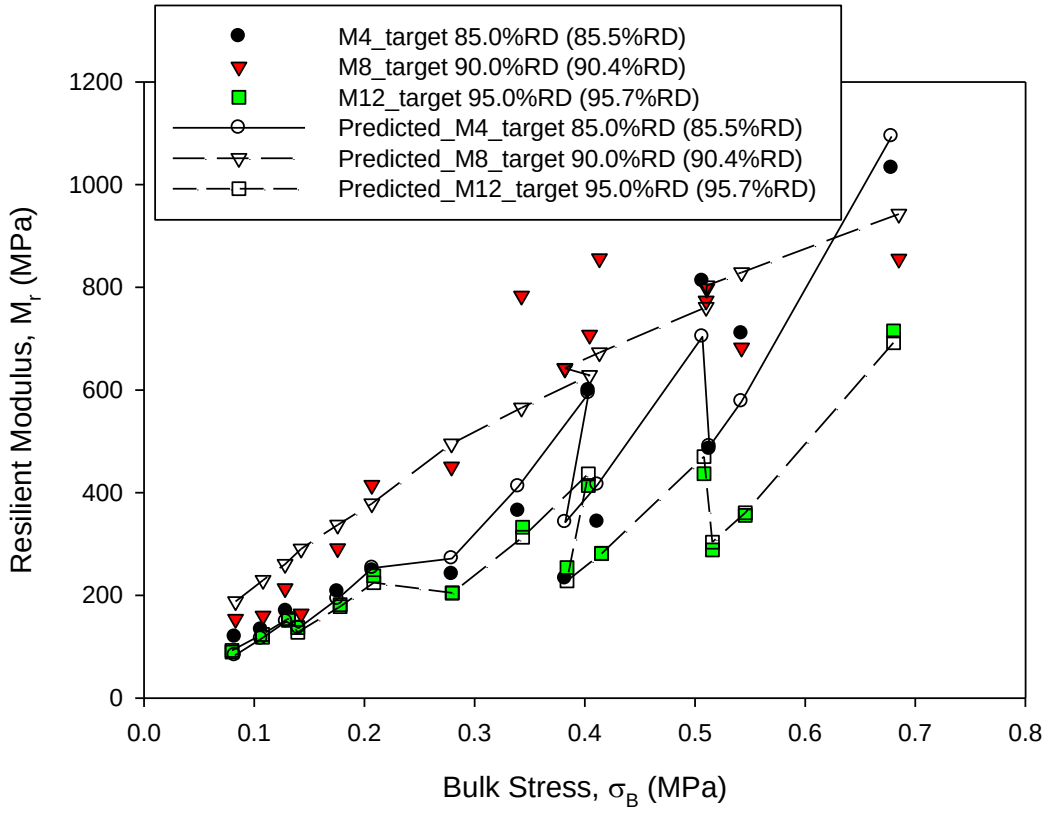

Figure 122. M_r vs. σ_B on crushed limestone sample with target 12% F_{200}

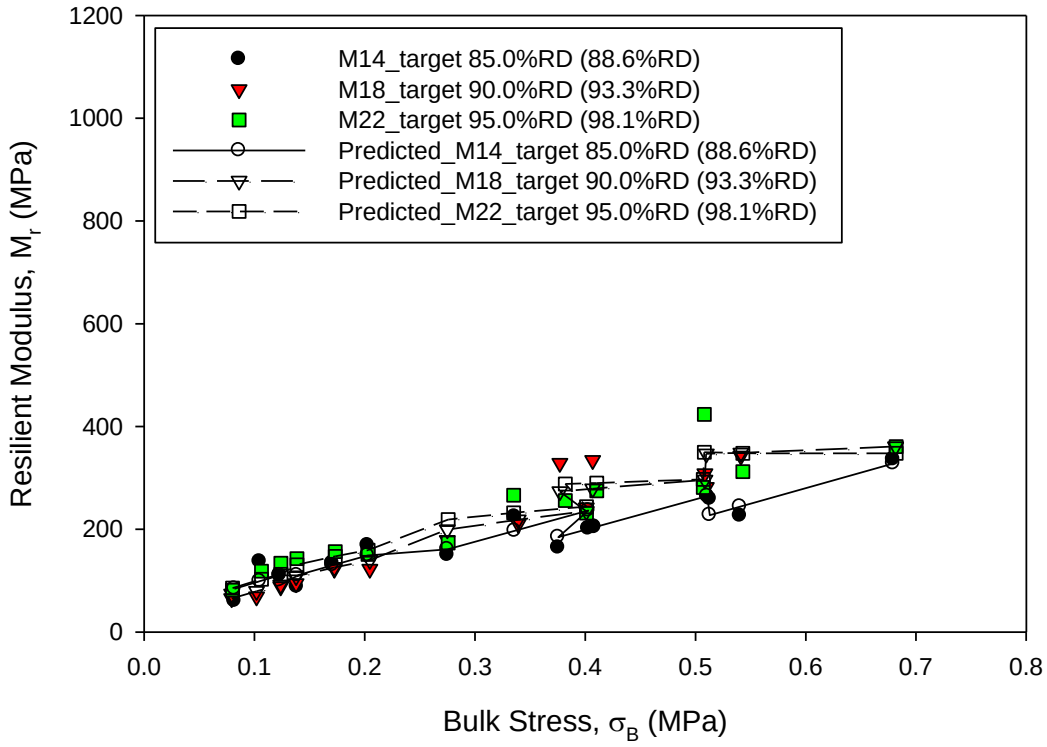

Figure 123. M_r vs. σ_B on RAP sample with natural F_{200}

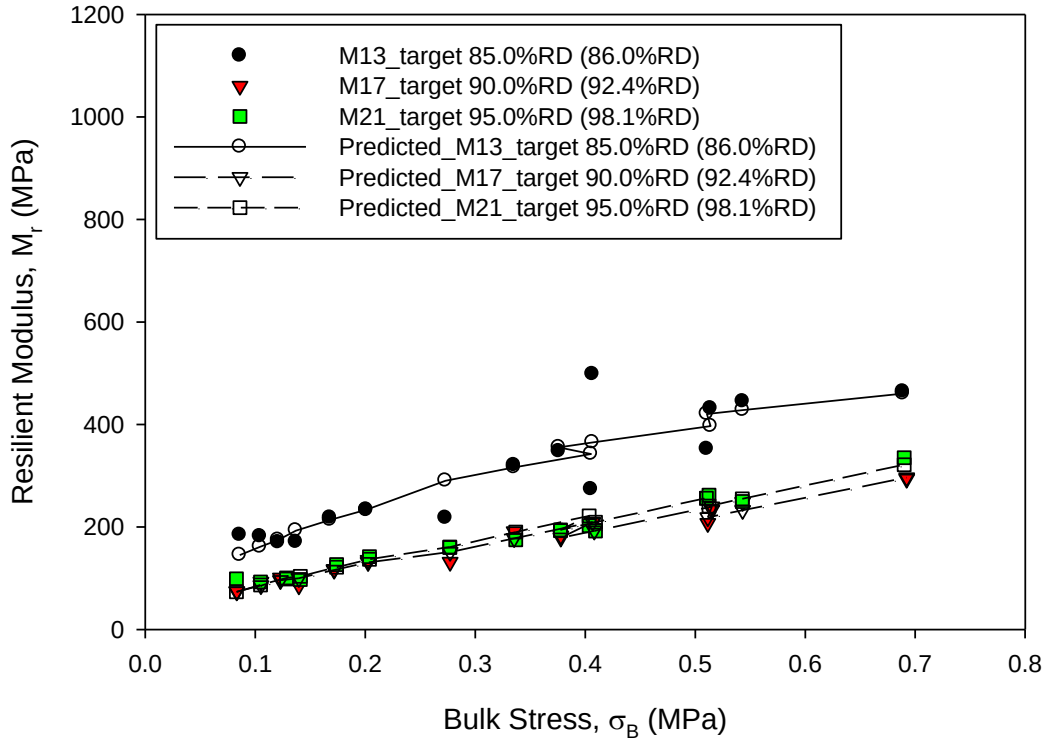

Figure 124. M_r vs. σ_B on RAP sample with 0% F_{200}

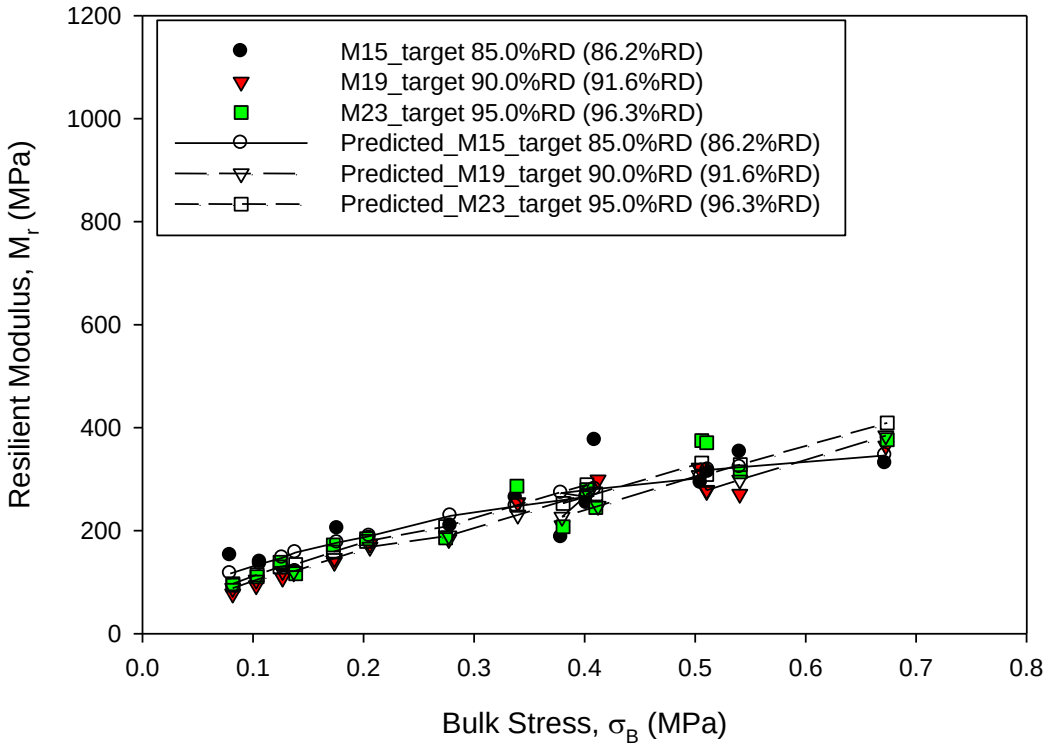

Figure 125. M_r vs. σ_B on RAP sample with 6% F_{200}

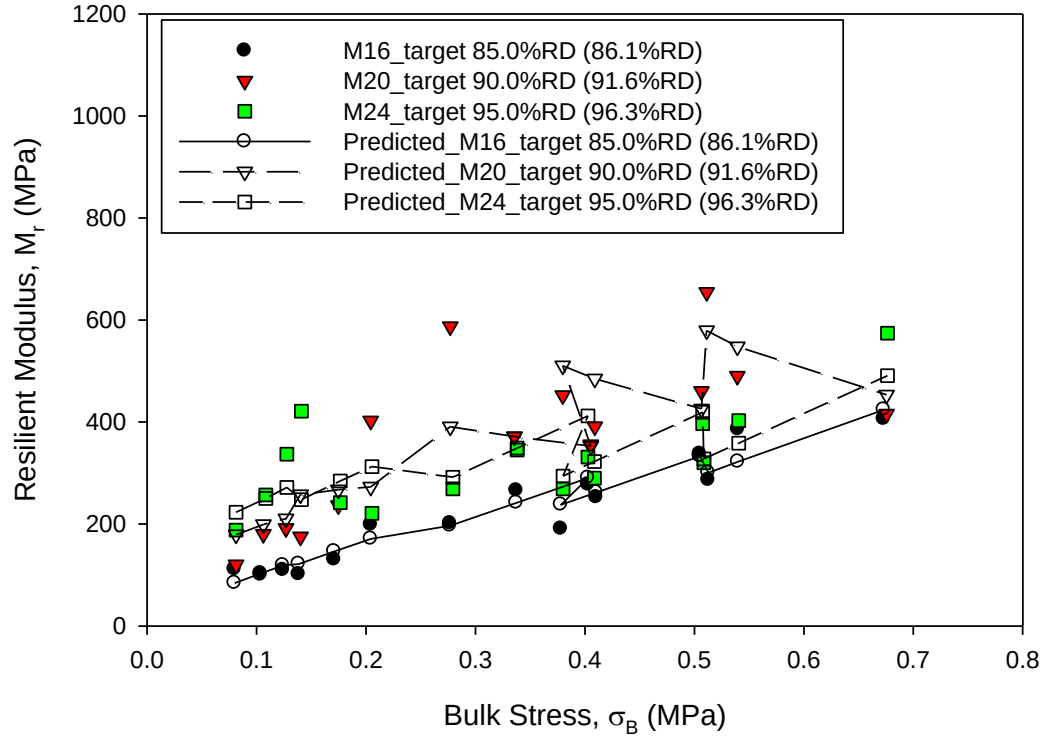

Figure 126. M_r vs. σ_B on RAP sample with 12% F_{200}

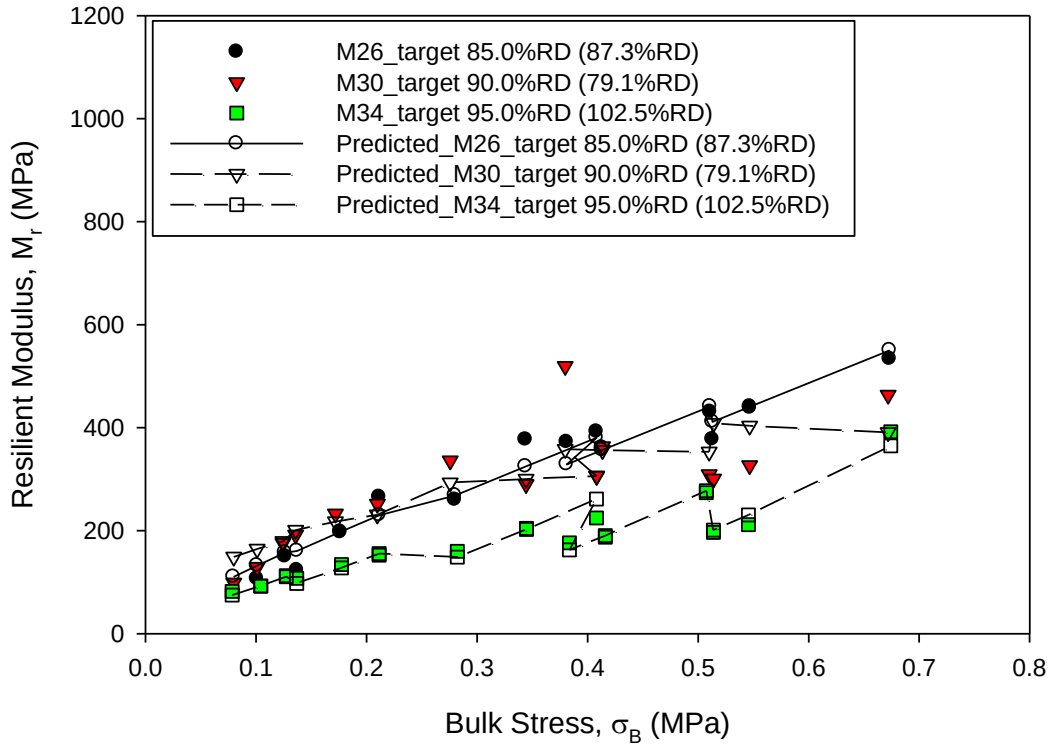

Figure 127. M_r vs. σ_B on RPCC/RAP sample with natural F_{200}

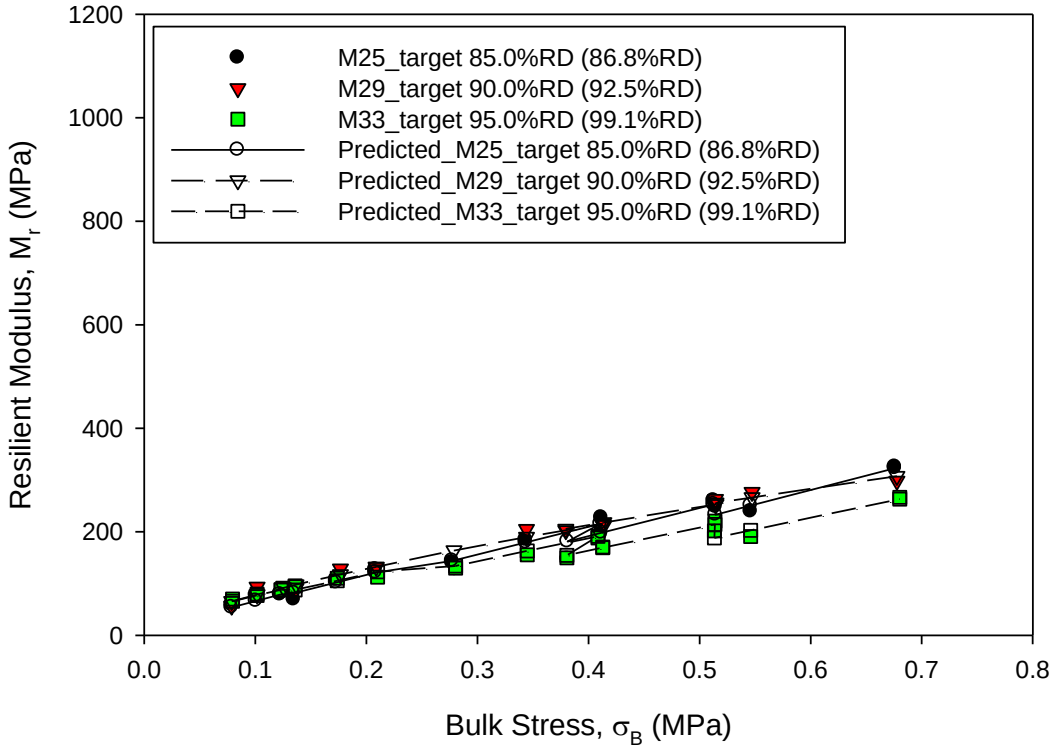

Figure 128. M_r vs. σ_B on RPCC/RAP sample with 0% F_{200}

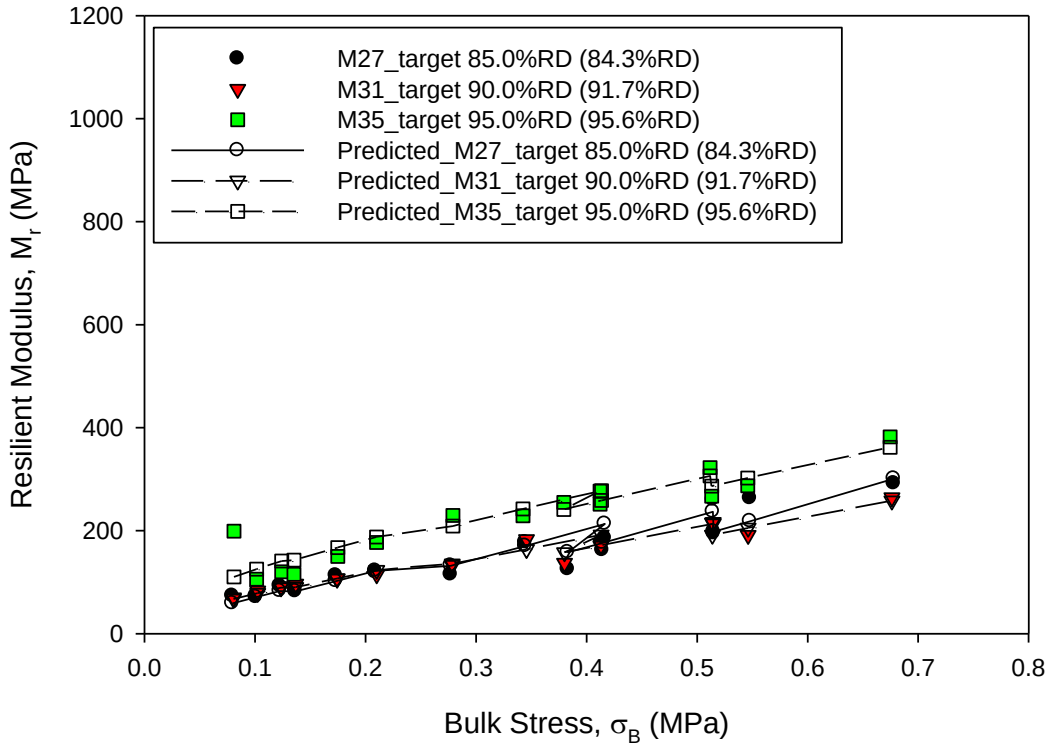

Figure 129. M_r vs. σ_B on RPCC/RAP sample with 6% F_{200}

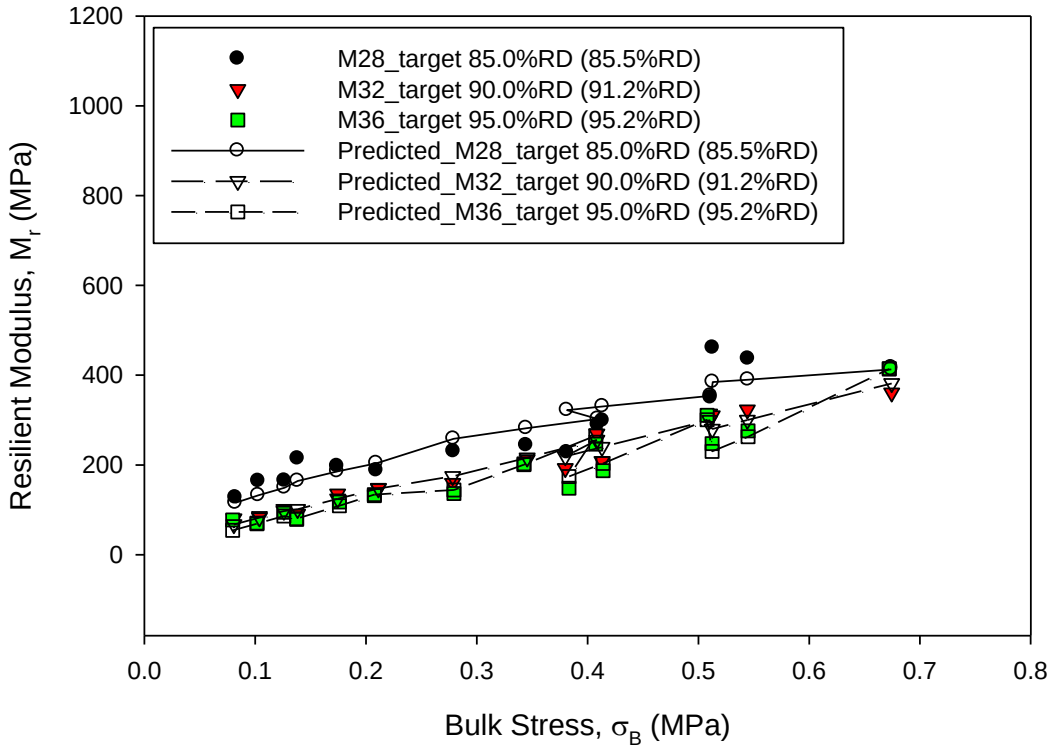

Figure 130. M_r vs. σ_B on RPCC/RAP sample with 12% F_{200}

Unconsolidated Undrained Shear Strength

According to AASHTO T307-99 (2009), the unconsolidated undrained shear strength (UU) tests were conducted when the accumulated permanent deformation is less than 5%. During the UU tests, the vertical displacements and the applied loads were recorded. The sample height should be modified for calculating the shear strain, because the original height was measure before the resilient modulus (M_r) test and the permanent strain was accumulated as the result of the M_r test loading.

The modified original height should be calculated using Equation 34.

$$H_0' = H_0 \times (1 - \varepsilon_p) \quad (34)$$

The accumulated permanent strain ε_p at the end of M_r test is 0.9243% and the original sample height (H_0) of the compacted sample before the M_r test is 7.9959 in.. The modified sample height (H_0') is calculated.

$$H_0' = 7.9959 \times (1 - 0.9243\%) = 7.9220\ in.$$

The shear strains were calculated using Equation 35.

$$\varepsilon = \frac{\Delta H}{H_0'} = \frac{9.54\times10^{-5}}{7.9220} \times 100\% = 1.2042 \times 10^{-3}\% \quad (35)$$

The corrected areas (A_c) were calculated with the shear strains using Equation 36.

$$A_c = \frac{A_0}{1-\varepsilon} = \frac{\pi\times(2)^2}{1-1.2042\times10^{-3}\%} = 12.5665\ in.^2 \quad (36)$$

The deviator stress (σ_d) is calculated using Equation 37.

$$\sigma_d = \sigma_1 - \sigma_3 = \frac{P}{A_c} = \frac{4.4569}{12.5665} = 0.3547\ psi \quad (37)$$

The membrane corrections ($\Delta\sigma_d$) were calculated using Equation 38. The Young's modulus for the membrane material (E_m) was 1400 kN/m^2 (203.05 psi) as suggested in ASTM D2850 (2007) and two membranes were used in the test to prevent confinement from leaking for the compacted samples.

$$\Delta\sigma_d = 4 \times E_m \times t_m \times \frac{\varepsilon}{D} \quad (38)$$

$$t_m = 2 \times 0.012 = 0.024\ in.$$

$$D = 2 \times \sqrt{\frac{A_c}{\pi}} = 2 \times \sqrt{\frac{12.5665}{\pi}} = 4.000021\ in.$$

$$\Delta\sigma_d = 4 \times 203.05 \times 0.024 \times \frac{1.2042 \times 10^{-3}\%}{4.000021} = 5.8683 \times 10^{-5} psi$$

The corrected deviator stresses (σ_d') were calculated using Equation 39.

$$\sigma_d' = \sigma_d - \Delta\sigma_d = 0.3547 - 5.8683 \times 10^{-5} = 0.3546 psi = 2.445 kPa \quad (39)$$

The shear stress and strain curve was plotted with the calculated corrected strains and deviator stresses (Figure 131).

The undrained shear strength (c_u) was calculated using Equation 40.

( )

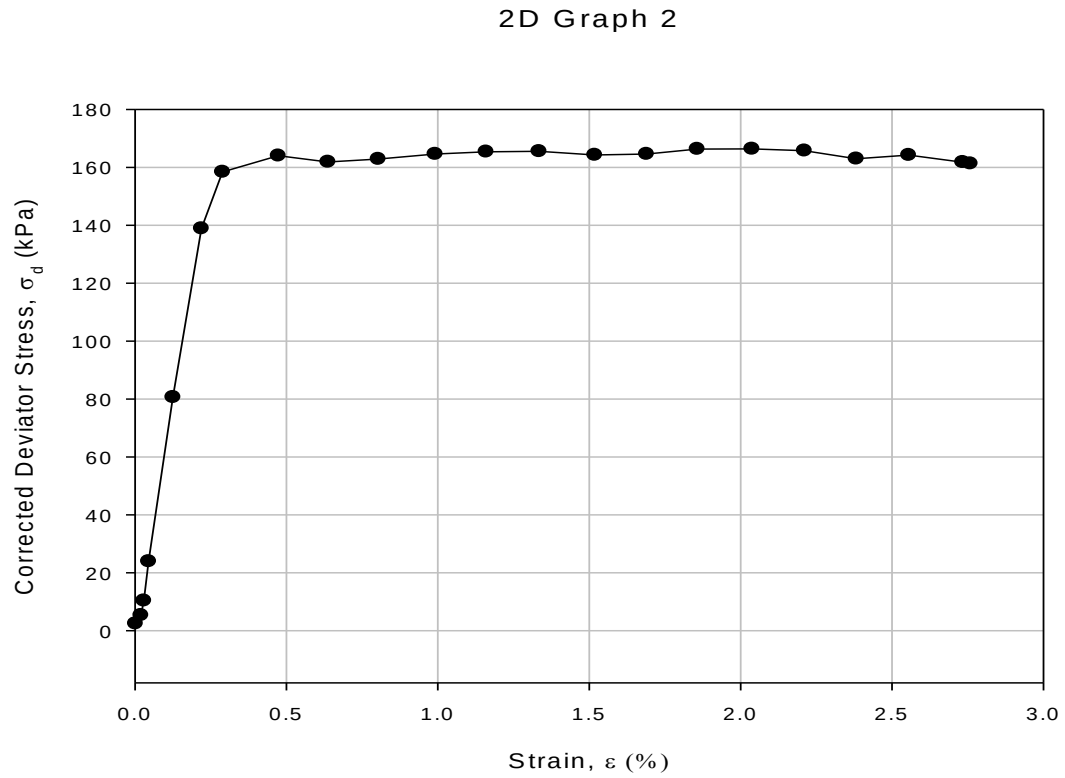

Figure 131. Stress and strain relationship with corrected data for a subbase sample

Limestone_85%RD_natural fines_strain vs Limesto

Statistical analysis of factors affecting undrained shear strength (c_u)

Whole Model

Actual by Predicted Plot

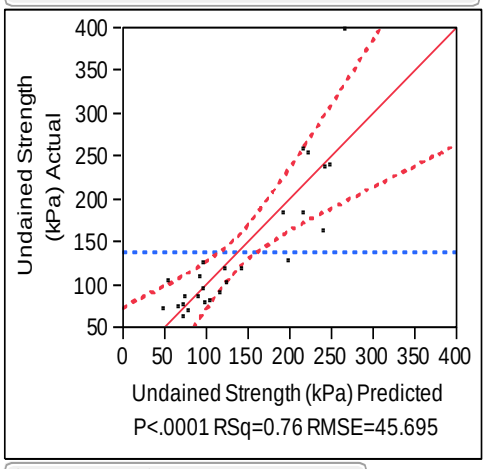

Summary of Fit

RSquare	0.75785
RSquare Adj	0.681382
Root Mean Square Error	45.69519
Mean of Response	137.5385
Observations (or Sum Wgts)	26

Analysis of Variance

Source	DF	Sum of Squares	Mean Square	F Ratio
Model	6	124163.50	20693.9	9.9106
Error	19	39672.96	2088.1	Prob > F
C. Total	25	163836.46		<.0001*

Parameter Estimates

Term	Estimate	Std Error	t Ratio	Prob>|t|
Intercept	136.70556	9.011213	15.17	<.0001*
Materials[Crushed Limestone]	89.738889	12.59115	7.13	<.0001*
Materials[RAP]	-53.92778	12.59115	-4.28	0.0004*
Target Fines Content (%)[0%]	-4.372222	12.59115	-0.35	0.7322
Target Fines Content (%)[12%]	14.966667	13.04367	1.15	0.2654
Target Relative Density (%)[85%]	-24.59444	12.59115	-1.95	0.0657
Target Relative Density (%)[90%]	-0.811111	13.04367	-0.06	0.9511

Effect Tests

Source	Nparm	DF	Sum of Squares	F Ratio	Prob > F
Materials	2	2	108619.48	26.0098	<.0001*
Target Fines Content (%)	2	2	2923.33	0.7000	0.5089
Target Relative Density (%)	2	2	11258.07	2.6958	0.0932

Figure 132. JMP results of least squares fit analysis for c_u

Materials

Leverage Plot

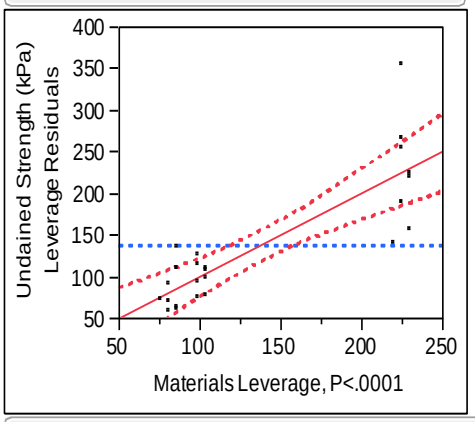

Least Squares Means Table

Level	Least Sq Mean	Std Error	Mean
Crushed Limestone	226.44444	15.231731	226.444
RAP	82.77778	15.231731	82.778
RPCC/RAP	100.89444	16.334211	99.125

LS Means Plot

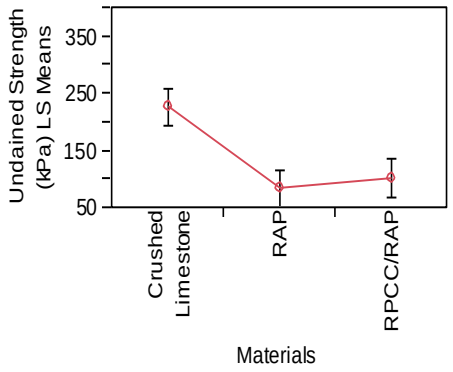

Figure 133. JMP results of least squares fit analysis of materials types effect on c_u

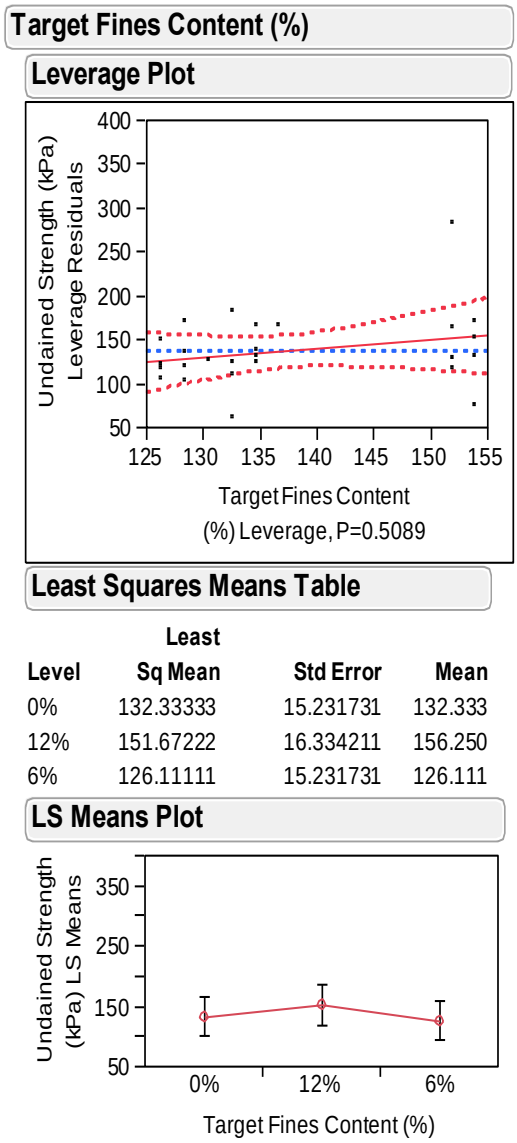

Figure 134. JMP results of least squares fit analysis of target fines contents effect on c_u

Target Relative Density (%)

Leverage Plot

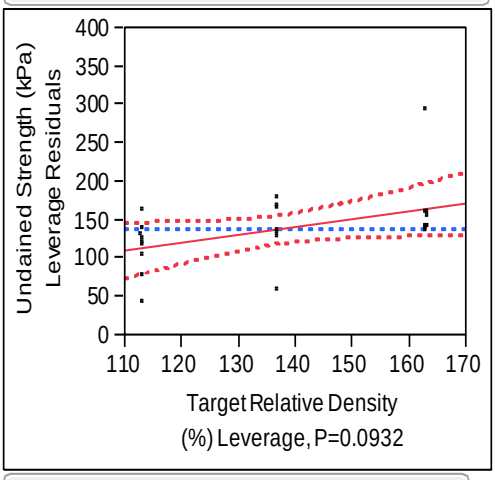

Least Squares Means Table

Level	Least Sq Mean	Std Error	Mean
85%	112.11111	15.231731	112.111
90%	135.89444	16.334211	138.500
95%	162.11111	15.231731	162.111

LS Means Plot

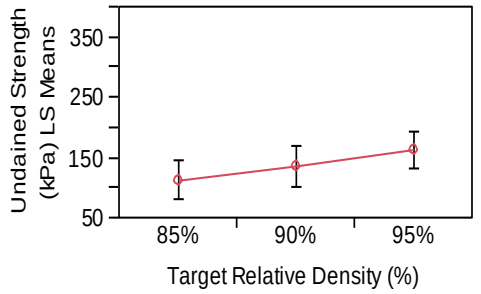

Figure 135. JMP results of least squares fit analysis of target relative density effect on c_u

Degradation

Degradations of the unbound granular materials were calculated to quantify the change particle size distribution of the tested materials after the permanent deformation tests.

Calculation

Area below the particle size distribution curve of untested material is denoted as A and of tested materials is denoted as B. The breakage index (BI) was calculated using Equation 41.

$$BI = \frac{A-B}{B} = \frac{1151.0-1169.6}{1169.6} \times 100\% = -1.59\% \quad (41)$$

Table 68. Breakage index calculation on a subbase sample

Sieve Size (mm)	Percent Passing (%)	Area between two points (%*mm)	Percent Passing (%)	Area between two points (%*mm)
100.0	576.5	100.0	575.6	100.0
77.4	209.7	77.1	210.1	77.4
62.4	235.0	63.0	242.8	62.4
36.6	78.9	39.2	85.4	36.6
29.4	10.4	32.2	11.3	29.4
28.2	28.2	30.8	30.8	28.2
20.8	7.8	22.8	8.6	20.8
16.1	2.6	17.6	2.8	16.1
13.5	1.2	14.5	1.3	13.5
11.5	0.8	12.3	0.8	11.5
9.6	—	10.1	—	9.6
Sum	A	1151.0	B	1169.6
BI			-1.59	

Note: — means no value calculated.

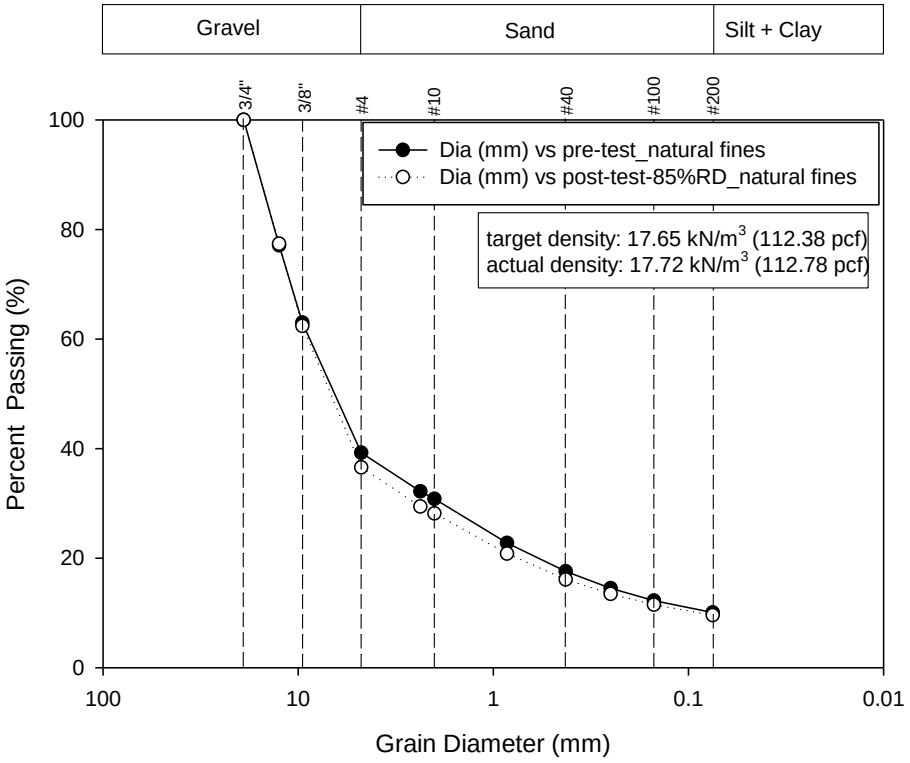

Figure 136. Particle size distribution change of a subbase sample

Particle size distribution change of all samples

For each permanent deformation test sample, wash sieve analyses were conducted on all materials from each sample and particle size distribution curves were plotted to compare with related particle size distribution curves for calculating breakage index.

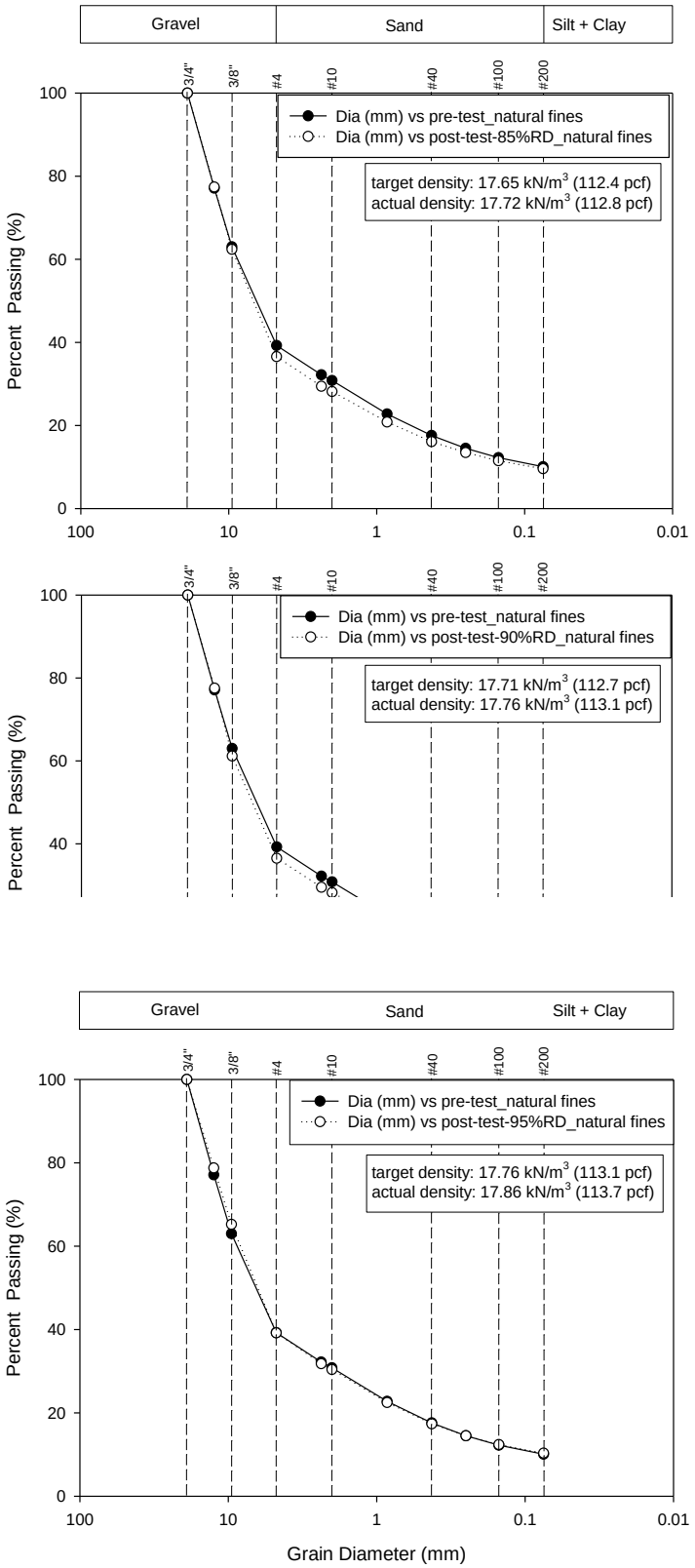

Figure 137. Particle size distributions on limestone with 7.9% fines content

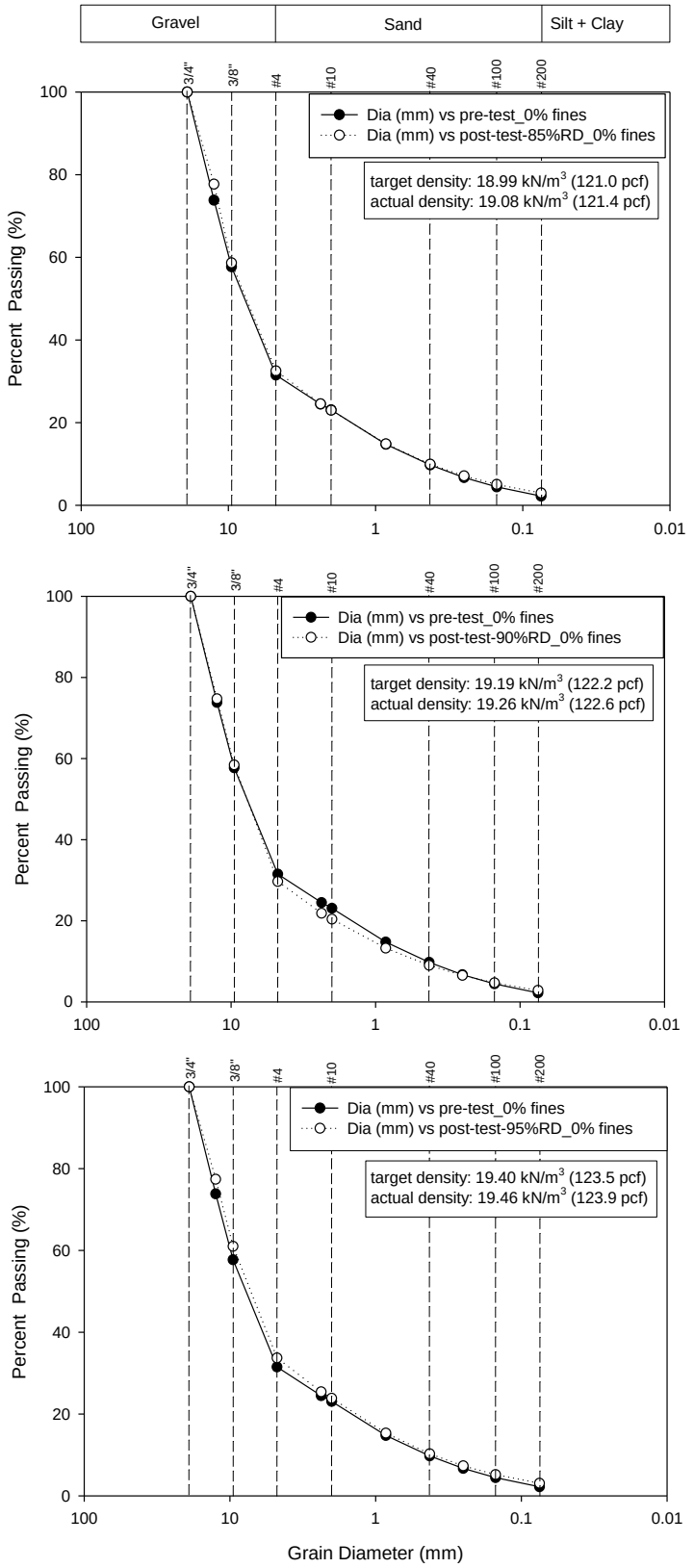

Figure 138. Particle size distributions on limestone with 2.2% fines content

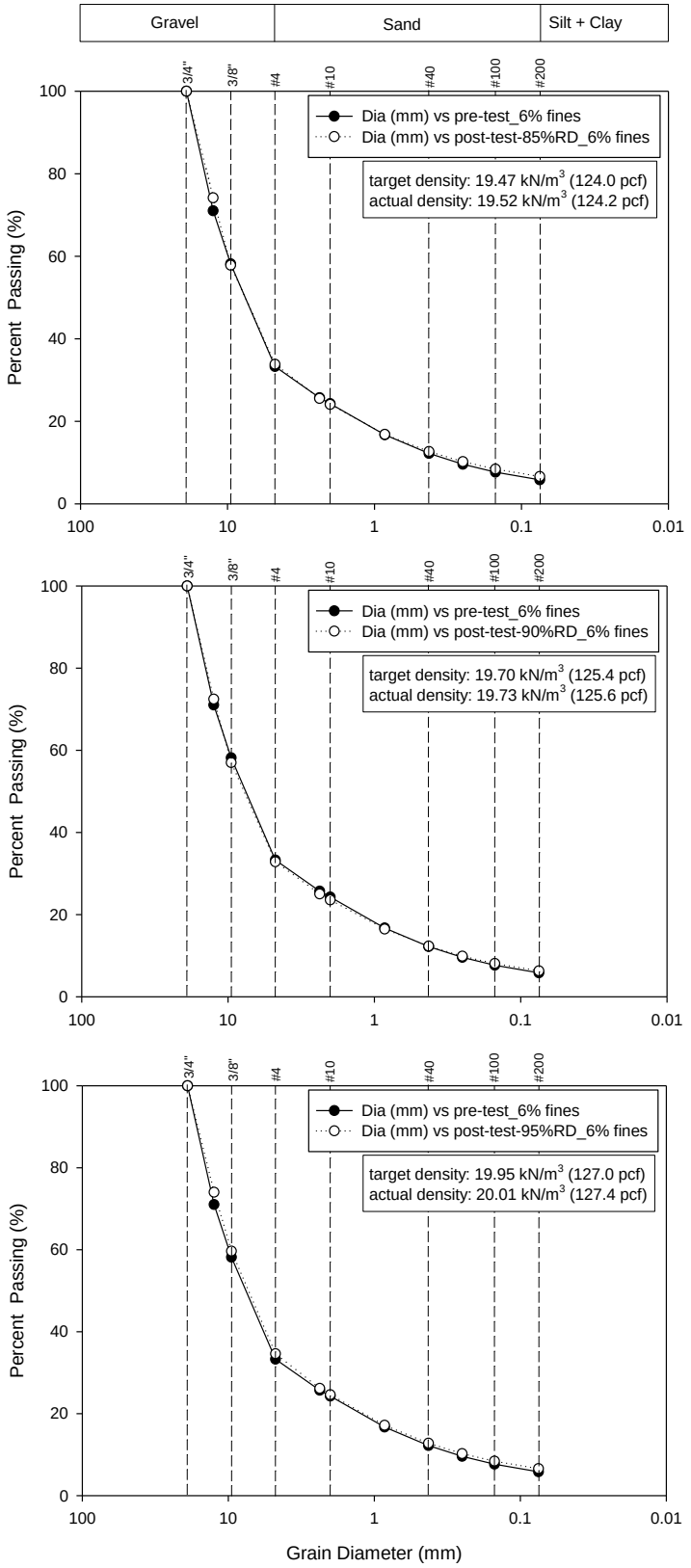

Figure 139. Particle size distributions on limestone with 5.8% fines content

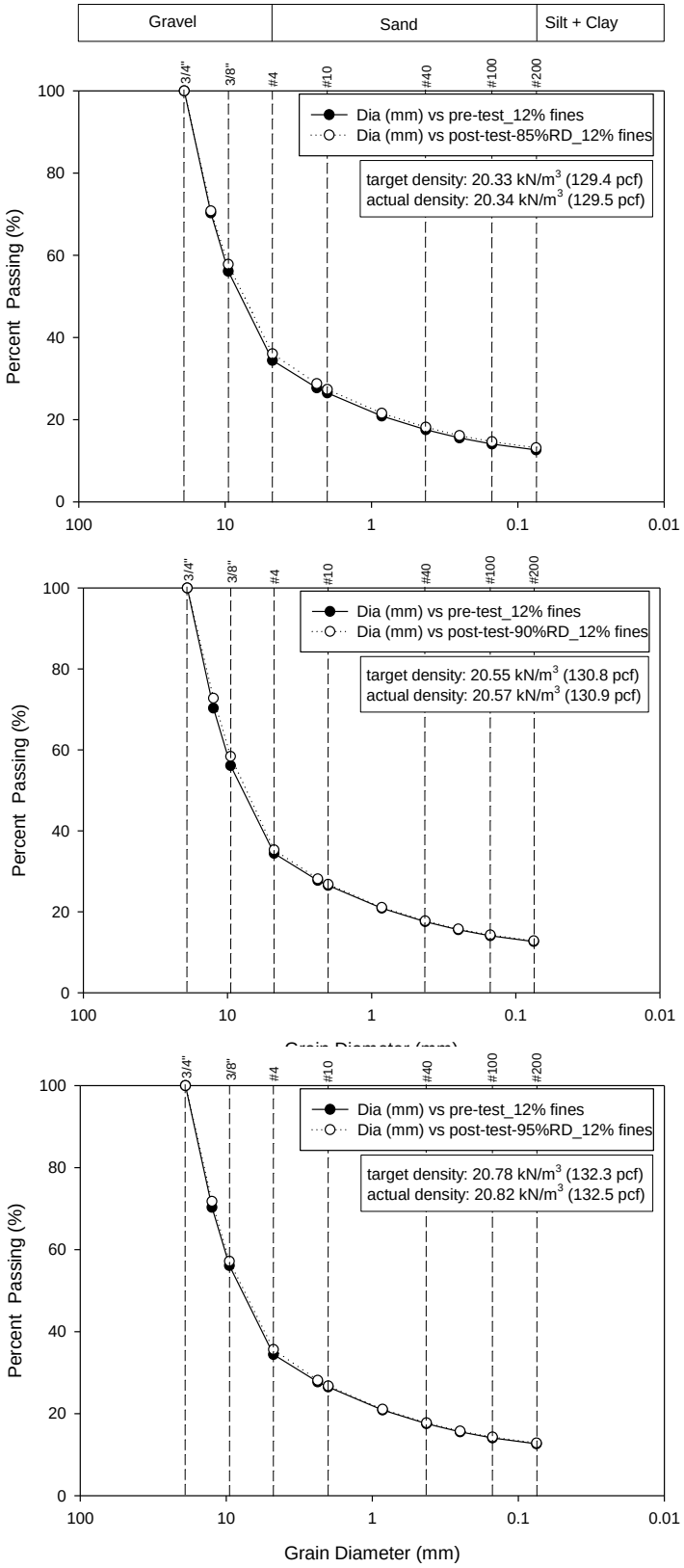

Figure 140. Particle size distributions on limestone with 12.6% fines content

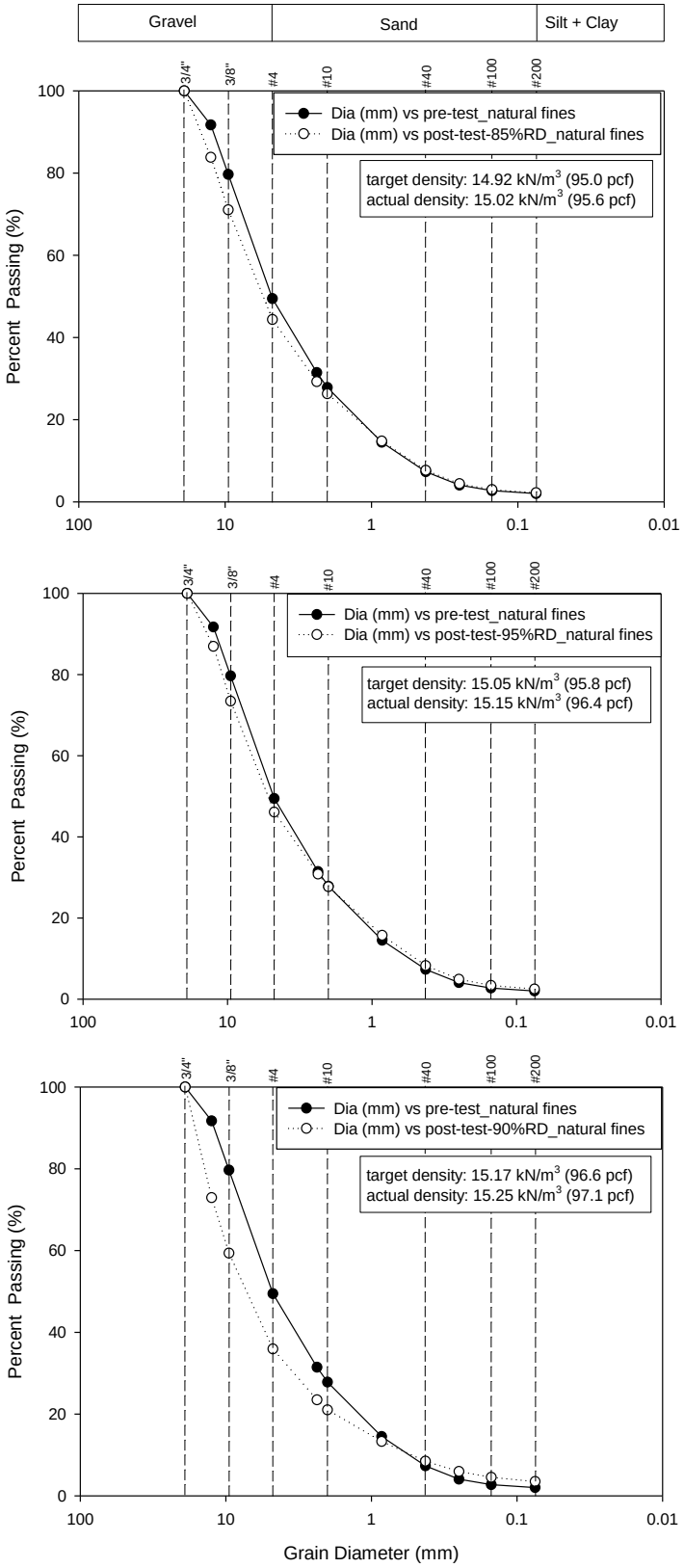

Figure 141. Particle size distributions on RAP with 2.0% fines content

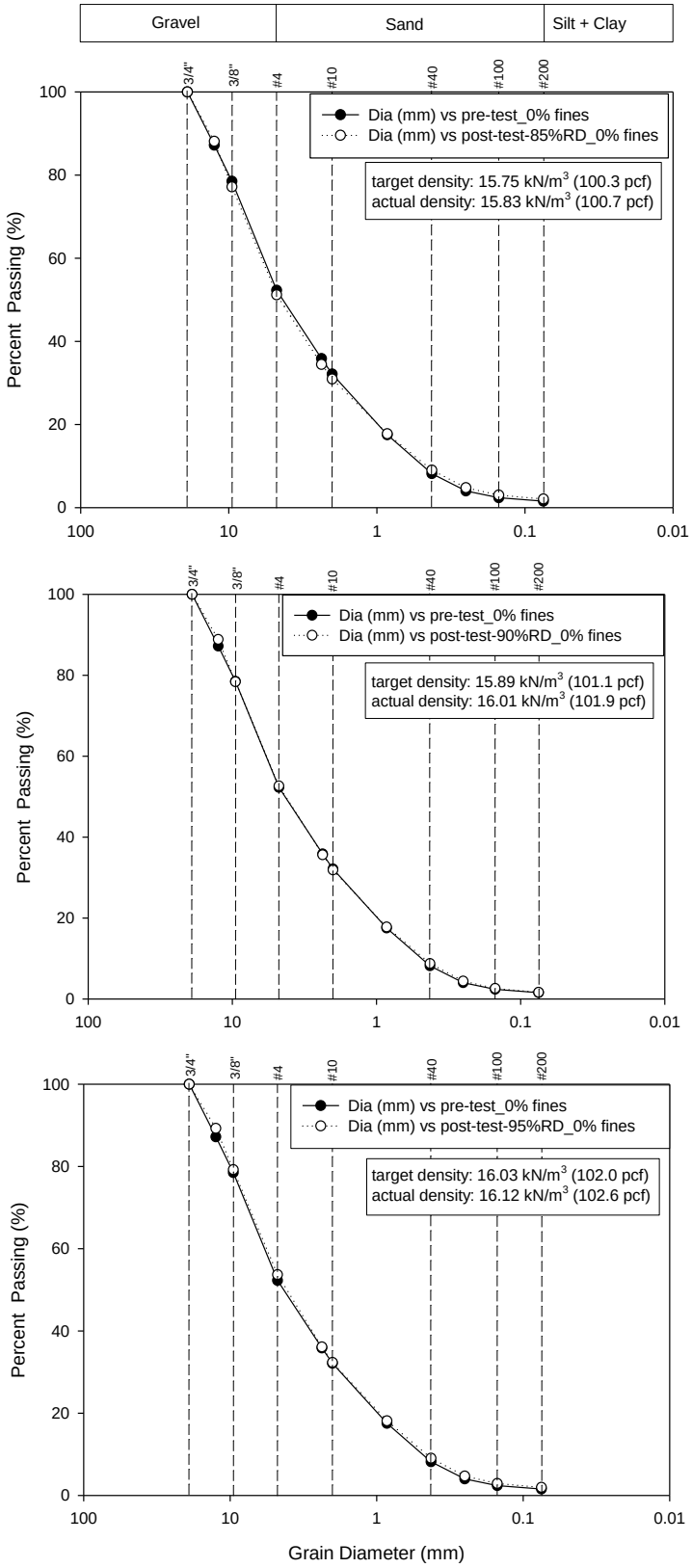

Figure 142. Particle size distributions on RAP with 1.6% fines content

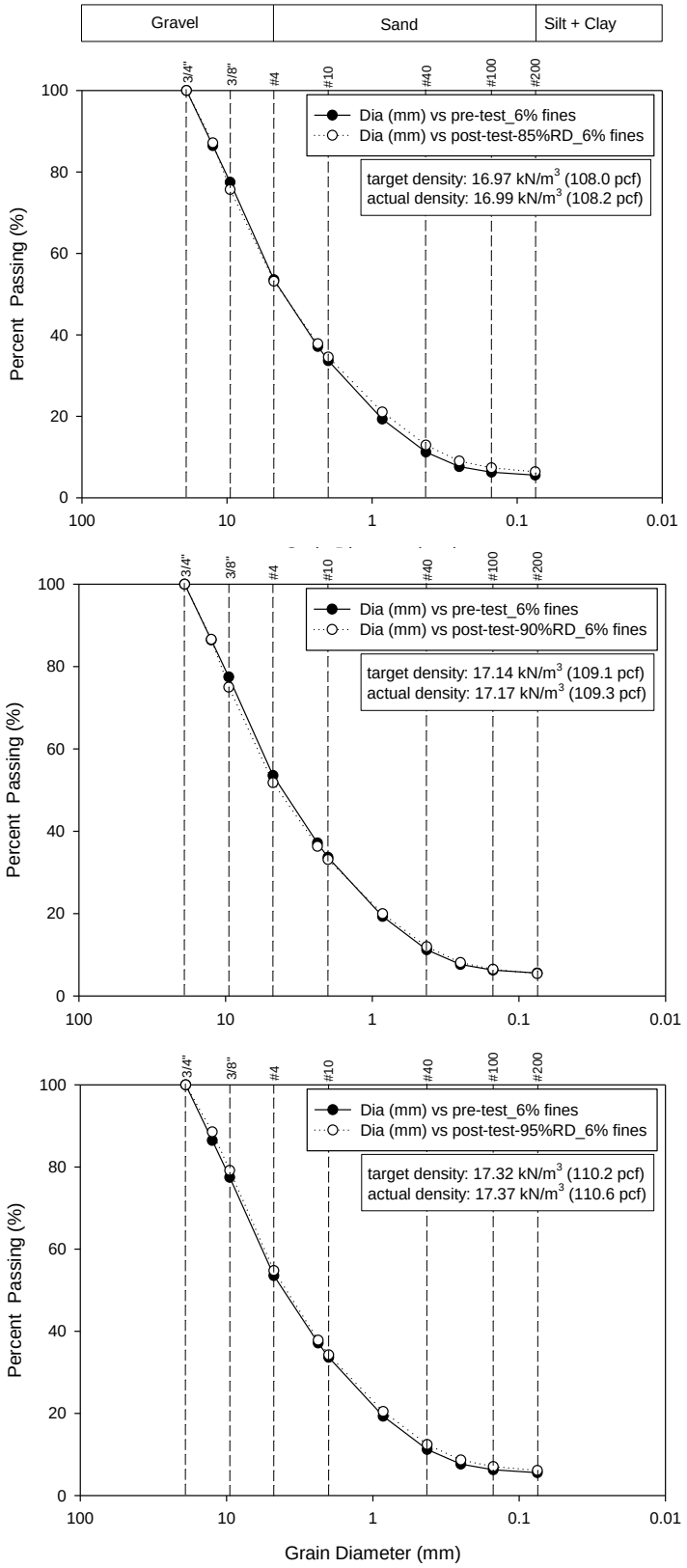

Figure 143. Particle size distributions on RAP with 5.6% fines content

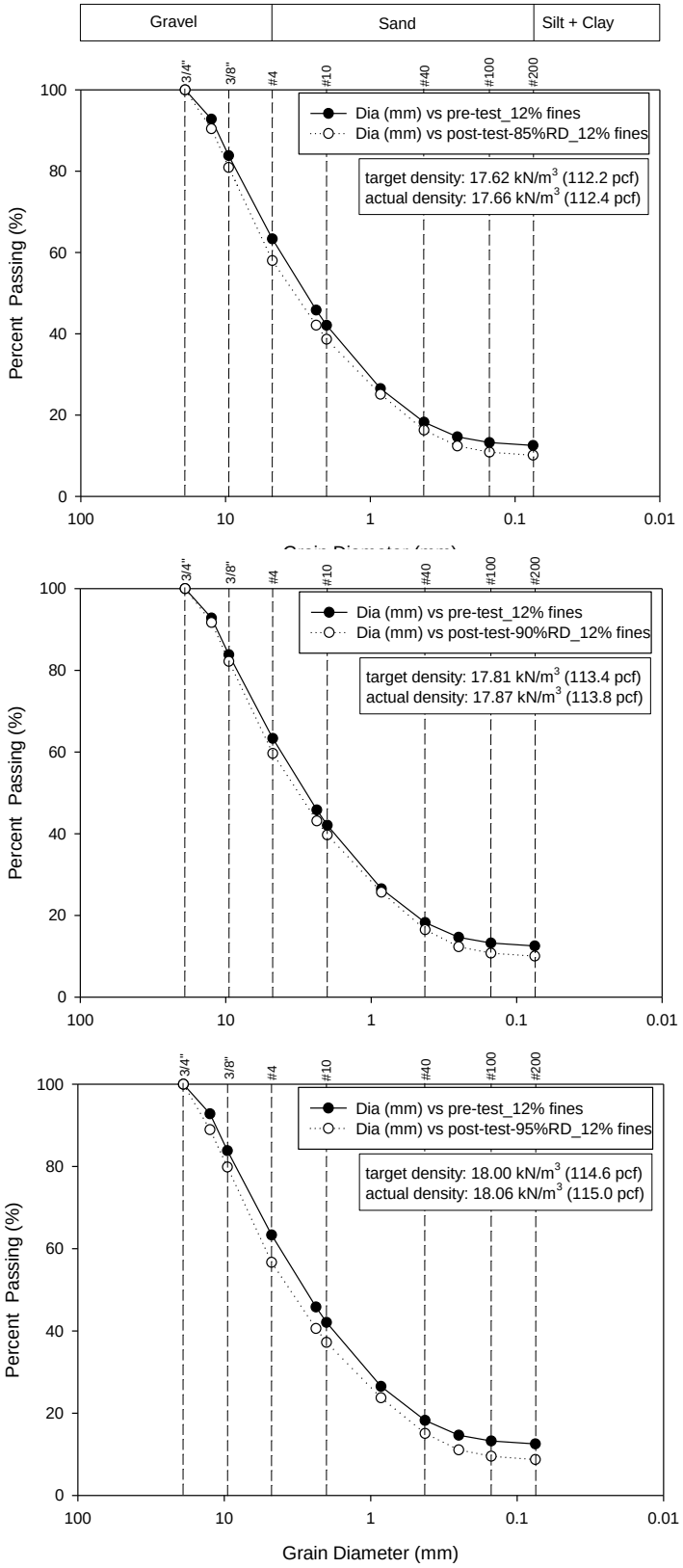

Figure 144. Particle size distributions on RAP with 12.5%fines content

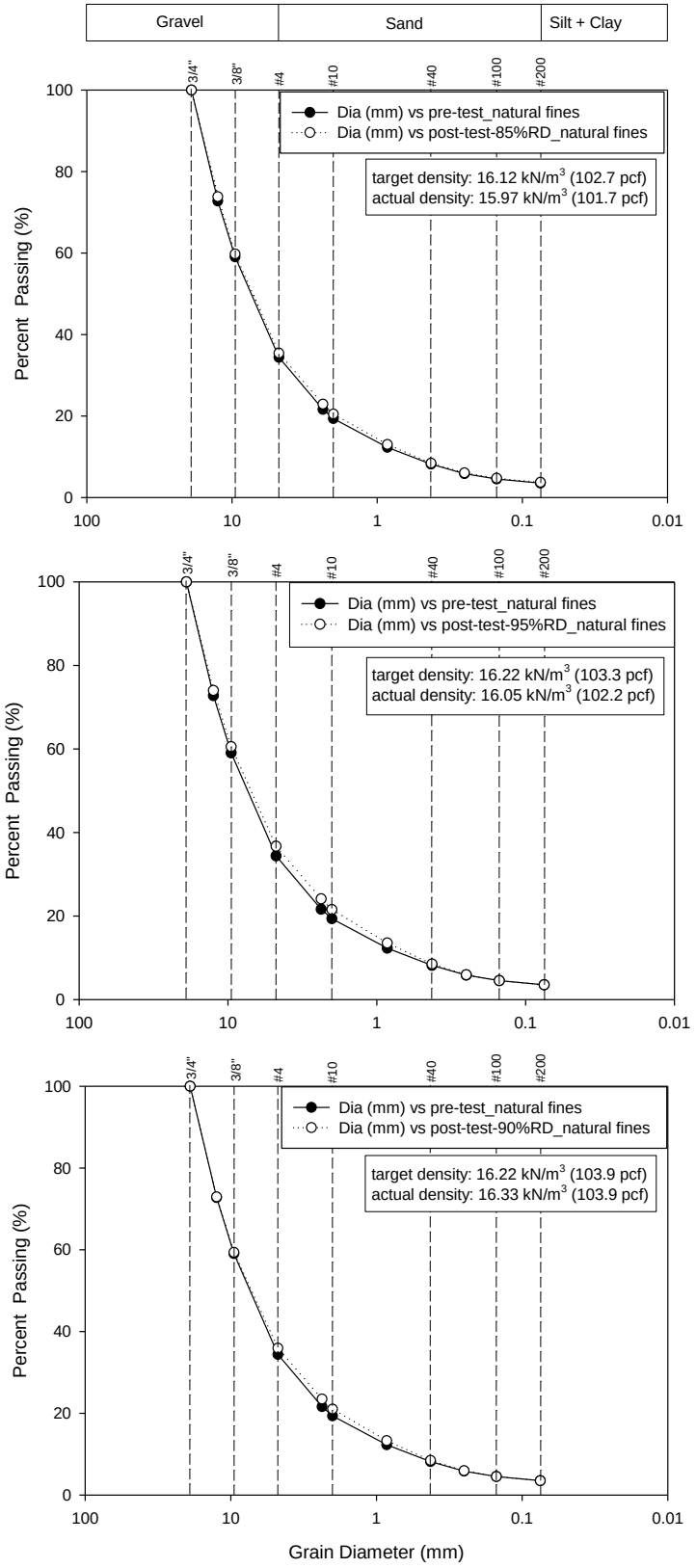

Figure 145. Particle size distributions on RPCC/RAP with 3.5% fines content

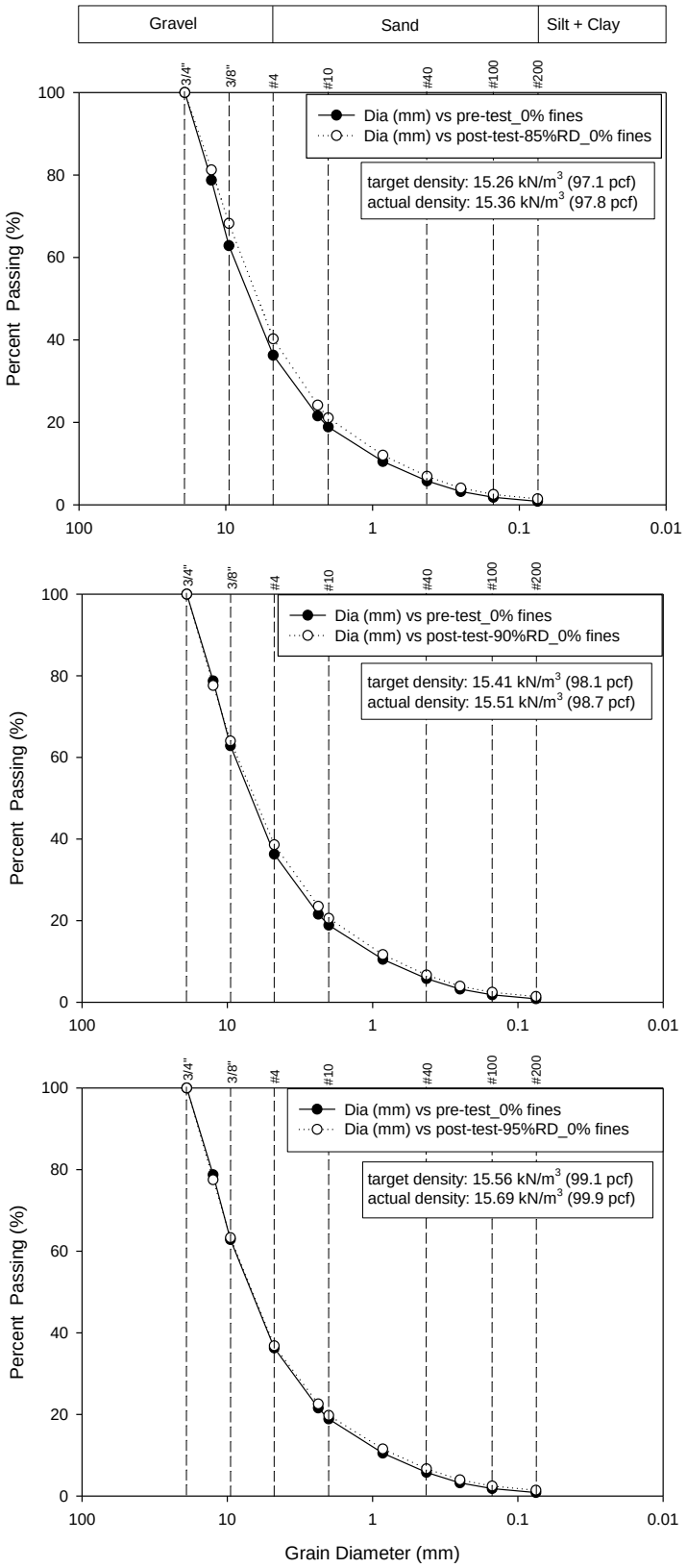

Figure 146. Particle size distributions on RPCC/RAP with 0.8% fines content

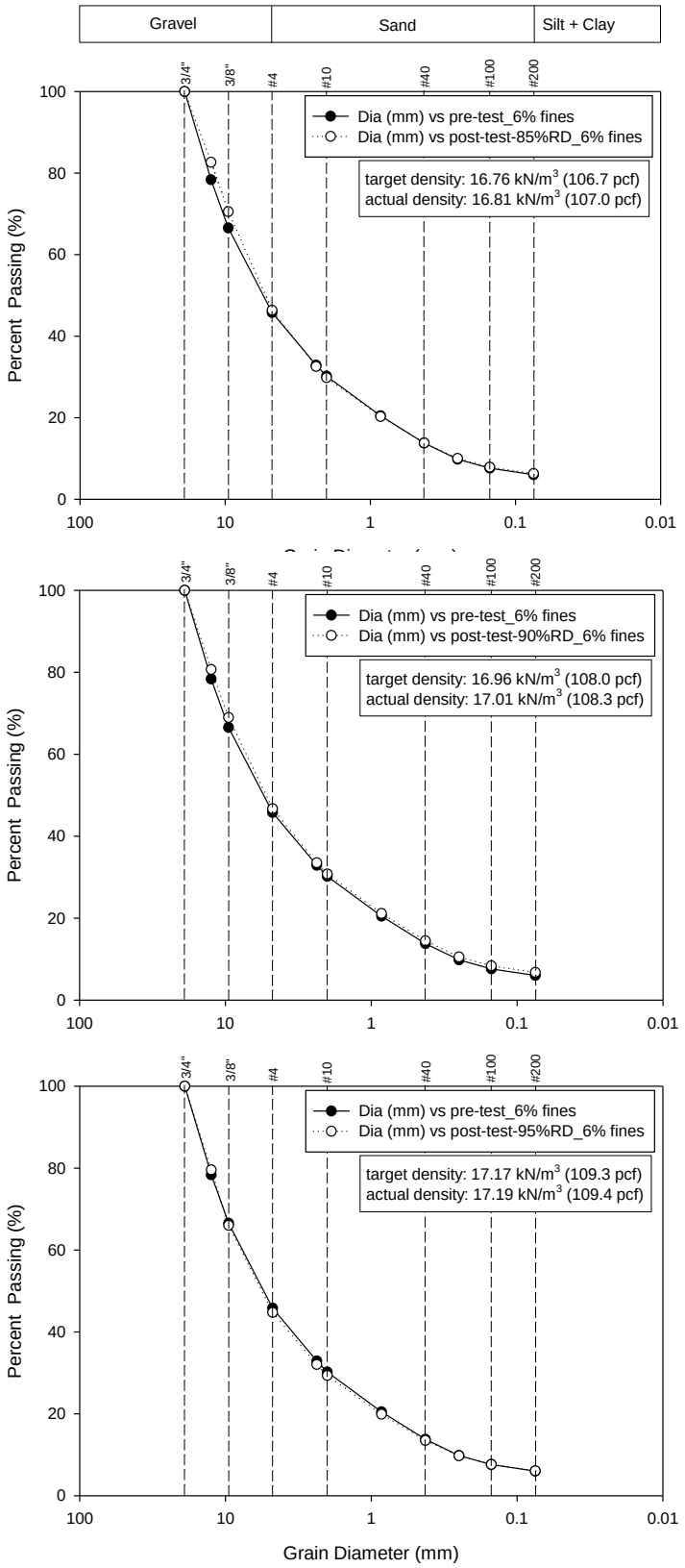

Figure 147. Particle size distributions on RPCC/RAP with 6.0% fines content

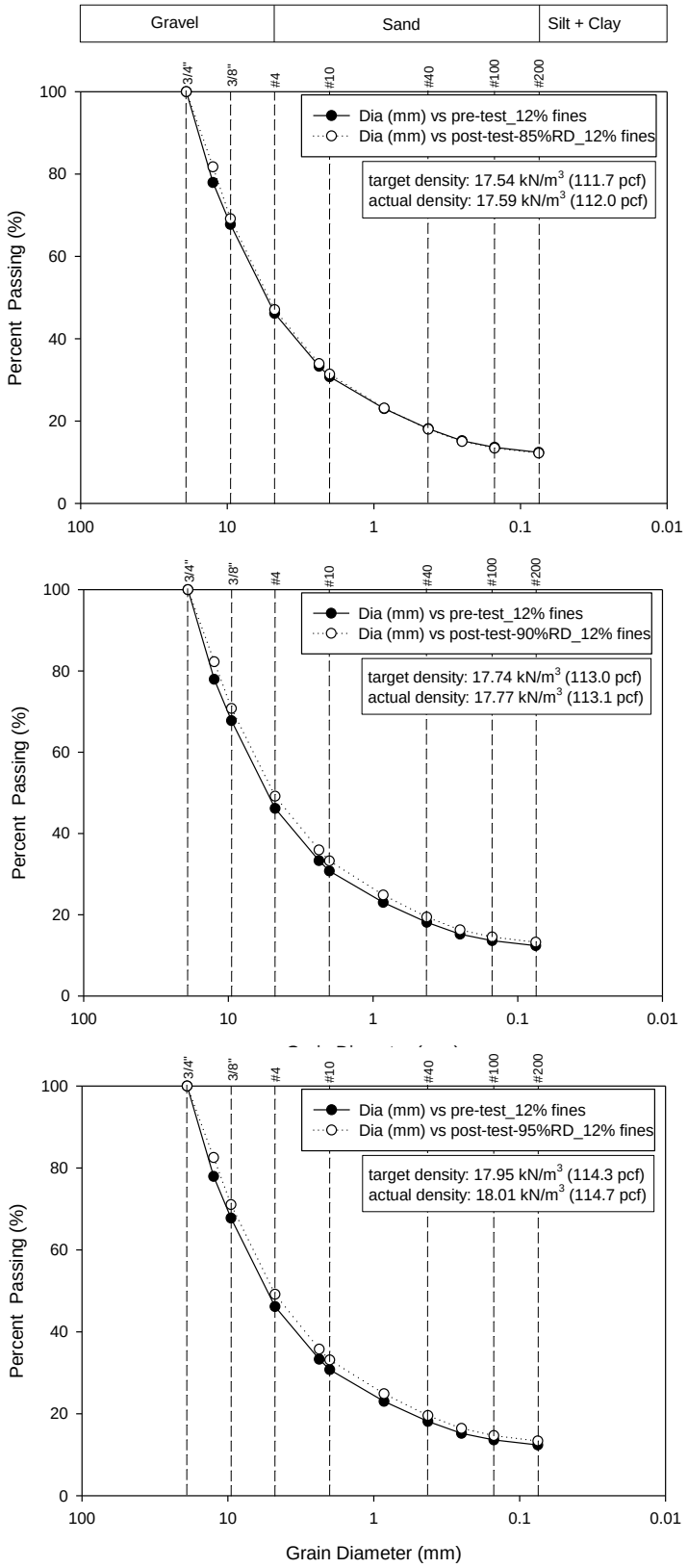

Figure 148. Particle size distributions on RPCC/RAP with 12.4% fines content

APPENDIX C. SYSTEM OUTPUTS

Permanent Deformation Tests

System outputs of the permanent deformation tests were reported for one sample using each method except 3 samples for NCHRP 598 tests.

Method #1 ISU 100k tests

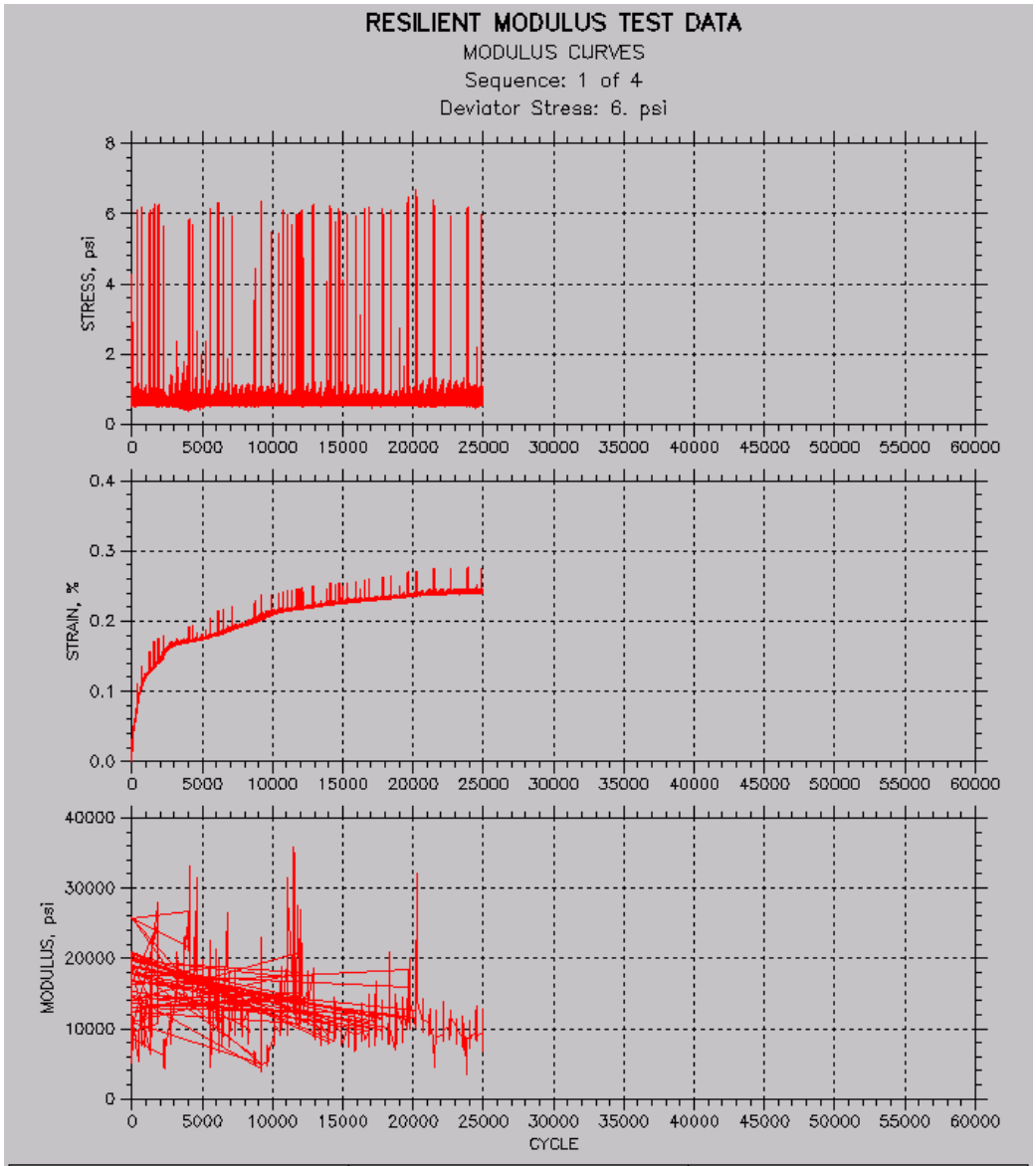

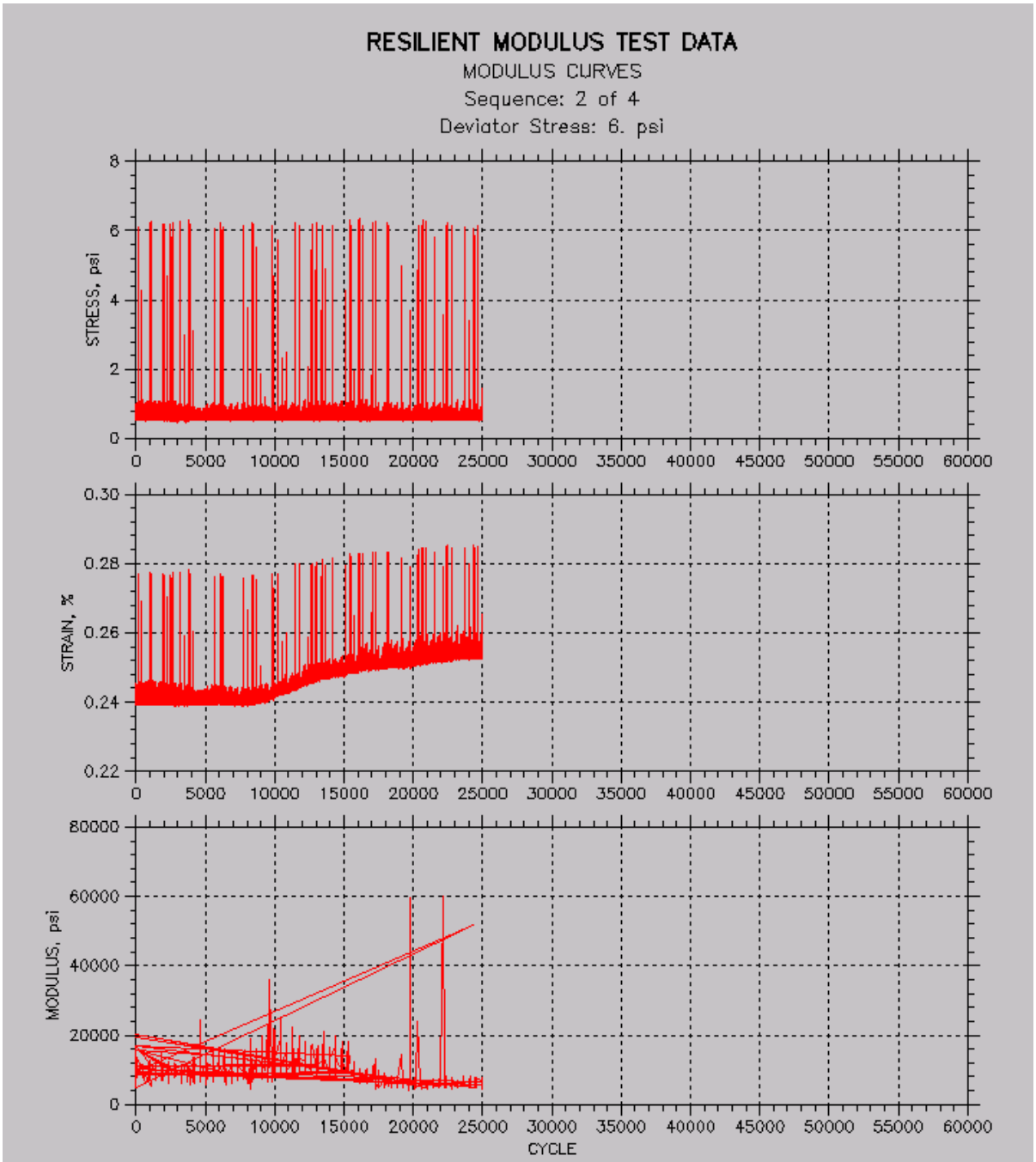

Project: MI I94	Location:	Project No.:
Boring No.:	Tested By: JL	Checked By:
Sample No.:	Test Date: 20110627	Depth:
Test No.:	Sample Type:	Elevation:
Description: TB3 Untrimmed Base material 3.3% 101.8pcf 8%fines		
Remarks:		
File: U:\Desktop\research\data\Cyclic Loading test results\MI\original dat data\Mr_MI-94_TB3_UntrimmedBase_101.8pcf_		

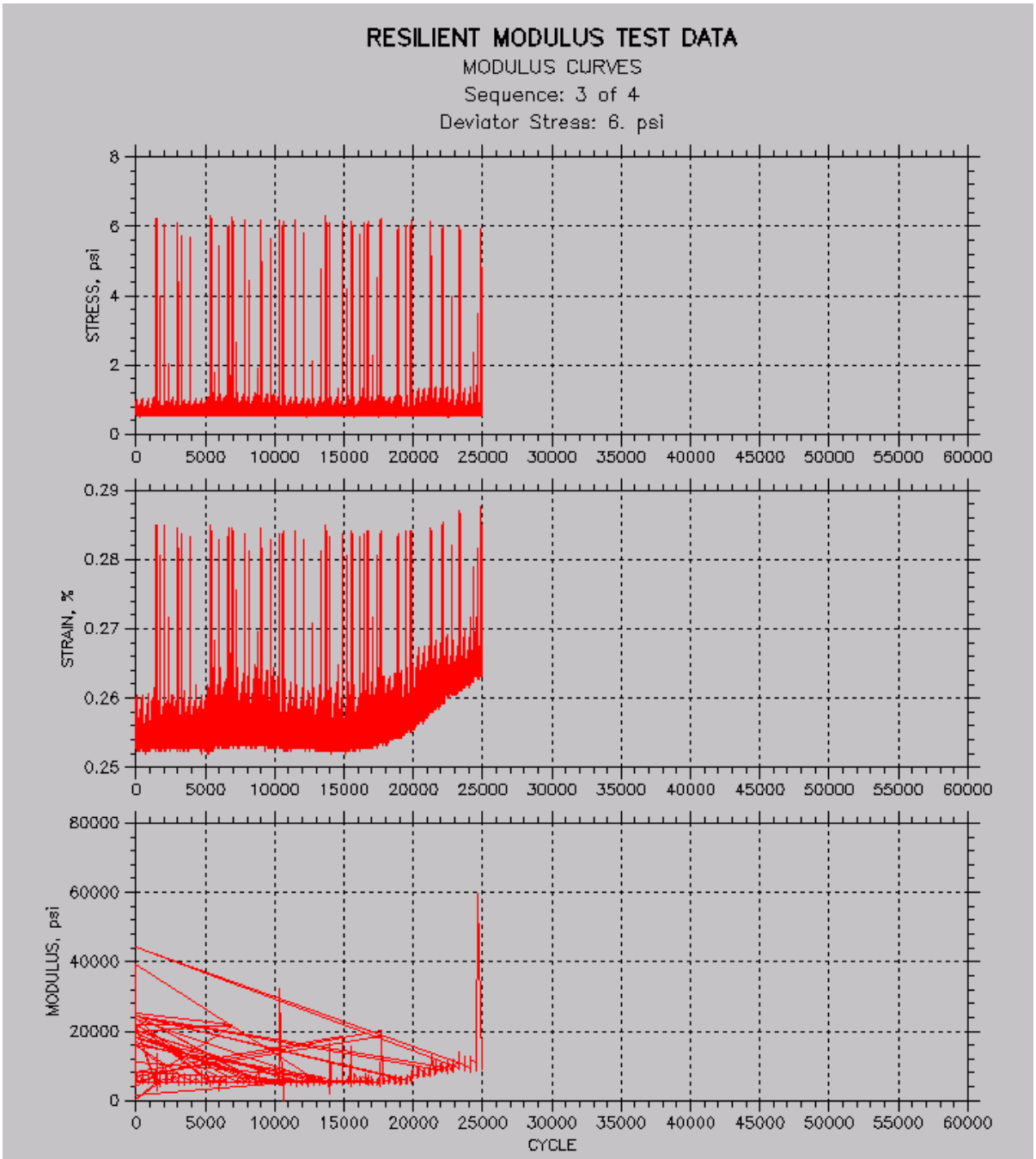

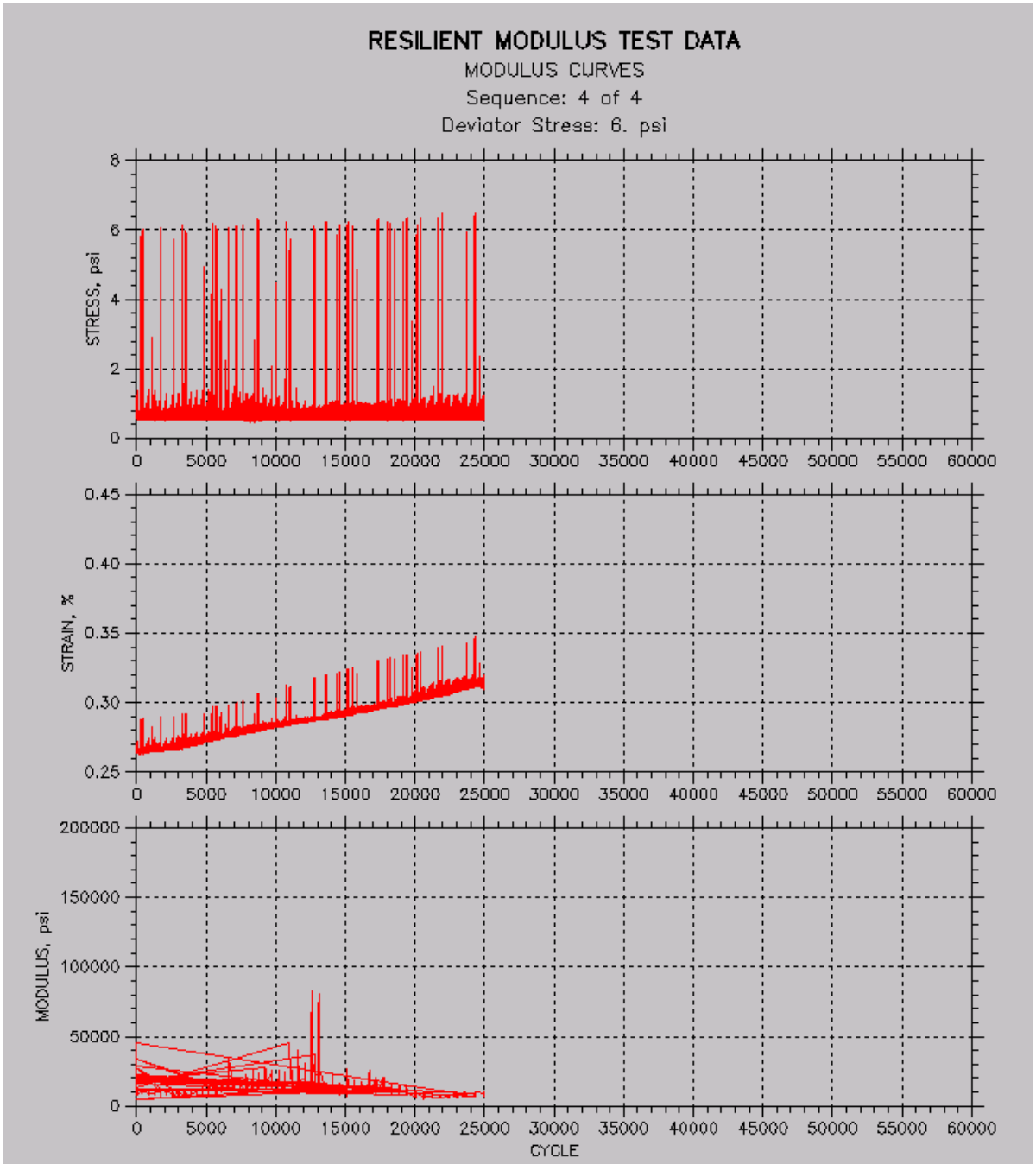

Project: MI I94	Location:	Project No.:
Boring No.:	Tested By: JL	Checked By:
Sample No.:	Test Date: 20110627	Depth:
Test No.:	Sample Type:	Elevation:
Description: TB3 Untrimmed Base material 3.3% 101.8pcf 8%fines		
Remarks:		
File: U:\Desktop\research\data\Cyclic Loading test results\MI\original dat data\Mr_MI-94_TB3_UntrimmedBase_101.8pct		

Method #2 ISU 1k tests

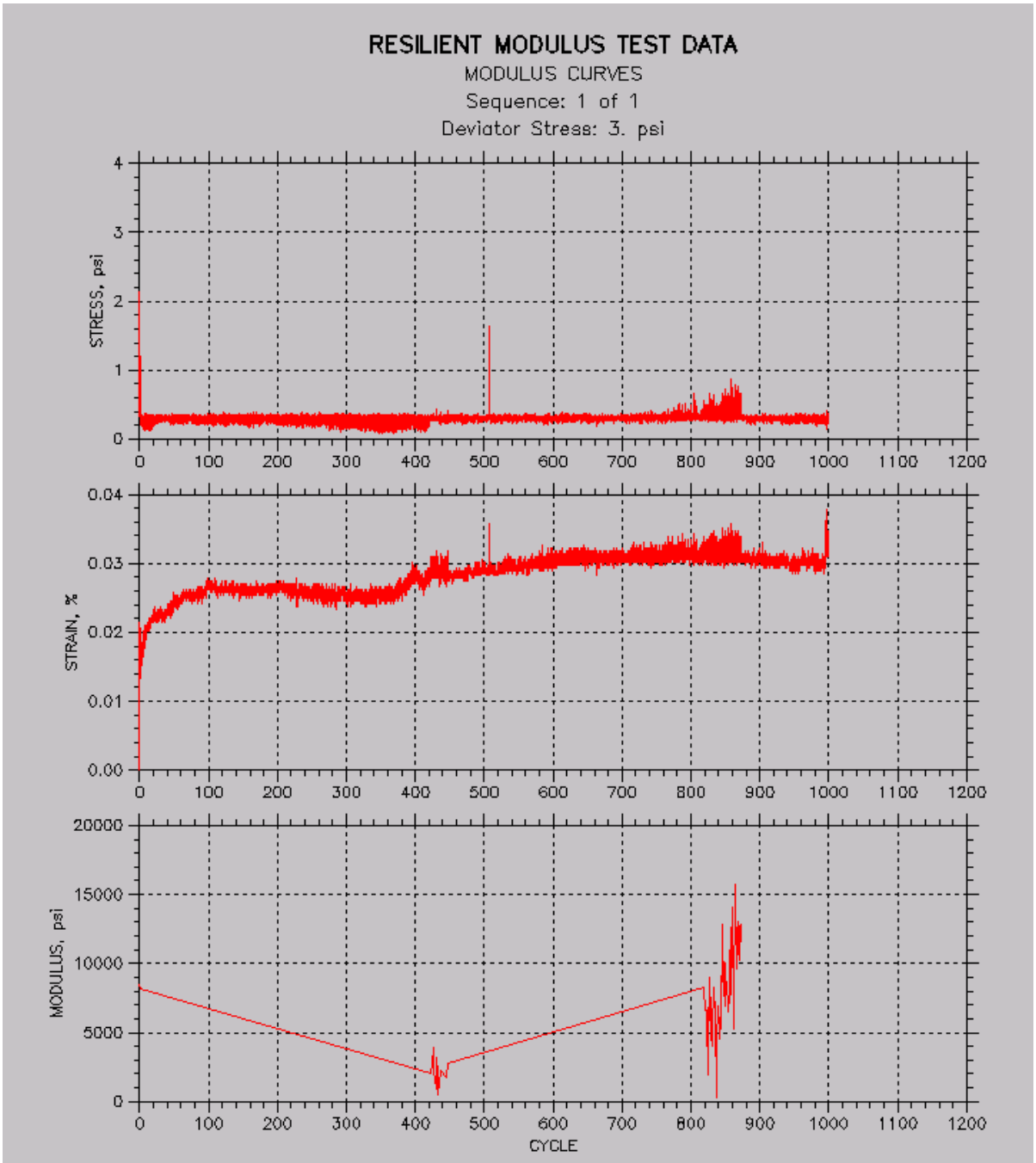

Method #3 NCHRP 598 tests

Crushed limestone

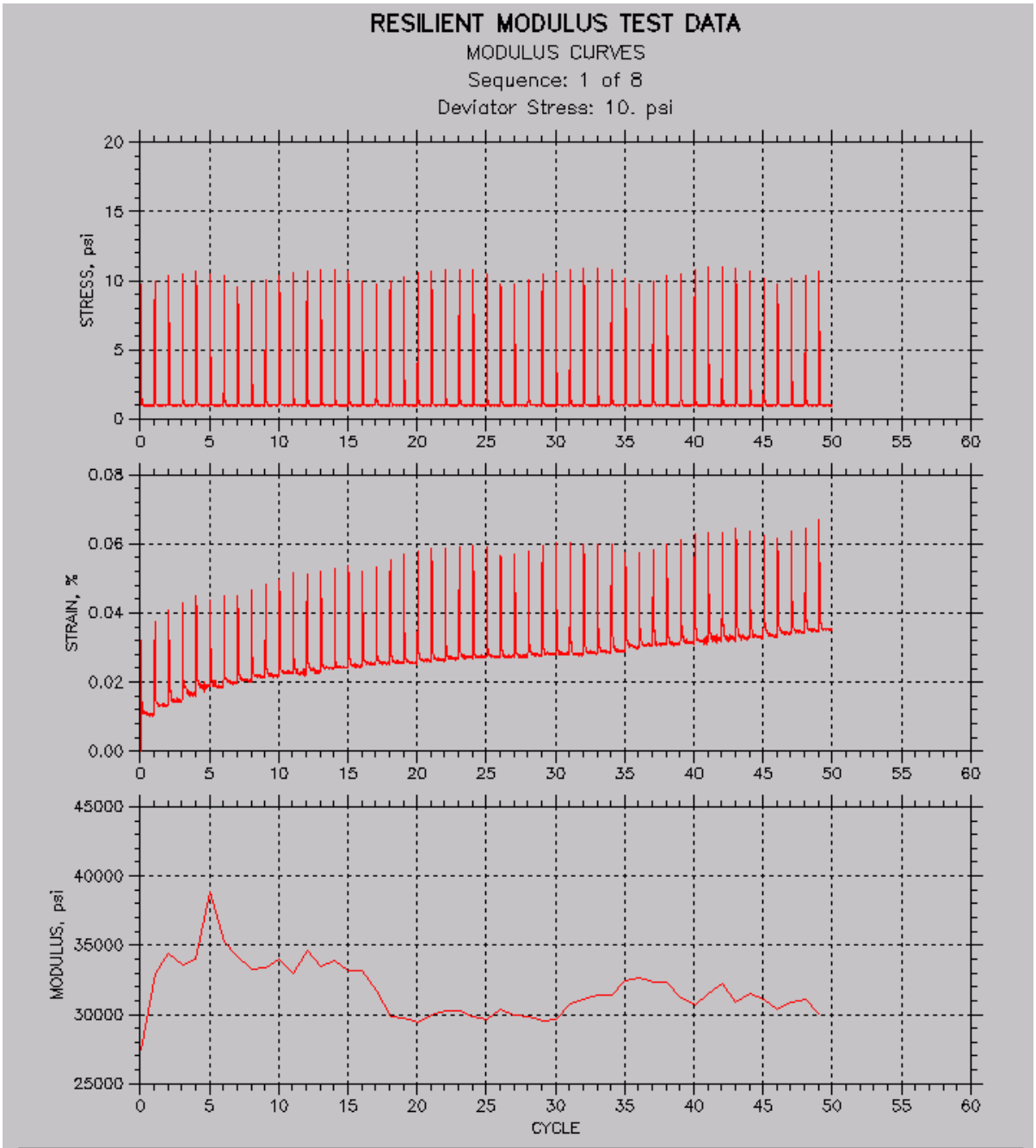

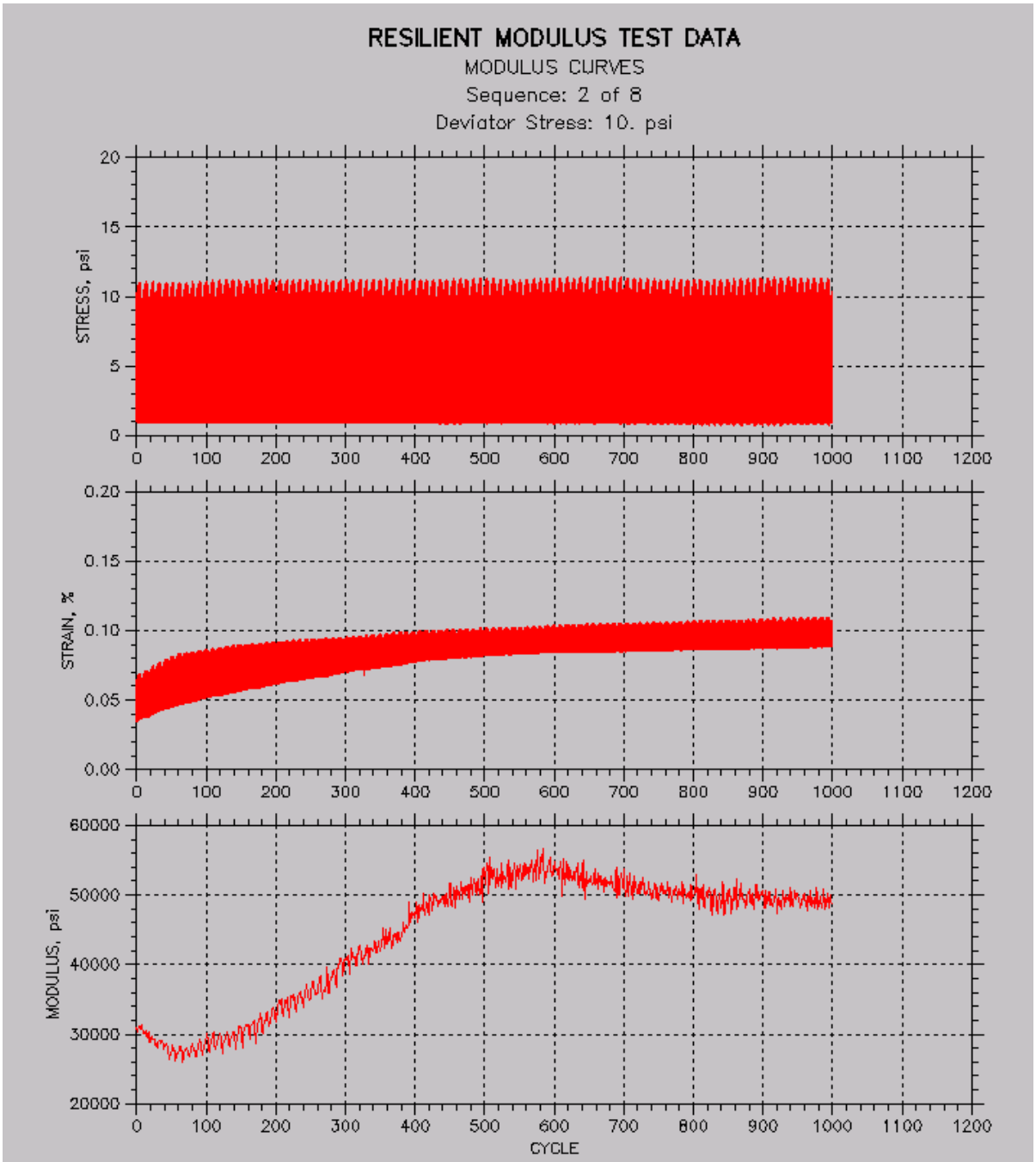

Project: PF2	Location: Ames	Project No.:
Boring No.:	Tested By: JL	Checked By:
Sample No.: 2	Test Date: 20120822	Depth:
Test No.:	Sample Type: Coarse	Elevation:
Description: Martin Marietta 950%RD 112.73pcf 2.32%w 7.90% fines permanent deformation test		
Remarks: Viracating compaction		
File: U:\Desktop\research\data\A New test plan\Permanent deformation tests\dat files\Crushed Limestone_Martin Marietta		

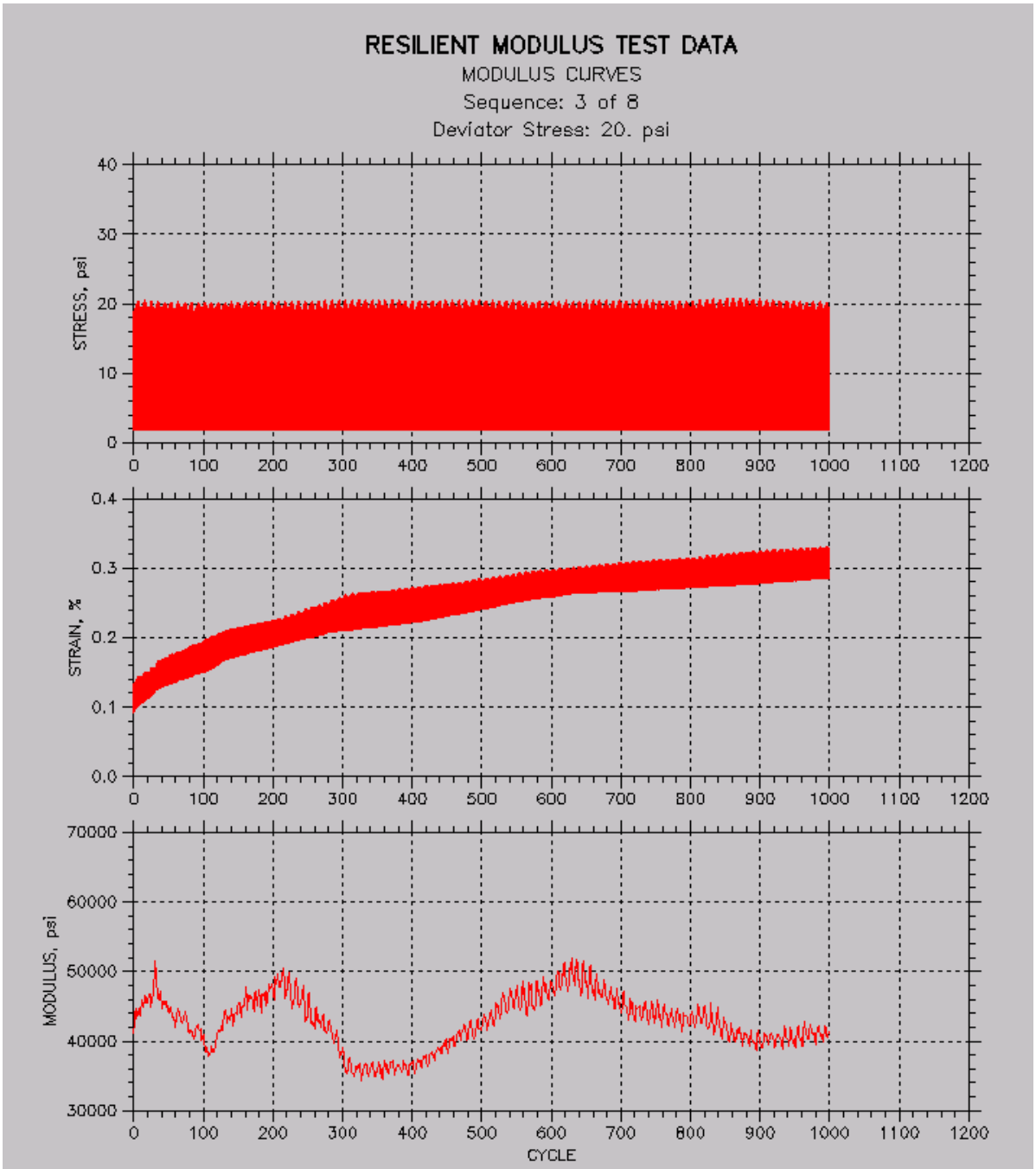

Project: PF2	Location: Ames	Project No.:
Boring No.:	Tested By: JL	Checked By:
Sample No.: 2	Test Date: 20120822	Depth:
Test No.:	Sample Type: Coarse	Elevation:
Description: Martin Marietta 950%RD 112.73pcf 2.32%w 7.90% fines permanent deformation test		
Remarks: Viracating compaction		
File: U:\Desktop\research\data\A New test plan\Permanent deformation tests\dat files\Crushed Limestone_Martin Marietta		

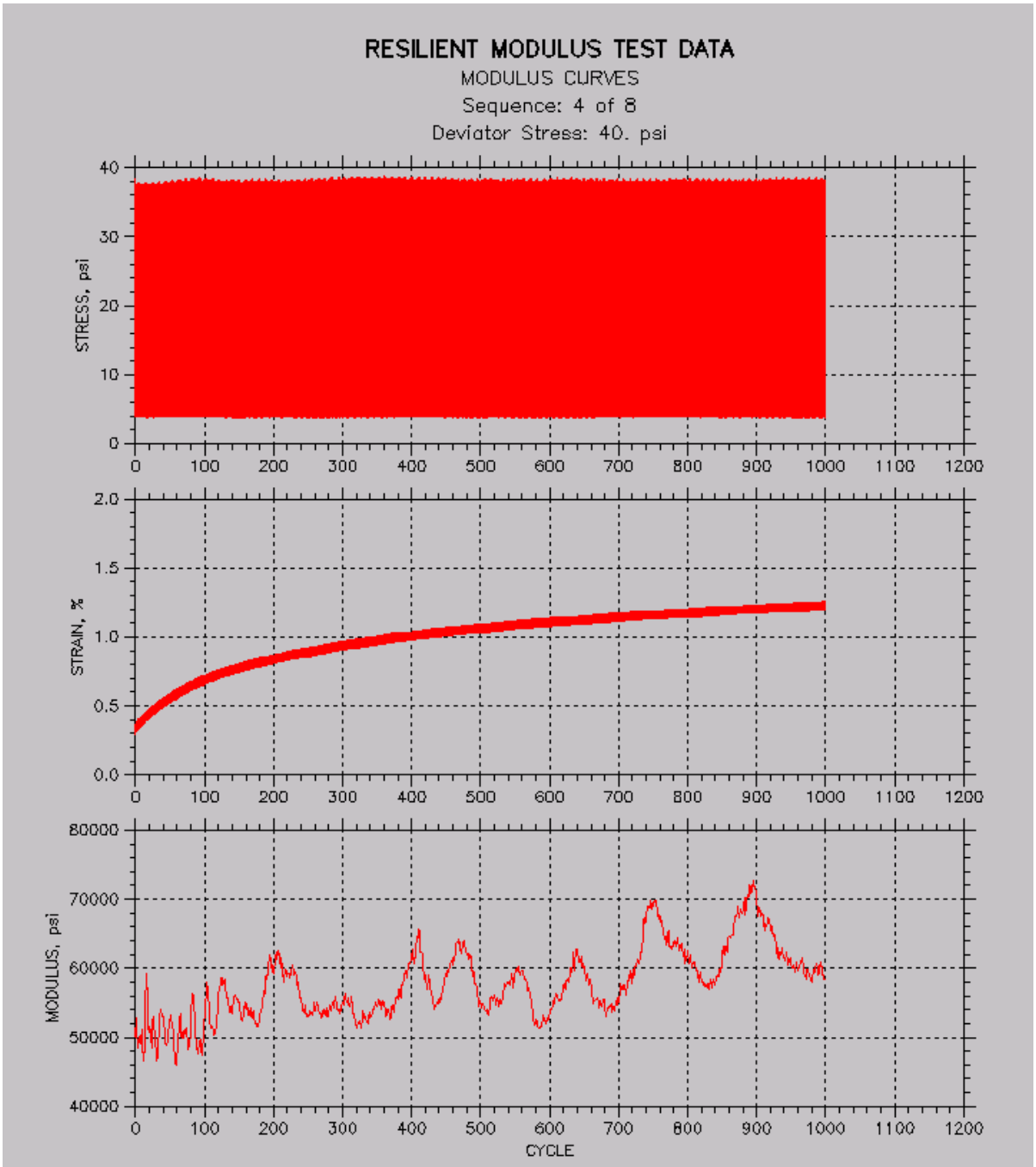

Project: PF2	Location: Ames	Project No.:
Boring No.:	Tested By: JL	Checked By:
Sample No.: 2	Test Date: 20120822	Depth:
Test No.:	Sample Type: Coarse	Elevation:
Description: Martin Marietta 950%RD 112.73pcf 2.32%w 7.90% fines permanent deformation test		
Remarks: Viracating compaction		
File: U:\Desktop\research\data\A New test plan\Permanent deformation tests\dat files\Crushed Limestone_Martin Marietta_		

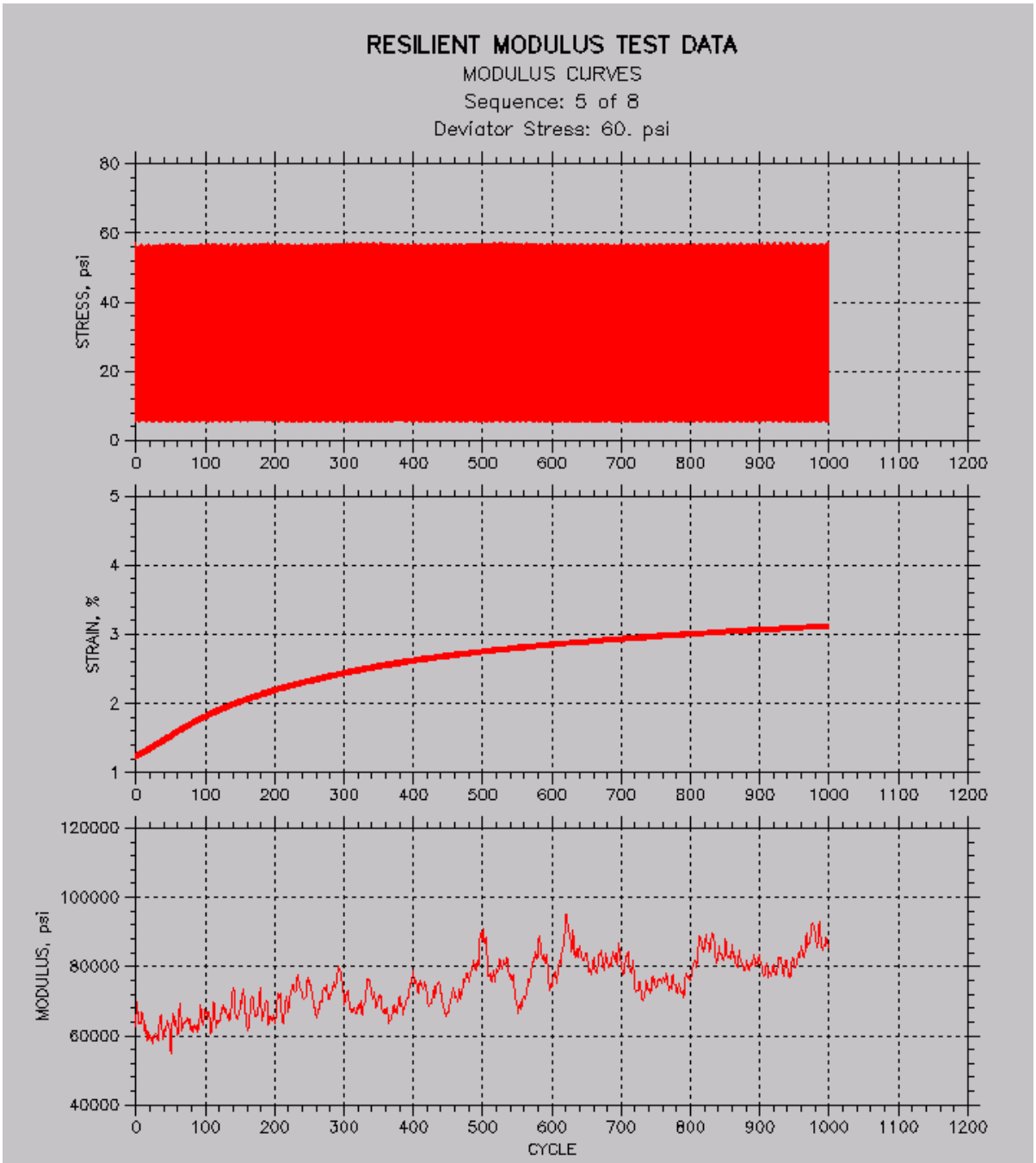

Project: PF2	Location: Ames	Project No.:
Boring No.:	Tested By: JL	Checked By:
Sample No.: 2	Test Date: 20120822	Depth:
Test No.:	Sample Type: Coarse	Elevation:
Description: Martin Marietta 950%RD 112.73pcf 2.32%w 7.90% fines permanent deformation test		
Remarks: Viracating compaction		
File: U:\Desktop\research\data\A New test plan\Permanent deformation tests\dat files\Crushed Limestone_Martin Marietta		

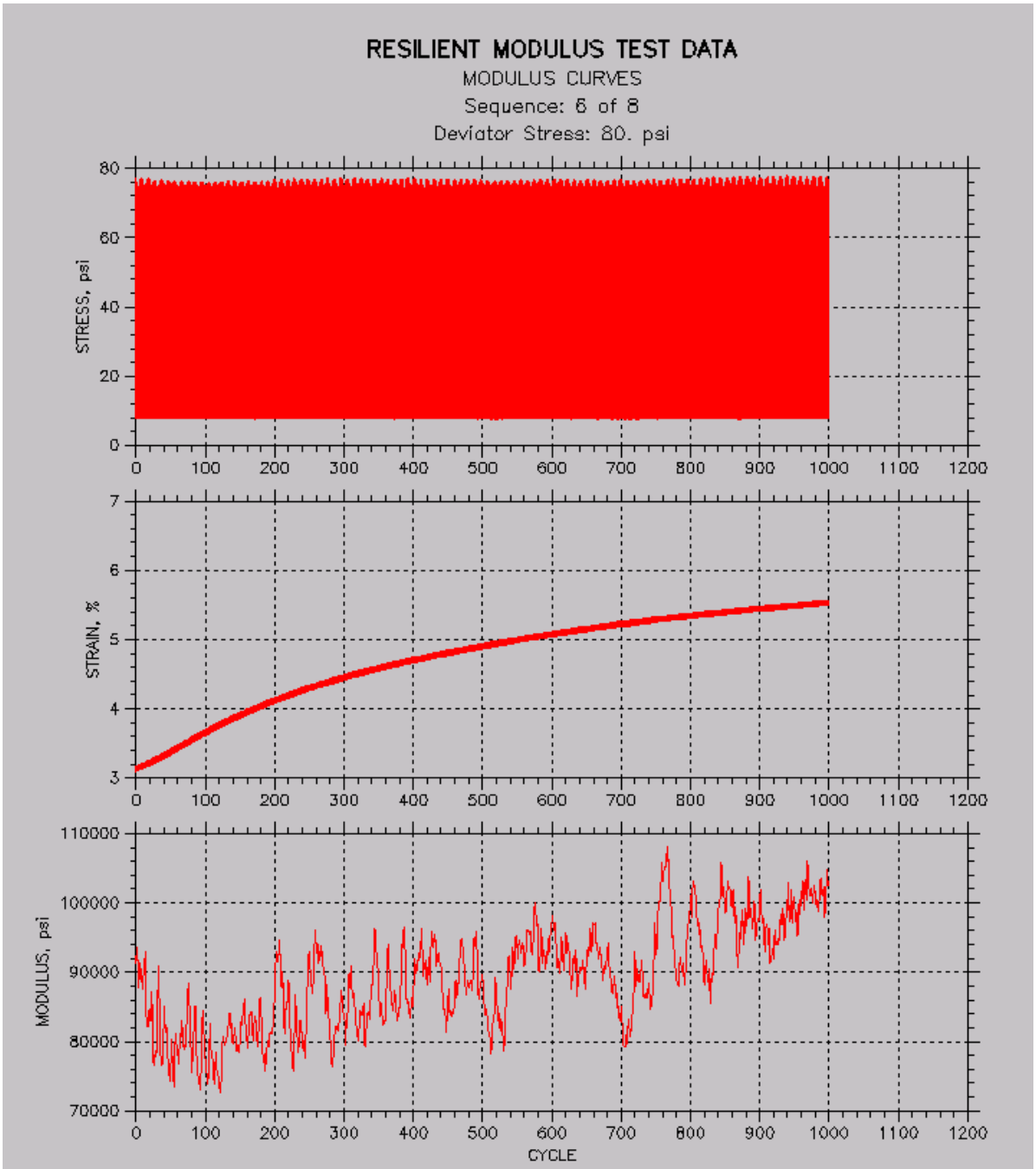

Project: PF2	Location: Ames	Project No.:
Boring No.:	Tested By: JL	Checked By:
Sample No.: 2	Test Date: 20120822	Depth:
Test No.:	Sample Type: Coarse	Elevation:
Description: Martin Marietta 950%RD 112.73pcf 2.32%w 7.90% fines permanent deformation test		
Remarks: Viracating compaction		
File: U:\Desktop\research\data\A New test plan\Permanent deformation tests\dat files\Crushed Limestone_Martin Marietta		

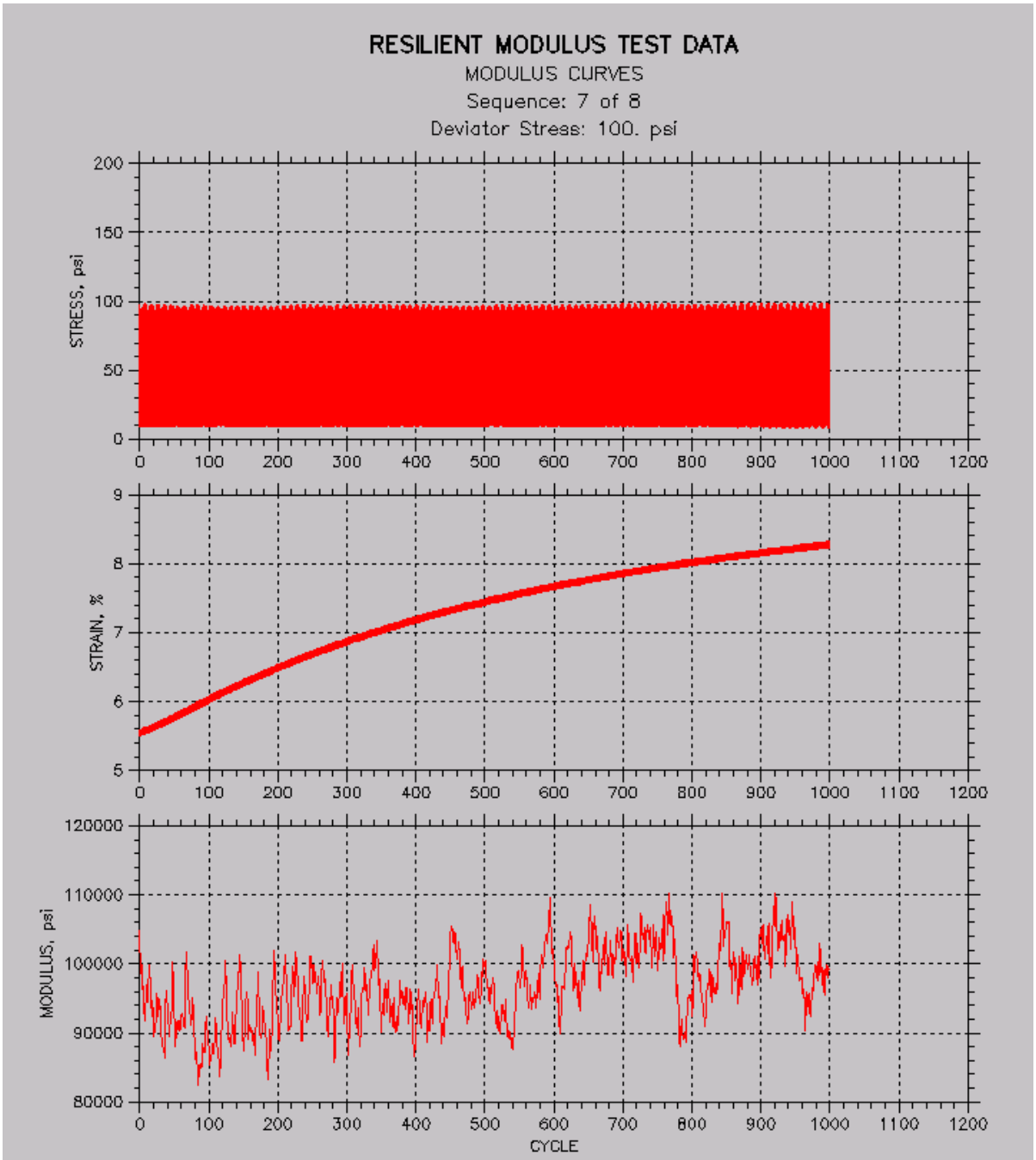

Project: PF2	Location: Ames	Project No.:
Boring No.:	Tested By: JL	Checked By:
Sample No.: 2	Test Date: 20120822	Depth:
Test No.:	Sample Type: Coarse	Elevation:
Description: Martin Marietta 950%RD 112.73pcf 2.32%w 7.90% fines permanent deformation test		
Remarks: Viracating compaction		
File: U:\Desktop\research\data\A New test plan\Permanent deformation tests\dat files\Crushed Limestone_Martin Marietta_		

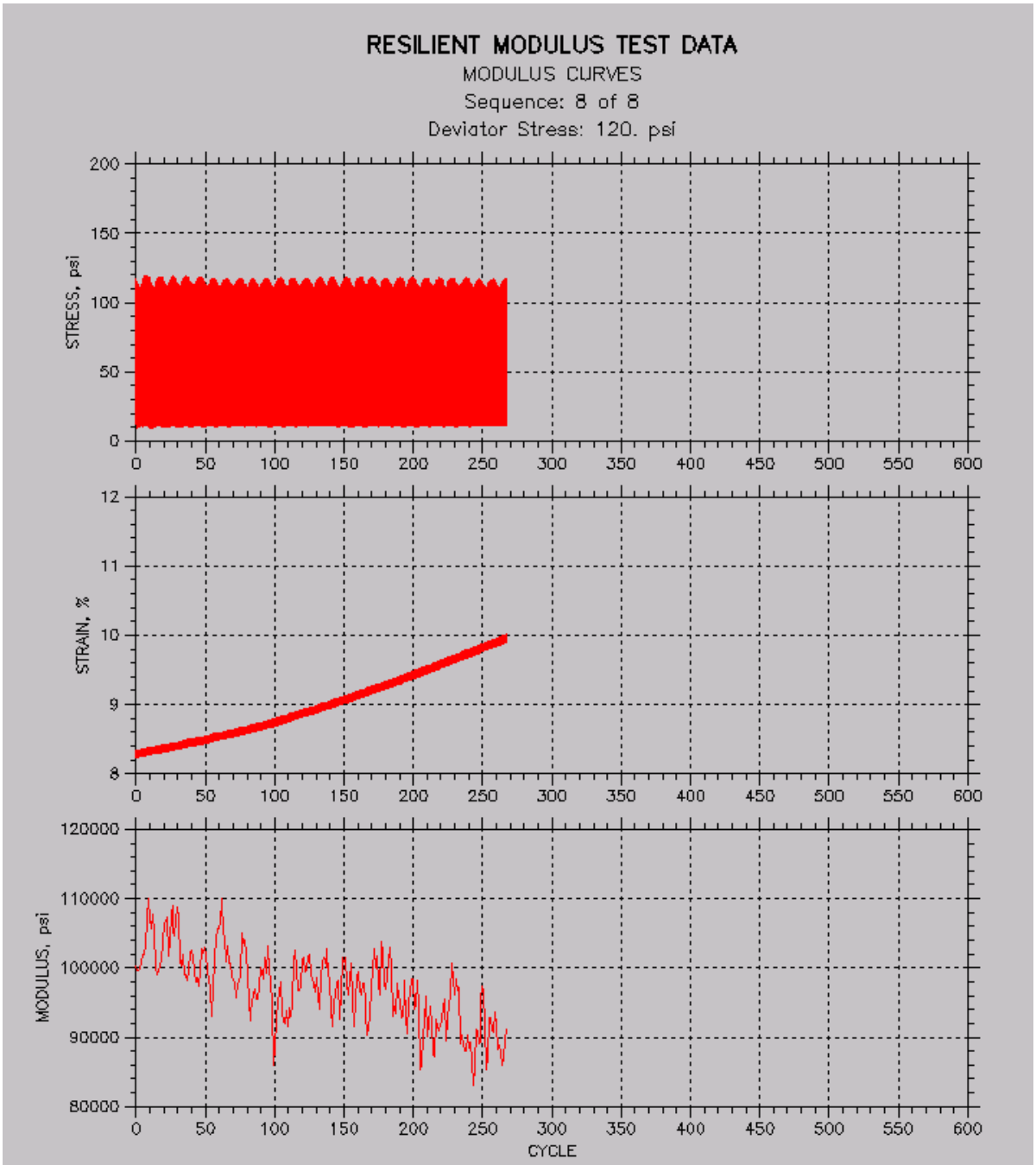

Project: PF2	Location: Ames	Project No.:
Boring No.:	Tested By: JL	Checked By:
Sample No.: 2	Test Date: 20120822	Depth:
Test No.:	Sample Type: Coarse	Elevation:
Description: Martin Marietta 950%RD 112.73pcf 2.32%w 7.90% fines permanent deformation test		
Remarks: Viracating compaction		
File: U:\Desktop\research\data\A New test plan\Permanent deformation tests\dat files\Crushed Limestone_Martin Marietta		

RAP

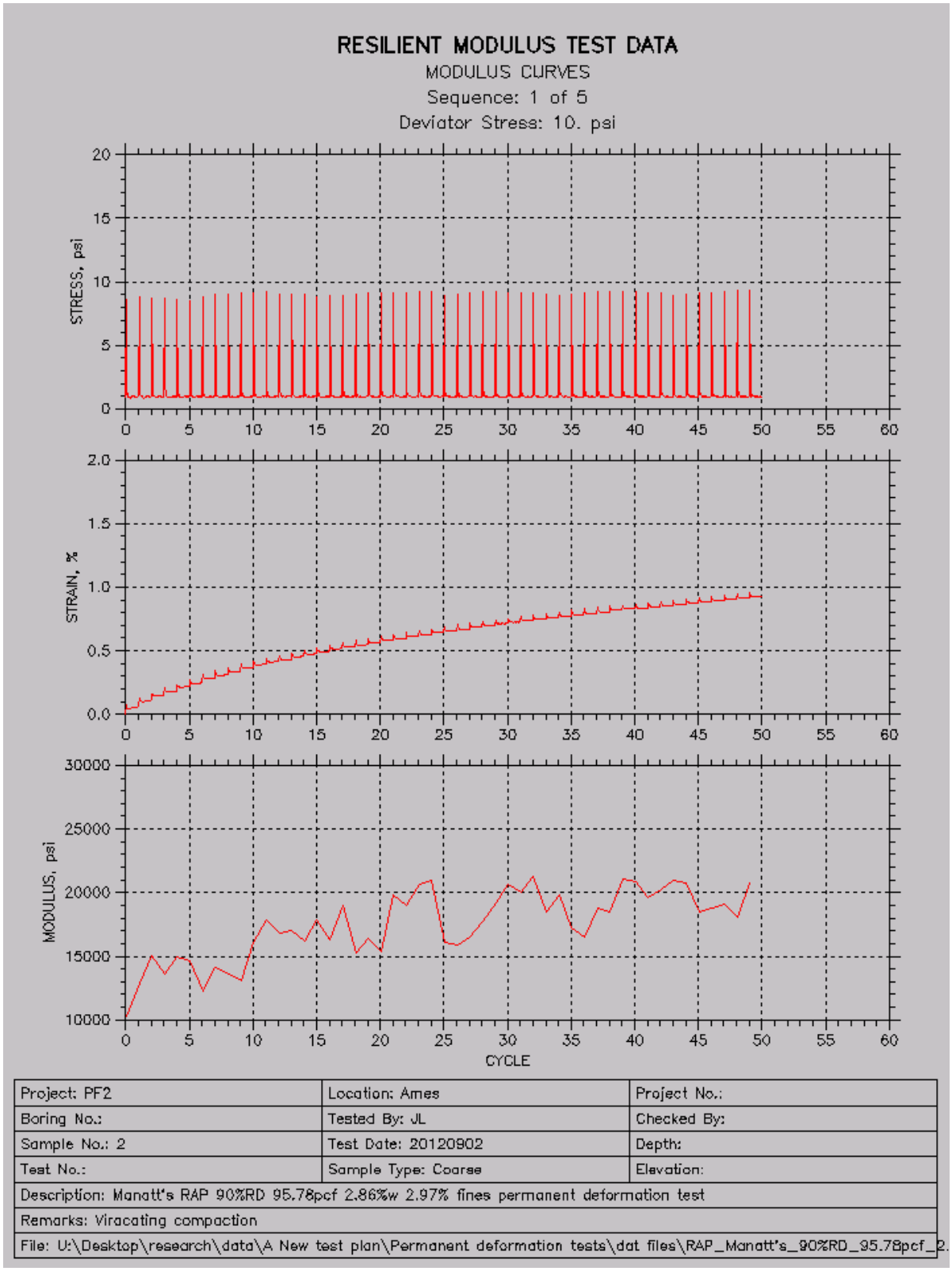

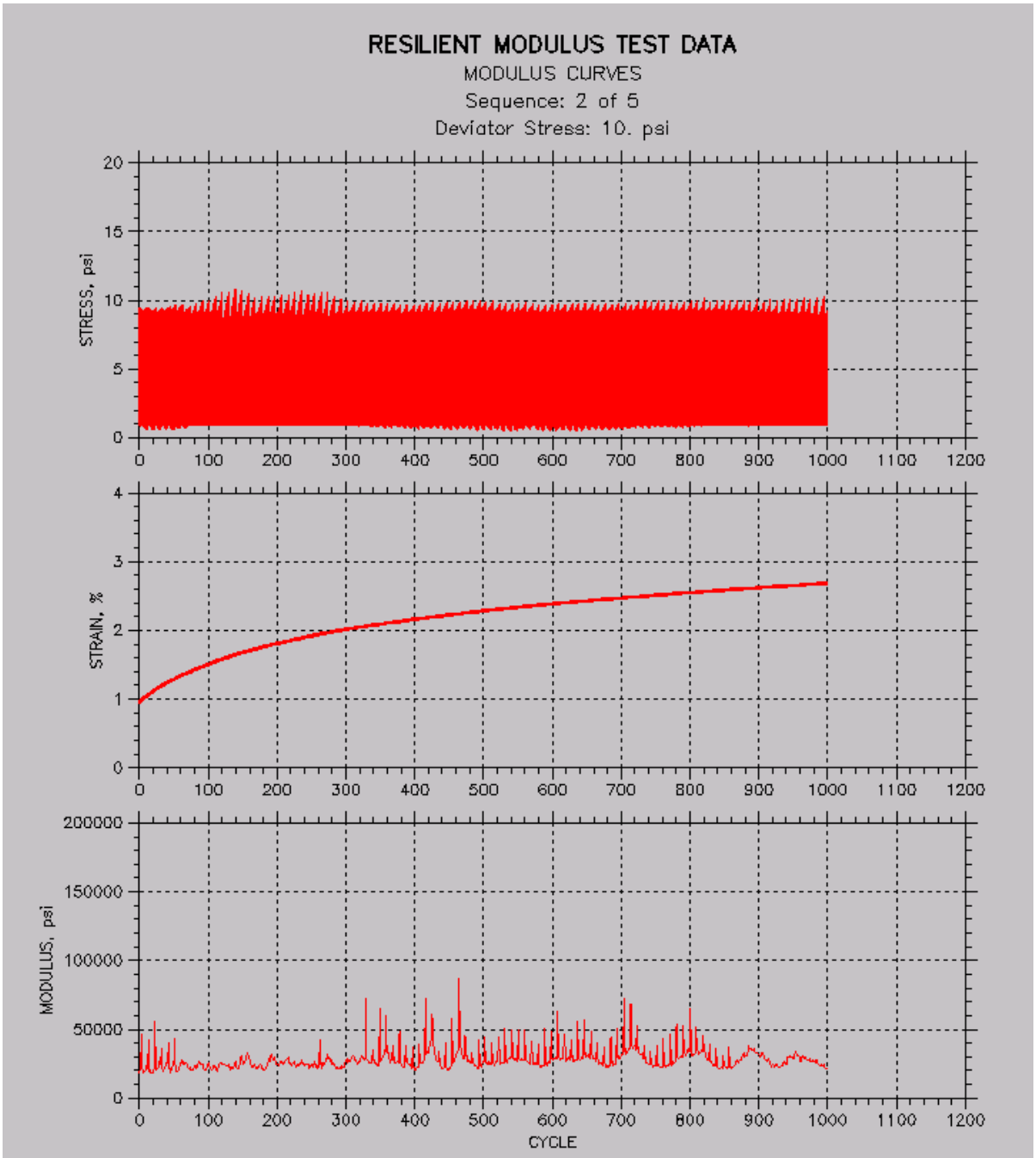

Project: PF2	Location: Ames	Project No.:
Boring No.:	Tested By: JL	Checked By:
Sample No.: 2	Test Date: 20120902	Depth:
Test No.:	Sample Type: Coarse	Elevation:
Description: Manatt's RAP 90%RD 95.78pcf 2.86%w 2.97% fines permanent deformation test		
Remarks: Viracating compaction		
File: U:\Desktop\research\data\A New test plan\Permanent deformation tests\dat files\RAP_Manatt's_90%RD_95.78pcf_2.		

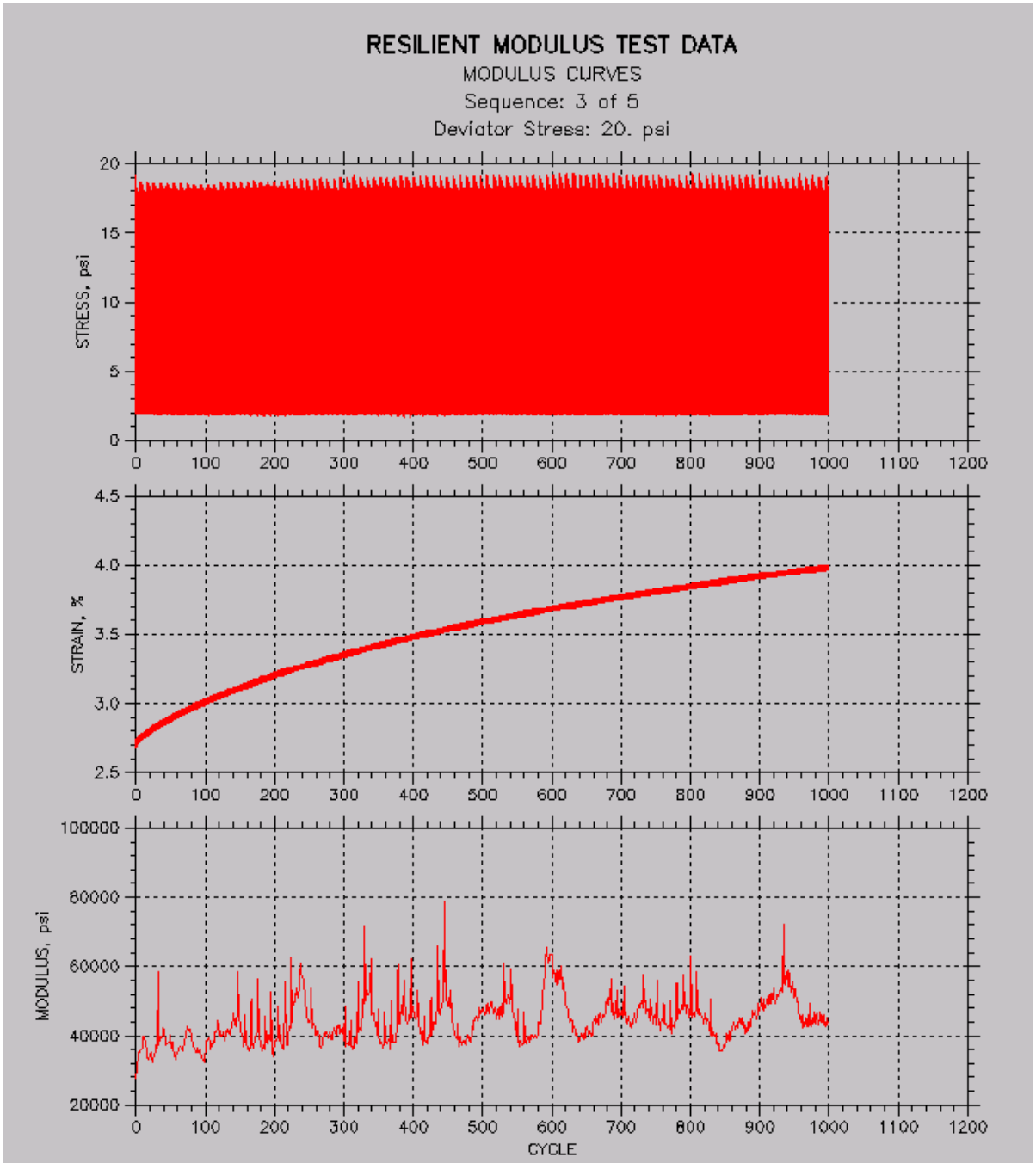

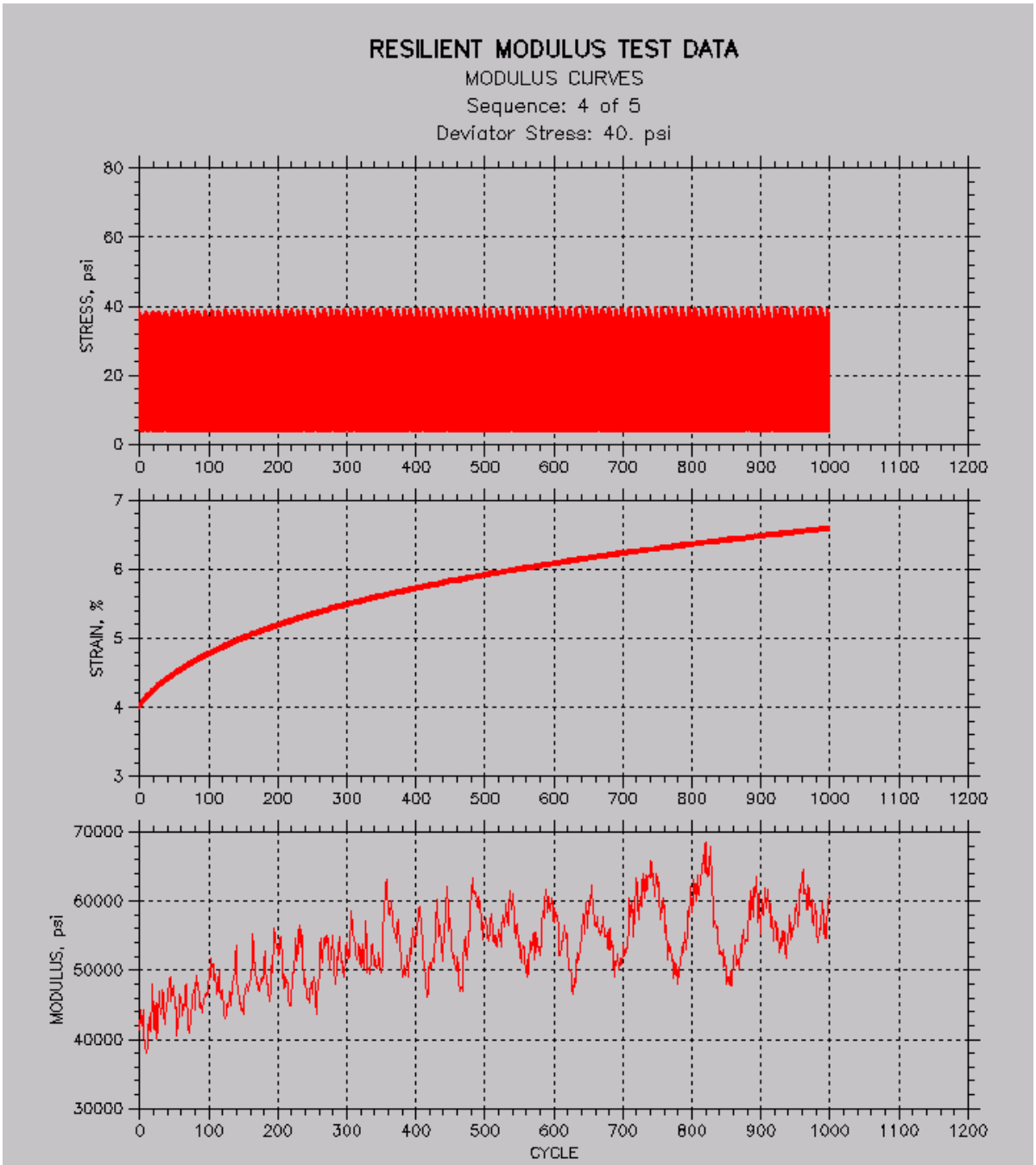

Project: PF2	Location: Ames	Project No.:
Boring No.:	Tested By: JL	Checked By:
Sample No.: 2	Test Date: 20120902	Depth:
Test No.:	Sample Type: Coarse	Elevation:
Description: Manatt's RAP 90%RD 95.78pcf 2.86%w 2.97% fines permanent deformation test		
Remarks: Viracating compaction		
File: U:\Desktop\research\data\A New test plan\Permanent deformation tests\dat files\RAP_Manatt's_90%RD_95.78pcf_2.		

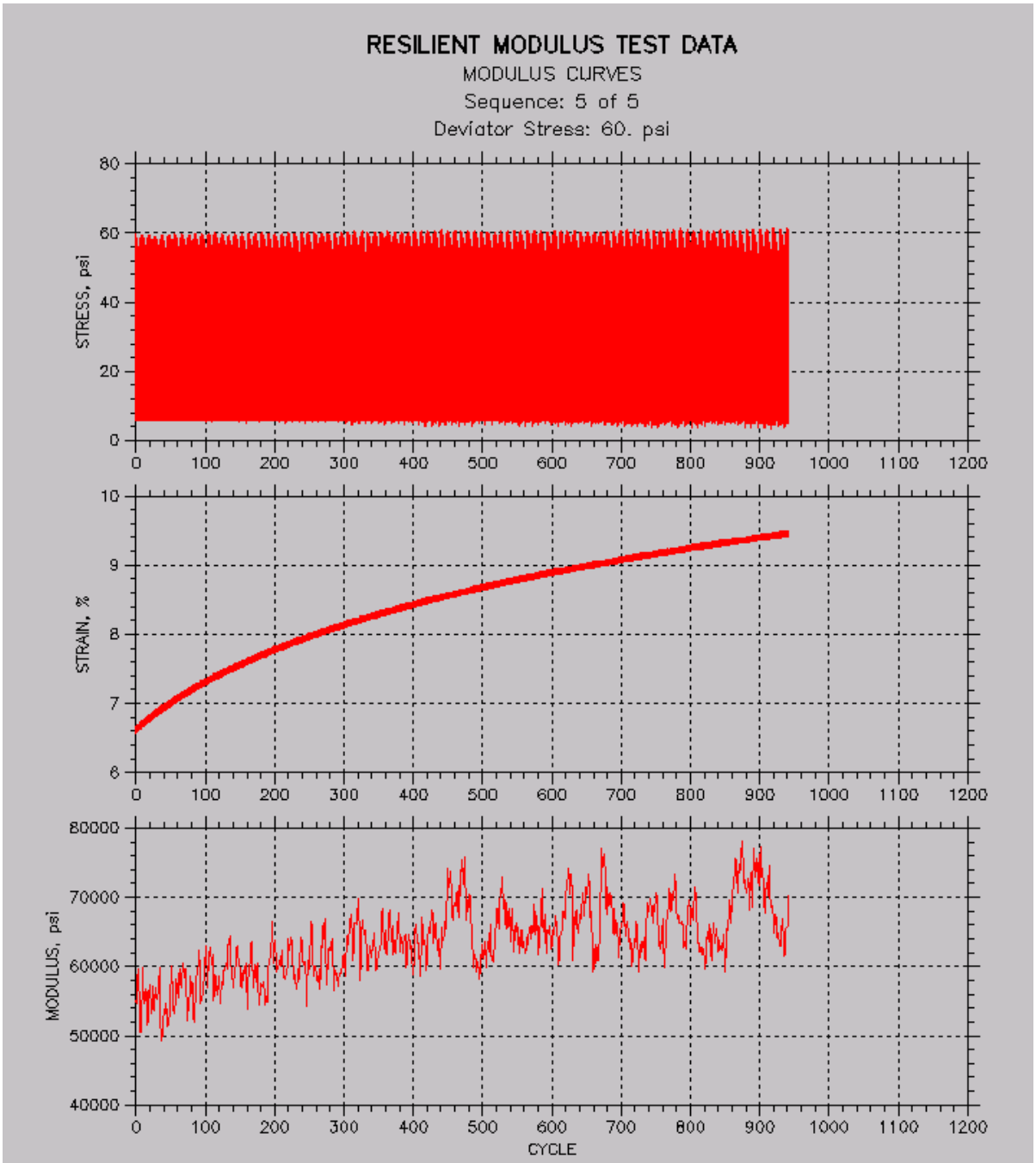

Project: PF2	Location: Ames	Project No.:
Boring No.:	Tested By: JL	Checked By:
Sample No.: 2	Test Date: 20120902	Depth:
Test No.:	Sample Type: Coarse	Elevation:
Description: Manatt's RAP 90%RD 95.78pcf 2.86%w 2.97% fines permanent deformation test		
Remarks: Viracating compaction		
File: U:\Desktop\research\data\A New test plan\Permanent deformation tests\dat files\RAP_Manatt's_90%RD_95.78pcf_2.		

RPCC/RAP

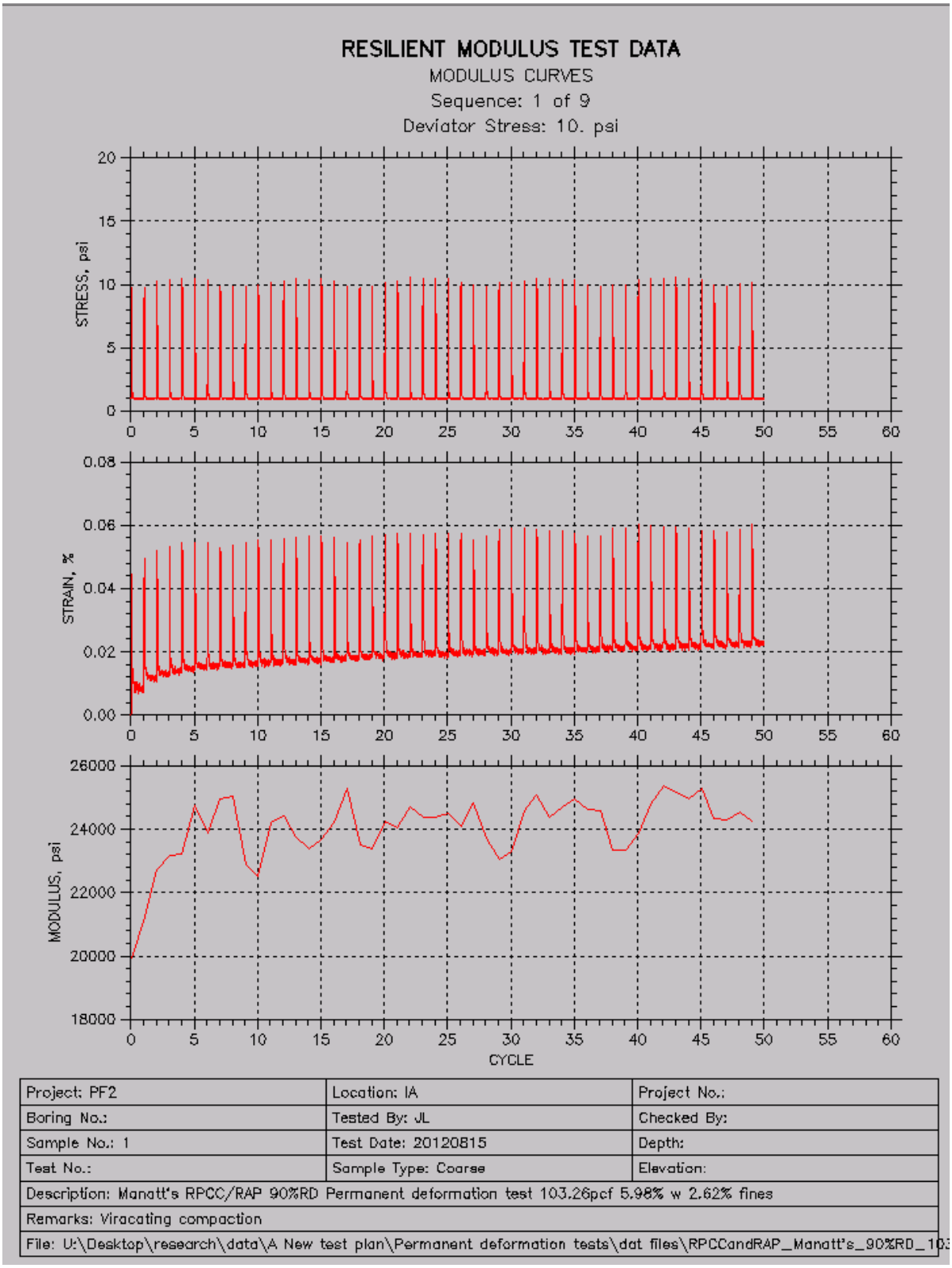

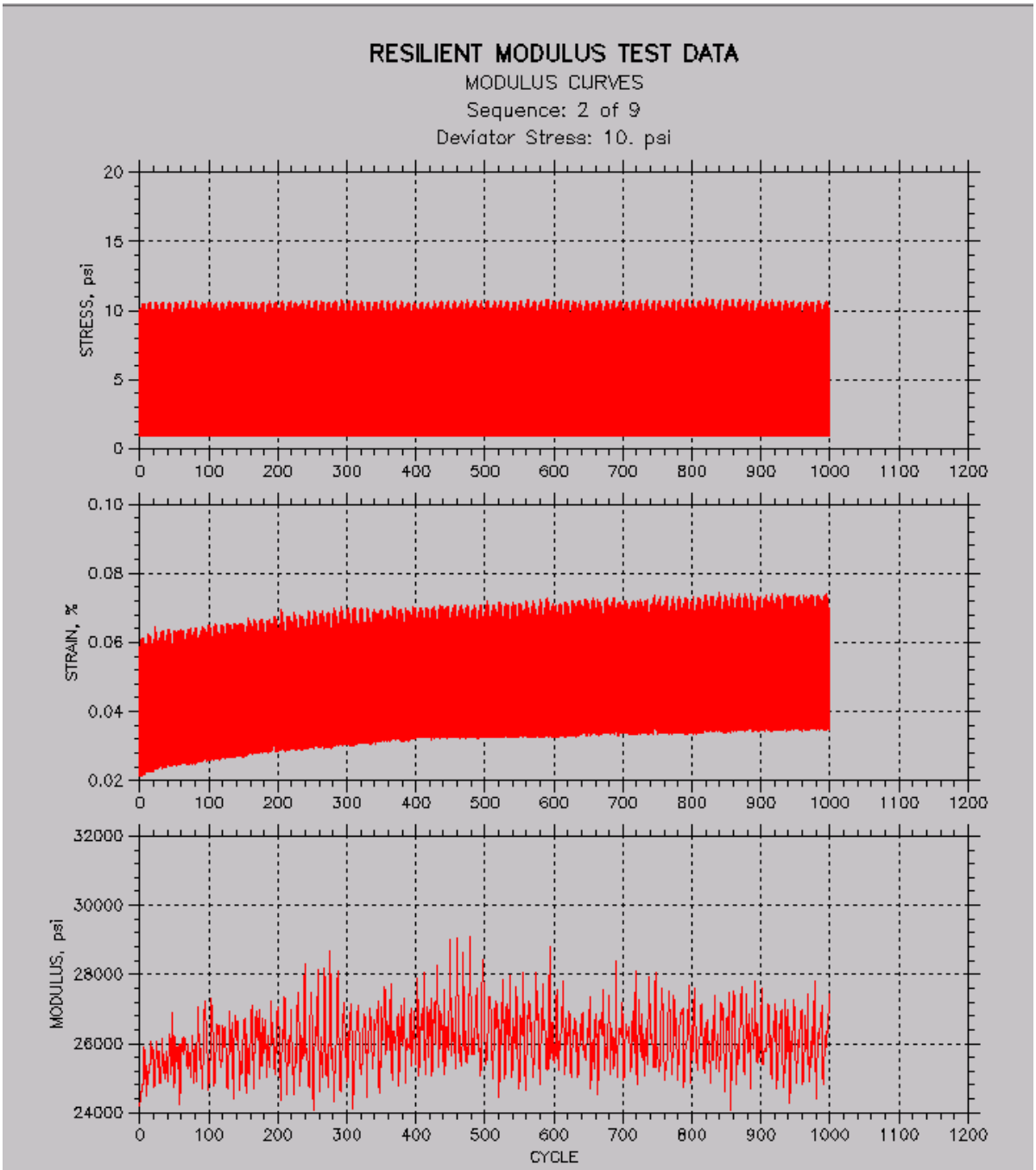

Project: PF2	Location: IA	Project No.:
Boring No.:	Tested By: JL	Checked By:
Sample No.: 1	Test Date: 20120815	Depth:
Test No.:	Sample Type: Coarse	Elevation:
Description: Manatt's RPCC/RAP 90%RD Permanent deformation test 103.26pcf 5.98% w 2.62% fines		
Remarks: Viracating compaction		
File: U:\Desktop\research\data\A New test plan\Permanent deformation tests\dat files\RPCCandRAP_Manatt's_90%RD_103		

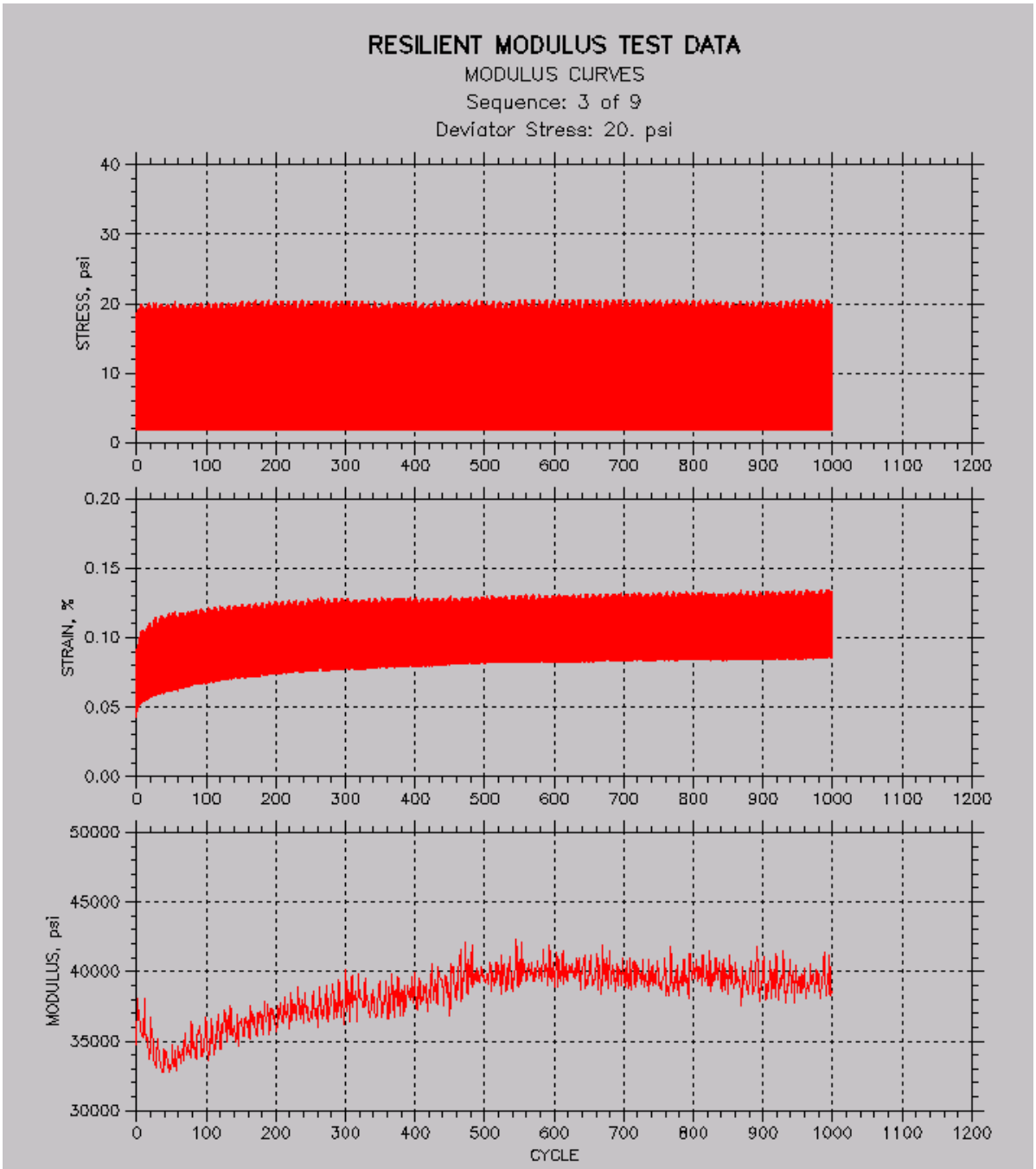

Project: PF2	Location: IA	Project No.:
Boring No.:	Tested By: JL	Checked By:
Sample No.: 1	Test Date: 20120815	Depth:
Test No.:	Sample Type: Coarse	Elevation:
Description: Manatt's RPCC/RAP 90%RD Permanent deformation test 103.26pcf 5.98% w 2.62% fines		
Remarks: Viracating compaction		
File: U:\Desktop\research\data\A New test plan\Permanent deformation tests\dat files\RPCCandRAP_Manatt's_90%RD_10		

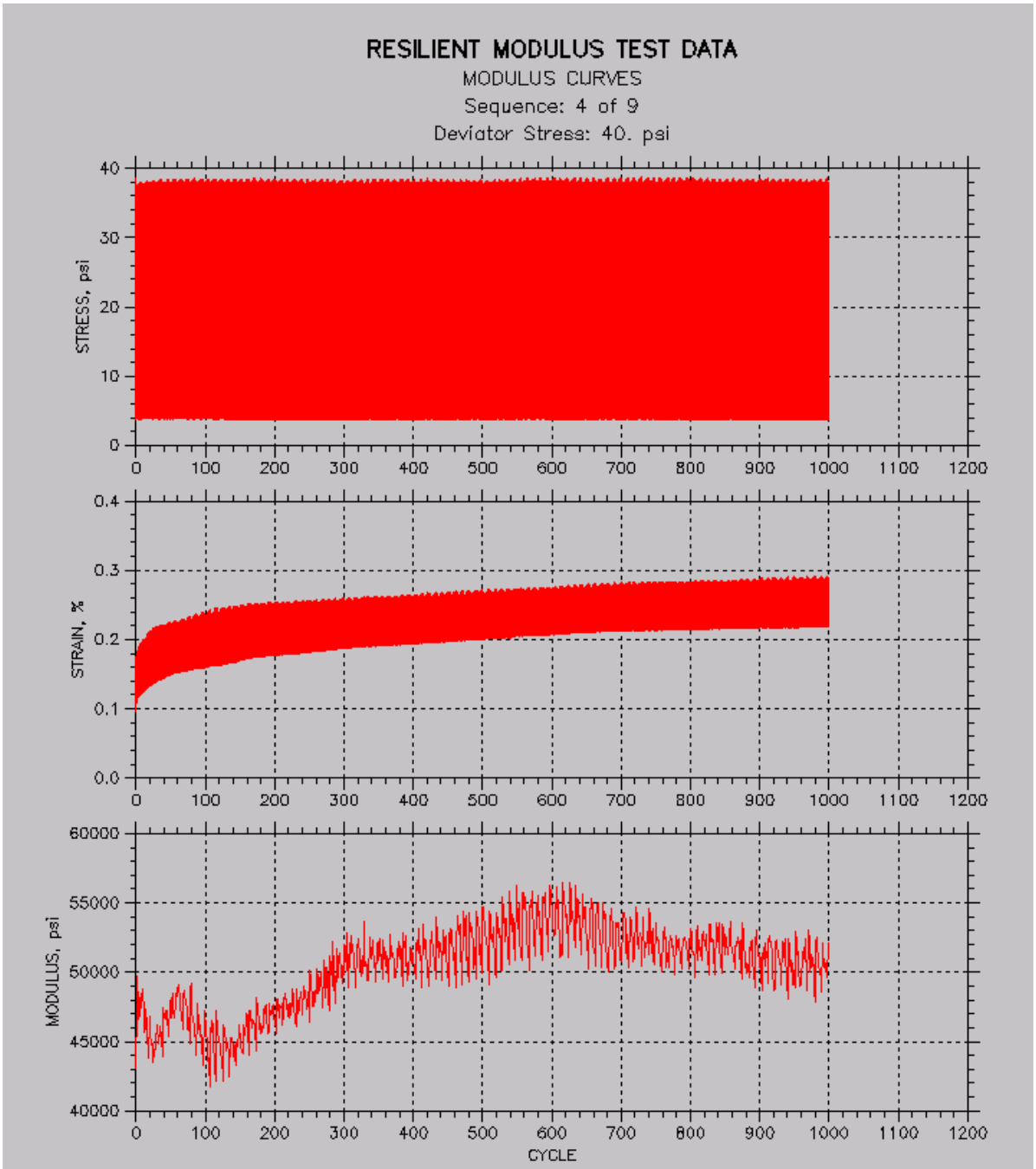

Project: PF2	Location: IA	Project No.:
Boring No.:	Tested By: JL	Checked By:
Sample No.: 1	Test Date: 20120815	Depth:
Test No.:	Sample Type: Coarse	Elevation:
Description: Manatt's RPCC/RAP 90%RD Permanent deformation test 103.26pcf 5.98% w 2.62% fines		
Remarks: Viracating compaction		
File: U:\Desktop\research\data\A New test plan\Permanent deformation tests\dat files\RPCCandRAP_Manatt's_90%RD_103		

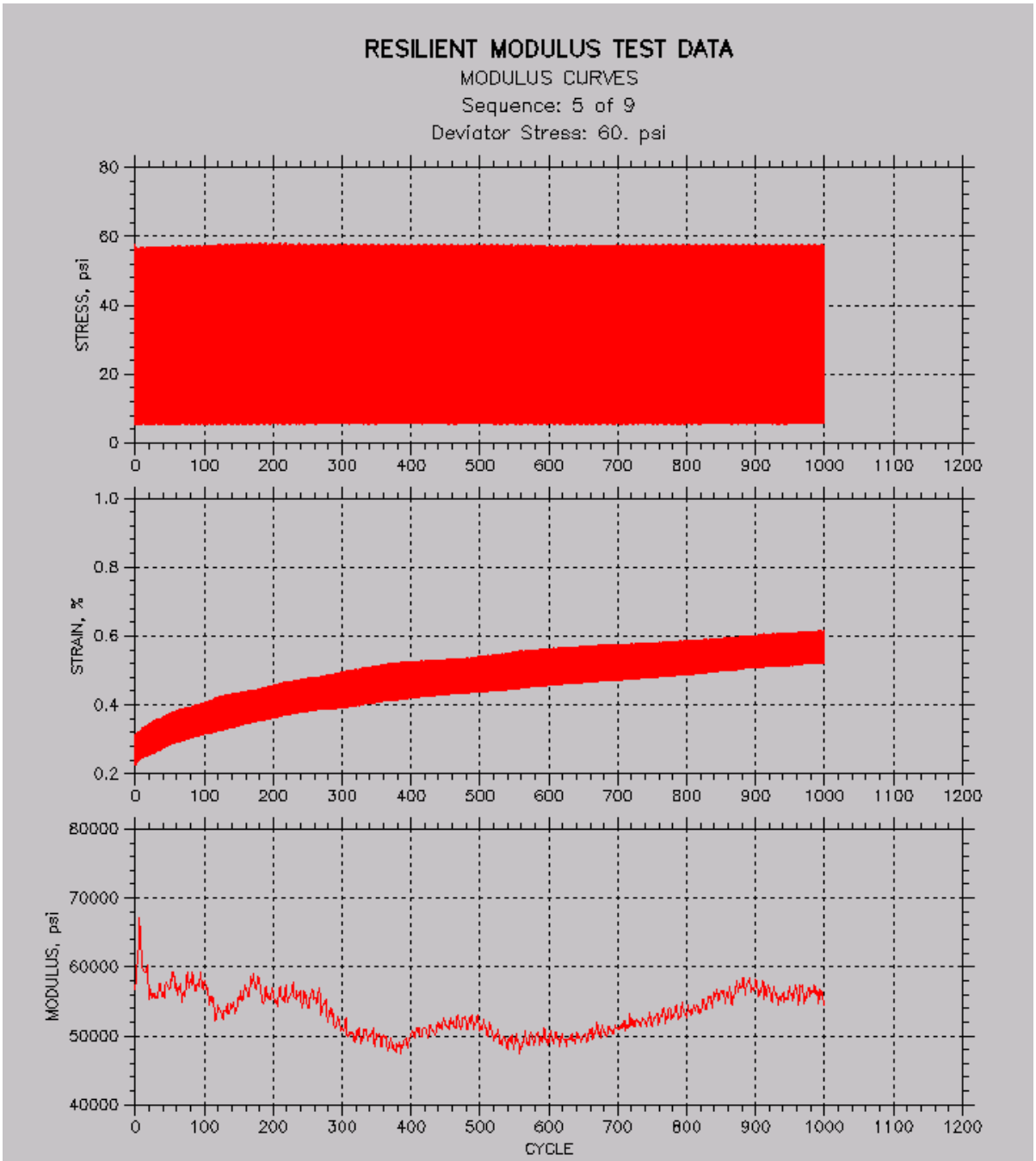

Project: PF2	Location: IA	Project No.:
Boring No.:	Tested By: JL	Checked By:
Sample No.: 1	Test Date: 20120815	Depth:
Test No.:	Sample Type: Coarse	Elevation:
Description: Manatt's RPCC/RAP 90%RD Permanent deformation test 103.26pcf 5.98% w 2.62% fines		
Remarks: Viracating compaction		
File: U:\Desktop\research\data\A New test plan\Permanent deformation tests\dat files\RPCCandRAP_Manatt's_90%RD_103.		

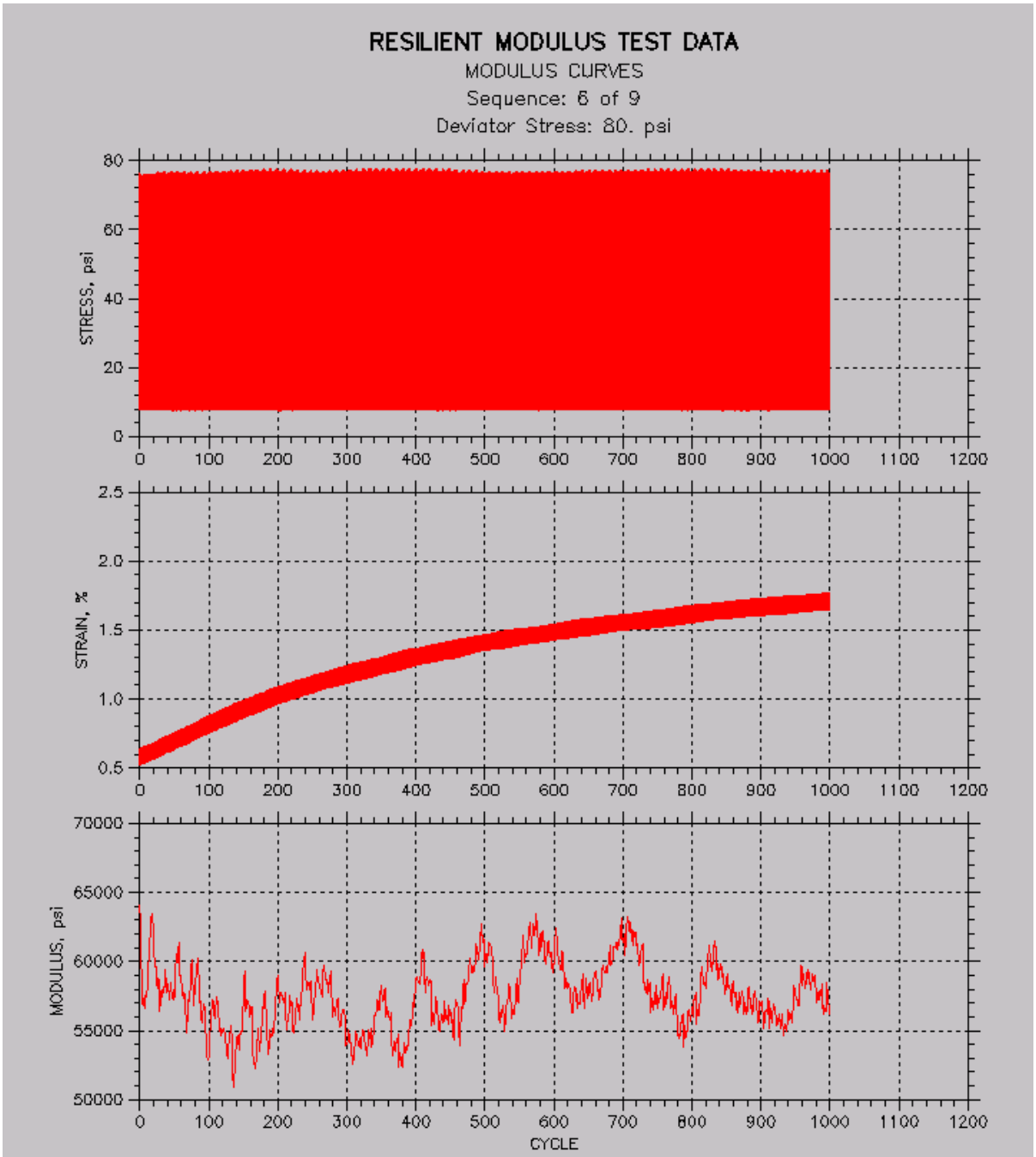

Project: PF2	Location: IA	Project No.:
Boring No.:	Tested By: JL	Checked By:
Sample No.: 1	Test Date: 20120815	Depth:
Test No.:	Sample Type: Coarse	Elevation:
Description: Manatt's RPCC/RAP 90%RD Permanent deformation test 103.26pcf 5.98% w 2.62% fines		
Remarks: Viracating compaction		
File: U:\Desktop\research\data\A New test plan\Permanent deformation tests\dat files\RPCCandRAP_Manatt's_90%RD_103		

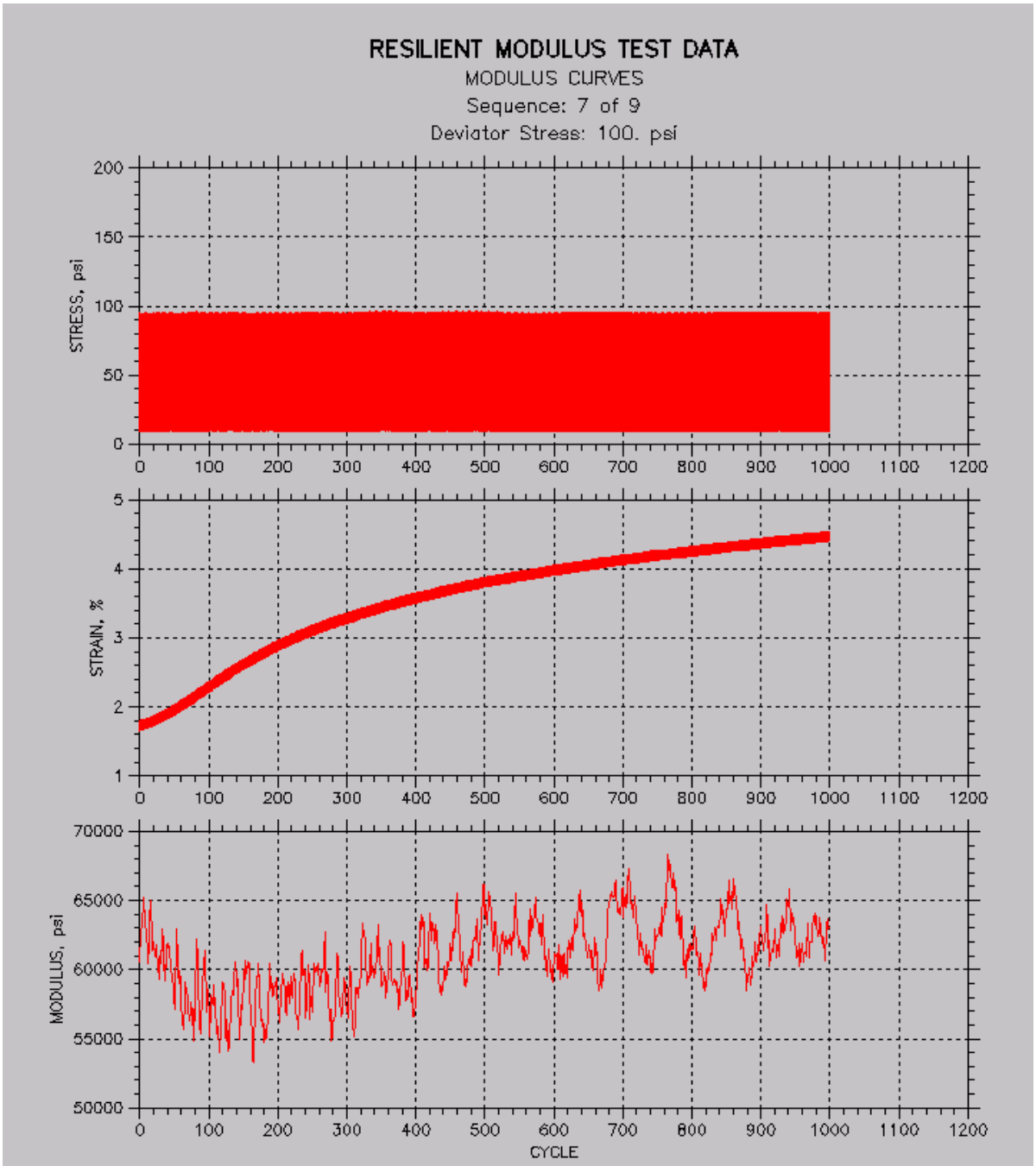

Project: PF2	Location: IA	Project No.:
Boring No.:	Tested By: JL	Checked By:
Sample No.: 1	Test Date: 20120815	Depth:
Test No.:	Sample Type: Coarse	Elevation:
Description: Manatt's RPCC/RAP 90%RD Permanent deformation test 103.26pcf 5.98% w 2.62% fines		
Remarks: Viracating compaction		
File: U:\Desktop\research\data\A New test plan\Permanent deformation tests\dat files\RPCCandRAP_Manatt's_90%RD_103		

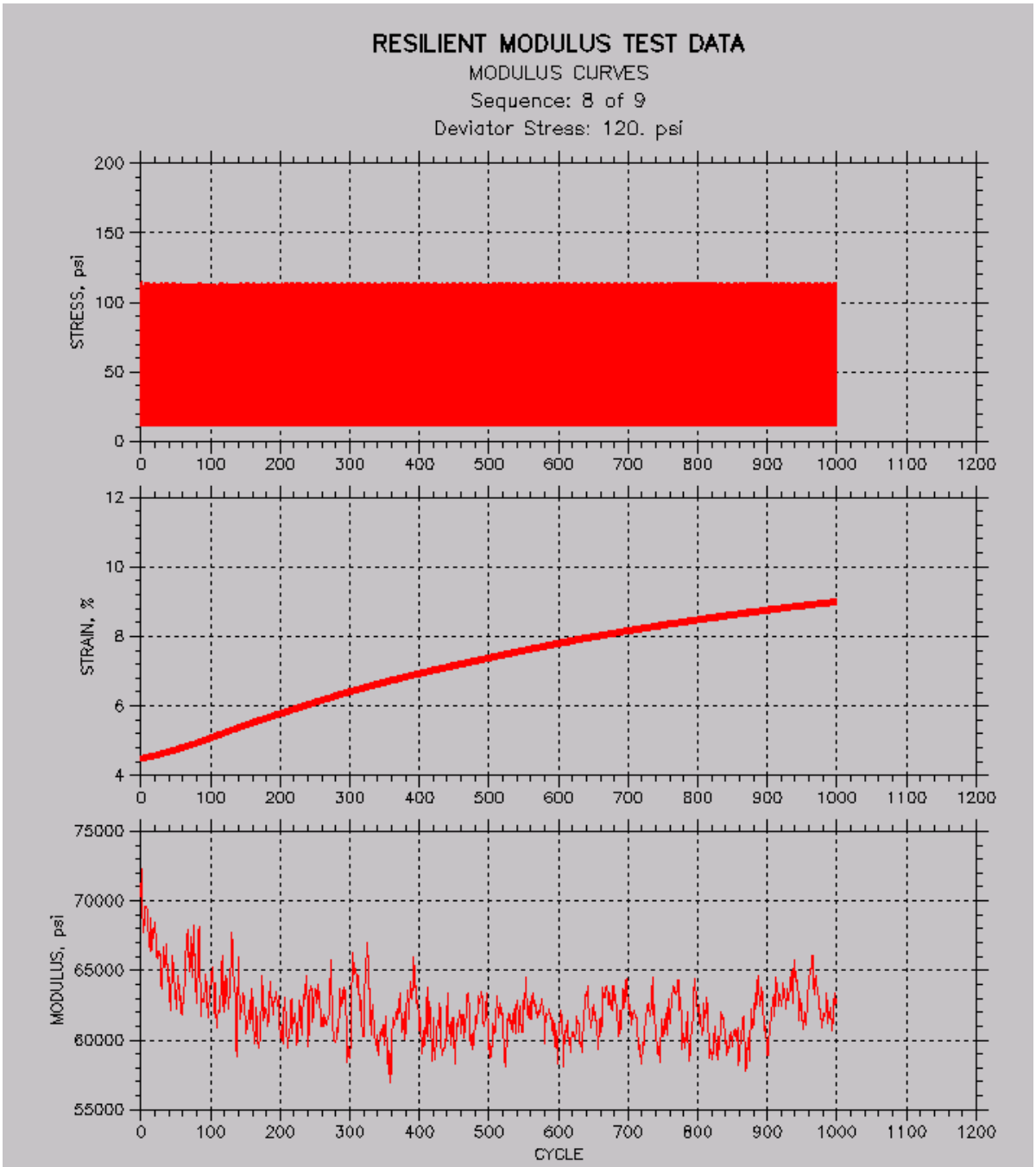

Project: PF2	Location: IA	Project No.:
Boring No.:	Tested By: JL	Checked By:
Sample No.: 1	Test Date: 20120815	Depth:
Test No.:	Sample Type: Coarse	Elevation:
Description: Manatt's RPCC/RAP 90%RD Permanent deformation test 103.26pcf 5.98% w 2.62% fines		
Remarks: Viracating compaction		
File: U:\Desktop\research\data\A New test plan\Permanent deformation tests\dat files\RPCCandRAP_Manatt's_90%RD_1		

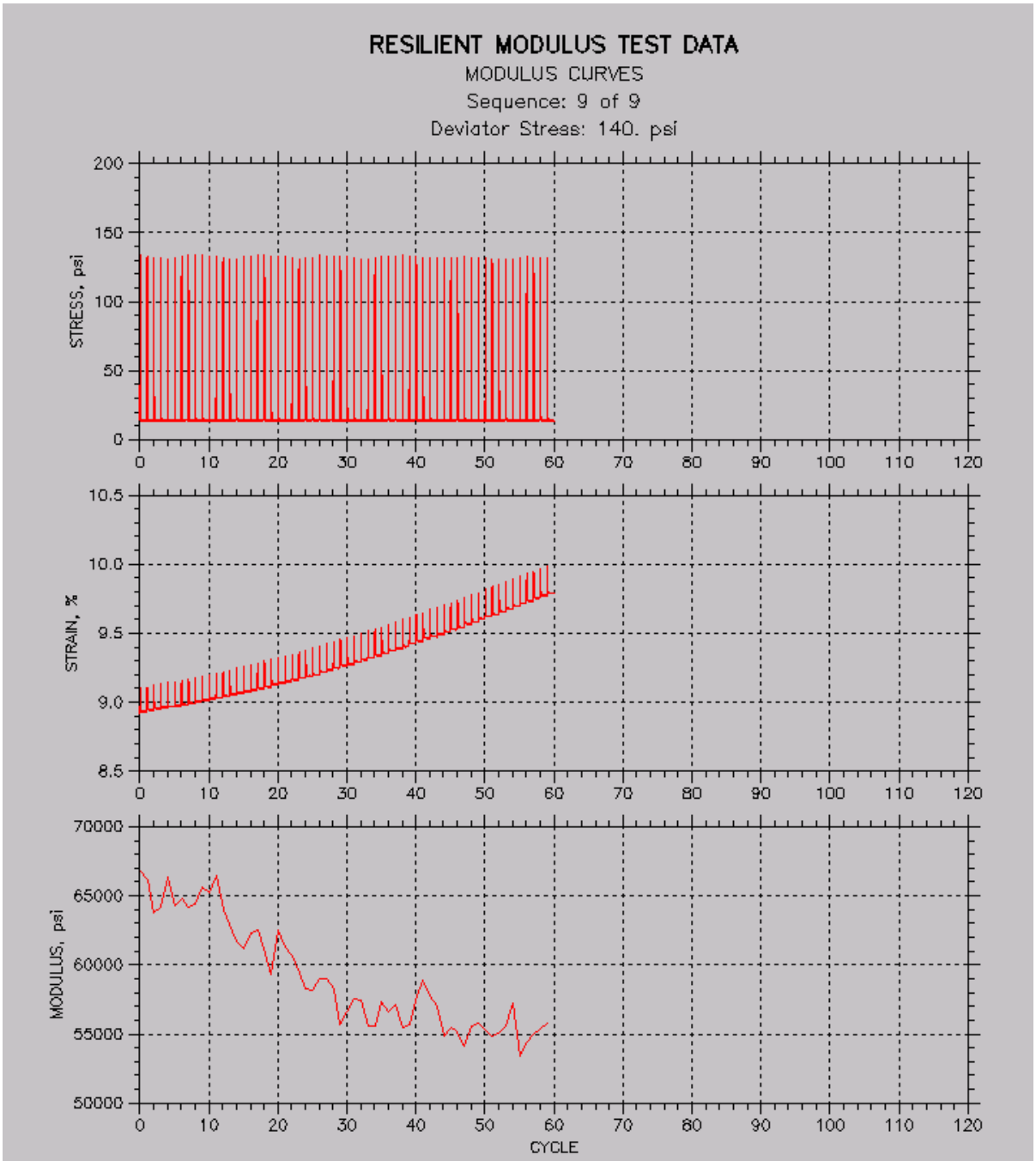

Project: PF2	Location: IA	Project No.:
Boring No.:	Tested By: JL	Checked By:
Sample No.: 1	Test Date: 20120815	Depth:
Test No.:	Sample Type: Coarse	Elevation:
Description: Manatt's RPCC/RAP 90%RD Permanent deformation test 103.26pcf 5.98% w 2.62% fines		
Remarks: Viracating compaction		
File: U:\Desktop\research\data\A New test plan\Permanent deformation tests\dat files\RPCCandRAP_Manatt's_90%RD_10		

Resilient Modulus Tests

System outputs of the resilient modulus tests were reported for each tested subbase material sample.

Crushed limestone

RESILIENT MODULUS TEST DATA

SUMMARY REPORT

$Mr = 1060.4 * Pa * (B/Pa)^{0.532} * (Sd/Pa)^{0.125}$ r = 0.979

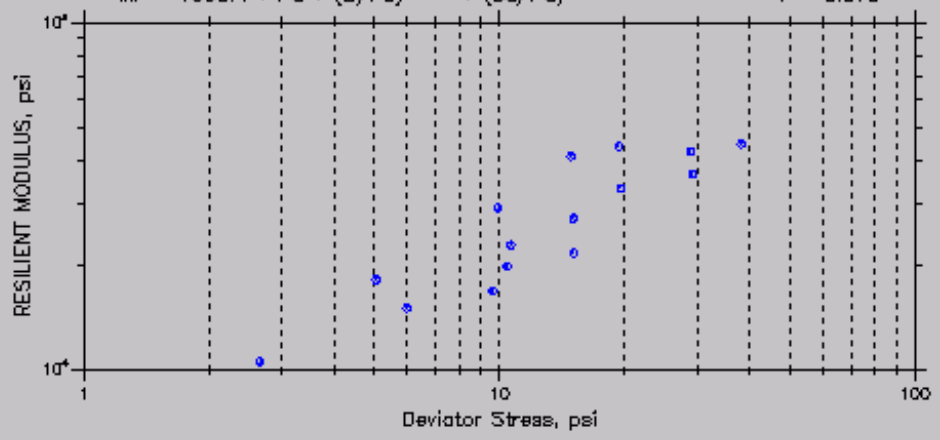

Confining Stress S3 (psi)	Nom. Max. Deviator Stress (psi)	Mean Deviator Stress (psi)	Std. Dev. Deviator Stress (psi)	Mean Bulk Stress (psi)	Mean Resilient Strain (%)	Std. Dev. Resilient Strain (%)	Mean Resilient Modulus (psi)	Std. Dev. Resilient Modulus (psi)
2.998	3	2.649	0.0584	11.64	0.02	0.00	10511	246.91
3.06	6	5.878	0.1429	15.16	0.04	0.00	14990	155.73
3.056	9	8.639	0.0580	18.81	0.05	0.00	16785	96.775
5.033	5	5.036	0.1641	20.13	0.03	0.00	18105	395.62
5.091	10	10.43	0.2817	25.7	0.05	0.00	19767	348.93
5.035	15	15.06	0.3856	30.16	0.06	0.00	21615	192.86
10.04	10	10.65	0.3059	40.78	0.04	0.00	22791	239.76
9.991	20	19.58	0.2381	49.56	0.05	0.00	33314	418.7
10.03	30	29.12	0.1158	59.22	0.07	0.00	38485	256.78
15.03	10	9.805	0.1490	55	0.03	0.00	29205	243.86
15.02	15	15.03	0.2976	60.09	0.05	0.00	27214	188.9
15.02	30	28.78	0.0420	73.84	0.06	0.00	42445	201.88
19.88	15	14.85	0.2227	74.49	0.03	0.00	41154	241.78
19.88	20	19.36	0.1020	79	0.04	0.00	43944	364.73
19.88	40	38.14	0.0181	97.77	0.08	0.00	44824	210.59

Project: PF2	Location: Ames	Project No.:
Boring No.:	Tested By: JL	Checked By:
Sample No.: 2	Test Date: 20120821	Depth:
Test No.:	Sample Type: Coarse	Elevation:
Description: Martin Marietta Crushed Limestone subbase 80% RD 112.73pcf 2.32% w 7.9% fines		
Remarks: Vibrating compaction		
File: U:\Desktop\research\data\A New test plan\MR& UU tests\MR tests\dat files\Crushed Limestone_Martin Marietta_80%		

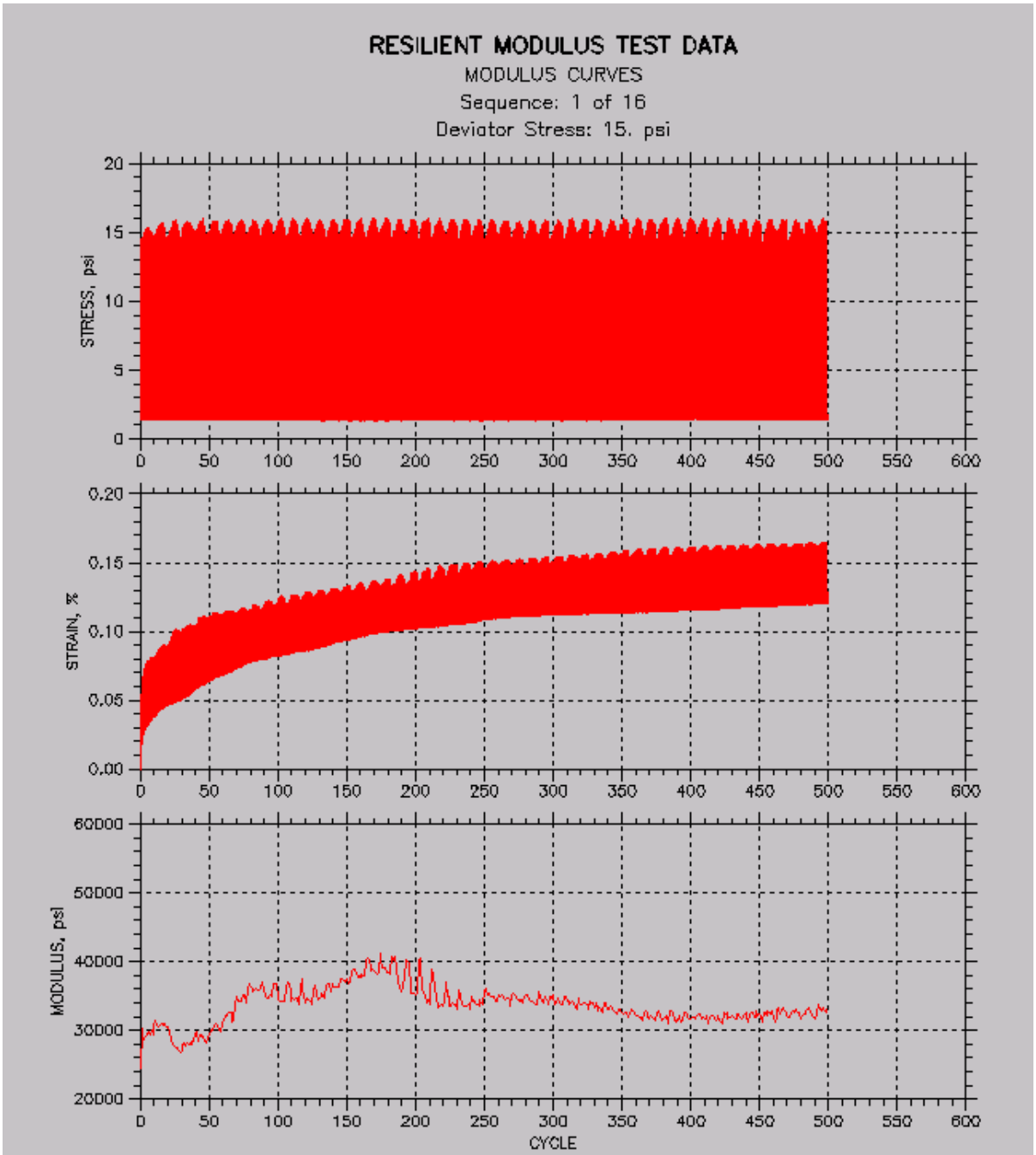

Project: PF2	Location: Ames	Project No.:
Boring No.:	Tested By: JL	Checked By:
Sample No.: 2	Test Date: 20120821	Depth:
Test No.:	Sample Type: Coarse	Elevation:
Description: Martin Marietta Crushed Limestone subbase 90% RD 112.73pcf 2.32% w 7.9% fines		
Remarks: Viracating compaction		
File: U:\Desktop\research\data\A New test plan\MR& UU tests\MR tests\dat files\Crushed Limestone_Martin Marietta_90%		

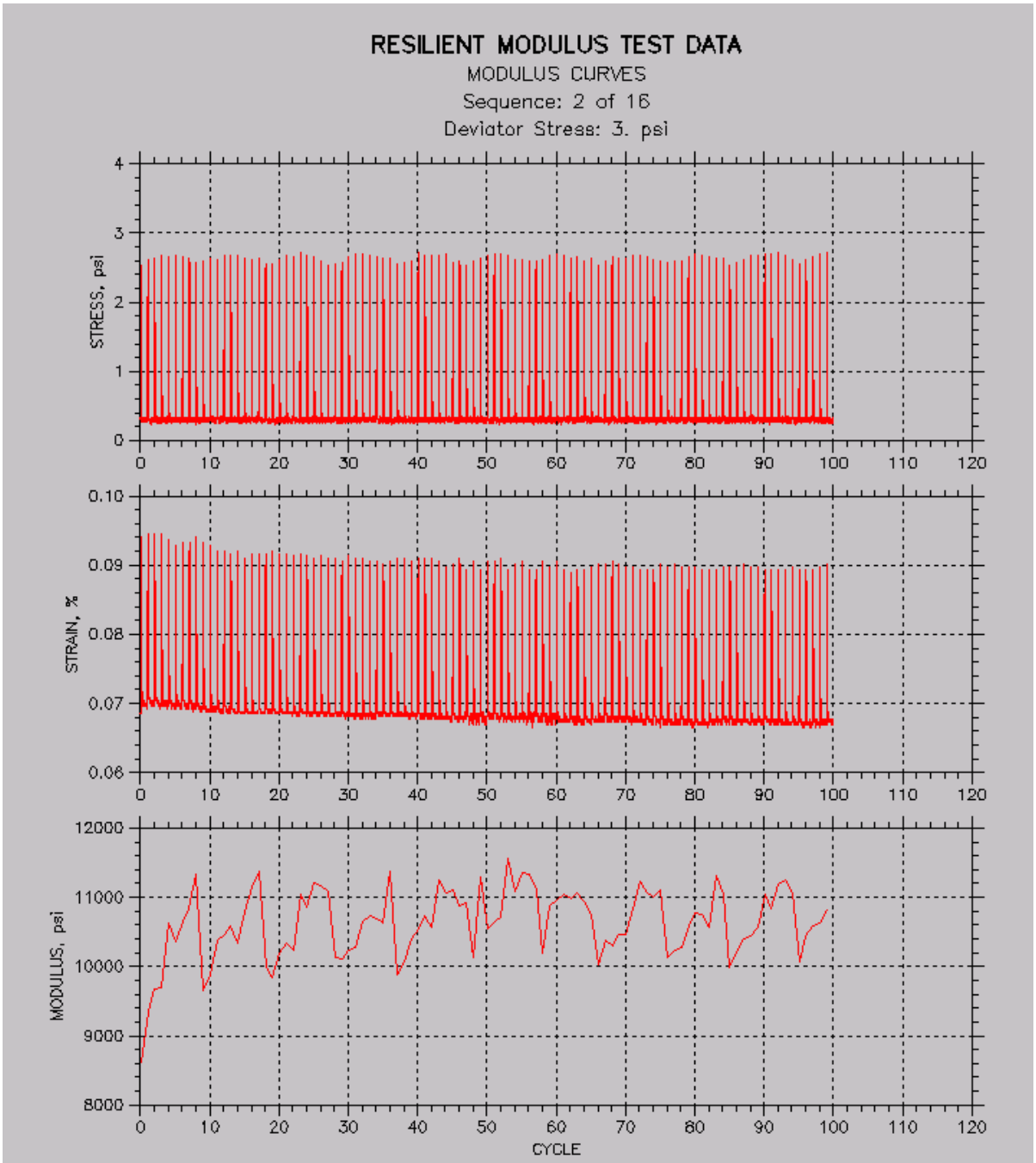

Project: PF2	Location: Ames	Project No.:
Boring No.:	Tested By: JL	Checked By:
Sample No.: 2	Test Date: 20120821	Depth:
Test No.:	Sample Type: Coarse	Elevation:
Description: Martin Marietta Crushed Limestone subbase 90% RD 112.73pcf 2.32% w 7.9% fines		
Remarks: Viracating compaction		
File: U:\Desktop\research\data\A New test plan\MR& UU tests\MR tests\dat files\Crushed Limestone_Martin Marietta_90%		

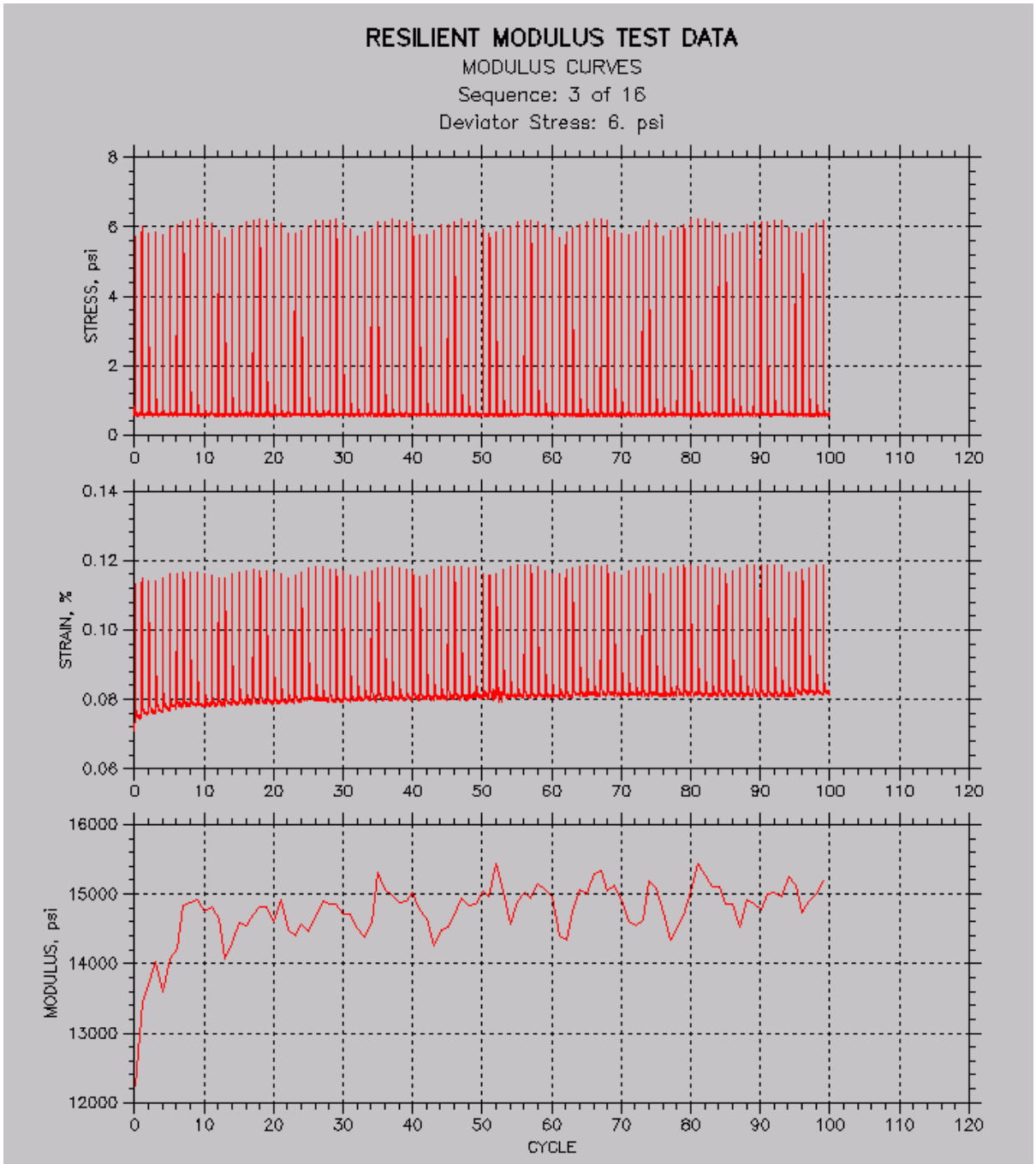

Project: PF2	Location: Ames	Project No.:
Boring No.:	Tested By: JL	Checked By:
Sample No.: 2	Test Date: 20120821	Depth:
Test No.:	Sample Type: Coarse	Elevation:
Description: Martin Marietta Crushed Limestone subbase 90% RD 112.73pcf 2.32% w 7.9% fines		
Remarks: Viracating compaction		
File: U:\Desktop\research\data\A New test plan\MR& UU tests\MR tests\dat files\Crushed Limestone_Martin Marietta_90%		

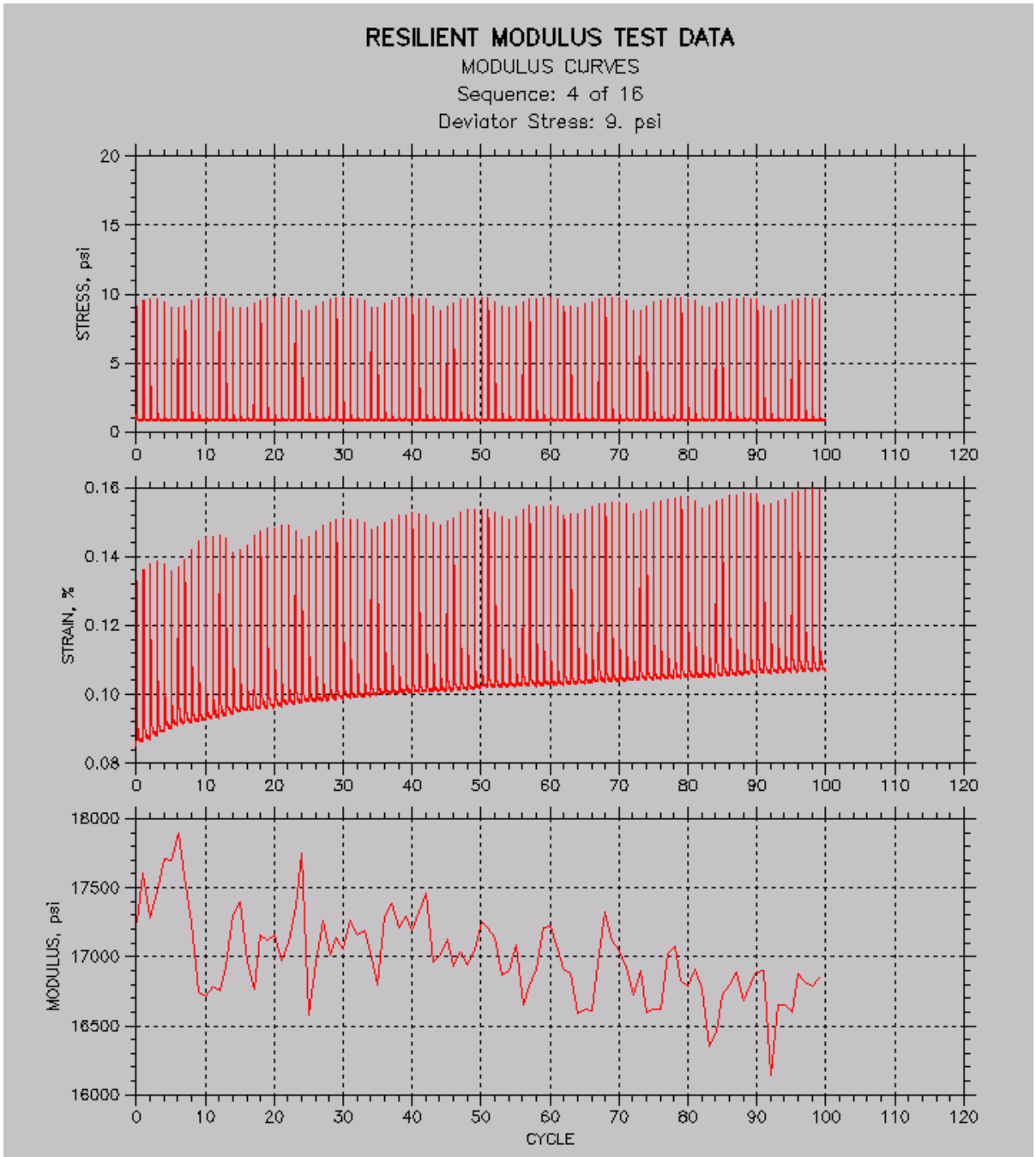

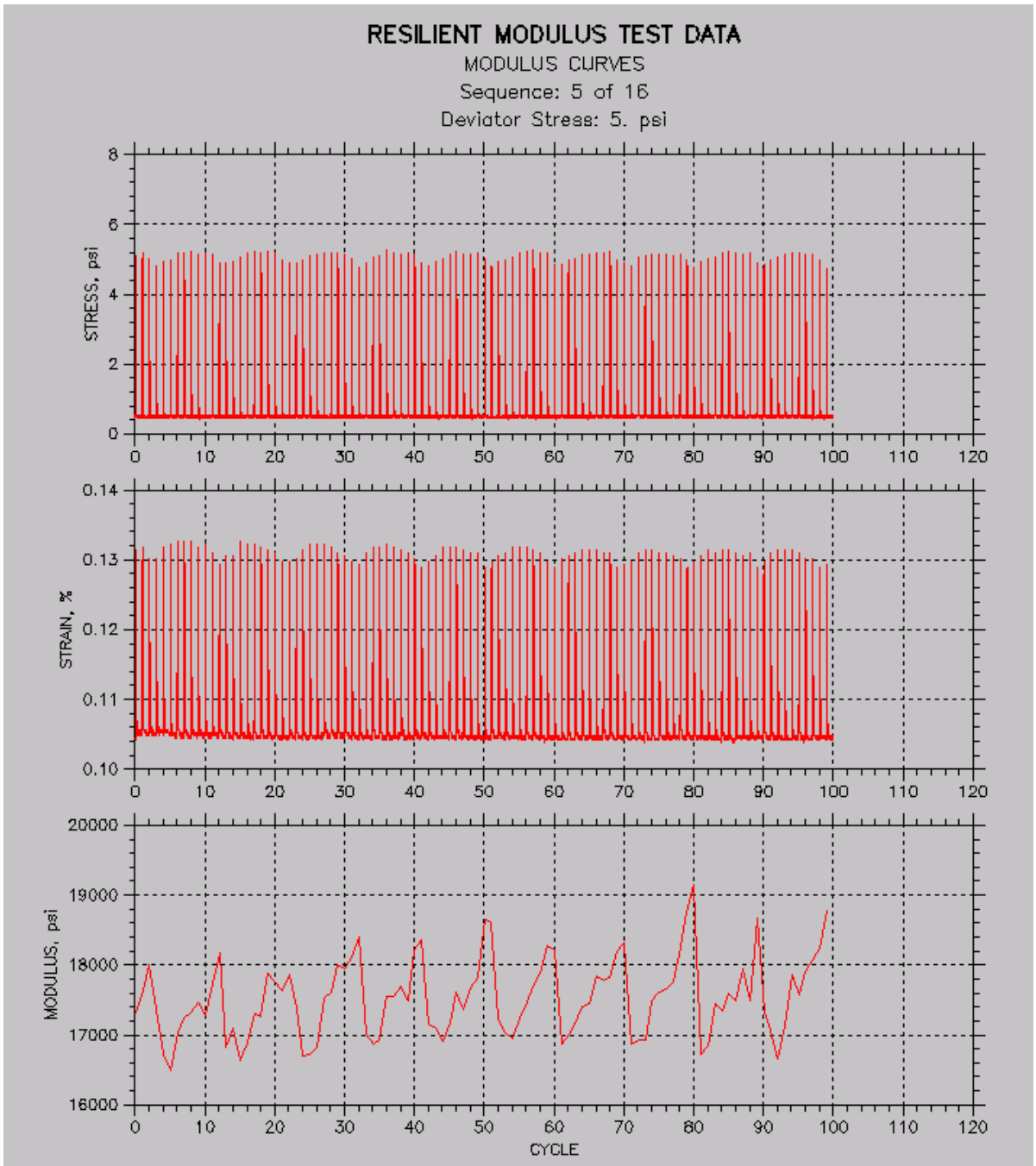

Project: PF2	Location: Ames	Project No.:
Boring No.:	Tested By: JL	Checked By:
Sample No.: 2	Test Date: 20120821	Depth:
Test No.:	Sample Type: Coarse	Elevation:
Description: Martin Marietta Crushed Limestone subbase 90% RD 112.73pcf 2.32% w 7.9% fines		
Remarks: Viracating compaction		
File: U:\Desktop\research\data\A New test plan\MR& UU tests\MR tests\dat files\Crushed Limestone_Martin Marietta_90%		

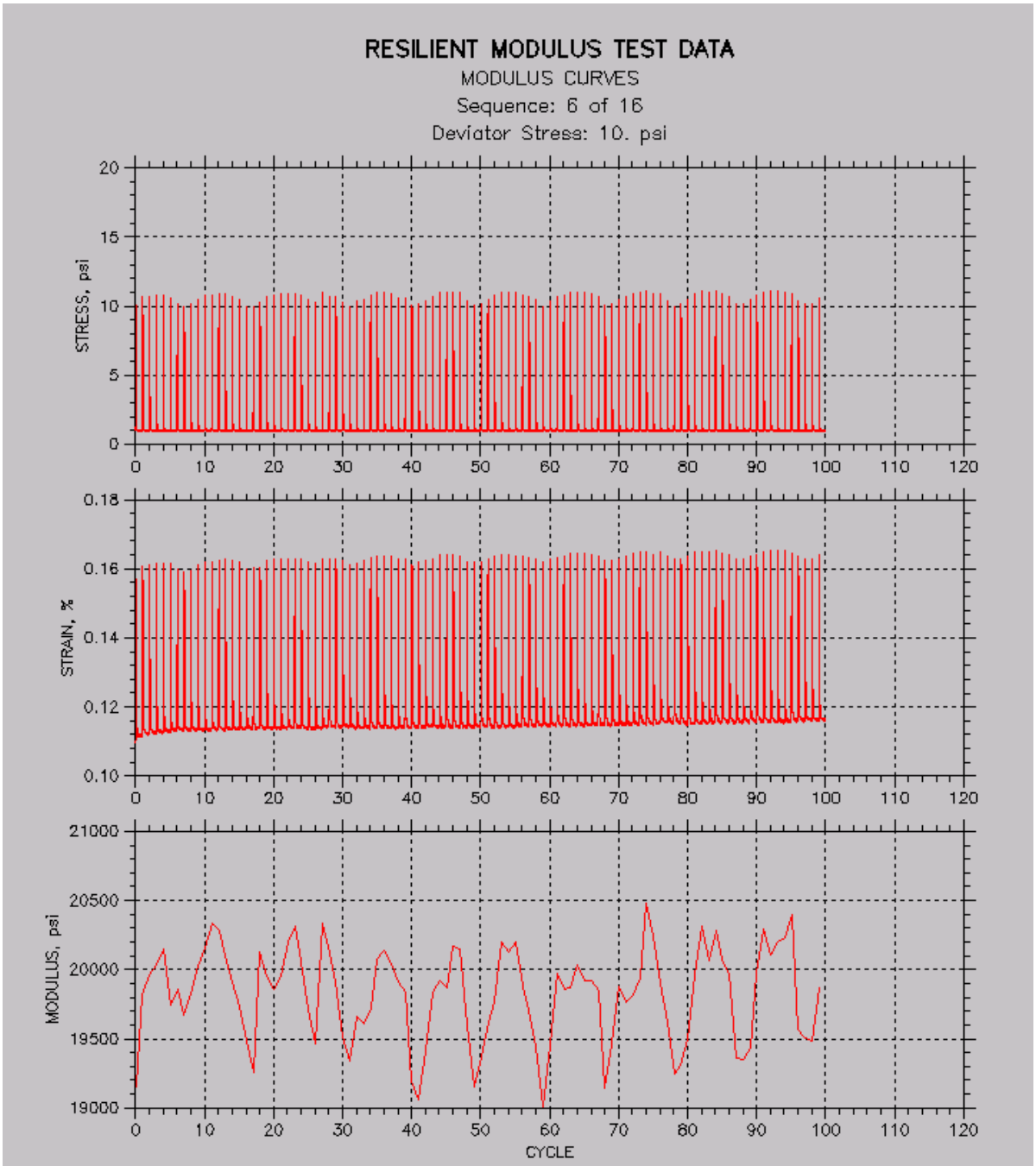

Project: PF2	Location: Ames	Project No.:
Boring No.:	Tested By: JL	Checked By:
Sample No.: 2	Test Date: 20120821	Depth:
Test No.:	Sample Type: Coarse	Elevation:
Description: Martin Marietta Crushed Limestone subbase 90% RD 112.73pcf 2.32% w 7.9% fines		
Remarks: Viracating compaction		
File: U:\Desktop\research\data\A New test plan\MR& UU tests\MR tests\dat files\Crushed Limestone_Martin Marietta_90%F		

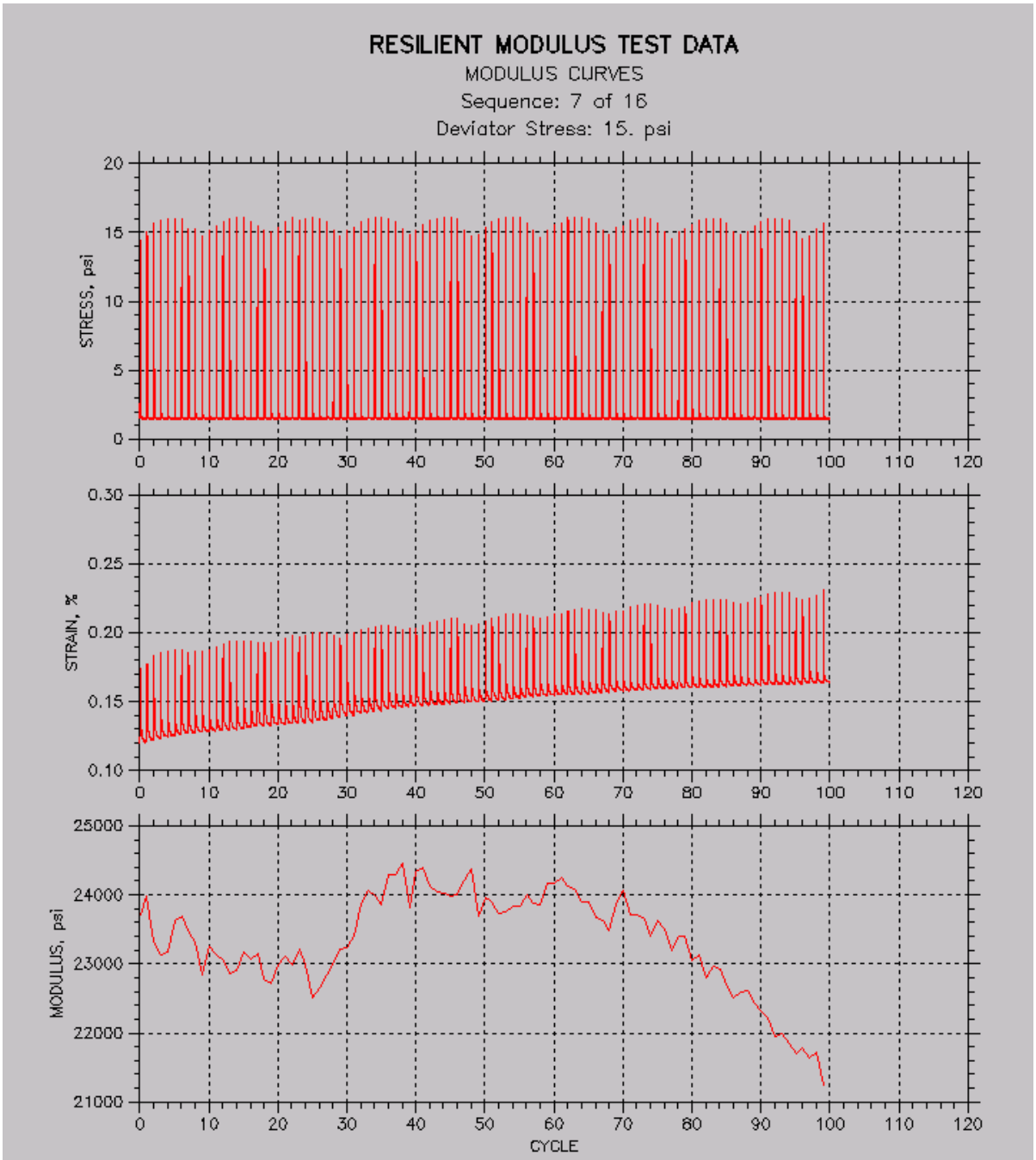

Project: PF2	Location: Ames	Project No.:
Boring No.:	Tested By: JL	Checked By:
Sample No.: 2	Test Date: 20120821	Depth:
Test No.:	Sample Type: Coarse	Elevation:
Description: Martin Marietta Crushed Limestone subbase 90% RD 112.73pcf 2.32% w 7.9% fines		
Remarks: Viracating compaction		
File: U:\Desktop\research\data\A New test plan\MR& UU tests\MR tests\dat files\Crushed Limestone_Martin Marietta_90%		

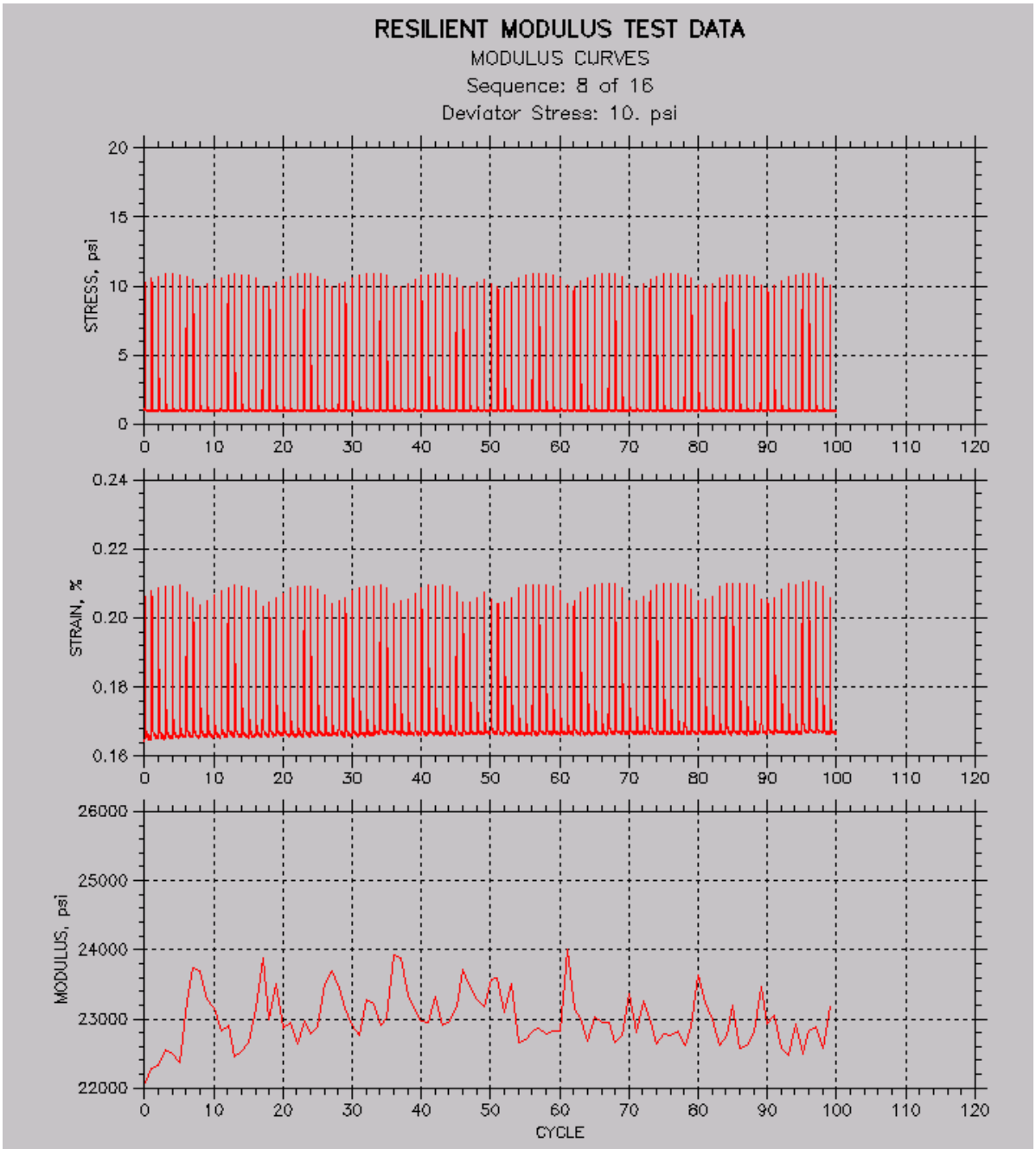

Project: PF2	Location: Ames	Project No.:
Boring No.:	Tested By: JL	Checked By:
Sample No.: 2	Test Date: 20120821	Depth:
Test No.:	Sample Type: Coarse	Elevation:
Description: Martin Marietta Crushed Limestone subbase 90% RD 112.73pcf 2.32% w 7.9% fines		
Remarks: Viracating compaction		
File: U:\Desktop\research\data\A New test plan\MR& UU tests\MR tests\dat files\Crushed Limestone_Martin Marietta_90		

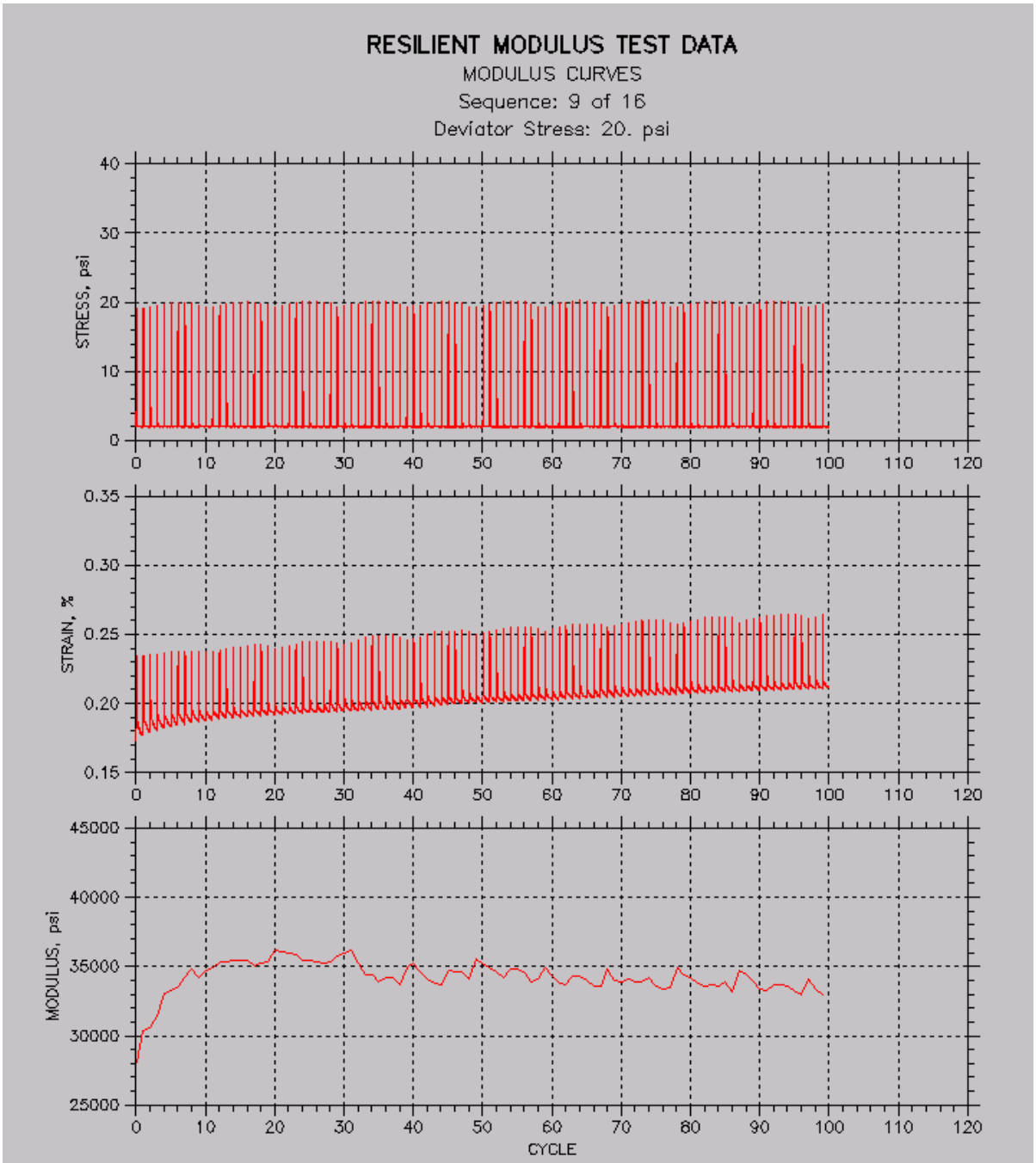

Project: PF2	Location: Ames	Project No.:
Boring No.:	Tested By: JL	Checked By:
Sample No.: 2	Test Date: 20120821	Depth:
Test No.:	Sample Type: Coarse	Elevation:
Description: Martin Marietta Crushed Limestone subbase 90% RD 112.73pcf 2.32% w 7.9% fines		
Remarks: Viracating compaction		
File: U:\Desktop\research\data\A New test plan\MR& UU tests\MR tests\dat files\Crushed Limestone_Martin Marietta_90%		

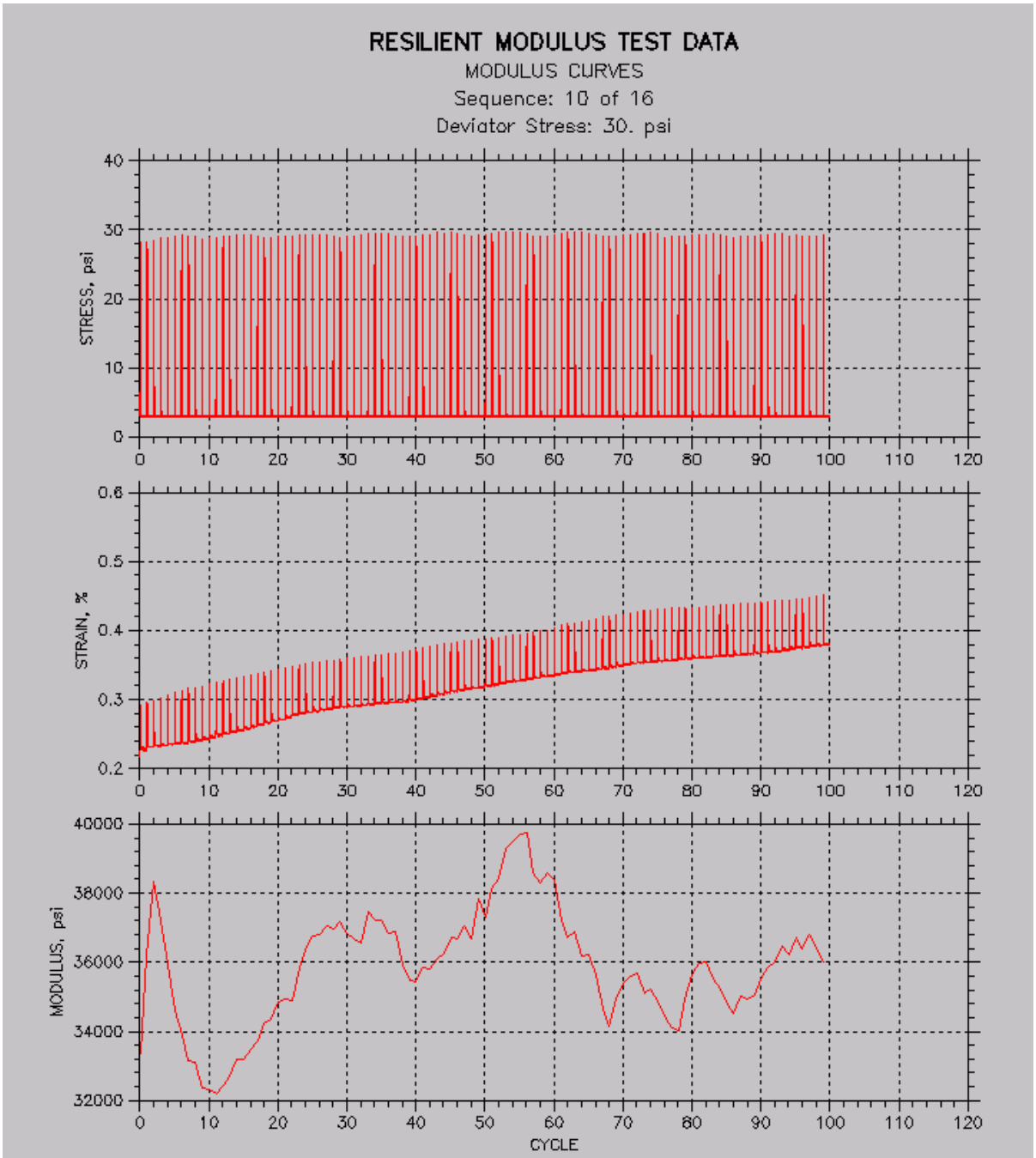

Project: PF2	Location: Ames	Project No.:
Boring No.:	Tested By: JL	Checked By:
Sample No.: 2	Test Date: 20120821	Depth:
Test No.:	Sample Type: Coarse	Elevation:
Description: Martin Marietta Crushed Limestone subbase 90% RD 112.73pcf 2.32% w 7.9% fines		
Remarks: Viracating compaction		
File: U:\Desktop\research\data\A New test plan\MR& UU tests\MR tests\dat files\Crushed Limestone_Martin Marietta_90%		

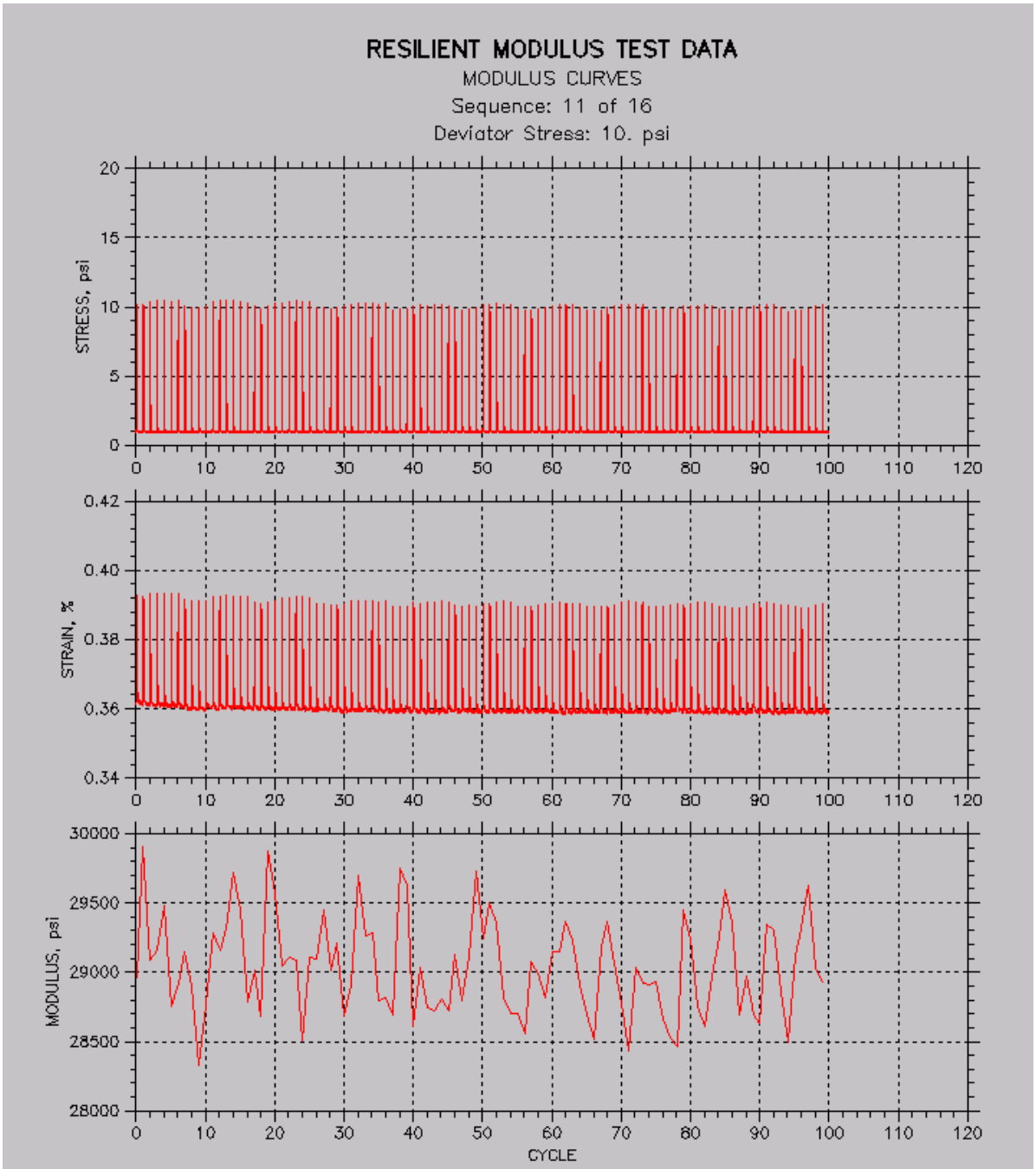

Project: PF2	Location: Ames	Project No.:
Boring No.:	Tested By: JL	Checked By:
Sample No.: 2	Test Date: 20120821	Depth:
Test No.:	Sample Type: Coarse	Elevation:
Description: Martin Marietta Crushed Limestone subbase 90% RD 112.73pcf 2.32% w 7.9% fines		
Remarks: Viracating compaction		
File: U:\Desktop\research\data\A New test plan\MR& UU tests\MR tests\dat files\Crushed Limestone_Martin Marietta_90%		

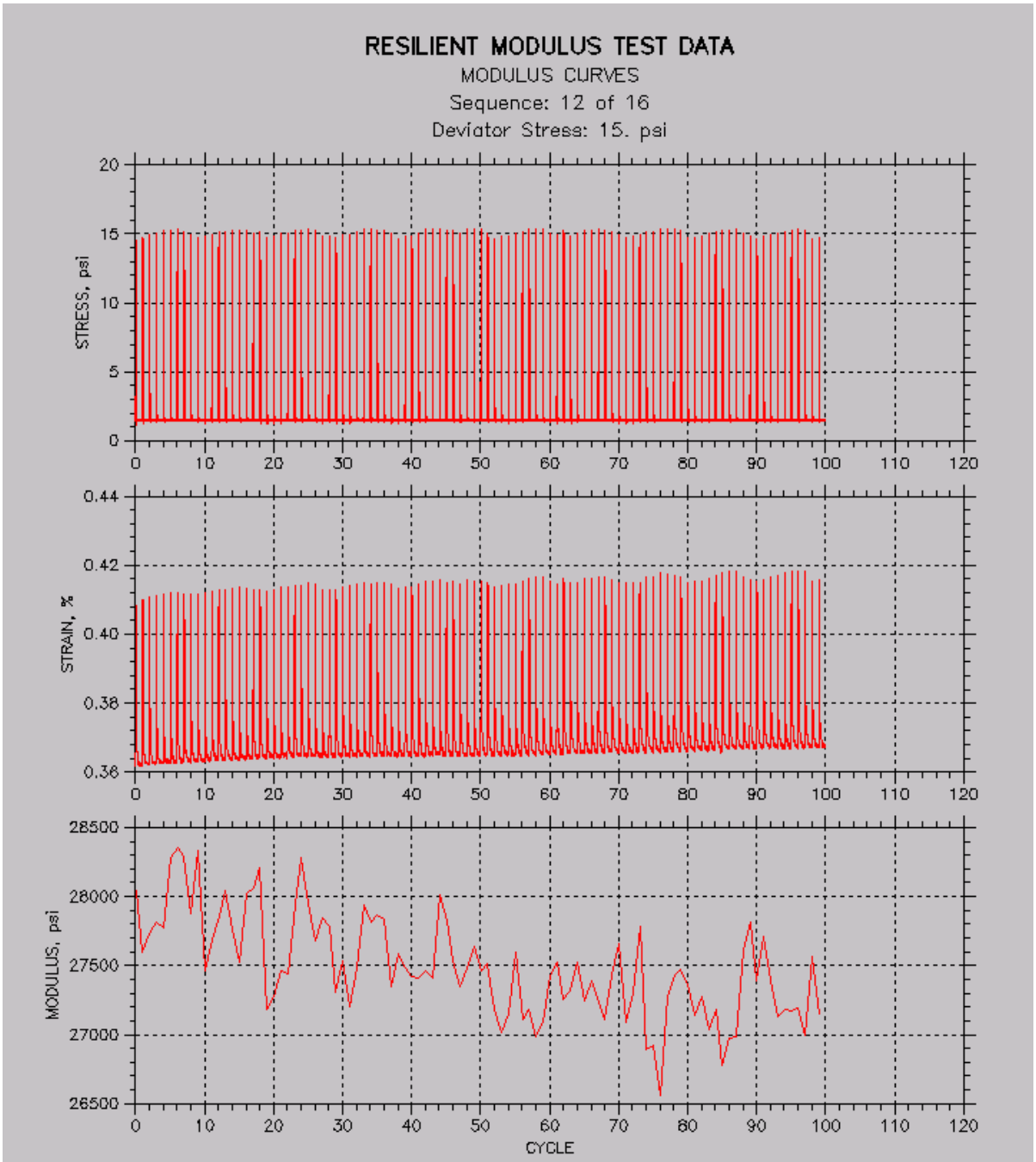

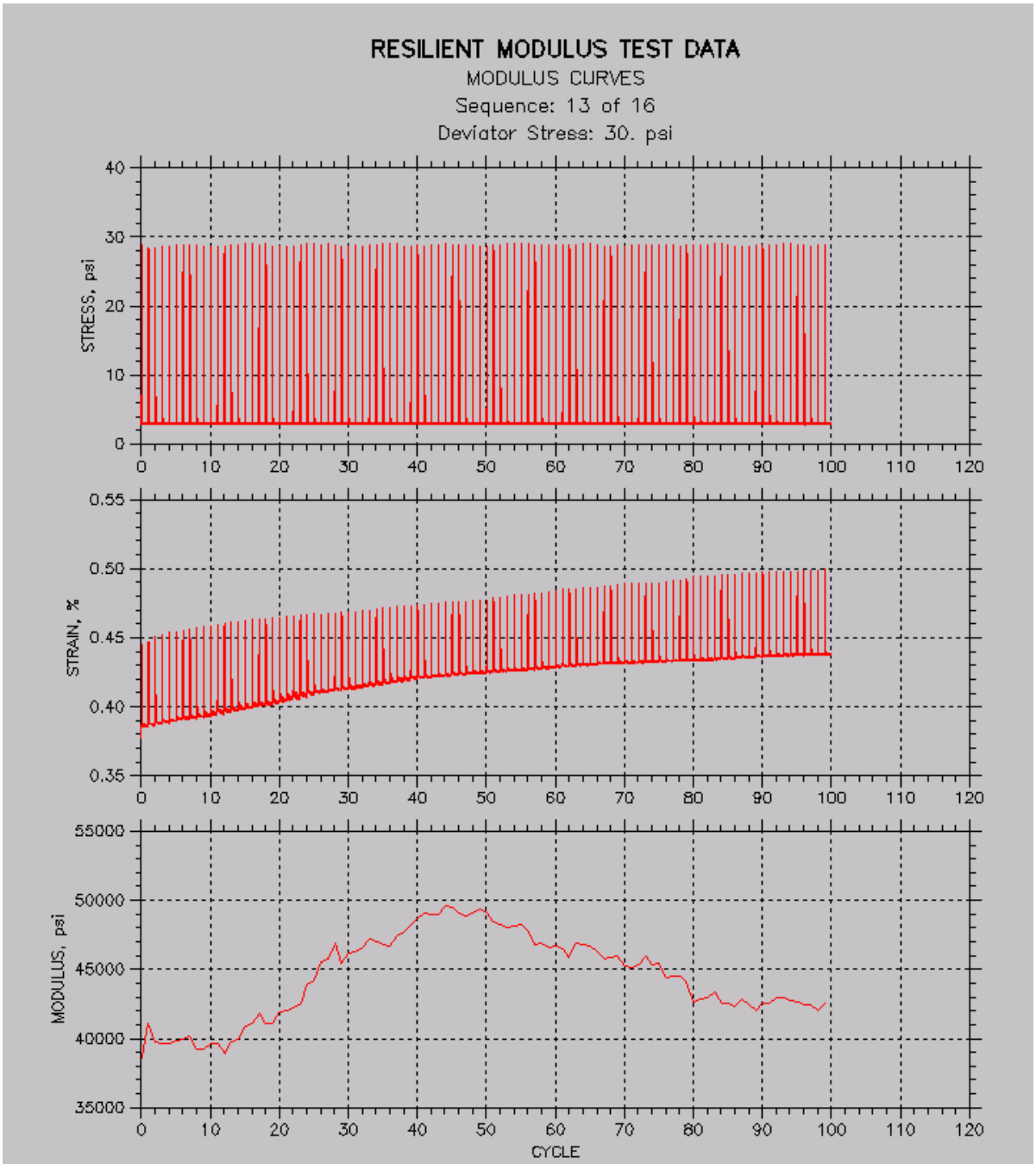

Project: PF2	Location: Ames	Project No.:
Boring No.:	Tested By: JL	Checked By:
Sample No.: 2	Test Date: 20120821	Depth:
Test No.:	Sample Type: Coarse	Elevation:
Description: Martin Marietta Crushed Limestone subbase 90% RD 112.73pcf 2.32% w 7.9% fines		
Remarks: Viracating compaction		
File: U:\Desktop\research\data\A New test plan\MR& UU tests\MR tests\dat files\Crushed Limestone_Martin Marietta_90%		

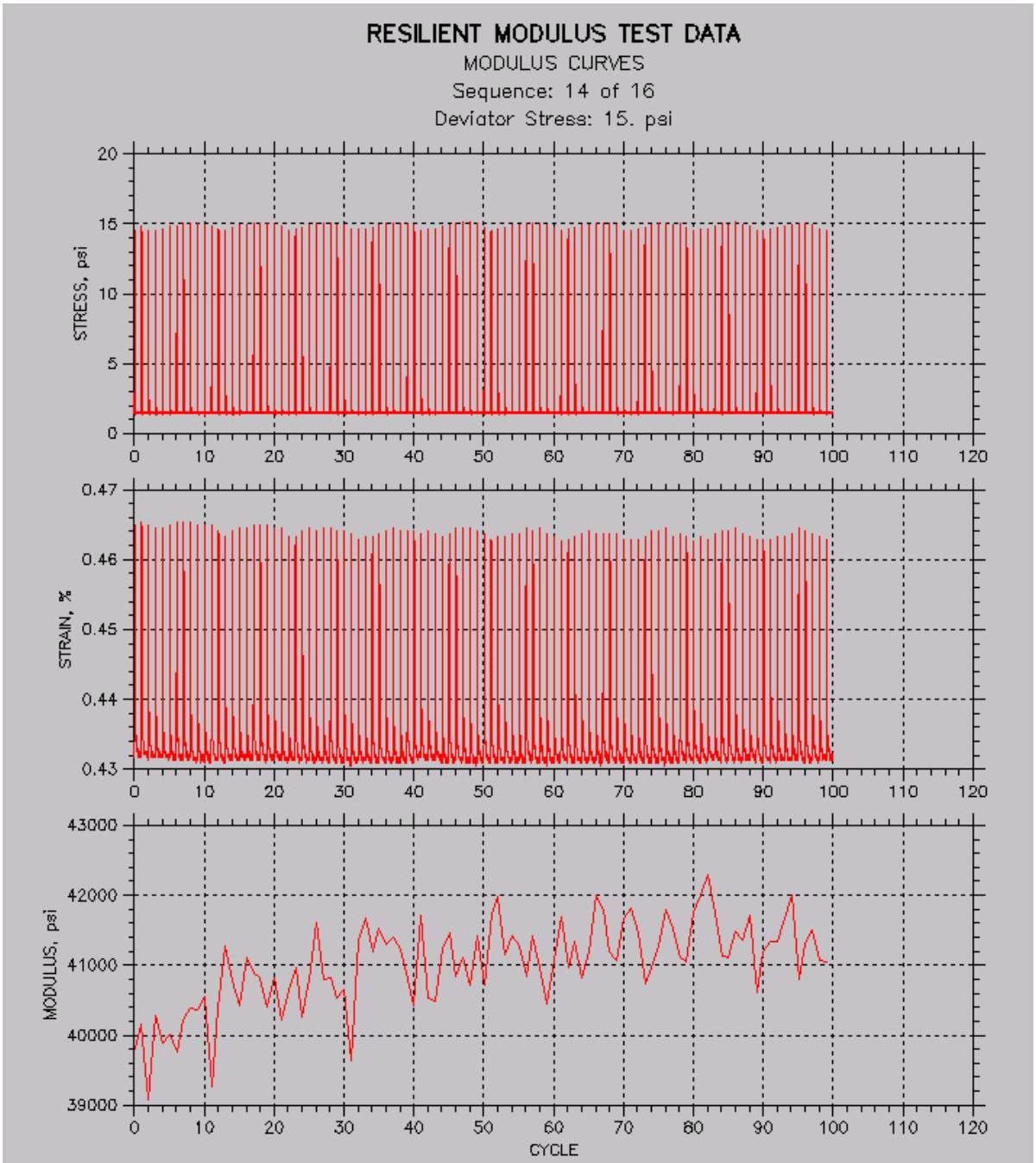

Project: PF2	Location: Ames	Project No.:
Boring No.:	Tested By: JL	Checked By:
Sample No.: 2	Test Date: 20120821	Depth:
Test No.:	Sample Type: Coarse	Elevation:
Description: Martin Marietta Crushed Limestone subbase 90% RD 112.73pcf 2.32% w 7.9% fines		
Remarks: Viracating compaction		
File: U:\Desktop\research\data\A New test plan\MR& UU tests\MR tests\dat files\Crushed Limestone_Martin Marietta_90%		

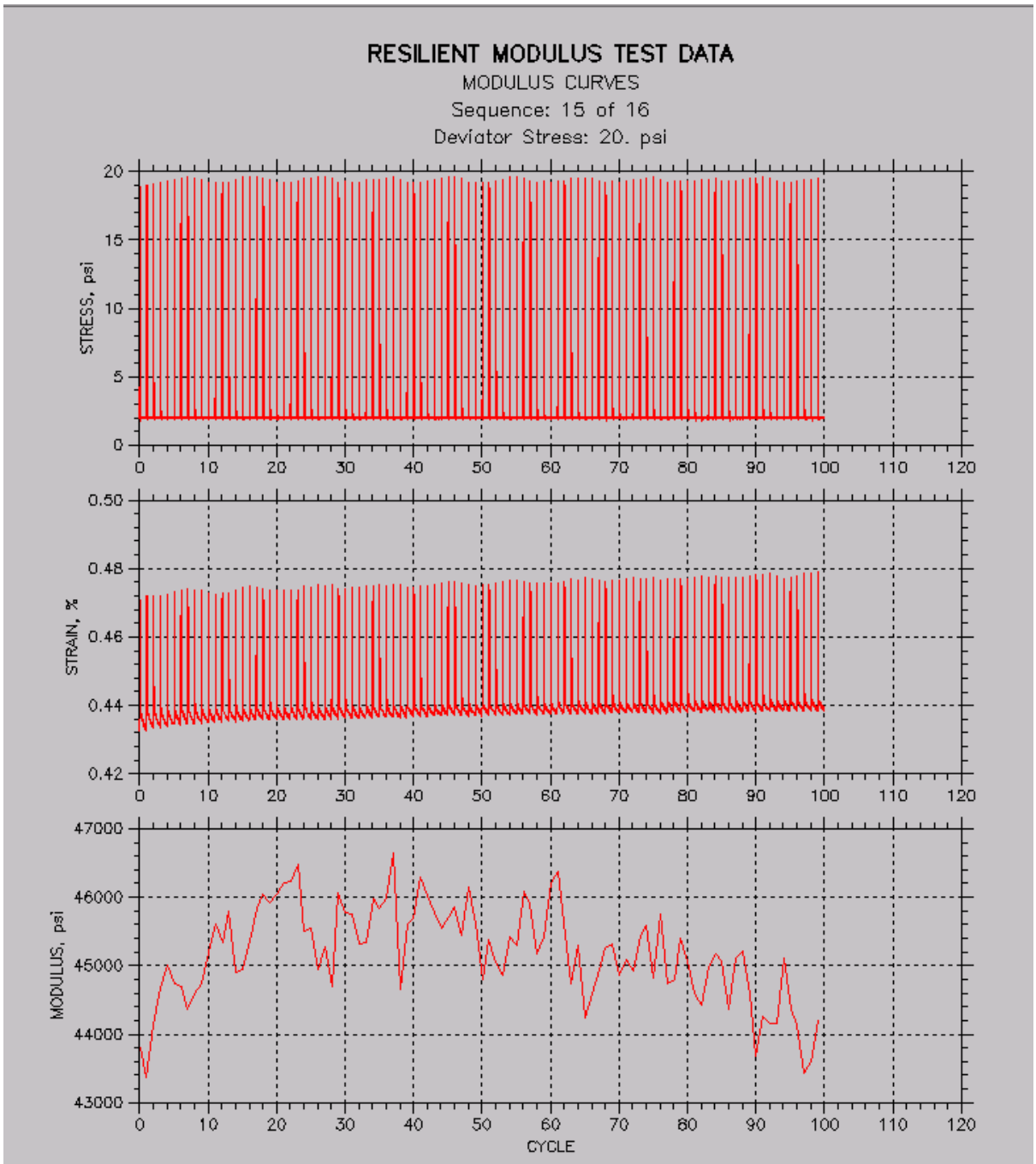

Project: PF2	Location: Ames	Project No.:
Boring No.:	Tested By: JL	Checked By:
Sample No.: 2	Test Date: 20120821	Depth:
Test No.:	Sample Type: Coarse	Elevation:
Description: Martin Marietta Crushed Limestone subbase 90% RD 112.73pcf 2.32% w 7.9% fines		
Remarks: Viracating compaction		
File: U:\Desktop\research\data\A New test plan\MR& UU tests\MR tests\dat files\Crushed Limestone_Martin Marietta_90%R		

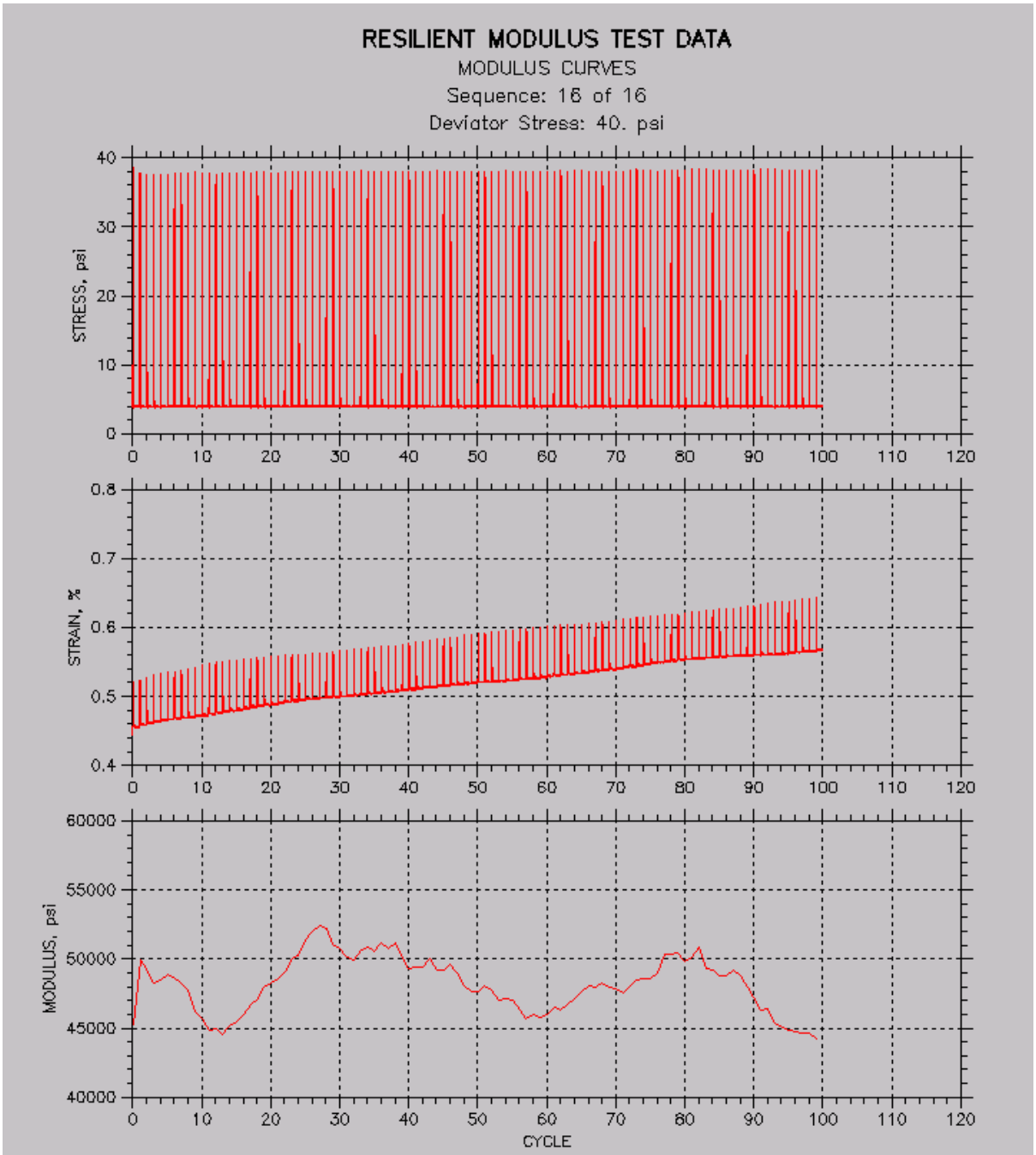

Project: PF2	Location: Ames	Project No.:
Boring No.:	Tested By: JL	Checked By:
Sample No.: 2	Test Date: 20120821	Depth:
Test No.:	Sample Type: Coarse	Elevation:
Description: Martin Marietta Crushed Limestone subbase 90% RD 112.73pcf 2.32% w 7.9% fines		
Remarks: Viracating compaction		
File: U:\Desktop\research\data\A New test plan\MR& UU tests\MR tests\dat files\Crushed Limestone_Martin Marietta_90%R		

RAP

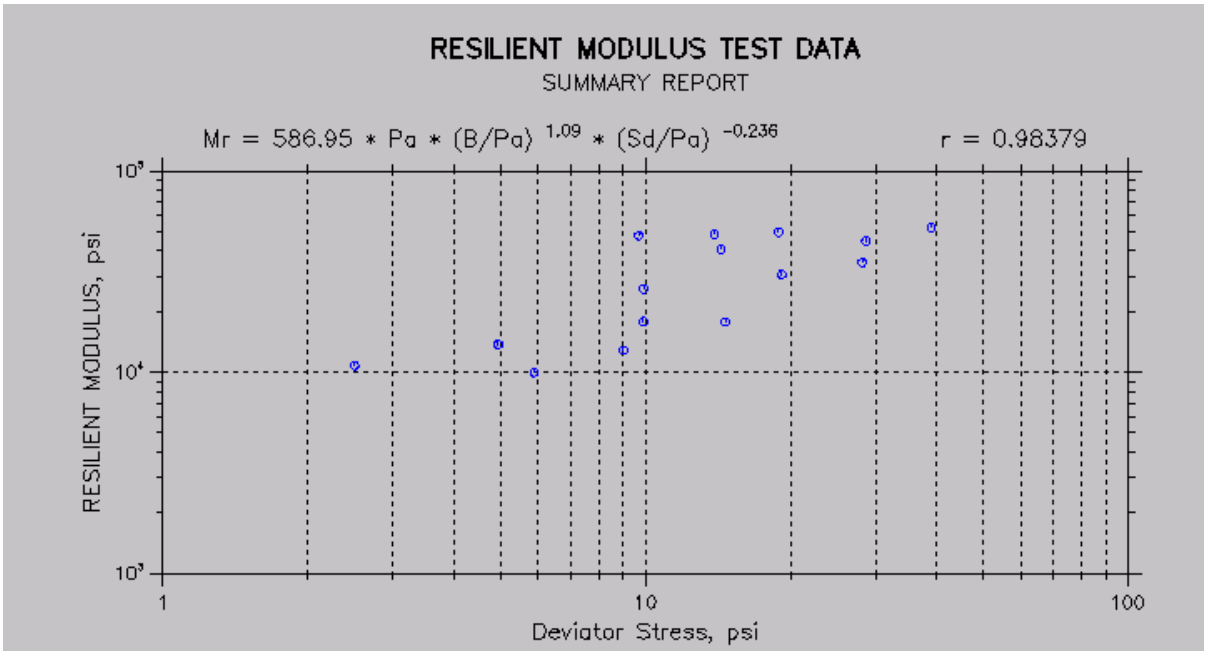

Confining Stress S3 (psi)	Nom. Max. Deviator Stress (psi)	Mean Deviator Stress (psi)	Std. Dev. Deviator Stress (psi)	Mean Bulk Stress (psi)	Mean Resilient Strain (%)	Std. Dev. Resilient Strain (%)	Mean Resilient Modulus (psi)	Std. Dev. Resilient Modulus (psi)
3.006	3	2.496	0.0444	11.52	0.02	0.00	10759	355.34
2.974	6	5.881	0.1257	14.8	0.05	0.00	9950.4	147
2.987	9	9.002	0.0661	17.96	0.06	0.00	12826	153.57
5.01	5	4.952	0.0441	19.98	0.03	0.00	13693	151.32
5.042	10	9.911	0.1833	25.04	0.05	0.00	17798	368.61
5.006	15	14.66	0.4125	29.68	0.07	0.00	17766	418.72
9.987	10	9.913	0.0465	39.87	0.03	0.00	25904	493.89
10.01	20	19.17	0.0253	49.19	0.06	0.00	30512	437.06
10	30	28.17	0.0337	58.17	0.07	0.00	35068	839.56
15	10	9.691	0.0584	54.69	0.02	0.00	47681	2221.3
15.03	15	13.9	0.0421	59	0.03	0.00	48448	1929.6
15.03	30	28.67	0.0219	73.74	0.06	0.00	44752	907.26
19.86	15	14.36	0.1401	73.95	0.03	0.00	40837	1942.1
19.87	20	18.88	0.0547	78.51	0.03	0.00	49679	1435.2
19.9	40	39.16	0.0439	98.86	0.07	0.00	52263	2451.3

Project: PF2	Location: IA	Project No.:
Boring No.:	Tested By: JL	Checked By:
Sample No.: 2	Test Date: 20120902	Depth:
Test No.:	Sample Type: Coarse	Elevation:
Description: Manatt's RAP 90%RD Mr test 95.78pcf 2.86% w 2.97% fines		
Remarks: Viracating compaction		
File: U:\Desktop\research\data\A New test plan\MR& UU tests\MR tests\dat files\RAP_Manatt's_90%RD_95.78pcf_2.86%w		

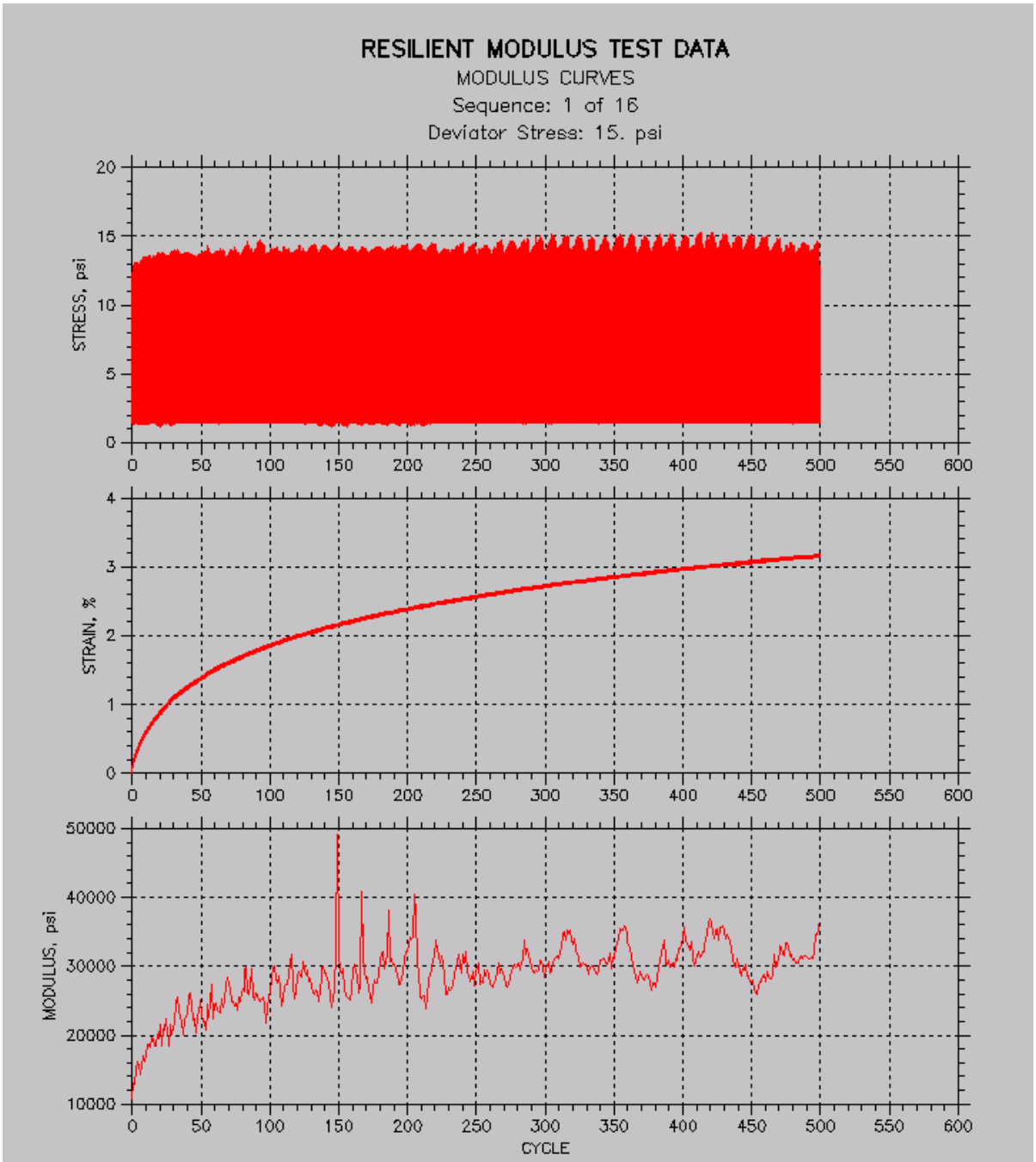

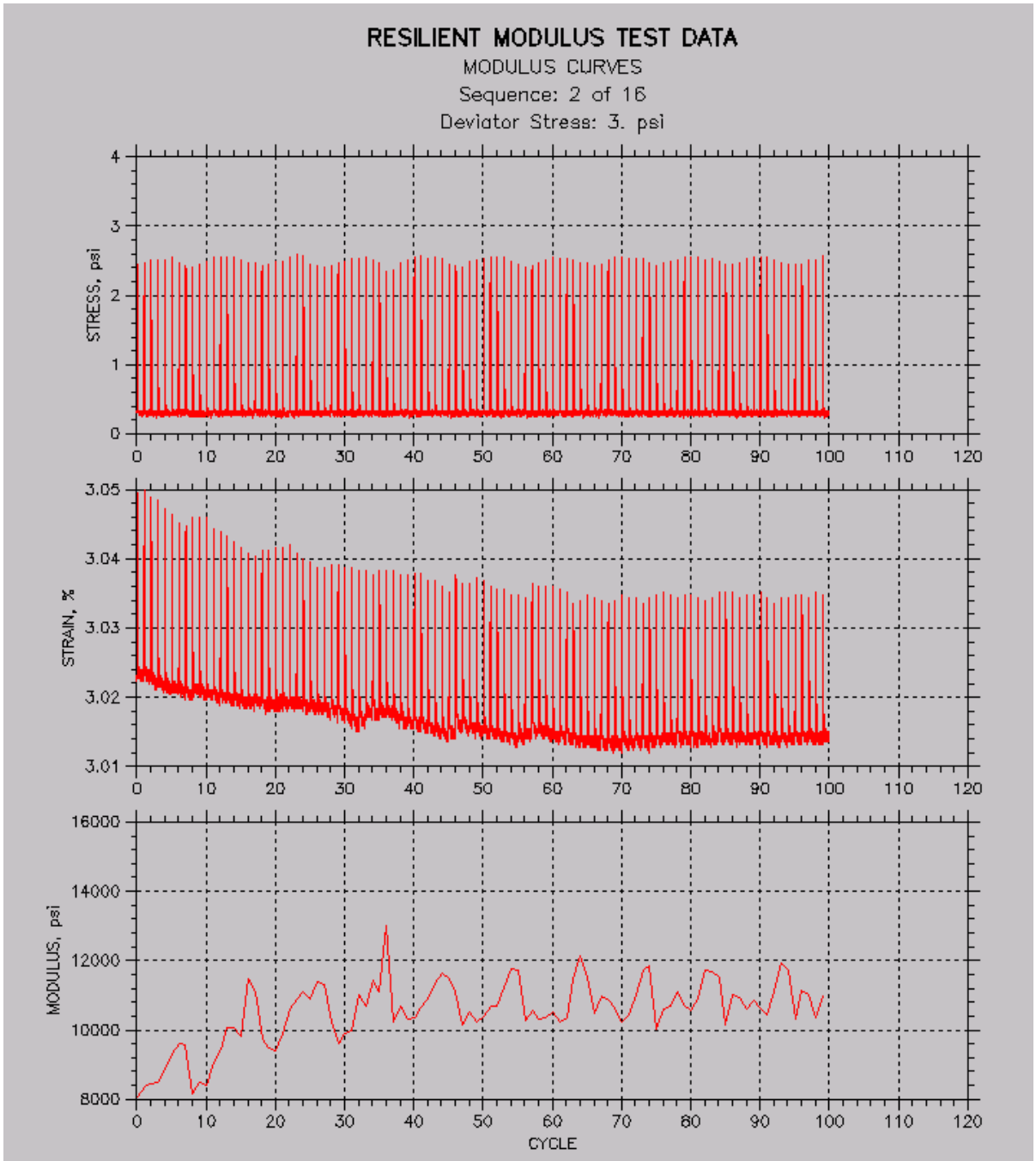

Project: PF2	Location: IA	Project No.:
Boring No.:	Tested By: JL	Checked By:
Sample No.: 2	Test Date: 20120902	Depth:
Test No.:	Sample Type: Coarse	Elevation:
Description: Manatt's RAP 90%RD Mr test 95.78pcf 2.86% w 2.97% fines		
Remarks: Viracating compaction		
File: U:\Desktop\research\data\A New test plan\MR& UU tests\MR tests\dat files\RAP_Manatt's_90%RD_95.78pcf_2.86%w		

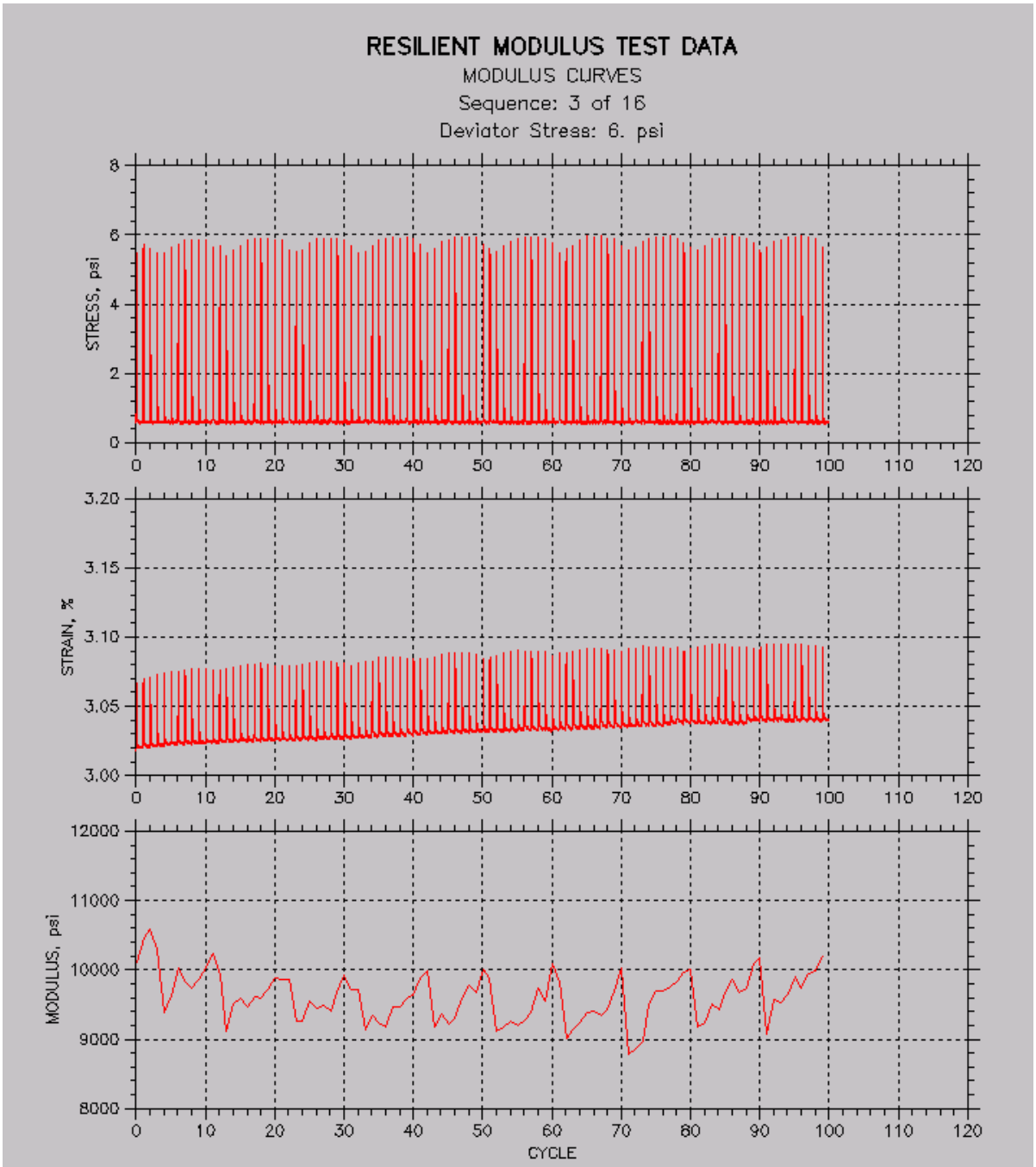

Project: PF2	Location: IA	Project No.:
Boring No.:	Tested By: JL	Checked By:
Sample No.: 2	Test Date: 20120902	Depth:
Test No.:	Sample Type: Coarse	Elevation:
Description: Manatt's RAP 90%RD Mr test 95.78pcf 2.86% w 2.97% fines		
Remarks: Viracating compaction		
File: U:\Desktop\research\data\A New test plan\MR& UU tests\MR tests\dat files\RAP_Manatt's_90%RD_95.78pcf_2.86%w		

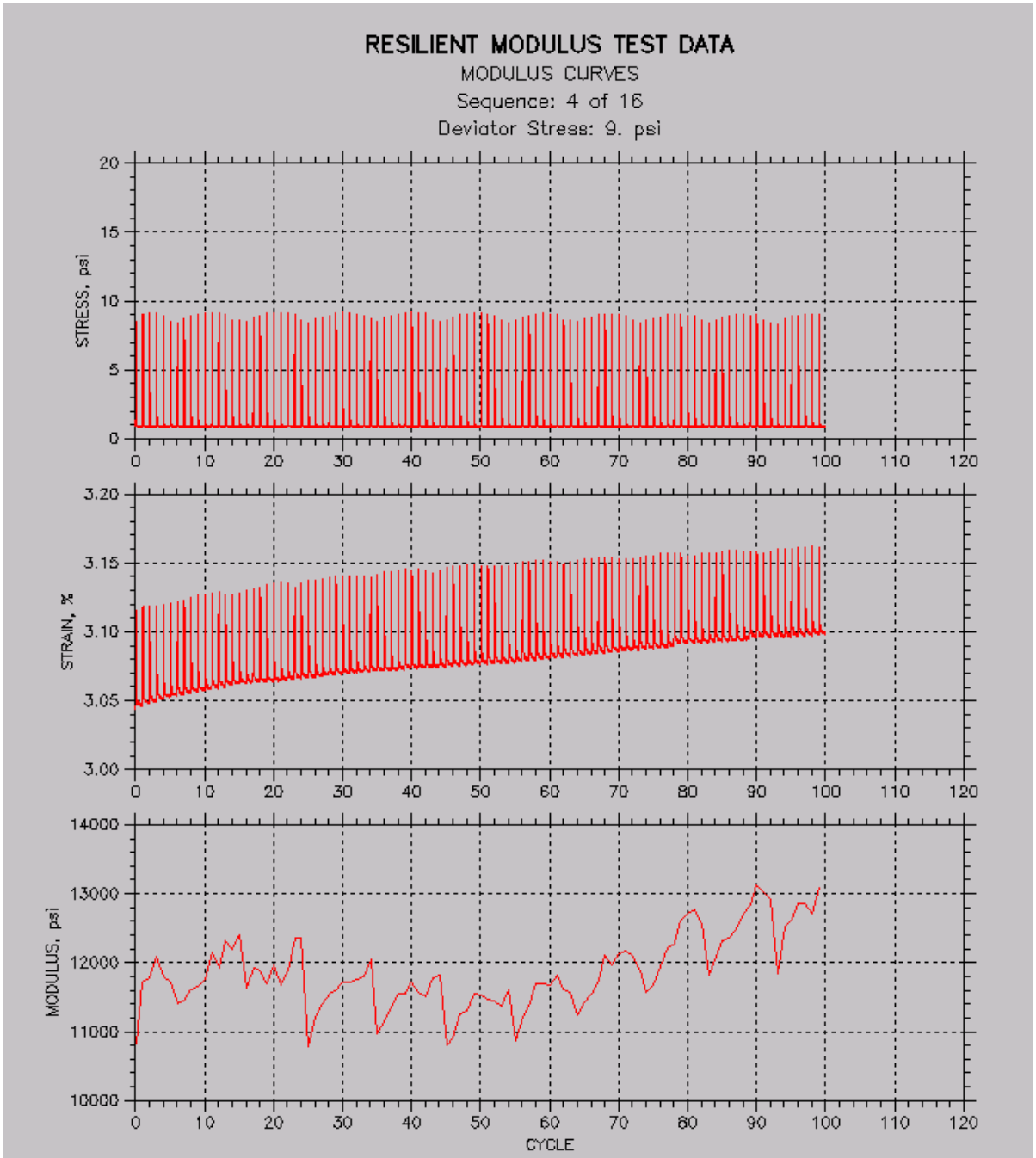

Project: PF2	Location: IA	Project No.:
Boring No.:	Tested By: JL	Checked By:
Sample No.: 2	Test Date: 20120902	Depth:
Test No.:	Sample Type: Coarse	Elevation:
Description: Manatt's RAP 90%RD Mr test 95.78pcf 2.86% w 2.97% fines		
Remarks: Viracating compaction		
File: U:\Desktop\research\data\A New test plan\MR& UU tests\MR tests\dat files\RAP_Manatt's_90%RD_95.78pcf_2.86%w		

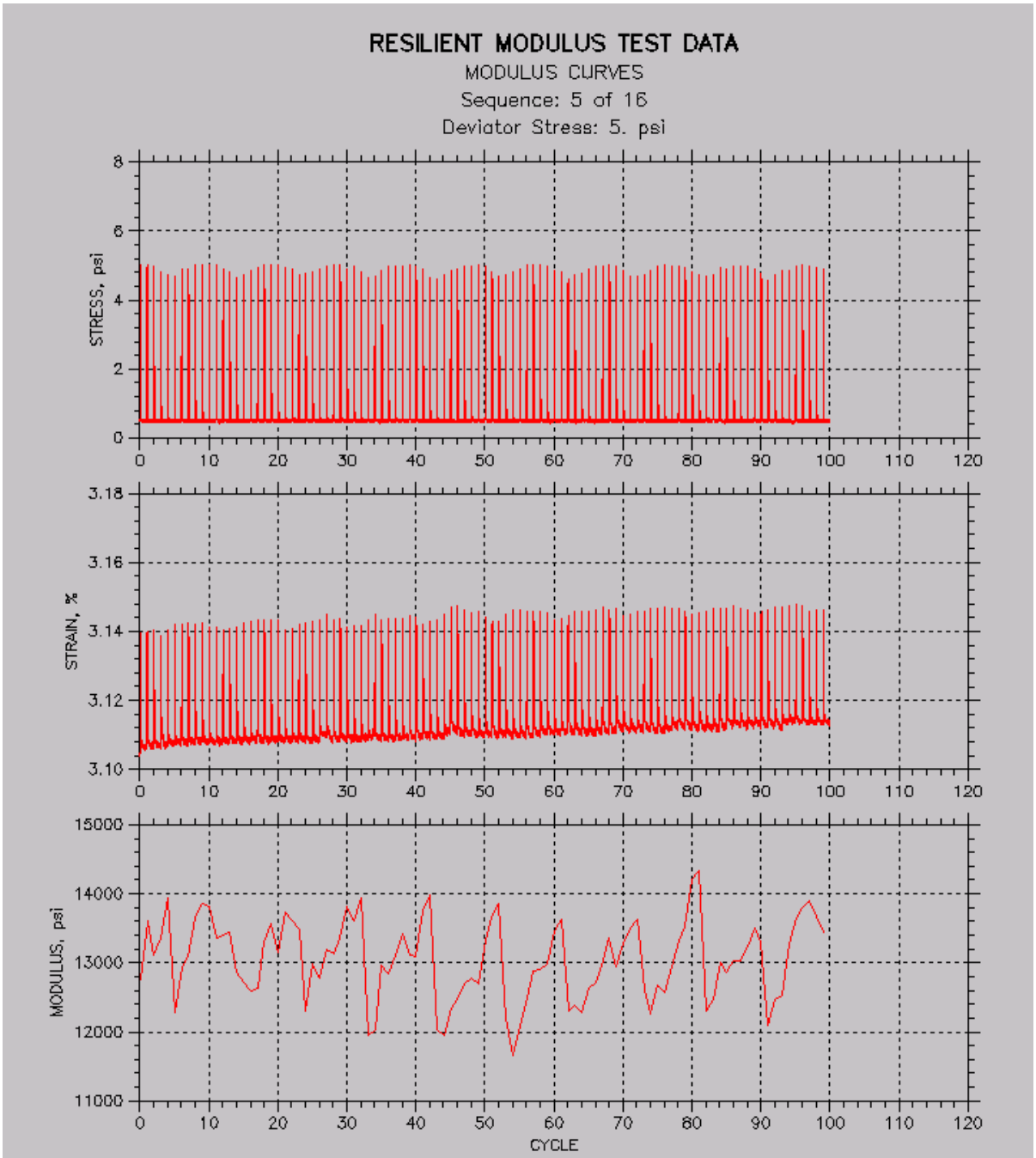

Project: PF2	Location: IA	Project No.:
Boring No.:	Tested By: JL	Checked By:
Sample No.: 2	Test Date: 20120902	Depth:
Test No.:	Sample Type: Coarse	Elevation:
Description: Manatt's RAP 90%RD Mr test 95.78pcf 2.86% w 2.97% fines		
Remarks: Viracating compaction		
File: U:\Desktop\research\data\A New test plan\MR& UU tests\MR tests\dat files\RAP_Manatt's_90%RD_95.78pcf_2.86%w		

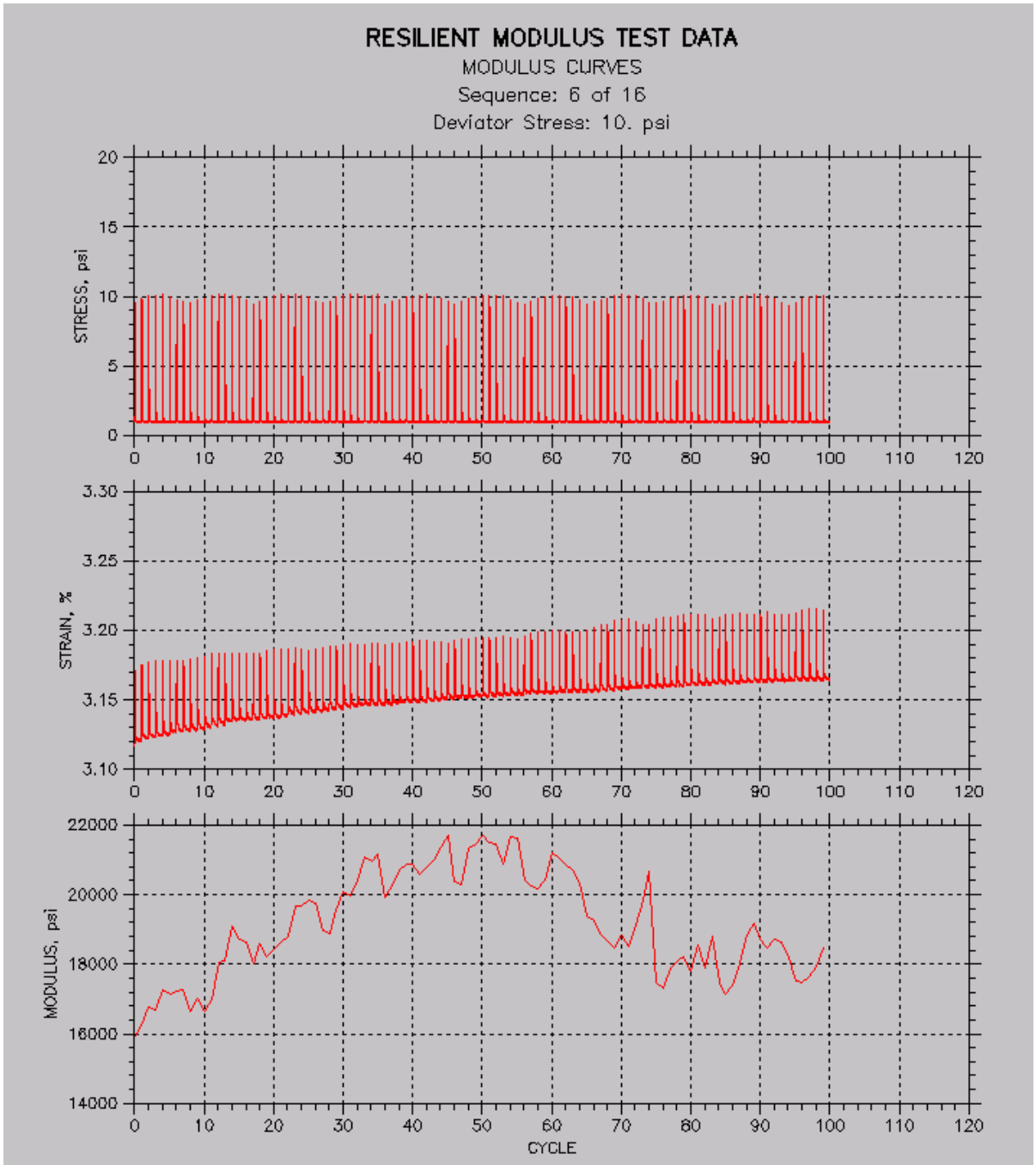

Project: PF2	Location: IA	Project No.:
Boring No.:	Tested By: JL	Checked By:
Sample No.: 2	Test Date: 20120902	Depth:
Test No.:	Sample Type: Coarse	Elevation:
Description: Manatt's RAP 90%RD Mr test 95.78pcf 2.86% w 2.97% fines		
Remarks: Viracating compaction		
File: U:\Desktop\research\data\A New test plan\MR& UU tests\MR tests\dat files\RAP_Manatt's_90%RD_95.78pcf_2.86%w		

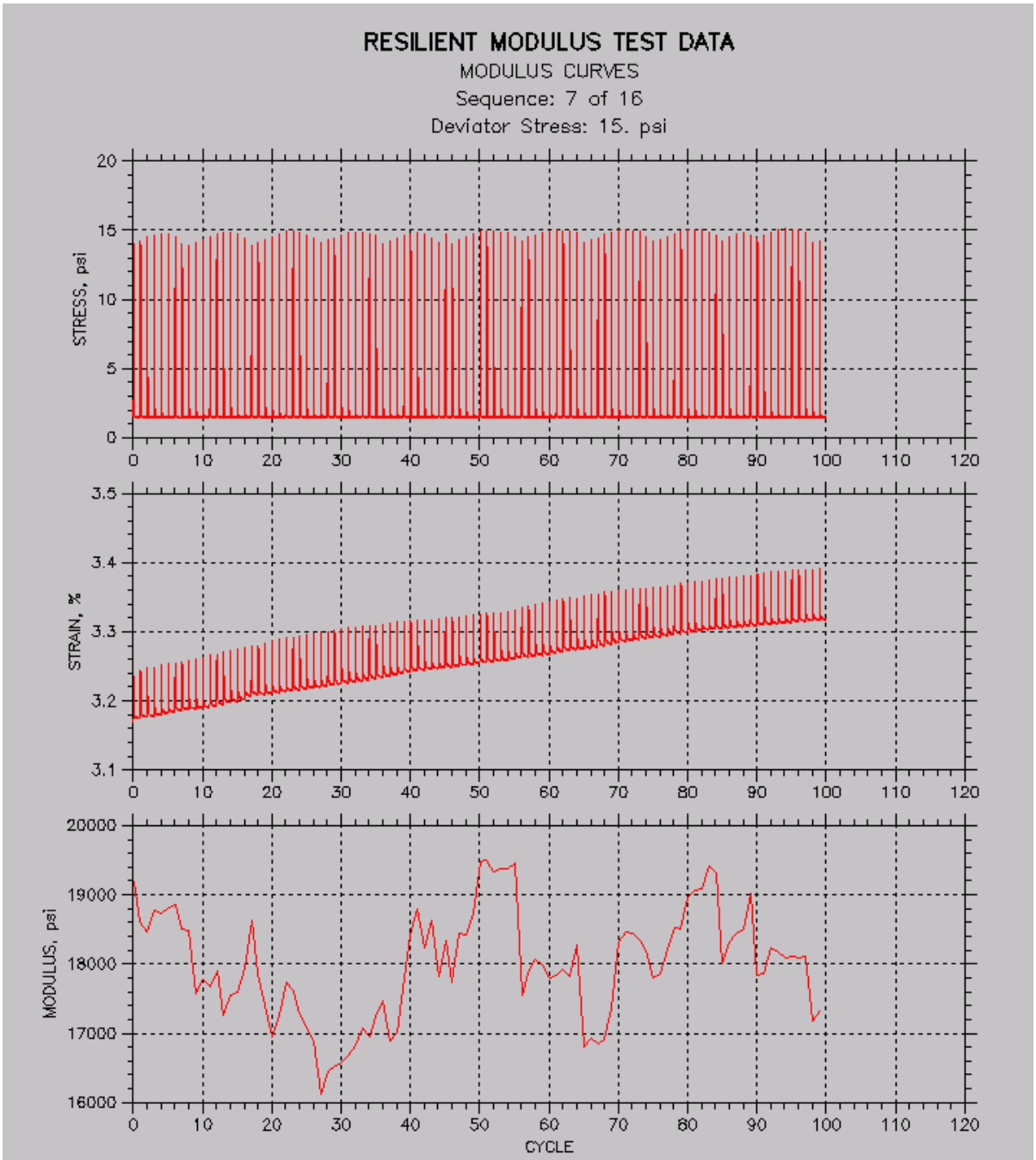

Project: PF2	Location: IA	Project No.:
Boring No.:	Tested By: JL	Checked By:
Sample No.: 2	Test Date: 20120902	Depth:
Test No.:	Sample Type: Coarse	Elevation:
Description: Manatt's RAP 90%RD Mr test 95.78pcf 2.86% w 2.97% fines		
Remarks: Viracating compaction		
File: U:\Desktop\research\data\A New test plan\MR& UU tests\MR tests\dat files\RAP_Manatt's_90%RD_95.78pcf_2.86%w		

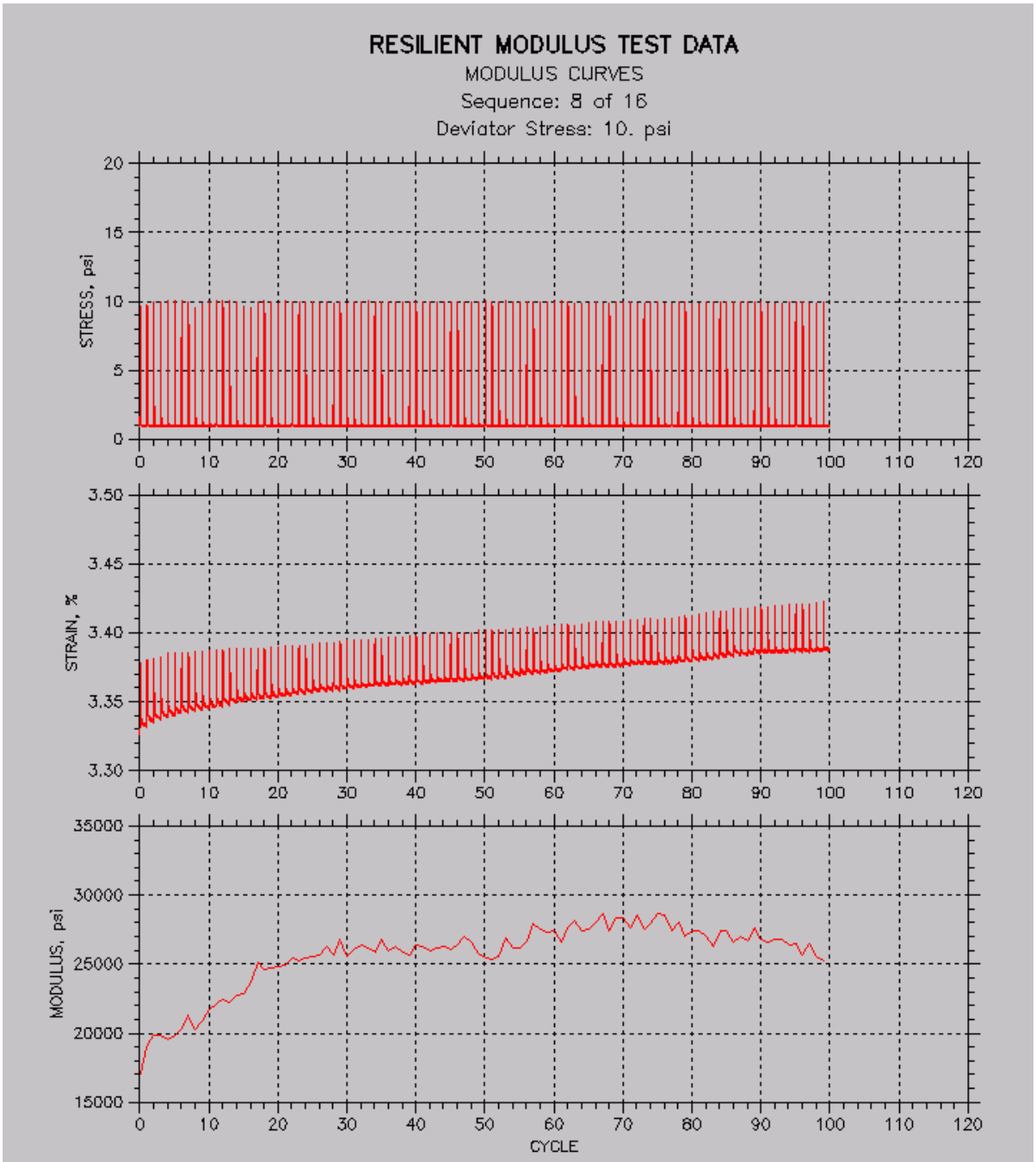

Project: PF2	Location: IA	Project No.:
Boring No.:	Tested By: JL	Checked By:
Sample No.: 2	Test Date: 20120902	Depth:
Test No.:	Sample Type: Coarse	Elevation:
Description: Manatt's RAP 90%RD Mr test 95.78pcf 2.86% w 2.97% fines		
Remarks: Viracating compaction		
File: U:\Desktop\research\data\A New test plan\MR& UU tests\MR tests\dat files\RAP_Manatt's_90%RD_95.78pcf_2.86%w		

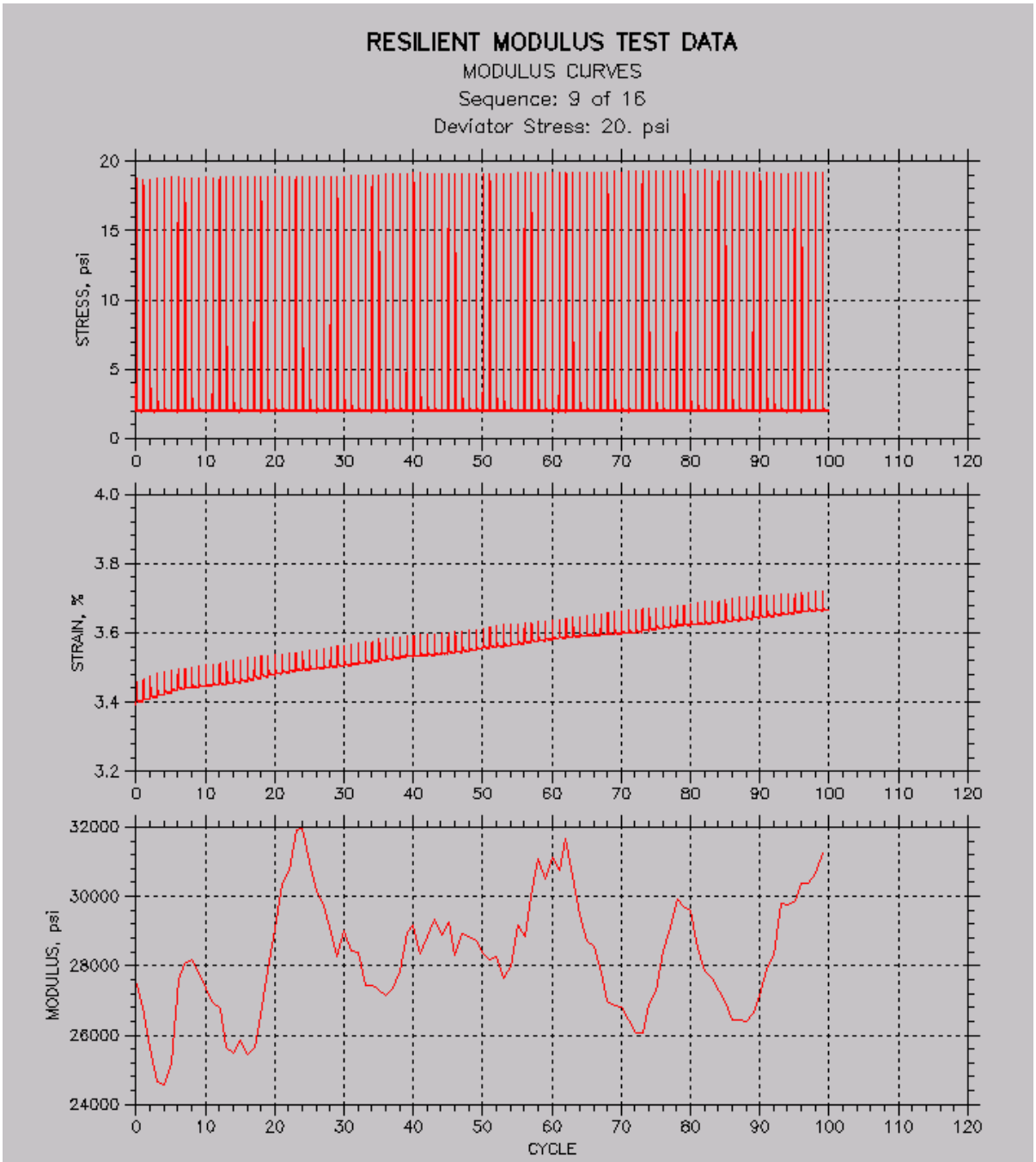

Project: PF2	Location: IA	Project No.:
Boring No.:	Tested By: JL	Checked By:
Sample No.: 2	Test Date: 20120902	Depth:
Test No.:	Sample Type: Coarse	Elevation:
Description: Manatt's RAP 90%RD Mr test 95.78pcf 2.86% w 2.97% fines		
Remarks: Viracating compaction		
File: U:\Desktop\research\data\A New test plan\MR& UU tests\MR tests\dat files\RAP_Manatt's_90%RD_95.78pcf_2.86%w		

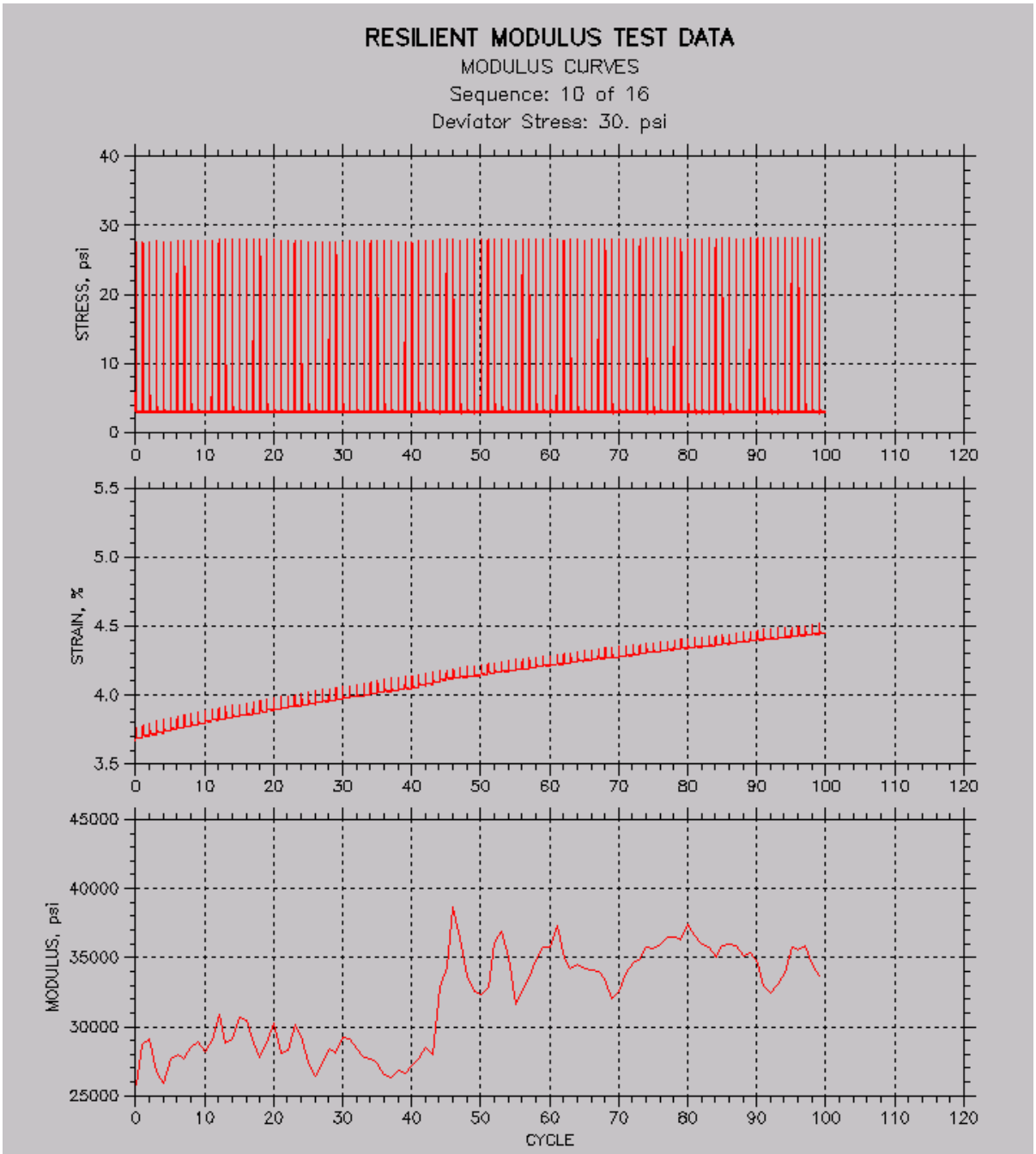

Project: PF2	Location: IA	Project No.:
Boring No.:	Tested By: JL	Checked By:
Sample No.: 2	Test Date: 20120902	Depth:
Test No.:	Sample Type: Coarse	Elevation:
Description: Manatt's RAP 90%RD Mr test 95.78pcf 2.86% w 2.97% fines		
Remarks: Viracating compaction		
File: U:\Desktop\research\data\A New test plan\MR& UU tests\MR tests\dat files\RAP_Manatt's_90%RD_95.78pcf_2.86%w.		

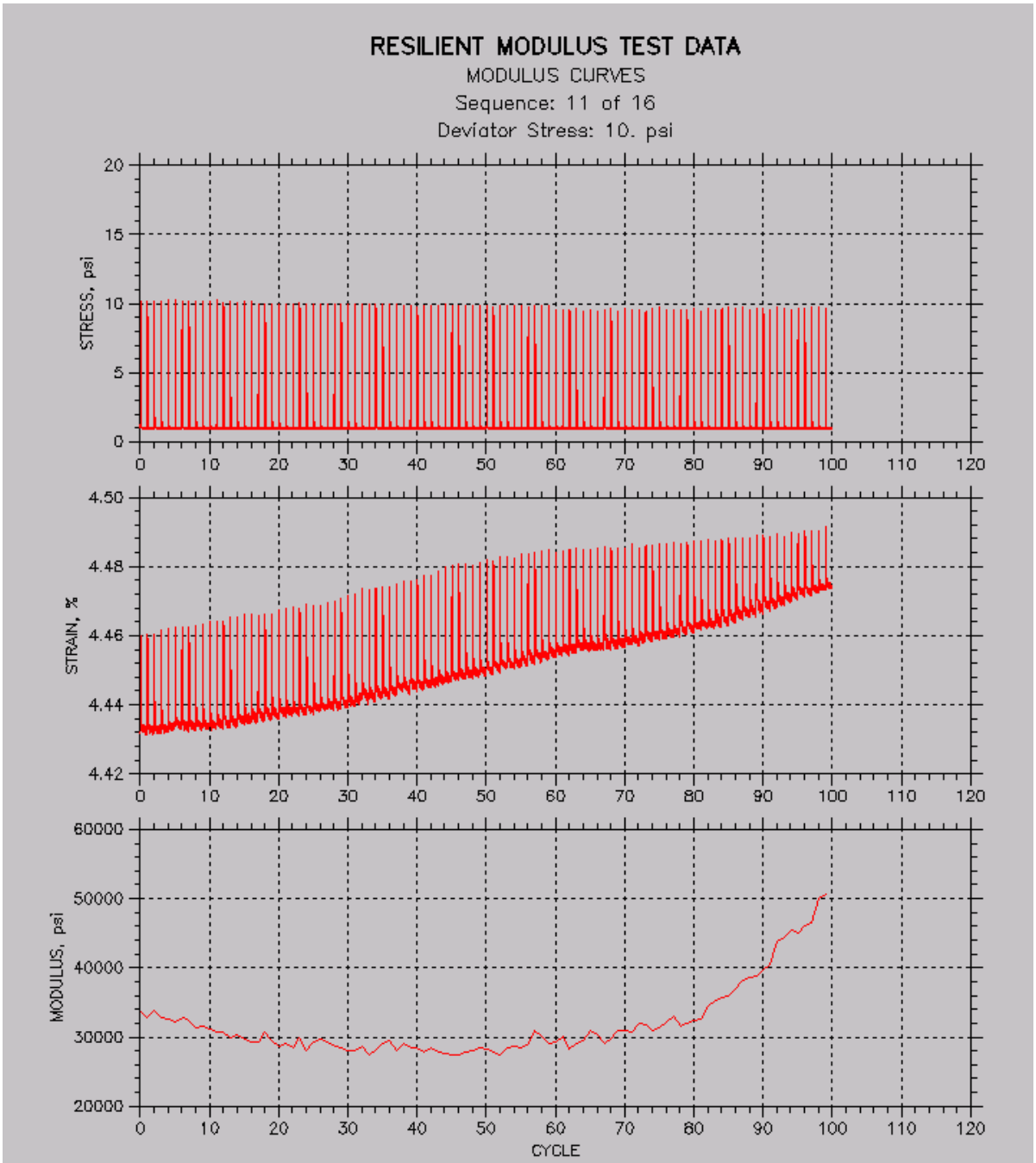

Project: PF2	Location: IA	Project No.:
Boring No.:	Tested By: JL	Checked By:
Sample No.: 2	Test Date: 20120902	Depth:
Test No.:	Sample Type: Coarse	Elevation:
Description: Manatt's RAP 90%RD Mr test 95.78pcf 2.86% w 2.97% fines		
Remarks: Viracating compaction		
File: U:\Desktop\research\data\A New test plan\MR& UU tests\MR tests\dat files\RAP_Manatt's_90%RD_95.78pcf_2.86%w		

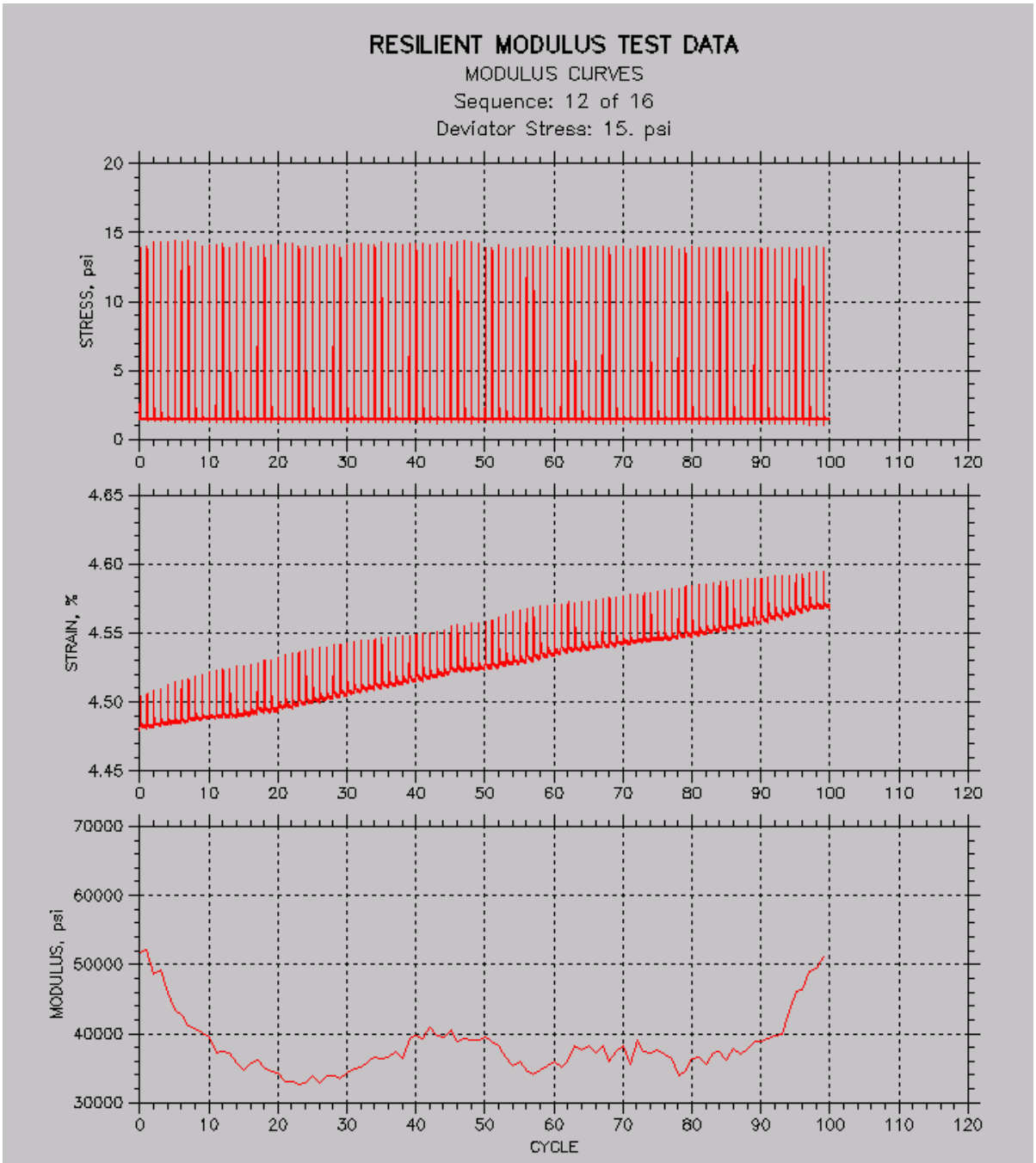

Project: PF2	Location: IA	Project No.:
Boring No.:	Tested By: JL	Checked By:
Sample No.: 2	Test Date: 20120902	Depth:
Test No.:	Sample Type: Coarse	Elevation:
Description: Manatt's RAP 90%RD Mr test 95.78pcf 2.86% w 2.97% fines		
Remarks: Viracating compaction		
File: U:\Desktop\research\data\A New test plan\MR& UU tests\MR tests\dat files\RAP_Manatt's_90%RD_95.78pcf_2.86%w		

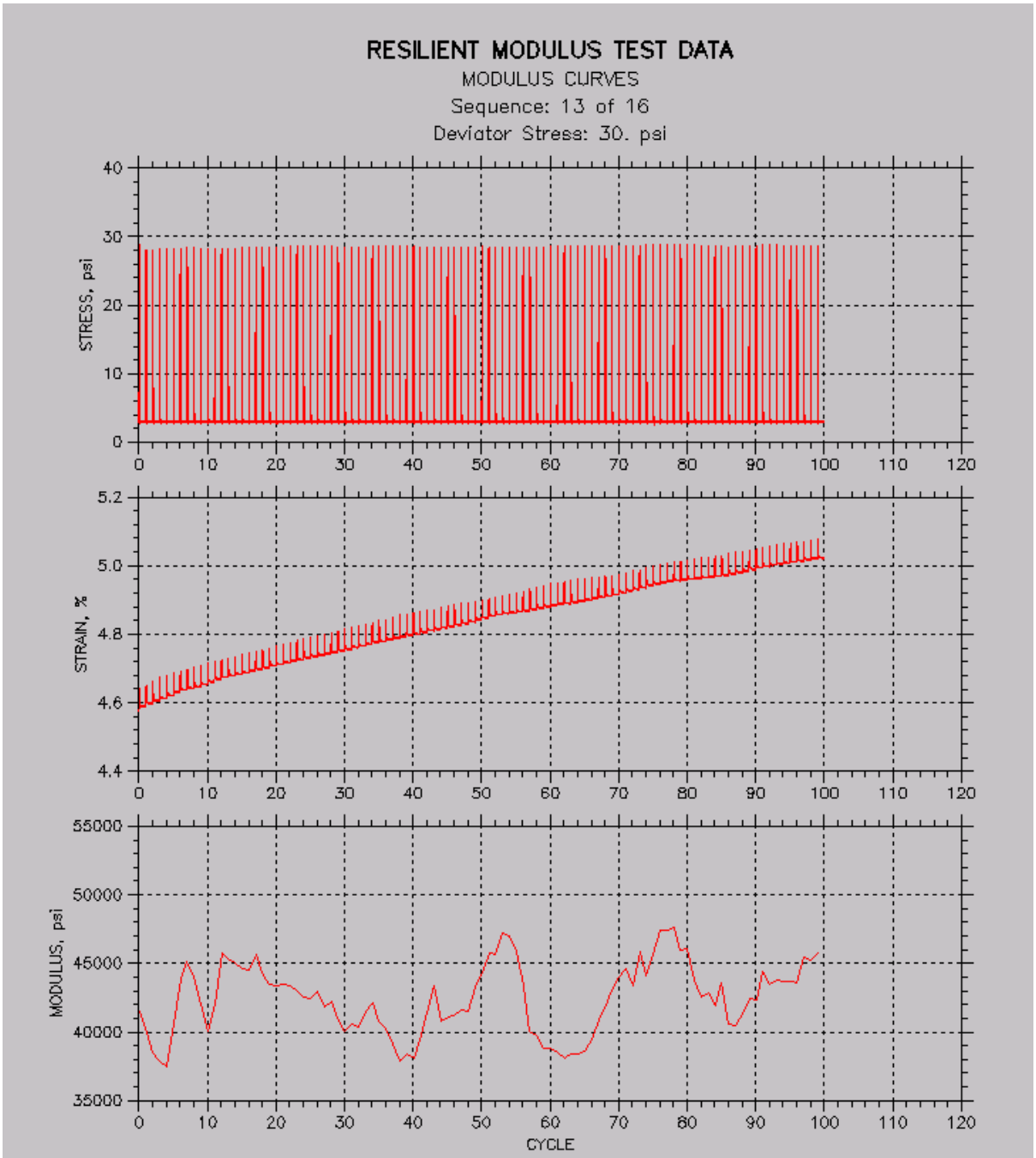

Project: PF2	Location: IA	Project No.:
Boring No.:	Tested By: JL	Checked By:
Sample No.: 2	Test Date: 20120902	Depth:
Test No.:	Sample Type: Coarse	Elevation:
Description: Manatt's RAP 90%RD Mr test 95.78pcf 2.86% w 2.97% fines		
Remarks: Viracating compaction		
File: U:\Desktop\research\data\A New test plan\MR& UU tests\MR tests\dat files\RAP_Manatt's_90%RD_95.78pcf_2.86%w_		

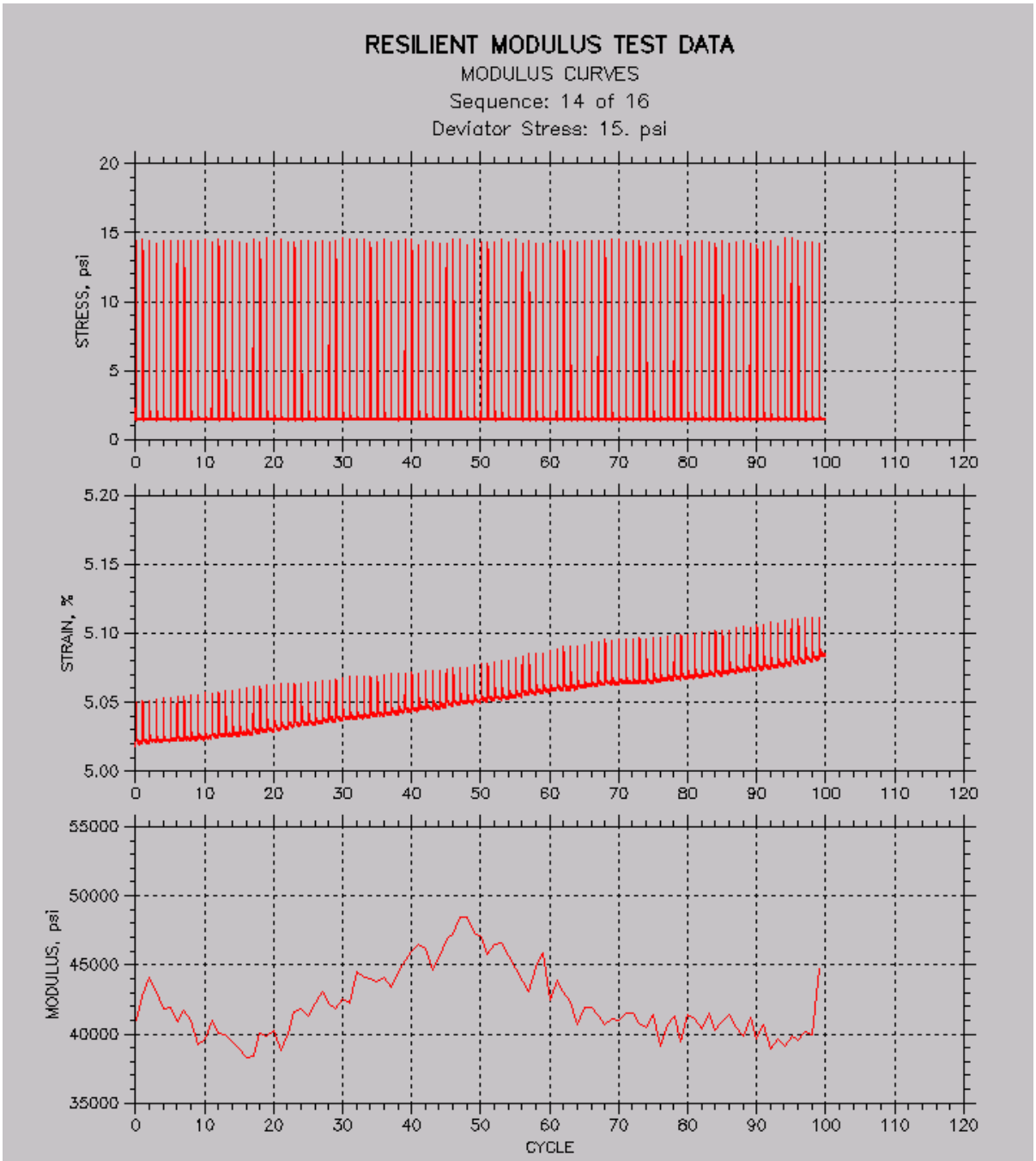

Project: PF2	Location: IA	Project No.:
Boring No.:	Tested By: JL	Checked By:
Sample No.: 2	Test Date: 20120902	Depth:
Test No.:	Sample Type: Coarse	Elevation:
Description: Manatt's RAP 90%RD Mr test 95.78pcf 2.86% w 2.97% fines		
Remarks: Viracating compaction		
File: U:\Desktop\research\data\A New test plan\MR& UU tests\MR tests\dat files\RAP_Manatt's_90%RD_95.78pcf_2.86%w		

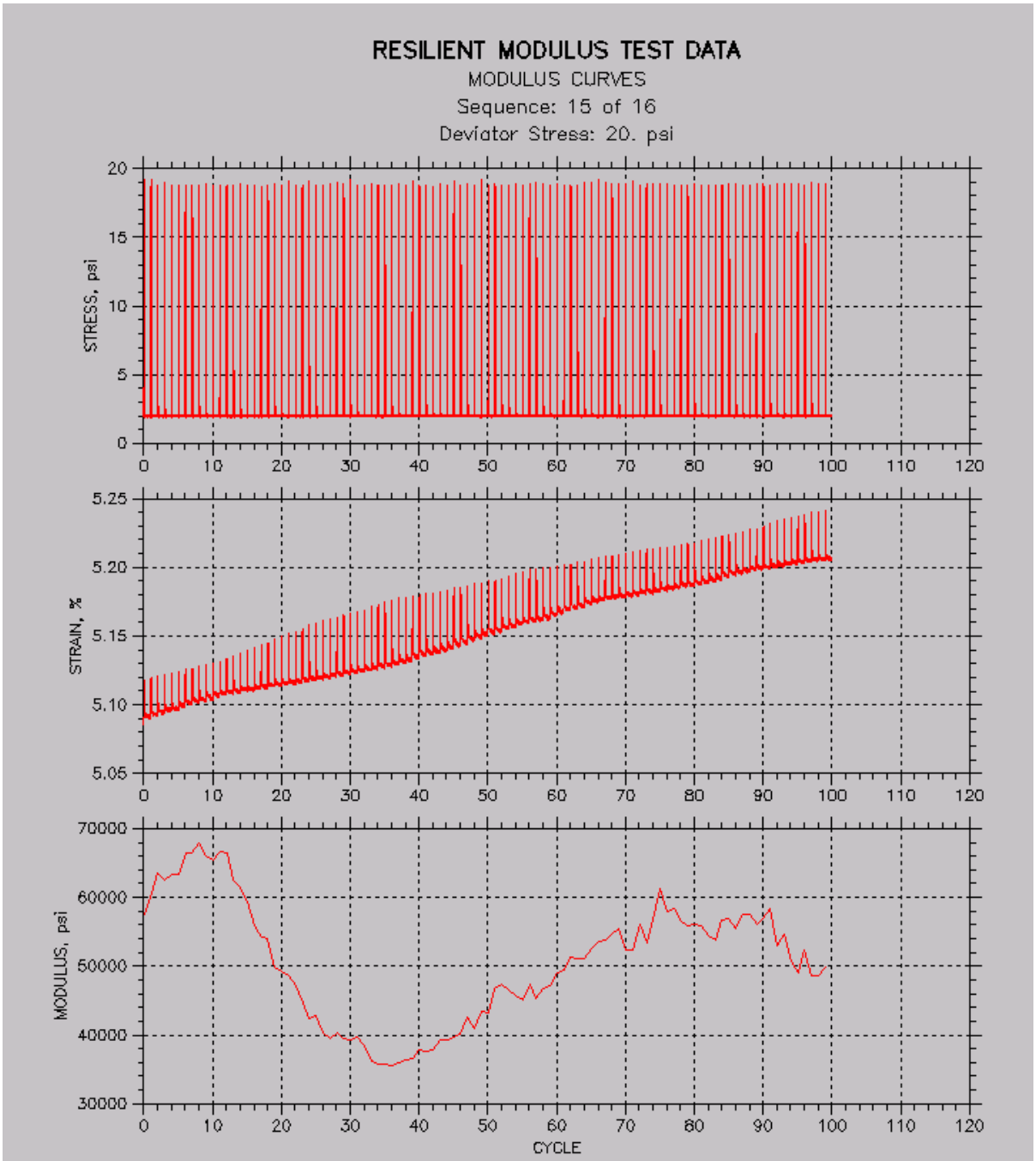

Project: PF2	Location: IA	Project No.:
Boring No.:	Tested By: JL	Checked By:
Sample No.: 2	Test Date: 20120902	Depth:
Test No.:	Sample Type: Coarse	Elevation:
Description: Manatt's RAP 90%RD Mr test 95.78pcf 2.86% w 2.97% fines		
Remarks: Viracating compaction		
File: U:\Desktop\research\data\A New test plan\MR& UU tests\MR tests\dat files\RAP_Manatt's_90%RD_95.78pcf_2.86%w		

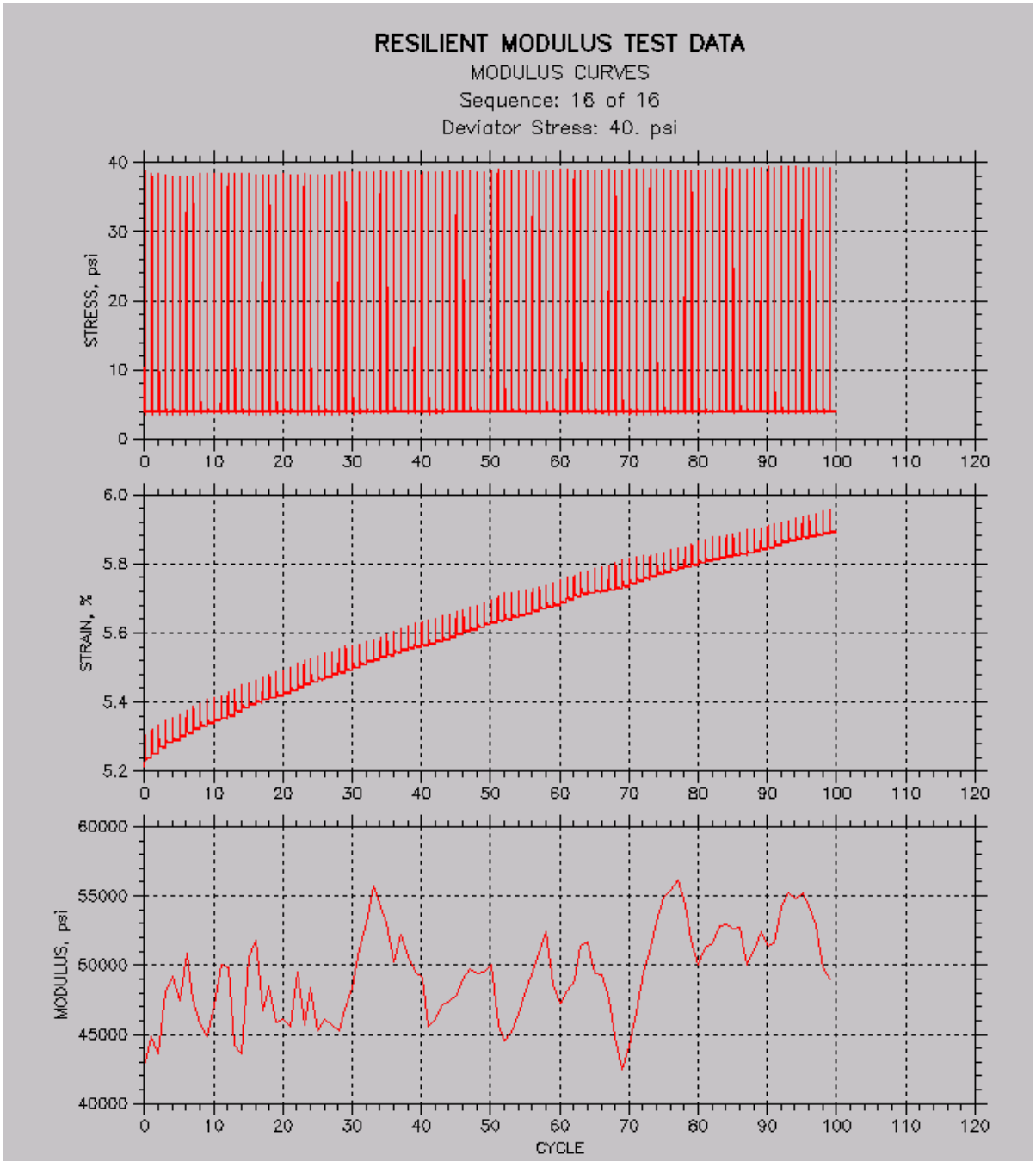

Project: PF2	Location: IA	Project No.:
Boring No.:	Tested By: JL	Checked By:
Sample No.: 2	Test Date: 20120902	Depth:
Test No.:	Sample Type: Coarse	Elevation:
Description: Manatt's RAP 90%RD Mr test 95.78pcf 2.86% w 2.97% fines		
Remarks: Viracating compaction		
File: U:\Desktop\research\data\A New test plan\MR& UU tests\MR tests\dat files\RAP_Manatt's_90%RD_95.78pcf_2.86%		

RPCC/RAP

RESILIENT MODULUS TEST DATA

SUMMARY REPORT

$Mr = 1355.1 * Pa * (B/Pa)^{0.653} * (Sd/Pa)^{-0.0675}$ r = 0.89366

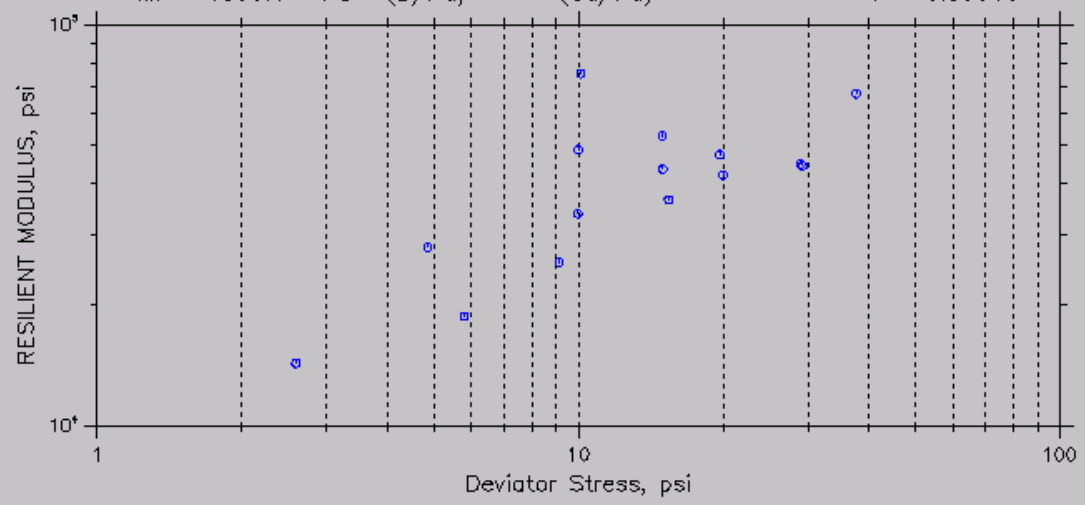

Confining Stress S3 (psi)	Nom. Max. Deviator Stress (psi)	Mean Deviator Stress (psi)	Std. Dev. Deviator Stress (psi)	Mean Bulk Stress (psi)	Mean Resilient Strain (%)	Std. Dev. Resilient Strain (%)	Mean Resilient Modulus (psi)	Std. Dev. Resilient Modulus (psi)
3.001	3	2.586	0.0488	11.59	0.02	0.00	14285	514.45
2.957	6	5.788	0.0752	14.66	0.03	0.00	18699	978.48
2.977	9	9.115	0.0706	18.05	0.03	0.00	25488	1788.1
4.947	5	4.863	0.0642	19.7	0.02	0.00	27842	1048.5
4.994	10	9.964	0.0675	24.94	0.03	0.00	33738	1762.7
5.013	15	15.4	0.2940	30.44	0.04	0.00	36536	1255.5
9.997	10	10	0.1410	39.99	0.02	0.00	48715	1956.6
9.986	20	20	0.2581	49.96	0.04	0.00	42039	1144.2
9.99	30	29.25	0.2797	59.21	0.06	0.00	44411	1229.9
14.99	10	10.11	0.2141	55.08	0.01	0.00	75323	8362.5
15.01	15	14.95	0.2282	59.97	0.03	0.00	52702	3108.7
15	30	28.96	0.1950	73.95	0.06	0.00	44844	940.02
19.86	15	14.97	0.1804	74.54	0.03	0.00	43598	1460.2
19.87	20	19.68	0.2072	79.28	0.04	0.00	47346	1014.2
19.88	40	37.82	0.0561	97.47	0.05	0.00	67214	759.03

Project: PF2	Location: Ames	Project No.:
Boring No.:	Tested By: JL	Checked By:
Sample No.: 1	Test Date: 20120808	Depth:
Test No.:	Sample Type: Coarse	Elevation:
Description: Manatt's RPCC/RAP 90%RD Mr test 103.26pcf 5.98% w 2.62% fines		
Remarks: Viracating compaction		
File: U:\Desktop\research\data\A New test plan\MR& UU tests\MR tests\dat files\RPCCandRAP_Manatt's_90%RD_103.26pc		

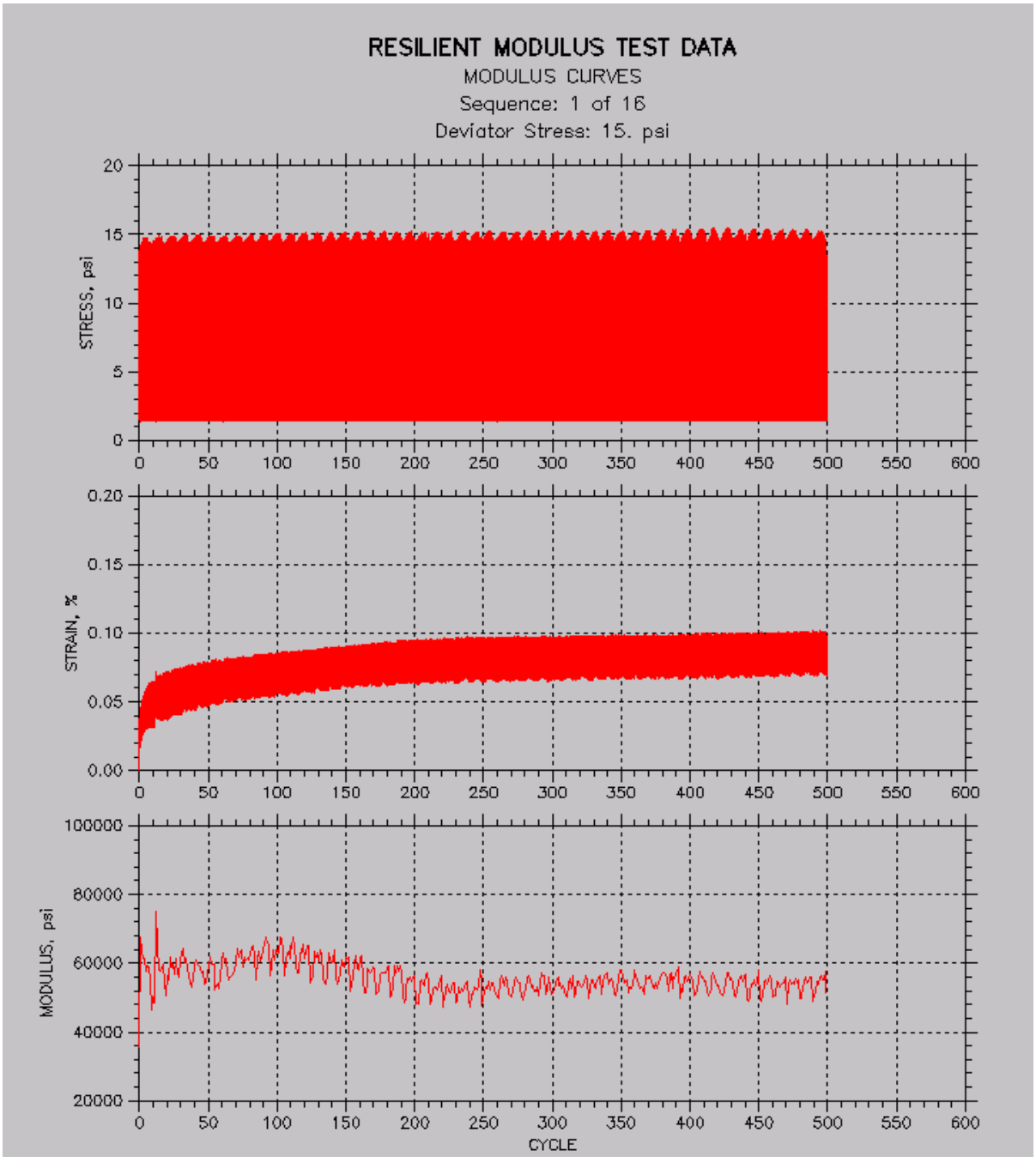

Project: PF2	Location: Ames	Project No.:
Boring No.:	Tested By: JL	Checked By:
Sample No.: 1	Test Date: 20120808	Depth:
Test No.:	Sample Type: Coarse	Elevation:
Description: Manatt's RPCC/RAP 90%RD Mr test 103.26pcf 5.98% w 2.62% fines		
Remarks: Viracating compaction		
File: U:\Desktop\research\data\A New test plan\MR& UU tests\MR tests\dat files\RPCCandRAP_Manatt's_90%RD_103.26pc		

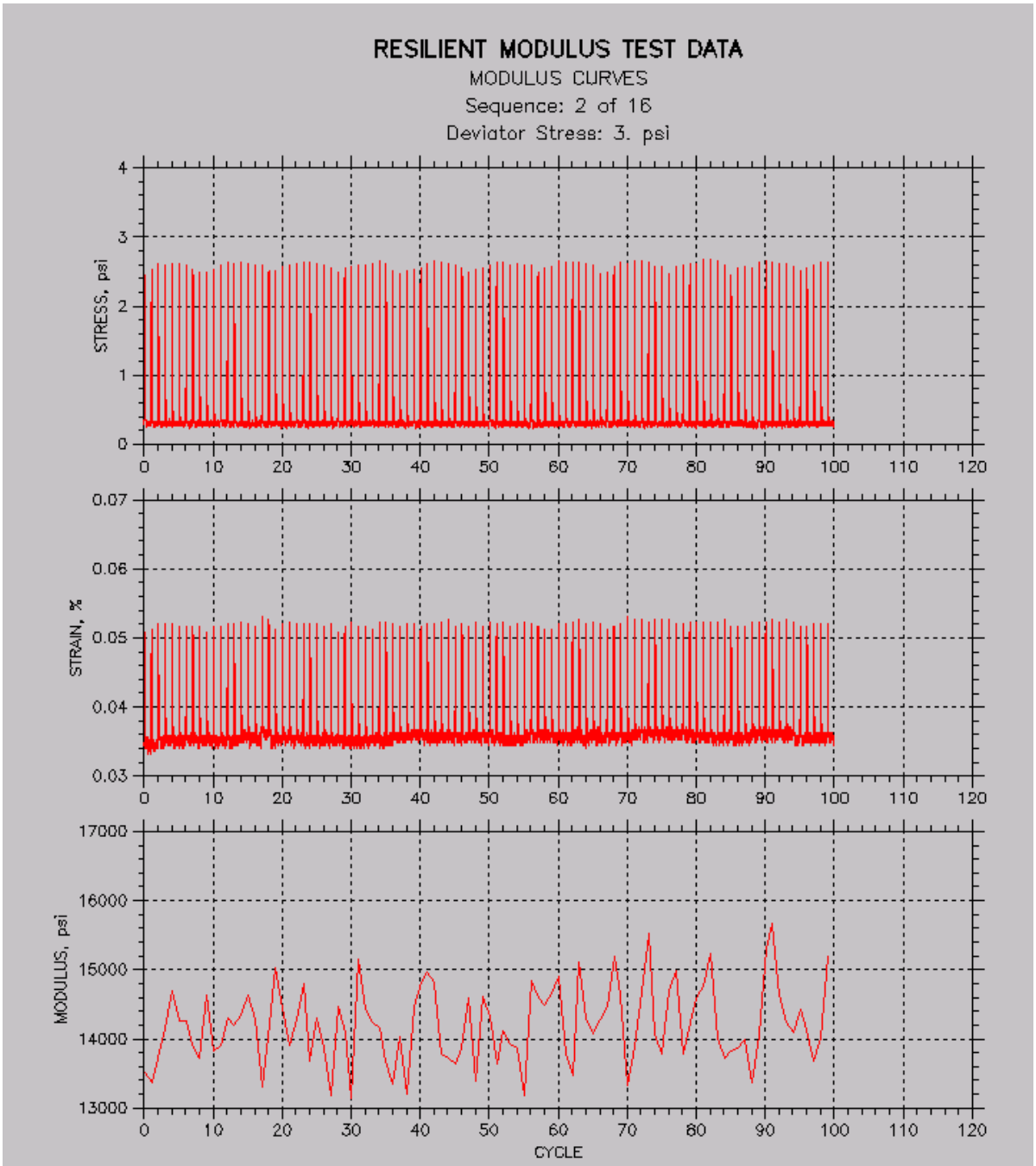

Project: PF2	Location: Ames	Project No.:
Boring No.:	Tested By: JL	Checked By:
Sample No.: 1	Test Date: 20120808	Depth:
Test No.:	Sample Type: Coarse	Elevation:
Description: Manatt's RPCC/RAP 90%RD Mr test 103.26pcf 5.98% w 2.62% fines		
Remarks: Viracating compaction		
File: U:\Desktop\research\data\A New test plan\MR& UU tests\MR tests\dat files\RPCCandRAP_Manatt's_90%RD_103.26p		

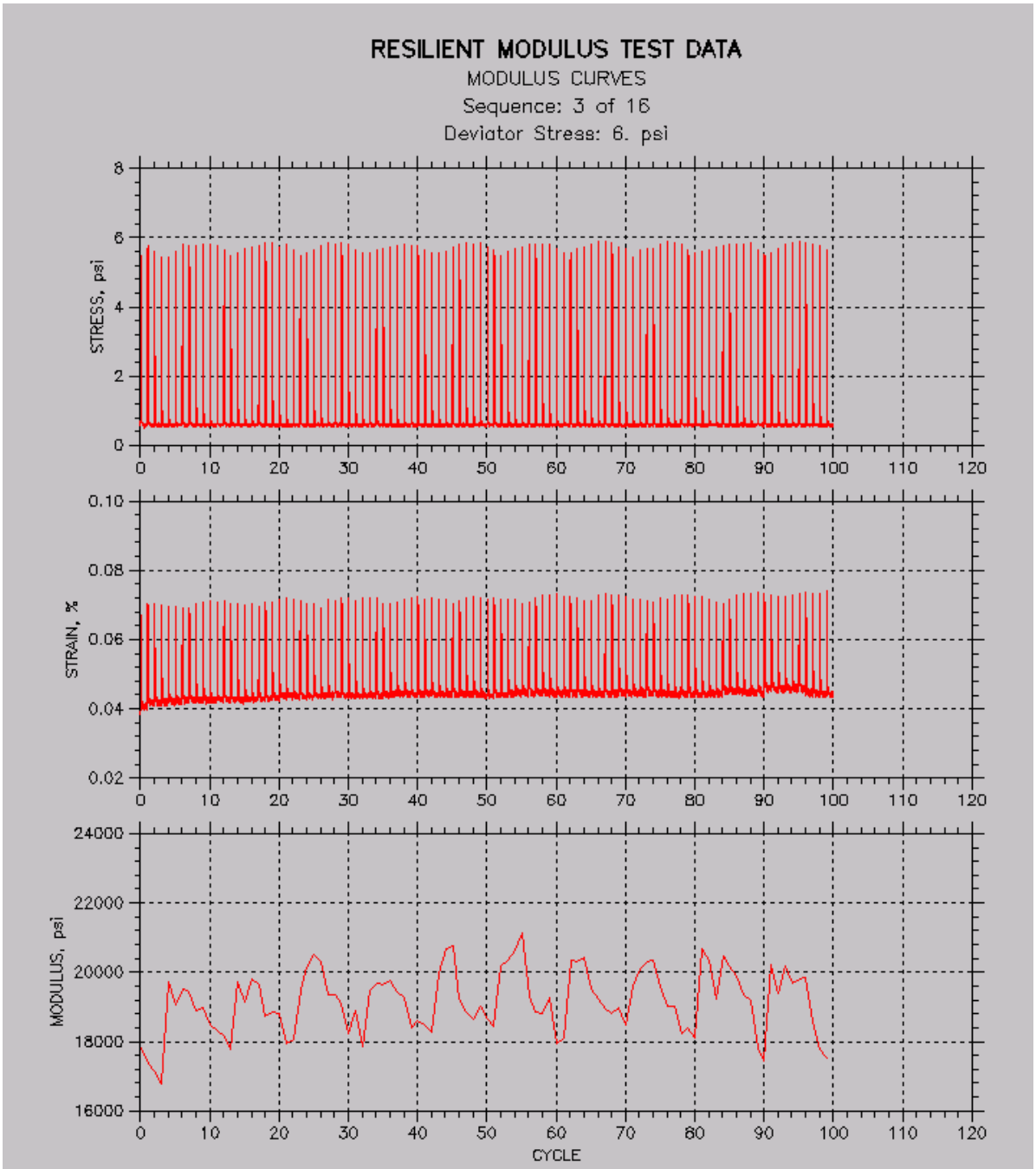

Project: PF2	Location: Ames	Project No.:
Boring No.:	Tested By: JL	Checked By:
Sample No.: 1	Test Date: 20120808	Depth:
Test No.:	Sample Type: Coarse	Elevation:
Description: Manatt's RPCC/RAP 90%RD Mr test 103.26pcf 5.98% w 2.62% fines		
Remarks: Viracating compaction		
File: U:\Desktop\research\data\A New test plan\MR& UU tests\MR tests\dat files\RPCCandRAP_Manatt's_90%RD_103.26p		

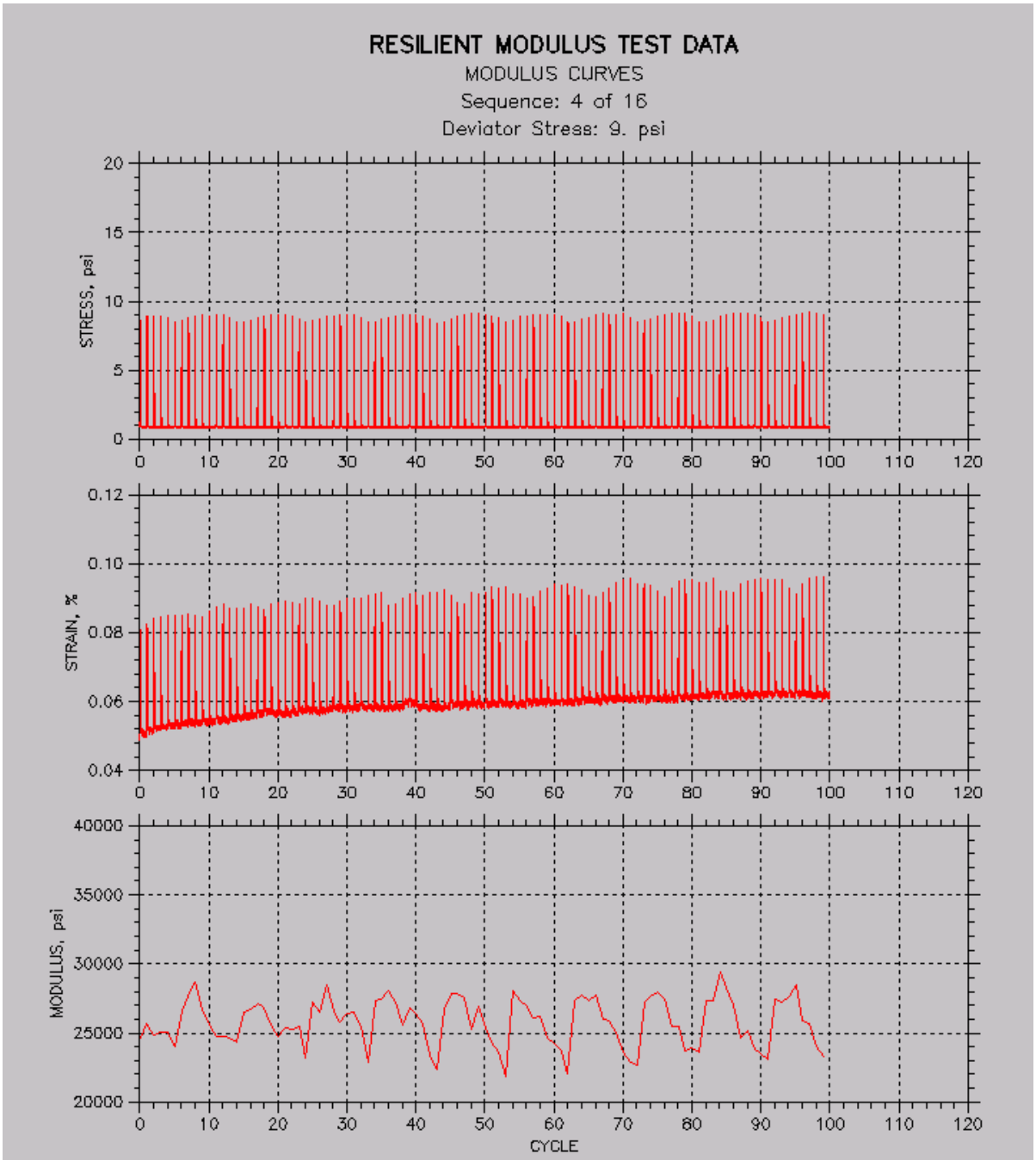

Project: PF2	Location: Ames	Project No.:
Boring No.:	Tested By: JL	Checked By:
Sample No.: 1	Test Date: 20120808	Depth:
Test No.:	Sample Type: Coarse	Elevation:
Description: Manatt's RPCC/RAP 90%RD Mr test 103.26pcf 5.98% w 2.62% fines		
Remarks: Viracating compaction		
File: U:\Desktop\research\data\A New test plan\MR& UU tests\MR tests\dat files\RPCCandRAP_Manatt's_90%RD_103.26p		

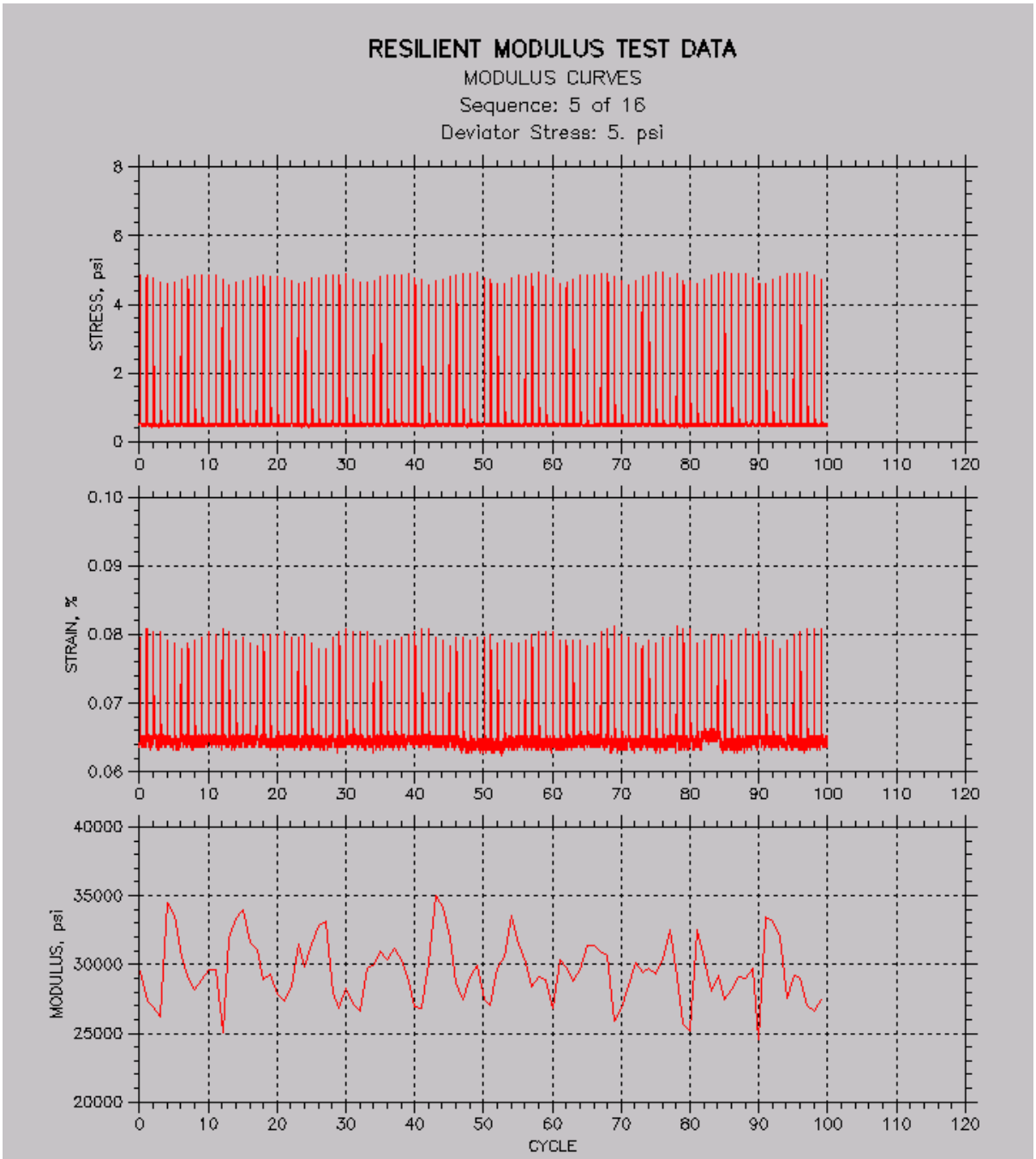

Project: PF2	Location: Ames	Project No.:
Boring No.:	Tested By: JL	Checked By:
Sample No.: 1	Test Date: 20120808	Depth:
Test No.:	Sample Type: Coarse	Elevation:
Description: Manatt's RPCC/RAP 90%RD Mr test 103.26pcf 5.98% w 2.62% fines		
Remarks: Viracating compaction		
File: U:\Desktop\research\data\A New test plan\MR& UU tests\MR tests\dat files\RPCCandRAP_Manatt's_90%RD_103.26pc		

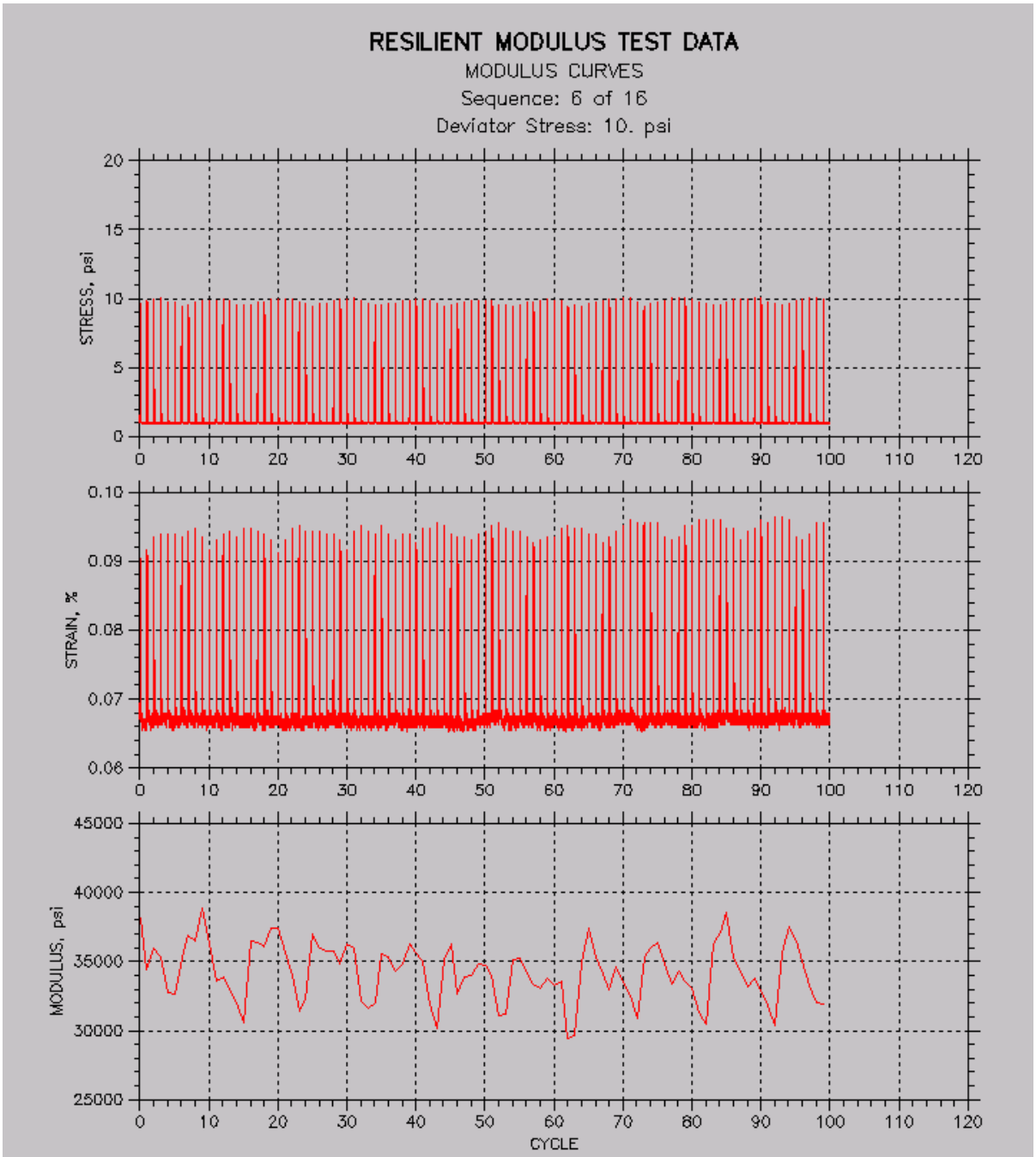

Project: PF2	Location: Ames	Project No.:
Boring No.:	Tested By: JL	Checked By:
Sample No.: 1	Test Date: 20120808	Depth:
Test No.:	Sample Type: Coarse	Elevation:
Description: Manatt's RPCC/RAP 90%RD Mr test 103.26pcf 5.98% w 2.62% fines		
Remarks: Viracating compaction		
File: U:\Desktop\research\data\A New test plan\MR& UU tests\MR tests\dat files\RPCCandRAP_Manatt's_90%RD_103.26p		

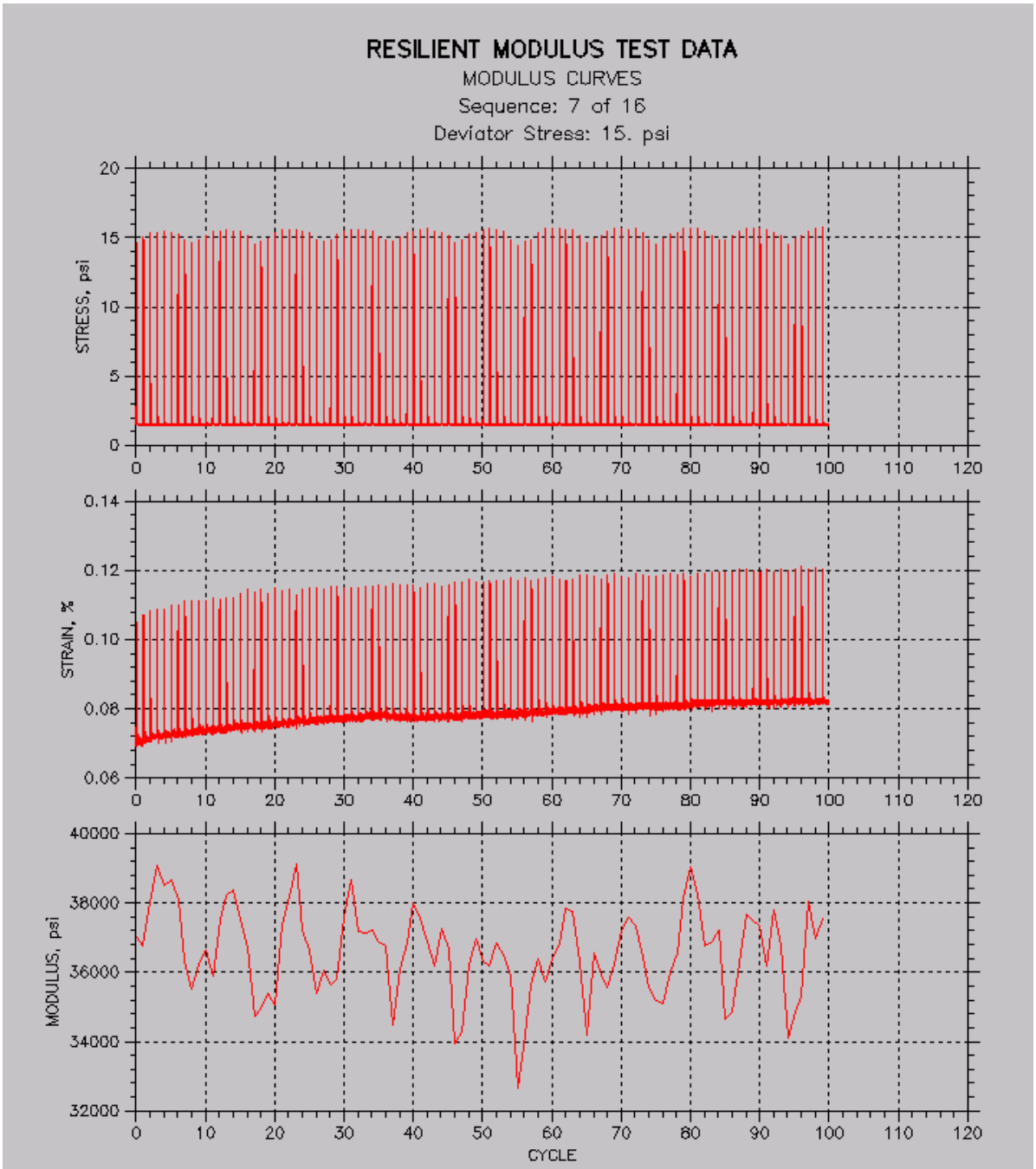

Project: PF2	Location: Ames	Project No.:
Boring No.:	Tested By: JL	Checked By:
Sample No.: 1	Test Date: 20120808	Depth:
Test No.:	Sample Type: Coarse	Elevation:
Description: Manatt's RPCC/RAP 90%RD Mr test 103.26pcf 5.98% w 2.62% fines		
Remarks: Viracating compaction		
File: U:\Desktop\research\data\A New test plan\MR& UU tests\MR tests\dat files\RPCCandRAP_Manatt's_90%RD_103.26p		

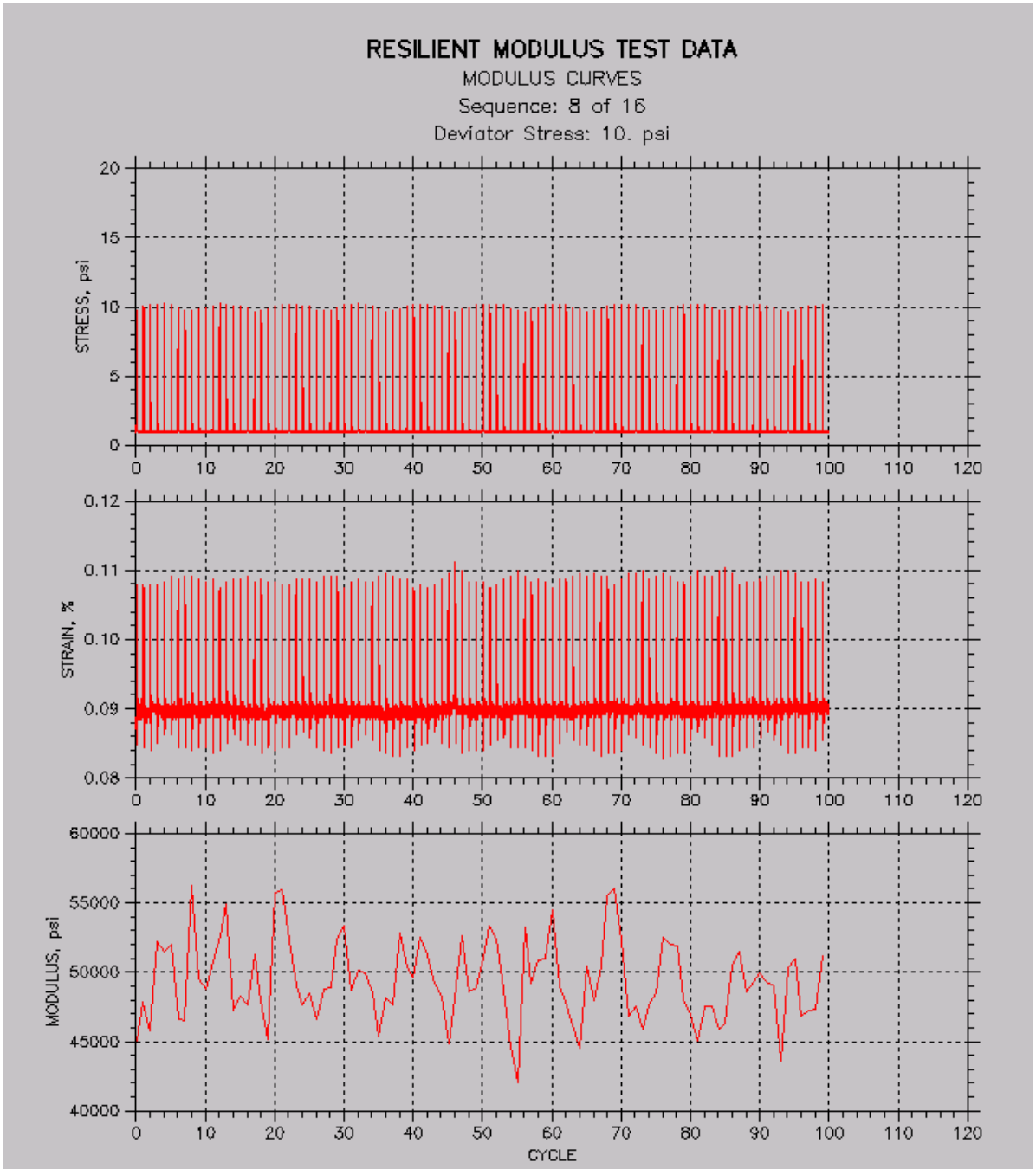

Project: PF2	Location: Ames	Project No.:
Boring No.:	Tested By: JL	Checked By:
Sample No.: 1	Test Date: 20120808	Depth:
Test No.:	Sample Type: Coarse	Elevation:
Description: Manatt's RPCC/RAP 90%RD Mr test 103.26pcf 5.98% w 2.62% fines		
Remarks: Viracating compaction		
File: U:\Desktop\research\data\A New test plan\MR& UU tests\MR tests\dat files\RPCCandRAP_Manatt's_90%RD_103.26p		

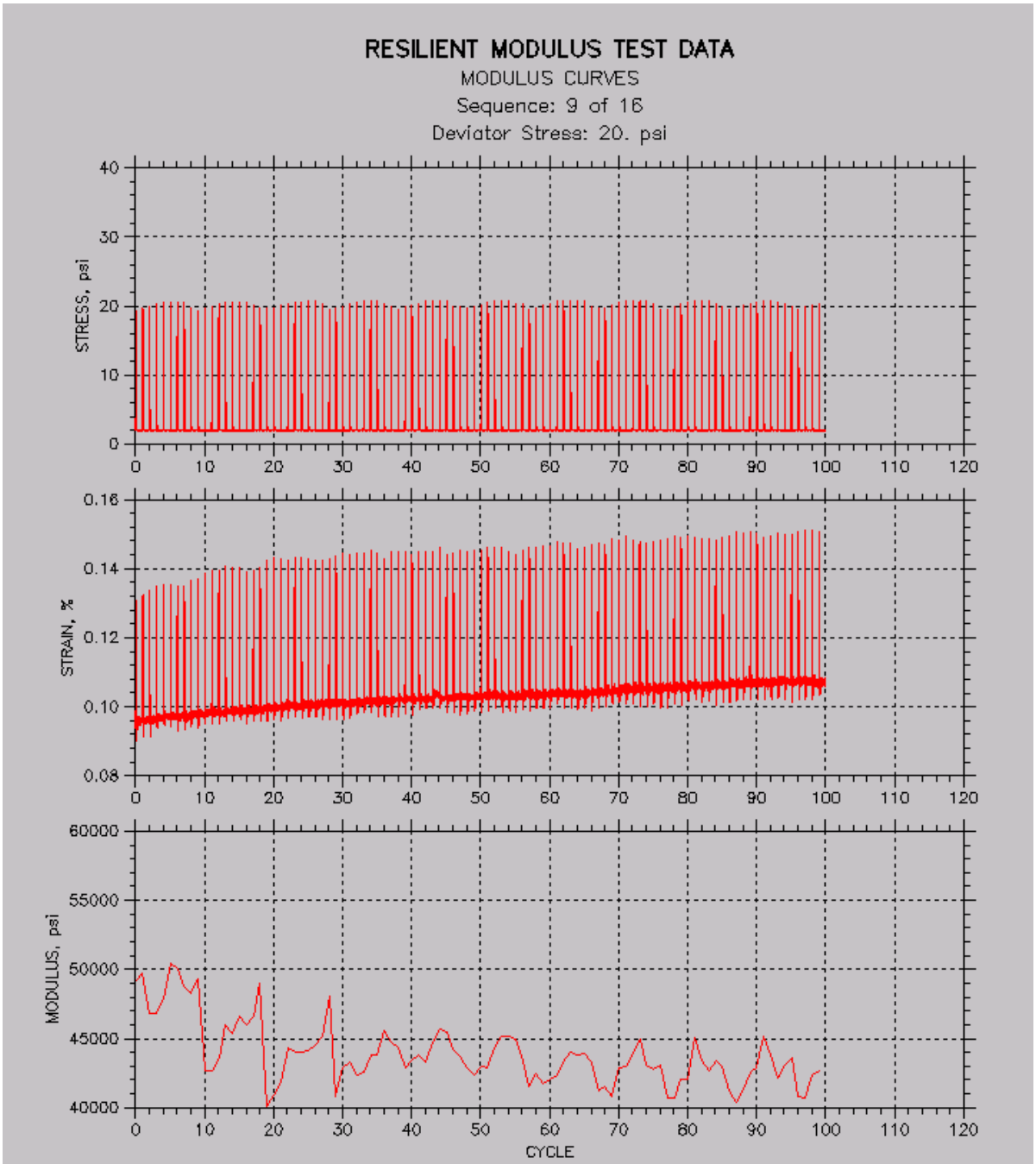

Project: PF2	Location: Ames	Project No.:
Boring No.:	Tested By: JL	Checked By:
Sample No.: 1	Test Date: 20120808	Depth:
Test No.:	Sample Type: Coarse	Elevation:
Description: Manatt's RPCC/RAP 90%RD Mr test 103.26pcf 5.98% w 2.62% fines		
Remarks: Viracating compaction		
File: U:\Desktop\research\data\A New test plan\MR& UU tests\MR tests\dat files\RPCCandRAP_Manatt's_90%RD_103.26pc		

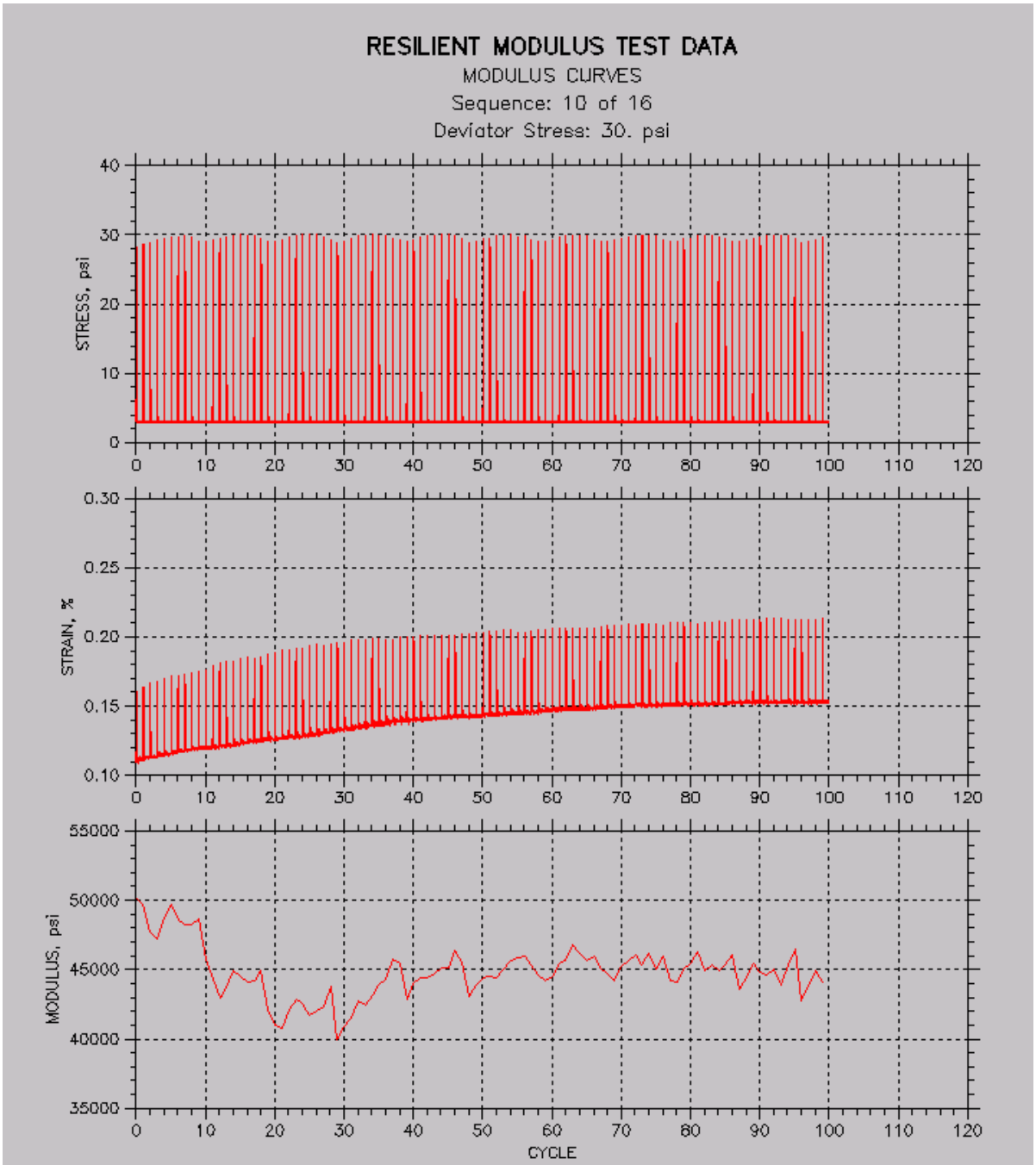

Project: PF2	Location: Ames	Project No.:
Boring No.:	Tested By: JL	Checked By:
Sample No.: 1	Test Date: 20120808	Depth:
Test No.:	Sample Type: Coarse	Elevation:
Description: Manatt's RPCC/RAP 90%RD Mr test 103.26pcf 5.98% w 2.62% fines		
Remarks: Viracating compaction		
File: U:\Desktop\research\data\A New test plan\MR& UU tests\MR tests\dat files\RPCCandRAP_Manatt's_90%RD_103.26p		

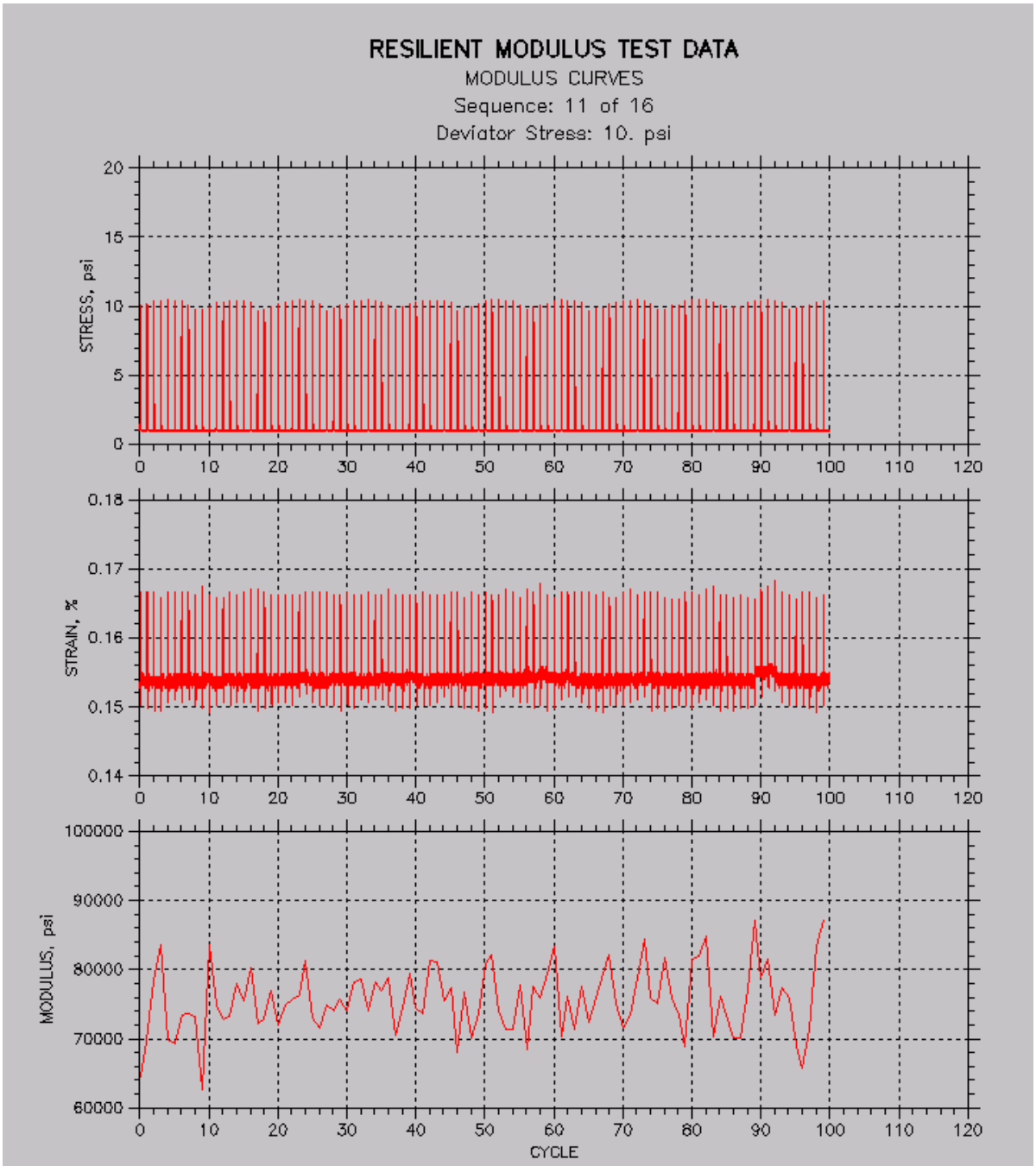

Project: PF2	Location: Ames	Project No.:
Boring No.:	Tested By: JL	Checked By:
Sample No.: 1	Test Date: 20120808	Depth:
Test No.:	Sample Type: Coarse	Elevation:
Description: Manatt's RPCC/RAP 90%RD Mr test 103.26pcf 5.98% w 2.62% fines		
Remarks: Viracating compaction		
File: U:\Desktop\research\data\A New test plan\MR& UU tests\MR tests\dat files\RPCCandRAP_Manatt's_90%RD_103.26p		

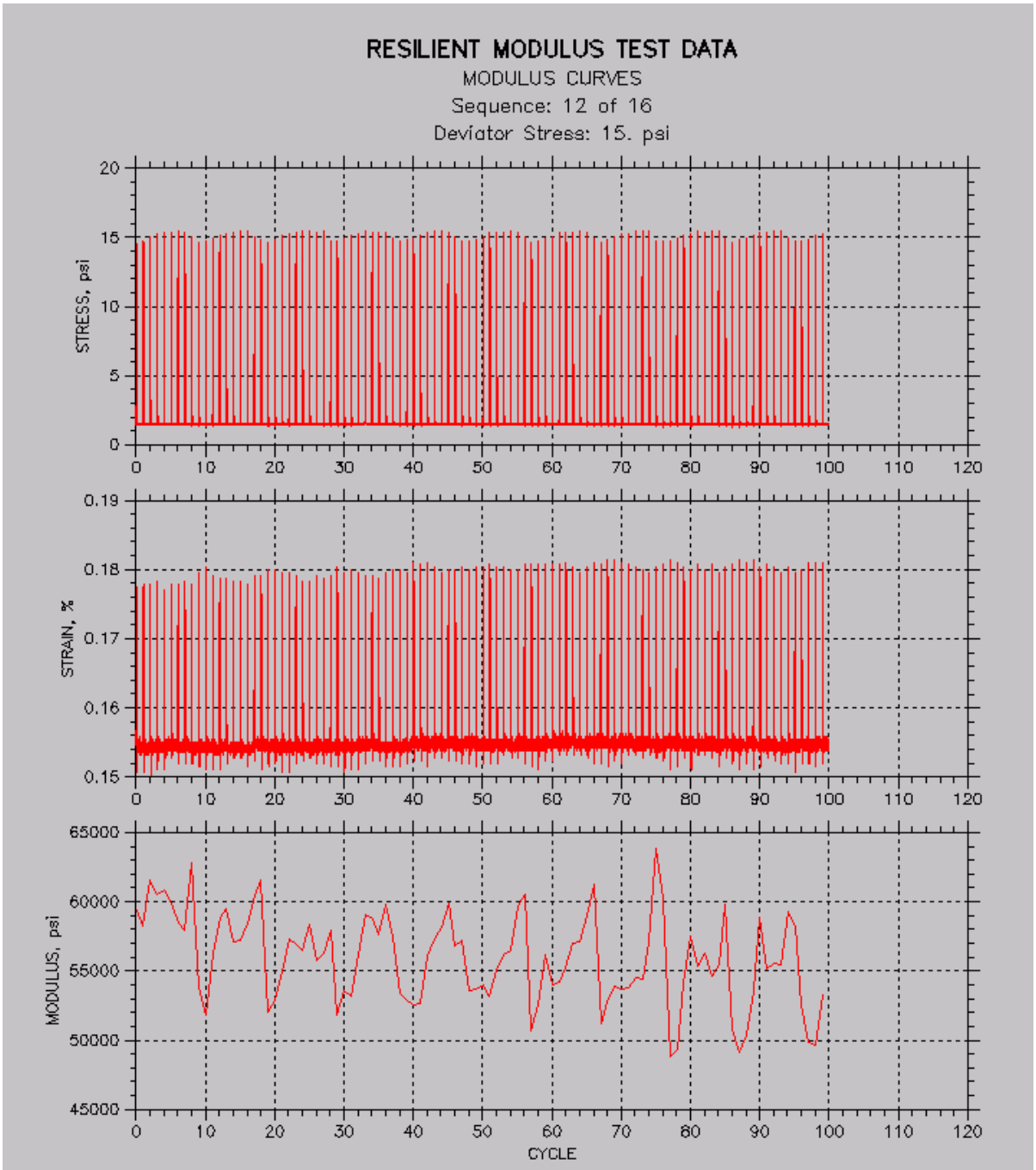

Project: PF2	Location: Ames	Project No.:
Boring No.:	Tested By: JL	Checked By:
Sample No.: 1	Test Date: 20120808	Depth:
Test No.:	Sample Type: Coarse	Elevation:
Description: Manatt's RPCC/RAP 90%RD Mr test 103.26pcf 5.98% w 2.62% fines		
Remarks: Viracating compaction		
File: U:\Desktop\research\data\A New test plan\MR& UU tests\MR tests\dat files\RPCCandRAP_Manatt's_90%RD_103.26p		

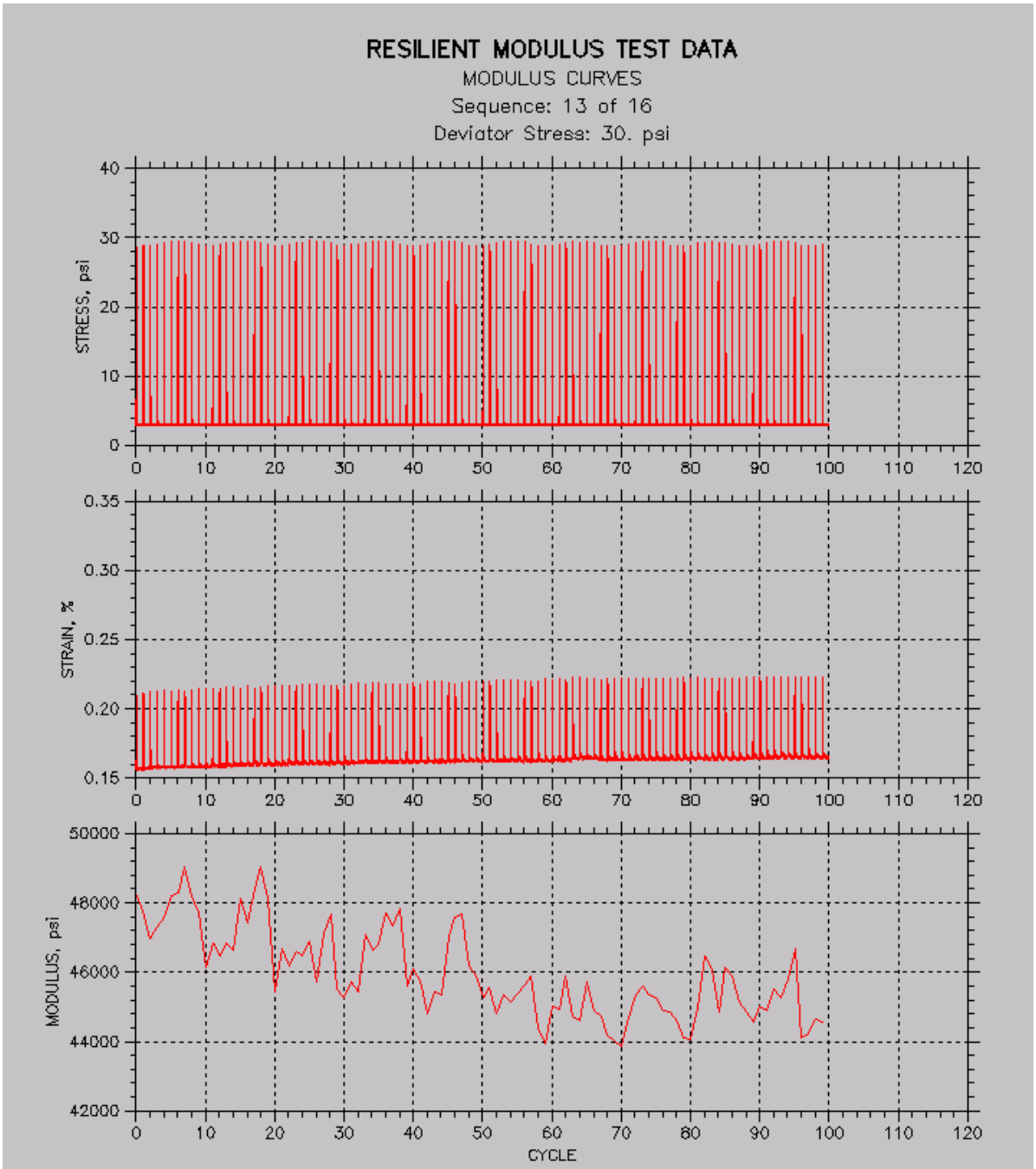

Project: PF2	Location: Ames	Project No.:
Boring No.:	Tested By: JL	Checked By:
Sample No.: 1	Test Date: 20120808	Depth:
Test No.:	Sample Type: Coarse	Elevation:
Description: Manatt's RPCC/RAP 90%RD Mr test 103.26pcf 5.98% w 2.62% fines		
Remarks: Viracating compaction		
File: U:\Desktop\research\data\A New test plan\MR& UU tests\MR tests\dat files\RPCCandRAP_Manatt's_90%RD_103.26p		

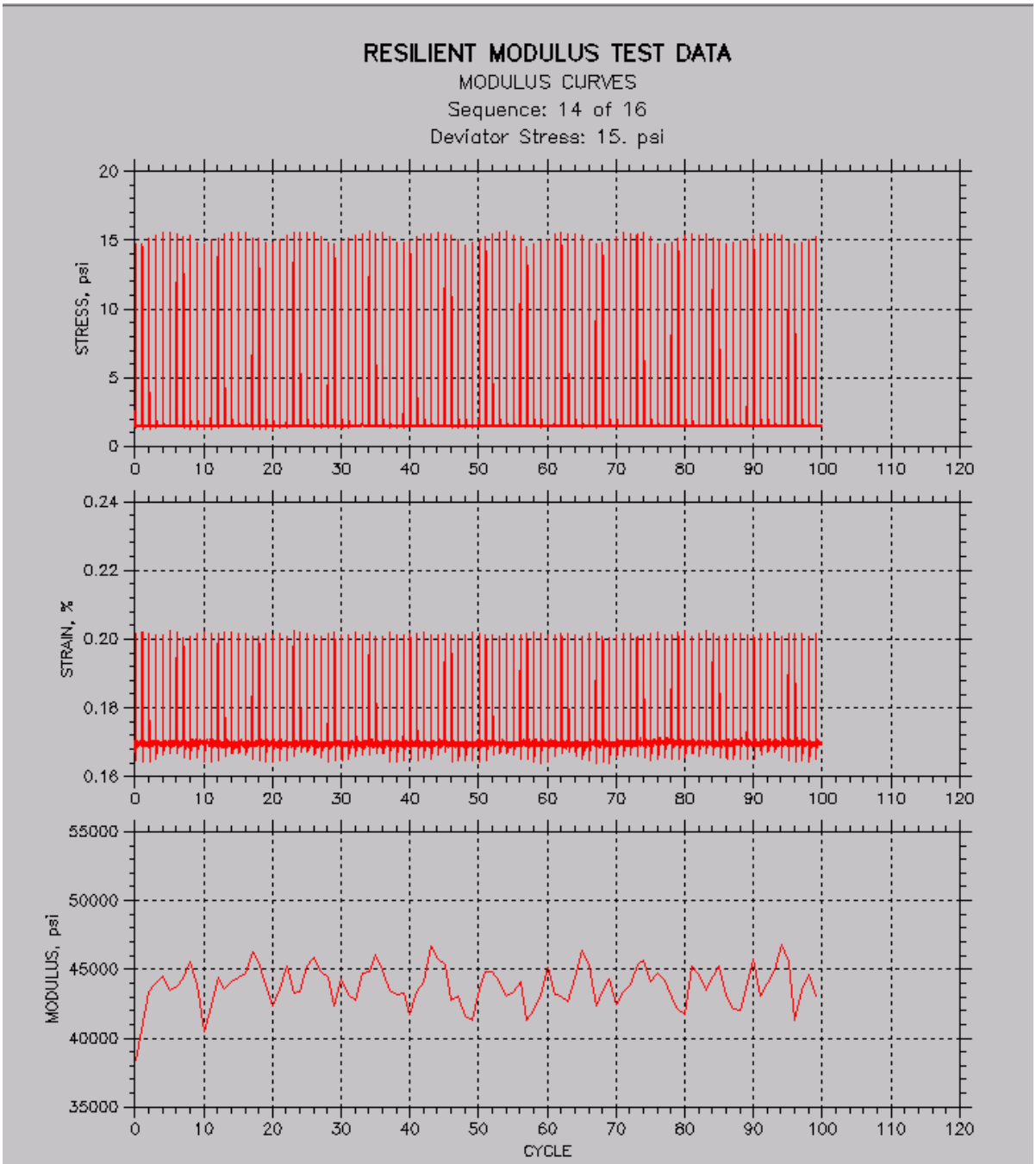

Project: PF2	Location: Ames	Project No.:
Boring No.:	Tested By: JL	Checked By:
Sample No.: 1	Test Date: 20120808	Depth:
Test No.:	Sample Type: Coarse	Elevation:
Description: Manatt's RPCC/RAP 90%RD Mr test 103.26pcf 5.98% w 2.62% fines		
Remarks: Viracating compaction		
File: U:\Desktop\research\data\A New test plan\MR& UU tests\MR tests\dat files\RPCCandRAP_Manatt's_90%RD_103.26pc		

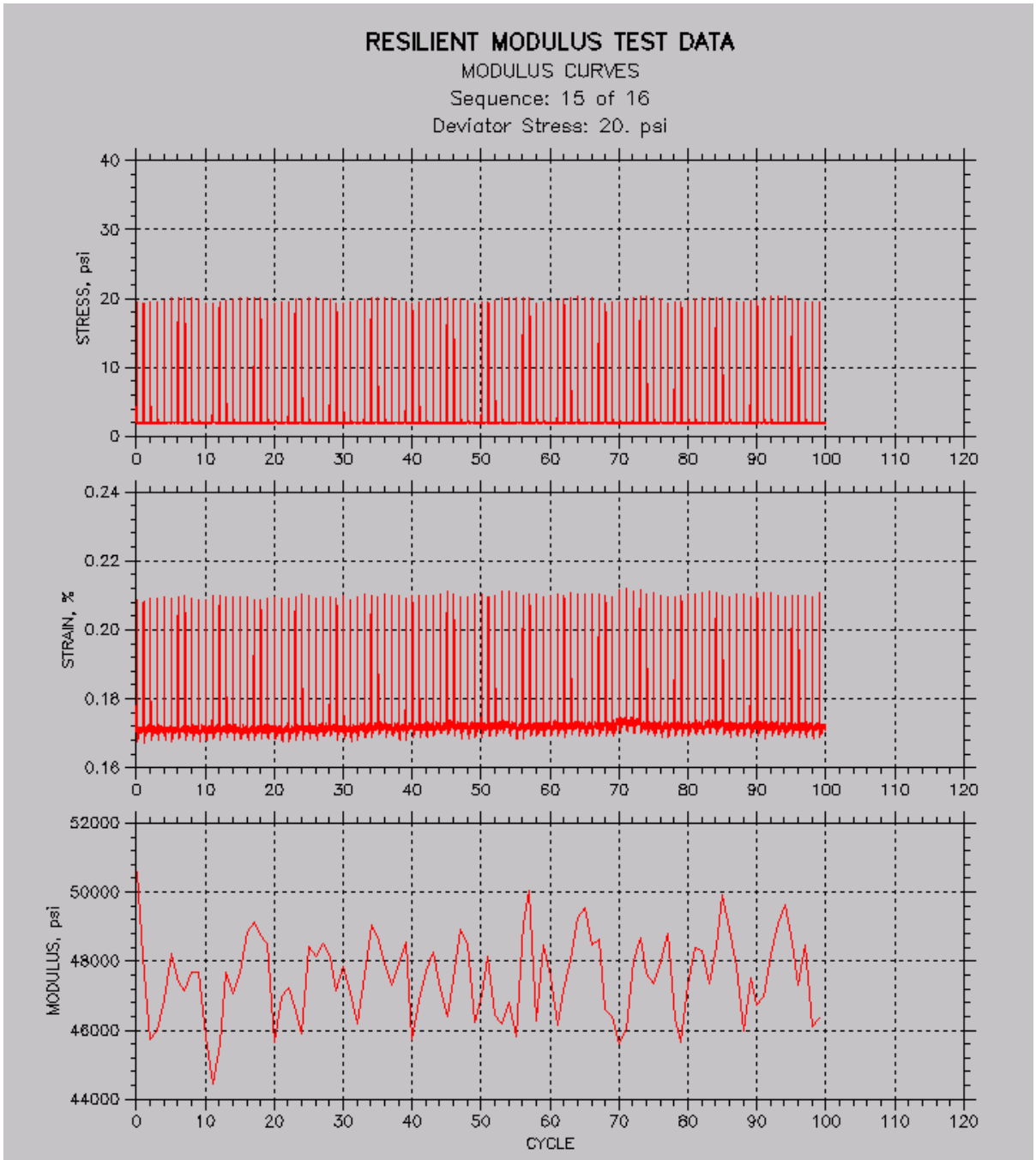

Project: PF2	Location: Ames	Project No.:
Boring No.:	Tested By: JL	Checked By:
Sample No.: 1	Test Date: 20120808	Depth:
Test No.:	Sample Type: Coarse	Elevation:
Description: Manatt's RPCC/RAP 90%RD Mr test 103.26pcf 5.98% w 2.62% fines		
Remarks: Viracating compaction		
File: U:\Desktop\research\data\A New test plan\MR& UU tests\MR tests\dat files\RPCCandRAP_Manatt's_90%RD_103.26pc		

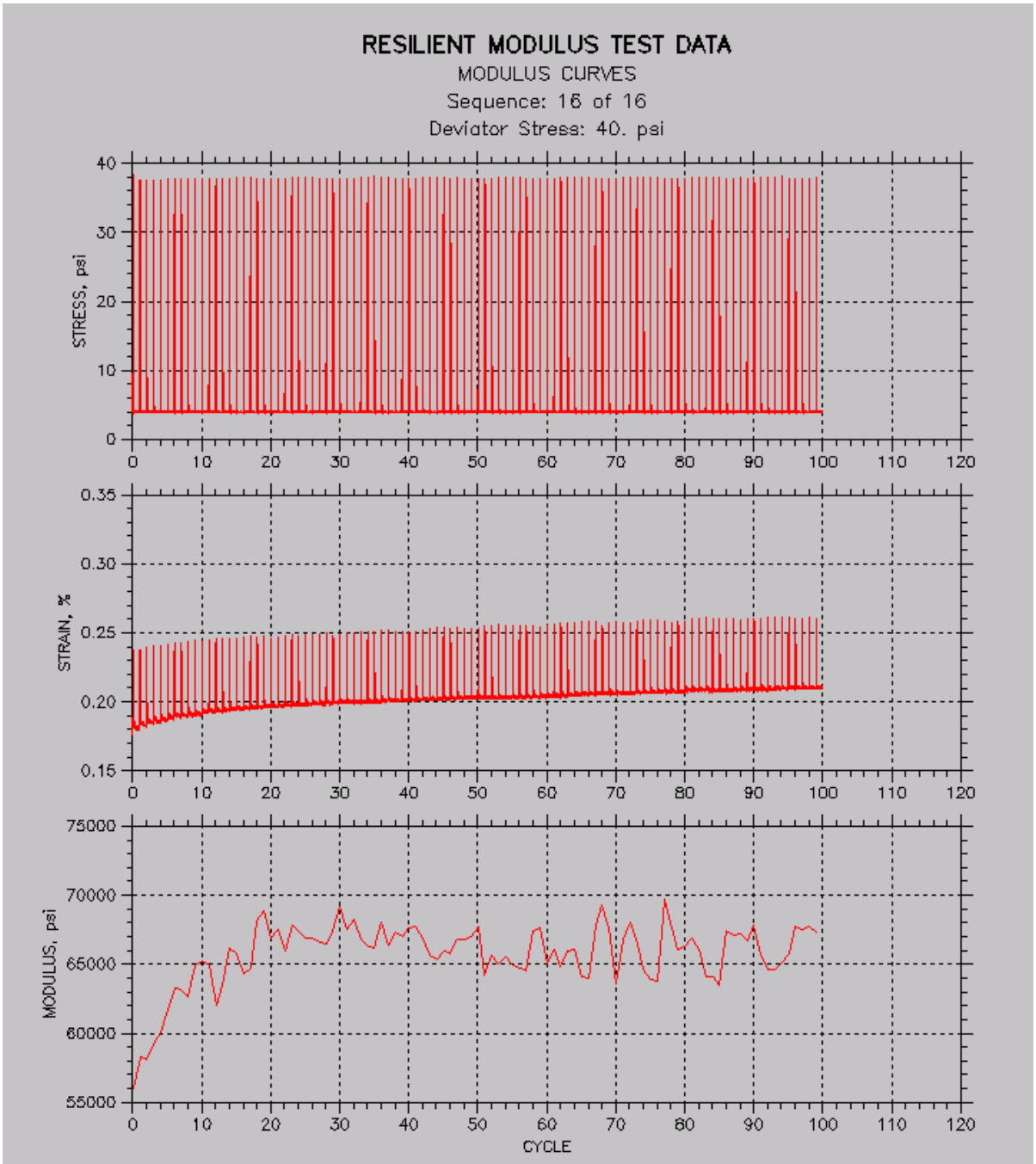

Project: PF2	Location: Ames	Project No.:
Boring No.:	Tested By: JL	Checked By:
Sample No.: 1	Test Date: 20120808	Depth:
Test No.:	Sample Type: Coarse	Elevation:
Description: Manatt's RPCC/RAP 90%RD Mr test 103.26pcf 5.98% w 2.62% fines		
Remarks: Viracating compaction		
File: U:\Desktop\research\data\A New test plan\MR& UU tests\MR tests\dat files\RPCCandRAP_Manatt's_90%RD_103.26pc		

APPENDIX D. LOAD CYCLES SELECTION STUDY

In order to see variance among the average resilient moduli of last five load repetitions (standard method), the maximum M_r and adjacent four load repetitions (max method), and the minimum M_r and adjacent four load repetitions (min method), one load sequence was randomly selected from each M_r test (Table 69) and determined according to system output.

Table 69. Randomly selected load sequence number of each resilient modulus test

Test No.	Target Fines (%)	Target Moisture (%)	RD (%)	Target γ_d (kN/m^3)	Target γ_d (pcf)	Sequence No.
M1	0.0	2.3	85.0	18.99	120.9	1
M2	6.0	2.3	85.0	19.47	123.9	15
M3	7.9	2.3	85.0	17.65	112.4	5
M4	12.0	2.3	85.0	20.33	129.4	7
M5	0.0	2.3	90.0	19.19	122.2	5
M6	6.0	2.3	90.0	19.70	125.4	14
M7	7.9	2.3	90.0	17.71	112.7	12
M8	12.0	2.3	90.0	20.55	130.8	15
M9	0.0	2.3	95.0	19.40	123.5	12
M10	6.0	2.3	95.0	19.95	127.0	13
M11	7.9	2.3	95.0	17.76	113.1	7
M12	12.0	2.3	95.0	20.78	132.3	10
M13	0.0	2.9	85.0	15.75	100.3	13
M14	2.0	2.9	85.0	14.92	95.0	10
M15	6.0	2.9	85.0	17.01	108.3	12
M16	12.0	2.9	85.0	17.62	112.2	5
M17	0.0	2.9	90.0	15.89	101.1	9
M18	2.0	2.9	90.0	15.05	95.8	8
M19	6.0	2.9	90.0	17.14	109.1	11
M20	12.0	2.9	90.0	17.81	113.4	13
M21	0.0	2.9	95.0	16.03	102.0	15
M22	2.0	2.9	95.0	15.17	96.6	10
M23	6.0	2.9	95.0	17.30	110.1	14
M24	12.0	2.9	95.0	18.00	114.6	13
M25	0.0	6.0	85.0	15.26	97.1	12
M26	3.5	6.0	85.0	16.12	102.7	9
M27	6.0	6.0	85.0	16.77	106.8	9
M28	12.0	6.0	85.0	17.54	111.7	5
M29	0.0	6.0	90.0	15.41	98.1	9
M30	3.5	6.0	90.0	16.22	103.3	4
M31	6.0	6.0	90.0	16.96	108.0	11
M32	12.0	6.0	90.0	17.74	113.0	6
M33	0.0	6.0	95.0	15.56	99.1	14
M34	3.5	6.0	95.0	16.32	103.9	15
M35	6.0	6.0	95.0	17.17	109.3	13
M36	12	6.0	95.0	17.95	114.3	7

Table 70. Resilient moduli summary for standard, max, and min methods

Test No.	Standard M_r	Max average	Max M_r					Min average	Min M_r				
	psi	psi	-2	-1	Max	1	2	psi	-2	-1	Min	1	2
1	18930.0	19085.4	19103.8	19115.4	19261.5	19161.5	18784.6	18489.2	18653.8	18692.3	18238.5	18346.2	18515.4
	Load No.		40	41	42	43	44		63	64	65	66	67
2	31917.0	34375.4	32846.2	34738.5	37230.8	34846.2	32215.4	32116.9	32200.0	31600.0	30430.8	32092.3	34261.5
	Load No.		22	23	24	25	26		67	68	69	70	71
3	84573.0	87946.1	85423.1	87403.8	89903.8	88500.0	88500.0	80946.1	84769.2	83557.7	71519.2	81615.4	83269.2
	Load No.		17	18	19	20	21		61	62	63	64	65
4	35004.0	35392.3	34815.4	35907.7	36269.2	34892.3	35076.9	34544.6	34692.3	34400.0	33723.1	34692.3	35215.4
	Load No.		57	58	59	60	61		83	84	85	86	87
5	42445.0	49215.4	49019.2	48923.1	49557.7	49480.8	49096.2	39592.3	39653.8	39653.8	38942.3	39750.0	39961.5
	Load No.		43	44	45	46	47		11	12	13	14	15
6	28978.0	29238.5	28384.6	28769.2	30615.4	29884.6	28538.5	27658.5	27923.1	27692.3	27176.9	27615.4	27884.6
	Load No.		75	76	77	78	79		11	12	13	14	15
7	92798.0	94969.2	93230.8	92500.0	99307.7	94769.2	95038.5	89215.4	99230.8	92500.0	79423.1	86307.7	88615.4
	Load No.		95	96	97	98	99		50	51	52	53	54
8	124050.0	126607.7	127653.8	128923.1	126769.2	126807.7	122884.6	121092.3	125480.8	121153.8	118365.4	119384.6	121076.9
	Load No.		11	12	13	14	15		89	90	91	92	93
9	25573.0	26155.4	26000	25884.6	26707.7	26707.7	25476.9	25390.8	26407.7	26023.1	24553.8	24969.2	25000.0

Test No.	Standard M_r	Max average	Max M_r					Min average	Min M_r				
	psi	psi	-2	-1	Max	1	2	psi	-2	-1	Min	1	2
	Load No.		15	16	17	18	19		54	55	56	57	58
10	72596.0	74757.7	74038.5	75288.5	74884.6	75461.5	74115.4	71326.9	71538.5	71250.0	70096.2	70673.1	73076.9
	Load No.		18	19	20	21	22		89	90	91	92	93
11	57184.0	58467.7	59869.2	57846.2	60769.2	57338.5	56515.4	57155.4	57800.0	56530.8	55484.6	57792.3	58169.2
	Load No.		27	28	29	30	31		60	61	62	63	64
12	36855.0	36869.2	36169.2	36600.0	38115.4	36769.2	36692.3	36221.5	35815.4	35630.8	34953.8	37046.2	37661.5
	Load No.		68	69	70	71	72		85	86	87	88	89
13	23807.0	30884.6	30576.9	30115.4	32115.4	31038.5	30576.9	23807.0	min=standard				
	Load No.		49	50	51	52	53						
14	51044.0	59523.1	73653.8	70961.5	74923.1	74461.5	3615.4	48407.7	49230.8	49153.8	47000.0	47884.6	48769.2
	Load No.		49	50	51	52	53		91	92	93	94	95
15	42436.0	57015.4	58269.2	61730.8	61846.2	52923.1	50307.7	38615.4	40115.4	37961.5	37692.3	38076.9	39230.8
	Load No..		62	63	64	65	66		27	28	29	30	31
16	18864.0	19504.6	20000.0	20069.2	21107.7	18230.8	18115.4	19033.8	20176.9	20692.3	17692.3	17961.5	18646.2
	Load No.		16	17	18	19	20		26	27	28	29	30
17	30512.0	31158.5	30723.1	31876.9	31953.8	31046.2	30192.3	25772.3	25492.3	25807.7	25453.8	25630.8	26476.9
	Load No.		23	24	25	26	27		15	16	17	18	19
18	30152.0	31692.3	32326.9	32923.1	33692.3	31923.1	27596.2	27838.5	31730.8	29711.5	25769.2	25730.8	26250.0

Test No.	Standard M_r	Max average	Max M_r					Min average	Min M_r				
	psi	psi	-2	-1	Max	1	2	psi	-2	-1	Min	1	2
	Load No.		69	70	71	72	73		13	14	15	16	17
19	43322.0	43965.4	43384.6	43884.6	45153.8	44480.8	42923.1	35076.9	35423.1	34846.2	34538.5	35000.0	35576.9
	Load No.		85	86	87	88	89		49	50	51	52	53
20	94894.0	104646.2	98846.2	97307.7	114153.8	108307.7	104615.4	88676.9	88769.2	90769.2	87307.7	89615.4	86923.1
	Load No.		67	68	69	70	71		93	94	95	96	97
21	37129.0	37129.0	max=standard					23676.9	23923.1	23538.5	22923.1	23615.4	24384.6
	Load No.								30	31	32	33	34
22	48616.0	48616.0	max=standard					40192.3	41942.3	41269.2	38096.2	39653.8	40000.0
	Load No.								32	33	34	35	36
23	45573.0	46538.5	46615.4	43846.2	43538.5	44076.9	54615.4	55461.6	53423.1	54230.8	63846.2	53076.9	52730.8
	Load No.		77	78	79	80	81		12	13	14	15	16
24	46426.0	64561.5	60384.6	60000.0	69038.5	67384.6	66000.0	46426.0	min=standard				
	Load No.		12	13	14	15	16						
25	37715.0	37903.9	38000.0	38269.2	38365.4	37788.5	37096.2	32050.0	31942.3	31942.3	31634.6	31846.2	32884.6
	Load No.		92	93	94	95	96		56	57	58	59	60
26	56879.0	60069.2	60038.5	59730.8	61576.9	59500.0	59500.0	56076.9	56442.3	55192.3	54038.5	56826.9	57884.6
	Load No.		11	12	13	14	15		39	40	41	42	43
27	26898.0	27507.7	27646.2	27946.2	28000.0	27546.2	26400.0	24727.7	25723.1	25776.9	24053.8	24084.6	24000.0
	Load No.		37	38	39	40	41		12	13	14	15	16

Test No.	Standard M_r	Max average	Max M_r					Min average	Min M_r				
	psi	psi	-2	-1	Max	1	2	psi	-2	-1	Min	1	2
28	28589.0	29048.5	29269.2	29384.6	29076.9	28723.1	28788.5	27992.3	28400.0	28861.5	27365.4	27507.7	27826.9
	Load No.		11	12	13	14	15		53	54	55	56	57
29	31020.0	32015.4	31826.9	32211.5	31961.5	32115.4	31961.5	25696.1	27250.0	26634.6	24634.6	24961.5	25000.0
	Load No.		61	62	63	64	65		16	17	18	19	20
30	27842.0	31561.5	26903.8	29942.3	34807.7	34153.8	32000.0	29934.6	29038.5	29769.2	24730.8	32884.6	33250.0
	Load No.		42	43	44	45	46		89	90	91	92	93
31	24625.0	24731.5	24269.2	24769.2	25119.2	24750.0	24750.0	24243.1	24330.8	24307.7	23903.8	24038.5	24634.6
	Load No.		88	89	90	91	92		26	27	28	29	30
32	21521.0	22209.6	22151.9	22336.5	22380.8	22321.2	21857.7	21408.4	21978.8	22000.0	20903.8	21173.1	20986.5
	Load No.		23	24	25	26	27		64	65	66	67	68
33	27662.0	29054.8	28811.5	28961.5	29307.7	29058.5	29134.6	27996.2	28538.5	28446.2	27338.5	27796.2	27861.5
	Load No.		23	24	25	26	27		84	85	86	87	88
34	56875.0	56875.0	max=standard					46526.9	46692.3	46865.4	45653.8	46153.8	47269.2
	Load No.								13	14	15	16	17
35	38725.0	39841.5	39638.5	39953.8	40469.2	39684.6	39461.5	38760.0	39400.0	39746.2	37384.6	38269.2	39000.0
	Load No.		34	35	36	37	38		27	28	29	30	31
36	19765.0	21090.8	20269.2	20930.8	23284.6	20638.5	20330.8	19733.9	20046.2	19692.3	19230.8	19669.2	20030.8
	Load No.		73	74	75	76	77		67	68	69	70	71

Statistical Analysis for Comparing Three Methods

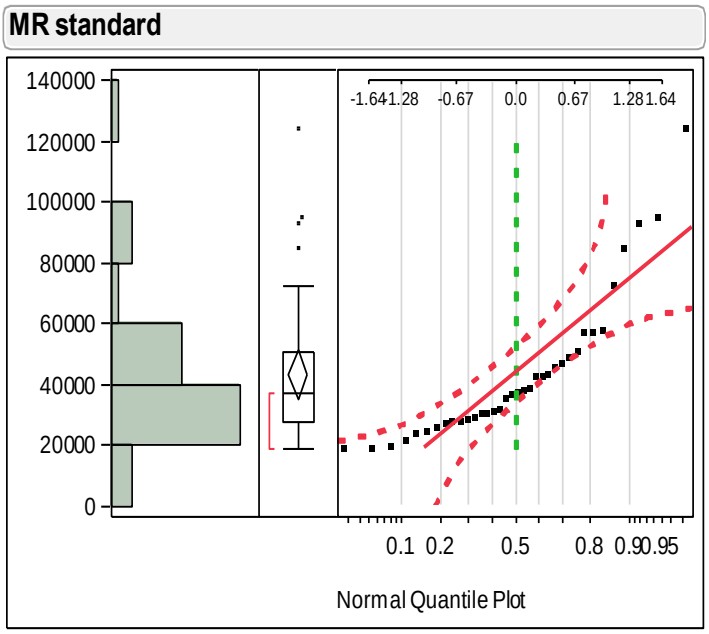

Quantiles

100.0%	maximum	124050
99.5%		124050
97.5%		124050
90.0%		87040.5
75.0%	quartile	50437
50.0%	median	36992
25.0%	quartile	27707
10.0%		20994.2
2.5%		18864
0.5%		18864
0.0%	minimum	18864

Moments

Mean	43383.167
Std Dev	23972.433
Std Err Mean	3995.4055
Upper 95% Mean	51494.271
Lower 95% Mean	35272.062
N	36

Figure 149. Distribution of standard M_r values

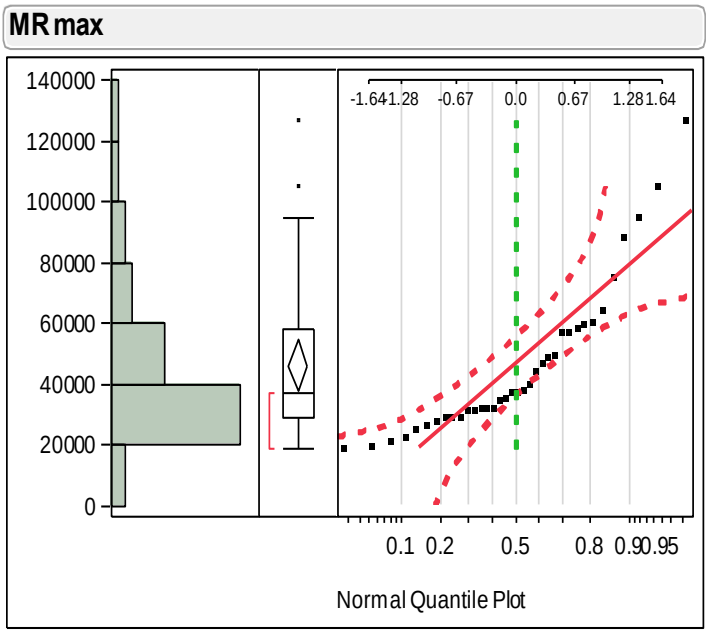

Quantiles

100.0%	maximum	126608
99.5%		126608
97.5%		126608
90.0%		90053
75.0%	quartile	58104.6
50.0%	median	36999.1
25.0%	quartile	29100.7
10.0%		21874
2.5%		19085.4
0.5%		19085.4
0.0%	minimum	19085.4

Moments

Mean	46117.347
Std Dev	25236.061
Std Err Mean	4206.0102
Upper 95% Mean	54656.002
Lower 95% Mean	37578.692
N	36

Figure 150. Distribution of maximum average M_r values

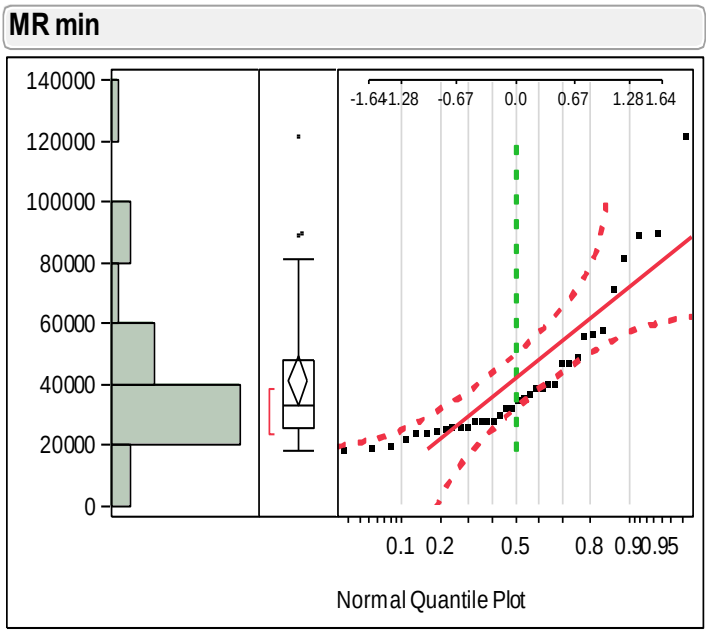

Quantiles

100.0%	maximum	121092
99.5%		121092
97.5%		121092
90.0%		83265.3
75.0%	quartile	47937.5
50.0%	median	33330.8
25.0%	quartile	25467.1
10.0%		20906.1
2.5%		18489.2
0.5%		18489.2
0.0%	minimum	18489.2

Moments

Mean	41163.369
Std Dev	23360.277
Std Err Mean	3893.3795
Upper 95% Mean	49067.35
Lower 95% Mean	33259.389
N	36

Figure 151. Distribution of minimum average M_r values

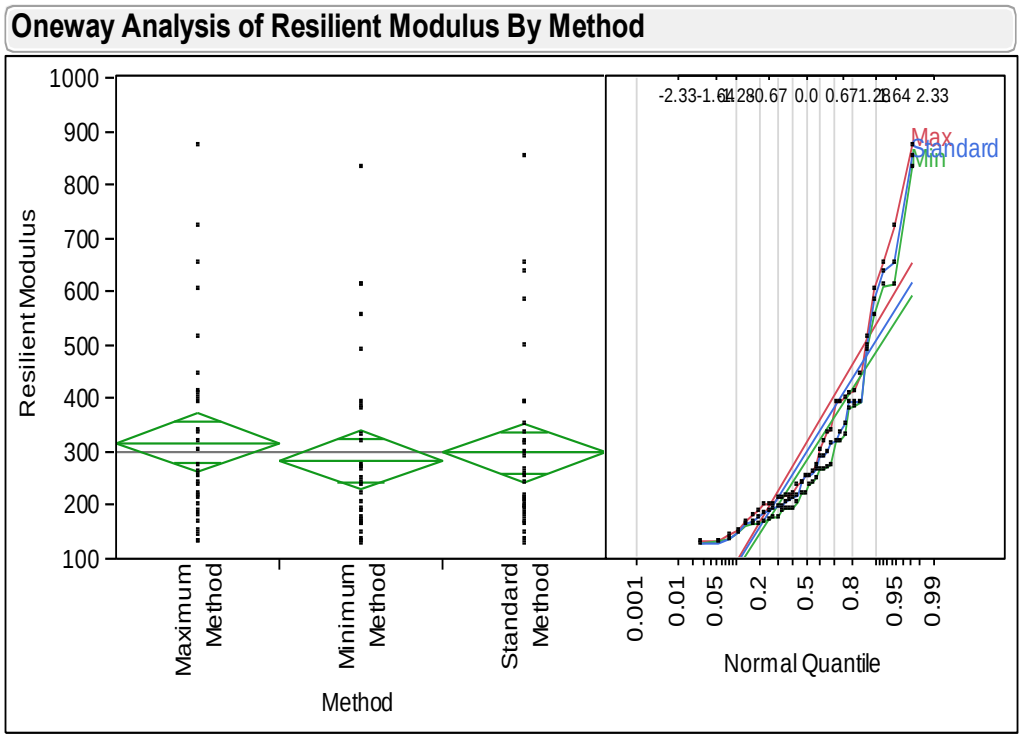

Oneway Anova

Summary of Fit

Rsquare	0.007157
Adj Rsquare	-0.01175
Root Mean Square Error	166.8683
Mean of Response	300.2986
Observations (or Sum Wgts)	108

Analysis of Variance

Source	DF	Sum of Squares	Mean Square	F Ratio	Prob > F
Method	2	21075.4	10537.7	0.3784	0.6859
Error	105	2923727.4	27845.0		
C. Total	107	2944802.8			

Means for Oneway Anova

Level	Number	Mean	Std Error	Lower 95%	Upper 95%
Maximum Method	36	317.968	27.811	262.82	373.11
Minimum Method	36	283.811	27.811	228.67	338.96
Standard Method	36	299.116	27.811	243.97	354.26

Std Error uses a pooled estimate of error variance

Figure 152. Comparing three methods for average M_r values at selected load sequences

APPENDIX E. HYDROMETER CORRECTIONS

A 152H hydrometer was used for all hydrometer tests in this study, and the temperature corrections were made by recording the readings of the hydrometer in pure distilled water and distilled water with dispersing agent (40g/L sodium hexametaphosphate solution). These solutions were placed in three glass cylinders which were placed in a water bath where the temperature was controlled (Figure 153). The hydrometer temperature corrections in distilled water with dispersing agent were plotted in Figure 154 and in distilled water were plotted in Figure 155. The hydrometer temperature corrections are negative values of hydrometer readings.

Figure 153. Glass cylinders in a water bath

Table 71. Readings of the hydrometer in distilled water with dispersing agent

Temperature °C	10.1	11.5	13.7	17.4	20.3	22.3	22.8	24.1
Reading	-6.33	-6.20	-6.00	-5.20	-4.38	-4.05	-4.00	-3.70
Temperature °C	25.9	29.0	29.8	30.8	33.6	35.4	40.1	
Reading	-3.03	-2.07	-1.97	-1.47	-0.07	0.87	3.00	

Table 72. Hydrometer temperature corrections in distilled water

Jar #B		Jar #E		Jar #G		Average	
T (ºC)	Correction	T (°C)	Correction	T (°C)	Correction	T(°C)	Correction
11.5	-1.00	11.5	-1.00	11.5	-1.00	11.5	-1.00
13.0	-0.80	13.0	-0.80	13.0	-0.80	13.0	-0.80
14.5	-0.55	14.5	-0.50	14.5	-0.50	14.5	-0.52
15.5	-0.55	15.5	-0.50	15.5	-0.45	15.5	-0.50
17.9	-0.10	17.9	-0.10	17.9	-0.10	17.9	-0.10
18.3	-0.10	18.3	-0.10	18.3	-0.05	18.3	-0.08
19.6	0.04	19.6	0.04	19.6	0.04	19.6	0.04
20.4	0.20	20.4	0.20	20.4	0.25	20.4	0.22
20.7	0.30	20.7	0.30	20.7	0.30	20.7	0.30
21.1	0.50	21.1	0.50	21.1	0.50	21.1	0.50
21.6	0.50	21.6	0.50	21.6	0.50	21.6	0.50
22.4	0.80	22.4	0.80	22.4	0.80	22.4	0.80
22.7	0.95	22.7	0.95	22.7	0.95	22.7	0.95
24.0	1.00	24.0	1.10	24.0	1.15	24.0	1.08
24.1	1.05	24.1	1.10	24.1	1.30	24.1	1.15
25.4	1.80	25.4	1.95	25.4	1.90	25.4	1.88
25.4	1.80	25.4	1.85	25.4	1.80	25.4	1.82
26.7	2.00	26.7	2.05	26.7	2.05	26.7	2.03
26.9	2.15	26.9	2.20	26.9	2.25	26.9	2.20
28.0	2.70	28.0	2.70	28.0	2.75	28.0	2.72
28.9	3.00	28.9	3.00	28.9	3.00	28.9	3.00
31.4	3.95	31.4	3.90	31.4	3.90	31.4	3.92
31.9	4.10	31.9	4.10	31.9	4.00	31.9	4.07
32.5	4.50	32.5	4.70	32.5	4.60	32.5	4.60
37.2	7.40	37.2	7.60	37.2	7.60	37.2	7.53

Note: T means temperature.

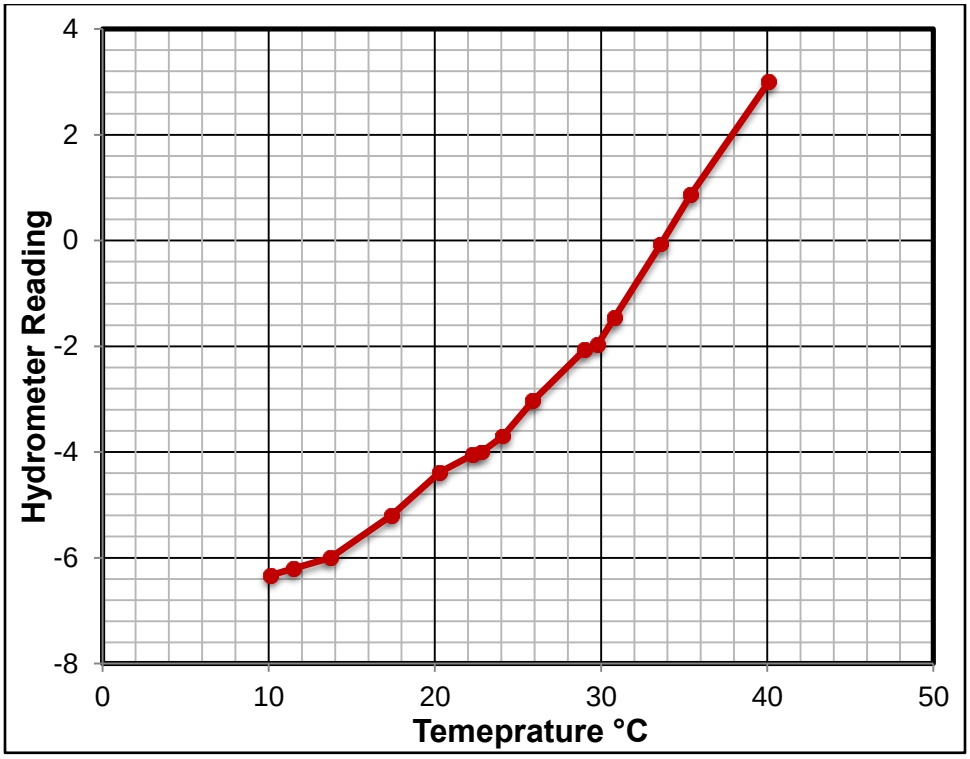

Figure 154. Hydrometer temperature correction in water with dispersing agent solution

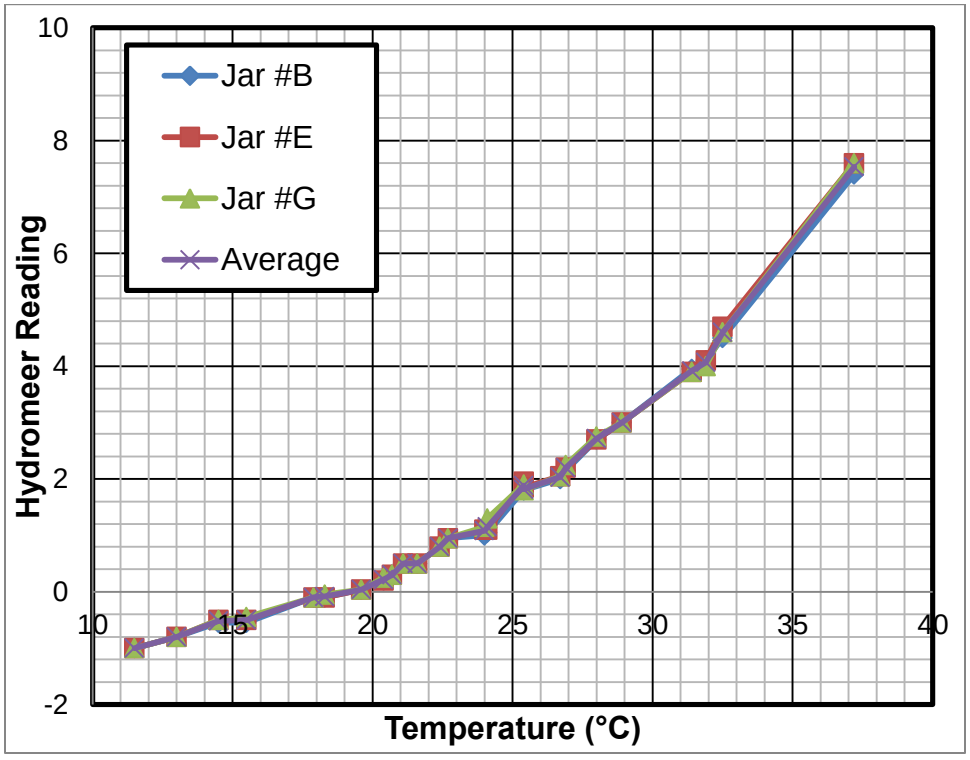

Figure 155. Hydrometer temperature corrections in distilled water

ACKNOWLEGEMENTS

I would like to express my deepest thanks to my mentor and advisor, Dr. David White, for his support and guidance throughout my research work. I am also very grateful to him for giving me opportunity to study and work with his research team and providing financial support for my studies, allowing me expand my knowledge on geotechnical engineering, skills on English communications, and experiences on field studies.

I would also like to thank the members on mu committee, Dr. Pavana Vennapusa and Dr. Robert Stephenson, who not only gave comments and suggestions on my thesis but who are also great instructors for answering my question with great knowledge and patience. Additionally, Dr. Pavana Vennapusa also instructed me on calibrating and using the tests apparatus and helped on managing materials. Moreover, Dr. Robert Stephenson gave me great guidance on analyzing the results in a scientific way by using statistical analysis and helps me confirm my conclusions with strong support.

I would like to express my gratitude toward Heath Gieselman who gave me instructions on lab works and Bob Steffes who helped me on modifying the test apparatus. Additionally, I am also very grateful to Dr. Christianna White for giving me instructions on learning technical writing skills.

Much appreciation is extended to the National Concrete Pavement Technology Center, for sponsoring this research. I would also to thank everyone I have met and worked with in the Earthworks Engineering Research Center and geotechnical laboratories at Iowa State University.

Last but certainly not least, I would like to thank my parents and my friends for their endless support and encouragement. The Master's degree is a long journey for me, and without their encouragement, this journey would be much more difficult.